EUROPEAN COMMISSION

SCIENCE
RESEARCH
DEVELOPMENT

technical steel research

Properties and in-service performance

Buckling curves of hot rolled H steel sections submitted to fire

Report

EUR 18380 EN

STEEL RESEARCH

EUROPEAN COMMISSION

Édith CRESSON, Member of the Commission
responsible for research, innovation, education, training and youth

DG XII/C.2 — RTD actions: Industrial and materials technologies — Materials and steel

Contact: Mr H. J.-L. Martin
Address: European Commission, rue de la Loi 200 (MO 75 1/10), B-1049 Brussels — Tel. (32-2) 29-53453; fax (32-2) 29-65987

European Commission

technical steel research

Properties and in-service performance

Buckling curves of hot rolled H steel sections submitted to fire

J.B. Schleich, L-G. Cajot
ProfilARBED-Recherches
66, rue de Luxembourg
L-4002 Esch/Alzette

J. Kruppa, D. Talamona
CTICM
Domaine de St. Paul
BP 1
F-78470 St.-Rémy-les-Chevreuse

W. Azpiazu, J. Unanue
LABEIN
Cuesta de Olabeaga 16
E-48013 Bilbao

L. Twilt, J. Fellinger, R-J. Van Foeken
TNO
PO Box 49
2600 AA Delft
The Netherlands

J-M. Franssen
Université de Liège
Quai Banning 6
B-4000 Liège

Contract No 7210-SA/316/515/618/931
1 July 1992 to 30 June 1995

Final report

Directorate-General
Science, Research and Development

1998

EUR 18380 EN

A great deal of additional information on the European Union is available on the Internet.
It can be accessed through the Europa server (http://europa.eu.int).

Cataloguing data can be found at the end of this publication.

Luxembourg: Office for Official Publications of the European Communities, 1998

ISBN 92-828-4603-2

Printed in Luxembourg

PRINTED ON WHITE CHLORINE-FREE PAPER

BUCKLING CURVES OF HOT ROLLED H STEEL SECTIONS SUBMITTED TO FIRE

C.E.C. Agreement N° 7210-SA/316/515/618/931

DRAFT FINAL REPORT (01.07.1992 to 30.06.1995)

S U M M A R Y

The research has lead to new formulae for the design of steel columns in case of fire:
- a new N/M interaction formula
- new buckling curves instead of the buckling curve c divided by 1,2 proposed in the present version of Eurocode 3 Part 1.2.

These formulae are presented in Design tables useful for the practical engineer. These formulae were deduced and calibrated from a very large amount of numerical simulations (more than 300 000) and from a database comprising 141 test results including the 29 tests made in the frame of the research.

For the study of the axially loaded columns, 21 tests have been performed in the Laboratory of LABEIN in Bilbao and 8 tests have been made in the CTICM laboratory in Maizières-les-Metz to analyse columns subjected to a normal force and a constant bending moment distribution.

The numerical simulations were made by using the five programs available in the different organizations: CEFICOSS and SAFIR (ProfilARBED Recherches and University of Liège), DIANA (TNO), LENAS and SISMEF (CTICM).

R É S U M É

La recherche a permis de définir de nouvelles formules pour le calcul des colonnes en acier soumises au feu:
- une nouvelle formule d'interaction N/M
- de nouvelles courbes de flambement à la place de la courbe c divisée par 1,2 de la version actuelle de l'Eurocode 3 Part 1.2.

Ces formules sont présentées sous forme d'abaques facilement utilisables par les ingénieurs de bureaux d'études. Ces formules ont été déduites et calibrées suite à un grand nombre de simulations numériques (plus de 300 000) et à partir d'une base de données comprenant les résultats de 141 tests incluant 29 tests réalisés dans le cadre de cette recherche.

Pour l'étude des colonnes chargées axiallement 21 tests ont été réalisés au laboratoire de LABEIN à Bilbao tandis que 8 tests ont eu lieu au laboratoire du CTICM à Maizières-les-Metz pour analyser les colonnes soumises à une force normale et à un moment fléchissant constant.

Les simulations ont été faites en utilisant 5 logiciels disponibles auprès des différents partenaires: CEFICOSS et SAFIR (ProfilARBED Recherches et Universitè de Liège), DIANA (TNO), LENAS et SISMEF (CTICM).

Z U S A M M E N F A S S U N G

Das vorliegende Projekt hat zu neuen Formeln zur Bemessung von Stahlstützen im Brandfall geführt:
- eine neue Formel zur N/M Interaktion
- neue Knickkurven, anstatt der empfohlene Kurve c geteilt durch 1,2 der jetzigen Fassung von EC 3 Teil 1.2.

Diese Formeln werden den Anwendern in praktische Bemessungstafeln vorgestellt. Diese Formeln wurden abgeleitet und kalibriert durch eine hohe Anzahl von numerischen Simulationen (über 300 000) und aus einer Datenbank mit den Resultaten von 141 Versuchen einschließlich der 29 Versuche im Rahmen dieses Projektes.

Für die Untersuchung der axial belasteten Stützen wurden 21 Versuche bei LABEIN in Bilbao sowie für die Untersuchung der axial belasteten Stützen mit konstantem Biegemoment wurden 8 Versuche bei CTICM in Maizières-les-Metz durchgeführt.

Die numerischen Simulationen wurden durchgeführt unter Zuhilfenahme von 5 den verschiedenen Partnern zur Verfügung stehenden Programmen: CEFICOSS und SAFIR (ProfilARBED Forschung und Universität Lüttich), DIANA (TNO), LENAS und SISMEF (CTICM).

TABLE OF CONTENTS

1. INTRODUCTION

The following financially independent partners have participated in the research:

- ProfilARBED Recherches, Luxembourg and University of Liège (Belgium) as sub-contractor
- CTICM, France
- TNO, The Netherlands
- LABEIN and ENSIDESA (SPAIN)

The technical coordination has been handled by ProfilARBED Department "Recherches et Promotion Techniques Structure (RPS)".

It was decided that only **one** final ECSC report will be written by the leader ProfilARBED-Recherches. This final report includes the contributions of

- Mr. J.-M Franssen for University of Liège,
- Mr. Azpiazu and Mr. Unanue for LABEIN,
- Mr. Talamona and Mr. Kruppa for CTICM,
- Mr Twilt, Mr Fellinger and Mr. van Foeken for TNO.

This research was composed of an experimental part and a theoretical part divided into three main subjects

- calculation models
- numerical simulations
- design rules

In all the items, the two following loadings were considered:

- axially loaded columns
- members subjected to a normal force and a bending moment distribution

In the experimental part, 21 tests on axially loaded columns have been performed in the LABEIN laboratory in Bilbao and 8 tests on eccentrically loaded columns in the CTICM laboratory of Maizières-les-Metz. Moreover 112 test results were obtained from different laboratories (Braunschweig, Berlin, Gent, Borehamwood, Rennes ...) and were stored in a database. This database includes 141 test results which have been used to calibrate the design formulae later.

As different software was available to the different partners (CEFICOSS, DIANA, LENAS, SAFIR and SISMEF), they were compared by using a set of calibration examples dealing with axial and eccentric loads. They were also used to simulate the 21 LABEIN tests and the 8 CTICM tests. Both exercises (calibration examples and comparison with test results) pointed out a good correspondence between the different numerical results and the measurements.

The software SAFIR was used to simulate the centrally loaded columns and the following cases were calculated.

- Two nominal yield strength, fy = 235 MPa and fy = 355 MPa, have been considered,
- H sections were given their nominal dimensions, according to the catalogue of the ARBED (1994) company, comprising European, American and British series,

- as the beam finite element does not allow local buckling to be taken into account, the sections which are classified under class 4 in pure compression according to EC3 1992 have not been considered. The fire resistance of class 4 profiles should therefore be assessed by means of experimental tests or by means of numerical simulations taking into account local buckling, which was beyond the scope of this project. Finally 339 sections of H steel profiles were considered for steel S235 and 258 sections for steel S355,
- for each section and each yield strength, buckling around the major axis, as well as around the minor axis, have been taken into account separately,
- for each section, yield strength and buckling axis, 10 different lengths have been considered, with the slenderness at ambient temperature λ equal to 20, 40, 60, ..., 200
  where $\lambda = H/i$ slenderness of the column,
  with i radius of gyration of the section.
- for each length, an average of 15 different load cases where applied, leading each time to a different value of the ultimate critical temperature.

The total number of single simulations is estimated to $(339 + 258) \times 2 \times 10 \times 15 \approx 180{,}000$ cases for centrally loaded columns at uniform temperature. In order to sort those results and derive some conclusions, it was necessary to establish an interpolation procedure which allows us to determine the ultimate load N_u as a function of the temperature θ and of the length H, once the cross section, the buckling plane and the yield strength have been chosen. The interpolation procedure is based on sinusoidal functions in the direction of H, owing to the fact that the buckling curves at each temperature have a very continuous and regular pattern. In the direction of θ on the other hand, the curves are made of multi linear segments, due to the fact that the material characteristics are linearly interpolated between values given every 100°C. In this direction the utilization of linear B-splines - and least square method in order to cope with redundant points - allowed us to calculate the ultimate loads leading to ultimate temperatures θ of 400, 500, ... 900°C.

For eccentrically loaded columns, the software LENAS was mainly used. Some checks were done by using DIANA.
Owing to the fact that the study on centrally loaded columns already showed a low dependency of the section type on the results when this work on eccentrically loaded columns started, and also because the number of parameters is here increased by 2 - the eccentricity of the load at each end of the column - , it was decided that not all the possible section types would be analysed. 28 steel sections were selected, covering the whole range from IPE 80 to HEM 1000.

- Three types of bending moment distribution (uniform, triangular and bi-triangular) over the length of the column have been analysed.
- 7 different eccentricities of the load were studied to find out the shape of the M-N interaction curve: $\delta = 0.00$, 0.05 , 0.10 , 0.50 , 1.00 , 3.00 , and 5.00 x i, with i the radius of gyration of the section.
- Because residual stresses have an influence only on centrally loaded columns, the effect of the yield strength on the shape of the M-N interaction curves was supposed to be negligible and only steel S235 has been considered.
- As for the axially loaded columns, an interpolation procedure was used to deduce the results for 400°C, 500°C, 600°C, 700°C, 800°C and 900°C.

In case of eccentrically loaded members, the effect of a thermal gradient on the N-M interaction curve was analysed by using DIANA.

The numerical simulations have allowed the proposal of an analytical formula for the buckling coefficient in case of central loading and an analytical expression for the interaction N-M curve in case of eccentrical loading. The expression for the buckling coefficient contains one scalar parameter, the severity factor β, which has been calibrated as to ensure the appropriate safety level. The interaction formula has also been validated against a large set of experimental results. Those calibration and verifications were made by using the tests database. Finally the comparison with the database has lead to Design formulae and Design tables useful for the practical engineer.

2. *EXPERIMENTAL WORK: FIRE TESTS ON STEEL COLUMNS*

2.1 INTRODUCTION

Of course some experimental test results are available in the literature and will be considered in the research. However, in order to avoid possible bias in the conclusions, it is desirable to obtain an experimental base as wide as possible, as well concerning the total number of tests as concerning the number of different independent sources, i.e. different laboratories. As it was not possible to find all the necessary experimental situations, it was decided to perform two new series of experimental tests;

- One series on columns with small eccentricity of the load. The same cross section was used for all the tests and the length of the column was changed in order to analyze the effect of this buckling length. In most of the available test results, the length of the column is fixed by the dimensions of the furnace, and the slenderness is changed by means of changes of the end supports and/or of the section type.
- One series on columns with very large eccentricities of the load. This situation has been seldom analyzed experimentally in the past.

2.2 GENERAL DESCRIPTION AND MAIN RESULTS

21 fire tests were performed in Spain in the LABEIN laboratory and 8 others at the Fire Station of CTICM (France).

The specimens were electrically heated by means of ceramic mat elements at a rate of;

- 5 K/min for the tests made by LABEIN,
- 10 K/min up to 400°C and 5 K/min beyond 400°C for the tests made by CTICM.

Automatic control of separate heating elements was present in order to ensure a uniform temperature distribution along the length of the elements. The temperature field has been measured with thermocouples welded on the specimens. The number of measurement points on each column varied from 17 to 35 depending on the length of the column. In the case that somewhat lower temperatures were recorded near the supports, the failure temperature of the element was estimated as the mean temperature of the thermocouples located in the central part of the column. The load as well as the axial expansion and horizontal displacements at mid level were monitored during the test. TABLE 2.2.1 is a summary of the tests made in LABEIN - first part of the table -and CTICM.

In this table;

- N° is the number of the test in the test report,
- Buc. axis defines the buckling axis as S for major and W for minor axis.
- i2 is the imperfection at L/4, i3 the imperfection at 2L/4, and i4 the imperfection at 3L/4,

TABLE 2.2.1 Results of the experimental tests made by LABEIN and CTICM.

N°	H	θ_u	Buc.	e	N	fy_w	fy_f	b	H	t_w	t_f	i2	i3	i4
	mm	°C	axis	mm	kN	MPa	MPa	mm	mm	mm	mm	mm	mm	mm
AL1	513	20	W	5	537	300	280	101.90	99.20	6.10	7.80		0.00	
BL1	513	532	W	5	362	300	286.5	101.85	98.85	5.92	7.61		0.00	
CL1	513	694	W	5	110	316	292.5	101.78	99.07	6.43	7.80		0.00	
DL1	513	863	W	5	40	309	282.5	102.28	99.12	6.13	7.68		0.00	
AL3	1270	20	W	5	490	300	280	101.95	99.08	5.97	7.67		0.00	
BL3	1272	390	W	5	292	300	286.5	101.93	98.90	5.97	7.64		0.20	
CL3	1271	474	W	5	251	316	292.5	101.90	99.25	6.13	7.82		0.40	
DL3	1269	749	W	5	24	309	282.5	102.15	99.15	6.02	7.73		0.30	
SL40	2020	525	W	5	170	286	280							
SL41	2026	509	W	5	174	286	280	101.84	98.97	5.73	7.58	0.60	0.70	0.70
SL42	2020	485	W	5	171	286	280	101.82	99.04	5.76	7.61	0.90	1.70	0.90
SL43	2021	20	W	5	366	286	280	101.84	98.89	5.80	7.57	-0.40	0.00	0.00
SL44	2023	495	W	5	173	286	280	101.68	99.17	5.73	7.60	0.50	1.10	0.60
AL5	2770	457	W	5	127	300	280	101.94	99.06	5.78	7.68	-0.07	-0.04	0.60
BL5	2772	587	W	5	73	300	286.5	101.76	98.95	5.76	7.62	0.30	1.00	0.80
CL5	2771	587	W	5	34	316	292.5	102.03	99.25	5.98	7.76	0.70	0.80	0.80
DL5	2772	886	W	5	7.7	309	282.5	102.15	99.16	5.96	7.72	0.80	1.60	0.80
AL6	3510	20	W	5	176	300	280	101.99	99.08	5.79	7.66	-0.70	-0.40	0.60
BL6	3510	446	W	5	105	300	286.5	101.88	98.93	5.93	7.63	0.80	1.00	0.30
CL6	3510	493	W	5	90	316	292.5	102.05	99.12	5.94	7.71	0.70	0.80	0.80
DL6	3510	727	W	5	11.5	309	282.5	101.68	99.17	5.73	7.60	0.80	1.60	0.80
P1	4000	664	W	100	100	314	275	200.2	201.4	9.04	15.04	-0.5	-0.5	-0.5
P2	4000	575	W	300	100	314	275	200.3	201.4	9.04	15	-1	-3	-3
P3	2000	599	S	650	100	314	275	200.3	201.3	9.04	14.96	-0.5	-0.5	-0.5
P4	2000	537	W	300	150	314	275	200.3	201.4	9.04	15	1.5	0.5	0.5
P5	2000	753	S	250	100	344	271	163.4	180.2	14	22.68	0.5	0	0
P6	5000	572	S	500	100	344	271	163.5	180.4	14	22.62	2	3	1.5
P7	2000	539	S	100	160	304	260	141.5	137.5	5.61	8.96	0	0	-0.5
P8	5000	507	S	100	100	304	260	139.8	133.8	5.61	8.28	1	0.5	0.5

Note;

- The values given for the ultimate temperature, the yield strengths and the dimensions of the section result from the average between several measured values.
- The elements were placed vertically. They were turned in such a way that the effect of the imperfection was added to the effect of the load eccentricity if the value of i2, i3 or i4 has a positive sign in TABLE 2.2.1.
- The measured residual stresses were in the order of magnitude of 0.10 x 235 MPa.

The sections were HEA100 profiles for the LABEIN tests and HEA140, HEM160 and HEB200 for the CTICM tests. Geometrical dimensions of the section and geometrical imperfections - i.e. out of straightness - of the column and were measured for each tested element. Residual stresses and yield strengths were measured from coupons belonging to the same production as the tested elements. The load was applied before the test and kept constant during the heating. It was applied with a well defined eccentricity through a very sharp knife support (or rollers at CTICM). The end rotation around this axis was free, and the rotation around the other axis was supposed to be restrained by the action of the knife (see FIGURE 2.2.1). Different buckling lengths from 510 to 5000 mm were considered, with different load levels.

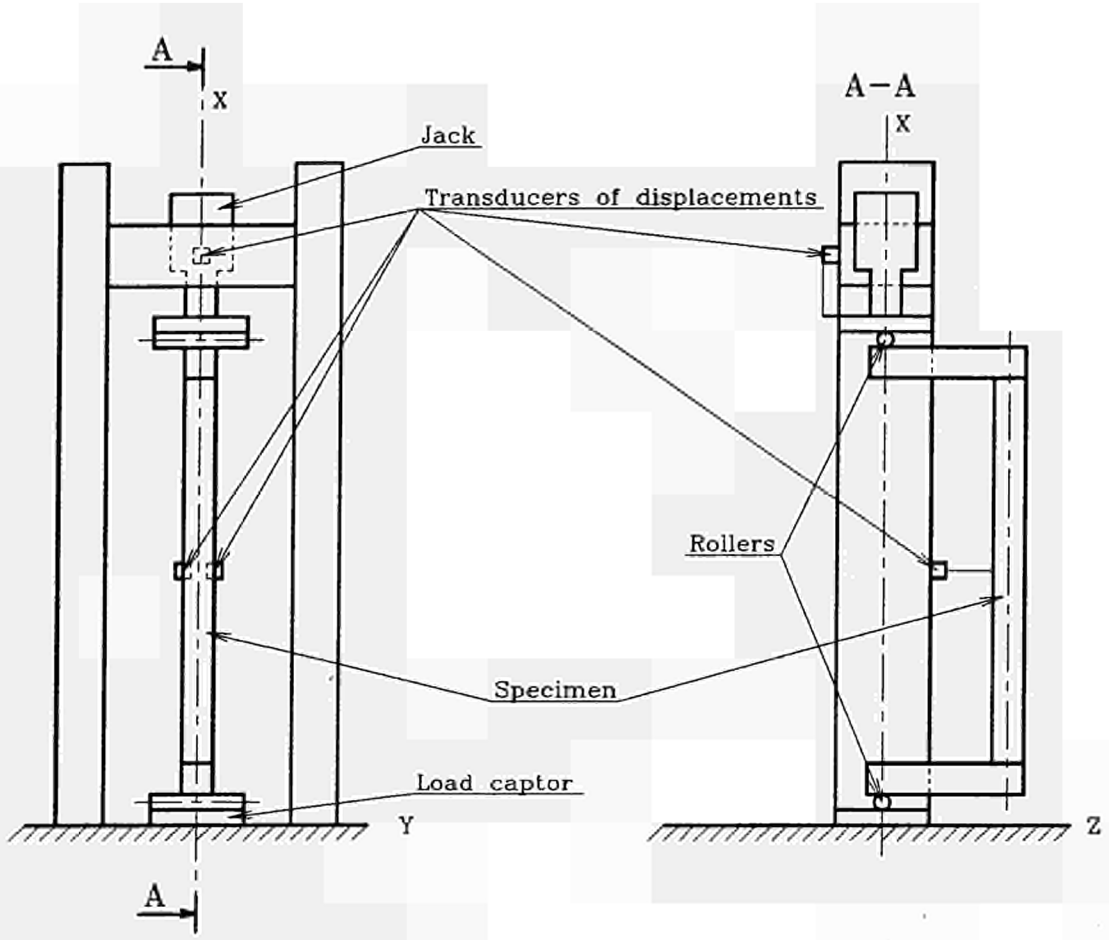

FIGURE 2.2.1 Experimental test rig.

Due to the fact that tests AL1, AL3, SL43 and AL6 were performed at ambient temperature, that test SL40 was a preliminary test performed to verify the heating equipment on an element which had not been precisely measured, and that some technical difficulties lead to uncertainties in tests DL3 and CL5, 14 tests from those performed at elevated temperature with a small eccentricity remain for consideration in the data base.

2.3 LABEIN TESTS

2.3.1 Data

Twenty-one HE100A specimens, with five different slenderness ratios, have been extracted from five primary profiles A, B, C, D and S and tested according to the following procedure.

		LENGTH (mm)						
		L1=510	L3=1270	L4=2020	L5=2770	L6=3510		
FAILURE TEMPERATUR EXPECTED (°C)	ROOM	AL1	AL3	SL4.3		AL6	Applied LOAD	0 → FAILURE LOAD
	400		BL3			BL6		Estimated b
	500	BL1	CL3	SL4.0/4.1/4.2/4.4	AL5	CL6		Numerical Simulations
	600				BL5			
	700	CL1			CL5			
	850	DL1	DL3		DL5	DL6		

The notations of the tests are xLy.z where x is A, B, C, D or S corresponding to the primary profile from which the specimens were obtained, where y is 1, 3, 4, 5 or 6 to identify the specimen length and where z is the number of the test in case of same length and same primary profile.

Four tests have been performed to determine the failure load at room temperature. For the other 17 tests, the procedure is represented in FIGURE 2.3.1:

- The load has been applied before heating. These loads have been provided for each specimen by the University of Liège so that the failure happens at the expected temperature.
- The load has been applied with an eccentricity of 5 mm.
- The buckling was along the weak axis.
- After loading the temperature has been increased by a ratio of 5°C/min until failure.
- A knife support has been used in top and bottom ends (FIGURE 2.3.2).

2.3.2 Measurements done before testing

2.3.2.1 Dimensional Measurements (See Annex 1)

2.3.2.2 Residual Stresses (See Annex 2)

2.3.2.3 Mechanical properties of steel.

Six tensile tests (three for the web and three for the flange) have been done by Ensidesa in each primary profile (A, B, C, D and S) from which the specimens were obtained. All the tensile test results are given in Annex 3. The measured yield stress fy is between 280 and 316 MPa.

2.3.3 Measurements done during testing

The temperature field has been measured with thermocouples welded on the specimens. The number of measurement points has been from 17 for 510 mm length specimens up to 23 for the length of 3500 mm. (See FIGURE 2.3.3 for test SL 4.2)

Load applied. (See FIGURE 2.3.4 for test SL 4.2)

Vertical displacement. (See FIGURE 2.3.4 for test SL 4.2)

The horizontal deflection in the middle cross section has been measured with two transducers attached to the flanges. (See FIGURE 2.3.4 for test SL 4.2)

The instrumentation used allows measuring to the 1 % uncertainty level. All the figures for the other tests are given in Annex 4.

2.3.4 Heating procedure

Ceramic mat heating elements (resistors) have been fixed on the web and on the flanges of the profiles and covered with an insulating fabric.

The resistors have been controlled by means of the thermocouples welded on the specimens in order to obtain a temperature field as uniform as possible.

2.3.5 Summary of results

Specimen type L1, 510 mm length

	Test	Failure load (kN)	Vertical disp. (mm)	Horizontal disp. 1 (mm)	Horizontal disp. 2 (mm)	Av. temperature (°C)	Expected temperature (°C)
AL1	Cold	536.55	4.37	2,90	2.65	ROOM	ROOM
BL1	Hot	361.51	6.23	14.14	13.93	532	500
CL1	Hot	109.95	5.82	20.22	21.34	664	700
DL1	Hot	40.07	11.55	32.25	30.43	863	850

Specimen type L3, 1270 mm length

	Test	Failure load (kN)	Vertical disp. (mm)	Horizontal disp. 1 (mm)	Horizontal disp. 2 (mm)	Av. temperature (°C)	Expected temperature (°C)
AL3	Cold	489.74	4.39	6.99	7.02	ROOM	ROOM
BL3	Hot	292.47	-1.33	14.65	12.33	372	400
CL3	Hot	250.97	-2.22	18.24	17.75	474	500
* DL3	Hot	24.05	0.10	40.62	40.68	749	850

Specimen type SL4, 2020 mm length

	Test	Failure load (kN)	Vertical disp. (mm)	Horizontal disp. 1 (mm)	Horizontal disp. 2 (mm)	Av. temperature (°C)	Expected temperature (°C)
** SL4.	Hot	170.00	--------	18.22	17.91	525	500
SL4.	Hot	174.17	-9.74	22.38	22.41	509	500
SL4.	Hot	170.76	-8.59	24.08	25.59	485	500
SL4.	Cold	365.97	4.22	11.03	9.83	ROOM	ROOM
SL4.	Hot	172.87	-8.25	26.22	22.62	495	500

Specimen type L5, 2770 mm length

	Test	Failure load (kN)	Vertical disp. (mm)	Horizontal disp. 1 (mm)	Horizontal disp. 2 (mm)	Av. temperature (°C)	Expected temperature (°C)
AL5	Hot	127.12	-12.58	34.99	36.70	457	500
BL5	Hot	72.72	-16.74	33.54	-------	587	600
*** CL5	Hot	34.49	-16.16	38.78	39.74	587	700
DL5	Hot	6.59	-14.17	76.18	-------	858	850

Specimen type L6, 3510 mm length

	Test	Failure load (kN)	Vertical disp. (mm)	Horizontal disp. 1 (mm)	Horizontal disp. 2 (mm)	Av. temperature (°C)	Expected temperature (°C)
AL6	Cold	175.91	3.23	30.59	-------	ROOM	ROOM
BL6	Hot	105.28	-------	32.49	-------	446	400
CL6	Hot	90.43	-13.48	45.70	-------	493	500
DL6	Hot	11.50	-13.62	94.69	-------	727	850

* This specimen has a sinusoidal imperfection of 7 mm in the middle cross section.

** This test was made in order to adjust the test equipment.

*** The buckling sections were 360 mm approx. from the ends, due to the temperature in the regions of thermocouples 19 and 20 being higher than the rest.

FIGURE 2.3.1 Procedure for hot tests

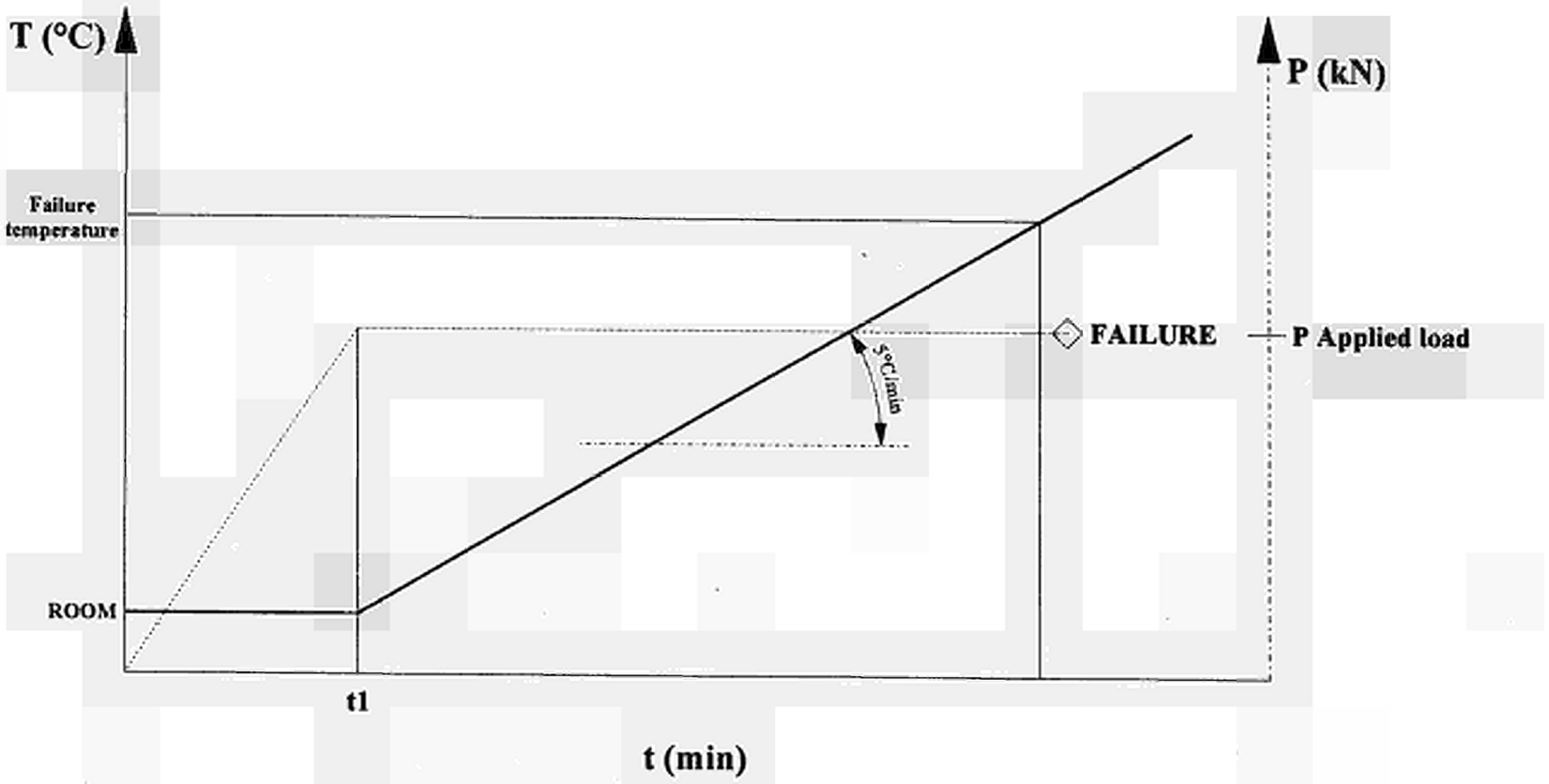

P: Applied load, corresponding to the expected failure temperature, provided by the University of Liege thanks to SAFIR simulations.

FIGURE 2.3.2 End conditions

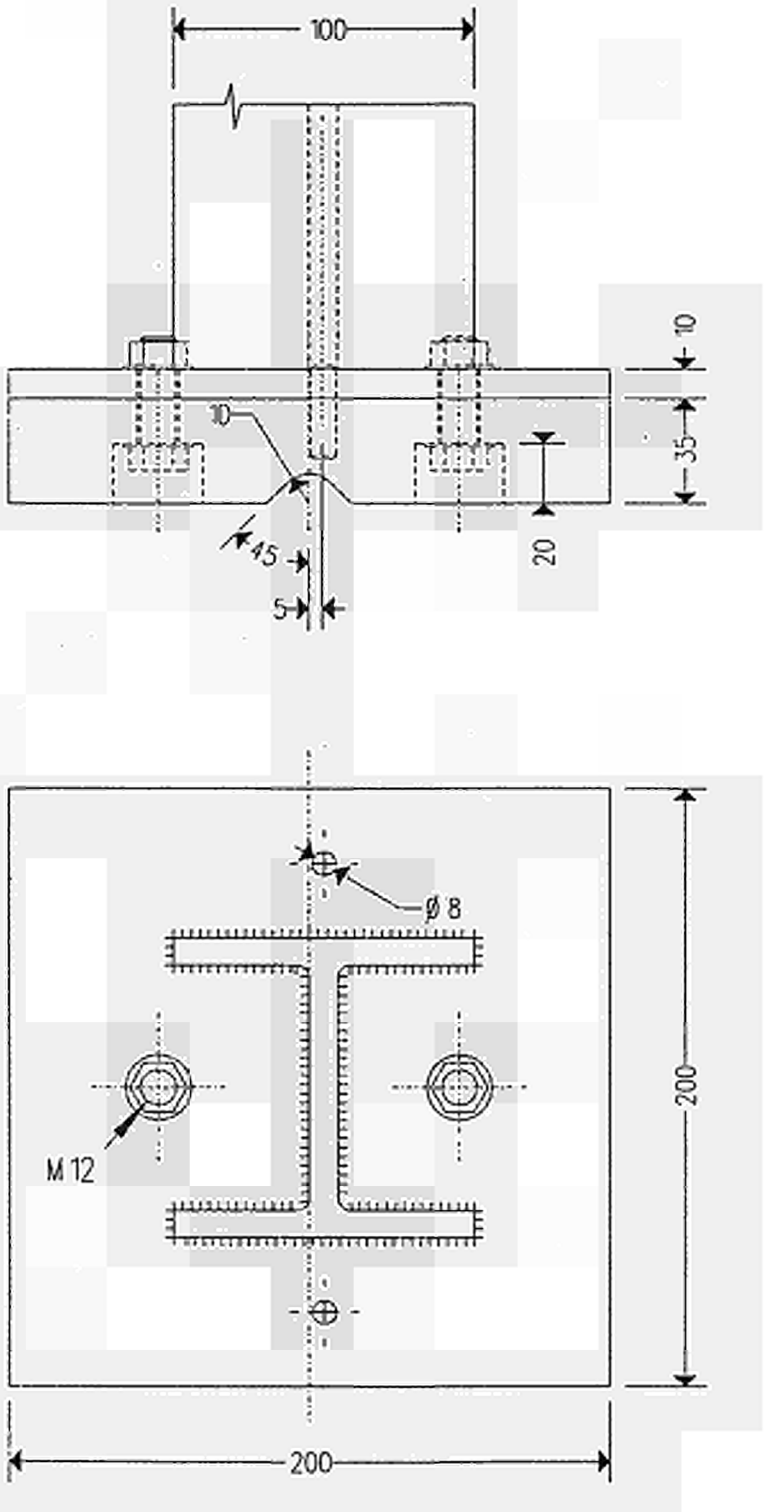

FIGURE 2.3.3 Thermocouple and resistor distribution for 2020 mm length specimens

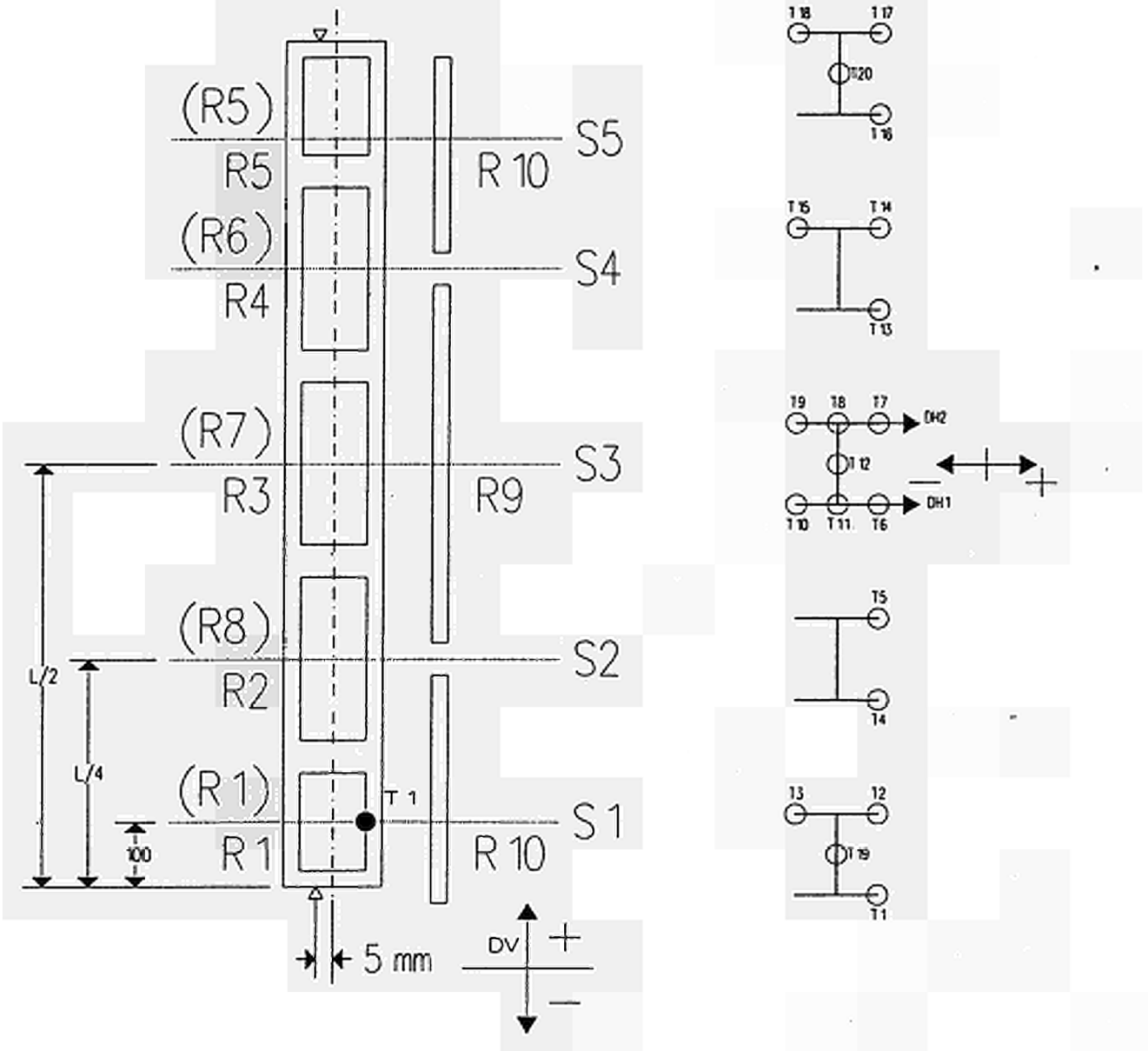

FIGURE 2.3.4 SPECIMEN SL4.2

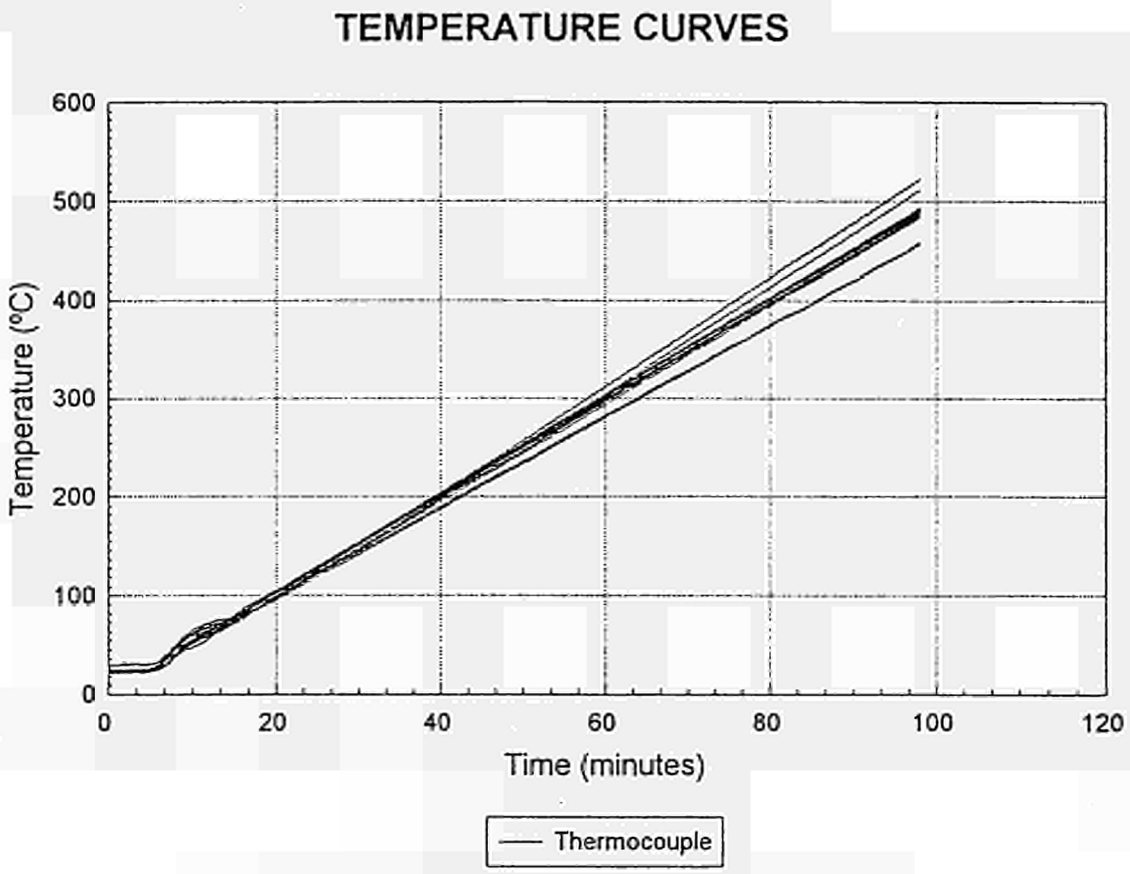

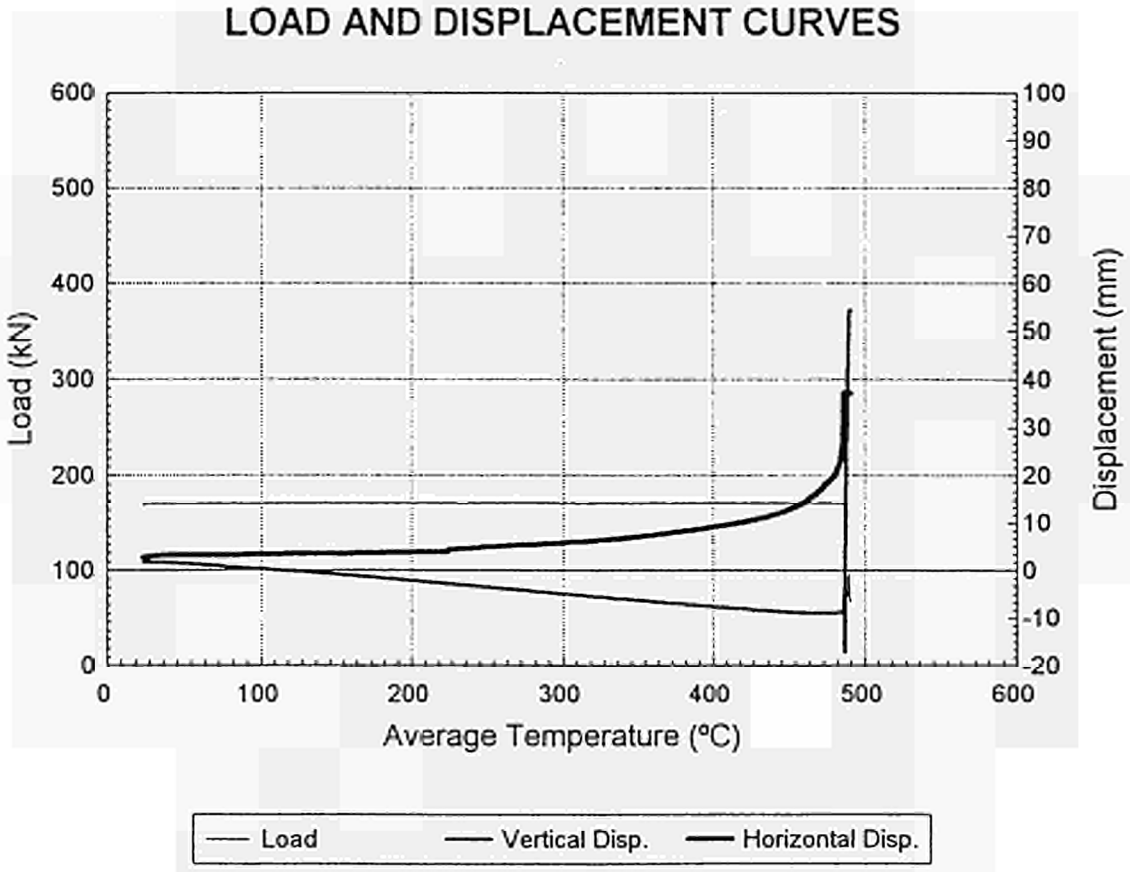

2.3.6 Southwell plot method applied to LABEIN tests

2.3.6.1 Theory of the Southwell plot for buckling tests (at 20°C)

During a column test we can draw f/P as a function of the horizontal displacement f (see FIGURE 2.3.6).

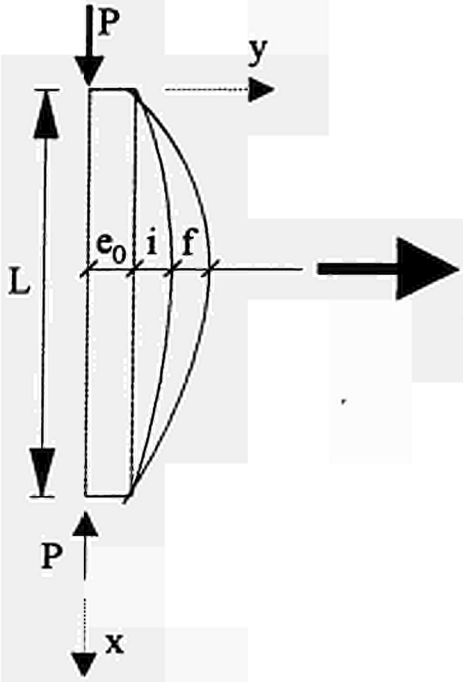

FIGURE 2.3.5

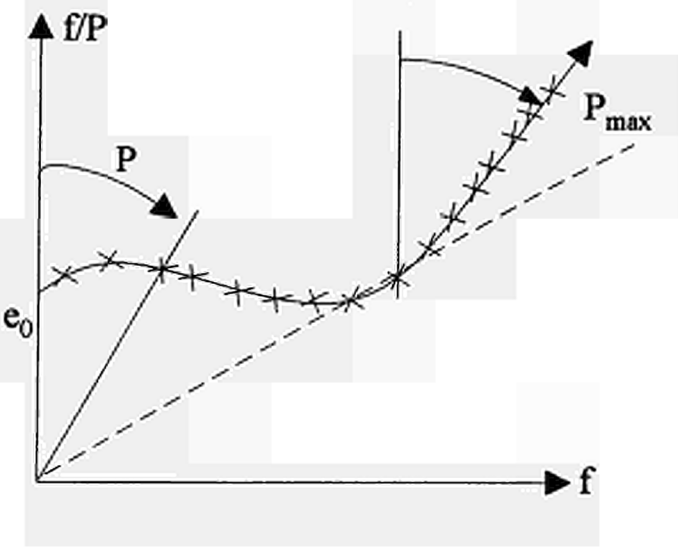

FIGURE 2.3.6

- if $e_i(x) = e_o + i \sin \frac{\pi x}{L}$ and $e_d(x) = f \sin \frac{\pi x}{L}$ then $e_T(x) = e_i + e_d$

- if $\frac{M}{EI} = \frac{-\delta^2 e_d}{\delta x^2}$

$$\frac{P}{EI}\left(e_o + i \sin \frac{\pi x}{L} + f \sin \frac{\pi x}{L}\right) = f \frac{\pi^2}{L^2} \sin \frac{\pi x}{L}$$

- In the point x = L/2

$$e_o + i + f = f/P \cdot \frac{\pi^2 EI}{L^2}$$

$$e_o + i + f = P_E \cdot f/P$$

$$f/P = \frac{1}{P_E}\left(f + (e_o + i)\right)$$

with:

$e_d(x)$	the horizontal displacement of the column
$e_i(x)$	the initial imperfection of the column
e_0	the eccentricity of the load
$e_T(x)$	the level arm of the load
f	the horizontal displacement at mid-height

i	the initial imperfection at mid-height
L	the buckling length of the column
P_E	the Euler load

- In case of a column test at room temperature, the FIGURE 2.3.6 becomes the FIGURE 2.3.7 where the curve is in fact a straight line with the equation: $Y = \frac{1}{P_E}(X + (e_0 + i))$

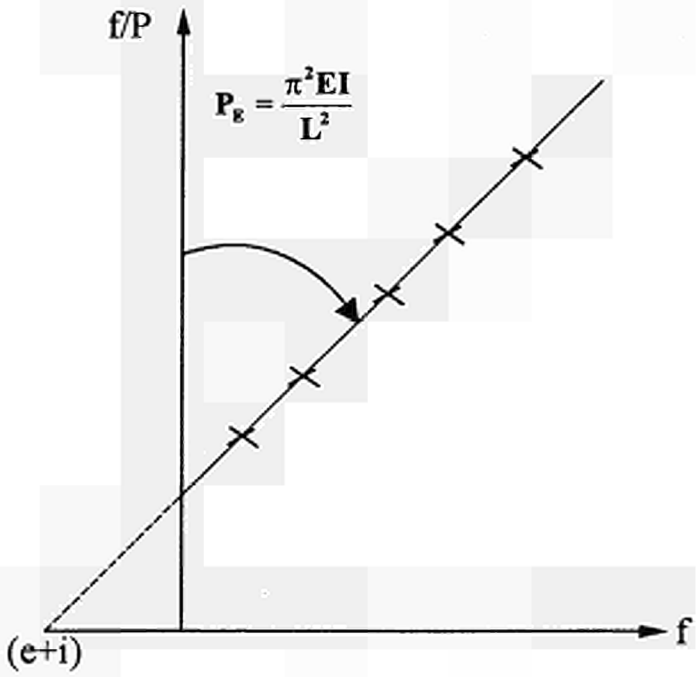

FIGURE 2.3.7

The slope of the line is the inverse of the Euler load and its intersection with the horizontal axis gives the effective eccentricity ($e_0 + i$).

These two values enable us to check the buckling length and the real eccentricity.

- In case of pure bending, the eccentricity e_0 is infinite and the FIGURE 2.3.7 becomes the FIGURE 2.3.8 The Southwell theory is not more valid because the deformed shape is in fact an arc of a circle instead of a sinusoïd.

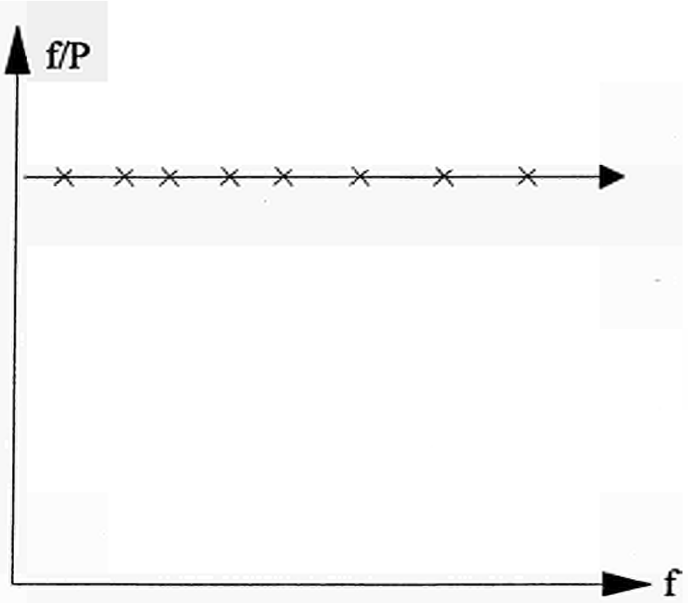

FIGURE 2.3.8

2.3.6.2 Southwell Plot for fire tests

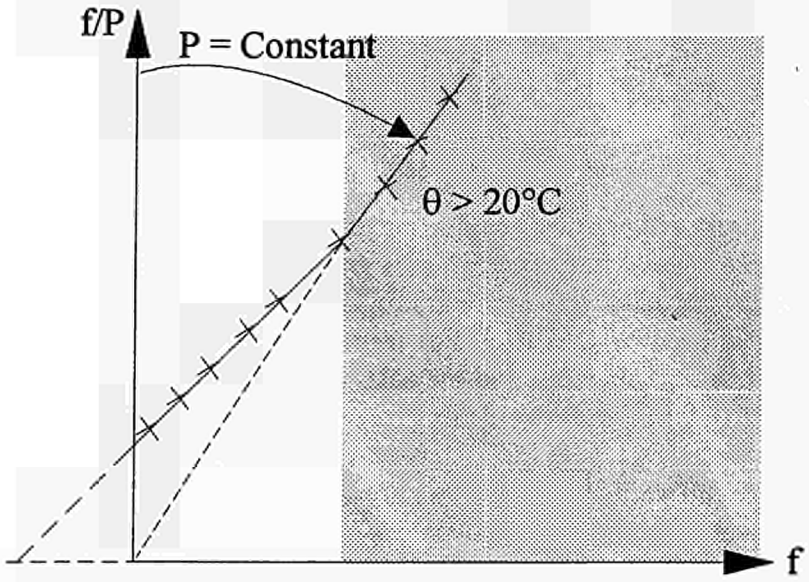

FIGURE 2.3.9

During a fire test, the load is kept constant during the heating phase. This implies that the Southwell plot becomes a straight line passing by the zero point and with a slope equal to the inverse of the applied load.

2.3.6.3 Southwell method applied to the measurements of the LABEIN tests

It was foreseen to apply the Southwell method to the LABEIN tests in order to check some tests for which the agreement between the simulation and the test results was not as good as the other tests. Unfortunately the measurements before heating of both tests are not precise enough to use the Southwell method. Moreover the Southwell method is only valid for rather small eccentricities as proved by the following table showing the application of that method to numerical results. In case of a buckling length of 3,5 m, an eccentricity of 3,5 mm appears to be the maximum value allowed to apply the Southwell method.

Length	End conditions	Eccentricity e_0	Imperfection e_i	Eccentricity		Buckling length	
				right	Southwell	right	Southwell
3.50 m	hinged-hinged	0.0 mm	3.5 mm	3.5 mm	3.5 mm	3.50 m	3.45 m
3.50 m	hinged-hinged	1.0 mm	3.5 mm	4.5 mm	4.7 mm	3.50 m	3.45 m
3.50 m	hinged-hinged	3.0 mm	3.5 mm	6.5 mm	7.3 mm	3.50 m	3.46 m
3.50 m	hinged-hinged	5.0 mm	3.5 mm	8.5 mm	9.7 mm	3.50 m	3.50 m
3.50 m	hinged-hinged	10.0 mm	3.5 mm	13.5 mm	16.0 mm	3.50 m	3.52 m
3.50 m	fixed-fixed	0.0 mm	3.5 mm	3.5 mm	3.0 mm	1.75 m	1.74 m

In conclusion, tests on axially loaded columns could be made with a very small eccentricity of which the precise value would be determined afterwards by the Southwell method. However this procedure needs to measure precisely the displacements during the loading before testing.

2.4 CTICM TESTS

2.4.1 Data

During May 1994, eight column tests subjected to fire were performed at the Fire Station of C.T.I.C.M. at Maizières-Lès-Metz. The columns were heated with electric flexiheaters and the temperatures were measured with thermocouples fixed on the columns. The heating procedure was similar to the one used by LABEIN. For more information about the implantation of the thermocouples, the heating programs and the tests arrangement refer to the reports [13 to 20] of the Fire Station of C.T.I.C.M or to **Annex 5**.

The columns were tested vertically. The tests are described in TABLE 2.4.1 The flexiheaters were fixed on one side of each flange and on one side of the web of the H profiles protected with Rockwool insulation. The heating rate was 10°C per minute up to 400°C and beyond 400°C only 5°C per minute, except for P2 the first column tested, which has a constant heating rate of 10°C per minute. For P1 an electrical breakdown of 4 minutes occurred after 86 minutes. For this reason the heating and all the measurements stopped. The transducers of displacement were reset when the electricity came back.

Name	P1	P2	P3	P4	P5	P6	P7	P8
Profile	HE200B	HE200B	HE200B	HE200B	HE160M	HE160M	HE140A	HE140A
Test n°	94-S-190	94-S-186	94-S-200	94-S-199	94-S-201	94-S-197	94-S-202	94-S-194
Length (m)	4	4	2	2	2	5	2	5
λ	78.9	78.9	23.42	39.5	27.59	70.63	34.9	87.26
N[kN]	100	100	100	150	100	100	160	100
Ecc. (m)	0.1	0.3	0.65	0.3	0.25	0.5	0.1	0.1
Steel	S 235	S 235	S 235	S 235	S 235	S 235	S 235	S 235
Buck. axis.	Weak	Weak	Strong	Weak	Strong	Strong	Strong	Strong

TABLE 2.4.1 Dimensions of the columns tested and load applied.

2.4.2 Measurements done before testing

2.4.2.1 Dimensional Measurements (see Annex 5)

2.4.2.2 Mechanical Properties (see Annex 5)

2.4.3 Measurements done during testing

The ultimate temperature and the load applied are given in table TABLE 2.2.1. Annex 5 explains in details how these ultimate temperatures were deduced from the measurements. The displacement of the mid-height of the column as a function of time is given in Annex 6.

2.5 DATABASE OF TESTS

This Database has been called SCOFIDAT for Steel Column in Fire/Database of Tests.

It is available on an EXCEL file and it contains 141 tests. The database field names and the whole database are given hereafter.

SCOFIDAT

Version 1.0 Date: 14.07.95

141 test results belong to the Database.

2.5.1 Field Names

1) **Profile Name**
2) **Insulating Material Description**
3) **Number of the test**
4) **Buckling Axis**
5) **Steelgrade: S 235, 355, 460**
6) **Measured yield point**
7) **Measured tensile strength**
8) **Length of the column**
9) **Buckling length**
10) **Applied load**
11) **Name of the Laboratory (City)**
12) **Name of the Country**
13) **Reference of the Laboratory report**
14) **Date of the test**
15) **Date of the report**
16) **Ultimate Load at room temperature (calculated according to EC3 part 1.1)**
17) **Imperfection of the column**
18) **Residual Stresses**
19) **Measured height of the steel section**
20) **Measured width of the steel section**
21) **Measured thickness of flange of the steel section**
22) **Measured thickness of web of the steel section**
23) **Time of fire resistance**
24) **Type of fire curve**
25) **Eccentricity of the load at the top of the column**
26) **Eccentricity of the load at the bottom of the column**
27) **Type of top end condition for the column**
28) **Type of bottom end condition for the column**
29) **Maximum of temperature in the column at the failure time**
30) **Minimum of temperature in the column at the failure time**
31) **Mean of temperature in the column at the failure time**

2.5.2 Explanations of the database field names

1. NAMEPROFIL

Designation of the steel section according to the catalogue : ARBED , Sales proprammе, Structural Shapes.

Ex: HD 210X210X198

Type = character *WIDTH: 18*

2. PROTECTION

Two possibilities are used: "n" or "y".

Type = character *WIDTH: 1*

3. NUMTEST

NUMTEST is the numerotation of this DATABASE FILE in DBASE4 (or EXCEL).

Type = numeric *WIDTH: 4 Dec: 0*

4. AXIS

Two possibilities are used: "W" or "S".

The letter "W" means that the buckling resistance with respect to the WEAK AXIS was tested.
The letter "S" means that the buckling resistance with respect to the STRONG AXIS was tested.

Type = character *WIDTH: 1*

5. STEELGRADE

The structural steel grades must be according to EN 10027

Ex: S 355 (S 235, S 275, S 355, S 420, S 460)

Type = character *WIDTH: 5*

6. M_YIELDSTR

Corresponds to the measured yield strength of the steel (in N/mm^2).

Ex: 364

Type = numeric *WIDTH: 3 Dec: 0*

7. M_ TENSISTR

Corresponds to the measured tensile strength of the steel (in N/mm²).

Ex: 523

Type = numeric *WIDTH: 3* *Dec: 0*

8. COLULENGTH

Corresponds to the total length (in mm) of the column.

Ex: 5700

Type = numeric *WIDTH: 6* *Dec: 0*

9. BUCKLENGTH

Corresponds to the buckling length (in mm) of the column.

Type = numeric *WIDTH: 6* *Dec: 0*

10. LOAD

Corresponds to the applied load during the test, expressed in kN.

Ex: 1100.0

Type = numeric *WIDTH: 6* *Dec: 1*

11. LABORATORY

Enter the name of the city where the test was performed.

Ex: BRAUNSCHWEIG

Type = character *WIDTH: 15*

12. COUNTRY

Country of the Laboratory.

Ex: Germany

Type = character *WIDTH: 15*

13. NUMREPORT

Reference of the Laboratory report.

Ex: 1618/8510

Type = character *WIDTH: 12*

14. TESTDATE

Date of the test written as follow: day / month / year

Ex: 02 / 09 / 88

Type = date *WIDTH: 8*

15. REPORTDATE

Date of the report written as follow: day / month / year

Ex 14 / 12 / 88

Type = date *WIDTH: 8*

16. NULT

N_{ult} is the ultimate load expressed in kN in cold condition (γ_{M0} =1,1 and γ_{M1} =1,1) according to EC3 Part 1.1 (April. 92) with the theoretical section sizes and the actual yield strength

Type = numeric *WIDTH: 7 Dec: 1*

17. IMPERFECTI

Note the imperfection (in mm) at the mid-height of the column in the buckling plane. (See FIGURE 2.5.1).

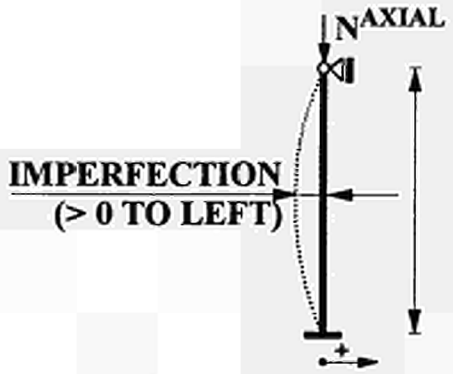

FIGURE 2.5.1

Type = numeric *WIDTH: 5 Dec: 1*

18. RESIDSTRES

Two possibilities are used: "N" or " Y " if the residual stresses have been measured.

Type = character *WIDTH: 4*

19 SIZES_H

Measured height of the steel section expressed in millimetres.

Ex: 270.3 (HD 210x210x198)

Type = numeric *WIDTH: 6 Dec: 1*

20 SIZES_B

Measured width of flange of the steel section expressed in millimetres.

Ex: 222.4 (HD 210x210x198)

Type = numeric *WIDTH: 6 Dec: 1*

21 SIZES_TF

Measured thickness of flange of the steel section expressed in millimetres.

Ex: 44.6 (HD 210x210x198)

Type = numeric *WIDTH: 5 Dec: 1*

22 SIZES_TW

Measured thickness of web of the steel section expressed in millimetres.

Ex: 44.6 (HD 210x210x198)

Type = numeric *WIDTH: 5* *Dec: 3*

23 FIRERESIST

Time of fire resistance expressed in minutes.

Ex: 38 (HD 210x210x198)

Type = numeric *WIDTH: 3* *Dec: 0*

24 FIRECURVE

Two possibilities are used: " ISO " or "."

Ex: ISO

Type = character *WIDTH: 7*

25 TOPECCENTR

Eccentricity of the load expressed in millimetres at the top of the column.
(> 0 TO THE RIGHT see FIGURE 2.5.2, a positive excentricity and a positive imperfection - see §17 - act in the same way)

Ex. 10

Type = numeric *WIDTH: 4*

26 BOTECCENTR

Eccentricity of the load expressed in millimetres at the bottom of the column.
(> 0 TO THE RIGHT see FIGURE 2.5.2, a positive excentricity and a positive imperfection - see § 17 - act in the same way)

Ex. 10

Type = numeric *WIDTH: 4*

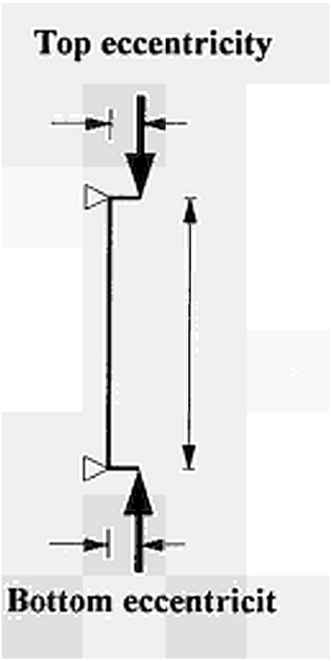

FIGURE 2.5.2

27 TOPSUPPORT

Type of top end condition for the column.

Ex: mcyl (See figure 3/II.2)

Write " knif " or " cyli " or" mcyl " or " fixe "

Type = character *WIDTH*: *4*

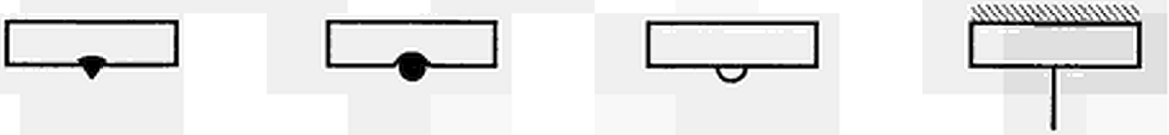

FIGURE 2.5.3

28 BOTSUPPORT

Type of bottom end condition for the column

Ex: mcyl (See FIGURE 2.5.3)

Write " knif " or " cyli " or" mcyl " or " fixe"

Type = character *WIDTH*: *4*

29 MAXCOLTEMP

Maximum of temperature in ° Celsius measured in the column at the failure time

Ex: 800

Type = numeric *WIDTH: 4*

30 MINCOLTEMP

Minimum of temperature in ° Celsius measured in the column at the failure time

Ex: 600

Type = numeric *WIDTH: 4*

31 MEANCOLTEMP

Mean of temperature in ° Celsius measured in the column at the failure time

Ex: 700

Type = numeric *WIDTH: 4*

	1	2	3	4	5	6	7	8	9	10	11	12	13	14	15	16	17	18	19	20	21	22	23	24	25	26	27	28	29	30	31
	NAMEPROFIL	PRT.	NUMTEST	AXIS	Steelgrade	M_YIELDSTR	M_TENSISTR	Collength	BUCKLENGTH	LOAD	LABORATORY	Country	Numreport	TESTDATE	Reportdate	MULT	IMPERFECTI	Residual	SIZES_H	SIZES_B	SIZES_TF	SIZES_TW	FIRERESIST	Firecurve	TOPECCENTR	BOTECCENTR	TOPSUPPORT	BOTSUPPORT	MAXCOLTEMP	MINCOLTEMP	MeanCOLTEMP
1	HD 210x210x198	n	1	W	S 355	364	523	5700	5700	1100	Braunschweig	Germany	1618/8610	02.09.88	04.12.88	3213.0	0	N	270.3	222.4	44.6	27.5	38.0	ISO	10	10	MCYL	MCYL	695	635	656
2	HD 310x310x500	n	2	S	S 355	296.5	490	4140	4140	2000	Gand	Belgium	5873	06.10.88	24.04.89	11716.0	0	N	427.0	335.0	73.0	42.0	58.0	ISO	85	85	CYLI	CYLI	795	630	700
3	HD 310x310x500	n	3	W	S 355	297	490	5700	5700	1850	Braunschweig	Germany	1618/8610	07.09.88	04.12.89	9544.0	0	N	428.0	335.0	73.6	42.0	60.0	ISO	34	34	MCYL	MCYL	885	755	784
4	HD 400x400x1086	n	4	W	S 355	390	574	4140	4140	4000	Gand	Belgium	5874	13.10.88	24.04.89	13824.0	0	N	568.0	446.0	125.0	71.0	68.0	ISO	227	227	CYLI	CYLI	740	545	644
5	W 360x410x314	n	5	W	S 355	401	536	4140	4140	1800	Gand	Belgium	5872	29.09.88	24.04.89	6086.0	1	N	402.8	401.7	39.0	20.8	34.5	ISO	120	120	CYLI	CYLI	862	501	652
6	W 360x410x314	n	6	W	S 460	496	676	4140	4140	1800	Gand	Belgium	5871	22.09.88	20.04.89	7326.0	-4	N	401.0	400.0	38.7	23.0	37.5	ISO	120	120	CYLI	CYLI	870	563	680
7	HEB 300	y	7	W	S 235	271	421	4380	1890	2000	Gand	Belgium	2704	29.06.79	09.08.79	.	0	N	306.0	298.0	18.4	11.0	58.0	ISO	0	0	FIXE	FIXE	666	566	588
8	IPE 160	y	8	W	S 235	270.6	405	4380	1890	106.2	Gand	Belgium	.	06.06.79	09.08.79	.	0	N	162.0	83.0	7.4	5.0	97.0	ISO	0	0	FIXE	FIXE	584	529	564
9	IPE 160	y	9	W	S 235	270.6	406	4380	1890	154.3	Gand	Belgium	.	18.06.79	09.08.79	.	0	N	163.0	82.0	8.0	4.0	64.0	ISO	0	0	FIXE	FIXE	525	440	475
10	IPE 200	y	10	W	S 235	277	430	4380	1890	203.2	Gand	Belgium	.	28.03.79	13.08.79	.	0	N	201.0	101.0	8.7	4.8	92.0	ISO	0	0	FIXE	FIXE	599	504	559
11	IPE 200	y	11	W	S 235	277	430	4380	1890	266.9	Gand	Belgium	.	07.03.79	13.08.79	.	0	N	201.0	101.0	8.7	4.8	45.0	ISO	0	0	FIXE	FIXE	404	389	394
12	IPE 200	y	12	W	S 235	271	430	4380	1815	323.5	Gand	Belgium	.	.	.	.	0	N	200.0	100.0	8.5	6.0	102.0	ISO	0	0	FIXE	FIXE	270	223	250
13	HEB 120	y	13	W	S 235	260	430	4380	1890	382.9	Gand	Belgium	.	16.06.79	14.08.79	.	0	N	124.0	120.0	10.5	6.7	55.0	ISO	.	.	FIXE	FIXE	531	506	519
14	HEB 120	y	14	W	S 235	260	430	4380	1890	267	Gand	Belgium	.	11.06.79	14.08.79	.	0	N	124.5	120.0	10.5	8.3	130.0	ISO	0	0	FIXE	FIXE	710	533	585
15	HEB 180	y	15	W	S 235	275	420	4380	1890	602.7	Gand	Belgium	.	19.04.79	14.08.79	.	0	N	180.0	180.0	13.2	10.0	90.0	ISO	0	0	FIXE	FIXE	675	578	616
16	HEB 180	y	16	W	S 235	275	420	4380	1890	892.9	Gand	Belgium	.	14.03.79	14.08.79	.	0	N	180.0	179.0	13.2	8.8	108.0	ISO	0	0	FIXE	FIXE	568	553	560
17	HEA 200	y	17	W	S 235	279	433	4380	1890	676.8	Gand	Belgium	.	07.06.79	14.08.79	.	0	N	193.3	198.0	9.4	4.7	85.0	ISO	0	0	FIXE	FIXE	573	551	556
18	HEA 300	y	18	W	S 235	269	442	4380	1890	1607.3	Gand	Belgium	.	02.06.79	20.08.79	.	0	N	296.3	299.0	13.4	7.7	110.0	ISO	0	0	FIXE	FIXE	.	.	561
19	HEA 220	y	19	W	S 235	262	.	4380	1915	972	Gand	Belgium	.	.	.	.	0	N	213.3	220.0	10.0	7.2	116.0	ISO	0	0	FIXE	FIXE	525	.	502
20	HEB 200	y	20	W	S 235	218	.	4380	1915	681	Gand	Belgium	.	.	.	.	0	N	200.0	200.0	15.0	9.2	231.0	ISO	0	0	FIXE	FIXE	567	529	549
21	HEB 140	y	21	W	S 235	247	.	4380	1915	641.7	Gand	Belgium	.	.	.	.	.	N	140.0	140.0	11.9	7.3	124.0	ISO	0	0	FIXE	FIXE	.	.	516
22	HEB 140	y	22	W	S 235	247	.	4380	1915	372	Gand	Belgium	.	.	.	.	.	N	140.0	140.0	11.9	7.4	115.0	ISO	0	0	FIXE	FIXE	.	508	576
23	IPE 220	y	23	W	S 235	273	.	4380	1915	319	Gand	Belgium	.	.	.	.	.	N	220.0	108.0	9.8	7.0	101.0	ISO	0	0	FIXE	FIXE	.	.	522
24	IPE 220	y	24	W	S 235	273	.	4380	1915	410	Gand	Belgium	.	.	.	.	.	N	220.0	108.0	9.6	7.0	82.0	ISO	0	0	FIXE	FIXE	525	231	360
25	HD 400x400x744	n	25	W	S 235	239	420	3950	4140	3400	Gand	Belgium	5091	02.10.84	17.06.85	7966.0	-4.1	N	500.0	427.0	88.0	51.0	45.0	ISO	180	180	CYLI	CYLI	666	474	566
26	HD 400x400x744	y	26	W	S 235	241	430	3950	4140	3400	Gand	Belgium	5092	14.01.86	22.05.86	8364.0	-4.1	N	500.0	427.0	88.5	51.0	145.0	ISO	180	180	CYLI	CYLI	674	428	608
27	HEM 220	n	27	S	S 235	268.5	.	5800	5800	1118	Braunschweig	Germany	148D1 1/I	1978-80	02.06.06	1914.4	0	N	240.0	226.0	26.0	15.5	23.0	ISO	49	49	MCYL	CYLI	.	.	530
28	HEB 120	n	28	S	S 235	266.4	.	5800	5800	103	Braunschweig	Germany	148D1 2/I	1978-80	02.06.06	240.7	0	N	120.0	120.0	11.0	6.5	11.0	ISO	45	45	MCYL	CYLI	.	.	555
29	HEB 220	n	29	S	S 235	242.9	.	3800	3800	551.6	Braunschweig	Germany	148D1 1/II	1978-80	02.06.06	849.9	0	N	220.0	220.0	16.0	9.5	9.0	ISO	102	102	MCYL	CYLI	.	.	550
30	HEB 220	n	30	S	S 235	242.3	.	3800	3800	386.4	Braunschweig	Germany	148D1 4/II	1978-80	02.06.06	847.4	0	N	220.0	220.0	16.0	9.5	12.0	ISO	102	102	MCYL	CYLI	.	.	610
31	HEB 120	n	31	S	S 235	257	.	3800	3800	317.8	Braunschweig	Germany	148D1 3	1976-77	30.06.06	510.6	0	N	120.0	120.0	11.0	6.5	12.0	ISO	0	0	MCYL	CYLI	.	.	560
32	HEM 220	n	32	S	S 235	269	.	3800	3800	1267.5	Braunschweig	Germany	148D1 4	1976-77	30.06.06	2131.0	0	N	240.0	226.0	26.0	15.5	18.0	ISO	12	12	MCYL	CYLI	.	.	600
33	HEB 220	n	33	S	S 235	261	.	3800	3800	767.1	Braunschweig	Germany	148D1 5	1976-77	30.06.06	1251.3	0	N	220.0	220.0	16.0	9.5	14.5	ISO	12	12	MCYL	CYLI	.	.	590
34	HEA 220	n	34	S	S 235	309	.	3800	3800	783.8	Braunschweig	Germany	148D1 6	1976-77	30.06.06	1613.7	0	N	210.0	220.0	11.0	7.0	11.5	ISO	12	12	MCYL	CYLI	.	.	560
35	HEM 220	n	35	S	S 235	269	.	4800	4800	695	Braunschweig	Germany	148D1 7	1976-77	30.06.06	1168.6	0	N	240.0	226.0	26.0	15.5	20.0	ISO	14	14	MCYL	CYLI	.	.	650
36	HEB 120	n	36	S	S 235	257	.	4800	4800	105	Braunschweig	Germany	148D1 8	1976-77	30.06.06	188.7	0	N	120.0	120.0	11.0	6.5	15.0	ISO	12	12	MCYL	CYLI	.	.	685
37	HEB 220	y	37	S	S 235	239.9	.	3800	3800	551.6	Braunschweig	Germany	148D1 2/II	1978-80	02.06.06	839.6	0	N	220.0	220.0	16.0	9.5	73.0	ISO	102	102	MCYL	CYLI	.	.	430
38	HEB 220	y	38	S	S 235	229.6	.	3800	3800	386.4	Braunschweig	Germany	148D1 3/II	1978-80	02.06.06	803.3	0	N	220.0	220.0	16.0	9.5	97.0	ISO	102	102	MCYL	CYLI	.	.	550
39	HEB 220	y	39	S	S 235	236.1	.	3800	3800	551.6	Braunschweig	Germany	148D1 5/II	1978-80	02.06.06	827.0	0	N	220.0	220.0	16.0	9.5	93.0	ISO	102	102	MCYL	CYLI	.	.	500
40	HEB 220	y	40	S	S 235	247.1	.	3800	3800	713.1	Braunschweig	Germany	148D1 1/III	1978-80	02.06.06	1123.0	0	N	220.0	220.0	16.0	9.5	94.0	ISO	55	55	MCYL	CYLI	.	.	545
41	HEB 120	y	41	S	S 235	275.9	.	5800	5800	138.3	Braunschweig	Germany	148D1 11/II	1978-80	02.06.06	243.9	0	N	120.0	120.0	11.0	6.5	49.0	ISO	55	55	MCYL	CYLI	.	.	350
42	HEB 120	y	42	S	S 235	246.6	.	5800	5800	138.3	Braunschweig	Germany	148D1 14/II	1978-80	02.06.06	217.8	0	N	120.0	120.0	11.0	6.5	43.5	ISO	55	55	MCYL	CYLI	.	.	325
43	HEB 120	y	43	S	S 235	287.5	.	5800	5800	97.1	Braunschweig	Germany	148D1 16/II	1978-80	02.06.06	263.5	0	N	120.0	120.0	11.0	6.5	66.5	ISO	55	55	MCYL	CYLI	.	.	520
44	HEB 120	y	44	S	S 235	276.8	.	5800	5800	164	Braunschweig	Germany	148D1 18/III	1978-80	02.06.06	288.2	0	N	120.0	120.0	11.0	6.5	63.0	ISO	30	30	MCYL	CYLI	.	.	498
45	HEB 120	y	45	S	S 235	255.2	.	5800	5800	290	Braunschweig	Germany	148D1 1/IV	1978-80	02.06.06	272.8	0	N	120.0	120.0	11.0	6.5	30.0	ISO	27	27	MCYL	CYLI	.	.	210
46	HEB 120	y	46	S	S 235	244.4	.	5800	5800	226	Braunschweig	Germany	148D1 2/IV	1978-80	02.06.06	215.2	0	N	120.0	120.0	11.0	6.5	25.5	ISO	55	55	MCYL	CYLI	.	.	160
47	HEM 220	y	47	S	S 235	270.3	.	5800	5800	781.1	Braunschweig	Germany	148D1 3/III	1978-80	02.06.06	1366.1	0	N	240.0	226.0	26.0	15.5	132.0	ISO	120	120	MCYL	CYLI	.	.	562
48	HEM 160	y	48	S	S 235	238.2	.	5800	5800	596.5	Braunschweig	Germany	148D1 4/III	1978-80	02.06.06	902.4	0	N	180.0	166.0	23.0	14.0	97.0	ISO	45	45	MCYL	CYLI	.	.	500
49	HEM 160	y	49	S	S 235	237.2	.	5800	5800	455	Braunschweig	Germany	148D1 5/III	1978-80	02.06.06	680.3	0	N	180.0	166.0	23.0	14.0	99.0	ISO	90	90	MCYL	CYLI	.	.	490
50	HEA 140	y	50	S	S 235	269.2	.	5800	5800	172.3	Braunschweig	Germany	148D1 6/III	1978-80	02.06.06	295.5	0	N	133.0	140.0	8.5	5.5	54.0	ISO	33	33	MCYL	CYLI	.	.	473
51	HEA 140	y	51	S	S 235	263.3	.	5800	5800	138.9	Braunschweig	Germany	148D1 7/III	1978-80	02.06.06	233.1	0	N	133.0	140.0	8.5	5.5	50.0	ISO	66	66	MCYL	CYLI	.	.	458
52	HEB 180	y	52	S	S 235	246.5	.	3860	3860	662	Braunschweig	Germany	148D1 BSII15	1981-83	06.06.06	.	0	N	180.0	180.0	14.0	8.5	68.0	ISO	30	30	MCYL	CYLI	.	.	418
53	HEB 180	y	53	S	S 235	259	.	3860	3860	664	Stuttgart	Germany	148D1 BII25	1981-83	06.06.06	.	0	N	180.0	180.0	14.0	8.5	67.5	ISO	30	30	MCYL	CYLI	.	.	417
54	HEB 180	y	54	S	S 235	267	.	3860	3860	891	Braunschweig	Germany	148D1 BSII25	1981-83	06.06.06	.	0	N	180.0	180.0	14.0	8.5	69.0	ISO	0	0	MCYL	CYLI	.	.	475
55	HEB 180	y	55	S	S 235	249	.	3860	3860	676	Stuttgart	Germany	148D1 BII15	1981-83	06.06.06	.	0	N	180.0	180.0	14.0	8.5	67.0	ISO	0	0	MCYL	CYLI	.	.	446
56	HEB 220	y	56	S	S 235	269	.	3700	3700	1489	Braunschweig	Germany	148D1 V 1	1981-83	06.06.06	2603.4	0	N	220.0	220.0	16.0	9.5	56.0	ISO	12	12	MCYL	CYLI	.	.	335
57	HEB 220	y	57	S	S 235	249.6	.	3700	3700	1628	Braunschweig	Germany	148D1 V 2	1981-83	06.06.06	2538.7	0	N	220.0	220.0	16.0	9.5	40.0	ISO	12	12	MCYL	CYLI	.	.	230
58	HEB 220	y	58	S	S 235	263.3	.	3700	3700	1136	Braunschweig	Germany	148D1 V 3	1981-83	06.06.06	1869.4	0	N	220.0	220.0	16.0	9.5	80.0	ISO	12	12	MCYL	CYLI	.	.	478
59	HEB 220	y	59	S	S 235	272	.	3700	3700	1039	Braunschweig	Germany	148D1 V 4	1981-83	06.06.06	1761.0	0	N	220.0	220.0	16.0	9.5	63.0	ISO	55	55	MCYL	CYLI	.	.	378
60	HEB 160	y	60	S	S 235	281.8	.	4700	4700	755	Braunschweig	Germany	148D1 VI 1	1981-83	06.06.06	1235.4	0	N	160.0	160.0	13.0	8.0	35.0	ISO	12	12	MCYL	CYLI	.	.	232

	1	2	3	4	5	6	7	8	9	10	11	12	13	14	15	16	17	18	19	20	21	22	23	24	25	26	27	28	29	30	31
	NAMEPROFIL	PRT.	M_MTEST	AXIS	Steelgrade	M_YIELDSTR	M_TENSISTR	Coulength	BUCKLENGTH	LOAD	LABORATORY	Country	Numreport	TESTDATE	Reportdate	MULT	IMPERFECTI	Residual	SIZES_H	SIZES_B	SIZES_TF	SIZES_TW	FIRERESIST	Firecurve	TOPECCENTR	BOTECCENTR	TOPSUPPORT	BOTSUPPORT	MAXCOLTEMP	MINCOLTEMP	MeanCOLTEMP
61	HEB 160	y	61	S	S 235	248.6	.	4700	4700	650	Braunschweig	Germany	148D1 VI 2	1981-83	06.06.06	1009.9	0	N	160.0	160.0	13.0	8.0	39.5	ISO	12	12	MCYL	CYLI	.	.	290
62	HEB 160	y	62	S	S 235	269.2	.	4700	4700	590	Braunschweig	Germany	148D1 VI 3	1981-83	06.06.06	955.8	0	N	160.0	160.0	13.0	8.0	54.5	ISO	12	12	MCYL	CYLI	.	.	412
63	HEB 280	y	63	S	S 235	238	.	4700	4700	991	Braunschweig	Germany	148D1 III 1	1981-83	06.06.06	1326.4	0	N	280.0	280.0	18.0	10.5	81.0	ISO	140	140	MCYL	CYLI	.	.	468
64	HEB 280	y	64	S	S 235	264	.	4700	4700	1143	Braunschweig	Germany	148D1 VII 2	1981-83	06.06.06	1814.5	0	N	280.0	280.0	18.0	10.5	54.0	ISO	140	140	MCYL	CYLI	.	.	305
65	HEB 100	y	65	S	S 235	260	.	4700	4700	169.5	Braunschweig	Germany	148D1 VII 5	1981-83	.	274.9	0	N	100.0	100.0	10.0	6.0	47.0	ISO	25	25	MCYL	CYLI	.	.	403
66	HEB 100	y	66	S	S 235	259.5	.	4700	4700	140.5	Braunschweig	Germany	148D1 VII 6	1981-83	06.06.06	227.9	0	N	100.0	100.0	10.0	6.0	36.0	ISO	50	50	MCYL	CYLI	.	.	298
67	HEA 180	y	67	S	S 235	297	.	5700	5700	320	Braunschweig	Germany	148D1 VIII 5	1981-83	06.06.06	594.0	0	N	171.0	180.0	9.0	6.0	54.5	ISO	86	86	MCYL	CYLI	.	.	438
68	HEA 120	y	68	S	S 235	240.8	.	5700	5700	112	Braunschweig	Germany	148D1 VIII 6	1981-83	06.06.06	168.6	0	N	114.0	120.0	8.0	5.0	43.5	ISO	57	57	MCYL	CYLI	.	.	422
69	HEA 220	y	69	S	S 235	270.8	.	3700	3700	601	Braunschweig	Germany	148D1 VIII 9	1981-83	06.06.06	847.9	0	N	210.0	220.0	11.0	7.0	64.0	ISO	105	105	MCYL	CYLI	.	.	485
70	HEA 220	y	70	S	S 235	277	.	3700	3700	814	Braunschweig	Germany	148D1 VIII 10	1981-83	06.06.06	1063.0	0	N	210.0	220.0	11.0	7.0	69.0	ISO	53	53	MCYL	CYLI	.	.	509
71	HEA 140	y	71	S	S 235	278	.	4700	4700	162.5	Braunschweig	Germany	148D1 VIII 14	1981-83	06.06.06	282.3	0	N	133.0	140.0	8.5	5.5	54.5	ISO	67	67	MCYL	CYLI	.	.	515
72	HEA 140	y	72	S	S 235	277	.	4700	4700	232	Braunschweig	Germany	148D1 VIII 15	1981-83	06.06.06	401.7	0	N	133.0	140.0	8.5	5.5	63.0	ISO	33	33	MCYL	CYLI	.	.	496
73	HEM 180	y	73	S	S 235	264	.	5700	5700	662	Braunschweig	Germany	148D1 VIII 1	1981-83	06.06.06	927.3	0	N	180.0	166.0	23.0	14.0	88.0	ISO	90	90	MCYL	CYLI	.	.	463
74	HEB 140	y	74	S	S 355	334.5	.	4700	4700	363	Braunschweig	Germany	.	1981-83	06.06.06	506.9	0	N	140.0	140.0	12.0	7.0	44.0	ISO	70	70	MCYL	CYLI	.	.	328
75	HEM 120	y	75	W	S 355	400.5	.	3800	3800	183	Braunschweig	Germany	.	1978-80	02.06.06	517.5	0	N	140.0	126.0	22.0	13.0	110.0	ISO	63	63	MCYL	CYLI	.	.	585
76	HEB 100	y	76	S	S 235	259.5	.	4700	4700	169.5	Braunschweig	Germany	.	1981-83	06.06.06	274.9	0	N	100.0	100.0	10.0	6.0	47.0	ISO	25	25	MCYL	CYLI	.	.	403
77	HEB 140	y	77	S	S 355	336	.	4700	4700	383	Braunschweig	Germany	.	1981-83	06.06.06	536.2	0	N	140.0	140.0	12.0	7.0	58.5	ISO	35	35	MCYL	CYLI	.	.	470
78	HEB 240	y	78	W	S 235	229.3	.	3700	3700	1230	Braunschweig	Germany	.	1981-83	06.06.06	1762.7	0	N	240.0	240.0	17.0	10.0	70.0	ISO	0	0	MCYL	CYLI	.	.	425
79	HEB 240	y	79	W	S 235	220.5	.	3700	1850	1195	Braunschweig	Germany	.	1981-83	06.06.06	1648.9	0	N	240.0	240.0	17.0	10.0	88.0	ISO	0	0	FIXED	FIXED	.	.	547
80	HEM 100	y	80	S	S 355	418.5	.	5700	5700	243	Braunschweig	Germany	.	1981-83	06.06.06	423.7	0	N	120.0	106.0	20.0	12.0	85.0	ISO	60	60	MCYL	CYLI	.	.	529
81	HEM 100	y	81	S	S 355	399.5	.	5700	5700	273	Braunschweig	Germany	.	1981-83	06.06.06	454.4	0	N	120.0	106.0	20.0	12.0	77.0	ISO	60	60	MCYL	CYLI	.	.	482
82	HEM 100	y	82	W	S 355	331.5	.	5700	2850	147	Braunschweig	Germany	.	1981-83	06.06.06	263.0	0	N	120.0	106.0	20.0	12.0	120.0	ISO	0	0	FIXED	FIXED	.	.	685
83	HEM 160	y	83	W	S 355	345.8	.	5700	2850	141	Braunschweig	Germany	.	1981-83	06.06.06	144.4	0	N	120.0	106.0	20.0	12.0	88.0	ISO	0	0	FIXED	FIXED	.	.	550
84	IPE 180	y	84	S	S 235	272.3	.	4700	4700	102	Braunschweig	Germany	.	1981-83	06.06.06	173.6	0	N	180.0	91.0	8.0	5.3	51.0	ISO	90	90	MCYL	CYLI	.	.	532
85	IPE 220	y	85	S	S 235	286.4	.	3700	3700	251	Braunschweig	Germany	.	1981-83	06.06.06	449.3	0	N	220.0	110.0	9.2	5.9	60.0	ISO	110	110	MCYL	CYLI	.	.	448
86	IPE 360	y	86	W	S 235	287.3	.	3700	3700	768	Braunschweig	Germany	.	1981-83	06.06.06	1379.0	0	N	360.0	170.0	12.7	8.0	37.0	ISO	9	9	MCYL	CYLI	.	.	290
87	IPE 360	y	87	W	S 235	272.8	.	3700	3700	610	Braunschweig	Germany	.	1981-83	06.06.06	1040.1	0	N	360.0	170.0	12.7	8.0	51.0	ISO	9	9	MCYL	CYLI	.	.	355
88	IPE 300	y	88	W	S 235	247.5	.	4700	4700	320	Braunschweig	Germany	.	1981-83	06.06.06	495.0	0	N	300.0	150.0	10.7	7.1	31.0	ISO	11	11	MCYL	CYLI	.	.	255
89	IPE 300	y	89	W	S 235	245.8	.	4700	4700	280	Braunschweig	Germany	.	1981-83	06.06.06	430.2	0	N	300.0	150.0	10.7	7.1	37.0	ISO	11	11	MCYL	CYLI	.	.	316
90	IPE 180	y	90	W	S 235	433	.	4700	4700	50	Braunschweig	Germany	.	1981-83	06.06.06	136.3	0	N	180.0	91.0	8.0	5.3	52.0	ISO	25	25	MCYL	CYLI	.	.	541
91	IPE 220	y	91	W	S 235	303.5	.	3700	3700	86	Braunschweig	Germany	.	1981-83	06.06.06	163.1	0	N	220.0	110.0	9.2	5.9	52.0	ISO	55	55	MCYL	CYLI	.	.	497
92	HEB 180	y	92	S	S 235	260	.	3860	2702	703	Braunschweig	Germany	.	1981-83	06.06.06	.	0	N	180.0	180.0	14.0	8.5	73.0	ISO	30	30	FIXED	CYLI	.	.	515
93	HEB 180	y	93	S	S 235	245	.	3860	2702	701	Stuttgart	Germany	.	1981-83	06.06.06	.	0	N	180.0	180.0	14.0	8.5	73.0	ISO	30	30	FIXED	CYLI	.	.	492
94	HEB 180	y	94	S	S 235	259	.	3860	2702	847	Braunschweig	Germany	.	1901-00	06.06.06	.	0	N	180.0	180.0	14.0	8.5	70.0	ISO	10	10	FIXED	CYLI	.	.	515
95	HEB 180	y	95	S	S 235	244	.	3860	2702	867	Stuttgart	Germany	.	1981-83	06.06.06	.	0	N	180.0	180.0	14.0	8.5	68.0	ISO	10	10	FIXED	CYLI	.	.	466
96	HEB 180	y	96	W	S 235	283	.	3860	1930	928	Braunschweig	Germany	.	1981-83	06.06.06	.	0	N	180.0	180.0	14.0	8.5	82.0	ISO	0	0	FIXED	FIXED	.	.	513
97	HEB 180	y	97	W	S 235	278	.	3860	1930	928	Braunschweig	Germany	.	1981-83	06.06.06	.	0	N	180.0	180.0	14.0	8.5	88.0	ISO	0	0	FIXED	FIXED	.	.	540
98	HEB 180	y	98	W	S 235	277	.	3860	1930	838	Stuttgart	Germany	.	1981-83	06.06.06	.	0	N	180.0	180.0	14.0	8.5	88.0	ISO	0	0	FIXED	FIXED	.	.	523
99	HEB 120	n	99	S	S 235	263.9	.	5800	5800	139.3	Braunschweig	Germany	.	1978-80	02.06.06	233.2	0	N	120.0	120.0	11.0	6.5	8.8	ISO	55	55	MCYL	CYLI	.	.	390
100	HEB 120	n	100	S	S 235	271.5	.	5800	5800	97.1	Braunschweig	Germany	.	1978-80	02.06.06	239.8	0	N	120.0	120.0	11.0	6.5	11.0	ISO	55	55	MCYL	CYLI	.	.	515
101	HEM 120	y	101	W	S 355	401	.	3800	3800	183	Braunschweig	Germany	.	01.01.78	31.12.80	143.6	0	N	.	.	.	.	110.0	ISO	63	63	MCYL	CYLI	.	.	585
102	HEB 140	y	102	S	S 355	330.5	.	4700	4700	302	Braunschweig	Germany	.	1981-83	06.06.06	415.9	0	N	140.0	140.0	12.0	7.0	56.0	ISO	70	70	MCYL	CYLI	.	.	437
103	HEA 100	n	103	W	.	300	.	.	1994	337	Rennes	France	.	.	.	.	.	N	.	.	.	.	.	.	0	0	MCYL	MCYL	.	.	365
104	HEA 100	n	104	W	.	300	.	.	1994	318	Rennes	France	.	.	.	.	.	N	.	.	.	.	.	.	0	0	MCYL	MCYL	.	.	400
105	HEA 100	n	105	W	.	300	.	.	1994	250	Rennes	France	.	.	.	.	.	N	.	.	.	.	.	.	0	0	MCYL	MCYL	.	.	510
106	HEA 100	n	106	W	.	300	.	.	1994	143	Rennes	France	.	.	.	.	.	N	.	.	.	.	.	.	0	0	MCYL	MCYL	.	.	550
107	HEA 100	n	107	W	.	300	.	.	1994	110	Rennes	France	.	.	.	.	.	N	.	.	.	.	.	.	0	0	MCYL	MCYL	.	.	600
108	HEA 100	n	108	W	.	300	.	.	1994	81	Rennes	France	.	.	.	.	.	N	.	.	.	.	.	.	0	0	MCYL	MCYL	.	.	680
109	HEA 100	n	109	W	.	300	.	.	1994	57	Rennes	France	.	.	.	.	.	N	.	.	.	.	.	.	0	0	MCYL	MCYL	.	.	750
110	HEA 100	n	110	W	.	300	.	.	1994	360	Rennes	France	.	.	.	.	.	N	.	.	.	.	22.0	.	0	0	MCYL	MCYL	.	.	235
111	HEA 100	n	111	W	.	300	.	.	1994	320	Rennes	France	.	.	.	.	.	N	.	.	.	.	42.0	.	0	0	MCYL	MCYL	.	.	440
112	HEA 100	n	112	W	.	300	.	.	1994	250	Rennes	France	.	.	.	.	.	N	.	.	.	.	43.0	.	0	0	MCYL	MCYL	.	.	450
113	HEA 100	n	113	W	.	300	.	.	1994	200	Rennes	France	.	.	.	.	.	N	.	.	.	.	46.0	.	0	0	MCYL	MCYL	.	.	480
114	HEA 100	n	114	W	.	300	.	.	1994	150	Rennes	France	.	.	.	.	.	N	.	.	.	.	53.0	.	0	0	MCYL	MCYL	.	.	552
115	HEA 100	n	115	W	.	300	.	.	1994	100	Rennes	France	.	.	.	.	.	N	.	.	.	.	60.0	.	0	0	MCYL	MCYL	.	.	618
116	HEA 100	n	116	W	.	300	.	.	1994	48	Rennes	France	.	.	.	.	.	N	.	.	.	.	68.0	.	0	0	MCYL	MCYL	.	.	701
117	UC 203	n	117	W	.	349	500	.	1500	550	Borehamhood	U.K	.	.	.	.	0	N	204.5	204.0	12.5	8.0	23.0	ISO	0	0	FIXED	FIXED	723	667	688
118	HEA 100	n	118	W	S 235	289.8	446.9	.	513	362	Labein	Spain	.	.	.	.	0	Y	98.9	101.9	7.6	5.9	105.0	.	5	5	KNIF	KNIF	.	.	532
119	HEA 100	n	119	W	S 235	288.4	450.2	.	513	110	Labein	Spain	.	.	.	.	0	Y	99.1	101.8	7.8	6.4	180.0	.	5	5	KNIF	KNIF	.	.	694
120	HEA 100	n	120	W	S 235	289.02	444.4	.	513	40	Labein	Spain	.	.	.	.	0	Y	99.1	102.3	7.7	6.1	160.0	.	5	5	KNIF	KNIF	.	.	863

	1	2	3	4	5	6	7	8	9	10	11	12	13	14	15	16	17	18	19	20	21	22	23	24	25	26	27	28	29	30	31
	NAMEPROFIL	PRT.	NUMTEST	AXIS	Steelgrade	M_YIELDSTR	M_TENSISTR	Colength	BUCKLENGTH	LOAD	LABORATORY	Country	Numreport	TESTDATE	Reportdate	NULT	IMPERFECTI	Residual	SIZES_H	SIZES_B	SIZES_TF	SIZES_TW	FIRERESIST	Firecurve	TOPECCENTR	BOTECCENTR	TOPSUPPORT	BOTSUPPORT	MAXCOLTEMP	MINCOLTEMP	MeanCOLTEMP
121	HEA 100	n	121	W	S 235	289.8	446.9	.	1272	292	Labein	Spain	.	.	.	.	0.2	Y	98.9	101.9	7.6	6.0	**87.0**	.	5	5	KNIF	KNIF	.	.	390
122	HEA 100	n	122	W	S 235	288.2	460.2	.	1271	261	Labein	Spain	.	.	.	.	0.4	Y	99.3	101.9	7.8	6.1	**92.0**	.	5	5	KNIF	KNIF	.	.	474
123	HEA 100	n	123	W	S 235	288.9	444.5	.	1269	24	Labein	Spain	.	.	.	.	0.3	Y	99.2	102.2	7.7	6.0	**166.0**	.	5	5	KNIF	KNIF	.	.	749
124	HEA 100	n	124	W	S 235	281.4	444.5	.	2026	174	Labein	Spain	.	.	.	.	0.7	Y	99.0	101.8	7.6	5.7	**83.0**	.	5	5	KNIF	KNIF	.	.	509
125	HEA 100	n	125	W	S 235	281.4	444.5	.	2020	171	Labein	Spain	.	.	.	.	1.7	Y	99.0	101.8	7.6	5.8	**97.0**	.	5	5	KNIF	KNIF	.	.	485
126	HEA 100	n	126	W	S 235	281.4	444.5	.	2023	173	Labein	Spain	.	.	.	.	1.1	Y	99.2	101.7	7.6	5.7	**92.0**	.	5	5	KNIF	KNIF	.	.	495
127	HEA 100	n	127	W	S 235	284.72	441.6	.	2770	127	Labein	Spain	.	.	.	.	-0.4	Y	99.1	101.9	7.7	5.8	**89.0**	.	5	5	KNIF	KNIF	.	.	457
128	HEA 100	n	128	W	S 235	289.7	446.9	.	2772	73	Labein	Spain	.	.	.	.	1	Y	99.0	101.8	7.6	5.8	**110.0**	.	5	5	KNIF	KNIF	.	.	587
129	HEA 100	n	129	W	S 235	298.2	460.2	.	2771	34	Labein	Spain	.	.	.	.	0.8	Y	99.3	102.0	7.8	6.0	**122.0**	.	5	5	KNIF	KNIF	.	.	587
130	HEA 100	n	130	W	S 235	288.8	444.5	.	2772	6.42	Labein	Spain	.	.	.	.	1.6	Y	99.2	102.2	7.7	6.0	**173.0**	.	5	5	KNIF	KNIF	.	.	858
131	HEA 100	n	131	W	S 235	289.8	446.9	.	3610	106	Labein	Spain	.	.	.	.	1.5	Y	98.9	101.9	7.6	5.9	**65.0**	.	5	5	KNIF	KNIF	.	.	446
132	HEA 100	n	132	W	S 235	288.1	460.2	.	3610	90	Labein	Spain	.	.	.	.	1.8	Y	99.1	102.1	7.7	5.9	**94.0**	.	5	5	KNIF	KNIF	.	.	493
133	HEA 100	n	133	W	S 235	288.7	444.5	.	3610	11.5	Labein	Spain	.	.	.	.	1.1	Y	99.2	101.7	7.6	5.7	**150.0**	.	5	5	KNIF	KNIF	.	.	727
134	HEB 200	n	134	W	S 235	275	458	4000	4000	100	CTICM	France	94-S-190	05.05.94	00.10.1994	.	1.5	N	201.4	200.2	15.0	9.0	**96.0**	.	100	100	MCYL	MCYL	.	.	664
135	HEB 200	n	135	W	S 235	275	458	4000	4000	100	CTICM	France	94-S-198	06.04.94	00.10.1994	.	2	N	201.4	200.3	15.0	9.0	**58.0**	.	300	300	MCYL	MCYL	600	540	575
136	HEB 200	n	136	S	S 235	275	458	2000	2000	100	CTICM	France	94-S-200	17.05.94	00.10.1994	.	1	N	201.3	200.3	15.0	9.0	**81.0**	.	650	650	MCYL	MCYL	634	544	599
137	HEB 200	n	137	W	S 235	275	458	2000	2000	150	CTICM	France	94-S-199	18.05.94	00.10.1994	.	1	N	201.4	200.3	15.0	9.0	**70.0**	.	300	300	MCYL	MCYL	574	467	537
138	HEM 160	n	138	S	S 235	271	463	2000	2000	100	CTICM	France	94-S-201	18.05.94	00.10.1994	.	2.5	N	180.2	163.4	22.7	14.0	**122.0**	.	250	250	MCYL	MCYL	777	732	753
139	HEM 160	n	139	S	S 235	271	463	5000	5000	100	CTICM	France	94-S-197	19.05.94	00.10.1994	.	1	N	180.4	163.5	22.7	14.0	**76.0**	.	500	500	MCYL	MCYL	599	484	572
140	HEA 140	n	140	S	S 235	260	410	2000	2000	100	CTICM	France	94-S-202	19.05.94	00.10.1994	.	1	N	137.5	141.5	9.0	5.6	**67.0**	.	100	100	MCYL	MCYL	577	512	539
141	HEA 140	n	141	S	S 235	260	410	5000	5000	100	CTICM	France	94-S-194	09.05.94	00.10.1994	.	1	N	133.8	139.8	8.3	5.6	**66.0**	.	100	100	MCYL	MCYL	560	443	507

ECSC Research 7210-SA 515 " Buckling Curves in Case of Fire "

Partners : **ProfilARBED Research** (Luxembourg) as leader of this Research

Université de Liège (Belgium)

TNO (The Netherlands)

CTICM (France)

LABEIN (Spain)

For information, please contact:

ProfilARBED Research
Service RPS
66, rue de Luxembourg
L-4221 Esch/Alzette

Telefax: --352 -5313-2199
Phone: --352 -5313-2183

3. CALCULATION MODELS

3.1 COMPARISON BETWEEN NUMERICAL PROGRAMS (SAFIR, CEFICOSS, LENAS, SISMEF, DIANA)

3.1.1 INTRODUCTION

As different programs are used in this research, a set of calibration examples has been established at the University of Liège and these examples have been calculated with the five programs available in the different organizations: CEFICOSS and SAFIR (ProfilARBED Recherches and University of Liège), DIANA (TNO), LENAS and SISMEF (CTICM).

3.1.2 Example Definition

Three types of structure (A, B, C) have been defined. For each type different kinds of heating have been analysed. The first structure A is a theoretical example called "Lee's Frame"; the other ones are a steel column with different load eccentricities. All the parameters needed for the simulations (material law and characteristics, loads, cross section, end conditions, heating conditions ...) are given hereafter:

STRUCTURE A: LEE'S FRAME

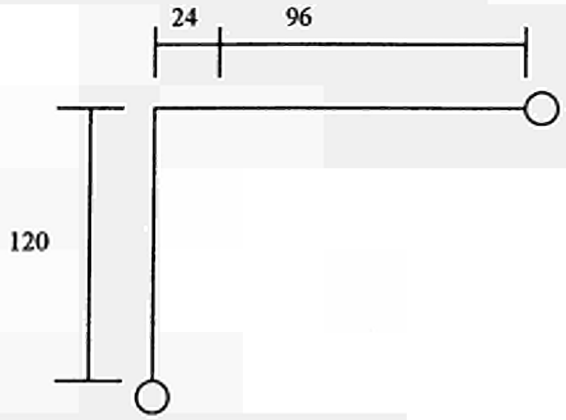

Section : rectangular : b = 3
h = 2

=> A = 6
I = 2

Units have to be consistent.

Test A.1. ambient temperature.

The material is elastic. E = 720.
Apply a vertical downward load on the horizontal beam, at a distance of 24 from the beam column connection.

Produce one EXCEL file showing the evolution of the vertical and the horizontal displacement under the load for every load step of 0.1 up to 1.7. for every converged point beyond 1.7.

Test A.2. uniform temperature.

The material is EC3 steel. E = 720, fy = 3.
Temperature is uniform in the section.
A vertical load of 0.2 is applied.
The temperature in the profile gradually increases.
Calculate the ultimate temperature (precision 0.5 °C).
Produce one EXCEL file showing the evolution of the vertical and the horizontal displacement under the load for every step of 32°C (20,52,84,..) up to 596°C, for every converged point beyond 596°C.

STRUCTURE B: ECCENTRICALLY LOADED COLUMN

Profile	:	HE200B.
Buckling	:	weak axis.
End conditions	:	pined at both ends.
f_y	:	235 MPa.
Dead weight	:	neglected (simulate one half of the column).
Total length	:	4 m.
Imperfection	:	4 mm, sinusoidal.
Loading	:	axial load N + bending moment M = N x 0.10 m. The bending moment has the same effect on transverse displacements as the imperfection.
Residual stresses	:	bitriangular, max. value = 117.5 MPa.
Material and thermal laws	:	EC3, part 10 $\varepsilon = 0.5$ and h = 25 when needed. no shadow effect.

Test B.1. ambient temperature

Calculate the ultimate axial load (precision 0.5 kN).
Produce one EXCEL file with;
- the shortening of one half of the column,
- the transversal displacement (both in mm)

for every step of 64 kN up to 320 kN,
for every converged point beyond 320 kN.

Test B.2. uniform temperature

Temperature is uniform in the section.
An axial load of 250 kN is applied (+ M = 25 kN m).
The temperature in the profile gradually increases.
Calculate the ultimate temperature (precision 0.5 °C).
Produce one EXCEL file with;
- the elongation of one half of the column (negative at 20°C),
- the transversal displacement (both in mm),

for every step of 32 °C (20, 52, 84,..) up to 404°C,
for every converged point beyond 404°C.

Test B.3. ISO curve

The profile is submitted to the ISO curve.
Apply a load of 250 kN (+ M = 25 kN m).
Calculate the fire resistance of the column (criteria = buckling) with a precision of 1 sec.
Produce one EXCEL file with;
- the elongation of one half of the column (negative at 20°c),
- the transversal displacement (both in mm),

for every step of 64" up to 576",
for every converged point beyond 576",

STRUCTURE C: CENTRICALLY LOADED COLUMN.

Profile	: HE200B.
Buckling	: weak axis.
End conditions	: pined at both ends.
f_y	: 235 MPa
Dead weight	: neglected (simulate one half of the column)
Total length	: 4 m
Imperfection	: 4 mm, sinusoidal.
Loading	: axial load.
Residual stresses	: bitriangular, max. value = 117.5 MPa
Material and thermal laws	: EC3, part 10 $\varepsilon = 0.5$ and h = 25 when needed. no shadow effect

Test C.1. ambient temperature

Calculate the ultimate load (precision 0.5 kN)
Produce one EXCEL file with;
- the shortening of one half of the column,
- the transversal displacement (both in mm)

for every step of 64 kN up to 1024 kN,
for every converged point beyond 1088 kN,

Test C.2. uniform temperature

Temperature is uniform in the section.
A load of 500 kN is applied.
The temperature in the profile gradually increases
Calculate the ultimate temperature (precision 0.5 °C)
Produce one EXCEL file with;
- the elongation of one half of the column (negative at 20°C),
- the transversal displacement (both in mm),

for every step of 32 °C (20, 52, 84,..) up to 500°C,

for every converged point beyond 500 °C,

Test C.3. ISO curve

The profile is submitted to the ISO curve.
Calculate the temperature distribution.
Show the obtained field of temperature after 960 sec by your own graphic tools.
Produce one EXCEL file showing the average temperature for every step of 320 sec. up to 1920 sec.
Apply a load of 500 kN.
Calculate the fire resistance of the column (criteria = buckling) with a precision of 1 sec.
Produce one EXCEL file with;
- the elongation of one half of the column (negative at 20°C),
- the transversal displacement (both in mm),

for every step of 64" up to 640",
for every converged point beyond 640",

3.1.3 Simulation Results

The following summary points out quite a good agreement between numerical models. All the results are described in the paper "A comparison between five structural Fire Codes applied to Steel Elements" [1] and given in Annex 7.

S U M M A R Y

	A - 1	A - 2	B - 1	B - 2	B - 3	C - 1	C - 2	C - 3
	LOAD	Temp.	LOAD	Temp.	Time	LOAD	Temp.	Time
SAFIR	1,85	626°C	417 kN	432°C	604 sec	1144 kN	524°C	745 sec
CEFICOSS	1,86	625°C	416 kN	433°C	606 sec	1154 kN	524°C	745 sec
DIANA	1,855	628°C	437kN	450°C	608 sec	1113 kN	515°C	717 sec
LENAS	1,84	621°C	414kN	428°C	589 sec	1166 kN	518°C	730 sec
SISMEF	1,84	625°C	414kN	427°C	589 sec	1117 kN	519°C	722 sec

3.2 NUMERICAL SIMULATIONS OF THE LABEIN TESTS

The following figure points out the good concordance between numerical results (SAFIR) and measurements provided by LABEIN.

FIGURE 3.2.1

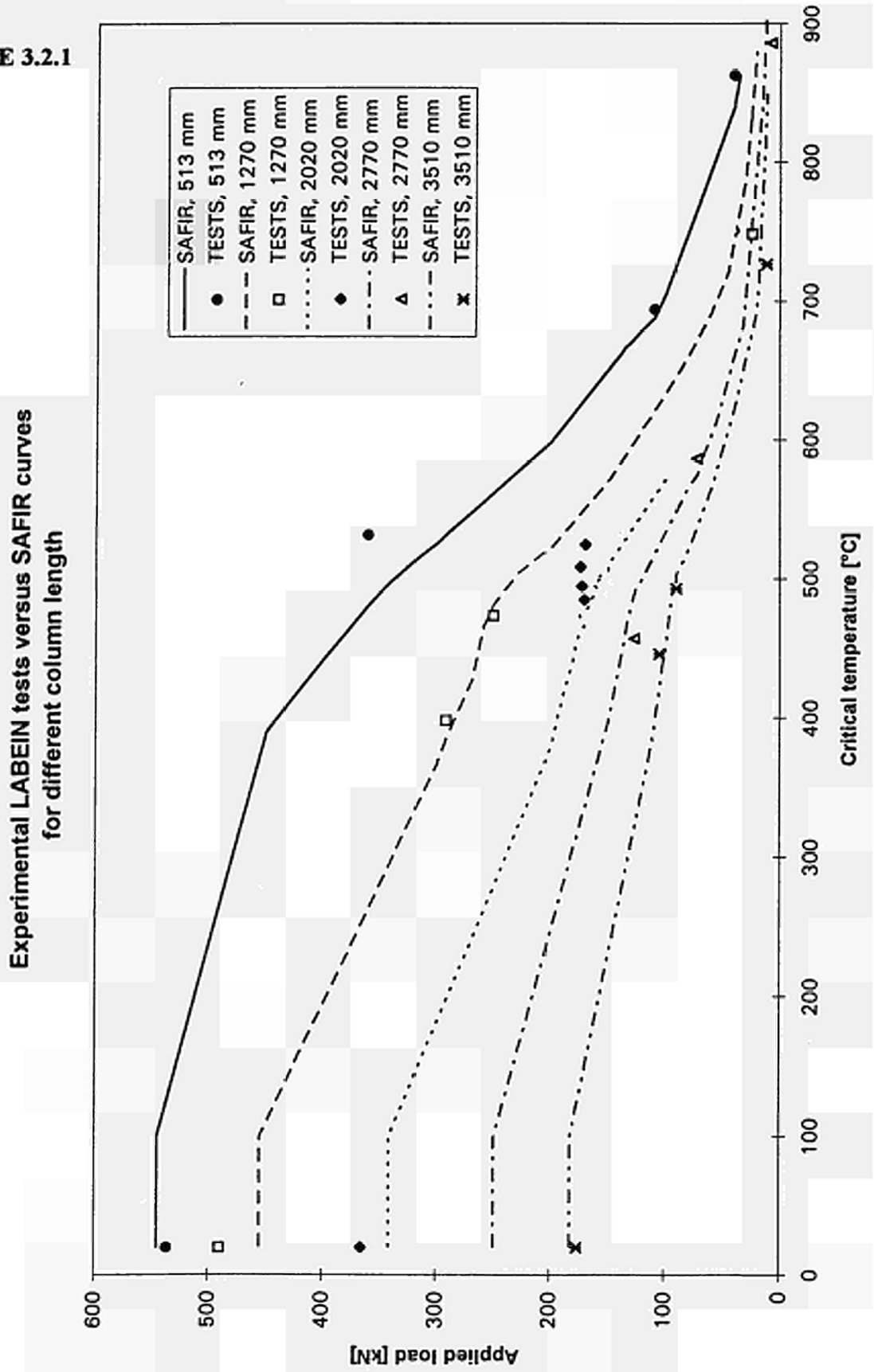

3.3 NUMERICAL SIMULATIONS OF THE CTICM TESTS.

Annex 6 presents the comparison between the horizontal displacements measured during the tests and the displacements calculated with LENAS. There were two transducers of displacement at mid height of the column (FIGURE 3.3.1a if the buckling is around the major axis and FIGURE 3.3.1b if the buckling is around the minor axis) to check that there was no rotation of the section of the column or lateral buckling.

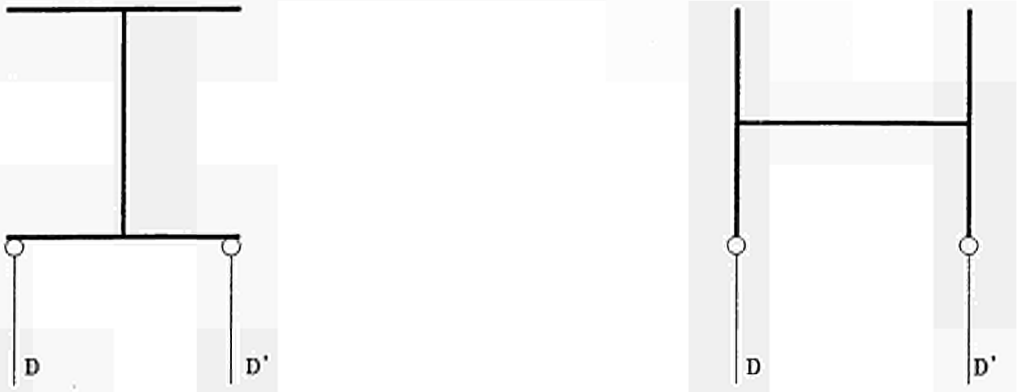

a) buckling around the major axis

b) buckling around the minor axis

FIGURE 3.3.1

The following comments have to be made to have a good understanding of this Annex 6.

For the column P1 the electric power broke down after 86 minutes and came back 4 minutes later. That's why there is no increasing of displacement between 86 and 90 minutes. This black out does not appear in LENAS simulation because the step of calculation was too large and because a linear interpolation is made between two points of the curve. As the transducers were reset, the curve after 90 minutes was "pasted", at the end of the first recording, with an offset equal to the oldest value recorded.

For the column P2 the computer did not record any displacement before 22 minutes and when it starts recording, the initial value was zero (the transducer was reset). There was only the relative displacement from the time t = 22 minutes. An additional displacement equal to the value calculated with LENAS (at t = 22) was added to the data recorded. From zero to 22 minutes the displacement kept constant and equal to the value calculated with LENAS at ambient temperature. For this reason, there is a small step after 22 minutes.

It is strange that for column P4 the initial displacement calculated with LENAS is the half of the displacement measured on the column. This difference seems to stay constant with the increasing of the temperature. It can come from incorrect initialisation of the transducers of displacement, or of local initial imperfection (material properties or geometry) that has not been measured.

For all the other tests there is a good agreement between simulation and experimentation.

The critical temperatures obtained with LENAS are on the safe side compared to the measured temperatures (TABLE 3.3.1 and FIGURE 3.3.1) except for column P6 where LENAS gives a temperature higher of 20°C than the one measured during this test.

COLUMN	$T_{LENAS\ SIMU} - T_{test}$ (°C)	$T_{LENAS\ SIMU}$ (°C)	Ttest (°C)
P1	-9	655	664
P2	-25	540	575
P3	-3	605	608
P4	-18	510	528
P5	-36	726	762
P6	+20	591	571
P7	-8	535	543
P8	0	520	520

TABLE 3.3.1 comparison LENAS (SIMU) and test

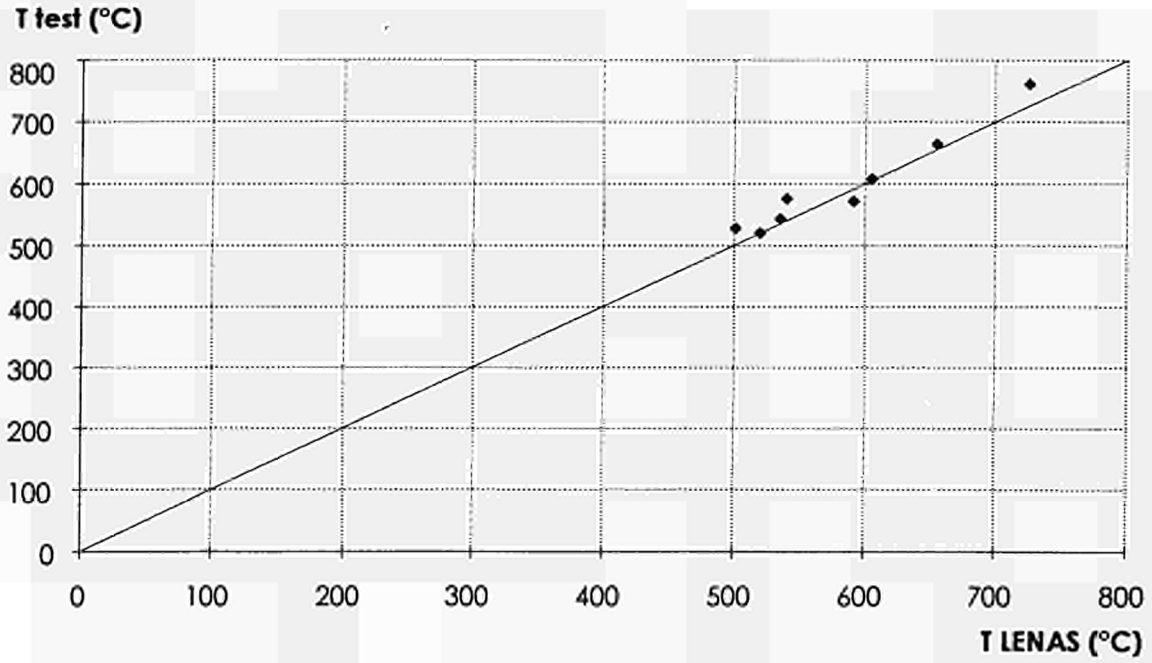

FIGURE 3.3.2 comparison of the critical temperatures (tests - LENAS)

Six calculations were made for each column. The results of these calculations are given in TABLE 3.3.2 and TABLE 3.3.3. TABLE 3.3.2 presents the time (in minutes) when the failure occurred and TABLE 3.3.3 presents the equivalent uniform temperature (at the time from TABLE 3.3.2). The six calculations were made with the following hypothesis:

- SIMU : The calculation is as close as possible to the real column tested. For this, the temperatures, the yield stress and the geometry measured were used in the calculation. The dead weight is neglected. (These results were plotted in FIGURE 3.3.2).

- TEMP. : It is the same as SIMU (see column in TABLE 3.3.2 and TABLE 3.3.3) except that the temperature is uniform in the cross section and along the column.

- GEO. : It is also the same as SIMU (see column in TABLE 3.3.2 and TABLE 3.3.3) but this time the geometry of the cross section is taken form ARBED's catalogue and the initial imperfection is equal to L/1000.

- SIG : It is the same as SIMU but $\sigma_y = 235$ MPa as given theoretically for a S235 steel profile.

- SIG1 : It is the same as SIG but σ_{yw} of the whole section is taken equal to the σ_{yf} measured for the flanges.

- SIG2 : It is the same as SIG but $\sigma_y = \dfrac{\sigma_{yf} S_f + \sigma_{yw} S_w}{S_f + S_w}$

The last column of TABLE 3.3.2 and TABLE 3.3.3 called ESSAI gives the time of failure (TABLE 3.3.2) of the column during the test performance and in TABLE 3.3.3 the equivalent critical temperature.

COLUMN	GEO	SIG	SIG1	SIG2	TEMP	SIMU	ESSAI
P1	94.75	91.12	95.0	95.75	94.62	95	96.75
P2	54.62	51.62	55.0	55.5	54.62	55.0	58.5
P3	82	74	80	81	80	80	80.56
P4	66.88	55.62	67.12	68.5	68.25	67.12	70.58
P5	115.9	109.6	114.3	116.5	115.3	115.3	122.4
P6	80.75	75.12	79.65	81.5	79.88	80.25	76.25
P7	60.88	59.88	64.25	65.62	65.75	65.12	66.7
P8	64.25	60.25	65.25	66.88	64.88	66.12	66.1

TABLE 3.3.2 Time of collapse of the columns (min)

COLUMN	GEO	SIG	SIG1	SIG2	TEMP	SIMU	ESSAI
P1	654	636	655	659	653	655	664
P2	535	505	540	545	536	540	575
P3	615	545	605	610	605	605	608
P4	509	543	510	517	516	510	528
P5	729	698	721	732	726	726	762
P6	594	565	588	597	589	591	571
P7	514	509	531	358	539	535	543
P8	511	491	516	524	514	520	520

TABLE 3.3.3 Equivalent temperature of collapse of the columns (°C)

From these calculations it can be concluded that it is not a bad approximation to take :

- The theoretical geometry.
- A uniform temperature in the column.
- A σ_y uniform in the cross section as defined for SIG1 or SIG2. Note that the fact of using σ_y equal to the theoretical value of 235 MPa is too safe.

4. NUMERICAL SIMULATIONS

4.1 CALCULATION OF AXIALLY LOADED MEMBERS: A PROPOSAL FOR AN ANALYTICAL PROPOSAL

4.1.1 INTRODUCTION

In Eurocode 3 - part 10 [2] two different calculation methods are presented to determine the fire resistance of axially loaded members;

- the general calculation model based on acknowledged principles and assumptions of the theory of structural mechanics, takes into account the effect of temperature. The application of this method requires the use of non linear computer programs,
- the simple calculation model, based on an analytical formula which can be applied with the use of tabulated data and/or a pocket calculator. This analytical formula has been recently amended in Eurocode 3 - Part 1.2. [3].

It is considered that, as stated in [2], " the general calculation models lead to a more realistic analysis of structures exposed to fire. Compared with simple calculation models, they give an improved approximation of the actual structural behaviour under fire conditions ". Simplified methods should therefore be allowed only if they prove to be safer than the more general methods.

One aim of the research is to verify the validity of the simplified method of [2] and [3] and to make an alternative proposal if necessary.
The methodology consisted of the application of the general model to a very large number of examples and to compare the results with the results provided by the analytical proposals and by real tests.

4.1.2 THE GENERAL MODEL

4.1.2.1 The numerical code

The general model has been applied by using of the computer code SAFIR, a non linear finite element program dedicated to the step by step simulation of the behaviour of structures submitted to fire. The 2D beam finite element that has been used in this study is based on the following formulations and hypotheses:

- Displacement type element.
- Prismatic element.
- The displacement of the node line is described by the displacements of 3 nodes:
  2 nodes at the ends of the element, supporting 2 translations and one rotation,
  1 node at mid length supporting the non linear part of the longitudinal displacement.
- The longitudinal displacement of the node line is a 2^{nd} order power function of the longitudinal co-ordinate.
- The transversal displacement of the node line is a 3^{rd} order power function of the longitudinal co-ordinate.
- The plane sections remain plane and perpendicular to the node line. i.e. the shear energy is not considered (Bernoulli hypothesis).

- The strains are small (Von Karman hypothesis), i.e.

$$\frac{1}{2}\frac{\delta u}{\delta x} << 1 \qquad (1)$$

- The non linear part of the strain is averaged on the length of the element to avoid locking, i.e.

$$\varepsilon_x = \frac{\delta u}{\delta x} + \frac{1}{2L}\int_{-L/2}^{+L/2}\left(\frac{\delta v}{\delta x}\right)^2 dx \qquad (2)$$

- The formulation is according to the total corrotational description.
- The angles between the deformed node line and the undeformed but translated node line are small, i.e.

$$\sin\varphi \cong \varphi$$
$$\cos\varphi \cong 1 \qquad (3)$$

- The longitudinal integration is numerically calculated by the method of Gauss.
- The cross section is discretized by means of triangular or quadrilateral fibres. At every longitudinal point of integration, all variables such as temperature, strain, stress, ... are uniform in each fibre.
- The tangent stiffness matrix is evaluated at each iteration of the convergence process (Newton - Raphson method).
- Residual stresses are considered by means of initial residual strains [4].

4.1.2.2 Hypotheses of the numerical simulations

- End conditions : simply supported, i.e. rotation not restrained.
- Load eccentricity : no eccentricity, i.e. axial load.
- Column imperfection : sinusoidal, maximum value = H/1000.
- Dead weight : neglected, i.e. only one half of the length is simulated, by means of 5 beam elements.
- Longitudinal integration : 2 points of Gauss
- Cross section : only one half is simulated. The dimensions are according to FIGURE 4.1.1, where only 1/4 of the section is represented.

FIGURE 4.1.1 Cross-section.

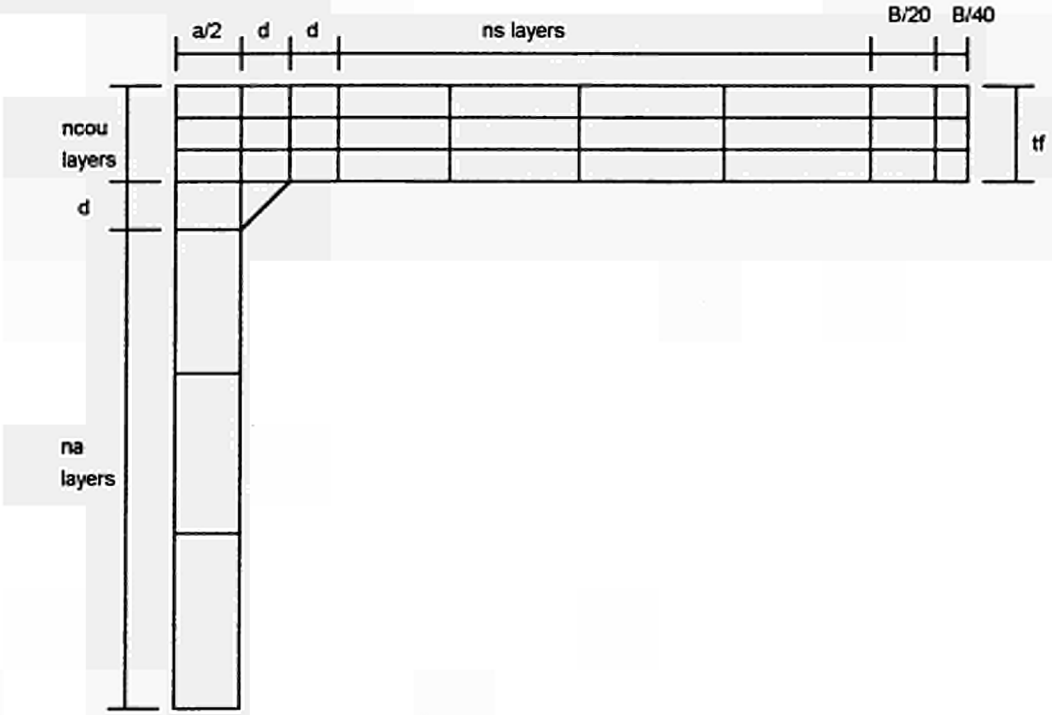

In FIGURE 4.1.1 dimension of the triangle having the same surface as the root fillet.

$$(2r)^2 - \pi r^2 = 4\left(d^2/2\right) \qquad (4)$$

d = 0.655 r

- ncou : number of layers on the thickness of the flange.
  dimension = tf/ncou
  where tf = flange thickness
- ns : number of layers on the length of one flange.
  dimension = (17 B / 40 - a/2 - 2d)/ns
  where B = width of the section,
  a = web thickness.
- na : number of layers on one half of the web.
  dimension = (H/2 - tf - d)/na
  where H = Height of the section.

The values for ncou, ns and na in the simulations have been set according to TABLE 4.1.1

TABLE 4.1.1 Parameters of the discretization.

Buckling around	major axis	minor axis
ncou	3	1
na	5	4
ns	5	10

- residual stresses:
  -constant across the thickness of the web and of the flanges,
  -triangular distribution,

-maximum value = 0.30 or 0.50 x 235 MPa depending on the value of H/B,
-no residual stress in the triangle accounting for the root fillet.

4.1.3 THE NUMERICAL SIMULATIONS IN CASE OF UNIFORM TEMPERATURE

The situation of uniform temperature has been considered as the limit case of insulated sections. With very important thermal insulation, the heating rate is so limited that the high thermal diffusivity of steel has time to homogenise the field of temperature in the section.
The other limit case leading to the most severe thermal gradient in the sections is when unprotected profiles are submitted to the ISO heating. It will be considered in another section.

4.1.3.1 S235

The nominal yield strength of 235 MPa has first been considered.
The nominal value has been adapted depending on the thickness of the flange according to EN.10025 [4], i.e.

$f_y = 235$ MPa if $t_f \leq 16$ mm
$f_y = 225$ MPa if $16 < t_f \leq 40$ mm
$f_y = 215$ MPa if $40 < t_f \leq 100$ mm
$f_y = 195$ MPa if $100 < t_f$

4.1.3.2 Strategy

The sections which are classified under class 4 according to EC3 part 1 [6] have not been considered because the beam element does not allow us to take local buckling into account whereas it is clearly stated in [1] that " *If there are failure modes, not covered by the general calculation model, they shall be excluded by appropriate detailing.* " The fire resistance of class 4 profiles should therefore be assessed by means of tests or by means of numerical simulations taking local buckling into account, which is beyond the scope of this project.

The **H** sections from the catalogue [7] of the Arbed company have been considered. In this catalogue, some sections have different names but same geometrical characteristics. In that case, one of the two twin profiles has been eliminated, which left 400 different **H** sections. For grade S235, 61 sections are classified as class 4 under axial loading according to [6]. 339 sections had thus to be considered;

34	HD	sections
128	HE	sections
6	HL	sections
28	HP	sections
41	IPE	sections
28	UB	sections
32	UC	sections
42	W	sections

For each section, buckling around the major axis as well as around the minor axis has been taken into account separately.

For each section and buckling axis, 10 different lengths have been considered, with the relative slenderness at ambient temperature $\overline{\lambda}$ equal to 0.20, 0.40, 0.60 ..... 2.00

For each length, an average of 12 different loads have been successively applied and the ultimate temperature corresponding to the loss of stability has been recorded.
When the applied load level is progressively decreased by very short time steps, the curve describing the decrease of the ultimate load as a function of temperature can be drawn. It appears that when the temperature is uniform in the section, this curve is made of linear segments of 100°C steps. Due to this fact, linear B-spline functions could be applied in order to determinate the loads which would lead to the ultimate temperatures of 400, 500, 600, 700, 800 and 900°C

Example:

For
- IPEA 80 section,
- buckling around the major axis,
- H = 1.272 m,
- fy = 235 MPa,

TABLE 4.1.2 gives the ultimate temperatures found for the 16 different loads that have been applied.

TABLE 4.1.2 Original points : ultimate temperatures.

Load [N]	Ult. temp. [°C]
84696	409.84
81167	431.14
77638	451.75
70580	492.84
63522	519.45
49406	567.12
39525	601.25
25409	668.89
18351	704.37
15528	736.86
12704	767.50
9881	798.56
9175	815.03
7764	852.48
7058	871.75
5646	920.66

TABLE 4.1.3 gives the loads corresponding to the ultimate temperatures of 400, 500 ... 900°C. Those loads have been found by application of linear β-spline functions and least square method in order to cope with redundant points.

TABLE 4.1.3 Computed points : ultimate load

Temp. [°C]	Ult. load [N]
400	86476
500	69288
600	39794
700	18822
800	9747
900	5988

FIGURE 4.1.2 Validation of the method of linear β-spline functions shows how well the original results from TABLE 4.1.2 and the computed results from TABLE 4.1.3 compare when plotted on the same graph.

FIGURE 4.1.2 Validation of the method of linear β-spline functions.

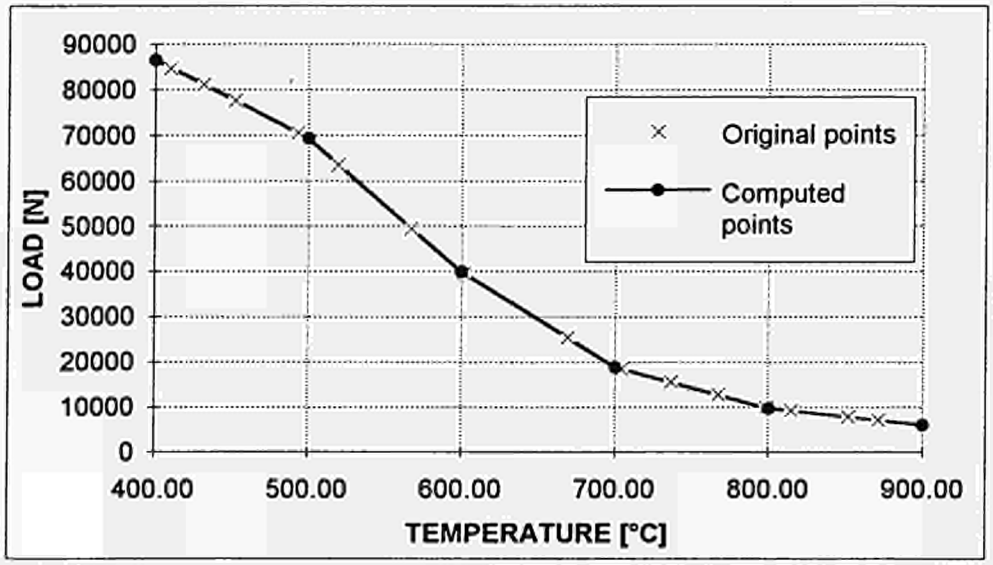

Note : In order to obtain sufficient precision on the computed values for N(400°C) and N(900°C), at least one original point must exist for a temperature between 400 and 430°C, and one point between 870 and 900°C.
For each section, each buckling axis and each nominal yield strength, a matrix was built such as the one found in TABLE 4.1.4.

TABLE 4.1.4 Computed matrix. Ultimate loads in kN for IPEA 80, major axis, S235.

	Length [m]										
Temp.	**0**	**0.636**	**1.272**	**1.908**	**2.544**	**3.180**	**3.816**	**4.452**	**5.088**	**5.724**	**6.360**
20	149.93	146.64	141.16	131.61	116.45	95.23	74.41	57.97	45.86	36.98	30.38
400	149.93	120.20	86.47	71.60	62.15	53.30	44.29	36.00	29.25	24.00	19.95
500	116.95	93.83	69.29	58.81	51.86	44.83	37.41	30.54	24.88	20.45	17.02
600	70.47	56.31	39.79	32.14	27.53	23.51	19.52	15.88	12.90	10.58	8.80
700	34.48	27.74	18.82	14.66	12.17	10.20	8.38	6.77	5.48	4.49	3.72
800	16.49	13.25	9.75	8.24	7.30	6.36	5.37	4.44	3.64	3.00	2.51
900	9.00	7.23	5.99	5.53	5.08	4.49	3.84	3.21	2.65	2.21	1.85

Each horizontal line of TABLE 4.1.4 is the buckling curve for the corresponding temperature. Those curves have a very regular and continuous shape. Therefore a sinusoidal expression is used when the ultimate load has to be found for a temperature belonging to the matrix (T = 600°C for example), but for intermediate length (H = 2 m for example) ;

$$N(T,H) = A_1(T) + A_2(T)\frac{H}{H_{max}} + \sum_{i=1}^{9} B_i(T)\sin\left(\frac{i\,\pi\,H}{H_{max}}\right) \qquad (5)$$

where N(T,H) axial load corresponding to temperature **T** (belonging to the matrix) and height **H**,

H_{max} maximum height (corresponding to $\bar{\lambda}$ = 2.00) for which calculations have been made (H_{max} = 6.360 m in TABLE 4.1.4),

$A_1(T)$, $A_2(T)$, $B_i(T)$ coefficients to be calculated from the 11 computed points at temperature **T**

note : it comes immediately that $A_1(T) = N(T,0)$

$A_2(T) = N(T,H_{max}) - N(T,0)$

When the ultimate load has to be found for a temperature and a length that do not belong to the matrix (t = 660°C and H = 3 m for example), eq. 5 is applied twice for the temperatures of the matrix immediately superior and inferior to the target temperature (600 and 700°C in this case) and a linear interpolation is made on the temperature between the two results.

4.1.3.3 Results for steel S235

In order to allow comparisons with the formula of [3], the results have first been presented in the form of buckling coefficient as a function of the relative slenderness evaluated at 20°C. The buckling coefficient is defined as ;

$$\frac{N}{N_{pl}(T)} = \frac{N}{fy(T)\,\Omega} = \frac{N}{Kfy\,fy\,\Omega} = \chi/\kappa \qquad (6)$$

where $N_{pl}(T)$ plastic load at temperature T,

fy(T) yield strength at temperature T,

fy yield strength at ambient temperature,

Ω cross sectional area

Kfy fy(T)/fy according to [1].

χ buckling coefficient calculated from the c-stut curve [1],

κ correction factor, equal to 1.20 in [1].

Ten different values of $\bar{\lambda}$, from 0.20 to 2.00, have been considered. For each relative slenderness, the buckling coefficient has been evaluated for the 339 sections, for 2 buckling axes, and for 5 ultimate temperatures (400, 500,..800°C).

Note : The temperature of 900°C has not been considered because it leads to higher buckling coefficients than the other temperatures and gives the false impression of a high scatter between the numerical results when presented in FIGURE 4.1.3. This temperature of 900°C corresponds in fact to very low load levels and is not very commonly reached in practical situations. As the results that are not considered give higher buckling coefficients than those that are used in the comparisons, the approximation is on the safe side anyway. 3390 buckling coefficients have thus been calculated for each relative slenderness.

In FIGURE 4.1.3, **SAFIR max** is the curve linking the maximum values that have been calculated by the general model, **SAFIR min** links the minimum values and **SAFIR 50%** means that 50% of the numerical results are below this curve. The analytical proposal made by the project team of EC3 - Part 10 in [1] is also drawn on FIGURE 4.1.3 (it corresponds in fact to the curve c of EC3 part 1 [6] divided by the correction factor of 1.20).

It can be observed that the analytical curve is too conservative for short columns ($\overline{\lambda} < 0.20$) whereas for intermediate length columns ($0.30 < \overline{\lambda} < 1.20$) the simplified model systematically provides results that are less safe than the general model. Also for very high columns ($1.20 < \overline{\lambda}$) the result provided by the simple model is unsafe when compared with the general model for more than 50 % of the cases.

The shape of the numerical buckling strand (i.e. the area between **SAFIR min** and **SAFIR max**) is too different from the shape of the analytical curve to let any hope that a modification of the correction factor that appears in the simple model could lead to a better correlation.

FIGURE 4.1.3. S235, uniform temperature, 339 sections, 2 axes, 5 ultimate temperatures.

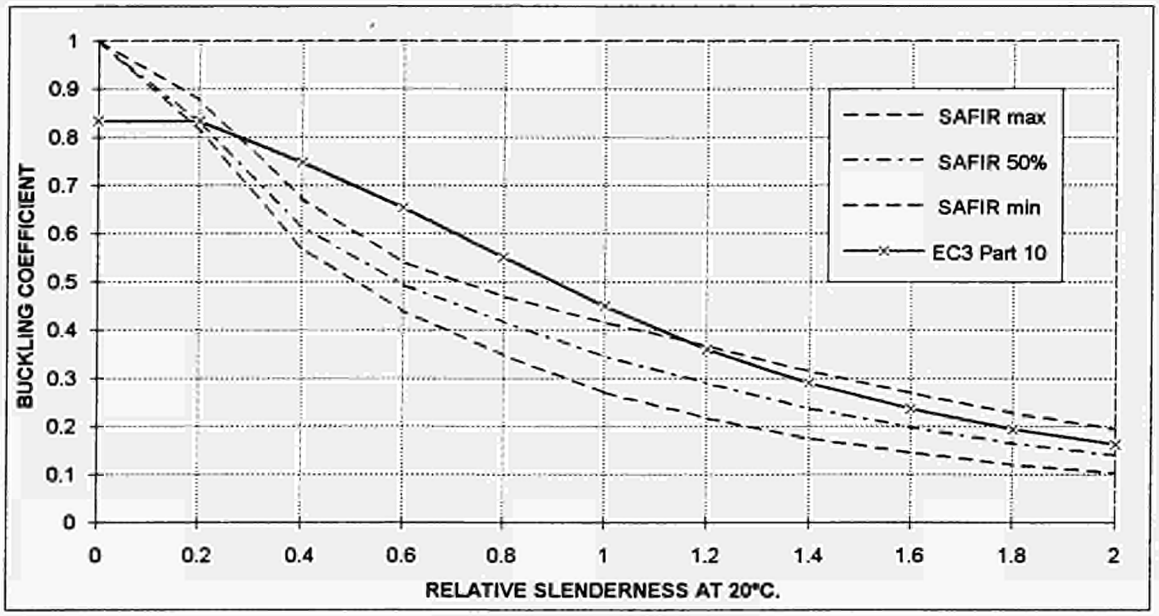

In order to allow comparisons with the analytical formula of [2], the results have then been presented in the form of buckling coefficient as a function of the relative slenderness evaluated at the ultimate temperature. FIGURE 4.1.4 presents the curves **SAFIR max, SAFIR min** and **SAFIR 50%** as well as the analytical proposal of EC3 - Part 1.2. [3] (it corresponds also to the curve c of EC3 part 1 [6] divided by the correction factor of 1.20 , but the variable on the horizontal axis of the diagram is evaluated at the ultimate temperature).

FIGURE 4.1.4. S235, uniform temperature, 339 sections, 2 axes, 5 ultimate temperatures.

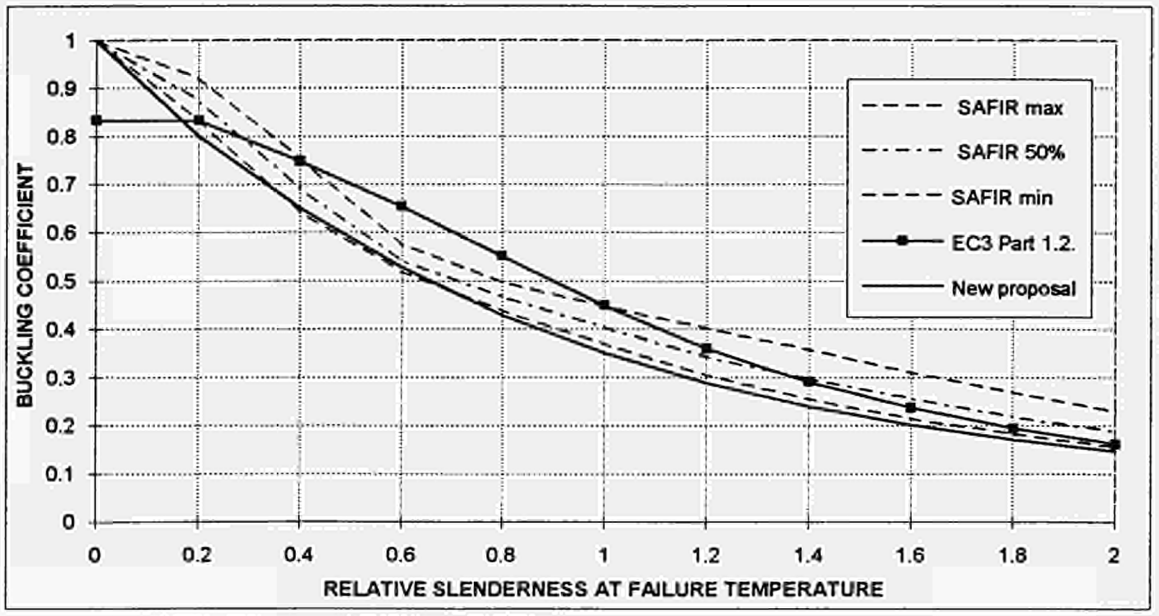

The analytical curve is also conservative for short columns ($\overline{\lambda} < 0.20$) whereas it systematically provides results that are less safe than the general model for $0.40 < \overline{\lambda} < 1.00$. For very high columns the result provided by the simple model tends to become safer when compared with the general model.
The buckling strand is thinner in FIGURE 4.1.4 than it was in FIGURE 4.1.3. This means that there is a better possibility to represent the results of the general model without excessive safety by an analytical expression in which the relative slenderness is evaluated at elevated temperature.

4.1.3.4 Results for steel S355

The nominal yield strength of 355 MPa has also been considered.
The nominal value has been adapted depending on the thickness of the flange according to EN.10025 [4], i.e.

fy = 355 MPa	if			tf ≤ 16 mm
fy = 345 MPa	if	16	<	tf ≤ 40 mm
fy = 335 MPa	if	40	<	tf ≤ 63 mm
fy = 325 MPa	if	63	<	tf ≤ 80 mm
fy = 315 MPa	if	80	<	tf ≤ 100 mm
fy = 295 MPa	if	100	<	tf

The sections which are classified under class 4 according to EC3 part 1 [6] have not been considered, which leaves 258 sections from the catalogue [6] to be considered.

34	HD	sections
106	HE	sections
4	HL	sections
23	HP	sections
25	IPE	sections
6	UB	sections
32	UC	sections
28	W	sections

FIGURE 4.1.5 presents the results when the relative slenderness is evaluated at the ultimate temperature. As 2 buckling axes and 5 ultimate temperatures are considered, 2580 buckling coefficients have been evaluated at each relative slenderness.

FIGURE 4.1.5. S355, uniform temperature, 258 sections, 2 axes, 5 ultimate temperatures.

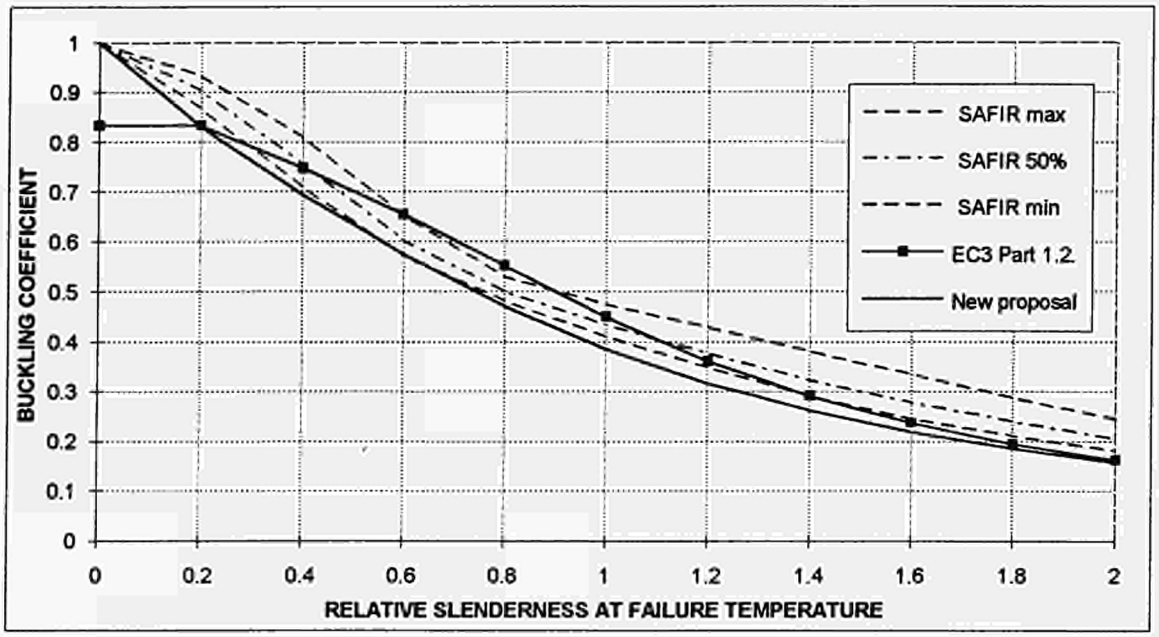

The numerical strand is higher on the vertical axis for S355 than it was for S235. This is due to the fact that the residual stresses do not depend on the yield strength. Their relative influence is therefore smaller when the yield strength is increased. This phenomena is not accounted for in the simplified model of [3], where the buckling coefficient does not vary with the yield strength.

4.1.4 A new proposal based on numerical results

The simplified models proposed in [2] or in [3] lead to safety levels that can be significantly lower than the general method. It appears that the safety level of the simple models is different at different slenderness. Therefore, a simple modification of the proposed method, such as a new value for the correction factor, would oblige to take a high value to ensure safety of intermediate length columns (see FIGURE 4.1.4) and would lead to an excessively uneconomical situation for short and long columns..

A new proposal has been made. The equation is;

$$N = \chi N_{pl}(T) = \chi Kfy\ fy\ \Omega \qquad (7)$$

The buckling coefficient χ is given by

$$\chi = \frac{1}{\varphi + \sqrt{\varphi^2 - \overline{\lambda}^2}} \qquad (8)$$

where $\varphi = \frac{1}{2}\left(1 + \alpha\,\overline{\lambda} + \overline{\lambda}^2\right)$ (9)

with α : imperfection factor

$= \beta\,\varepsilon$, $\beta = 1{,}2$ in this chapter: the value of the severity factor β will be fixed by comparing with the database of test (see chapter 5)

$\varepsilon = \sqrt{235/fy}$ (fy in MPa)

$\lambda_E(T) = \pi \sqrt{E(T)/fy(T)}$

$\bar{\lambda}$: relative slenderness evaluated at temperature T

$\bar{\lambda} = \lambda / \lambda_E(T) = \bar{\lambda}(20°C) \sqrt{Kfy / K_E}$

with $K_E = E(T)/E$ according to [1]

The buckling curve calculated according to Eq. 8 has been drawn in FIGURE 4.1.4 and FIGURE 4.1.5. This curve varies with the yield strength due to the parameter ε that appears in the imperfection factor. Eq. 8 is exactly the same as the one defined at ambient temperature in [6], except that the threshold limit of 0.20 for $\bar{\lambda}$ does not appear in Eq. 9. This makes the new curve start at χ = 1.00 for $\bar{\lambda}$ = 0.00 but makes it decrease even for very low slenderness instead of having an horizontal plateau up to $\bar{\lambda}$ = 0.20.

For the situations where the temperature is known, Eq. 9, 8 and 7 allow to the direct calculation of the ultimate load. If the ultimate temperature is the unknown, an iterative process has to be applied owing to the fact that the relative slenderness is evaluated at the ultimate temperature. This process is no problem for pocket calculators or for computers. It converges very quickly (one iteration necessary) , especially if the initial value of the slenderness is chosen according to;

$\bar{\lambda}$ = 1.20 x $\bar{\lambda}$(20°C).

The determination of the ultimate load is even faster with the help of tabulated data. Eq. 7 can indeed be rewritten in the form;

$$N = \chi \, Kfy \, fy \, \Omega = f'_{y,\theta,\bar{\lambda}} \cdot \Omega \qquad (10)$$

where Ω is the area of the cross section

$f'_{y,\theta,\bar{\lambda}}$ is the critical compression stress for a given temperature and a given slenderness, $f'_{y,\theta,\bar{\lambda}} = \chi \, K_{fy} \, f_y$

It is possible to draw directly tables providing the critical stress **as a function of the relative slenderness evaluated at 20°C**. The effect of the reduction of the material properties as well as the effect of buckling are simultaneously incorporated. Such tables are given in chapter 6.

Notes.

1. Low temperatures:
The formula should probably be adapted in the temperature range from 20 to 400°C. From 20 to 100°C for example, the stress - strain relationship of steel is not modified (Kfy = Kfp = KE = 1.00) and there is no reason why the failure load should decrease. From 100 to 400°C, a linear interpolation could be proposed between the load calculated at 100°C (= to the load at 20°C, calculated according to [6]) and the load calculated at 400°C by the simple model for elevated temperature. This is true whatever the analytical proposal at elevated temperature.

2. Linear interpolations:
Strictly speaking, the interpolation on the temperature in the tables of chapter 6 for the calculation of $f_{y,\theta,\bar{\lambda}}$ should not be linear because of the temperature dependency of the relative slenderness. In fact, the influence of Kfy is overwhelming in the determination of the overall buckling coefficient, and a linear interpolation is amply sufficient.

3. Different buckling curves:
A more detailed analysis of the numerical results shows that the classification established at ambient temperature between different buckling curves a, b, c and d tends to vanish at elevated temperature. The fact of using a different severity factor, and therefore a different buckling curve, according to the same classification as at 20°C would therefore not reduce the significant safety level that is achieved in some cases. Two other options have been considered without better success : either considering a different buckling curve for each ultimate temperature or differentiating between both buckling axes.

4.1.5 Unprotected sections submitted to ISO heating

The case of unprotected profiles submitted to ISO heating leads to the most severe thermal gradients in the steel section, except if a more severe heating curve is applied (hydrocarbon curve for example). All the other cases of thermally protected profiles should have results between those calculated previously in chapter 4.1 for uniform temperature (totally protected) and those that could be calculated for unprotected profiles.
The general model has been used to calculate the temperature distribution in the steel sections heated by the ISO curve The boundary conditions have been taken according to Eurocode Actions, Chapter 20 [54] and the thermal properties of steel according to Eurocode 3 Part 1.2 [27]. For S235 steel, for all the sections, for both buckling axes and for 10 different column lengths, 8 different loads have been applied and the fire resistance noted. The average temperature of the non uniform distribution at the moment of failure, T_{mean} , has also been noted. For the 50.000 odd non uniform results calculated by the general model, the load leading to the same ultimate temperature in the uniform situation has been calculated, as well as the ratio between both values $N^{iso}(T_{mean},H)$ and $N^{uniform}(T_{mean},H)$. Values higher than 1.00 indicate that the ISO heating is not as severe as the uniform heating, whereas values lower than 1.00 indicate that the ISO heating leads to a lower ultimate temperature. FIGURE 4.1.6 representing the distribution of the $N^{iso}/N^{uniform}$ ratio shows that the difference between ISO and uniform temperature seldom exceeds 1,15.

FIGURE 4.1.7 representing the cumulative distribution shows that in 95% of cases, the ISO load is equal to at least 90% of the UNIFORM load.
In fact, the question is whether the new analytical proposal made in chapter 4.1.4 for totally protected sections (uniform temperatures) can be safely applied to unprotected profiles submitted to the ISO fire, and hence to normally protected profiles as well. Thus, the

meaningful ratio is between $N^{iso}(T_{mean},H)$ calculated by the general model and $N^{analyt.}(T_{mean},H)$ calculated by the new proposal (eqn. 7). FIGURE 4.1.8 representing the distribution of the $N^{iso}/N^{analyt.}$ ratio shows that the ISO buckling load is generally higher than that calculated by eqn. 7.

FIGURE 4.1.8 representing the cumulative distribution shows us that in 95% of the cases, the ISO load is higher than the load calculated according to eqn. 7. That means that the new proposal can be safely used for unprotected steel profiles, although it has been established from results based on the uniform temperature distribution.

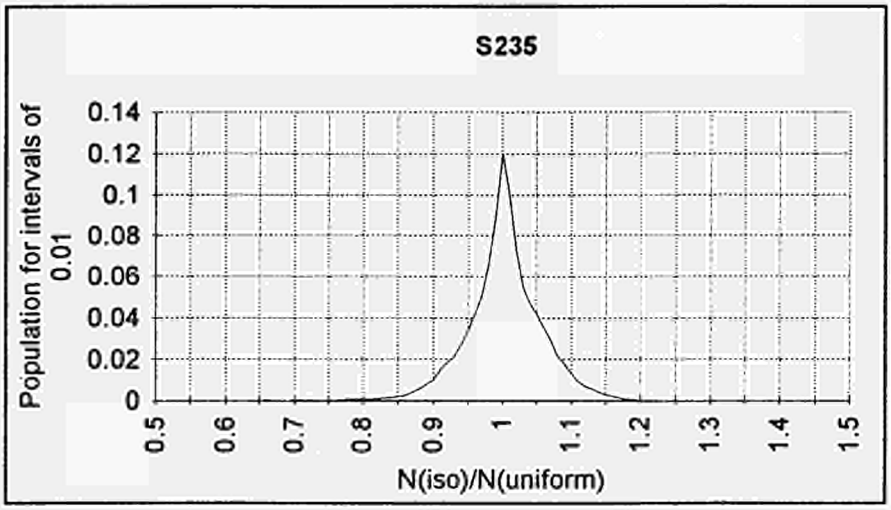

FIGURE 4.1.6 Distribution of the ISO/UNIFORM ratio. N(iso) and N(uniform) calculated by the general model.

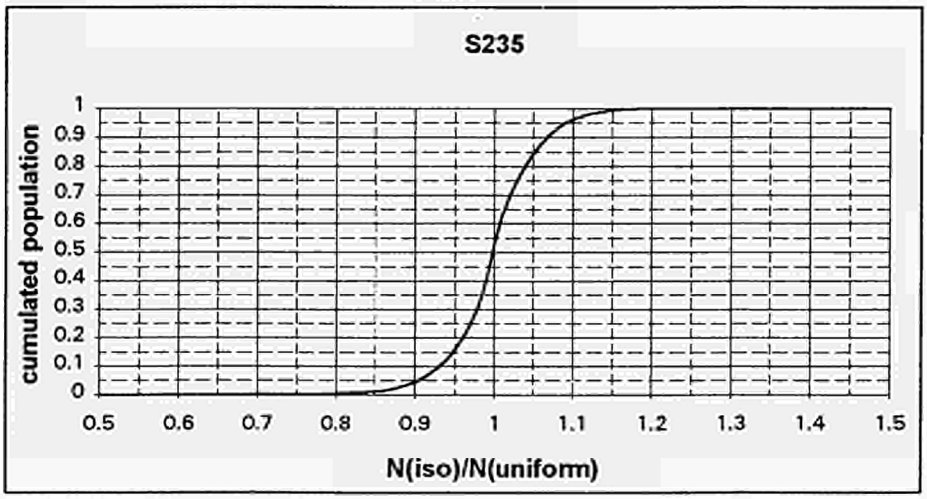

FIGURE 4.1.7 Cumulative distribution of the ISO/UNIFORM ratio. N(iso) and N(uniform) calculated by the general model.

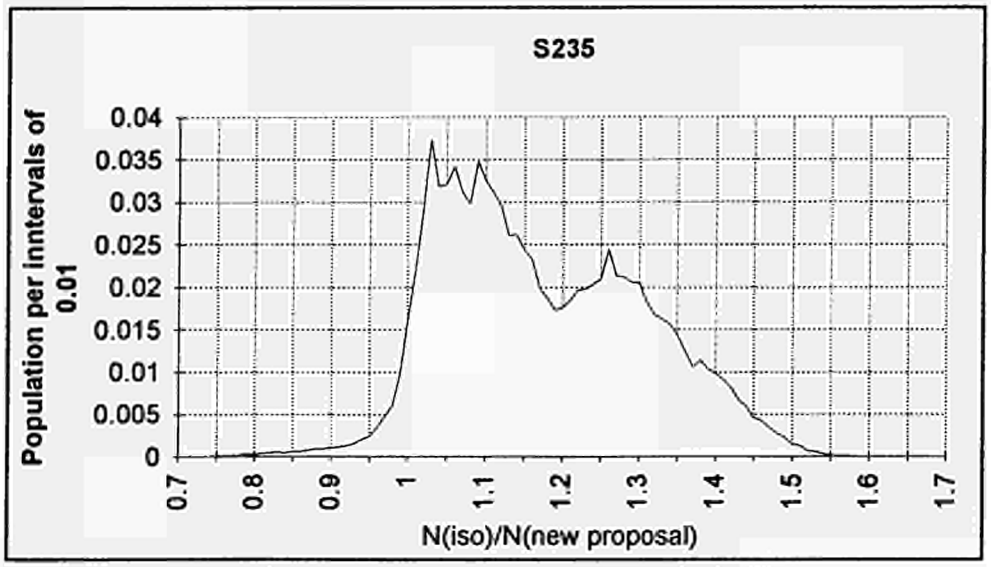

FIGURE 4.1.8 Distribution of the ISO/New proposal ratio

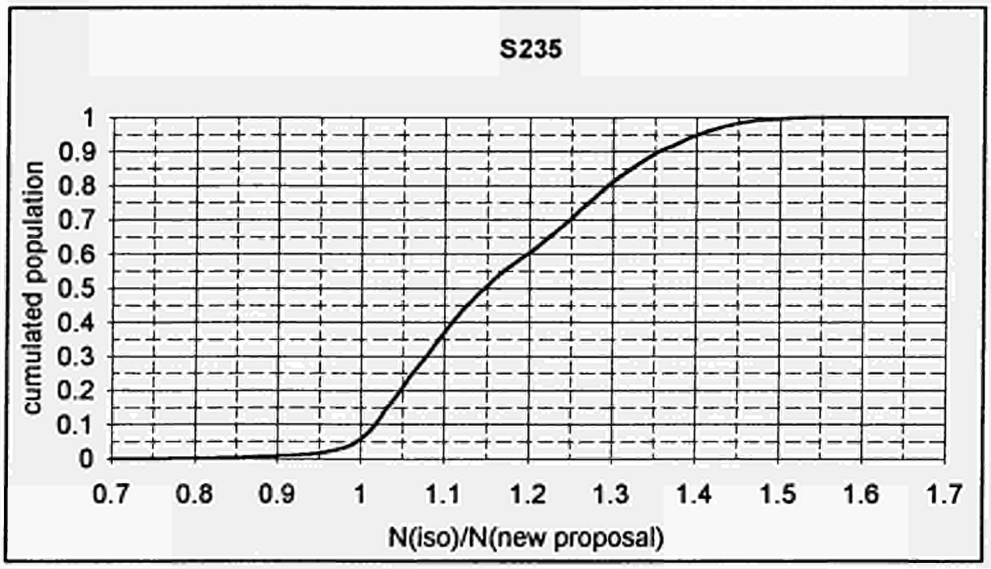

FIGURE 4.1.9 Cumulative distribution of the ISO/new proposal ratio

4.2 CALCULATION OF COLUMNS IN COMPRESSION AND BENDING: A FORMULA FOR M-N INTERACTION

After the validation of the LENAS software used for this research (see chapter 3), it is possible to check the M-N interaction formula of Eurocode 3 Part 1.2 in order to find out if the simple transposition to hot conditions of the formulae developed with columns in ambient temperature is correct.

However, since the results from finite element calculations depend on the way a structure is discretized, the determination of an optimum mesh necessary for the calculations was carried out.

4.2.1 Sensitiveness analysis of the results in relation to the column discretization

The sensitiveness analysis of the failure temperature in relation to the fineness of the discretization of the column (over its length and in section) was carried out with 8 different mesh types (4 about the minor axis and 4 about the major axis) submitted to 4 different loads (2 generating a buckling of the column about its minor axis and 2 about its major axis).

These load cases consisted of an axial compressive force combined with a uniform or bi-triangular moment distribution over the column height.

The dimensions of the analysed column were as follows:

- steel section : HE 200 B
- steel : S235
- length : 4 m
- initial deformation : $e_0 = l / 1000$ (sinusoidal deformation)
- residual stress : bi-triangular distribution in the web and flanges (maximum value 0.5 x 235 MPa)

The load types under analysis were as follows :

- As concerns buckling about the major axis :
- an axial compressive force N=100 kN combined with a uniform moment distribution M=10 kN.m
- an axial compressive force N=100kN combined with a bi-triangular moment distribution M=10kN.m
- As concerns buckling about the minor axis:
- an axial compressive force N=10 kN combined with a uniform moment distribution M=40 kN.m
- an axial compressive force N=50kN combined with a bitriangular moment distribution M=50kN.m

The discretization into a number of beam elements and of section divisions (fibers) is defined in TABLE 4.2.1 as concerns buckling about the minor axis, and in TABLE 4.2.2 as concerns buckling about the minor axis.

reference of discretization	T1	T2	T3	T4
number of elements over the length	20	20	10	6
number of fibers in section	80	60	60	60
discretization in section	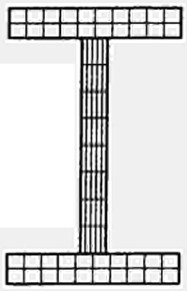	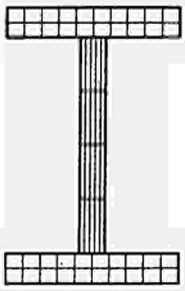		

TABLE 4.2.1 Discretization for the analysis of buckling about the minor axis

reference of discretization	T5	T6	T7	T8
number of elements over the length	20	20	10	6
number of fibers in section	146	60	60	60
discretization in section	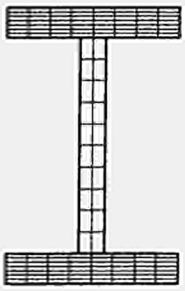	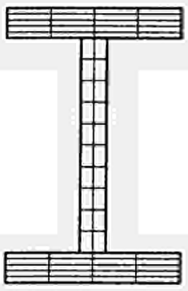		

TABLE 4.2.2 Discretization for buckling about the major axis

FIGURE 4.2.1 to FIGURE 4.2.4 show the results of the numerical simulations for these 8 cases of discretization of the column.

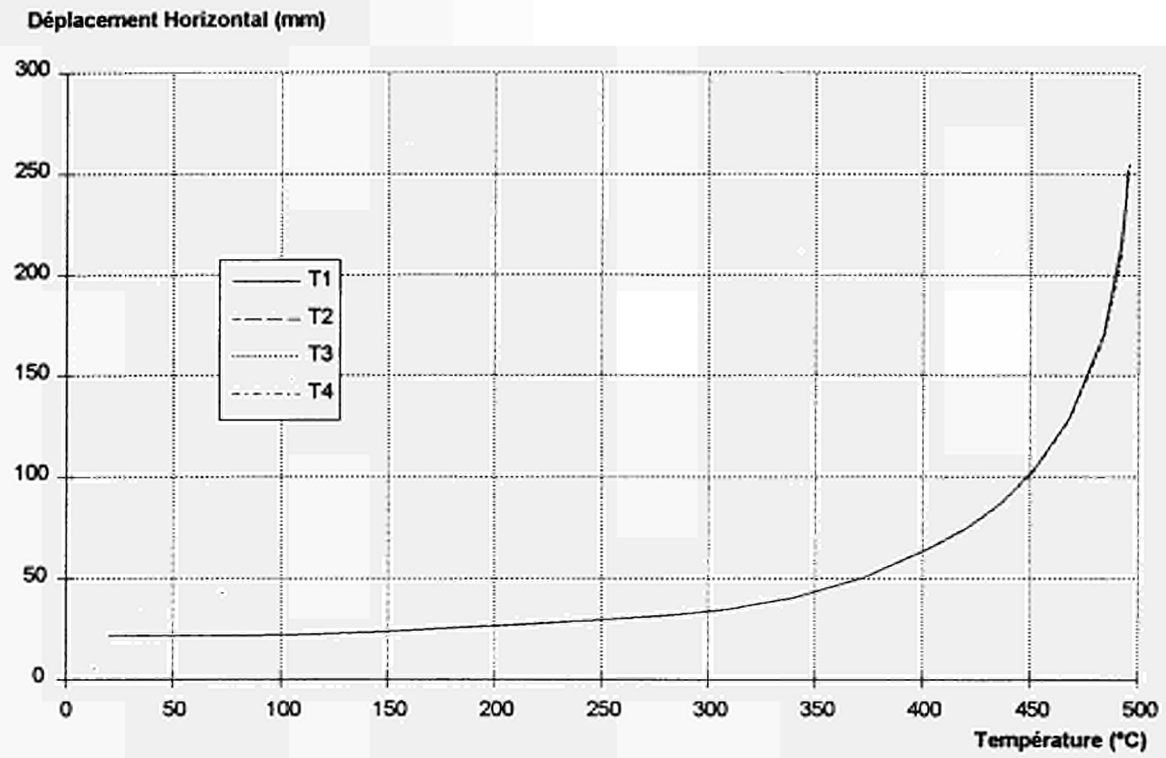

FIGURE 4.2.1 Influence of the mesh - buckling about the minor axis and uniform moment distribution

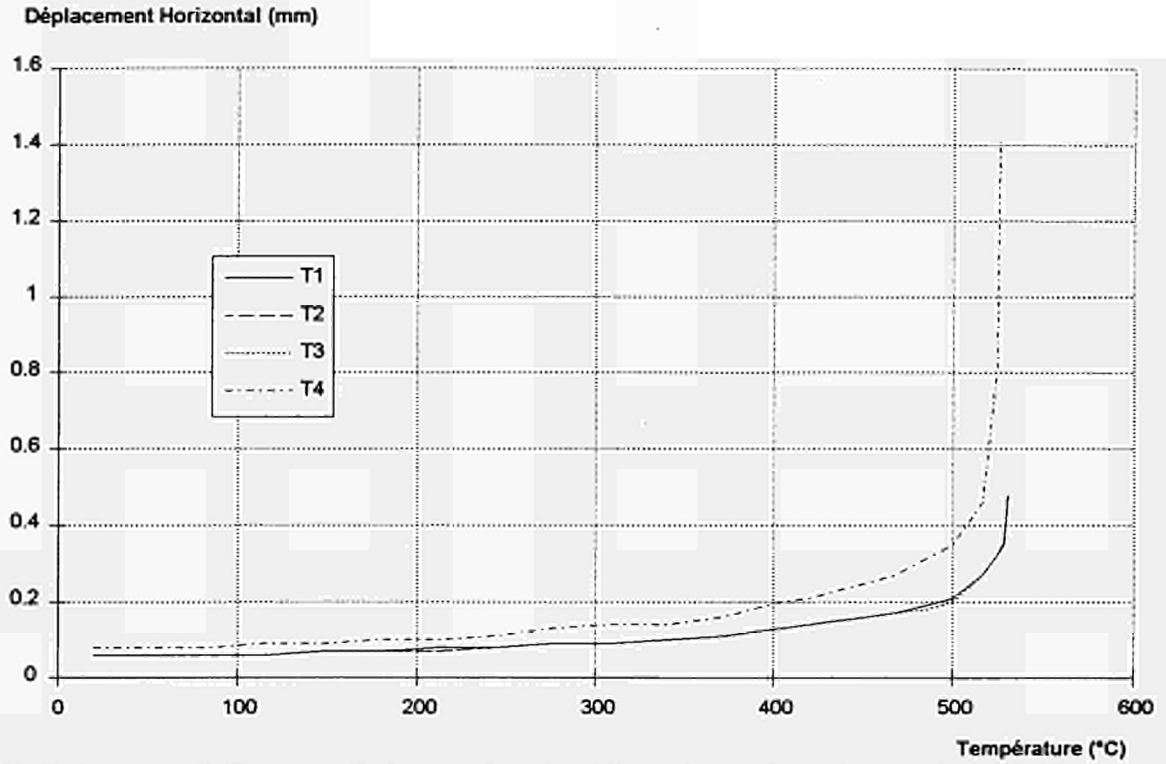

FIGURE 4.2.2 Influence of the mesh - buckling about the minor axis and bi-triangular moment distribution

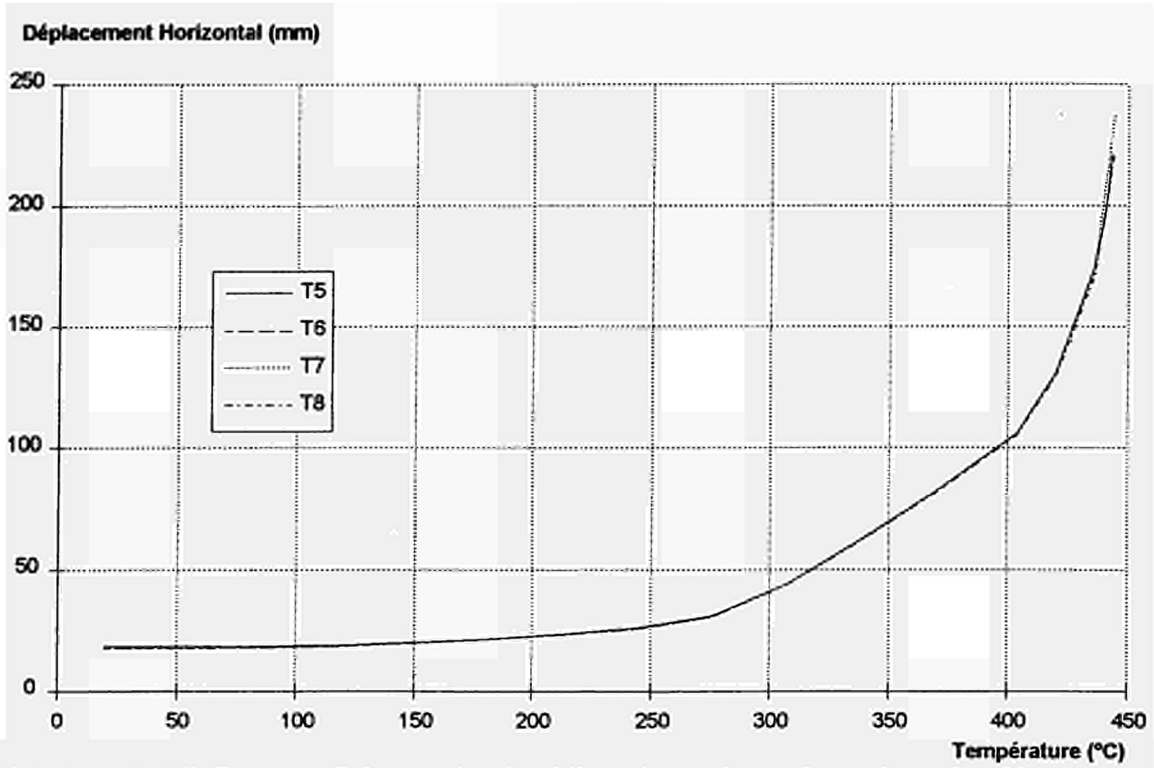

FIGURE 4.2.3 Influence of the mesh - buckling about the major axis and uniform moment distribution

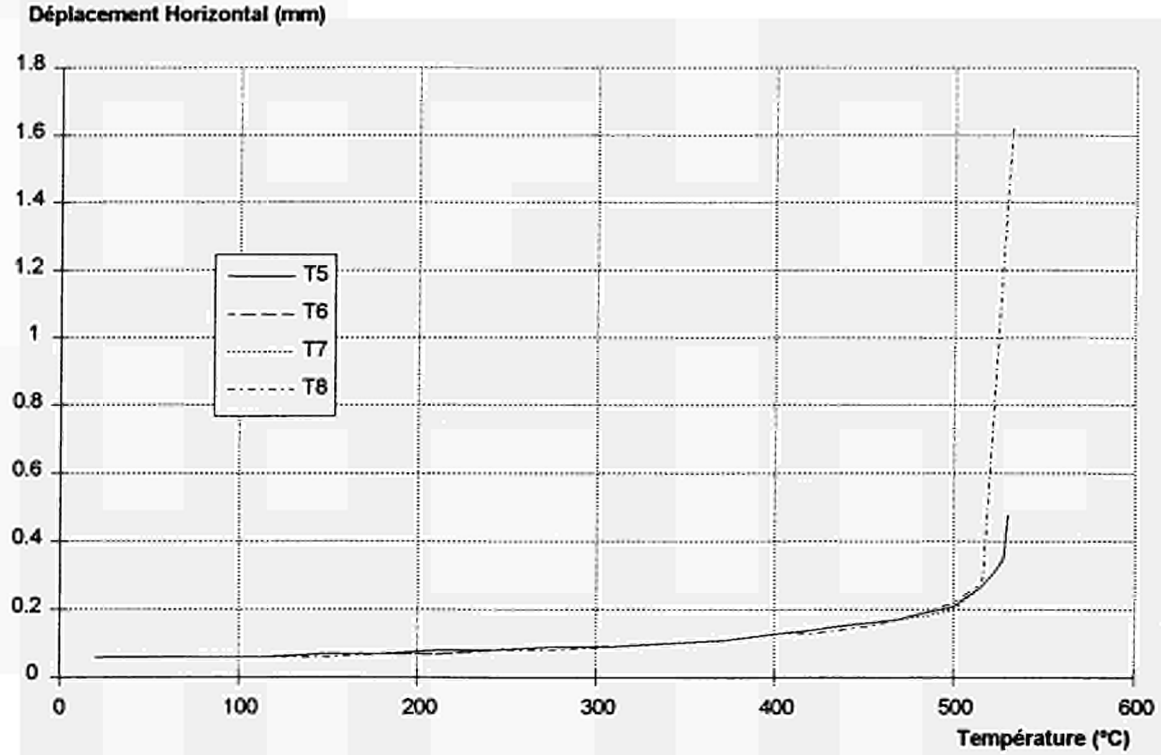

FIGURE 4.2.4 Influence of the mesh - buckling about the major axis and bi-triangular moment distribution

On FIGURE 4.2.2 and FIGURE 4.2.4, it can be seen that the meshes with only 6 elements over the length of the column give calculation results quite different from those carried out with 10 and 20 elements. The difference in failure temperature between these meshes is

however only 1%, but the difference in displacement is very large, especially for a bi-triangular moment distribution about the minor axis. Meshes with 10 and 20 elements give very similar results.

As concerns the discretization in section, neither the increase of the number of fibers over the web depth (case T1 for buckling about the minor axis), nor the increase of the number of fibers over the flange width (case T5 for buckling about the major axis), generated a change in the results.

Consequently, a mesh into 10 elements over the column height with a section division Type T3 (TABLE 4.2.1) for buckling about the minor axis, and T7 (TABLE 4.2.2) for buckling about the major axis, shall be used.

Since the columns subject to a uniform moment over their height are perfectly symmetrical, they may be simulated by taking only half a length. Since the columns subject to a triangular or bi-triangular moment do not have any symmetry (because of the load), it shall be necessary to discretize the whole column.

4.2.2 Numerical Analysis

Taking into account some gaps in the formulae of Part 1.2 of Eurocode 3 as concerns the fire resistance of steel columns in compression and bending, a numerical analysis must be carried out on a sufficiently representative set of specimens.

However, this analysis will be restricted to the columns subject to temperatures ranging from 400 to 900°C, since below 400°C steel does not lose much of its strength (the yield point remains unchanged and the modulus of elasticity decreases by 30%). In addition, in Eurocode 3 Part 1.2, a conventional temperature of 350°C is recommended for Class 4 steel sections. Besides, beyond 900°C, the interest of calculations is much limited since such a critical temperature means that the column is practically not loaded (less than 10% in relation to its failure load at ambient temperature).

The survey of the laws of variation of the mechanical properties of steel according to Eurocode 3 Part 1.2 shows that these properties vary linearly by steps of 100°C.

Calculations carried out on an HEB 200 (FIGURE 4.2.5) show that the failure temperature also varies linearly by steps of 100°C. It is therefore possible, from two numerical results within a range of 100°C (e.g. the 600-700°C range) to extrapolate the failure load to both ends of this range. Thus, with a reduced number of calculations between 400°C and 900°C, it is possible to determine the failure loads for temperatures of 400, 500, 600, 700, 800 and 900°C. This method was retained for the following part of this survey.

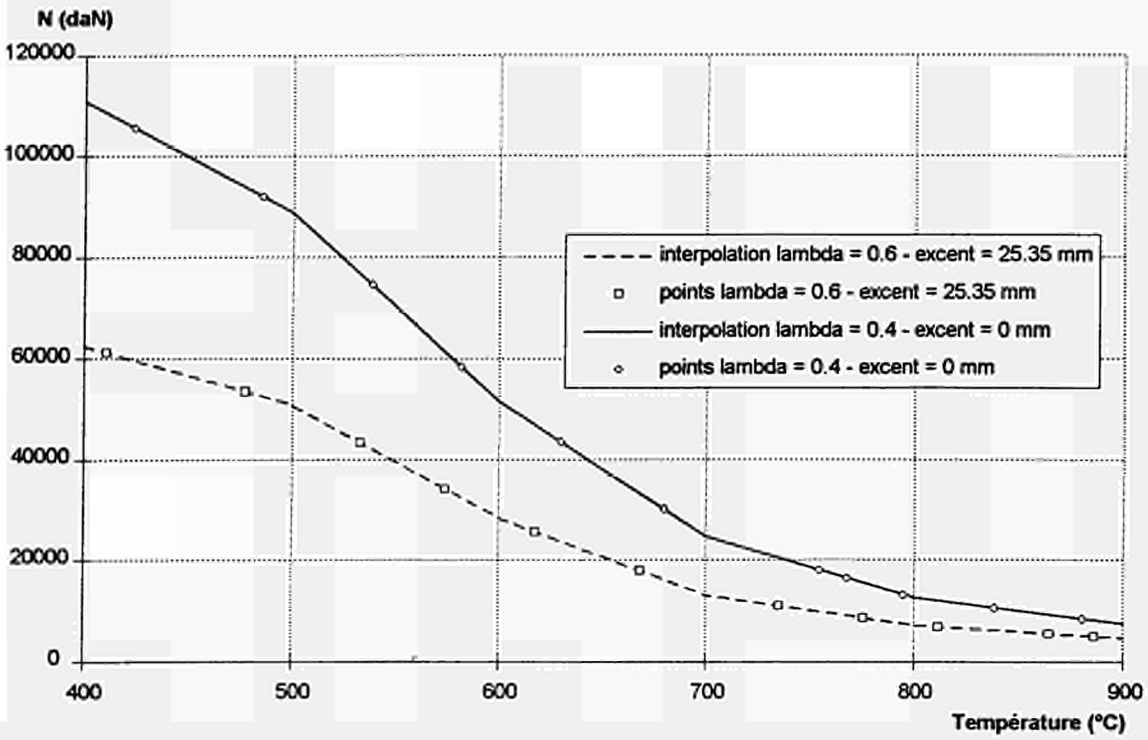

FIGURE 4.2.5 Example of linear interpolation between the results obtained with LENAS

4.2.2.1 Calculation assumptions

The calculations were carried out on the following steel sections :

- HE AA 100, 200, 400, 600 and 1000
- HE A 100, 200, 400, 600 and 1000
- HE B 100, 200, 400, 600 and 1000
- HE M 100, 200, 400, 600 and 1000
- IPE 80, 200, 400, 600, IPE 750x137, IPE 750x147, IPE 750x173, and IPE 750x193

Though some of the selected steel sections are Class 3 (e.g. HE 400 AA) or 4 (HE 1000 B is Class 4 in pure compression and Class 1 in pure bending), this cannot lead to errors in the results since the numerical model used (on the basis of "beam" finished elements) does not take the risk of local instability into account. These steel sections were not selected for their Class, but in order to cover a complete range of steel section dimensions.

The calculation assumptions are as follows :

- buckling lengths equivalent to reduced slenderness ratios of $\lambda = 0.2$ to 2.0 with a 0.2 step.
- sinusoidal initial deformation with a maximum deformation $e_0 = l / 1000$

- residual stresses with a bi-triangular distribution in the flanges and in the web, with a maximum value of 0.5 x 235 MPa or 0.3 x 235 MPa depending on the section dimensions of the steel section (as recommended in Eurocode 3 Part 1.1 of 1984)

- column pinned at both ends

- eccentricity of the load of : $\delta = 0$, 0.05 x r, 0.1 x r, 0.5 x r, 1 x r, 3 x r, 5 x r, 20 x r and 50 x r (r is the radius of gyration of the column).

- dead weight of the column disregarded.

- radii in section disregarded.

- the yield point of the steel varies depending on the thickness of the flanges t_f (in conformity with standard EN 10025 [5]), i.e.:

- f_y = 235 MPa	if	t_f	$\leq$	16 mm		
- f_y = 225 MPa	if	16	<	t_f	$\leq$	40 mm
- f_y = 215 MPa	if	40	<	t_f	$\leq$	100 mm
- f_y = 195 MPa	if	100	<	t_f		

Three types of moment distribution over the height of the column are analysed :

- uniform.

- triangular.

- bi-triangular.

FIGURE 4.2.6 shows an example of results of these calculations (see also Annex 8). The value of the plastic moment M_{pl} was calculated for each steel section by using the proper yield point (defined above) and disregarding the radii (since they are disregarded in the calculations carried out with LENAS).

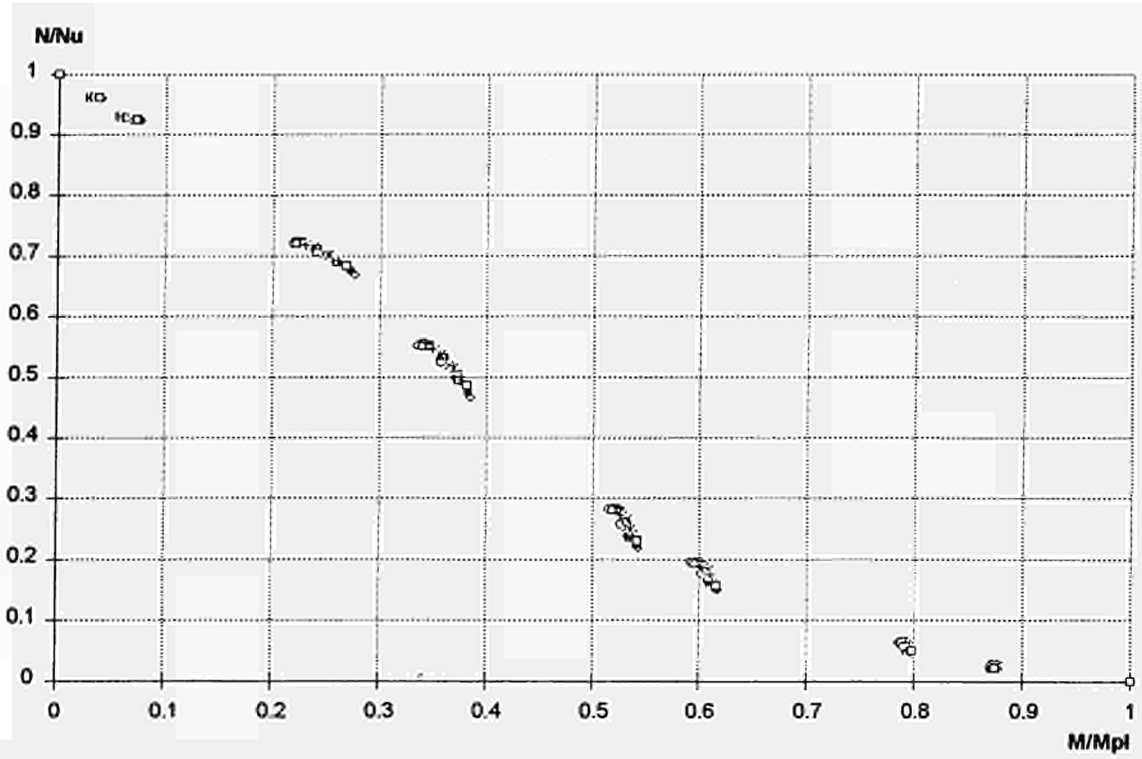

FIGURE 4.2.6 Example of results of interaction between normal force and bending moment buckling about the minor axis, uniform moment distribution, $\lambda_{20} = 0.6$ and temperature of 400°C

4.2.2.2 Interpretation of the results

The analysis of the numerical results allows us to distinguish three main ranges:

- A) The variation of the M-N interaction curve depending on the failure temperature.
- B) The evolution of the M-N interaction curve depending on the slenderness ratio of the column.
- C) The dispersion of the results depending on the section of the column.

A) Influence of the failure temperature

FIGURE 4.2.7, FIGURE 4.2.8 and FIGURE 4.2.9 show the M-N interaction curves from 400°C to 900°C, for an HE 200 B steel section with a reduced slenderness ratio of 1.4 (at ambient temperature), in which buckling occurs about the minor axis. Each figure shows a moment distribution type (uniform moment distribution on FIGURE 4.2.7, triangular on FIGURE 4.2.8 and bi-triangular on FIGURE 4.2.9).

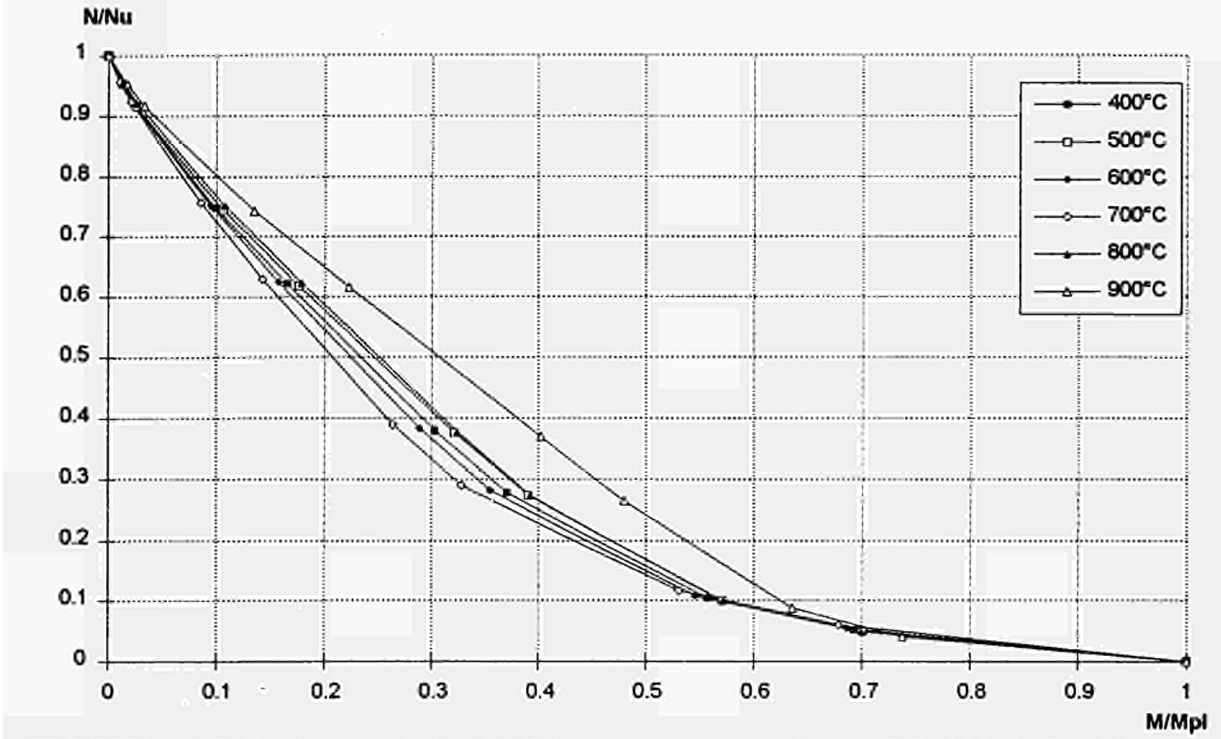

FIGURE 4.2.7 Evolution of the M-N interaction curve for an HE 200 B (buckling about minor axis, $\lambda_{20} = 1.4$ and uniform moment) depending on the failure temperature

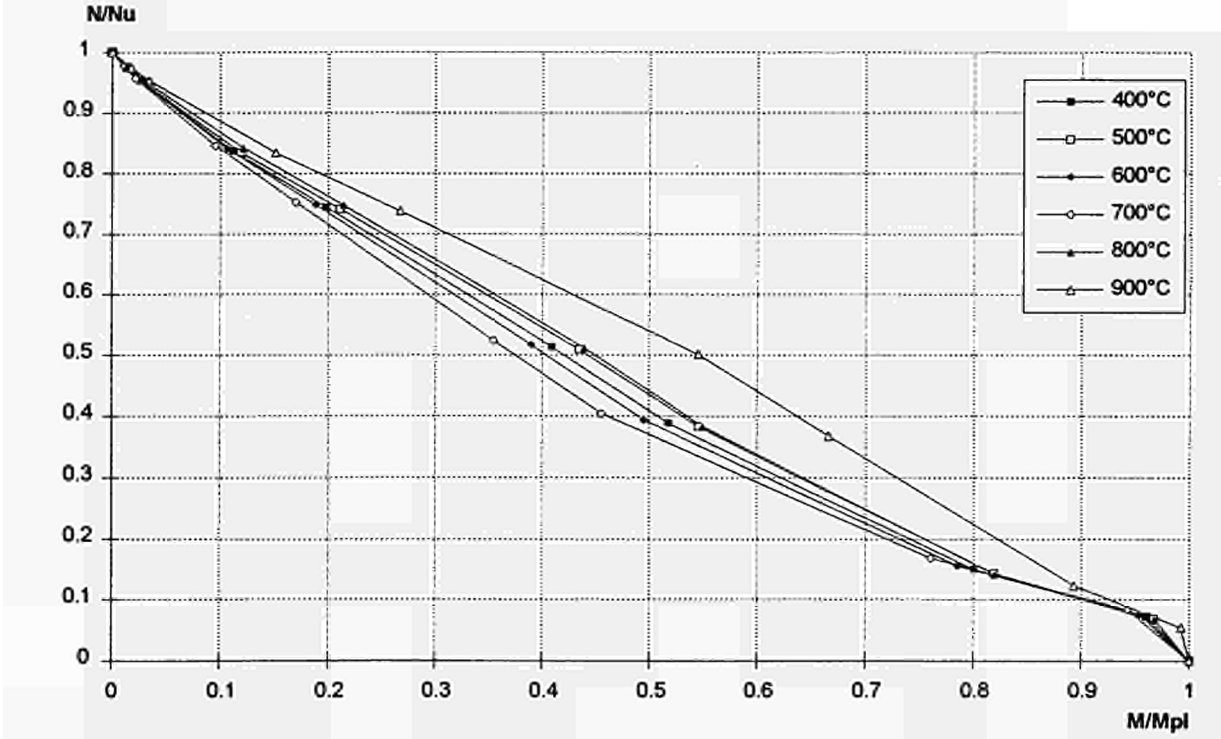

FIGURE 4.2.8 Evolution of the M-N interaction curve for an HE 200 B (buckling about minor axis, $\lambda_{20} = 1.4$ and triangular moment) depending on the failure temperature

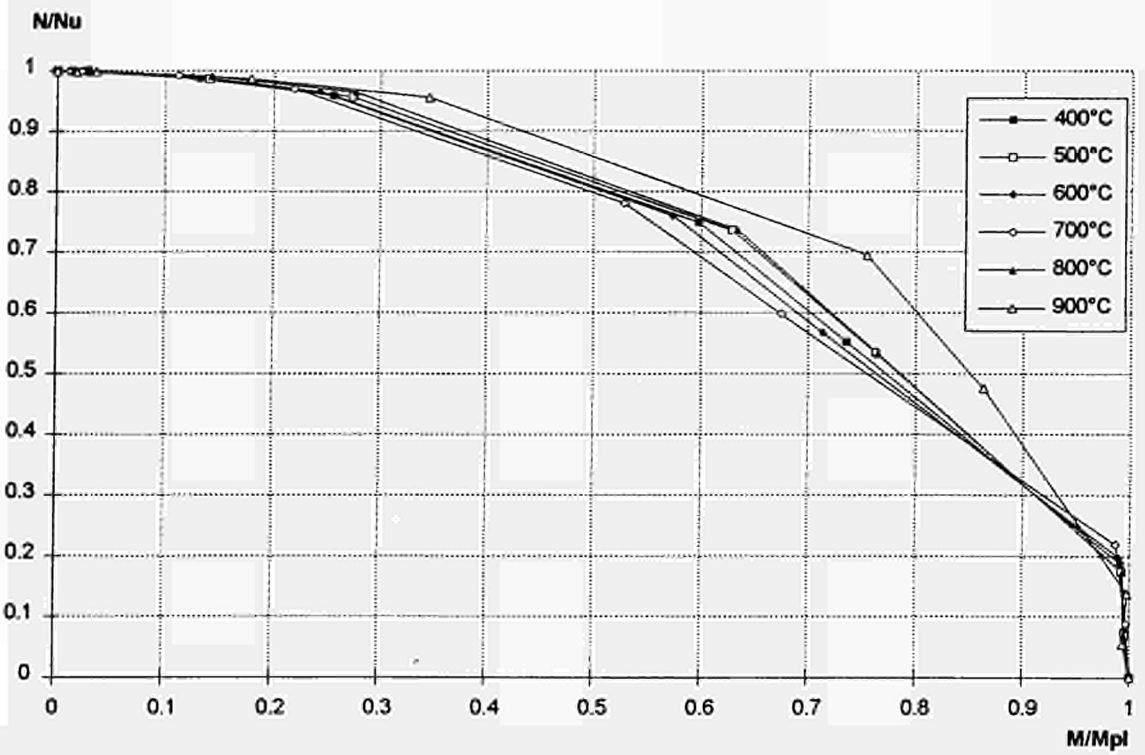

FIGURE 4.2.9 Evolution of the M-N interaction curve for an HE 200 B (buckling about minor axis, $\lambda_{20} = 1.4$ and bi-triangular moment) depending on the failure temperature

It can be noted that :

- The dispersion of the results is not very large depending on the temperature, except for the curve obtained at a failure temperature of 900°C which always give a greater strength.
- The relative position of the curves changes depending on the ratio $\sqrt{\frac{k_{y,\theta}}{k_{E,\theta}}}$. That is to say, the greater this ratio, the more concave the M-N interaction curve will be. In fact, for a fixed ratio N/N_u, the greater the ratio $\sqrt{\frac{k_{y,\theta}}{k_{E,\theta}}}$, the lower the value M/M_{pl} will be. If N/N_u is taken as 0.3, for instance, for a failure temperature of 700°C, the result will be $\sqrt{\frac{k_{y,\theta}}{k_{E,\theta}}} = 1.33$ and $M/M_{pl} = 0.32$, while at 900°C, $\sqrt{\frac{k_{y,\theta}}{k_{E,\theta}}} = 0.94$ and $M/M_{pl} = 0.455$.

Because of the relatively low dispersion of the results, it seems possible to limit the analysis to one only interaction curve. Hence, the average curve, obtained for a failure temperature of 400°C, was retained. In fact, if the results obtained for a failure temperature of 900°C are disregarded, the ratio $\sqrt{\frac{k_{y,\theta}}{k_{E,\theta}}}$ varies from 1.33 (at 700°C) to 1.1 (at 800°C) at the most, and it is equal to 1.19 for a failure temperature of 400°C, which corresponds approximately to the average of both extreme values.

B) Influence of the slenderness ratio

FIGURE 4.2.10, FIGURE 4.2.11 and FIGURE 4.2.12 show the evolution of the M-N interaction curves, for a failure temperature of 400°C and the buckling about the minor axis of an HE 200 B steel section depending on the slenderness ratio.

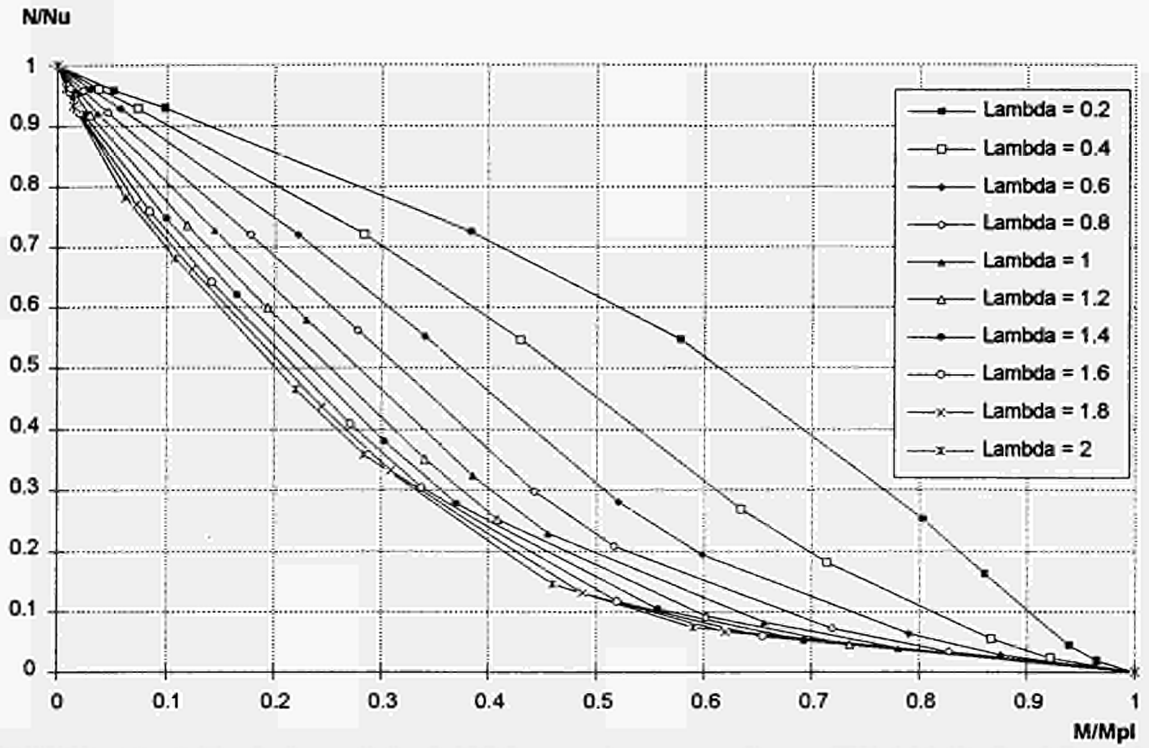

FIGURE 4.2.10 Evolution of the M-N interaction curve for an HE 200 B (buckling about minor axis, a temperature of 400°C and uniform moment) depending on λ

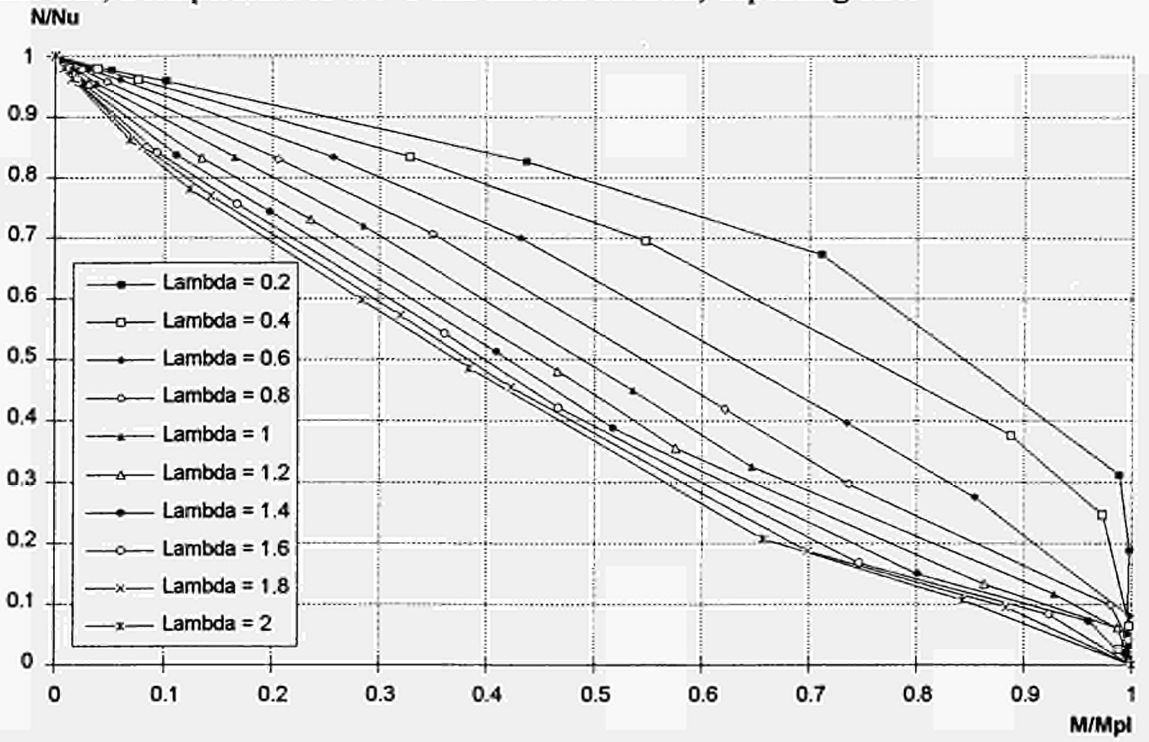

FIGURE 4.2.11 Evolution of the M-N interaction curve for an HE 200 B (buckling about minor axis, a temperature of 400°C and triangular moment) depending on λ

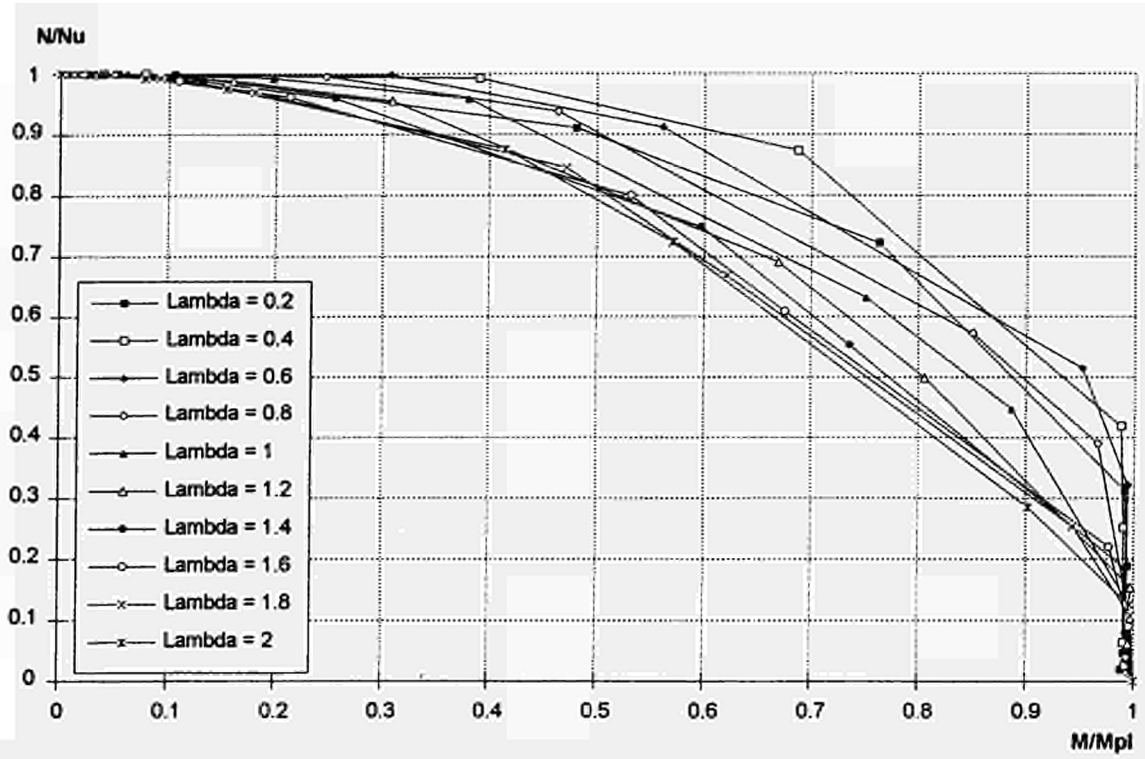

FIGURE 4.2.12 Evolution of the M-N interaction curve for an HE 200 B (buckling about minor axis, a temperature of 400°C and bi-triangular moment) depending on λ

Generally, the more the slenderness ratio increases, the more the curves takes on a concave shape. It can also be noted that for a small increase in the slenderness ratio for values of λ ranging from 0.2 to 0.6, the variation of the curve is large. On the other hand, a variation of the slenderness ratio, when λ is high (1.2 to 2), does not alter the M-N interaction curve much.

C) Influence of the shape of the section

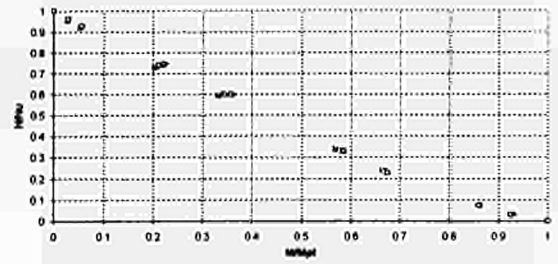

a - uniform moment, major axis

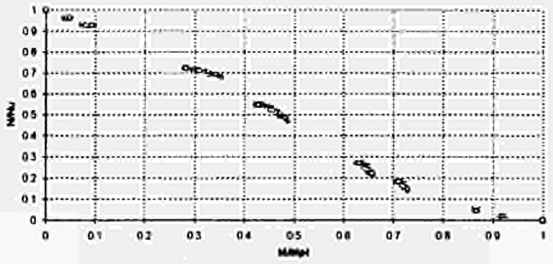

b - uniform moment, minor axis

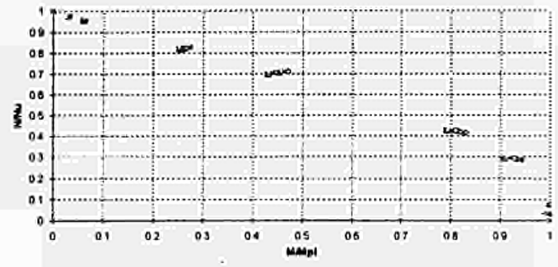

c - triangular moment, major axis

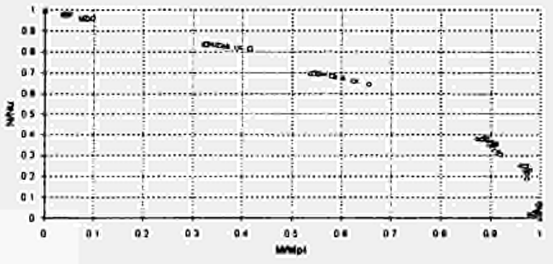

d - triangular moment, minor axis

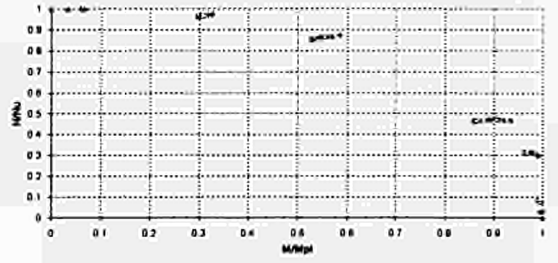

e - bi-triangular moment, major axis

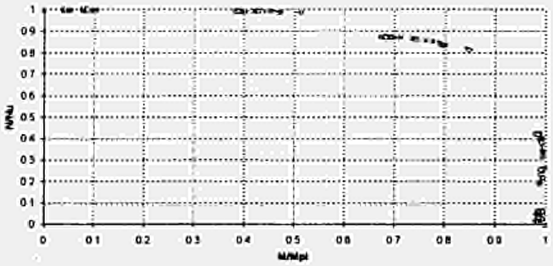

f - bi-triangular moment, minor axis

FIGURE 4.2.13 Results for all the sections = 0.4, Temperature of 400°C

It can be seen that the dispersion of the results for buckling about the major axis is relatively low. In the case of buckling about the minor axis, this dispersion is somewhat higher. In addition, for both buckling axes, the dispersion increases from the uniform moment distribution to the bi-triangular moment distribution. However, in all cases, it seems possible to define only one interaction law for all the steel sections.

4.2.3 Determination of a formula for M-N interaction

From the results obtained through numerical simulations for about 150 000 different cases, an analytical expression was worked out to allow the determination of the fire resistance of steel columns subject to the combined effects of an axial force and of a bending moment.

For the first stage, an alteration of the formula of Eurocode 3 - Part 1.2 will be proposed. And, for the second stage, a new formulation, on the basis of a different approach, will be given.
For each of these formulae, a preliminary sensitivity analysis in relation to the various parameters used in these formulae will be carried out in order to obtain adjusted factors.

4.2.3.1 Analysis of the parameters of Eurocode 3 Part 1.2

The formulation for Class 1 and 2 steel sections is :

$$\frac{N_{Sd}}{\chi(\theta)_{min}\, A\, f_{y,\theta}} + k_y \frac{M_{y,Sd}}{W_{pl,y}\, f_{y,\theta}} \leq 1 \qquad (11)$$

with :

$$k_y = 1 - \frac{\mu_y\, N_{Sd}}{\chi(\theta)_y\, A\, f_{y,\theta}} \qquad \text{but } k_y \leq 1.5 \qquad (12)$$

$$\mu_y = \bar{\lambda}_{y,\theta}\left(2\,\beta_{M,y} - 4\right) + \frac{W_{pl} - W_{el}}{W_{el}} \qquad \text{but } \mu_y \leq 0.9 \qquad (13)$$

In a first step, we shall study the influence of some parameters such as k_y, μ_y , or the influence of the ratio of the modulus of plastic bending divided by the modulus of elastic bending.

A) Influence of the ratio modulus of plastic bending - Modulus of elastic bending

As a rule, the ratio $\frac{W_{pl} - W_{el}}{W_{el}}$ generates but a very small variation of μ_y since it must be added to λ_y (2β - 4). This ratio varies between 0.08 and 0.22 if we consider buckling about the major axis, and between 0.51 and 0.59 for buckling about the minor axis. It seems simpler to take this ratio as equal to a constant C.

For instance, C = 0.15 (major axis), and C = 0.55 (minor axis).

B) Influence of μ_y

μ_y mainly depends on the bending moment distribution and on the slenderness ratio (but also on the modulus of elastic and plastic bending, which is practically equal to a constant). For the values of $\beta_{M,y}$ between 1.1 and 2, the value of μ_y is negative, and if $\beta_{M,y}$ is between 2 and 2.5, then μ_y is positive (if $\beta_{M,y} = 2$, then $\mu_y = 0$).

We try to determine the maximum and minimum values of μ_y . These values are obtained for the maximum value of the slenderness ratio.

Now, in our analysis, the fixed limit is $\lambda = 2$. In addition, λ is a function of the ratio $\sqrt{\frac{k_y}{k_E}}$, which gives a maximum λ of 2.66 at 700°C. Thus we can find the values of $\mu_{y,mini}$ = -4.8 a $\mu_{y,maxi}$ = 2.66.

But, since μ_y is limited to 0.9 (equation 13), the value of 2.66 is never reached. This limitation generates a maximum interaction curve which can never be exceeded in any case.

It can be noted on FIGURE 4.2.14 that the deviation is smaller between the curves obtained with μ_y equal to -2 and -4 than for those obtained with μ_y equal to 0.8 and 0.9. This type of curve is very sensitive to a small variation of μ_y when this value is near 0.9, whereas if μ_y is negative, a small variation of μ_y generates but a small alteration of the curve.

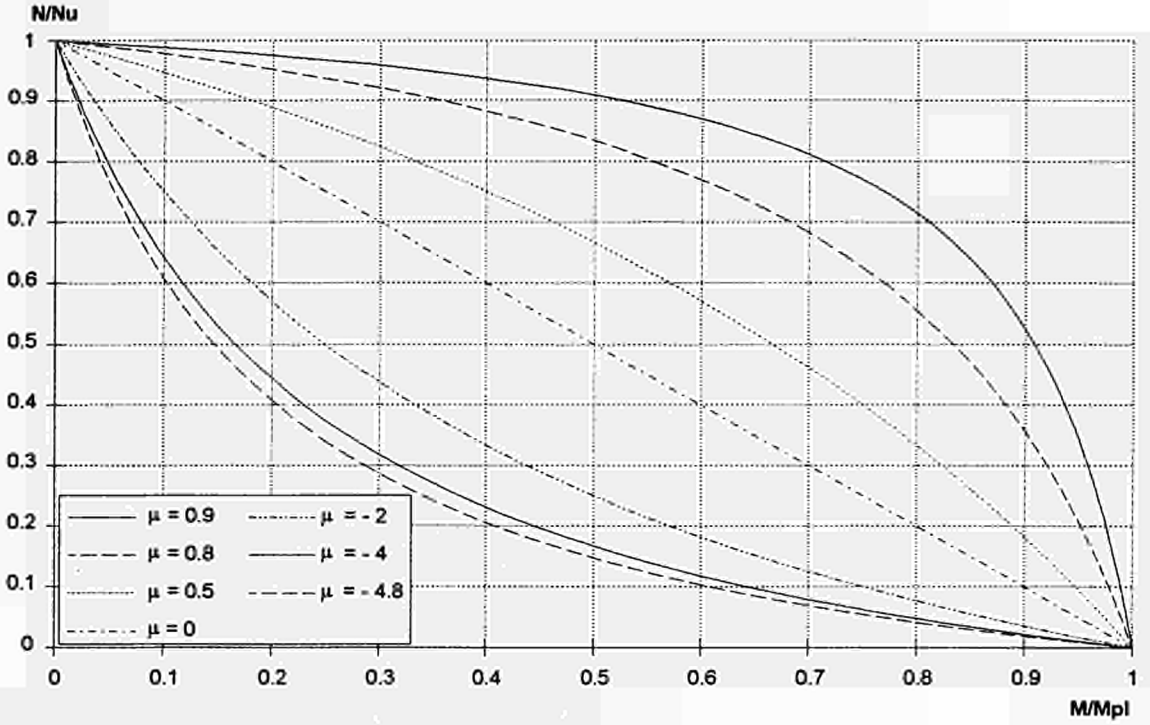

FIGURE 4.2.14 Sensitiveness of the formula to μ_y

C) Influence of k_y

In the formulation of Eurocode 3 Part 1.2, the value of k_y must be less than or equal to 1.5. This limitation creates a linear part on the M-N interaction curve, as soon as the value calculated from equation 5.2 is greater than 1.5 (FIGURE 4.2.15).

The equation of this linear part is :

$$\frac{N}{N_u} = -1.5\frac{M}{M_{pl}} + 1 \qquad (14)$$

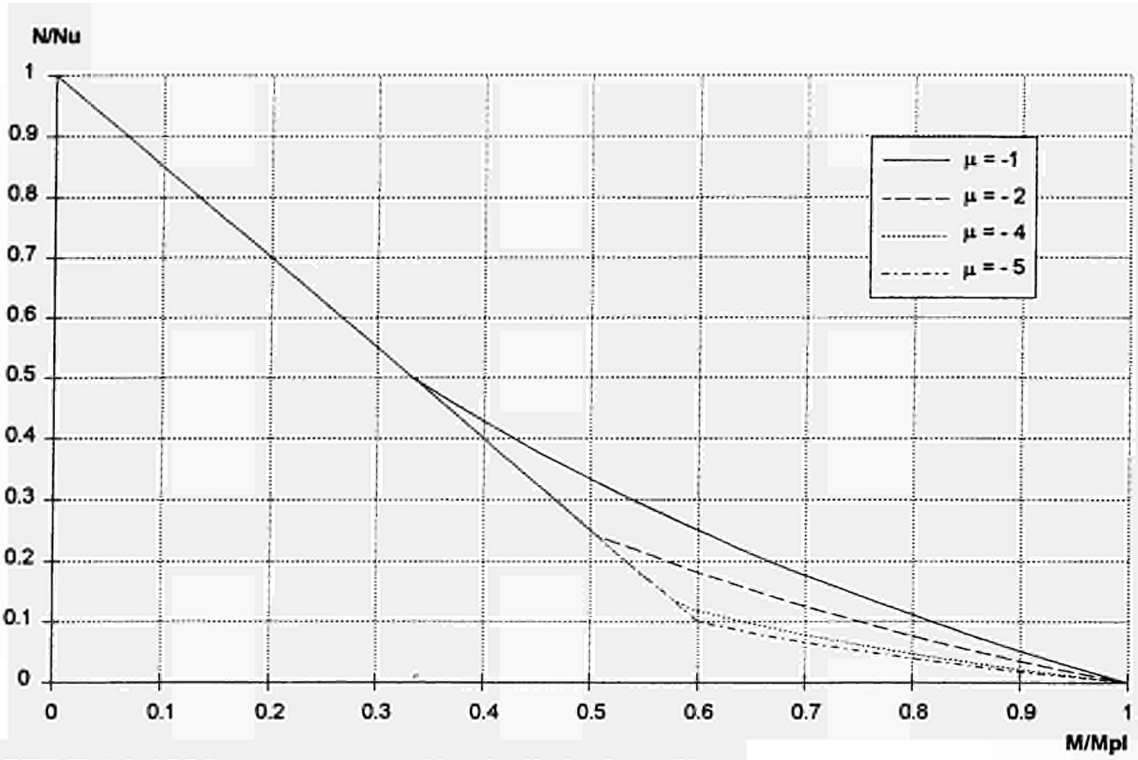

FIGURE 4.2.15 Linear part created by the limitation of k_y

The value of $k_y = 1.5$ is reached when the loading of the column tends towards a uniform moment distribution (since μ_y is negative). The greater the slenderness ratio of the column, the more preponderant this phenomenon becomes.

4.2.3.2 Evolution of the formula of Eurocode 3 Part 1.2

In order to work out an evolution of the formula of Eurocode 3 Part 1.2, the maximum value that k_y can reach must be found during the first stage. Then, a formula is developed (depending on the slenderness ratio of the column) for each load case and about both buckling axes. Eventually, a global M-N interaction formula is developed.

A) Determination of the maximum value of k_y

A first analysis of the M-N interaction curves (FIGURE 4.2.16) shows that when a column is subject to a uniform moment distribution and when its slenderness ratio is large enough, the limitation of factor k_y to 1.5 leads to an overestimation of the strength of the column as compared to its actual strength. Indeed, for this type of column, it shows a linear part when M stays relatively low, but k_y should be limited to 3 (FIGURE 4.2.16).

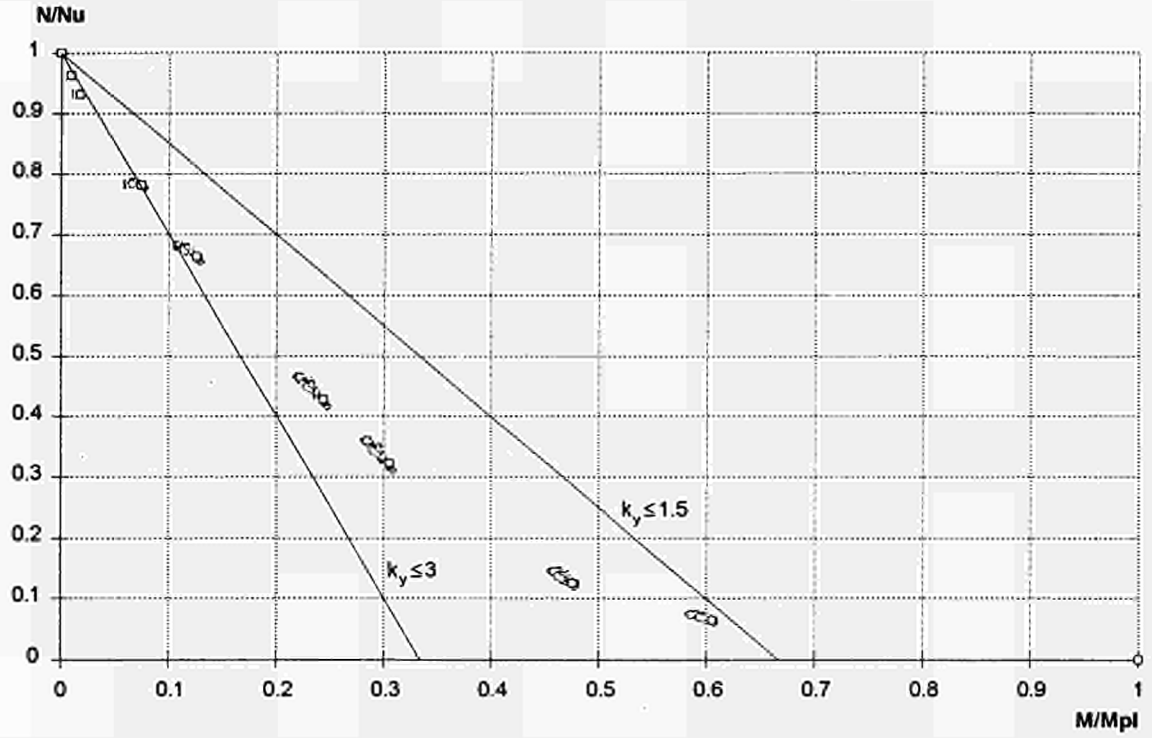

FIGURE 4.2.16 Maximum value of k_y (buckling about minor axis - uniform moment distribution - $\lambda_{20} = 2$ - 400 °C)

B) Equation for each load case

From all the available results on the one hand, and the general formulation of the interaction curve (equation 15) on the other hand, it is possible to determine the value of μ_y (formula 16).

$$\frac{N_{Sd}}{\chi(\theta)_{min}\, A\, f_{y,\theta}} + \left(1 - \mu_y \frac{N_{Sd}}{\chi(\theta)_y\, A\, f_{y,\theta}}\right) \frac{M_{y,Sd}}{W_{pl,y}\, f_{y,\theta}} \leq 1 \qquad (15)$$

hence:

$$\mu_y = \left[\frac{N_{Sd}}{\chi(\theta)_{min}\, A\, f_{y,\theta}} + \frac{M_{y,Sd}}{W_{pl,y}\, f_{y,\theta}} - 1\right] \frac{\chi(\theta)_y\, A\, f_{y,\theta}}{N_{Sd}} \frac{W_{pl,y}\, f_{y,\theta}}{M_{y,Sd}} \qquad (16)$$

For the results obtained the dispersion of the points is acceptable if we disregard the points found out for the very large load eccentricities (20 x r and 50 x r) which lead to eccentricities of up to 20 metres (FIGURE 4.2.17).

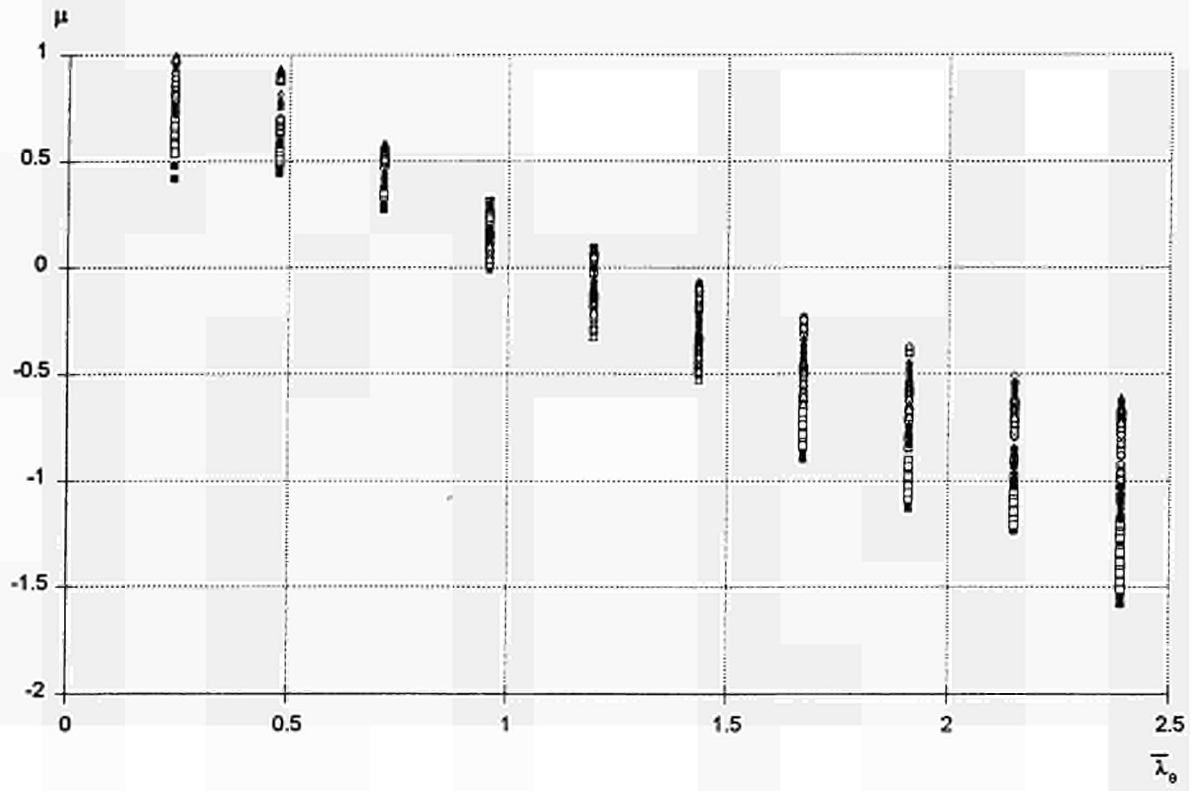

FIGURE 4.2.17 Evolution of μ according to the slenderness ratio (buckling about minor axis - triangular moment) (see also Annex 10).

The calculations carried out for large load eccentricities do not reach the failure load of the column, but underestimate it, due to the fact that it is numerically extremely difficult to simulate failure through pure bending : the failure of the structure generally occurs through the considerable deformations generated by bending, and not through the creation of a plastic hinge due to the total plasticization of a section. This phenomenon is particularly distinct for a load with a uniform or triangular moment distribution.

In order to estimate the evolution of factor μ_y as a function of λ, the average of all μ_y is calculated for each slenderness ratio (disregarding both maximum eccentricities of each column) and for each load type (FIGURE 4.2.18 and FIGURE 4.2.19)

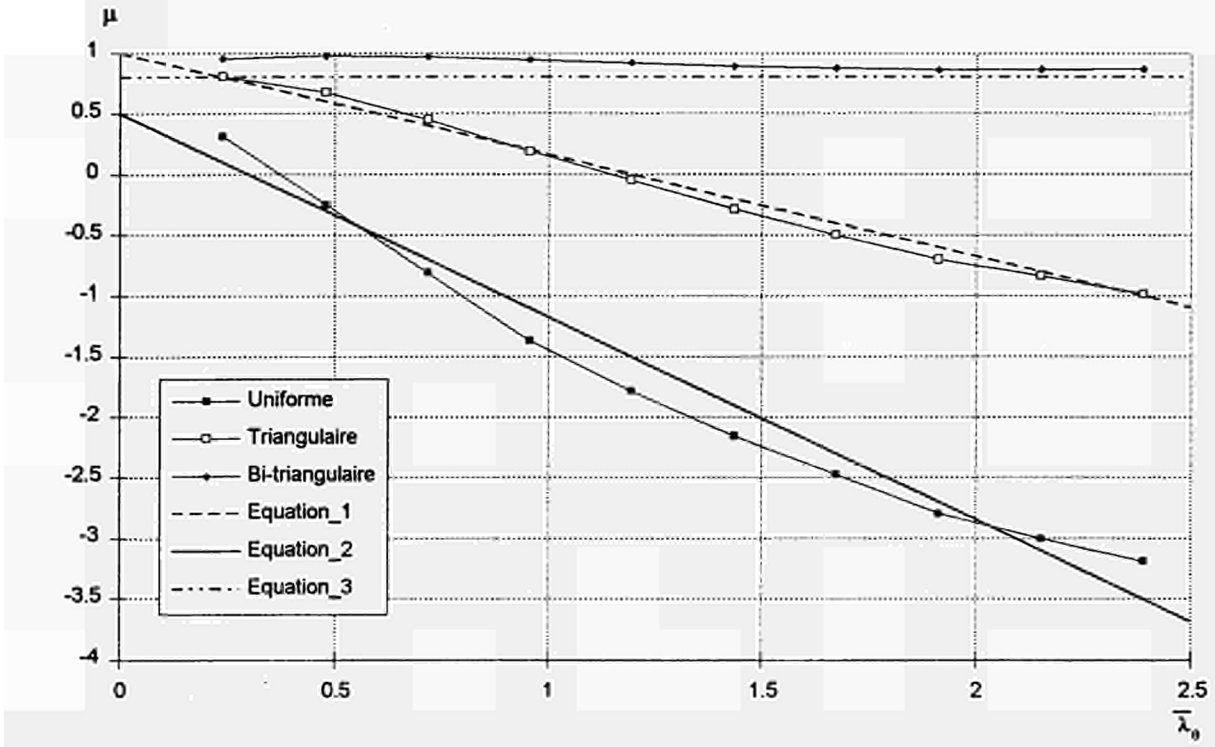

FIGURE 4.2.18 Average of μ_y according to the slenderness ratio and selected approximations for buckling about the minor axis

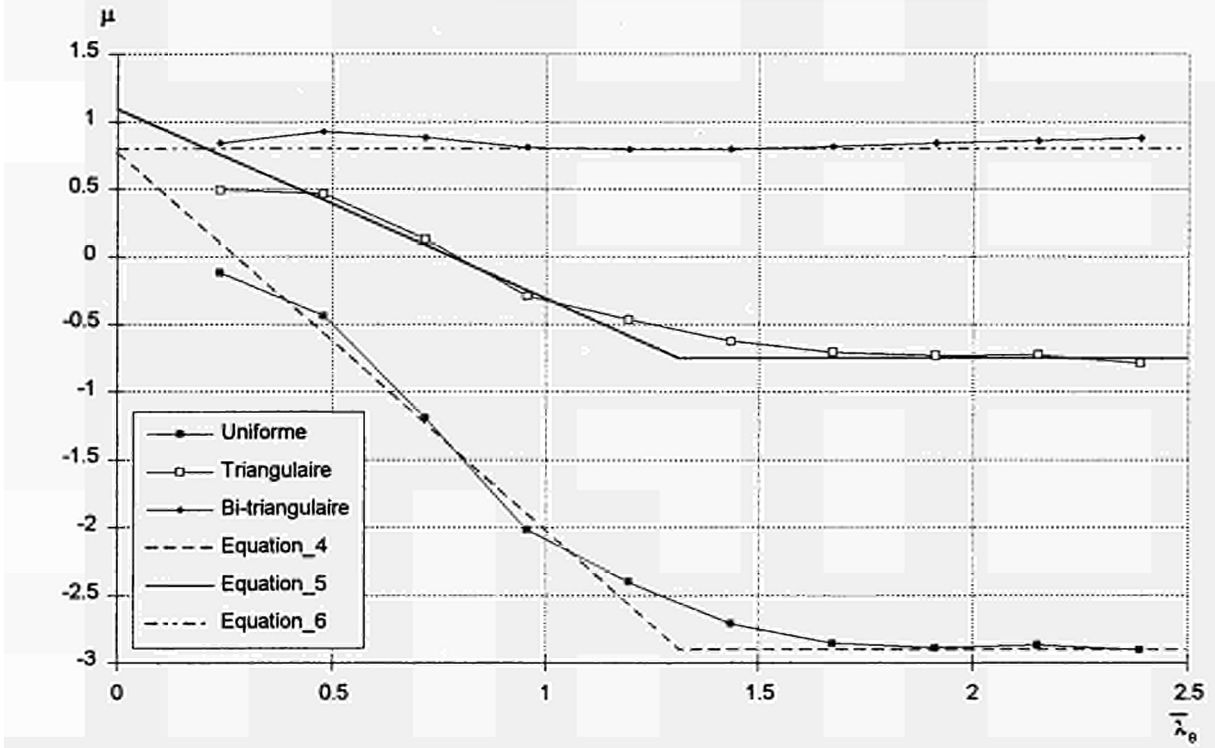

FIGURE 4.2.19 Average of μ_y according to the slenderness ratio and selected approximations for buckling about the major axis

From the points calculated through an average of factors μ_y , the following interpolation functions can be determined:

- **About the minor axis:**

- Uniform moment:

Equation_1 $\mu = -1.68\,\bar{\lambda}_\theta + 0.5$ (17)

- Triangular moment:

Equation_2 $\mu = -0.84\bar{\lambda}_\theta + 1$ (18)

- Bi-triangular moment:

Equation_3 $\mu = 0.8$ (19)

- About the major axis:

- **Uniform moment:**

Equation_4 $\mu = -2.8\,\bar{\lambda}_\theta + 0.78$ but $\bar{\lambda}_{20} \leq 1.1$ (20)

- Triangular moment:

Equation_5 $\mu = -1.4\,\bar{\lambda}_\theta + 1.09$ but $\bar{\lambda}_{20} \leq 1.1$ (21)

- Bi-triangular moment:

Equation_6 $\mu = 0.8$ (22)

Equations (17) to (22) define the starting point which is indispensable for developing a global formula.

C) Final equation

The final formula must be a function of the load type, i.e. it must include factor $\beta_{M,y}$. For this purpose, we shall keep the principle of the formula of Eurocode 3 Part 1.2, that is to say that we shall carry out, for the calculation of μ_y , a linear interpolation between $\beta_{M,y} = 1.1$ and 1.8 which is extended for values greater than 1.8, μ_y being limited to a maximum value.

The formulation of μ_y is determined about the minor axis by solving two systems of two equations with two unknown values:

$$1.1\,A + B = -1.68$$
$$1.8\,A + B = -0.84 \qquad (23)$$

$$1.1\,C + D = 1$$
$$1.8\,C + D = 0.5 \qquad (24)$$

Thus, we find out : A = 1.2, B = 3, C = 0.71 and D = 0.29

The formulation of μ_y is then as follows :

$$\mu_y = \left(1.2\,\beta_{M,y} - 3\right)\bar{\lambda}_\theta + 0.71\,\beta_{M,y} - 0.29 \qquad \text{with } \mu_y \le 0.8 \qquad (25)$$

Similarly, we can obtain the formulation of μ_y about the major axis, i.e. :

$$\mu_y = \left(2\,\beta_{M,y} - 5\right)\bar{\lambda}_\theta + 0.44\,\beta_{M,y} + 0.29 \qquad \text{with } \mu_y \le 0.8 \text{ and } \bar{\lambda}_{20} \le 1.1 \qquad (26)$$

From the equations above and the definition of β (β = 1,8-0,7ψ and $\psi = \frac{M_2}{M_1}$ with $|M_1| \ge |M_2|$, M_1 and M_2 being the end bending moments), we can obtain the following equation system:

$$\frac{N_{Sd}}{\chi(\theta)_{min}\,A\,f_{y,\theta}} + k_y\,\frac{M_{y,Sd}}{W_{pl,y}\,f_{y,\theta}} \le 1 \qquad (27)$$

with:

$$k_y = 1 - \frac{\mu_y\,N_{Sd}}{\chi(\theta)_y\,A\,f_{y,\theta}} \qquad \text{but } k_y \le 3 \qquad (28)$$

If buckling occurs about the minor axis:

$$\mu_y = -0,84\,\bar{\lambda}_\theta(\psi + 1) - 0,5\psi + 1,00 \qquad \text{with } \mu_y \le 0.8 \qquad (29)$$

If buckling occurs about the major axis:

$$\mu_y = -1,40\,\bar{\lambda}_\theta(\psi + 1) - 0,31\psi + 1,09 \qquad \text{but } \mu_y \le 0.8 \text{ and } \bar{\lambda}_{20} \le 1.1 \qquad (30)$$

D) Formula - Numerical results comparison

These formulae developed for a failure temperature of 400°C have the advantage of showing the same type of curve evolution (from convex to concave) depending on the temperature.

A comparison is carried out between the failure temperature obtained numerically, and that obtained analytically with the formulation above (for temperatures from 400 to 900°C). This comparison is carried out through an adimensional standard (FIGURE 4.2.20) defined by:

$$D_{numerical} = \sqrt{N_a^2 + M_a^2} \quad (31)$$

$$D_{analytical} = \sqrt{N_p^2 + M_p^2} \quad (32)$$

These graphs (FIGURE 4.2.21) show on the x-axis the value of standard $D_{numerical}$ in relation to the numerical results, and on the y-axis the value of standard $D_{analytical}$ obtained with the formula defined above. The 45° straight line represents a perfect equality between these two values. While the straight line which is slightly above represents an error of +10% of the analytical value as compared to the numerical value (therefore unconservative), the straight line which is slightly below the bisectrix represents, on the other hand, an error of -10% of the analytical value as compared to the numerical value (conservative).

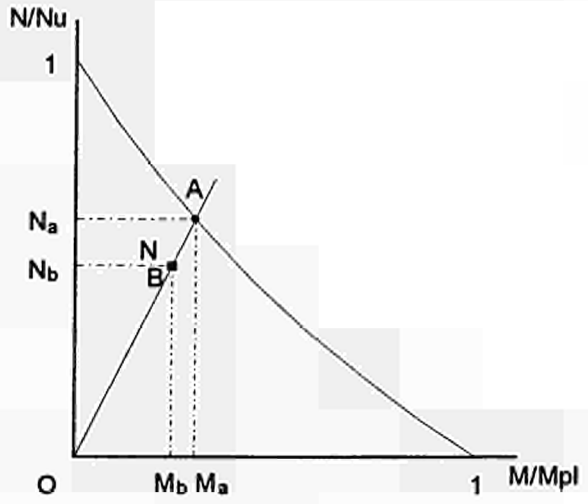

FIGURE 4.2.20 $\overline{OB}$ = numerical result; $\overline{OA}$ = analytical result

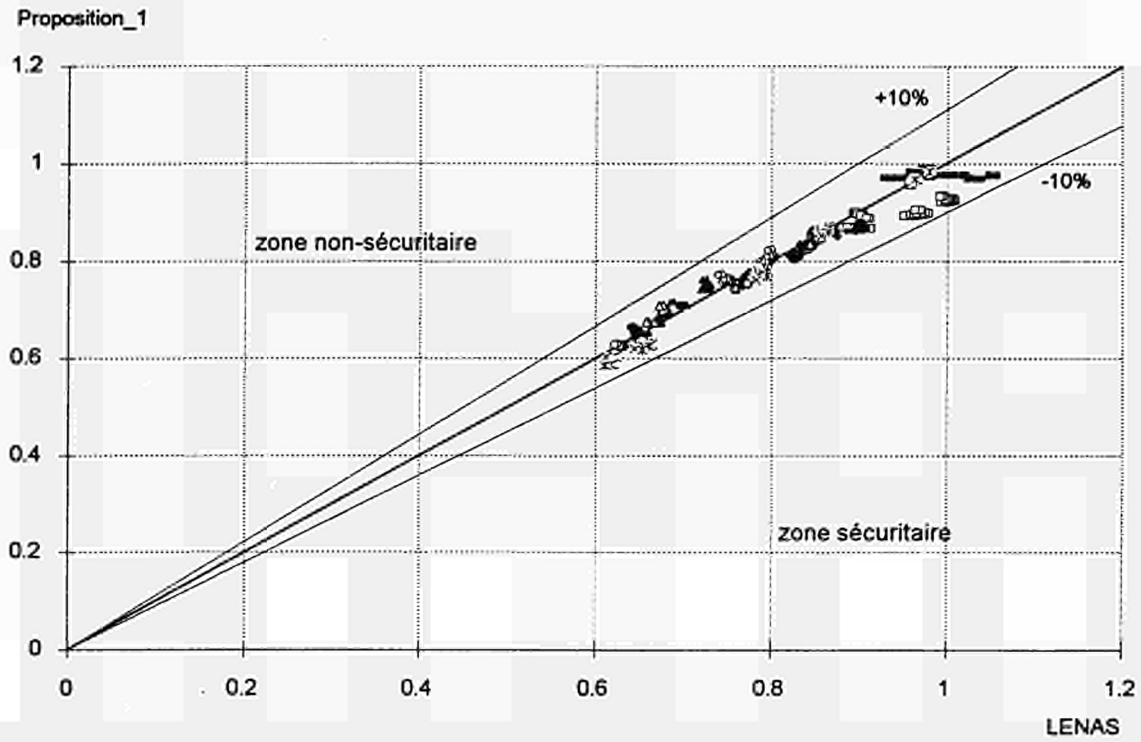

FIGURE 4.2.21 Analytical formula - numerical results comparison at 400°C for buckling about minor axis and triangular moment distribution (See also Annex 11)

In this annex, it can be noted that, as a rule, most points can be found in between those two straight lines, except in the case of buckling about the minor axis where some points are slightly above the permissible maximum. Actually, these points correspond to the values of both largest eccentricities.

For a bi-triangular moment distribution, it can be noted that the clouds of points form a straight line. This is due to the fact that the analytical formula gives a curve with the shape of an arc of a circle for a value of μ_y of 0.8. The calculated value $D_{analytical}$ is therefore constant.

E) Other formulation

Another approach based on the equation $\left(\frac{N_{Sd}}{\chi_{min}\ A\ f_{y,\theta}}\right)^{\alpha} + \frac{M_{y,Sd}}{W_{pl,y}\ f_{y,\theta}} \leq 1$ has been analysed (see Annex 12). However the formulation defined in C (see (27) to (30)) has been kept in the following because it is easier to extend it for 3D behaviour.

5. CALIBRATION OF THE FORMULAE BY COMPARISON WITH EXPERIMENTAL RESULTS

5.1 INTRODUCTION

In the previous chapter numerical models have been applied on virtually all the combinations of yield strength, buckling axis, buckling length, ultimate temperature and cross section for the basic case of simply supported steel columns. The effects of initial deflections, residual stresses and large displacements have been considered and the non linear stress-strain relationships were taken from EC3 Part 1.2.

This work has allowed the proposal of an analytical formula for the buckling coefficient in case of central loading and an analytical expression for the interaction N-M curve in case of eccentrical loading. The expression for the buckling coefficient contains one scalar parameter, the severity factor β, which has to be calibrated as to ensure the appropriate safety level. It is also desirable that the interaction formula is validated against a large set of experimental results before any real confidence can be placed in the proposed method. Those calibration and verifications are really necessary for various reasons;

- any analytical, numerical or theoretical model is much more likely to be accepted by authorities if it is backed and supported by a set of good old real life tests - although it can be questioned that a furnace test is closer to real life than a numerical test -,
- the numerical tests have been made with characteristic values for the initial out of straightness and for the residual stresses, which are likely to produce excessively severe results,
- the parameters of the material taken from Eurocode 1995 are linearly interpolated between values given every 100°C. It would be amazing if mother nature had provided us with such a strange material. The only thing we can take for granted about this material model is that it can surely not correspond to reality. It is hoped, and the model has been formulated in a manner that, the model is a reasonable approximation of reality.

Therefore the proposed formulae were compared with available experimental tests results from literature (see chapter 3). This has allowed us to determine the severity factor to be used in order to obtain the desired safety level.
Only tests when the actual yield strength had been measured were considered. When not measured, the nominal values have been used for the geometrical dimensions of the cross section. A recent sensitive analysis by Talamona [32] has shown that the yield strength is largely predominant before other characteristics such as geometrical imperfections, cross sectional area, residual stresses, ...
As only a limited number of tests have been made on simply supported axially loaded columns, the results of the tests made with other end conditions were supposed to represent a test made on an equivalent simply supported column with its length equal to the buckling length of the actual element. The analyses that will be detailled in this chapter have been repeated with the results sorted in three groups according to the support conditions , pinned - pinned, pinned - fixed , and fixed - fixed , and no significant difference emerged between the three groups, which seems as an indication that it was valid to consider the tests that are not simply supported.

One scalar parameter is present in the proposed formula to calibrate the model: the severity factor β which has an influence on the buckling coefficient χ , i.e. on the ultimate load under

central compression. Strictly speaking, the severity factor should be experimentally evaluated only from tests made on centrally loaded columns.

Tests when the load has been applied with a defined eccentricity have been considered provided that this eccentricity is sufficiently small. This was judged by the fact that, when the column is calculated by an interaction formula such as the one from Eurocode 3 [25], the stress produced by the axial load is at least equal to 75% of the total stress. Tests where the stress produced by the bending moment is larger than 25% of the total stress were considered to be too sensitive to the interaction and were dismissed. It has also been verified at the end of this project that the 33 tests with a small eccentricity lead to the same conclusion as the 40 tests made on axially loaded column.
Only full scale tests were considered. As the majority of available furnaces have a height in the range 3 to 4 meters, a large number of different cross section types have been tested, but very often with the same length of the column. In order to circumvent that fact, it was decided to perform an original set of experimental tests made on the same cross section, but for different length and different load factors as already mentioned in chapter 2.

5.2 RESULTS OF THE EXPERIMENTAL TESTS

5.2.1 Test from Borehamwood.

One test result was found in the Compendium [35] published by BSC and BRE in the United Kingdom. Columns with blocked-in web which are also reported were not considered here because of the high thermal gradient existing in the section. The test which could be used is labelled as 41 in ref [35]. It is labelled as 117 in the database given in chapter 2.5. The actual dimensions of the section have been measured, as well as the yield strength in the flange. The ends of the column were encased in concrete caps and, as the element was restrained in rotation by the loading system, end fixity was assumed and an effective length of ½ of the exposed length has been adopted in this paper in order to be consistent with the interpretation of the tests made in Gent, although 0.70 of the exposed length was chosen in the interpretation of ref [35].

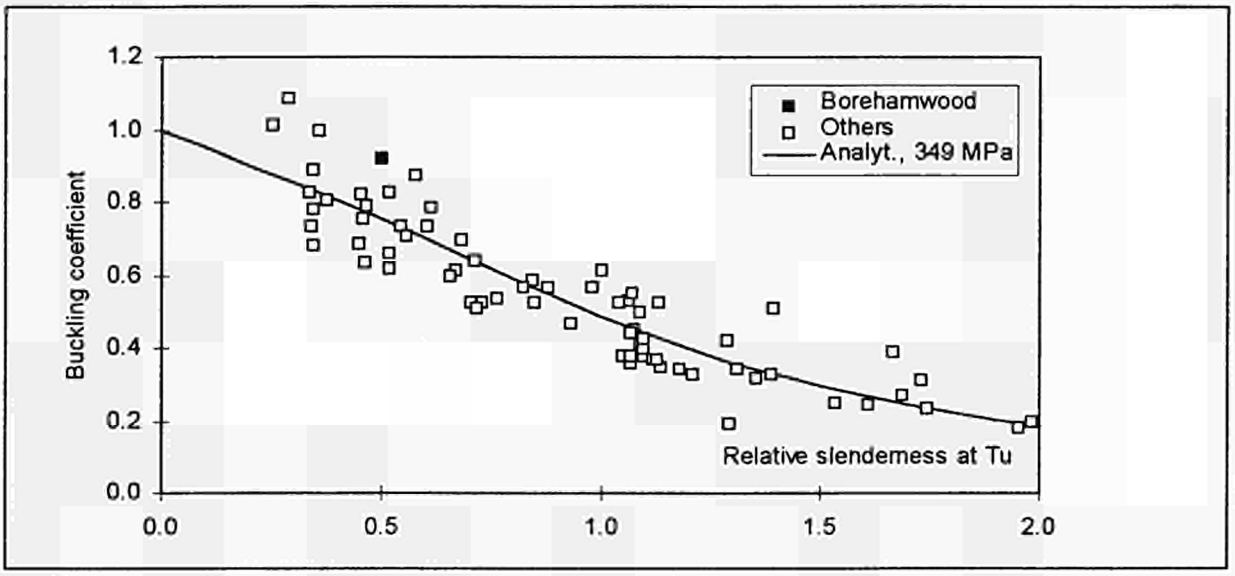

FIGURE 5.2.1 Test of Borehamwood

FIGURE 5.2.1 shows the experimental buckling coefficients plotted versus the relative slenderness at the ultimate temperature. 2 tests results are not visible on the figure because the relative slenderness was higher than 2. The result of Borehamwood is highlighted on this figure and it appears that it is one of the more favourable results. Had the test been interpreted as having a buckling length of 0.70 L as in ref [35] , this point would have been shifted to the right and would have appeared as even more favourable. The analytical curve has been drawn with the yield strength of the Borehamwood test and with the severity factor ensuring that the ratio between the analytical results and the experimental results has an mean value of 1.00, see the following paragraph 5.2.4 «Determination of the severity factor». The general trend of all the experimental tests is practically the same as the analytical curve.

5.2.2 Tests from Gent.

16 test results from Gent are considered. The results have been taken from the original test reports from the laboratory of Professor Minne at the University of Gent and some values may differ slightly from what has been reported elsewhere.
The test labelled as N° 2.4 in ref [36] has not been considered here because of the uncertainty mentioned in the original test report on the position of the load resulting from problems in the welding of the end plates on the specimen.
The test labelled as N° 2.18 in ref [36] has not been considered because of the very severe longitudinal gradients existing in the temperature distribution. A difference of almost 300°C is found in the test report between two different cross sections.
The geometrical dimensions have been measured in each element and the yield strength was measured for each section type. In the evaluation of each fire test, the mean value of the available tension test results was used. The columns were clamped in special end fixtures intended to provide a perfect rotational restraint at both ends. This hypothesis of rotational fixity was experimentally verified by 4 tests made at room temperature, see ref [31], and was also confirmed by the shape of the elements observed after the fire tests.
The tests were therefore interpreted as tests made on simply supported elements with a length equal to 0.50 the exposed length of the actual elements, and buckling around the minor axis.

FIGURE 5.2.2 shows the buckling coefficients derived from the tests of Gent in function of the relative slenderness at the ultimate temperature

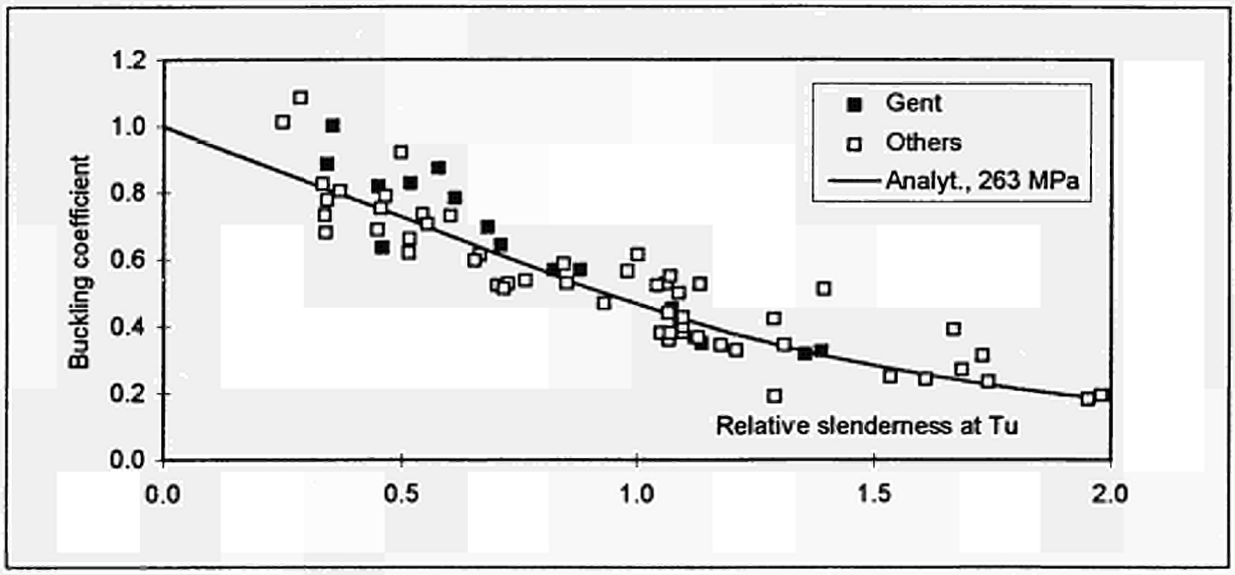

FIGURE 5.2.2 Tests of Gent

5.2.3 Tests from Germany.

25 test results from the Technische Universität Braunschweig and 3 test results from Stuttgart were obtained. The results of those tests have been collected and transmitted to the authors by Dorn [39], with the exception of test N° 1, see the database given in chapter 2.5, taken from ref [41]. Most of the results from Braunschweig have been published in the reports [42] of Sonderforschungsbereich 148.
FIGURE 5.2.3 shows how the tests made in Braunschweig are located on the graph whereas FIGURE 5.2.4 refers to the tests made in Stuttgart.

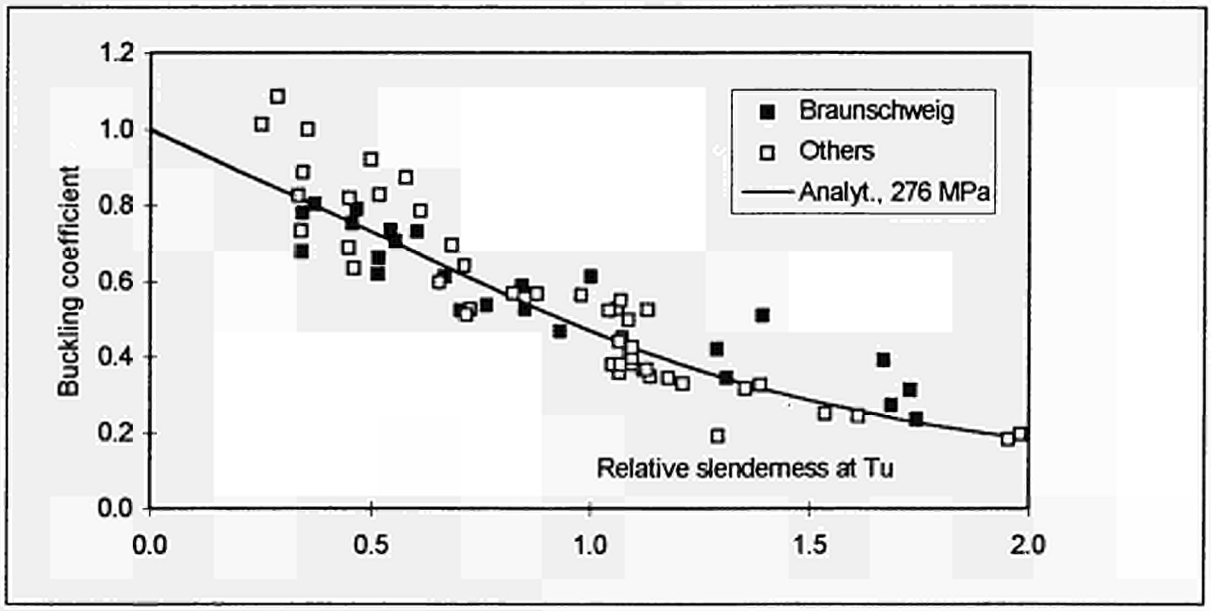

FIGURE 5.2.3 Tests of Braunschweig

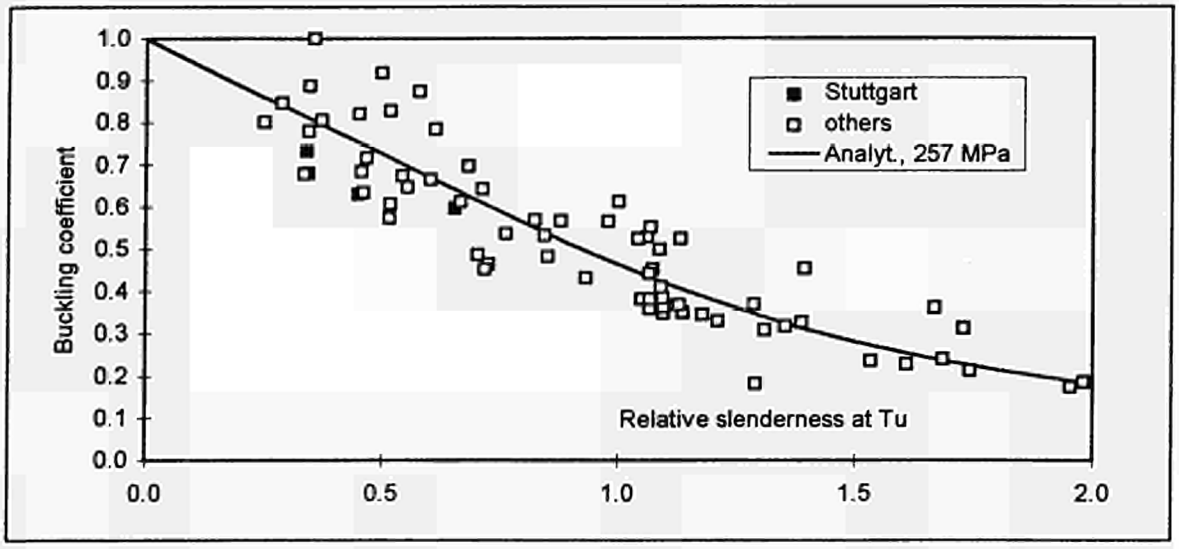

FIGURE 5.2.4 Tests of Stuttgart

5.2.4 Test from Rennes.

14 axially loaded simply supported columns were tested at the INSA in Rennes and reported by Aribert and Randriantsara [37]. All the tests were made on HEA100 sections, half of them under increasing temperature and constant load, half of them at constant temperature and increasing load. The length of all the elements was 1.994 m, which gives for one slenderness the influence of the load level on the ultimate temperature. One measured value is reported for the yield strength as well as the second moment of area and the sectional area.

The fact that all the tests have been made on the same cross section type and for one buckling length is clearly reflected on FIGURE 5.2.5. The points are not exactly at the same horizontal distance because the relative slenderness is evaluated at the ultimate temperature and this one was not the same in the different tests. The fact that the higher values from Rennes are shifted to the left and the lower values to the right when the slenderness is evaluated at the ultimate temperature indeed reduce the scattering from the analytical curve.

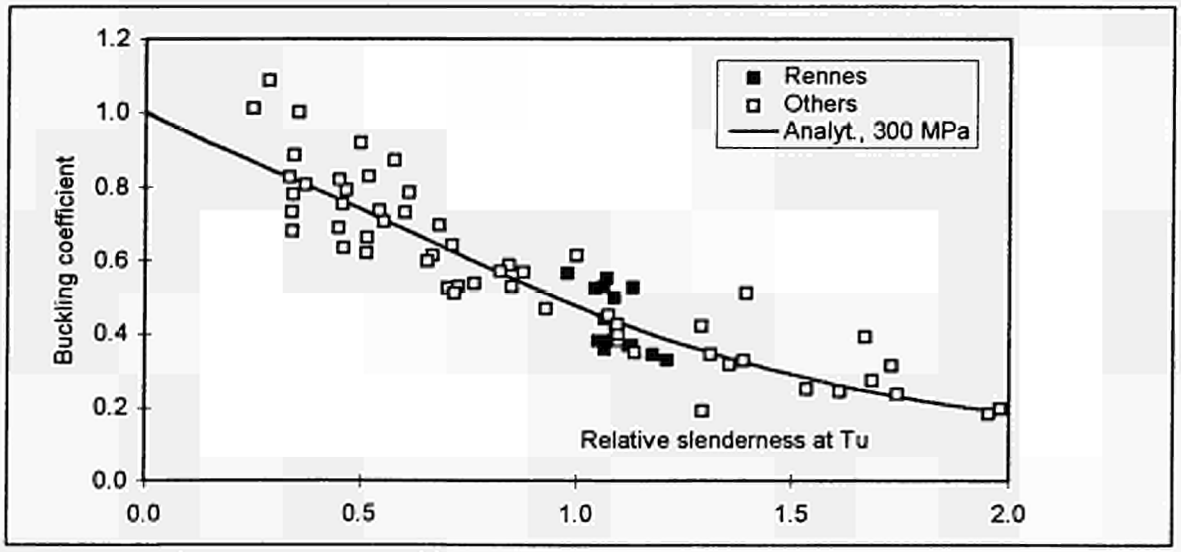

FIGURE 5.2.5 Tests of Rennes

5.2.5 Test from Bilbao.

These tests have already been described in chapter 3. Only the main items are given here.

- The values given for the ultimate temperature, the yield strengths and the dimensions of the section result from the average between several measures on the specimen.
- The elements were placed vertically. They were turned in such a way that the effect of the imperfection was added to the effect of the load eccentricity.
- The measured residual stresses were in the order of magnitude of 0.10 x 235 Mpa.

Tests N° AL1, AL3, SL43 and AL6 were performed at ambient temperature and will not be considered in the evaluation of the analytical formula for buckling at elevated temperatures. They were conducted to verify the loading equipment and to provide reference points at 20°C. Test N° SL40 was a preliminary test performed to verify the heating equipment. It was performed on an element which had not been precisely measured.

The specimen N° DL3 was accidentally heated when the elongation was restrained in the loading system. This was recognised early and the temperature was decreased before the test was restarted with free axial displacement. Due to this preheating history, the specimen had an initial sinusoidal imperfection of 7 mm before the actual test. If an imperfection of H/1000 = 2 mm could be regarded as a usual structural imperfection, it can be considered that the load had been applied with a first order eccentricity of 5 + (7 - 2) = 10 mm. The test can therefore be used for the validation of computer programs or for M-N interaction formula but in this case, it leads to a bending stress that is too important before the axial stress and this test can no longer be regarded as representative of axial buckling, see § 5.1 Introduction.

In test N° CL5, the temperature was significantly higher in the regions near the supports than in the middle of the column. This was confirmed by the fact that the buckling sections were 360 mm approximately from the ends. Because of the uncertainty on the real buckling length, this test will not be used in the comparison with the simple model.

Due to this severe examination of the 17 hot tests, 14 tests performed at elevated temperature remain for consideration in the data base. They are plotted on FIGURE 5.2.6.

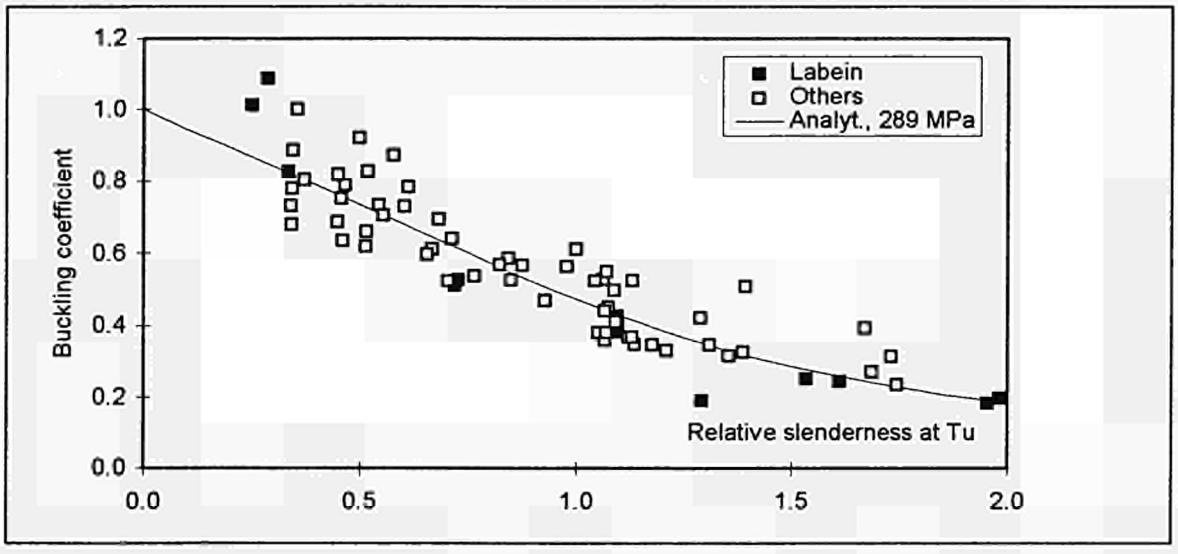

FIGURE 5.2.6 Tests of Bilbao

5.2.6 Summary of the available tests.

The 73 experimental test results that have been considered for the evaluation of the analytical formula and the determination of the severity factor have been noted in bold in the chapter 2.5.

5.3 CALIBRATION: DETERMINATION OF THE SEVERITY FACTOR

If a value of the severity factor is chosen, say β_1 , it is possible to calculate for each test the ratio between the value of the ultimate load calculated with the use of the analytical formula (see Eq. 7 to 10 of chapter 4.1) and the experimental load. The analytical load is of course evaluated at the ultimate temperature of the test. This ratio is also the ratio between the analytical and the experimental buckling coefficient.

$$x_i = \frac{N_{ui}^{ana.lyt.}}{N_{ui}^{exp.}} = \frac{\chi_i^{analyt.}}{\chi_i^{exp.}} \qquad i = 1,\ldots,73 \tag{33}$$

The analytical proposal is safe if it leads to values of x_i lower than 1, and unsafe for values higher than 1. For each chosen severity factor, the average value and the standard deviation of the 73 x_i are calculated.

$$Mx = \frac{\sum_{i=1}^{73} x_i}{73} \qquad dx = \sqrt{\frac{(x_i - Mx)^2}{72}} \tag{34}$$

FIGURE 5.3.1 shows how the mean value Mx varies depending on the choice that has been made for the severity factor β. This figure confirms what has already been mentioned, that the value of 1.20 is very safe because it leads to an analytical load that is equal, on average, to 82.5% of the experimental load. In order to calibrate the analytical proposal to obtain, on average, the same ultimate loads as in experimental tests, β has to be given the value of 0.65

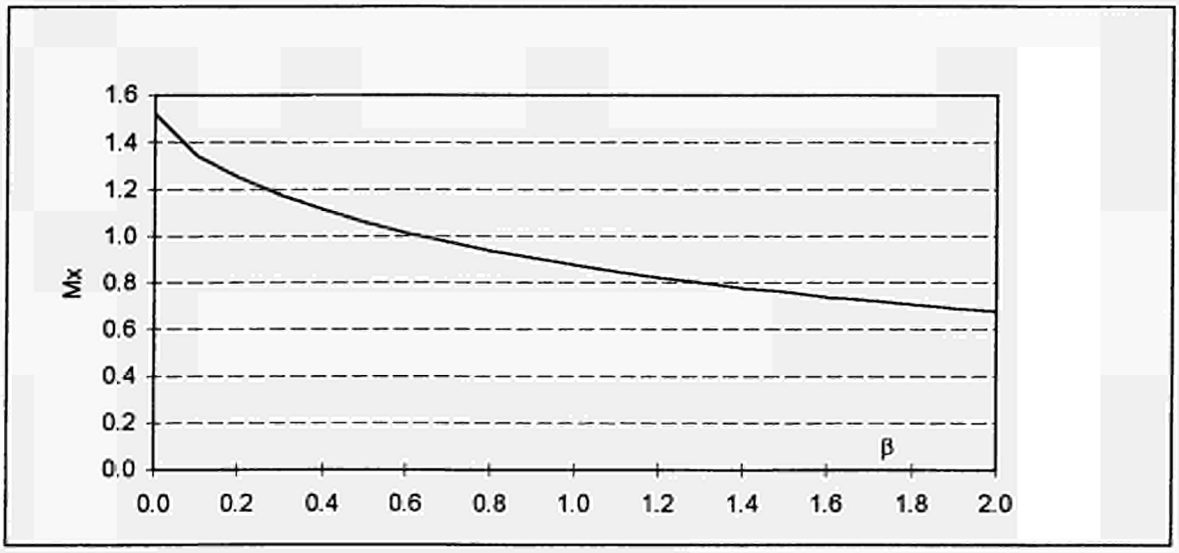

FIGURE 5.3.1 Evolution of the mean value with β.

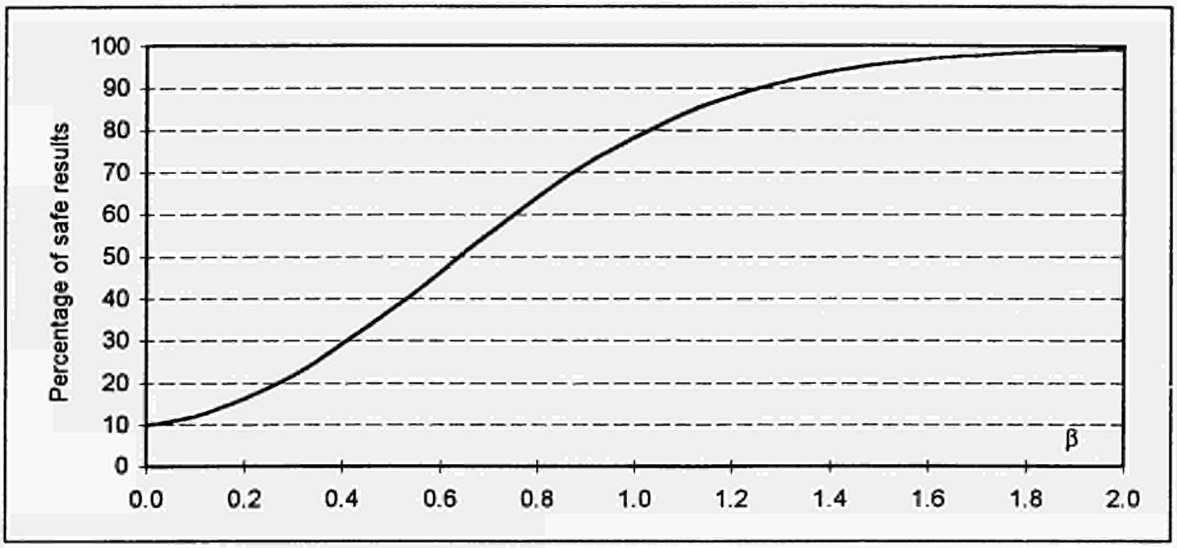

FIGURE 5.3.2 Percentage of safe results

On the base of the mean value and the standard deviation, and assuming a normal distribution, it is possible to calculate the proportion of tests which are safely calculated by the analytical formula. FIGURE 5.3.2 shows the evolution of this percentage with the severity factor. It comes immediately from FIGURE 5.3.1 that a severity factor of 0.65 leads to 50% of safe results. It can be noticed that the value of 1.20, which ensures that the formula is safe with respect to the numerical simulations performed with characteristic imperfections, also leads to a safe result with respect to the tests in 88% of the cases. In order to reach a safety level of 95%, β has to be given the value of 1.46, which leads to the very conservative value of 0.77 for the average result

It is the opinion of the authors that for practical applications a value of 0.65 should be chosen, in order to represent the tests results as close as possible and that no additional safety margin should be added when the fire resistance of an element is assessed by means of an analytical formula.

The first reason for choosing the mean value when establishing the analytical formula is that the same objective is in fact used when the assessment of the fire resistance is made by experimental testing. When a new structural system or a separating element has to be tested against fire, it is seldom the case that a statistically significant series of tests is performed and the element is required to succeed in 95% of the tests. Usually, one single positive result is enough for the authorities.

The other reason is that the formula has been calibrated using the *actual* yield strength as measured on the tested specimens. In a real life use of the formula, the *nominal* yield strength of the material would be used, which for commonly delivered elements introduces an additional safety margin. Recognising that a discrepancy existed when the fire resistance of a steel column was determined on one hand by a standard fire resistance test and on the other hand by the E.C.C.S. analytical approach [45] based on characteristic values, Petterson and Witteveen [46] had already developed a correction procedure in order to obtain improved consistency between analytically and experimentally determined fire resistance values.

Moreover axially loaded columns without any eccentricity are very seldom met in practice. In real situations, bending moments are practically always present. In the case of eccentrically loaded columns, the safety is still increased as explained in chapter 5.5.

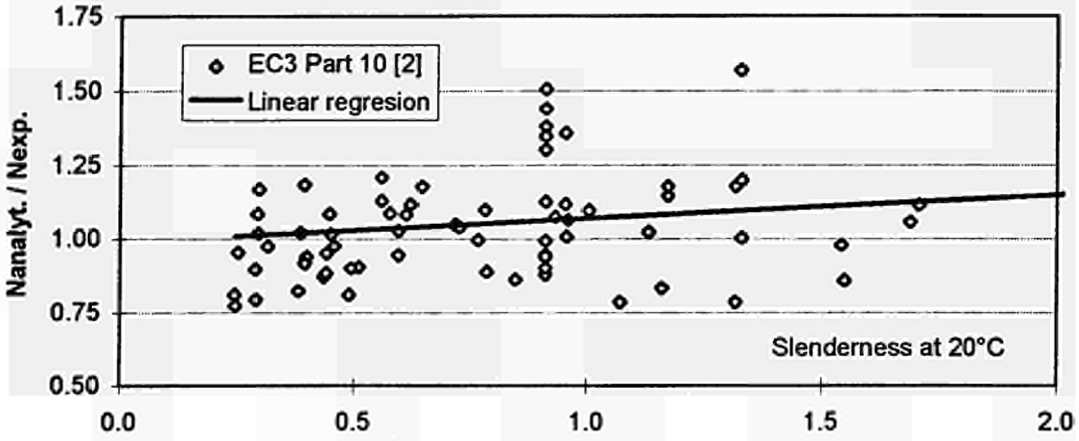

FIGURE 5.3.3 EC3 proposal

When the analytical loads was calculated according to EC3 part 1.2 as proposed in ref. [2], i.e. with the buckling curve c divided by 1.20, then the average value of the ratio between the analytical and the experimental load was equal to 1.06. FIGURE 5.3.3 illustrates that this proposal tended to be unsafe and that the safety level was not uniform with the slenderness, decreasing with higher buckling lengths (one test, not seen on FIGURE 5.3.3, has a ratio of 2.1 for a slenderness of 1.7).

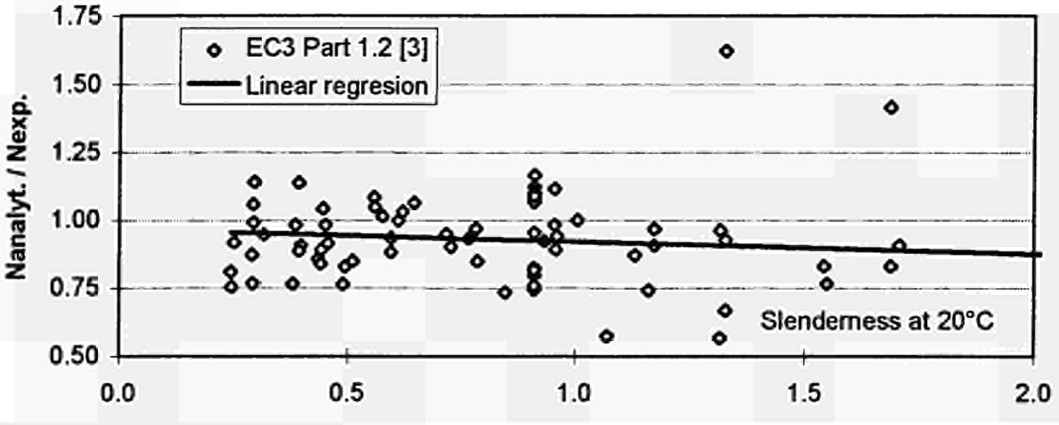

FIGURE 5.3.4 Dublin proposal

When the relative slenderness is evaluated at the ultimate temperature [3], then the average value of the ratio between the analytical and the experimental load is equal to 0.93. FIGURE 5.3.4 illustrates that this proposal tends to be eccessively safe. Due to the fact that the relative slenderness is evaluated at the ultimate temperature, the safety level is more uniform, slightly increasing for increasing slenderness.

The values 1.06 and 0.93 indicate that those analytical methods had also been calibrated in such a way that the calculated loads are, more or less, equal to the experimental loads.

The value of b = 0.65 has been used to draw the analytical line on FIGURE 5.2.1 to FIGURE 5.2.6. It has to be mentioned that the analytical curve depends on the yield strength of steel,

see Eq. 9. In each of those figures, a choice had to be made and the mean value of the yield strength for the tests highlighted on the figure was considered.
FIGURE 5.3.5 summarises all the test results as well as the analytical proposal, drawn with the characteristic value of the severity factor, $\beta = 1.20$, as well as with the value for practical applications, $\beta = 0.65$. The curves have been drawn with a yield strength of 281 Mpa, average value of all the experimental tests. It must be mentioned that FIGURE 5.3.5 gives an excessive impression of variation around the mean value because the analytical curve could be drawn for one single value of the yield strength. In fact, when calculating the ratio of analytical and experimental test, the actual value of the yield strength is considered for each test, which tends to reduce the scatter. This can unfortunately not be put on a single graph.

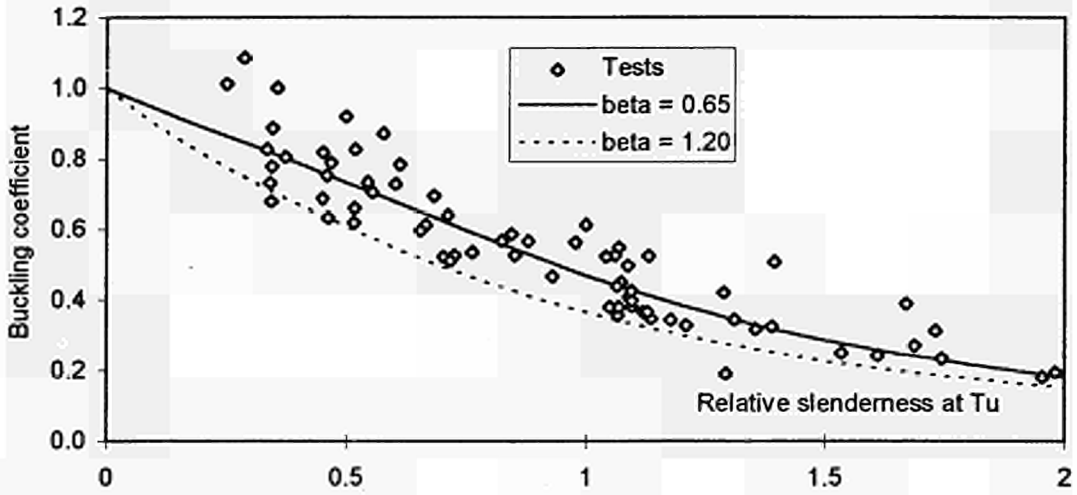

FIGURE 5.3.5 All the test results

It comes as no surprise on FIGURE 5.3.6 that the average value of the ratio between the analytical and the experimental load is equal to 1.00 when the analytical load is calculated according to the present proposal and with $\beta = 0.65$. More significant is the fact that the analytical expression deduced from the extensive numerical simulations leads to a safety level that is totally independent of the slenderness.

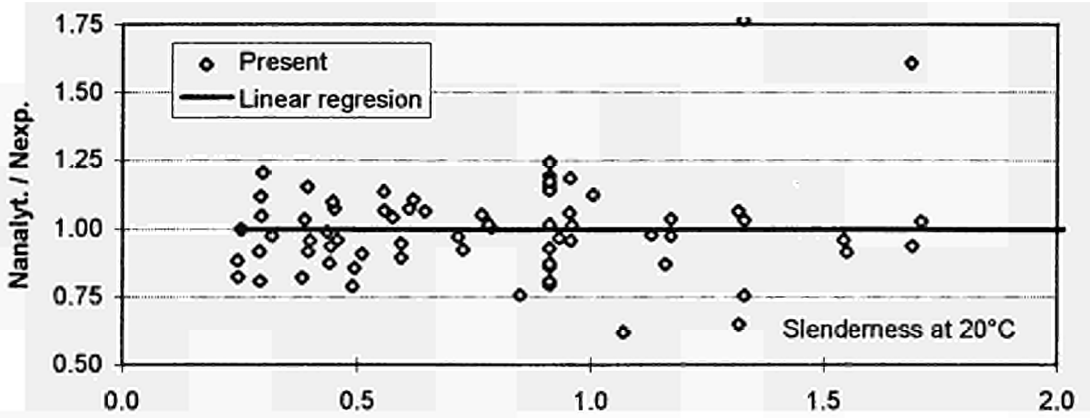

FIGURE 5.3.6 The present proposal

FIGURE 5.3.7 shows the experimental results when the discrimination has been made on the fact that the nominal eccentricity of the load was 0 or that there was a small but acceptable eccentricity. It can be noticed that the general trend is the same, which is an a posteriori justification to the fact that tests with small eccentricities were taken into account in the calibration of the formula established for centrally loaded columns.

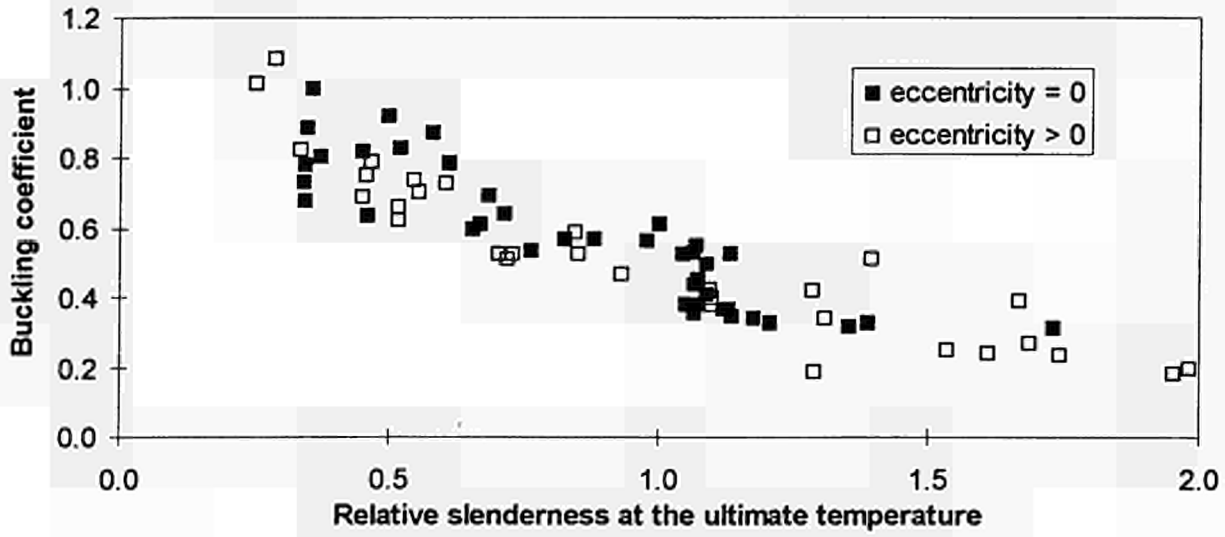

FIGURE 5.3.7 Influence of a small eccentricity

The fact that a value of 0,65 has to be chosen to be in line with the test database while the numerical simulations lead to a higher value of β (see chapter 4) confirm that assumptions considered in the numerical simulations, especially the structural imperfection and the residual stresses, are too severe and don't correspond to the values generally met during the tests. In fact the assumptions corresponded to the characteristic values while the average values have to be used to better represent the experimental results.
That's why it is advised to consider an initial imperfection of 0,25 . H/1000 (H being the length column) and residual stresses equal to 0,25 . 235 N/mm^2 when using the advanced calculation method to determine the behaviour of a column in case of fire.

5.4 INFLUENCE OF THE YIELD STRENGTH

The proposed formula for the buckling coefficient (see chapter 4) is dependant upon the yield strength (see factor ε in formula (9) in chapter 4.1) The formula has been deduced by numerical simulations on steel S235 and S355 (see chapter 4). Simulations with CEFICOSS for steel S460 have confirmed the beneficial effect of high yield strength on the buckling coefficient and have proved that the formula can be also used for S460.
FIGURE 5.4.1 is an experimental validation of the fact that the buckling coefficient is favorably influenced by increasing nominal yield strength. On this figure, tests are only plotted if the yield strength at ambient temperature differs by more than 10% from the average value of the complete tests series. It can be noticed that the 4 tests with a high yield strength have higher buckling coefficients than the 12 tests with a low yield strength.

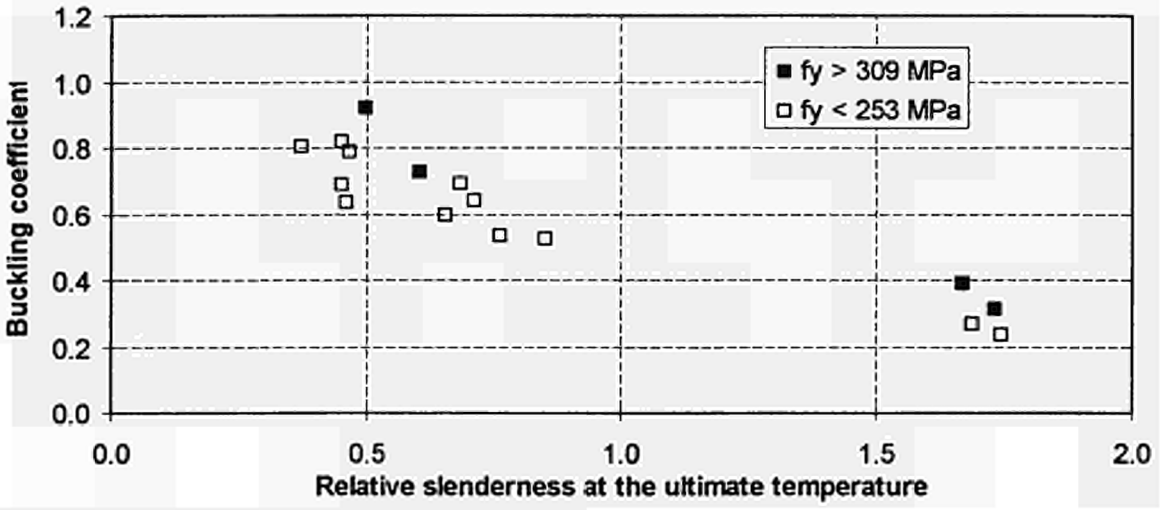

FIGURE 5.4.1 Influence of the yield strength

5.5 VERIFICATION OF THE PROPOSED FORMULAE IN CASE OF ECCENTRICALLY LOADED COLUMNS

The calibration has been made on the central load only. The global formula, including the bending term, has to be compared with experimental evidence. When all admissible results are considered, no matter the eccentricity of the load, the data base comprises 141 results of full scale experimental tests. For each test the ultimate temperature corresponding to the applied load has been estimated by the new analytical proposal. Each test is represented by one point on FIGURE 5.5.1. Most of the evaluated ultimate temperatures are within 10% of the experimental temperature (when expressed in °C).

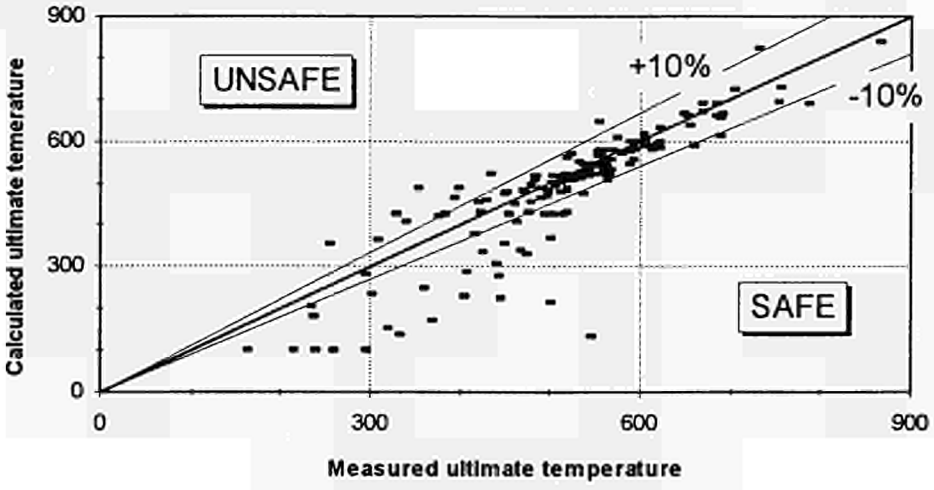

FIGURE 5.5.1 Comparison for all the available tests

FIGURE 5.5.2 is another presentation of the comparison. The histogram shows that most of the points are on the safe side and very few of them overestimate the ultimate temperature by 10%. This is another reason why the value of 0.65 could be accepted for the severity factor. When bending moments are introduced, as is practically always the case in real situations, a

new safety margin appears compared to the cases of centrally loaded columns. The average of all the temperature ratio, including the 71 centrally loaded test results, is now less than 95%. When only eccentrically loaded columns are considered, the average value of the temperature ratio becomes 87%.

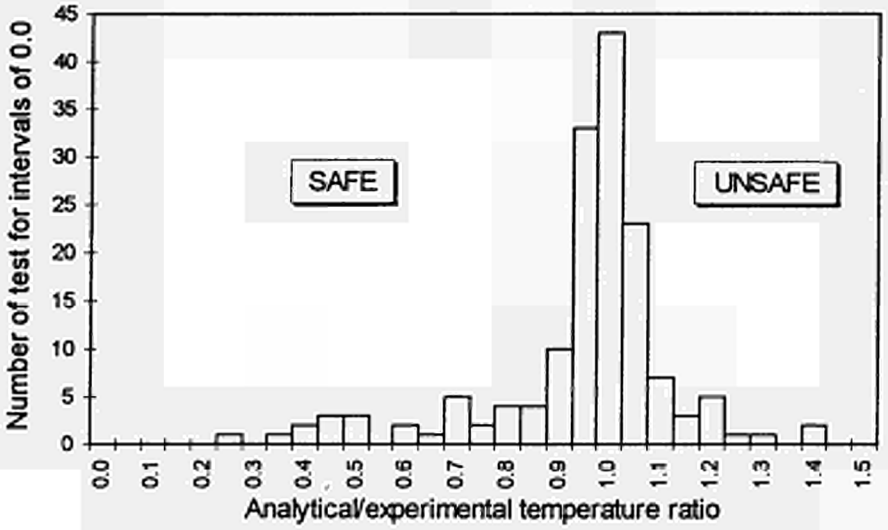

FIGURE 5.5.2 Histogram for all the available tests

6. DESIGN RULES

6.1 ANALYTICAL FORMULA

6.1.1 Centrally loaded column

In fire

$$N_{b,fi} = \chi_\theta \, A \, k_{max,\theta} \, f_y \quad (35)$$

•) with, for $\theta \geq 400$ °C

$$\chi_\theta = \frac{1}{\Phi(\theta) + \left[\Phi(\theta)^2 - \bar{\lambda}_\theta^2\right]^{0,5}} \quad \text{but } \chi \leq 1 \quad (36)$$

$$\text{where } \Phi(\theta) = 0,5\left[1 + \alpha \bar{\lambda}_\theta + \bar{\lambda}_\theta^2\right] \quad (37)$$

$\alpha = 0,65\,\varepsilon$ is an imperfection factor

$$\bar{\lambda}_\theta = k_{\lambda,\theta}\,\bar{\lambda} \quad (38)$$

with $\bar{\lambda}$ is the slenderness for the relevant buckling mode at 20°C

$$k_{\lambda,\theta} = \sqrt{\frac{k_{max,\theta}}{k_{E,\theta}}}\,\bar{\lambda} \quad (39)$$

$$\varepsilon = \sqrt{\frac{235}{f_y}} \quad \text{fy in MPa is the nominal yield} \quad (40)$$

strength, i.e. not reduced according to EN 10025[34] depending on the flange thickness.

•) for $\theta \leq 100$°C,
χ is calculated according to Eurocode 3 Part 1.1.[25], as for $\theta = 20$°C

•) for 100°C < θ < 400°C,
χ is linearly interpolated between the values calculated for 100 and 400°C

Simplification for $\bar{\lambda} \leq 0,8$
$\bar{\lambda}_\theta$ can be considered constant and equal to $1,2\bar{\lambda}$ if $\bar{\lambda}$ is smaller than 0,8 (see Annex 14)

At room temperature
ENV 1993-1-1 [6]

$$N_{b,Rd} = \chi A f_y / \gamma_{M1}$$

with

$$\chi = \frac{1}{\Phi + \left[\Phi^2 - \bar{\lambda}_\theta^2\right]^{0,5}} \quad \text{but } \chi \leq 1$$

$$\text{where } \Phi = 0,5\left[1 + \alpha(\bar{\lambda} - 0,2) + \bar{\lambda}^2\right]$$

α is an imperfection factor

$$\bar{\lambda} = \left[A f_y / N_{cr}\right]^{0,5} = \lambda / \lambda_1$$

λ is the slenderness for the relevant buckling mode

$$\lambda_1 = \pi\left[E/f_y\right]^{0,5} = 93,9\,\varepsilon$$

$$\varepsilon = \left[235/f_y\right]^{0,5} \quad (f_y \text{ in N/mm}^2)$$

and N_{cr} is the elastic critical force for the relevant buckling mode.

6.1.2 Eccentrically loaded column

6.1.2.1 Bending moment and buckling around the strong axis

In fire	At room temperature ENV 1993-1-1[6]
$\frac{N_{fi,Ed}}{\chi_{y,\theta} A k_{max,\theta} f_y} + k_y \frac{M_{y,fi,Ed}}{W_{pl,y} k_{max,\theta} f_y} \le 1$	$\frac{N_{Sd}}{\chi_y A f_y/\gamma_{M1}} + k_y \frac{M_{y,Sd}}{W_{pl,y} f_y/\gamma_{M1}} \le 1$
where	where
$k_y = 1 - \frac{\mu_y N_{fi,Ed}}{\chi_{y,\theta} A k_{max,\theta} f_y}$ but $k_y \le 3$	$k_y = 1 - \frac{\mu_y N_{Sd}}{\chi_y A f_y}$ but $k_y \le 1,5$
$\mu_y = (2\beta_{M,y} - 5)\bar{\lambda}_\theta + 0,44\beta_{M,y} + 0,29$	$\mu_y = (2\beta_{M,y} - 4)\bar{\lambda}_y + \frac{W_{pl,y} - W_{el,y}}{W_{el,y}}$ but $\mu_y \le 0,9$
but $\mu_y \le 0,8$ and $\bar{\lambda} \le 1,1$	

with $\beta_{M,y}$, the equivalent uniform moment factor for flexural buckling. In case of end moments, $\beta_{M,y} = 1,8\text{-}0,7\psi$

Note: 1) The formula has been deduced from numerical simulations on column subjected to axial compression combined with uniform, triangular and bi-triangular bending moment distributions. Moreover, thanks to the $\beta_{M,y}$, the formulae could be extended to other type of bending moment distributions as though it is at room temperature.

2) For cross sections in class 3, $W_{pl,y}$ has to be replaced by $W_{el,y}$ as though it is at room temperature.

6.1.2.2 Bending moment and buckling around the weak axis

In fire	At room temperature ENV 1993-1-1[6]
$\frac{N_{fi,Ed}}{\chi_{z,\theta} A k_{max,\theta} f_y} + k_z \frac{M_{z,fi,Ed}}{W_{pl,z} k_{max,\theta} f_y} \le 1$	$\frac{N_{Sd}}{\chi_z A f_y/\gamma_{M1}} + k_z \frac{M_{z,Sd}}{W_{pl,z} f_y/\gamma_{M1}} \le 1$
where	where
$k_z = 1 - \frac{\mu_z N_{fi,Ed}}{\chi_{z,\theta} A k_{max,\theta} f_y}$ but $k_z \le 3$	$k_z = 1 - \frac{\mu_z N_{Sd}}{\chi_z A f_y}$ but $k_z \le 1,5$
$\mu_z = (1,2\beta_{M,z} - 3)\bar{\lambda}_\theta + 0,71\beta_{M,z} - 0,29$	$\mu_z = (2\beta_{M,z} - 4)\bar{\lambda}_z + \left[\frac{W_{pl,z} - W_{el,z}}{W_{el,z}}\right]$ but $\mu_z \le 0,9$
but $\mu_z \le 0,8$	

with $\beta_{M,z}$, the equivalent uniform moment factor for flexural buckling. In case of end moments, $\beta_{M,z} = 1,8\text{-}0,7\psi$

Note: 1) The formula has been deduced from numerical simulations on column subjected to axial compression combined with uniform, triangular and bi-triangular bending moment distributions. Moreover, thanks to the $\beta_{M,z}$, the formulae could be extended to other type of bending moment distributions as though it is at room temperature.

2) For cross sections in class 3, $W_{pl,z}$ has to be replaced by $W_{el,z}$ as though it is at room temperature.

6.1.2.3 Bending moments and axial compression

In fire

$$\frac{N_{fi,Ed}}{\chi_{min,\theta} A k_{max,\theta} f_y} + k_y \frac{M_{y,fi,Ed}}{W_{pl,y} k_{max,\theta} f_y} + k_z \frac{M_{z,fi,Ed}}{W_{pl,z} k_{max,\theta} f_y} \le 1$$

in which

$$k_y = 1 - \frac{\mu_y N_{fi,Ed}}{\chi_{y,\theta} A k_{max,\theta} f_y} \quad \text{but} \quad k_y \le 3$$

$$\mu_y = (2\beta_{M,y} - 5)\bar{\lambda}_\theta + 0{,}44\beta_{M,y} + 0{,}29$$

but $\mu_y \le 0{,}8$ and $\bar{\lambda} \le 1{,}1$

$$k_z = 1 - \frac{\mu_z N_{fi,Ed}}{\chi_{z,\theta} A k_{max,\theta} f_y} \quad \text{but} \quad k_z \le 3$$

$$\mu_z = (1{,}2\beta_{M,z} - 3)\bar{\lambda}_\theta + 0{,}71\beta_{M,z} - 0{,}29$$

but $\mu_z \le 0{,}8$

χ_{min} is the lesser of $\chi_{y,\theta}$ and $\chi_{z,\theta}$

At room temperature
ENV 1993-1-1[6]

$$\frac{N_{Sd}}{\chi_{min} A f_y/\gamma_{M1}} + k_y \frac{M_{y,Sd}}{W_{pl,y} f_y/\gamma_{M1}} + k_z \frac{M_{z,Sd}}{W_{pl,z} f_y/\gamma_{M1}} \le 1$$

in which

$$k_y = 1 - \frac{\mu_y N_{Sd}}{\chi_y A f_y} \quad \text{but} \quad k_y \le 1{,}5$$

$$\mu_y = (2\beta_{M,y} - 4)\bar{\lambda}_y + \left[\frac{W_{pl,y} - W_{el,y}}{W_{el,y}}\right] \quad \text{but} \quad \mu_z \le 0{,}9$$

$$k_z = 1 - \frac{\mu_z N_{Sd}}{\chi_z A f_y} \quad \text{but} \quad k_z \le 1{,}5$$

$$\mu_z = (2\beta_{M,z} - 4)\bar{\lambda}_z + \left[\frac{W_{pl,z} - W_{el,z}}{W_{el,z}}\right] \quad \text{but} \quad \mu_z \le 0{,}9$$

χ_{min} is the lesser of χ_y and χ_z
and $\beta_{M,y}$ and $\beta_{M,z}$ are equivalent uniform moment factors for flexural buckling.

Note: 1) The formulae has been deduced from numerical simulations on columns subjected to axial compression with bending moment in the buckling plane (M_z and buckling about weak axis or M_y and buckling about strong axis). The formulae has been extended here to bending moments about both axes as though it was at room temperature.

2) For cross sections in class 3, $W_{pl,y}$ and $W_{pl,z}$ have to be replaced respectively by $W_{el,y}$ and $W_{el,z}$.

6.2 DESIGN TABLES

6.2.1 Design tables (S235, S355, S460)

As already explained in chapter 4 (see equation 10), the analytical formula can be rewritten in the following way:

$$N_{b,fi} = \chi_\theta A k_{max,\theta} f_y = f'_{y,\theta,\bar{\lambda}} A \quad (41)$$

where A is the area of the cross section

and $f'_{y,\theta,\bar{\lambda}} = \chi_\theta k_{max,\theta} f_y$ is the critical compression stress for a given temperature θ and a given slenderness ratio $\bar{\lambda}$.

Table 6.2.1. gives the critical compression stress for S235 steel, Table 6.2.2. can be used for S355 steel and Table 6.2.3. for 460. It should be added that the yield stress f_y has to be reduced according to EN 10025[34] for large flange thickness; in that case, this reduction factor stress had to multiply the critical compression stress given in the tables.

TABLE 6.2.1 Critical compression stress $f'_{y,\theta,\bar{\lambda}}$ for S235 steel

	Temperature θ					
	400°C	500°C	600°C	700°C	800°C	900°C
$\bar{\lambda}$ (20°C)	$f'_{y,\theta,\bar{\lambda}}$ [N/mm^2]					
0.0	235	183	110	54	26	14
0.1	218	171	102	50	24	13
0.2	202	159	94	46	22	13
0.3	187	147	87	42	21	12
0.4	171	136	80	38	19	11
0.5	156	124	72	34	18	10
0.6	140	113	65	30	16	10
0.7	126	102	58	26	15	9
0.8	112	91	51	23	13	8
0.9	99	81	45	20	12	7
1.0	88	73	40	18	11	7
1.1	78	65	35	16	9	6
1.2	70	58	31	14	8	6
1.3	62	52	28	12	8	5
1.4	56	47	25	11	7	5
1.5	50	42	22	10	6	4
1.6	45	38	20	9	6	4
1.7	41	35	18	8	5	4
1.8	37	31	17	7	5	3
1.9	34	29	15	7	4	3
2.0	31	26	14	6	4	3

TABLE 6.2.2 Critical compression stress $f'_{y,\theta,\bar{\lambda}}$ for S355 steel

	Temperature θ					
	400 °C	500 °C	600 °C	700 °C	800 °C	900 °C
$\bar{\lambda}$ (20°C)	$f'_{y,\theta,\bar{\lambda}}$ [N/mm²]					
0.0	355	277	167	82	39	21
0.1	334	261	157	76	37	20
0.2	313	246	147	71	35	19
0.3	293	231	137	66	33	18
0.4	272	215	126	60	31	17
0.5	250	199	116	54	28	16
0.6	227	182	105	49	26	15
0.7	204	165	94	43	24	14
0.8	182	148	83	38	21	13
0.9	161	132	73	33	19	12
1.0	143	118	65	29	17	11
1.1	126	105	57	25	15	10
1.2	112	93	51	22	14	9
1.3	100	83	45	19	12	8
1.4	89	75	40	17	11	8
1.5	80	67	36	15	10	7
1.6	72	61	32	14	9	6
1.7	65	55	29	13	8	6
1.8	59	50	26	11	7	5
1.9	54	46	24	10	7	5
2.0	49	42	22	9	6	4

TABLE 6.2.3 Critical compression stress $f'_{y,\theta,\bar{\lambda}}$ for S460 steel

	Temperature θ					
	400 °C	500 °C	600 °C	700 °C	800 °C	900 °C
$\bar{\lambda}$ (20°C)	$f'_{y,\theta,\bar{\lambda}}$ [N/mm²]					
0.0	460	359	216	106	51	28
0.1	435	341	204	100	48	26
0.2	412	323	193	93	46	25
0.3	388	305	181	87	43	24
0.4	362	286	169	80	41	23
0.5	335	266	155	73	38	22
0.6	305	245	141	66	35	21
0.7	276	222	127	58	32	19
0.8	246	200	112	51	29	18
0.9	218	179	99	44	26	16
1.0	193	159	87	39	23	15
1.1	170	142	77	34	21	14
1.2	151	126	68	30	19	12
1.3	134	112	60	26	17	11
1.4	119	100	54	23	15	10
1.5	107	90	48	21	13	9
1.6	96	81	43	18	12	8
1.7	87	73	39	17	11	8
1.8	79	67	35	15	10	7
1.9	72	61	32	14	9	6
2.0	66	56	29	12	8	6

TABLE 6.2.4 Parameters of the stress strain relationship of steel [3]

Temperature (°C)	$k_{max,\theta}$	$k_{E,\theta}$	$k_{\lambda,\theta}$
20	1.00	1.00	1.00
100	1.00	1.00	1.00
200	1.00	0.90	1.05
300	1.00	0.80	1.12
400	1.00	0.70	1.20
500	0.78	0.60	1.14
600	0.47	0.31	1.23
700	0.23	0.13	1.33
800	0.11	0.09	1.11
900	0.06	0.0675	0.94

6.3 DESIGN EXAMPLES

The proposed examples apply to the following element;

- Section HE 220 A
- radius of gyration $i_z = 5.51$ cm
- sectional area $\Omega = 64.34$ cm²
- Buckling axis minor
- Length L = 3.30 m
- Yield strength fy = 355 Mpa

Preliminary calculations are;

$$\varepsilon = \sqrt{\frac{235}{fy}} = 0.814 \qquad \text{see Eq. (40)}$$

$$\bar{\lambda}(20°C) = \frac{\lambda}{\lambda_E(20°C)} = \frac{L/i_z}{93.91\,\varepsilon} = \frac{3300/55.1}{93.91 \text{ x } 0.814} = 0.784$$

EXAMPLE 1.

N_d = 150 kN, determine the **ultimate temperature**.

Method 1 : critical compression stress (TABLE 6.2.2).

$$f'_{y,\theta,\bar{\lambda}} = \frac{N_{fi,Ed}}{A} = \frac{150000}{6434} = 23{,}3 \text{ N/mm}^2 \qquad \text{see Eq. (41)}$$

The ultimate temperature has to be found by interpolations in table 4

At 700°C;	for $\bar{\lambda} = 0.70$,	$f'_{y,\theta,\bar{\lambda}} = 43$	
	for $\bar{\lambda} = 0.80$,	$f'_{y,\theta,\bar{\lambda}} = 38$	
⇒	for $\bar{\lambda} = 0.784$,	$f'_{y,\theta,\bar{\lambda}} = 38{,}3$	
At 800°C;	for $\bar{\lambda} = 0.70$,	$f'_{y,\theta,\bar{\lambda}} = 24$	
	for $\bar{\lambda} = 0.80$,	$f'_{y,\theta,\bar{\lambda}} = 21$	
⇒	for $\bar{\lambda} = 0.784$,	$f'_{y,\theta,\bar{\lambda}} = 21{,}7$	
⇒	for $\bar{\lambda} = 0.784$ and	$f'_{y,\theta,\bar{\lambda}} = 23{,}3$	$\theta = 790$ °C

Method 2 : analytical expression.

$N_{b.fi} = \chi_\theta \, A \, k_{max,\theta} \, f_y$ see Eq. (35)

is rewritten in the form

$$k_{max,\theta} = \frac{N_{b,fi}}{\chi_\theta A f_y} \qquad (42)$$

First calculation with the initial assumption;

$\bar{\lambda}_\theta = 1{,}20\,\bar{\lambda} = 1{,}20 \times 0{,}784 = 0{,}941$

The calculation is then made as shown hereafter.

$$\phi(\theta) = \frac{1}{2}\left(1 + \alpha\,\bar{\lambda}_\theta + \bar{\lambda}_\theta^2\right) \qquad \text{see Eq. (37)}$$

$$\phi(\theta) = \frac{1}{2}\left(1 + 0{,}65 \times 0{,}814 \times 0{,}941 + 0{,}941^2\right) = 1{,}191$$

$$\chi(\theta)\frac{1}{\phi(\theta) + \sqrt{\phi^2(\theta) - \bar{\lambda}_\theta^2}} \qquad \text{see Eq. (36)}$$

$$\chi(\theta) = \frac{1}{1{,}191 + \sqrt{1{,}191^2 - 0{,}941^2}} = 0{,}520$$

$$k_{max,\theta} = \frac{N_{b,fi}}{\chi_\theta A f_y} \qquad \text{see Eq. (42)}$$

$$k_{max,\theta} = \frac{150000}{0{,}520 \times 6434 \times 355} = 0{,}126$$

From the values of TABLE 6.2.4, $k_{max,\theta} = 0.126$ gives $\theta = \mathbf{786°C}$

For this temperature, TABLE 6.2.4 yields $k_{E,\theta} = 0.095$

The relative slenderness at 786°C is then calculated, according to Eq. (39), as;

$$\bar{\lambda}(786°C) = \sqrt{\frac{0.126}{0.095}}\,0.784 = 0.902$$

It can be noticed that a direct interpolation on $k_{\lambda,\theta}$ in TABLE 6.2.4 gives a very good approximation.

As the first calculation has been made with the assumption of $\bar{\lambda}_\theta = 0{,}941$, an iteration will be made.

Iteration 1.

$$\phi(\theta) = \frac{1}{2}\left(1 + 0.65 \times 0.814 \times 0.902 + 0.902^2\right) = 1.145$$

$$\chi(\theta) = \frac{1}{1.145 + \sqrt{1.145^2 - 0.902^2}} = 0.540$$

$$k_{max,\theta} = \frac{150\,000}{0.540 \times 6434 \times 355} = 0.122$$

From the values of TABLE 6.2.4, $k_{max,\theta} = 0.122$ gives $\theta = \mathbf{790°C}$

For this temperature, TABLE 6.2.4, yields $k_{E,\theta} = 0.094$

The relative slenderness at 790°C is then calculated, according to Eq. (39), as;

$$\bar{\lambda}(790°C) = \sqrt{\frac{0.122}{0.094}}\,0.784 = 0.892$$

Iteration 2.

$$\phi(\theta) = \frac{1}{2}(1 + 0.65 \text{ x } 0.814 \text{ x } 0.892 + 0.892^2) = 1.134$$

$$\chi(\theta) = \frac{1}{1.134 + \sqrt{1.134^2 - 0.892^2}} = 0.545$$

$$k_{max,\theta} = \frac{150\,000}{0.545 \text{ x } 6434 \text{ x } 355} = 0.120$$

From the values of TABLE 6.2.4, $k_{max,\theta} = 0.120$ gives $\theta = 791°C$

For this temperature, TABLE 6.2.4, yields $k_{E,\theta} = 0.093$

The relative slenderness at 791°C is then calculated, according to Eq. (39), as;

$$\bar{\lambda}(791°C) = \sqrt{\frac{0.120}{0.093}}\,0.784 = 0.890$$

This value of 791°C is the converged solution of the analytical equations. The utilisation of the critical compression stress as well as the analitycal calculation limited to one iteration provide answers with a precision of 1°C.

EXAMPLE 2.

Determine the ultimate load knowing that the ultimate temperature is equal to 653°C.
N.B : this temperature exists in the unprotected HE 220 A section after an exposure of 15 minutes to the ISO fire.

Method 1 : critical compression stress (TABLE 6.2.2).

The ultimate temperature has to be found by interpolations in TABLE 6.2.2

At 600°C; for $\bar{\lambda} = 0.70$, $f'_{y,\theta,\bar{\lambda}} = 94$

for $\bar{\lambda} = 0.80$, $f'_{y,\theta,\bar{\lambda}} = 83$

$\Rightarrow$ for $\bar{\lambda} = 0.784$, $f'_{y,\theta,\bar{\lambda}} = 84{,}8$

At 700°C; for $\bar{\lambda} = 0.70$, $f'_{y,\theta,\bar{\lambda}} = 43$

for $\bar{\lambda} = 0.80$, $f'_{y,\theta,\bar{\lambda}} = 38$

$\Rightarrow$ for $\bar{\lambda} = 0.784$, $f'_{y,\theta,\bar{\lambda}} = 38{,}8$

$\Rightarrow$ for $\bar{\lambda} = 0.784$ and $\theta = 653°C$, $f'_{y,\theta,\bar{\lambda}} = 60{,}3$

$N_{b,fi} = A\, f'_{y,\theta,\bar{\lambda}} = 6434 \times 60{,}3 = 387970$ Newtons see Eq. (41)

Method 2 : analytical expression.

From the values of TABLE 6.2.4, $\theta = 653°C$ gives $k_{max,\theta} = 0.343$ and $k_{E,\theta} = 0.215$

$$\bar{\lambda}(653°C) = \sqrt{\frac{k_{max,\theta}}{k_{E,\theta}}}\,\bar{\lambda}(20°C) \qquad \text{see Eq. (39)}$$

$$= \sqrt{\frac{0{,}343}{0{,}215}}\,0{,}784 = 1{,}264 \times 0{,}784 = 0{,}991$$

$$\phi(\theta) = \frac{1}{2}\left(1 + \alpha\,\bar{\lambda}_\theta + \bar{\lambda}_\theta^2\right) \qquad \text{see Eq. (37)}$$

$$\phi(\theta) = \frac{1}{2}\left(1 + 0.65 \times 0.814 \times 0.991 + 0.991^2\right) = 1.253$$

$$\chi(\theta) = \frac{1}{\phi(\theta) + \sqrt{\phi^2(\theta) - \bar{\lambda}_\theta^2}} \qquad \text{see Eq. (36)}$$

$$\chi(\theta) = \frac{1}{1.253 + \sqrt{1.253^2 - 0.991^2}} = 0.495$$

$N_{b,fi} = \chi_\theta\, A\, k_{max,\theta}\, f_y$ see Eq. (35)

$N_{b,fi}\,(653°C) = 0{,}495 \times 6434 \times 0{,}343 \times 355 = 387736$ Newtons

No iteration is required in this case where the ultimate temperature belongs to the data. The utilisation of the tables with the compression stress gives virtually the same ultimate load as the use of the analytical formula.

6.4 NOMOGRAM

The ECCS (European Convention for Constructional Steelwork) has published the ECCS Technical Note No 89 which describes how to calculate unprotected and protected internal Steelwork by using a Nomogram based on the European Prestandard ENV 1993-1-2 [3]. This Technical Note No 89 is given in Annex 16. The result of this research can be very easily included in the nomogram if the following changes are made.

Technical Note No 89	Improvement based on the ESCS research 7210 SA 316/515/618/931
2.3 Temperature Distribution	**2.3 Temperature Distribution**
An adaptation factor κ is introduced to take account of a non-uniform temperature distribution over the height and alongside the steel section. The value of the adaptation factor κ should be taken as follows:	An adaptation factor κ is introduced to take account of a non-uniform temperature distribution over the height and alongside the steel section. The value of the adaptation factor κ should be taken as follows:
- beams: · exposed on all four sides: $\kappa = 1,0$ · exposed on three sides, with a composite or concrete slab on side four: $\kappa = 0,7$ - statically indeterminate beams at support: · exposed on all four sides: $\kappa = 0,85$ · exposed on three sides, with a composite or concrete slab on side four: $\kappa = 0,6$ - stability problems: $\kappa = 1,2$	- beams: · exposed on all four sides: $\kappa = 1,0$ · exposed on three sides, with a composite or concrete slab on side four: $\kappa = 0,7$ - statically indeterminate beams at support: · exposed on all four sides: $\kappa = 0,85$ · exposed on three sides, with a composite or concrete slab on side four: $\kappa = 0,6$ - lateral torsional buckling $\kappa = 1,2$ - column: $\kappa = 1,0$
3. Calculation procedure	**3. Calculation procedure**
$R_{fi,d,o}$ is calculated using $\overline{\lambda}_{fi,\theta,max}$ as given above, the yield strength f_y at room temperature and buckling curve c	$R_{fi,d,o}$ is calculated using $\overline{\lambda}_{fi,\theta,max}$ as given above, the yield strength f_y at room temperature and the buckling curve established in the scope of the ECSC research 7210 SA 316/515/618/931 (see chapter 6.1.1).

The table 1b and 1c has to be adapted and become

Tab. 1b Critical steel temperature of internal columns for $\ell_{cr,fi,o} = 0,5$ L

$\mu_{o,c}$	$\overline{\lambda}_{o,c}$									
	0,20	0,40	0,60	0,80	1,00	1,20	1,40	1,60	1,80	2,00
0,30	670	678	688	699	714	729	744	758	771	781
0,35	647	655	665	677	689	701	715	727	738	747
0,40	627	635	645	657	670	682	692	700	709	717
0,45	609	617	628	640	653	666	676	684	690	695
0,50	592	601	612	625	638	651	661	670	676	681
0,55	577	586	598	611	625	637	648	657	663	668
0,60	563	572	584	598	612	625	636	645	652	657

Tab. 1c Critical steel temperature of top storey columns for $\ell_{cr,fi,o} = 0,7$ L

$\mu_{o,c}$	$\overline{\lambda}_{o,c}$									
	0,20	0,40	0,60	0,80	1,00	1,20	1,40	1,60	1,80	2,00
0,30	636	640	643	648	652	656	659	660	661	662
0,35	612	617	621	626	631	635	638	640	641	642
0,40	591	596	601	606	613	617	621	623	624	625
0,45	572	578	583	589	596	601	605	607	609	610
0,50	554	561	566	573	581	587	591	593	595	596
0,55	537	544	550	558	566	573	577	580	582	584
0,60	520	528	535	544	553	560	565	568	570	572

$\mu_{o,c}$ = design load in fire / design buckling resistance for $\theta = 20°C$, $\ell_{fi} = 1,0$ L, buckling curve ECSC 7210 SA 316/515/618/931, $\gamma_{M,fi} = 1,0$

$\overline{\lambda}_{o,c}$ = non dimensional slenderness of column for $\ell_{fi} = 1,0$ L.

In the nomogram, the curve corresponding to the columns is thanks to this ECSC research, the curve noted $\kappa = 1,0$ instead of the curve noted $\kappa = 1,2$ which is required by the present Technical Note No 89.

7. *CONCLUSIONS*

The behavior of centrally and eccentrically loaded steel column at elevated temperatures has been investigated by a very wide series of numerical tests. The buckling of steel columns at elevated temperatures has been the subject of quite a lot of investigations and publications in the last decades. The most distinctive aspects of the work that has been reported here are:

- the numerical study has considered virtually every possible combination of all the parameters such as the profile section, the yield strength, the buckling axis, the thermal distribution, the slenderness and the load level.

- the numerical study was based on non linear stress - strain relationships, whereas most of the previous works on the subject sticked to bilinear behaviour. The influence of the residual stresses has been considered on the basis of principles of structural mechanics, see ref. [49].

For centrally loaded columns,
- the shape of the buckling curve is different from the shape observed at ambient temperature,
- the results are more consistently presented when the relative slenderness is evaluated at the ultimate temperature. In this case, the buckling curve does not depend significantly on the temperature,
- the buckling coefficient increases with increasing nominal yield strength,
- the scatter between different section or different buckling planes is not significant.

For eccentrically loaded columns, the following additional observations could be made;
- in case of uniform bending moment distribution, the unsymetrical character of the interaction curve in the M-N plane is more pronounced than at ambient temperature,
- the slenderness and the shape of the bending moment diagram have a very great importance, as is the case at 20°C,
- the shape of the interaction curve is different in each buckling plane.

An analytical proposal has been made for the design in case of fire of centrally and eccentrically loaded columns. The research has lead to a new formula for the buckling coefficient which depends upon the yield strength and to a new formula for the N-M interaction. These analytical formulae have been made, similar in its form, to what exists for room temperature in ENV 1993-1-2[3].

This proposal, based on the extensive numerical study of the problem, has been calibrated on the basis of 73 experimental tests made on centrally loaded columns in order to obtain, on average, the same result with the formula than those observed in the tests. When test results from eccentrically loaded columns are also considered, an additional safety margin appears to be provided by the analytical proposal.
The safety level does not depend on the slenderness ratio. The parameters which were identified as significant by the numerical study have seen their role confirmed by the comparison with experimental tests.
It should be noted the calibration of the proposed analytical solution was founded on a significant number of carefully scrutinized experimental results from 6 different laboratories. 80% of those tests come from sources that are independent from the partners of the research.

In addition to the new analytical formula which can be easily used by hand (as illustrated by the design examples) or programmed in a computer, design tables have been provided for the practical designers which enable them to calculate very quickly a column in case of fire.
The benefit of this research is illustrated by the two following figures which compares the ESCS 7210 SA / 316/515/618/931 proposal to the ENV 1993-1-2 proposal [3].

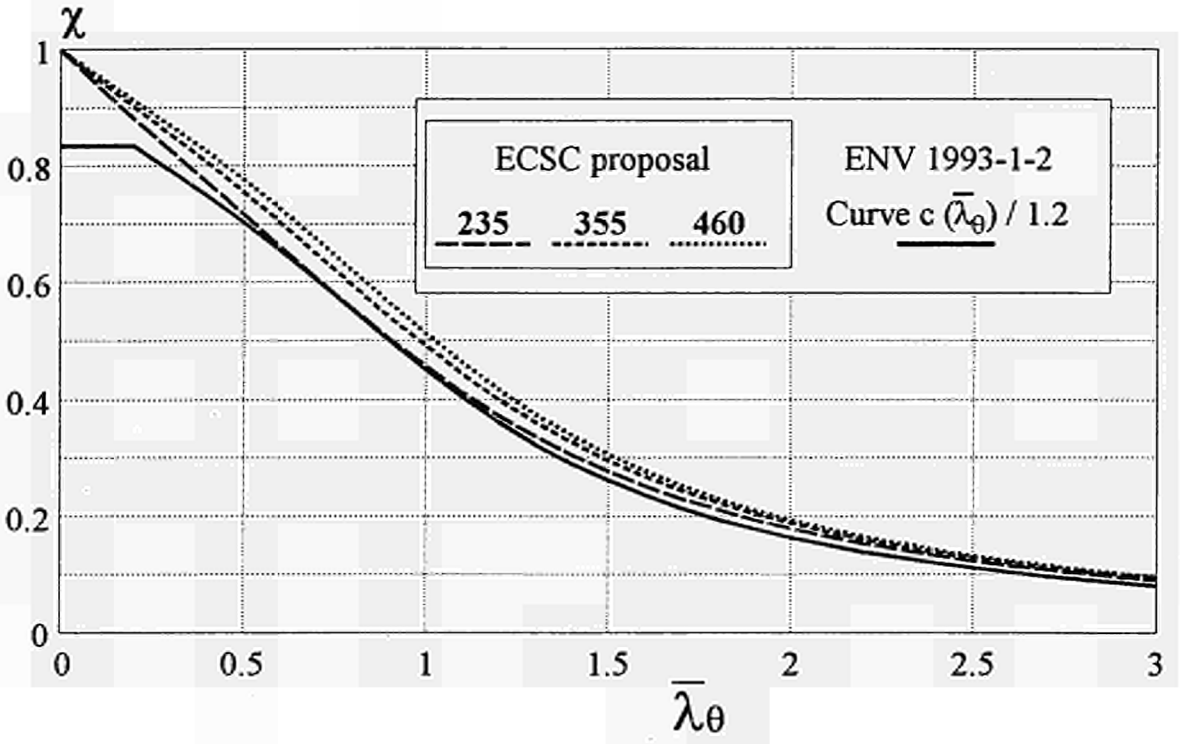

FIGURE 7.1 ECSC 7210 SA 316,515,931,618 proposal for Buckling Curves in Case of Fire

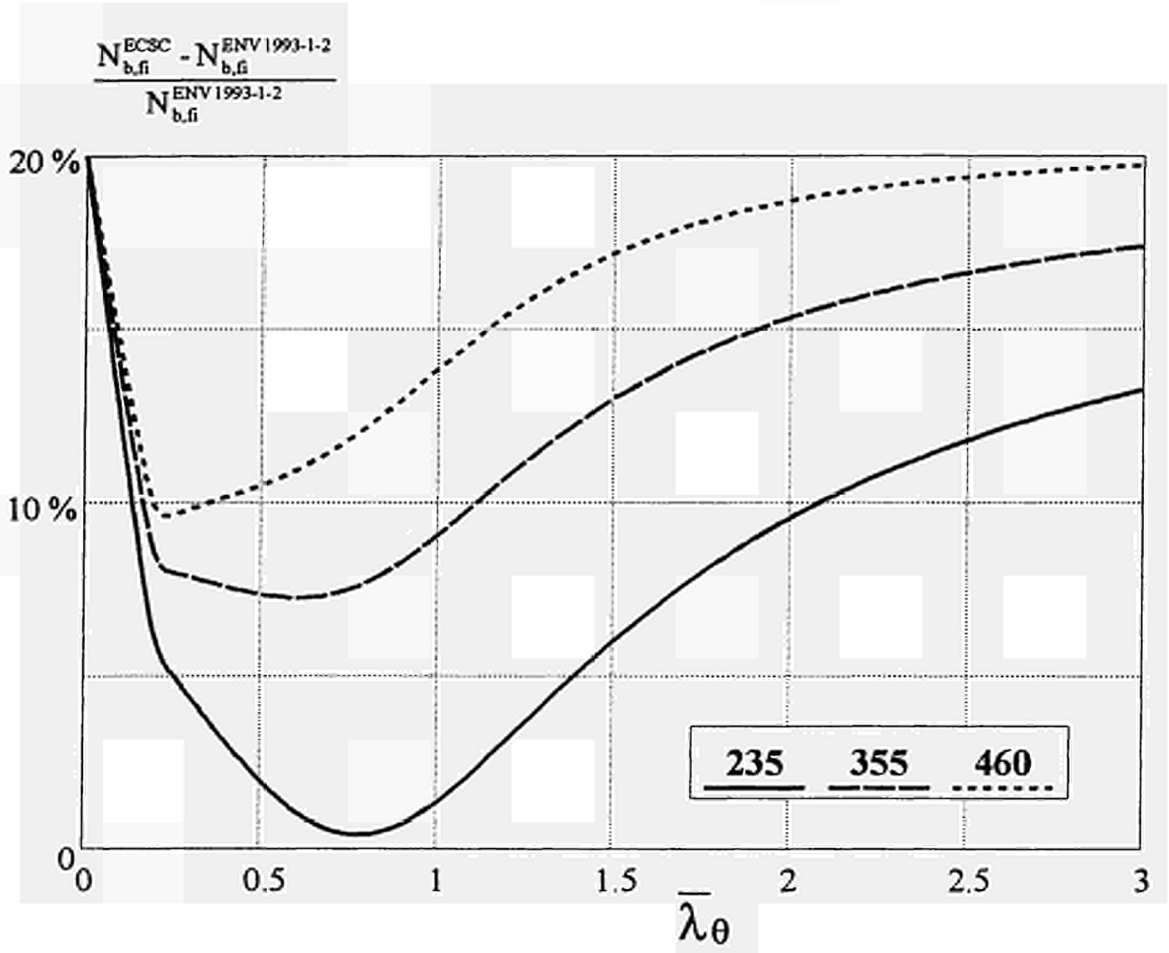

FIGURE 7.2

Moreover this research has provided design formulae and tables which have been checked with a database of 141 tests, which enables us to avoid any suspicious comments because formulae and tables have been deduced from both numerical simulations (made by five different software) and experimental tests.

8. *NOTATIONS*

Latin case letters

A	Area of the cross section
$D_{numerical}$	failure temperature obtained numerically
$D_{analytical}$	failure temperature obtained analytically
e	eccentricity of the load [mm]
e_o	sinusoïdal initial imperfection
$e_d(x)$	horizontal displacement of the column
$e_i(x)$	initial imperfection of the column
$e_T(x)$	level arm of the load
f	horizontal displacement at mid-height of the column
f_y	yield strength at room temperature [MPa]
$f'_{y,\theta,\bar{\lambda}}$	critical compression stress for a given temperature θ and a given slenderness ratio $\bar{\lambda}$
$f_y(T)$	yield strength at temperature [T]
k_E	reduction factor of the Young's Modulus with the temperature
k_{max}	reduction factor of the yield stress with the temperature
k_y	factor multiplying the bending moment M in the N/M interaction formula
$k_{\bar{\lambda}}$	reduction factor of $\bar{\lambda}$ with the temperature
H	Length of the column[m]
H_{max}	maximum height [m]
i	radius of gyration of the section
i2	imperfection at L/4
i3	imperfection at 2.L/4
i4	imperfection at 3.L/4
L	buckling length of the column
M_{Sd}	design applied bending moment
N_{cr}	elastic critical force for the relevant buckling curve
$N_{(T,H)}$	axial load at temperature T and for a column length H
$N_{pl}(T)$	plastic load at temperature T
N_{Sd}	design applied normal force
N_u	ultimate load
P_E	Euler load
r	radius of gyration of the column
t	time [min]
T	temperature [°C]
W_{pl}	modulus of plastic bending
W_e	modulus of elastic bending

Greek lower case letters

α	imperfection factor
β	severity factor

β_M	equivalent uniform moment for flexural buckling in case non uniform bending distribution
ε	$=\sqrt{\frac{235}{f_y}}$ (fy in MPa)
μ_y	factor multiplying N_{Sd} in the k_y formula
δ	eccentricity of the load
κ	correction factor
$\bar{\lambda}$	relative slenderness ratio at room temperature (20°C)
χ	buckling coefficient
θ	temperature [°C]

Greek upper case letters

Ω	cross sectional area

Indices

Latin case letters

b	buckling
cr	critical
d	design
el	elastic
E	relative to the Young's Modulus
fi,E_d	design action in case of fire
fi	in case of fire
min	minimum
max	maximum
pl	plastic
Rd	design resistance
u	ultimate
y	relative to strong axis yy
z	relative to weak axis zz

Greek case letters

λ	relative slenderness
θ	temperature [°C]

9. *REFERENCES*

[1] Franssen J.M., Schleich J.B., Cajot L.G., Talamona D., Zhao B., Twilt L., Both K. "A Comparison between five Structural Fire Codes applied to Steel Elements". Fire Safety Science-Proceeding of the fourth international symposium, pp 1125-1136.

[2] Kruppa J., Law M. and Twilt L., Eurocode No. 3 Design of Steel Structures. Part 10: Structural Fire Design, Commission of the European Communities, Draft April 1990.

[3] prENV 1993-1-2. Eurocode 3. Design of steel structures. Draft part 1.2. Structural fire design, July 1993 version, CEN, 1993.

[4] Franssen J.M., "Modélisation et influence des contraintes résiduelles dans les profils métalliques soumis à l'incendie" Construction Métallique: 3, 35-42, 1989.

[5] EN 10025, Hot rolled products of non-alloy structural steels: Technical delivery conditions, CEN, Brussels, 1990.

[6] ENV 1993-1-1. Eurocode 3: Design of steel structures. Part 1.1: General rules and rules for buildings. CEN, April 1992.

[7] ARBED. Sale programme. Structural shapes, ARBED, Luxembourg, January 1993.

[8] Talamona D., CTICM. SA 316 Interaction M-N, Comparison between LENAS and the EC3 formulas, October 1993.

[9] Cajot L.G., Chantrain Ph., Mathieu J,. Schleich J.B.; REFAO III. Practical Design Tools for Unprotected Steel Columns Submitted to ISO-Fire. / C.E.C Research 7210-SA/505; Final Report. Eur 14348 EN, Luxembourg 1992, RPS Report n° 11/91.

[10] Schlussbericht Teilprojekt D1. Sicherheitstheoretische Untersuchungen zur Versagenswahrscheinlichkeit von brandbeanspruchten Bauteilen bzw. Bauwerk-abschnitten. Karl Kordina, Volker Henke, Braunschweig. April 1987.

[11] Dorn T., Institut für Baustoffe, Massivbau und Brandschutz, Braunschweig; data discs 3,5", file: Datenb2.xls, Dezember 1993.

[12] Minne R., Laboratorium voor Aanwending der Brandstoffen en Warmte-overdracht; University of Gent; Reports: 5091 to 5099, 5871 to 5874, 5925 to 5927.

[13] Station d'Essais du C.T.I.C.M., Rapport d'essai n° 94-S-186, France, 1994.

[14] Station d'Essais du C.T.I.C.M., Rapport d'essai n° 94-S-190, France, 1994.

[15] Station d'Essais du C.T.I.C.M., Rapport d'essai n° 94-S-194, France, 1994.

[16] Station d'Essais du C.T.I.C.M., Rapport d'essai n° 94-S-197, France, 1994.

[17] Station d'Essais du C.T.I.C.M., Rapport d'essai n° 94-S-199, France, 1994.

[18] Station d'Essais du C.T.I.C.M., Rapport d'essai n° 94-S-200, France, 1994.

[19] Station d'Essais du C.T.I.C.M., Rapport d'essai n° 94-S-201, France, 1994.

[20] Station d'Essais du C.T.I.C.M., Rapport d'essai n° 94-S-202, France, 1994.

[21] Ossenbruggen, P., J., Aggarwal, V. and Culver, C., G., "Steel Column Failure Under Thermal Gradients.", ASCE, J. struct. division, Vol. 99, No. ST4, pp. 727-739, 1973.

[22] Aribert, J.-M. and Abdel Aziz, M. "Simulation du comportement à l'incendie de poteaux comprimés et fléchis en présence de gradients quelconques de température.", CTICM, Construction Métallique, N°2, 1987.

[23] Culver, C., Aggarwal, V, and Ossenbruggen, P, "Buckling of Steel Columns at Elevated Temperatures.", ASCE, J. Str. Division, , Vol. 99, No. ST4, pp. 715-726, 1973.

[24] ECCS-Technical Committee 3 - Fire Safety of Steel Structures, "European Recommendations for the Fire Safety of Steel Structures.", Elsevier, 1983.

[25] ENV 1993-1-1. Eurocode 3 : Design of Steel structures. Part 1.1 : General rules and rules for buildings. CEN, April 1992.

[26] Kruppa, J., Law, M. and Twilt, L., Eurocode No. 3 Design of Steel Structures. Part 10: Structural Fire Design, Commission of the European Communities, Draft April 1990.
[27] prENV 1993-1-2. Eurocode 3. Design of steel structures. Draft part 1.2. Structural fire design, July 1993 version, CEN, 1993.
[28] C.E.C. Agreement 7210-SA / 316 / 515 / 618 / 931, Buckling Curves of Hot Rolled H Steel Sections Submitted to Fire, semestrial report n° 3.
[29] Rubert, A. and Schaumann, P., "Temperaturabhängige Werkstoffeigenshaften von Baustahl bei Brandbeanspruchung.", Stahlbau 54, Heft 3, S.81-86, 1985.
[30] Olesen, F., B., "Fire tests on steel columns.", Inst. of Building Techn. and Struct. Eng., Aalborg, Denmark; 1980.
[31] Vandamme, M., Janss, J., "Buckling of Axially Loaded Steel Columns in Fire Conditions.", IABSE Periodica, 3/1981.
[32] Talamona, D.,"SA 316. Interaction M-N. Comparison between LENAS and tests.",CTICM report INC - 94/246 - DT, 1994.
[33] Burgess, I., W., Olawale, A., O. and Plank, R., J., "Failure of Steel Columns in Fire.", Fire Safety Journal, 1991.
[34] EN 10025, Hot rolled products of non-alloy structural steels : Technical delivery conditions, CEN, Brussels, 1990.
[35] Compendium of UK Standard Fire Test Data. Unprotected Structural Steel - 1, BSC Swinden Laboratories, Rotherham, 1988
[36] Janss, J. and Minne, R. "Buckling of Steel Columns in Fire Conditions.", Fire Safety Journal, Vol. 4, 1982.
[37] Aribert, J.-M., and Randriantsara , C., "Etude du flambement à des températures d'incendie. Action du fluage.", CTICM, Construction Métallique, N°4, 1980.
[38] Azpiazu, W., and Unanue, J., A., "Buckling curves of hot rolled H steel sections submitted to fire.", LABEIN, Report n° 97.798-2-ME/V, 1993.
[39] Dorn, T., IBMB, Braunschweig, letter Dn/Dn 9341, private communication, 1993.
[40] Olawale, A., O, and Plank, R., J., "The collapse analysis of steel columns in fire using a finite strip method.", Int. j. num. meth. in eng., Vol. 26, 2755-2764, 1988.
[41] Cajot, L.-G., Chantrain, Ph., Mathieu, J. and Schleich, J.-B., "REFAO-III, Practical Design Tools for Unprotected Steel Columns Submitted to ISO-Fire.", Research 7210-SA/505, Final Report Eur 14348 EN, C.E.C., Luxembourg, 1992
[42] Sonderforschungsbereich 148. Brandverhalten von Bauteilen. TU-Braunschweig, from 1977.
[43] Evaluation du risque d'incendie. Méthode de calcul., Société suisse des ingénieurs et des architectes, document SIA 81.
[44] Kruppa, J., "Calcul des températures critiques des structures en acier.", Construction Métallique, CTICM, Sept. 1976.
[45] European Recommendations for Steel Constructions. E.C.C.S., 1978.
[46] Petterson, O., and Witteveen, J., "On the fire resistance of structural steel elements derived from standard fire tests or by calculation.", Fire Safety Journal, 73-87, Vol. 2, 1980.
[47] Setti, P., "Buckling of axially loaded steel columns with imperfections at elevated temperature.", Third Int. Colloquium on Stability of metal structures, Paris, CTICM, preliminary report, 167-174,1983.
[48] Burgess, I., W. and Najjar, S., R., "A Simple Approach to the Behaviour of Steel Columns in Fire.", J. Construct. Steel Research, 31, 115-134, 1994.
[49] Franssen, J.-M., "Modélisation et influence des contraintes résiduelles dans les profils métal-liques soumis à l'incendie.", Construction Métallique, 3, 35-42, 1989.

[50] Aasen, B., "An Experimental Study on Steel Columns Behaviour at Elevated Temperatures.". The Norwegian Inst. of Technology, Trondheim, 1985.
[51] Margaret Law & Turlogh O'Brien *Fire Safety of Bare External Structural Steel* Constructional Steel Research and Development Organisation Constrado May 1981
[52] Joris Fellinger & Kees Both *Modellering van Straling en Convective in Holle Ruimten in Potentiaalstroomberekeningen volgens de Eindige Elementen Methode* TNO Bouw report 95-CVB-R0392 April 1995
[53] DIANA User's Manual Volume 7: Potential Flow Analysis TNO: Release 5.1; Revision A, Delft April 1993
[54] Eurocode 1 Basis of Design and Actions on Structures, Part 2.2: Actions on Structures Exposed to Fire ENV 1991-2-2 April 1993
[55] ECCS Technical Note No 89, Fire Resistance of Steel Structures, Brussels 1996

ANNEX 1:

1. LABEIN TESTS - DIMENSIONAL MEASUREMENTS

1.1 MEASUREMENTS MADE ON THE SPECIMENS

Twenty HE 100 A specimens to be tested, with five different slenderness ratio, have been measured in order to determine the variation in cross-sectional area and shape and the initial curvature of the web.

The specimens with buckling lengths of 510 and 1,270 mm have been measured in three cross sections, the two end sections and the mean section (see FIGURE 1.1). The rest of the specimens have been measured in five cross sections according FIGURE 1.2. The dimensions taken in each cross sections appears in FIGURE 1.3.

1.2 PROCEDURE

The measurements have been taken according to ECCS report n° 36 "TESTING PROCEDURES" part 3.4.

All cross section measurements have been taken with a digital calibre TESA DIGIT CAL n/s 2, certificate 01.02.93 Departamento de Metrologia. Dossier 52/01/93.

The initial curvature of the web (imperfection) has been measured with a theodolite ZEISS Ni 1 s/n 160103 stationed in line with the column and near one of the ends.

1.3 RESULTS

In TABLE 1.1 to TABLE 1.20 appear the results of the readings. All dimensions are in millimeters.

The location on the measurements are shown on FIGURE 1.1 to FIGURE 1.3.

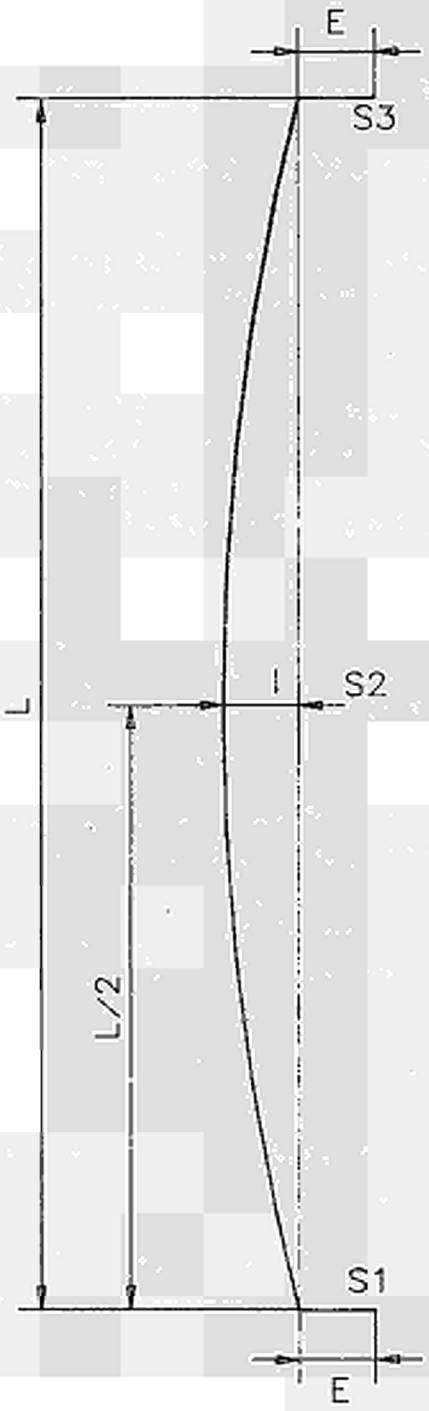

CROSS SECTIONS Si IN SPECIMENS A_DL1 AND A_DL3

FIGURE 1.1

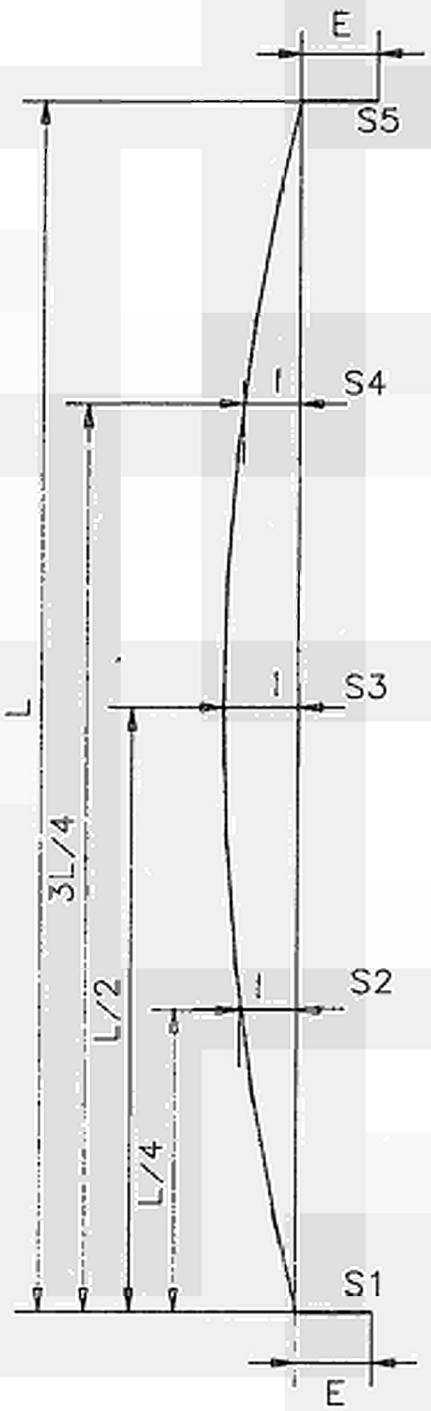

CROSS SECTIONS Si IN SPECIMENS A_DL5, SL41_4 AND A_DL6

FIGURE 1.2

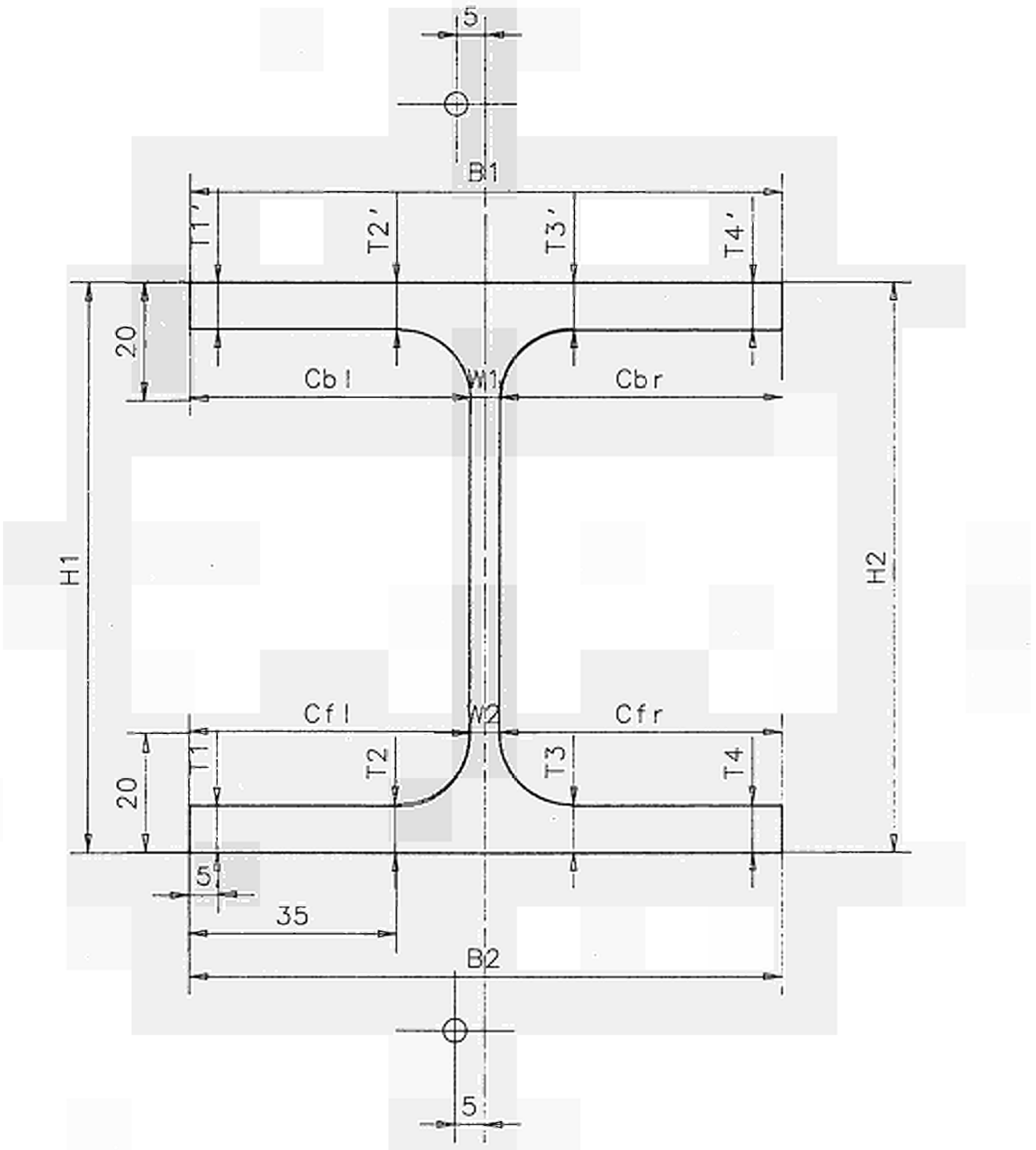

CROSS SECTION MEASUREMENTS

FIGURE 1.3

SPECIMEN	AL1
BUCKLING LENGHT	513.0
EXCENTRICITY	5.0

CROSS SECTION MEASUREMENTS																			
CROSS SECTION	B1	B2	H1	H2	W1	W2	T1	T2	T3	T4	T1'	T2'	T3'	T4'	Cbl	Cbr	Cfl	Cfr	I
S1	101.6	102.3	98.8	99.6	6.1	6.6	7.2	7.9	8.2	7.5	7.7	8.6	8.1	7.7	47.7	47.8	49.0	46.7	0.0
S2	101.6	102.3	99.1	99.3	5.7	6.0	7.2	8.1	7.9	7.5	7.5	8.2	8.2	7.7	47.9	48.0	48.9	47.4	0.0
S3	101.6	102.1	99.3	99.1	5.9	6.2	7.3	8.4	8.1	7.5	7.6	8:2	8.1	7.7	47.8	47.9	48.7	47.2	0.0

TABLE 1.1

SPECIMEN	BL1
BUCKLING LENGHT	513.0
EXCENTRICITY	5.0

CROSS SECTION MEASUREMENTS																			
CROSS SECTION	B1	B2	H1	H2	W1	W2	T1	T2	T3	T4	T1'	T2'	T3'	T4'	Cbl	Cbr	Cfl	Cfr	I
S1	101.9	101.8	98.8	98.9	6.0	6.0	7.4	8.0	8.1	7.4	7.1	7.9	7.8	7.2	48.4	47.5	48.0	47.8	0.0
S2	102.0	101.8	98.8	98.7	5.8	5.9	7.4	8.1	8.0	7.4	7.1	7.7	7.7	7.3	48.8	47.4	48.1	47.8	0.0
S3	101.9	101.7	98.9	99.0	6.0	5.8	7.4	8.2	8.0	7.5	7.1	7.8	7.8	7.3	48.8	47.1	48.2	47.7	0.0

TABLE 1.2

SPECIMEN	CL1
BUCKLING LENGHT	513.0
EXCENTRICITY	5.0

CROSS SECTION MEASUREMENTS																		
CROSS SECTION	B1	B2	H1	H2	W1	W2	T1	T2	T3	T4	T1'	T2'	T3'	T4'	Cbl	Cbr	Cfl	Cfr	l
S1	101.6	101.9	98.9	99.6	6.6	7.2	7.4	8.1	7.8	7.5	7.6	8.5	8.1	7.5	46.0	49.0	46.0	48.7	0.0
S2	101.6	102.1	99.1	99.4	5.9	6.3	7.3	8.1	7.8	7.4	7.6	8.6	8.1	7.5	45.8	49.9	46.8	49.0	0.0
S3	101.5	102.0	98.1	99.3	6.2	6.4	7.4	8.2	7.8	7.4	7.6	8.3	8.2	7.5	45.4	49.9	46.4	49.2	0.0

TABLE 1.3

SPECIMEN	DL1
BUCKLING LENGHT	513.0
EXCENTRICITY	5.0

CROSS SECTION MEASUREMENTS																		
CROSS SECTION	B1	B2	H1	H2	W1	W2	T1	T2	T3	T4	T1'	T2'	T3'	T4'	Cbl	Cbr	Cfl	Cfr	l
S1	102.0	102.7	98.8	99.4	5.8	6.4	7.3	7.9	7.8	7.3	7.5	8.1	8.0	7.5	48.0	48.2	49.0	47.3	0.0
S2	102.0	102.7	98.9	99.3	6.0	6.3	7.2	7.8	7.8	7.4	7.5	8.1	8.1	7.5	48.0	48.0	48.9	47.5	0.0
S3	101.8	102.5	99.2	99.1	5.9	6.4	7.1	7.7	7.8	7.3	7.6	8.2	8.1	7.6	47.9	48.0	48.9	47.2	0.0

TABLE 1.4

SPECIMEN	AL3
BUCKLING LENGHT	1,270.0
EXCENTRICITY	5.0

CROSS SECTION MEASUREMENTS																		
CROSS SECTION	B1	B2	H1	H2	W1	W2	T1	T2	T3	T4	T1'	T2'	T3'	T4'	Cbl	Cbr	Cfl	Cfr	I
S1	101.5	102.2	99.8	98.5	5.7	6.1	7.4	7.9	7.9	7.2	7.6	8.0	8.2	7.4	47.8	48.0	47.0	49.1	0.0
S2	101.7	102.4	99.6	98.7	5.9	6.1	7.3	7.7	7.9	7.1	7.5	8.0	8.1	7.5	47.8	48.0	47.1	49.2	0.0
S3	101.7	102.2	99.3	98.6	6.0	6.0	7.2	8.1	8.0	7.2	7.4	8.0	8.2	7.3	48.0	47.7	47.3	48.9	0.0

TABLE 1.5

SPECIMEN	BL3
BUCKLING LENGHT	1,272.0
EXCENTRICITY	5.0

CROSS SECTION MEASUREMENTS																		
CROSS SECTION	B1	B2	H1	H2	W1	W2	T1	T2	T3	T4	T1'	T2'	T3'	T4'	Cbl	Cbr	Cfl	Cfr	I
S1	102.0	101.7	98.4	99.5	6.1	6.1	7.4	8.4	8.1	7.4	7.1	8.0	8.1	7.3	48.9	47.0	48.2	47.4	0.0
S2	102.1	101.9	98.3	99.6	5.7	5.8	7.3	8.0	8.0	7.4	7.0	7.9	7.6	7.2	49.1	47.3	48.3	47.8	0.2
S3	102.0	101.9	98.4	99.2	6.0	6.1	7.3	8.0	8.4	7.4	7.1	7.9	7.9	7.1	48.7	47.3	47.7	48.1	0.0

TABLE 1.6

SPECIMEN	CL3
BUCKLING LENGHT	1,271.0
EXCENTRICITY	5.0

CROSS SECTION MEASUREMENTS																		
CROSS SECTION	B1	B2	H1	H2	W1	W2	T1	T2	T3	T4	T1'	T2'	T3'	T4'	Cbl	Cbr	Cfl	Cfr	I
S1	101.4	101.8	99.5	99.0	6.1	6.0	7.4	8.1	8.2	7.3	7.7	8.3	8.4	7.5	49.0	46.3	48.4	47.4	0.0
S2	101.7	102.2	99.6	99.0	6.0	6.3	7.4	7.9	8.0	7.2	7.7	8.3	8.4	7.7	49.1	46.6	48.2	47.7	0.4
S3	102.0	102.3	99.8	98.6	6.1	6.3	7.2	7.7	8.0	7.2	7.6	8.4	8.4	7.6	49.1	46.8	47.7	48.3	0.0

TABLE 1.7

SPECIMEN	DL3
BUCKLING LENGHT	1,269.0
EXCENTRICITY	5.0

CROSS SECTION MEASUREMENTS																		
CROSS SECTION	B1	B2	H1	H2	W1	W2	T1	T2	T3	T4	T1'	T2'	T3'	T4'	Cbl	Cbr	Cfl	Cfr	I
S1	102.7	101.9	99.8	98.5	6.2	5.7	7.6	8.2	8.2	7.5	7.5	7.9	8.0	7.2	47.3	49.2	48.0	48.2	0.0
S2	102.5	101.7	99.7	98.8	6.2	6.0	7.5	8.1	8.1	7.6	7.4	7.8	8.0	7.2	47.3	49.0	47.9	47.8	0.3
S3	102.4	101.7	99.5	98.6	6.0	6.0	7.5	8.2	8.2	7.4	7.4	7.9	7.9	7.2	47.3	49.1	48.0	47.7	0.0

TABLE 1.8

TABLE 1.9

SPECIMEN	SL41
BUCKLING LENGHT	2,026.0
EXCENTRICITY	5.0

CROSS SECTION MEASUREMENTS																		
CROSS SECTION	B1	B2	H1	H2	W1	W2	T1	T2	T3	T4	T1'	T2'	T3'	T4'	Cbl	Cbr	Cfl	Cfr	l
S1	101.8	101.7	98.5	99.4	5.5	5.8	7.1	7.8	7.8	7.2	7.4	8.0	8.0	7.5	48.0	48.3	48.7	47.2	0.0
S2	102.0	101.9	98.4	99.4	5.9	5.5	7.0	7.9	7.7	7.2	7.2	8.0	8.0	7.4	48.0	48.1	49.0	47.4	0.6
S3	102.0	102.0	98.3	99.7	5.7	5.7	7.1	7.8	7.7	7.2	7.3	7.9	8.0	7.3	48.0	48.3	48.9	47.4	0.7
S4	101.9	101.8	98.5	99.6	5.8	5.9	7.1	7.8	7.7	7.3	7.4	8.0	8.2	7.4	47.6	48.5	48.6	47.3	0.7
S5	101.8	101.5	98.5	99.4	5.9	5.6	7.1	7.9	7.8	7.2	7.4	8.0	8.0	7.4	47.6	48.3	48.5	47.4	0.0

TABLE 1.10

SPECIMEN	SL42
BUCKLING LENGHT	2,020.0
EXCENTRICITY	5.0

CROSS SECTION MEASUREMENTS																		
CROSS SECTION	B1	B2	H1	H2	W1	W2	T1	T2	T3	T4	T1'	T2'	T3'	T4'	Cbl	Cbr	Cfl	Cfr	I
S1	101.8	101.7	98.4	99.5	6.2	5.6	7.4	8.4	8.1	7.4	7.0	7.7	7.7	7.2	48.5	47.1	48.1	48.0	0.0
S2	101.9	101.7	98.5	99.7	5.7	5.7	7.4	8.0	8.1	7.5	7.1	7.9	7.8	7.2	48.7	47.5	48.0	48.0	0.9
S3	101.7	101.8	98.6	99.6	5.4	5.7	7.4	8.0	8.1	7.5	7.1	7.9	7.8	7.3	48.6	47.7	47.9	48.2	1.7
S4	101.9	101.9	98.3	99.6	5.6	5.8	7.5	8.1	8.0	7.5	7.0	7.8	7.6	7.2	48.8	47.5	47.8	48.3	0.9
S5	102.0	101.8	98.5	99.7	6.1	5.8	7.3	8.1	8.0	7.3	7.0	7.8	7.8	7.4	48.5	47.4	47.8	48.2	0.0

TABLE 1.11

SPECIMEN	SL43
BUCKLING LENGHT	2,021.0
EXCENTRICITY	5.0

CROSS SECTION MEASUREMENTS																		
CROSS SECTION	B1	B2	H1	H2	W1	W2	T1	T2	T3	T4	T1'	T2'	T3'	T4'	Cbl	Cbr	Cfl	Cfr	I
S1	102.2	101.7	98.6	99.2	5.9	5.5	7.2	7.7	7.8	7.1	7.3	8.0	8.0	7.4	48.2	48.1	47.8	48.4	0.0
S2	102.0	101.9	98.8	98.6	5.8	5.6	7.2	7.7	7.8	7.0	7.4	8.0	7.9	7.3	48.1	48.1	47.8	48.5	-0.4
S3	102.1	101.8	99.1	98.7	6.1	5.9	7.2	7.6	7.7	7.0	7.4	8.0	8.0	7.3	48.2	47.8	47.5	48.4	0.0
S4	101.8	101.7	99.2	98.8	6.1	5.7	7.2	7.7	7.8	7.1	7.4	8.0	8.1	7.4	48.2	47.5	47.4	48.6	0.0
S5	101.7	101.5	99.8	98.1	5.7	5.7	7.3	7.7	7.8	7.0	7.4	8.3	8.0	7.4	48.3	47.7	47.2	48.6	0.0

TABLE 1.12

SPECIMEN	SL44
BUCKLING LENGHT	2,023.0
EXCENTRICITY	5.0

CROSS SECTION MEASUREMENTS																		
CROSS SECTION	B1	B2	H1	H2	W1	W2	T1	T2	T3	T4	T1'	T2'	T3'	T4'	Cbl	Cbr	Cfl	Cfr	I
S1	101.7	101.7	99.4	99.4	5.7	6.0	7.0	7.7	7.7	7.2	7.3	8.0	8.0	7.4	47.6	48.4	48.2	47.5	0.0
S2	101.7	101.7	99.0	99.3	5.7	5.4	7.0	7.8	7.6	7.2	7.4	8.0	8.0	7.3	47.8	48.2	48.7	47.6	0.5
S3	101.7	101.8	99.4	98.6	5.8	5.6	7.0	7.8	7.7	7.2	7.4	8.1	8.0	7.4	47.8	48.1	48.8	47.4	1.1
S4	101.6	101.7	99.0	99.6	5.7	5.8	7.2	7.9	7.7	7.2	7.4	8.3	8.0	7.4	47.6	48.3	48.5	47.4	0.6
S5	101.6	101.6	98.6	99.4	5.7	5.9	7.1	7.8	8.1	7.3	7.4	8.2	8.2	7.5	47.6	48.3	48.3	47.4	0.0

TABLE 1.13

SPECIMEN	AL5
BUCKLING LENGHT	2,770.0
EXCENTRICITY	5.0

CROSS SECTION MEASUREMENTS																		
CROSS SECTION	B1	B2	H1	H2	W1	W2	T1	T2	T3	T4	T1'	T2'	T3'	T4'	Cbl	Cbr	Cfl	Cfr	I
S1	102.3	101.6	99.5	98.6	6.1	5.6	7.4	8.0	8.2	7.3	7.3	7.8	7.8	7.1	47.0	49.2	47.9	48.1	0.0
S2	102.2	101.7	99.3	98.7	5.6	5.6	7.4	8.0	8.1	7.5	7.3	7.9	8.0	7.2	47.4	49.2	47.9	48.2	-0.7
S3	102.4	101.7	99.8	98.4	5.9	5.7	7.4	8.1	8.3	7.4	7.4	8.3	7.9	7.1	47.2	49.3	47.8	48.2	-0.4
S4	102.4	101.5	99.8	98.5	6.0	5.7	7.5	8.1	8.3	7.5	7.3	7.9	8.0	7.1	47.2	49.2	47.7	48.1	0.6
S5	102.1	101.5	99.5	98.5	5.9	5.7	7.5	8.1	8.1	7.4	7.4	7.8	7.9	7.2	47.2	49.0	47.9	47.9	0.0

TABLE 1.14

SPECIMEN	BL5
BUCKLING LENGHT	2,772.0
EXCENTRICITY	5.0

CROSS SECTION MEASUREMENTS																		
CROSS SECTION	B1	B2	H1	H2	W1	W2	T1	T2	T3	T4	T1'	T2'	T3'	T4'	Cbl	Cbr	Cfl	Cfr	I
S1	101.7	101.5	99.6	98.2	6.0	6.0	7.5	8.0	8.3	7.5	7.3	7.7	8.0	7.2	47.0	48.7	47.7	47.8	0.0
S2	101.8	101.5	99.6	98.5	5.6	5.7	7.3	8.3	8.1	7.4	7.2	7.8	7.9	7.1	47.4	48.8	47.8	48.0	0.8
S3	102.0	101.8	99.4	98.4	5.8	5.7	7.4	8.1	8.2	7.4	7.3	7.9	7.7	7.0	47.5	48.7	48.2	47.9	1.0
S4	102.1	101.8	99.5	98.3	5.7	5.5	7.4	8.1	8.0	7.3	7.2	7.6	7.8	7.0	47.3	49.1	48.0	48.3	0.3
S5	101.8	101.6	99.5	98.5	5.8	5.8	7.4	8.0	8.2	7.4	7.2	7.6	7.8	7.0	47.3	48.7	47.8	48.0	0.0

TABLE 1.15

SPECIMEN	CL5
BUCKLING LENGHT	2,771.0
EXCENTRICITY	5.0

CROSS SECTION MEASUREMENTS																		
CROSS SECTION	B1	B2	H1	H2	W1	W2	T1	T2	T3	T4	T1'	T2'	T3'	T4'	Cbl	Cbr	Cfl	Cfr	I
S1	102.0	101.8	99.2	99.4	6.2	5.8	7.7	8.4	8.4	7.7	7.1	7.9	7.9	7.3	48.1	47.7	47.3	48.7	0.0
S2	102.2	102.0	98.9	99.5	6.3	5.8	7.5	8.3	8.3	7.6	7.1	7.8	7.9	7.3	48.5	47.4	47.9	48.3	0.7
S3	102.3	102.0	98.8	99.6	6.0	5.7	7.6	8.3	8.2	7.6	7.1	7.9	7.7	7.2	48.9	47.4	47.9	48.4	0.8
S4	102.1	101.8	99.0	99.6	5.9	5.9	7.7	8.4	8.3	7.6	7.0	7.8	7.8	7.3	48.8	47.4	47.8	48.1	0.8
S5	102.2	101.9	98.8	99.7	6.2	6.0	7.7	8.4	8.5	7.7	7.0	7.8	7.9	7.5	48.9	47.1	47.9	48.0	0.0

TABLE 1.16

SPECIMEN	DL5
BUCKLING LENGHT	2,772.0
EXCENTRICITY	5.0

CROSS SECTION MEASUREMENTS																		
CROSS SECTION	B1	B2	H1	H2	W1	W2	T1	T2	T3	T4	T1'	T2'	T3'	T4'	Cbl	Cbr	Cfl	Cfr	I
S1	102.4	101.9	99.6	98.6	5.9	5.9	7.5	8.1	8.3	7.4	7.3	7.9	8.0	7.1	47.3	49.2	47.9	48.1	0.0
S2	102.4	102.0	99.8	98.5	5.8	5.8	7.5	8.1	8.3	7.5	7.3	7.8	8.0	7.0	47.4	49.2	48.1	48.1	0.8
S3	102.3	101.9	99.6	98.6	5.8	5.8	7.5	8.1	8.5	7.5	7.4	7.8	7.9	7.1	47.1	49.4	47.8	48.3	1.6
S4	102.4	101.6	99.8	98.7	5.9	5.7	7.5	8.2	8.3	7.5	7.4	7.9	8.0	7.1	47.1	49.4	47.8	48.1	0.8
S5	102.6	102.0	99.5	98.9	6.1	6.9	7.5	8.2	8.3	7.5	7.4	7.8	8.0	7.1	47.2	49.3	48.0	47.1	0.0

TABLE 1.17

SPECIMEN	AL6
BUCKLING LENGHT	3,510.0
EXCENTRICITY	5.0

CROSS SECTION MEASUREMENTS																		
CROSS SECTION	B1	B2	H1	H2	W1	W2	T1	T2	T3	T4	T1'	T2'	T3'	T4'	Cbl	Cbr	Cfl	Cfr	I
S1	102.4	101.8	98.7	99.5	5.7	5.9	7.5	8.2	8.1	7.5	7.1	7.9	7.8	7.3	49.6	47.1	48.1	47.8	0.0
S2	102.2	101.7	98.8	99.4	5.9	5.7	7.4	8.3	8.0	7.5	7.1	7.9	7.9	7.3	49.3	47.0	48.1	47.9	1.3
S3	102.1	101.4	98.7	99.6	5.9	5.5	7.4	8.2	8.1	7.4	7.1	7.8	7.8	7.4	49.1	47.1	48.0	47.9	1.0
S4	102.4	101.6	98.7	99.5	5.9	5.6	7.5	8.2	8.1	7.4	7.0	7.8	7.8	7.3	49.1	47.4	48.2	47.8	0.2
S5	102.5	101.8	99.1	98.8	6.0	5.8	7.5	8.2	8.0	7.5	7.1	7.8	7.8	7.3	48.9	47.6	48.4	47.6	0.0

TABLE 1.18

SPECIMEN	BL6
BUCKLING LENGHT	3,510.0
EXCENTRICITY	5.0

CROSS SECTION MEASUREMENTS																		
CROSS SECTION	B1	B2	H1	H2	W1	W2	T1	T2	T3	T4	T1'	T2'	T3'	T4'	Cbl	Cbr	Cfl	Cfr	I
S1	101.8	102.0	99.0	98.8	5.9	6.0	7.1	8.0	7.8	7.3	7.4	8.2	8.0	7.5	47.9	48.0	48.5	47.5	0.0
S2	101.9	102.1	98.4	99.3	5.8	5.9	7.0	7.8	7.7	7.2	7.3	8.2	8.1	7.4	47.9	48.2	48.7	47.5	1.4
S3	101.7	101.9	98.6	99.3	5.6	5.8	7.0	7.9	7.9	7.3	7.4	8.1	8.1	7.4	47.9	48.2	48.7	47.4	1.5
S4	101.6	101.8	98.5	99.7	5.8	6.8	7.0	7.9	7.8	7.2	7.5	8.2	8.2	7.5	47.8	48.0	47.7	47.3	0.5
S5	101.9	102.1	98.5	99.2	5.9	5.8	7.0	7.8	7.7	7.2	7.3	8.2	8.1	7.4	48.0	48.0	48.8	47.5	0.0

TABLE 1.19

SPECIMEN	CL6
BUCKLING LENGHT	3,510.0
EXCENTRICITY	5.0

CROSS SECTION MEASUREMENTS																		
CROSS SECTION	B1	B2	H1	H2	W1	W2	T1	T2	T3	T4	T1'	T2'	T3'	T4'	Cbl	Cbr	Cfl	Cfr	I
S1	101.8	102.3	99.2	98.6	6.1	6.2	7.2	8.0	8.0	7.3	7.5	8.2	8.2	7.4	48.1	47.6	48.6	47.5	0.0
S2	101.9	102.5	98.6	99.6	5.8	6.1	7.0	7.9	7.8	7.3	7.5	8.2	8.2	7.5	48.3	47.8	49.1	47.3	0.8
S3	101.7	102.3	98.9	99.7	5.9	6.1	7.1	8.0	7.9	7.4	7.5	8.3	8.2	7.6	48.1	47.7	49.2	47.0	1.8
S4	101.7	102.2	99.0	99.4	5.7	6.0	7.1	7.9	7.8	7.3	7.5	8.1	8.2	7.6	48.3	47.7	49.2	47.0	1.6
S5	101.8	102.3	98.7	99.5	5.7	5.8	7.1	7.9	8.0	7.3	7.4	8.1	8.2	7.5	48.1	48.0	49.2	47.3	0.0

TABLE 1.20

SPECIMEN	DL6
BUCKLING LENGHT	3,510.0
EXCENTRICITY	5.0

CROSS SECTION MEASUREMENTS																		
CROSS SECTION	B1	B2	H1	H2	W1	W2	T1	T2	T3	T4	T1'	T2'	T3'	T4'	Cbl	Cbr	Cfl	Cfr	I
S1	101.7	101.7	99.4	99.4	5.7	6.0	7.0	7.7	7.7	7.2	7.3	8.0	8.0	7.4	47.6	48.4	48.2	47.5	0.0
S2	101.7	101.7	99.0	99.3	5.7	5.4	7.0	7.8	7.6	7.2	7.4	8.0	8.0	7.3	47.8	48.2	48.7	47.6	0.5
S3	101.7	101.8	99.4	98.6	5.8	5.6	7.0	7.8	7.7	7.2	7.4	8.1	8.0	7.4	47.8	48.1	48.8	47.4	1.1
S4	101.6	101.7	99.0	99.6	5.7	5.8	7.2	7.9	7.7	7.2	7.4	8.3	8.0	7.4	47.6	48.3	48.5	47.4	0.6
S5	101.6	101.6	98.6	99.4	5.7	5.9	7.1	7.8	8.1	7.3	7.4	8.2	8.2	7.5	47.6	48.3	48.3	47.4	0.0

ANNEX 2:

2. LABEIN TESTS-RESIDUAL STRESSES MEASUREMENTS ON HOT ROLLED HE 100 A PROFILES

2.1 SPECIMENS

Residual stresses have been measured on five one meter length specimens marked as A, B, C, D and S. Each one of them were obtained from the same primary profile from which the specimens to be tested later were obtained.

On 29.03.93 the test specimens were received from ENSIDESA, cutted from five primary rolling lengths according to TABLE 2.1 below.

MAIN PROFILE	TEST SPECIMENS RECEIVED					
	FOR TESTING					FOR R.S. MEASUREMENT
	510 mm	1270	2020	2770	3520	1000 mm
A	1	1		1	1	1
B	1	1		1	1	1
C	1	1		1	1	1
D	1	1		1	1	1
S			5			1

TABLE 2.1

2.2 MEASUREMENT PROCEDURE

The slicing method has been chosen. Electrical strain gages have been used as measurement devices. These were set at the cross sections of each one meter length specimens (see FIGURE 2.1, FIGURE 2.2 and FIGURE 2.3).

The first step was to measure the resistance of the strain gages with a high accuracy digital Wheatstone bridge. The second step was to cut the one meter specimens to obtain 120 mm samples, which were later sliced to obtain thirteen "Unstrained" coupons (see FIGURE 2.1 FIGURE 2.2 and FIGURE 2.3).

The resistance of the gages was then remeasured in the third step to obtain the residual stresses as reported in the following pages.

The differences in resistance between first and second records give the residual stresses values reported.

In order to avoid interferences by temperature and other effects during measuring a precision resistance was used to calibrate the Wheatstone bridge and an identical strain gage was set on a strip with the same dimensions and material properties than the strips used for measurements. This permitted to correct temperature effects.

On specimen marked as A, strain gages were fastened in pairs on both sides of flanges and web. For the rests of the specimens strain gages were only set on one side (see FIGURE 2.2 and FIGURE 2.3)

For each strain gage four measurement were made in each step in order to obtain statistical data to calculate measurement uncertainty.

2.3 EQUIPMENT AND MEASURING CONDITIONS

STRAIN GAGES

MICRO-MEASUREMENTS DIVISION	: CEA-06-250 UW-350
RESISTANCE AT 24°C	: 350.0±0.3% Ω
GAGE FACTOR AT 24°C	: 2.085±0.5%
K_t	: +0.4±0.2%
ADHESIVE	: M-BOND 200
COAT	: M-COAT D

MEASUREMENT INSTRUMENT

HBM DMP39 precision Wheatstone bridge	: n/s 23905
CALIBRATION ERROR	: $\leq \pm 5.10^{-6}$
RESOLUTION FOR 350 Ω RANGE	: 10^{-4} Ω
UNCERTAINTY	: < 10^{-4} of measured value
CERTIFICATE	: LNE Dossier n° 2050058 DMI/16 27.05.92

RESISTANCE STANDARD

TETTEX 3276/KT	: n/s 132412
RESISTANCE AT 24°C	: 99.9999 Ω
UNCERTAINTY	: 8.4 ppm
CERTIFICATE	: Laboratorio Central Oficial de Electrotecnia. Dossier SCI 01975, 06.03.92

ENVIRONMENTAL CONDITIONS

TEMPERATURE	: 20±0.5°C
HUMIDITY	: 57±2%
CONDITIONING TIME	: 24 hours prior to making measurements.

2.4 CALCULATION PROCEDURE

$$\Delta R_{i1} = R'_{i1} - R_{i1}$$

$$\varepsilon_{i1} = \frac{\Delta R_{i1}}{R_{i1}} \cdot \frac{1}{K} \qquad K = gage\ factor$$

$$\sigma_{i1} = \varepsilon_{i1} \cdot E \qquad E = 205800\ N/mm^2$$

i = A1 to A24, B1 to B13, C1 to C13, D1 to D13 and S1 to S13.

$$\sigma_{imean} = \frac{\sum_{j=1}^{4} \sigma_{ij}}{4}$$

– Uncertainty:

The uncertainty of the standard was evaluated at 10^{-4} of the measured value for the complete measurement chain (including wheatstone bridge and standard resistor).

Uncertainty $\in$ 95 % confidence interval = U

$$U = \sqrt{U^2_{standard} + 4S^2_{n-1}(\sigma_1 \ldots \sigma_4)}$$

$U_{standard}$ = 2.85 X 10^{-4} % or $\pm$ 0.30 N/mm^2
S_{n-1} = Standard Deviation of measured values.

2.5 RESULTS

STRAIN GAGE	RESIDUAL STRESSES (N/mm²)					U (N/mm²)
	σ_1	σ_2	σ_3	σ_4	σ_{mean}	
A1	-30.80	-30.80	-29.79	-30.08	-30.37	1.06
A2	-7.35	-7.20	-7.20	-6.91	-7.17	0.47
A3	69.97	69.82	69.97	69.97	69.93	0.33
A4	-36.38	-36.52	-36.52	-36.52	-36.49	0.33
A5	-8.93	-8.93	-8.93	-8.79	-8.90	0.33
A6	-10.22	-10.22	-9.79	-9.79	-10.00	0.58
A7	-29.94	-29.80	-29.80	-29.80	-29.83	0.33
A8	-4.33	-4.18	-4.62	-4.18	-4.33	0.51
A9	-33.17	-33.31	-33.17	-33.17	-33.21	0.33
A10	30.14	29.99	29.56	29.70	29.85	0.60
A11	-10.09	-10.09	-10.09	-10.09	-10.09	0.30
A12	24.95	24.95	24.95	25.09	24.99	0.33
A13	9.94	10.23	10.23	9.94	10.09	0.45
A14	-8.21	-8.21	-8.21	-8.06	-8.17	0.33
A15	-3.74	-3.89	-3.60	-3.60	-3.71	0.41
A16	-10.07	-10.22	-10.07	-10.36	-10.18	0.41
A17	13.54	13.68	13.82	13.54	13.64	0.41
A18	-0.43	-0.43	-0.43	-0.29	-0.40	0.33
A19	7.63	7.77	7.77	7.77	7.74	0.33
A20	-31.66	-31.52	-31.66	-31.66	-31.63	0.33
A21	-20.85	-20.85	-20.85	-20.99	-20.88	0.33
A22	23.61	23.61	23.61	23.75	23.64	0.33
A23	17.57	17.43	17.72	17.72	17.61	0.41
A24	-15.97	-15.97	-15.82	-15.82	-15.90	0.34

Specimen A

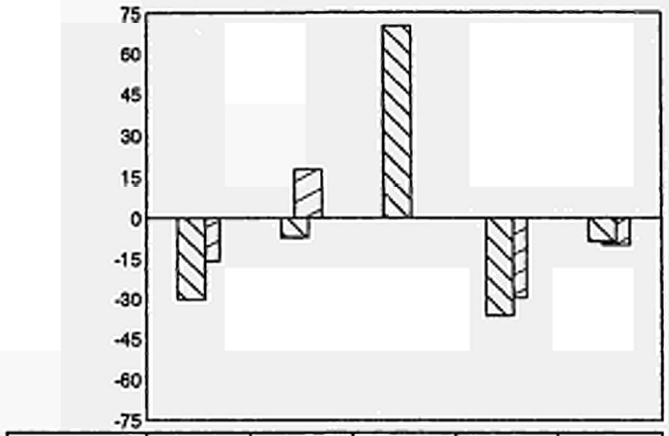

EXTERIOR	-30,37	-7,17	69,93	-36,49	-8,9
INTERIOR	-15,9	17,61		-29,83	-10

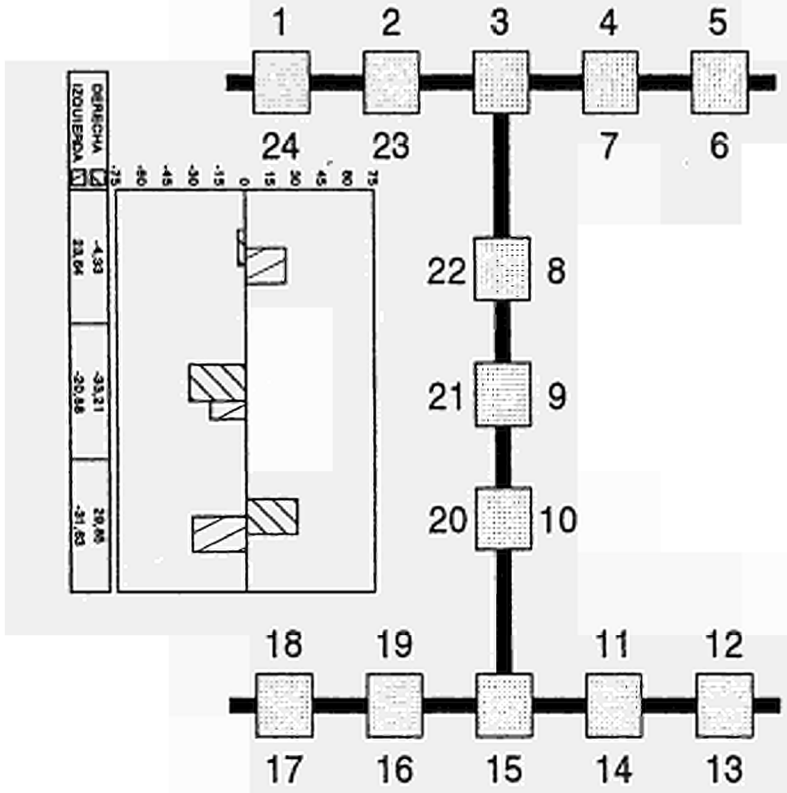

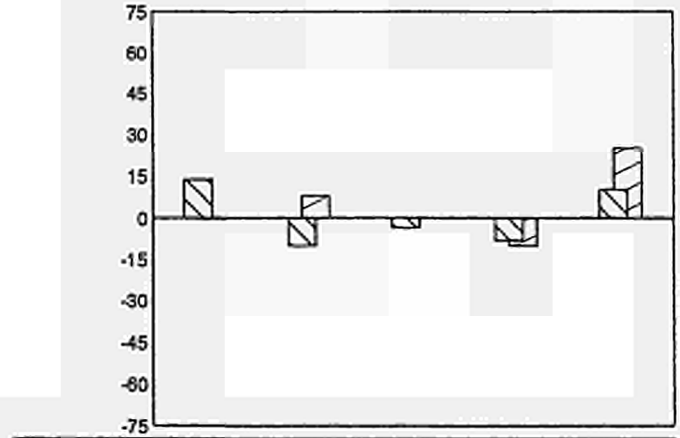

EXTERIOR	13,64	-10,18	-3,71	-8,17	10,09
INTERIOR	-0,4	7,74		-10,09	24,99

STRAIN GAGE	RESIDUAL STRESSES (N/mm²)					U (N/mm²)
	σ_1	σ_2	σ_3	σ_4	σ_{mean}	
B1	-8.20	-8.49	-8.35	-8.64	-8.42	0.48
B2	-8.93	-8.93	-8.93	-8.93	-8.93	0.30
B3	21.73	21.73	21.73	21.73	21.73	0.30
B4	-4.75	-4.75	-4.46	-4.75	-4.68	0.42
B5	14.39	14.68	14.54	14.54	14.54	0.38
B6	44.87	44.87	44.87	44.73	44.84	0.33
B7	-13.10	-13.10	-13.10	-12.81	-13.03	0.42
B8	25.90	25.90	25.75	25.75	25.82	0.34
B9	-6.62	-6.48	-6.48	-6.48	-6.51	0.33
B10	-29.23	-29.08	-29.08	-29.23	-29.15	0.34
B11	49.22	49.22	49.22	49.22	49.22	0.30
B12	-1.01	-1.15	-1.01	-1.15	-1.08	0.34
B13	-7.63	-7.20	-6.91	-7.05	-7.20	0.69

Specimen B

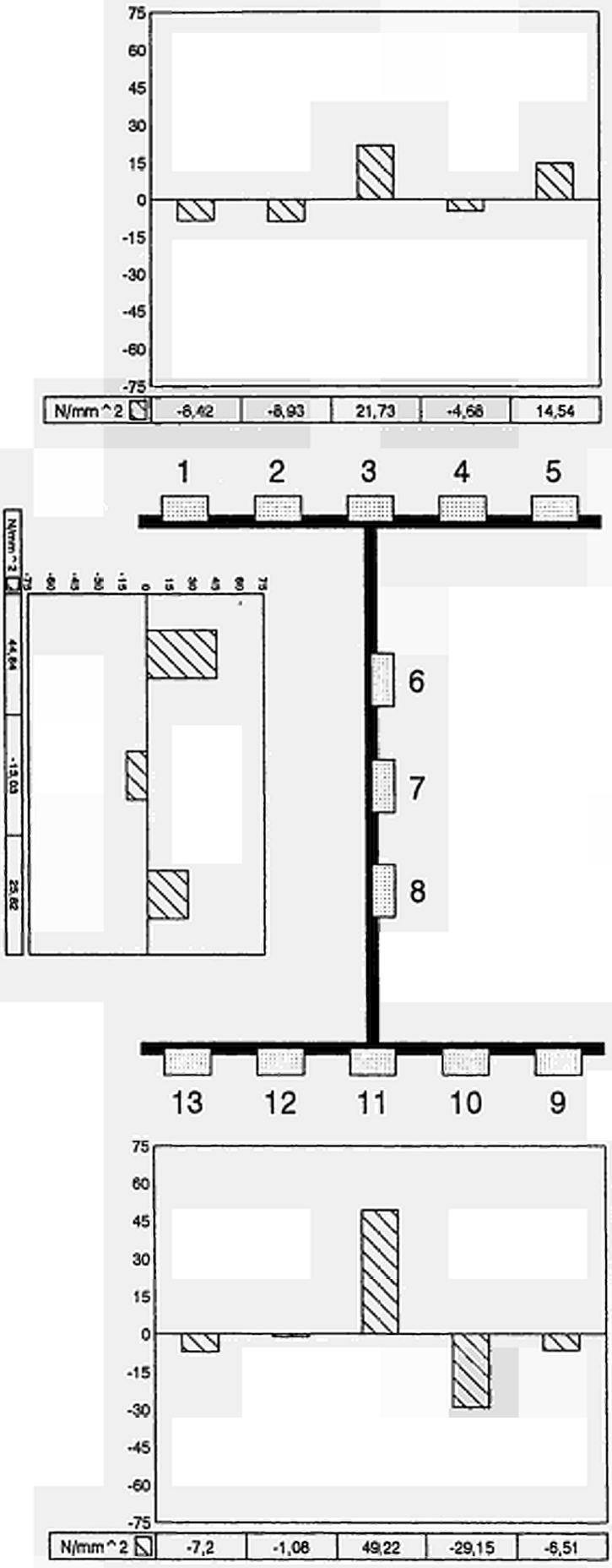
75
60
45
30
15
0
-15
-30
-45
-60
-75
N/mm^2
-6,42
-8,93
21,73
-4,68
14,54
1
2
3
4
5
6
7
8
13
12
11
10
9
N/mm^2
44,84
-13,03
25,82
-7,2
-1,08
49,22
-29,15
-6,51

STRAIN GAGE	RESIDUAL STRESSES (N/mm²)					U (N/mm²)
	σ_1	σ_2	σ_3	σ_4	σ_{mean}	
C1	10.94	10.94	10.79	10.79	10.86	0.34
C2	0.72	0.86	0.72	0.72	0.76	0.33
C3	4.03	3.89	3.74	3.74	3.85	0.41
C4	-4.32	-4.32	-4.32	-4.32	-4.32	0.30
C5	16.86	16.86	16.86	16.86	16.86	0.30
C6	-64.21	-64.35	-63.78	-63.63	-63.99	0.75
C7	-20.44	-20.44	-20.58	-20.30	-20.44	0.38
C8	-5.04	-5.04	-5.18	-8.20	-5.87	3.12
C9	-27.63	-27.78	-27.63	-27.63	-27.67	0.33
C10	-3.17	-3.31	-3.17	-3.17	-3.21	0.33
C11	74.13	74.13	74.13	74.13	74.13	0.30
C12	-26.62	-26.76	-26.76	-26.76	-26.73	0.33
C13	-0.58	-0.58	-0.58	-0.29	-0.50	0.42

Specimen C

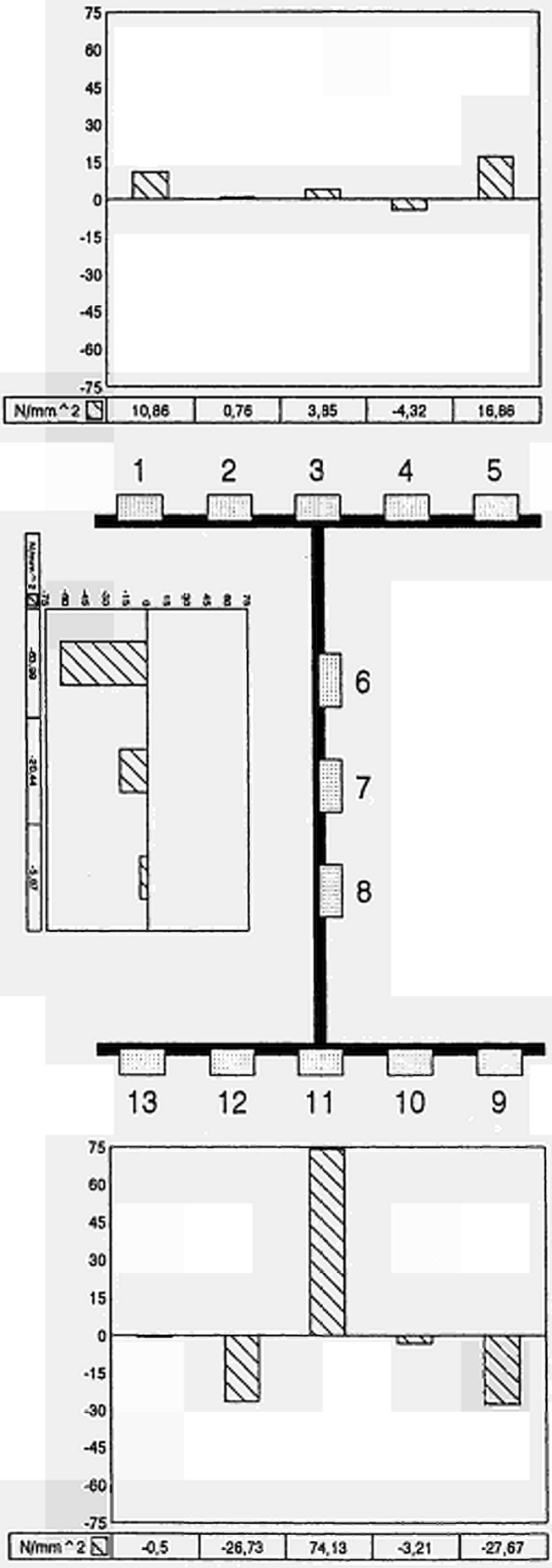
75
60
45
30
15
0
-15
-30
-45
-60
-75
N/mm^2
10,86
0,76
3,85
-4,32
16,86
1
2
3
4
5
6
7
8
13
12
11
10
9
N/mm^2
-0,5
-26,73
74,13
-3,21
-27,67

STRAIN GAGE	RESIDUAL STRESSES (N/mm²)					U (N/mm²)
	σ_1	σ_2	σ_3	σ_4	σ_{mean}	
D1	-8.94	-9.37	-9.37	-9.37	-9.26	0.52
D2	-41.22	-41.51	-41.51	-41.22	-41.37	0.45
D3	69.92	69.92	69.92	69.78	69.88	0.33
D4	-1.58	-1.73	-1.58	-1.73	-1.66	0.34
D5	-23.92	-23.92	-23.63	-23.78	-23.81	0.41
D6	3.03	3.03	3.03	3.17	3.06	0.33
D7	-18.17	-18.17	-18.32	-18.32	-18.24	0.34
D8	-38.20	-38.20	-38.20	-38.48	-38.27	0.42
D9	9.07	9.36	9.50	9.36	9.32	0.47
D10	1.01	1.15	1.01	1.15	1.08	0.34
D11	-3.46	-3.46	-3.60	-3.46	-3.49	0.33
D12	-4.32	-4.61	-4.46	-4.89	-4.57	0.57
D13	24.47	24.18	24.18	24.18	24.25	0.41

Specimen D

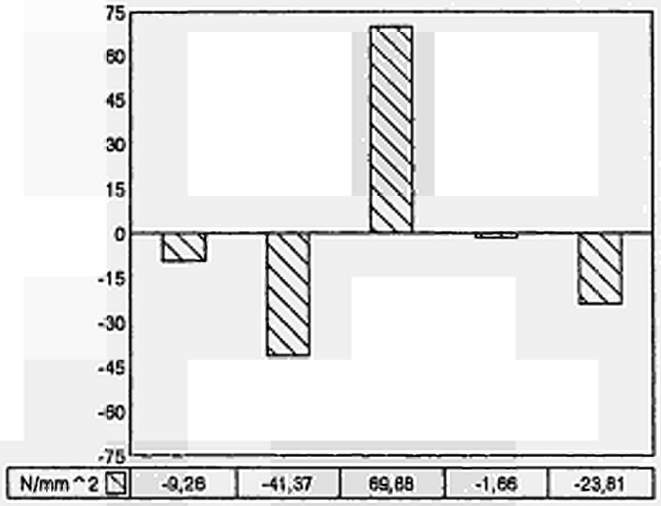
75
60
45
30
15
0
-15
-30
-45
-60
-75
N/mm^2
-9,26
-41,37
69,88
-1,66
-23,81

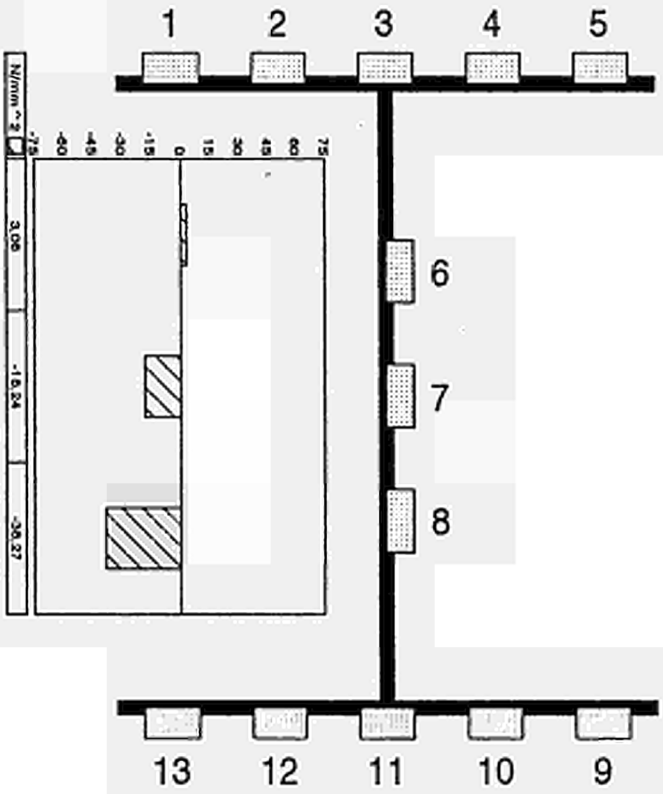
1
2
3
4
5
6
7
8
N/mm^2
3,06
-16,24
-36,27

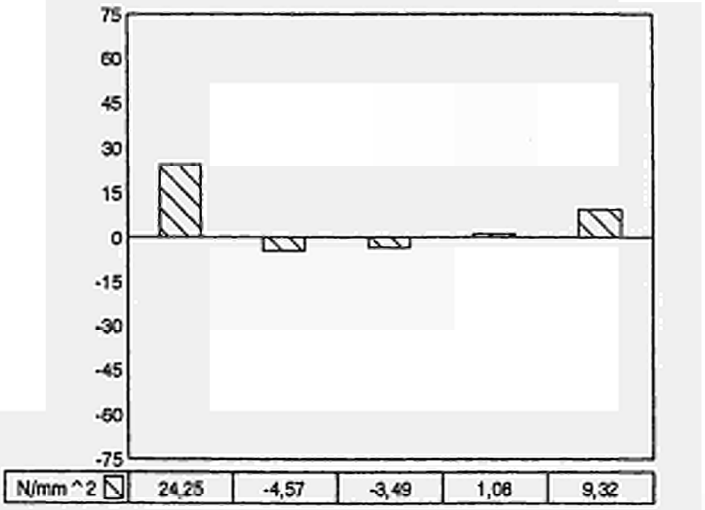
13
12
11
10
9

75
60
45
30
15
0
-15
-30
-45
-60
-75
N/mm^2
24,25
-4,57
-3,49
1,08
9,32

STRAIN GAGE	RESIDUAL STRESSES (N/mm²)					U (N/mm²)
	σ_1	σ_2	σ_3	σ_4	σ_{mean}	
S1	-13.25	-13.39	-13.25	-12.96	-13.21	0.47
S2	-10.94	-10.94	-10.94	-10.65	-10.87	0.41
S3	33.85	33.71	33.85	33.85	33.82	0.33
S4	-11.09	-10.80	-10.94	-10.80	-10.91	0.41
S5	-8.20	-8.34	-8.49	-8.49	-8.38	0.41
S6	32.40	32.11	31.96	31.96	32.11	0.50
S7	-31.54	-31.68	-31.25	-31.54	-31.50	0.47
S8	-23.91	-23.91	-23.91	-23.63	-23.84	0.42
S9	-25.08	-25.08	-25.08	-25.08	-25.08	0.30
S10	6.19	6.05	6.19	5.90	6.08	0.41
S11	19.03	19.03	18.88	19.03	18.99	0.33
S12	-30.68	-30.54	-30.54	-30.68	-30.61	0.34
S13	34.69	34.69	34.83	35.12	34.83	0.50

Specimen S

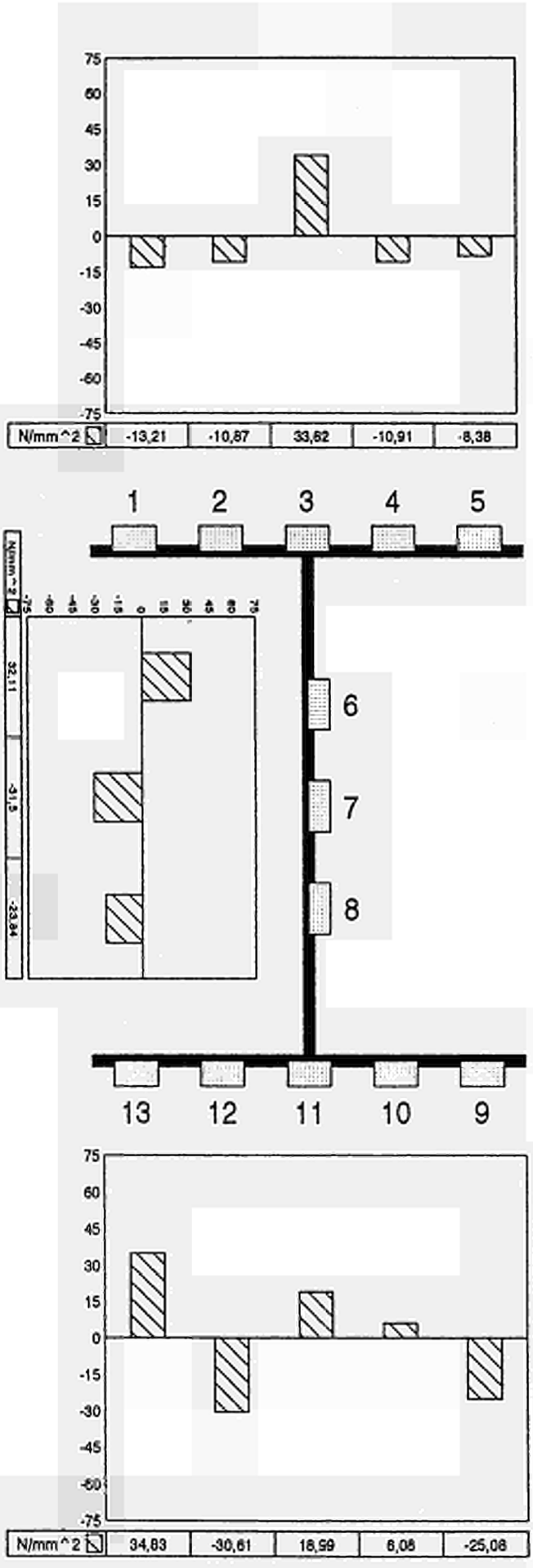
75
60
45
30
15
0
-15
-30
-45
-60
-75
N/mm^2
-13,21
-10,87
33,62
-10,91
-8,38
1
2
3
4
5
6
7
8
13
12
11
10
9
32,11
-31,5
-23,84
34,83
-30,61
16,99
6,08
-25,08

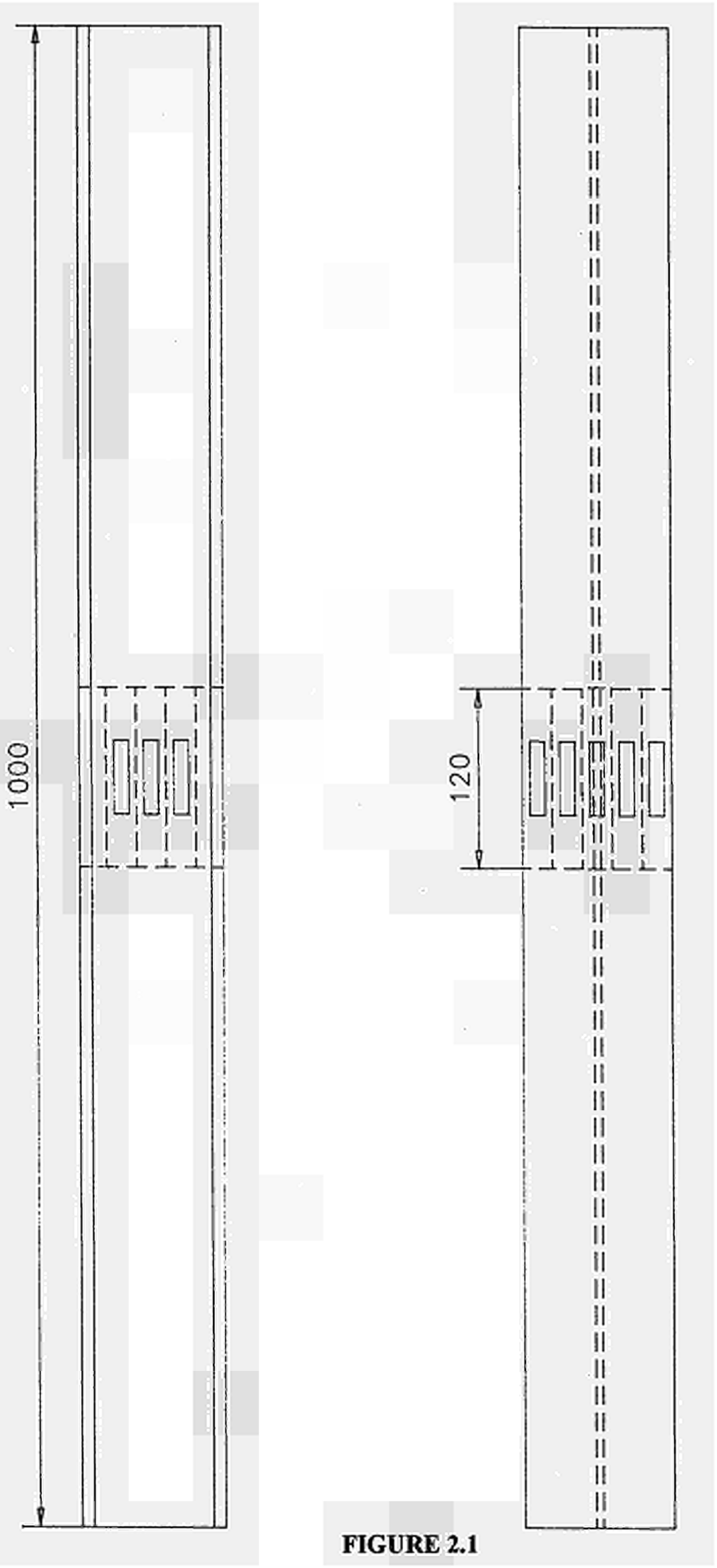

FIGURE 2.1

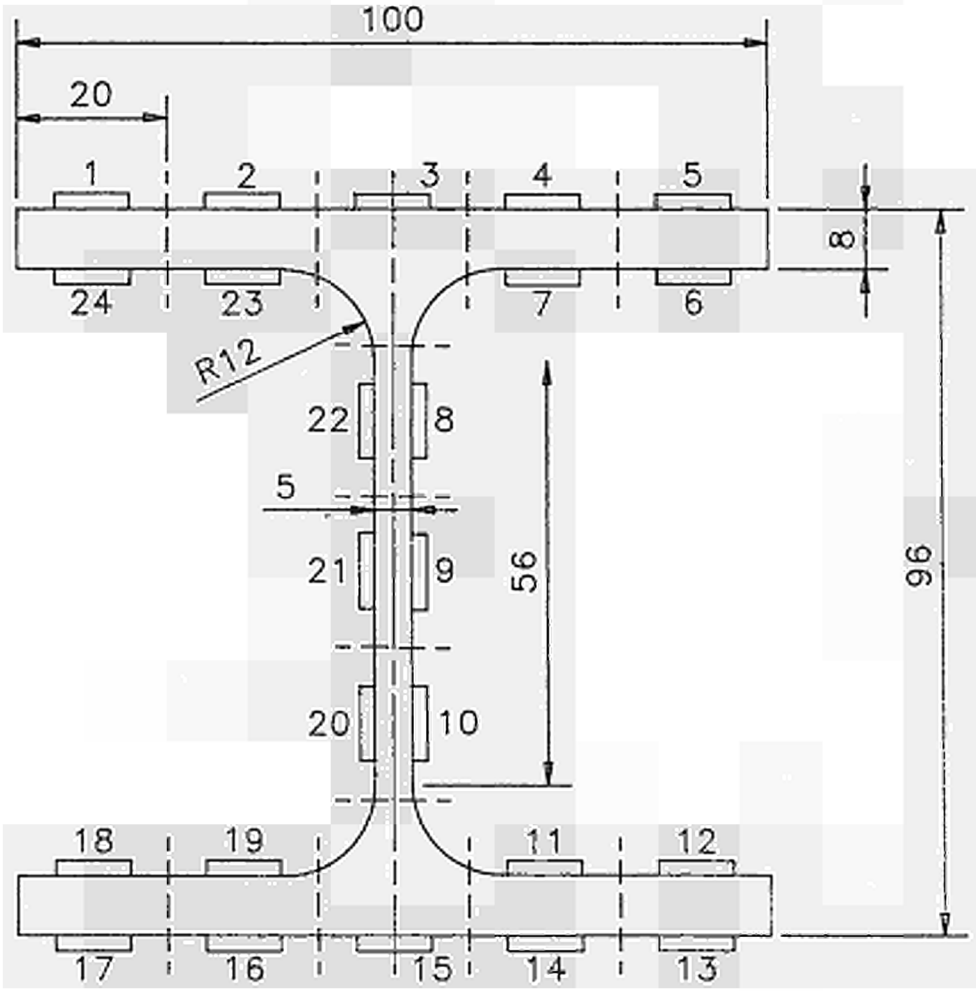

STRAIN GAGES IN SPECIMEN A

FIGURE 2.2

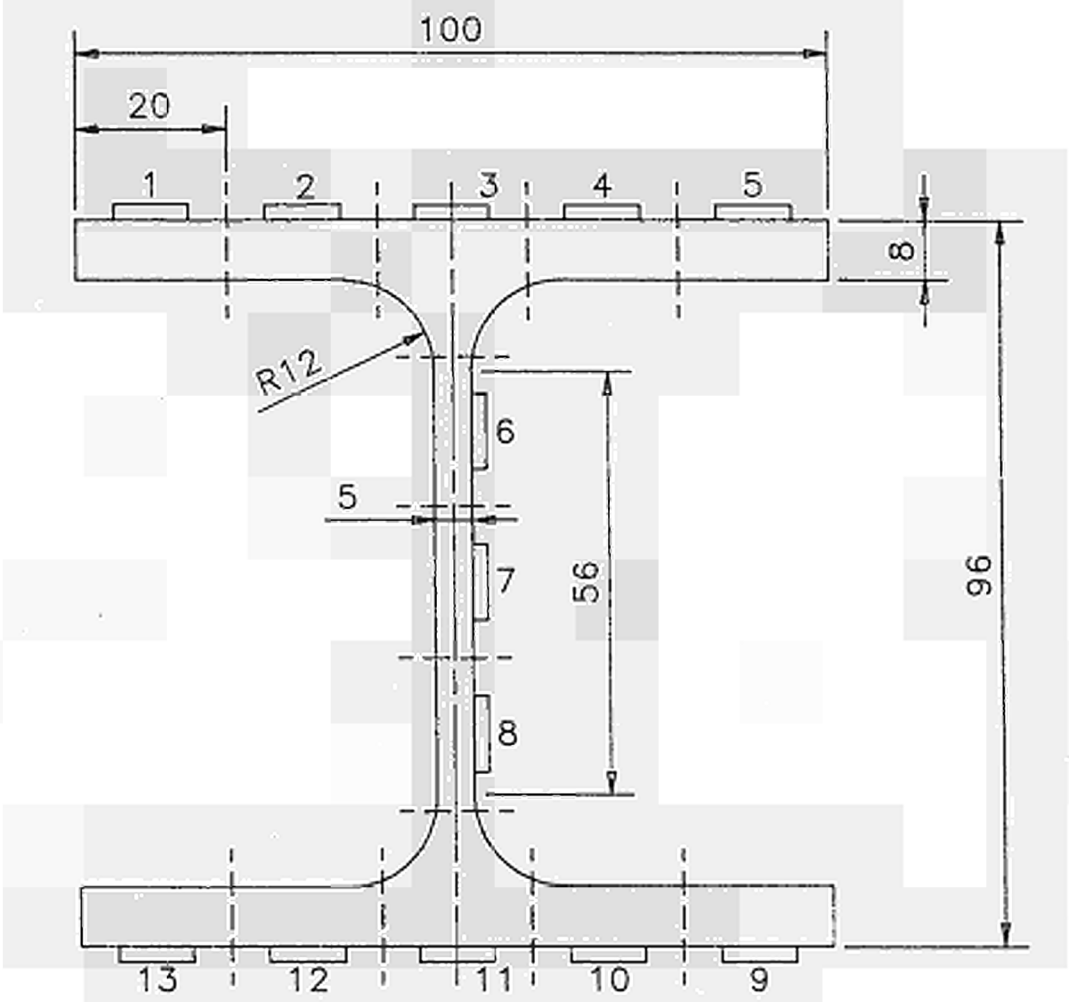

STRAIN GAGES IN SPECIMENS B, C, D AND S

FIGURE 2.3

ANNEX 3:

3. LABEIN TESTS - MECHANICAL PROPERTIES OF STEEL

ENSIDESA AVILES	INSPECCION DE PRODUCTOS/E.MECANICOS	4/3/93
	Muestras de PERFIL Para PROYECTO"CURVAS DE PANDEO DE VIGAS SOMETIDAS AL FUEGO" Enviadas por D. BENJAMIN FERNANDEZ	

MUESTRA		PERFIL HEA 100					
COLADA		223892					
CALIDAD		A-42b					
PROBETA		200x25	200x25	200x25	200x25	200x25	200x25
DENOMINACION		AM1	AM2	AM3	AL1	AL2	AL3
ORIENTACION		ALMA	ALMA	ALMA	ALA	ALA	ALA
ESPESOR (mm)		6.0	6.0	6.0	7.0	7.1	7.0
ANCHO (mm)		25.0	25.0	25.0	25.0	25.0	25.0
LONGITUD (mm)		200.0	200.0	200.0	200.0	200.0	200.0
LONGITUD FINAL(mm)		256.0	252.0	252.0	252.0	253.0	255.0
LIMITE ELASTICO 0,2%	Kg.	4.656	4.560	4.560	5.040	5.088	4.920
	MPa	304.5	298.2	298.2	282.5	281.2	275.8
CARGA DE ROTURA	Kg	6.900	6.780	6.760	7.840	8.020	7.820
	MPa	451.3	443.4	442.1	439.5	443.2	438.4
ALARGAMIENTO %		28.0	26.0	26.0	26.0	26.5	27.5
ESPESOR FINAL (mm)		3.4	3.6	3.2	4.1	4.5	4.3
ANCHO FINAL (mm)		17.7	18.0	18.0	17.0	17.0	17.0
Σ %		59.9	56.8	57.6	60.2	56.9	58.2

VoBo	Observaciones: MAIN PROFILE A	

ENSIDESA AVILES	INSPECCION DE PRODUCTOS/E.MECANICOS	4/3/93
	Muestras de PERFIL Para PROYECTO"CURVAS DE PANDEO DE VIGAS SOMETIDAS AL FUEGO" Enviadas por D. BENJAMIN FERNANDEZ	

MUESTRA		PERFIL HEA 100					
COLADA		223892					
CALIDAD		A-42b					
PROBETA		200x25	200x25	200x25	200x25	200x25	200x25
DENOMINACION		BM1	BM2	BM3	BL1	BL2	BL3
ORIENTACION		ALMA	ALMA	ALMA	ALA	ALA	ALA
ESPESOR (mm)		5.9	5.9	5.9	7.1	7.1	7.0
ANCHO (mm)		25.0	25.0	25.0	25.0	25.0	25.0
LONGITUD (mm)		200.0	200.0	200.0	200.0	200.0	200.0
LONGITUD FINAL(mm)		248.0	255.0	257.0	258.0	255.0	256.0
LIMITE ELASTICO 0,2%	Kg.	4.464	4.560	4.512	5.256	5.136	5.088
	MPa	296.9	303.3	300.1	290.5	283.8	285.2
CARGA DE ROTURA	Kg	6.760	6.840	6.840	8.020	8.040	7.980
	MPa	449.6	454.9	454.9	443.2	444.3	447.3
ALARGAMIENTO %		24.0	27.5	28.5	29.0	27.5	28.0
ESPESOR FINAL (mm)		3.3	3.3	3.5	4.4	4.3	4.2
ANCHO FINAL (mm)		18.0	17.5	17.5	17.0	17.0	17.5
Σ %		59.7	60.8	58.4	57.8	58.2	58.0

VºBº	Observaciones: MAIN PROFILE B	

ENSIDESA AVILES	INSPECCION DE PRODUCTOS/E.MECANICOS	4/3/93
	Muestras de PERFIL Para PROYECTO"CURVAS DE PANDEO DE VIGAS SOMETIDAS AL FUEGO" Enviadas por D. BENJAMIN FERNANDEZ	

MUESTRA		PERFIL HEA 100					
COLADA		223892					
CALIDAD		A-42b					
PROBETA		200x25	200x25	200x25	200x25	200x25	200x25
DENOMINACION		CM1	CM2	CM3	CL1	CL2	CL3
ORIENTACION		ALMA	ALMA	ALMA	ALA	ALA	ALA
ESPESOR (mm)		6.2	6.1	6.1	7.1	7.0	7.5
ANCHO (mm)		25.0	25.0	25.0	25.0	25.0	25.0
LONGITUD (mm)		200.0	200.0	200.0	200.0	200.0	200.0
LONGITUD FINAL(mm)		253.0	252.0	254.0	252.0	257.0	250.0
LIMITE ELASTICO 0,2%	Kg.	5.328	4.752	4.752	5.376	5.376	5.328
	MPa	337.2	305.7	305.7	297.1	301.4	278.8
CARGA DE ROTURA	Kg	7.240	6.960	6.960	8.100	8.120	8.540
	MPa	458.2	447.7	447.4	447.7	455.2	446.8
ALARGAMIENTO %		26.5	26.0	27.0	26.0	28.5	25.0
ESPESOR FINAL (mm)		3.7	3.7	4.0	4.7	4.8	4.8
ANCHO FINAL (mm)		17.5	17.5	17.2	17.0	17.2	17.0
Σ %		58.2	57.5	54.9	55.0	52.8	56.5

VoBo	Observaciones: MAIN PROFILE C	

ENSIDESA AVILES	INSPECCION DE PRODUCTOS/E.MECANICOS	1/3/93
	Muestras de PERFIL . Para PROYECTO"CURVAS DE PANDEO DE VIGAS SOMETIDAS AL FUEGO" Enviadas por D. BENJAMIN FERNANDEZ	

MUESTRA		PERFIL HEA 100					
COLADA		223892					
CALIDAD		A-42b					
PROBETA		200x25	200x25	200x25	200x25	200x25	200x25
DENOMINACION		DM1	DM2	DM3	DL1	DL2	DL3
ORIENTACION		ALMA	ALMA	ALMA	ALA	ALA	ALA
ESPESOR (mm)		6.1	6.1	6.1	7.1	7.1	7.1
ANCHO (mm)		25.0	25.0	25.0	25.0	25.0	25.0
LONGITUD (mm)		200.0	200.0	200.0	200.0	200.0	200.0
LONGITUD FINAL(mm)		252.0	253.0	255.0	252.0	255.0	254.0
LIMITE ELASTICO 0,2%	Kg.	4.800	4.752	4.848	5.112	5.088	5.136
	MPa	308.8	305.7	311.9	282.5	281.2	283.8
CARGA DE ROTURA	Kg	6.920	6.820	6.840	7.980	8.080	8.120
	MPa	445.1	438.7	440.0	441.0	446.6	448.8
ALARGAMIENTO %		26.0	26.5	27.5	26.0	27.5	27.0
ESPESOR FINAL (mm)		4.2	3.9	4.0	4.5	4.6	4.8
ANCHO FINAL(mm)		17.6	17.5	17.4	17.0	17.2	17.0
Σ %		51.5	55.2	54.4	56.9	55.4	54.0

VºBº	Observaciones: MAIN PROFILE D

ENSIDESA AVILES	INSPECCION DE PRODUCTOS/E.MECANICOS	8/3/93
	Muestras de PERFIL Para PROYECTO"CURVAS DE PANDEO DE VIGAS SOMETIDAS AL FUEGO" Enviadas por D. BENJAMIN FERNANDEZ	

MUESTRA		PERFIL HEA 100					
COLADA		223892					
CALIDAD		A-42b					
PROBETA		200x25	200x25		200x25	200x25	
DENOMINACION		SM1	SM1		SL1	SL2	
ORIENTACION		ALMA	ALMA		ALA	ALA	
ESPESOR (mm)		6.0	6.0		7.1	7.1	
ANCHO (mm)		25.0	25.0		25.0	25.0	
LONGITUD (mm)		200.0	200.0		200.0	200.0	
LONGITUD FINAL(mm)		254.0	261.0		254.0	252.0	
LIMITE ELASTICO 0,2%	Kg.	4.320	4.440		5.040	5.088	
	MPa	282.5	290.4		278.5	281.2	
CARGA DE ROTURA	Kg	6.760	6.740		8.040	8.080	
	MPa	442.4	440.5		444.4	446.4	
ALARGAMIENTO %		27.0	30.5		27.0	26.0	
ESPESOR FINAL (mm)		4.2	4.1		4.4	4.2	
ANCHO FINAL (mm)		17.9	17.0		17.0	16.5	
Σ %		49.8	53.5		57.8	60.9	

VºBº	Observaciones: MAIN PROFILE S

ANNEX 4:

4. LABEIN TESTS-MEASUREMENTS DONE DURING TESTING (APPLIED LOAD, VERTICAL DISPLACEMENTS, HORIZONTAL DEFLECTION AT MID-HEIGHT)

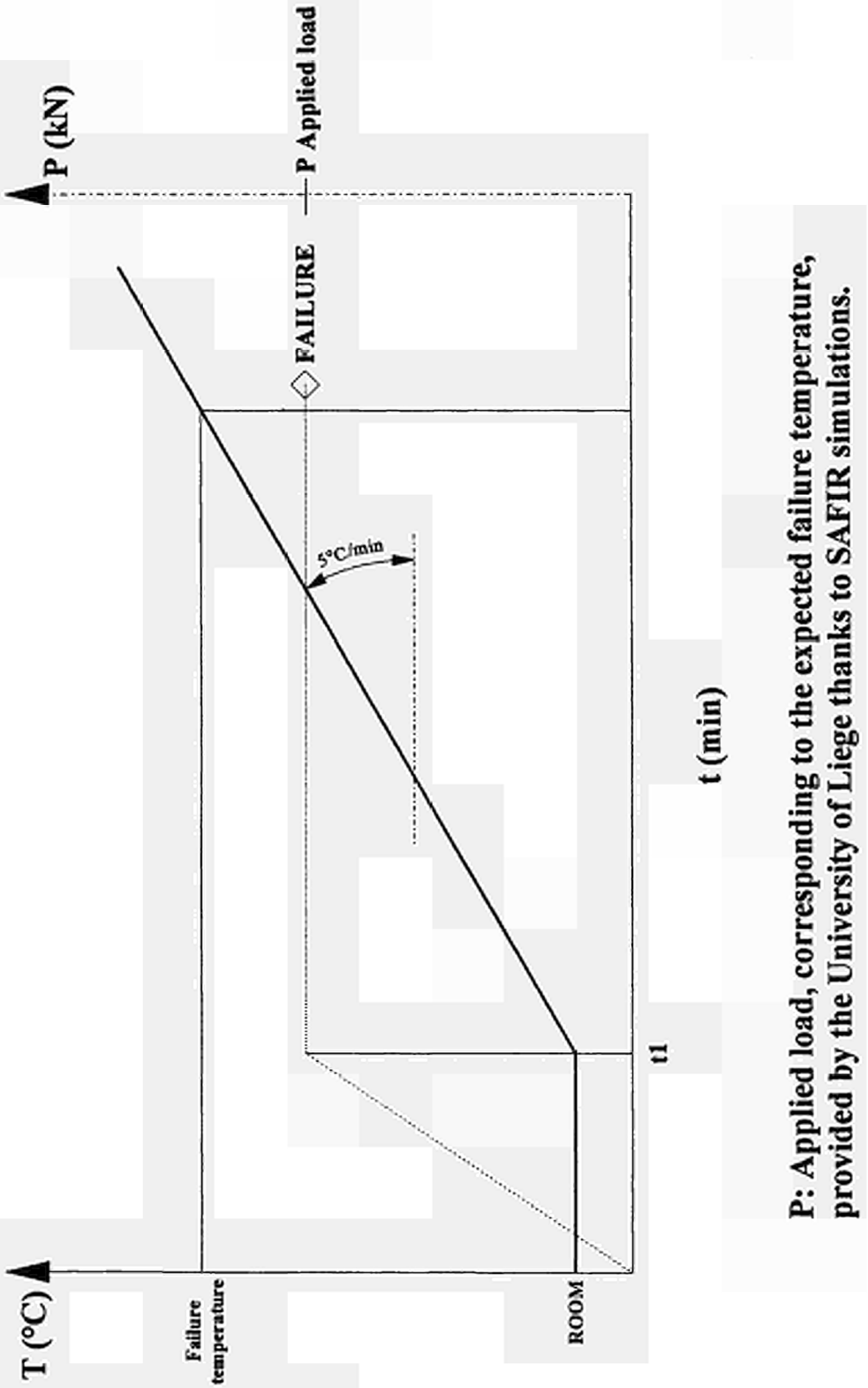

FIGURE 4.1 Procedure for hot tests

FIGURE 4.2 End conditions

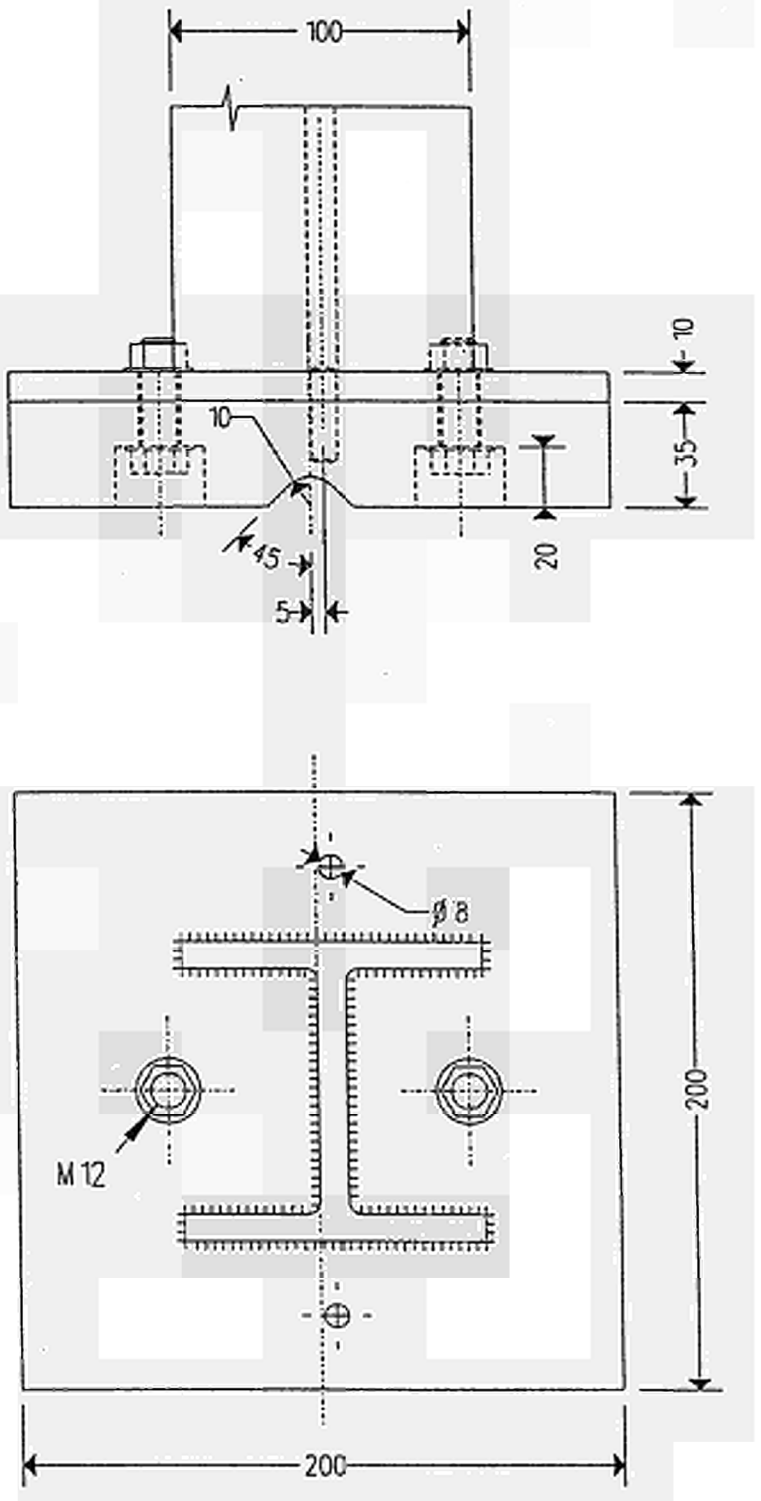

FIGURE 4.3 Thermocouples and resistors distribution for 510 mm length specimens

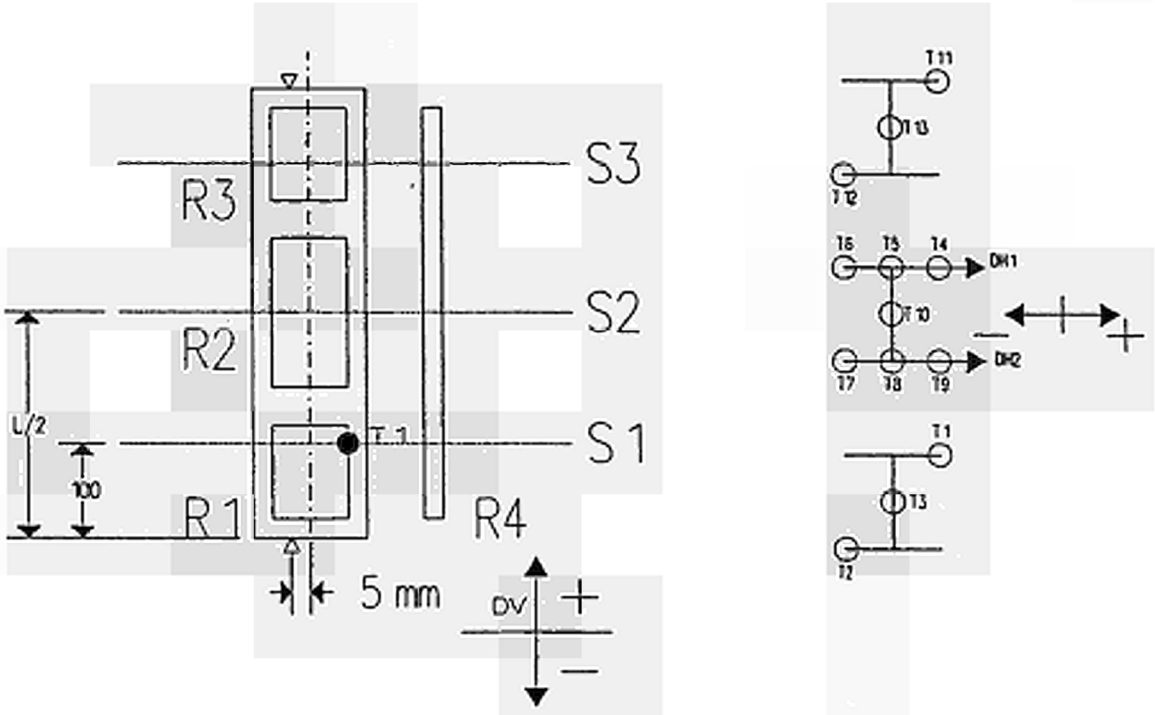

FIGURE 4.4 SPECIMEN AL1 (cold test)

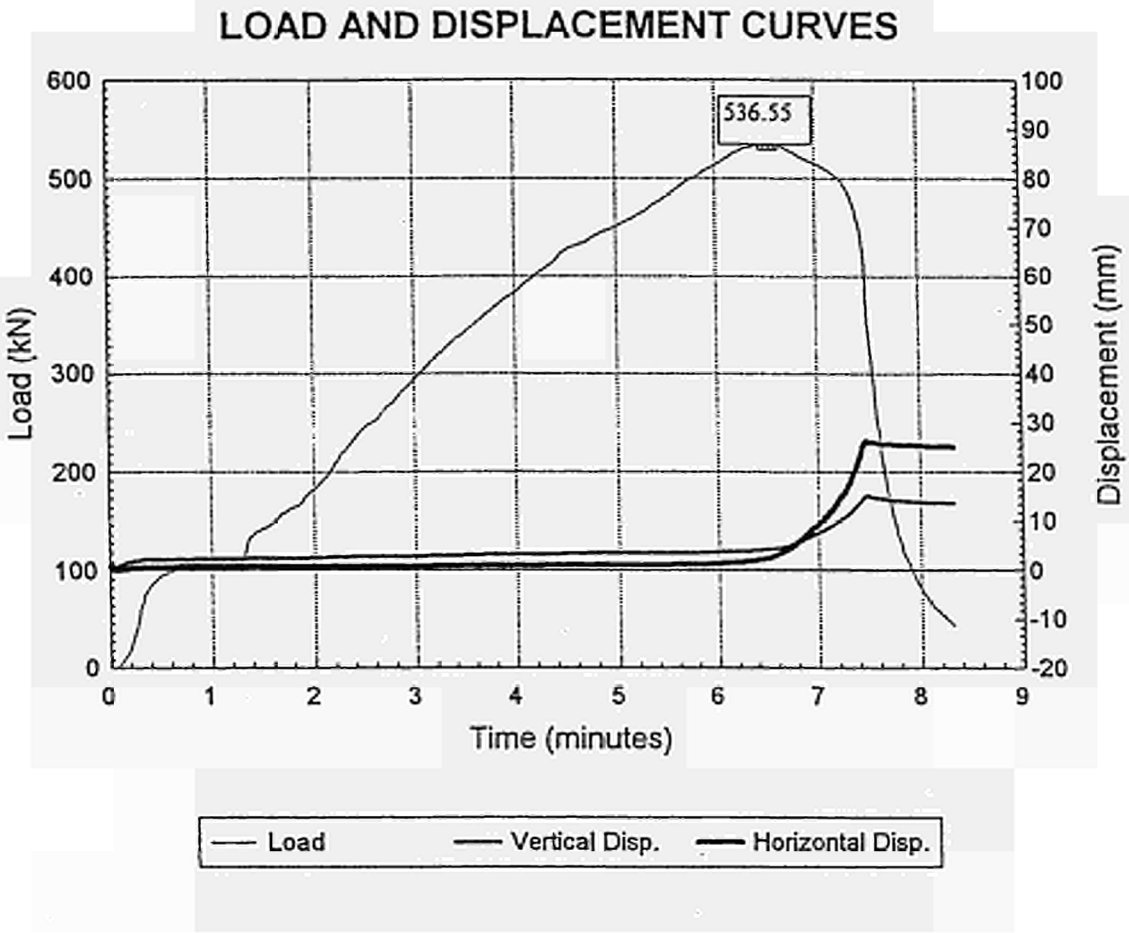

FIGURE 4.5 SPECIMEN BL1

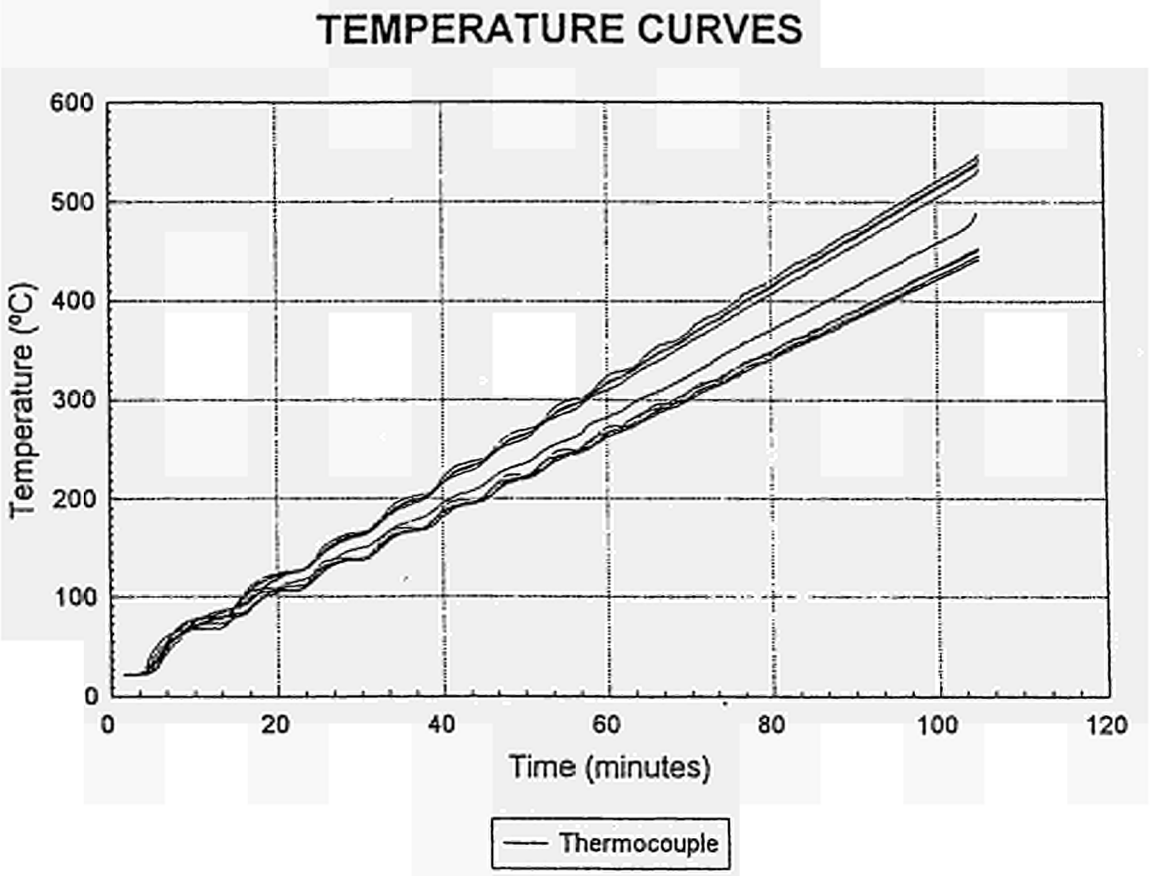

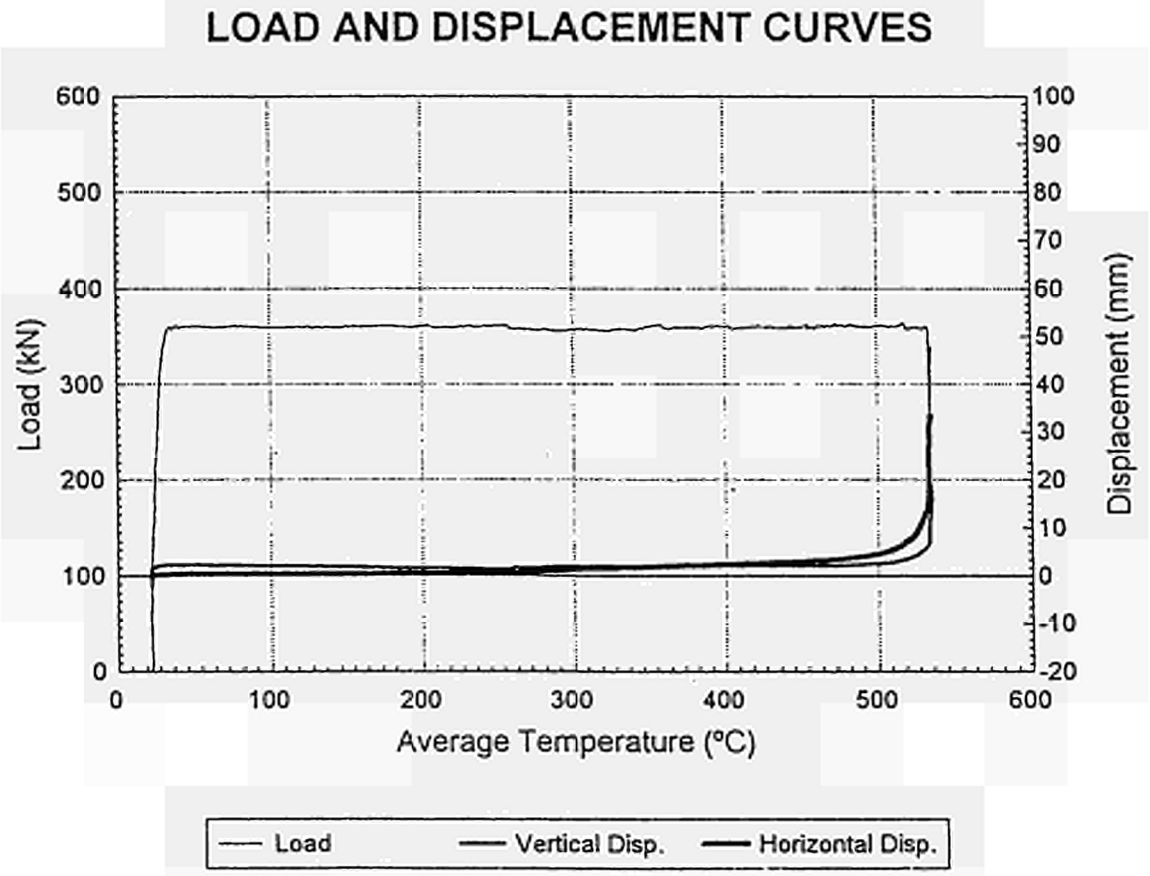

FIGURE 4.6 SPECIMEN CL1

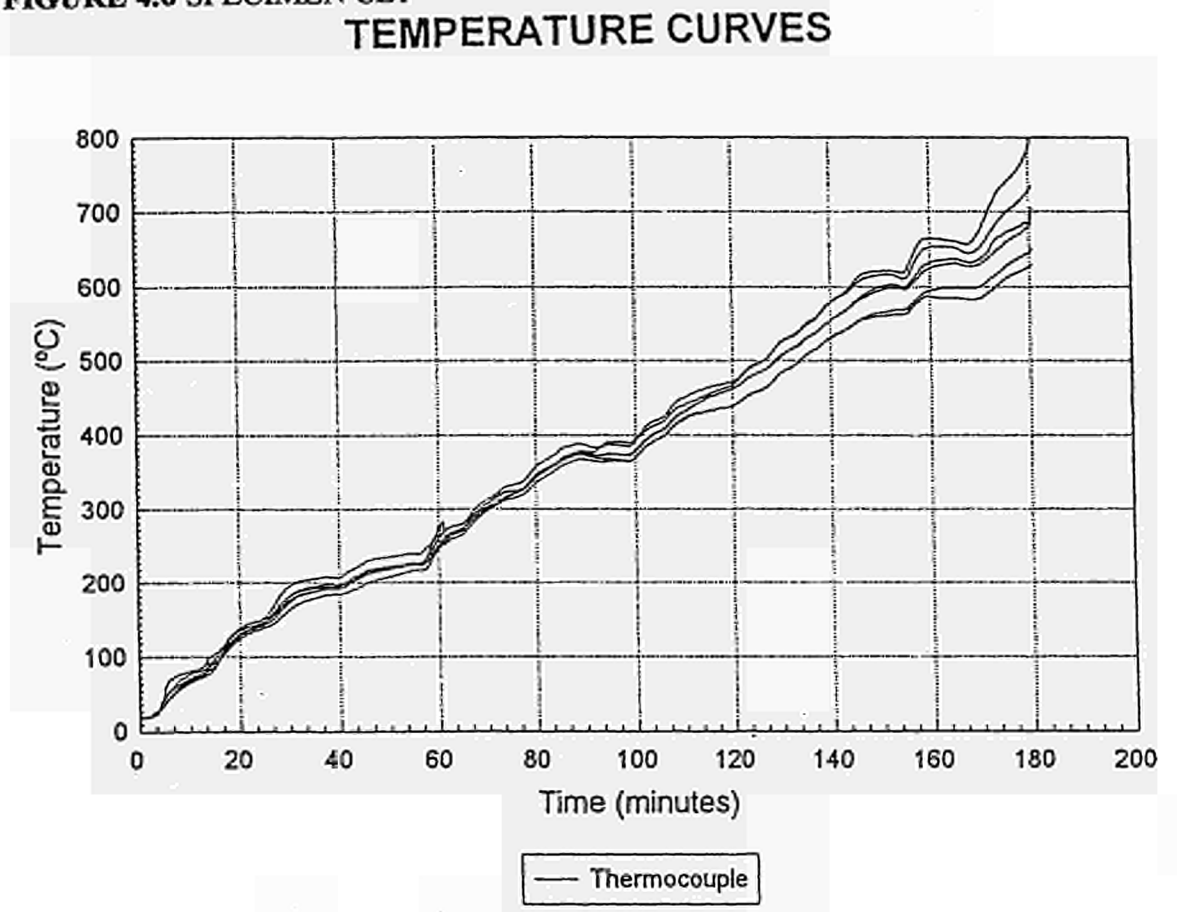

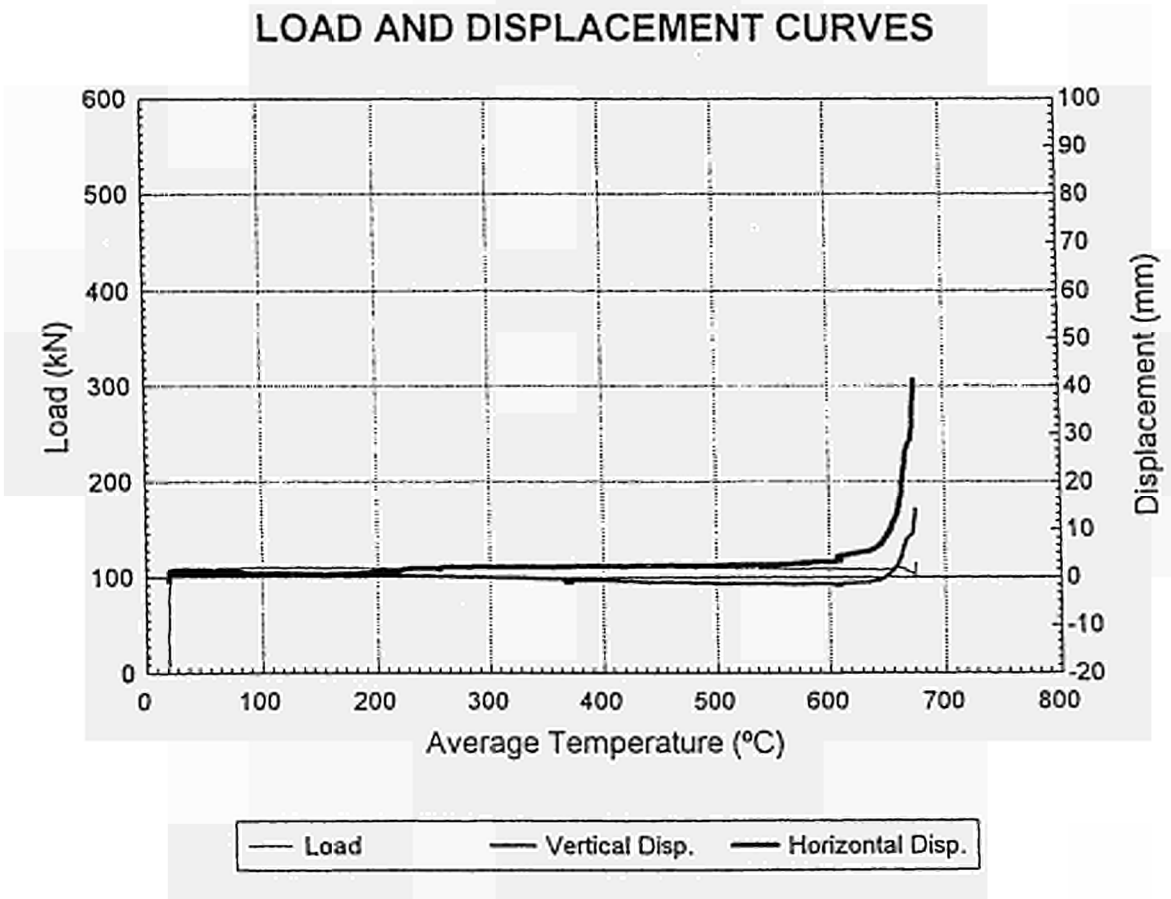

FIGURE 4.7 SPECIMEN DL1

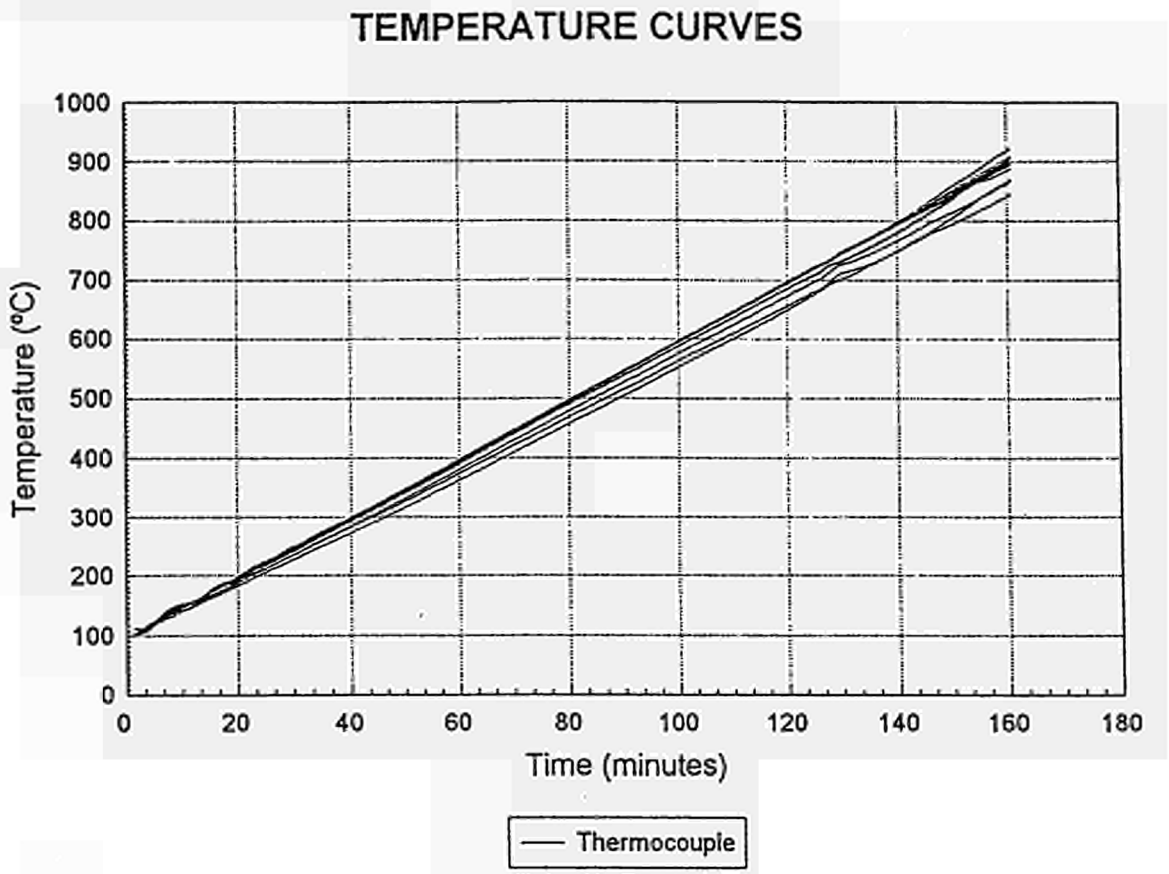

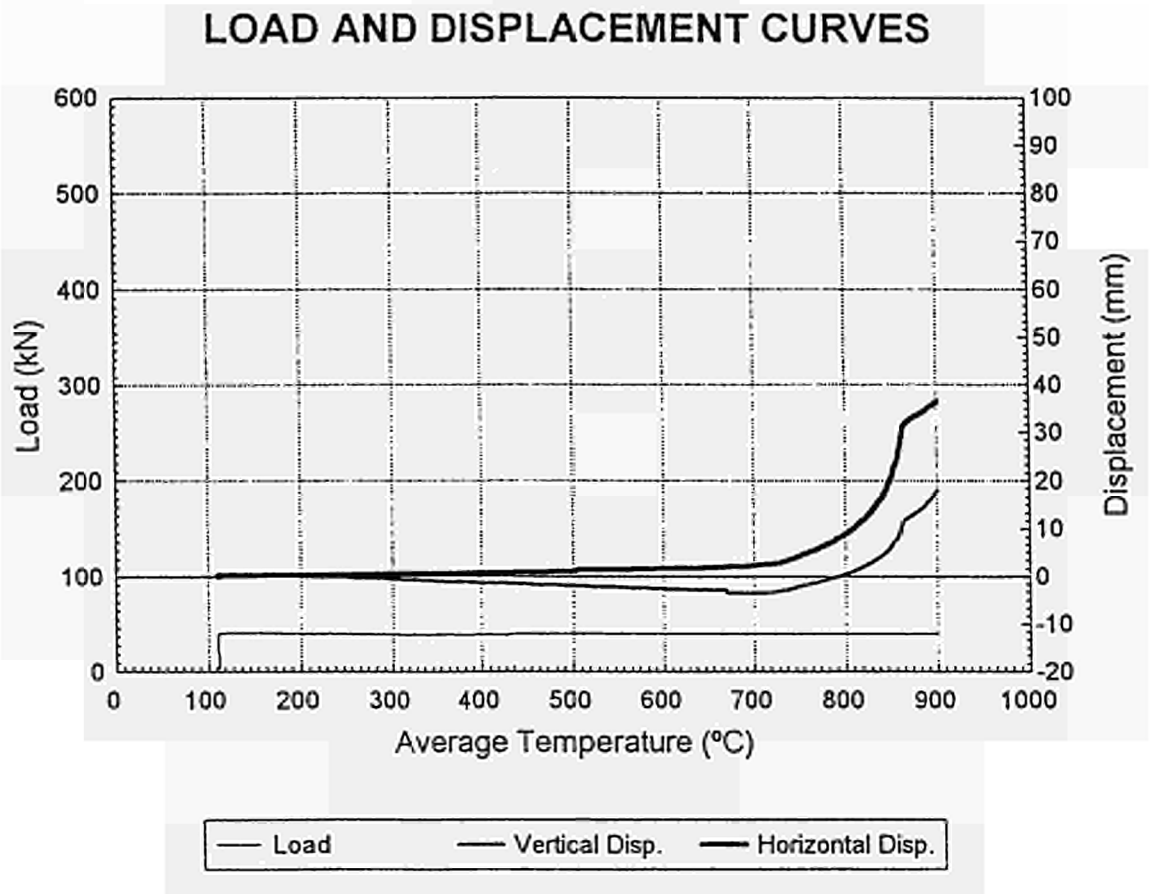

FIGURE 4.8 Thermocouples and resistors distribution for 1270 mm length specimens

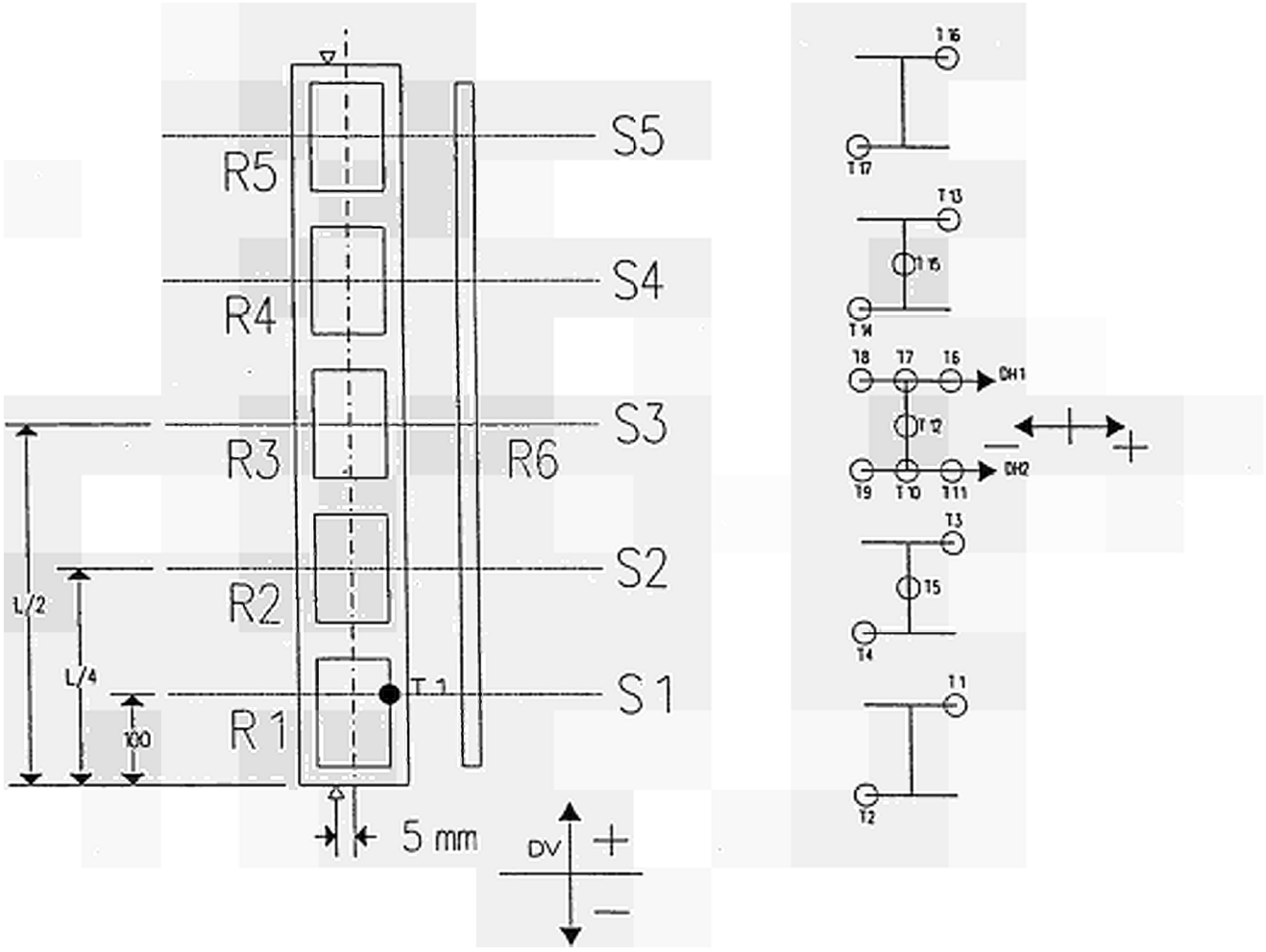

FIGURE 4.9 SPECIMEN AL3 (cold test)

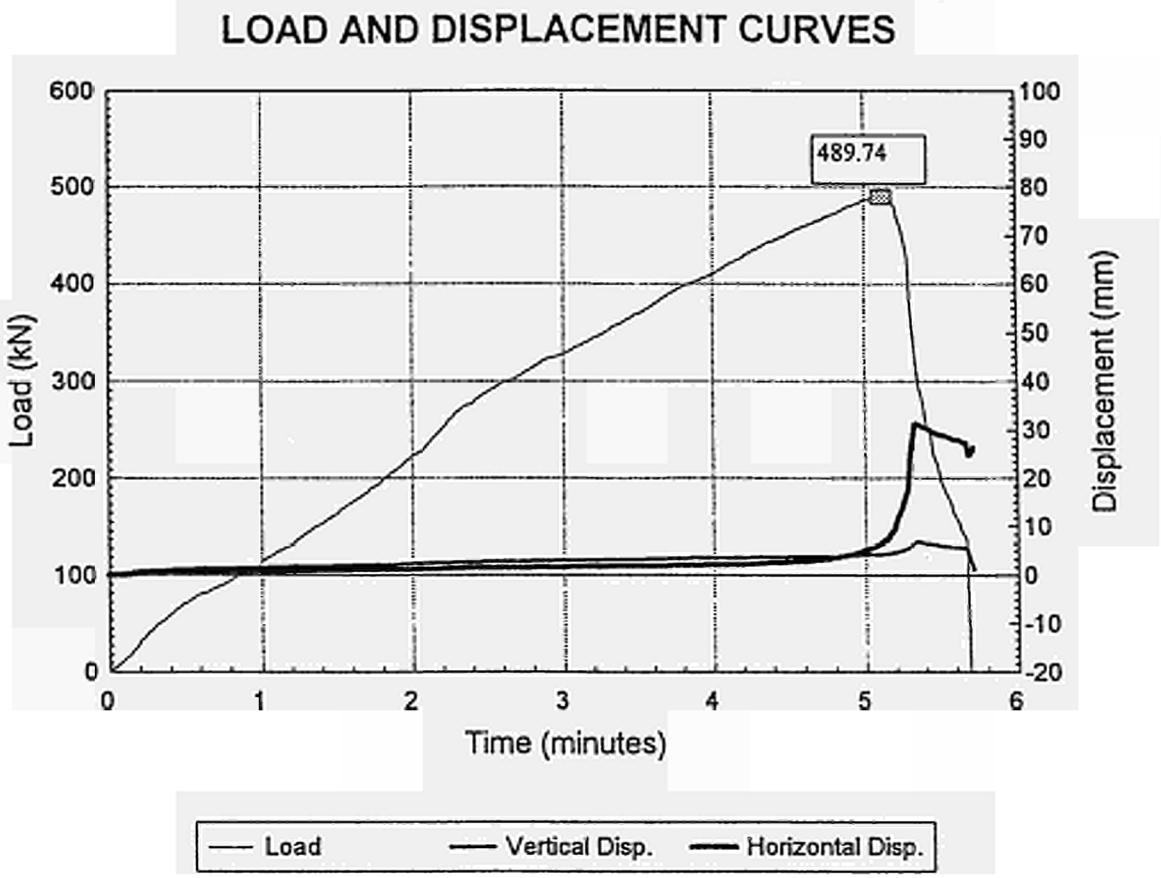

FIGURE 4.10 SPECIMEN BL3

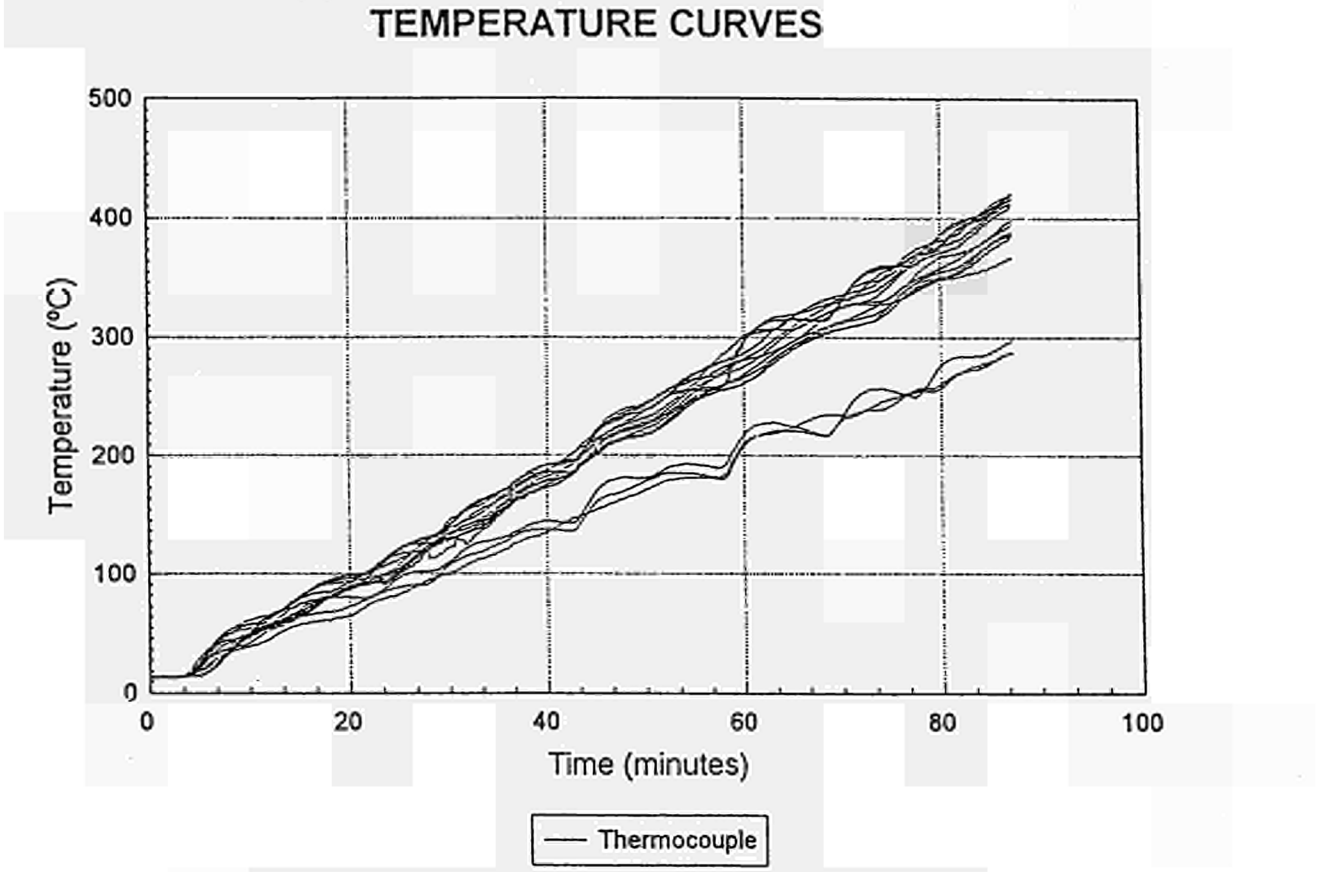

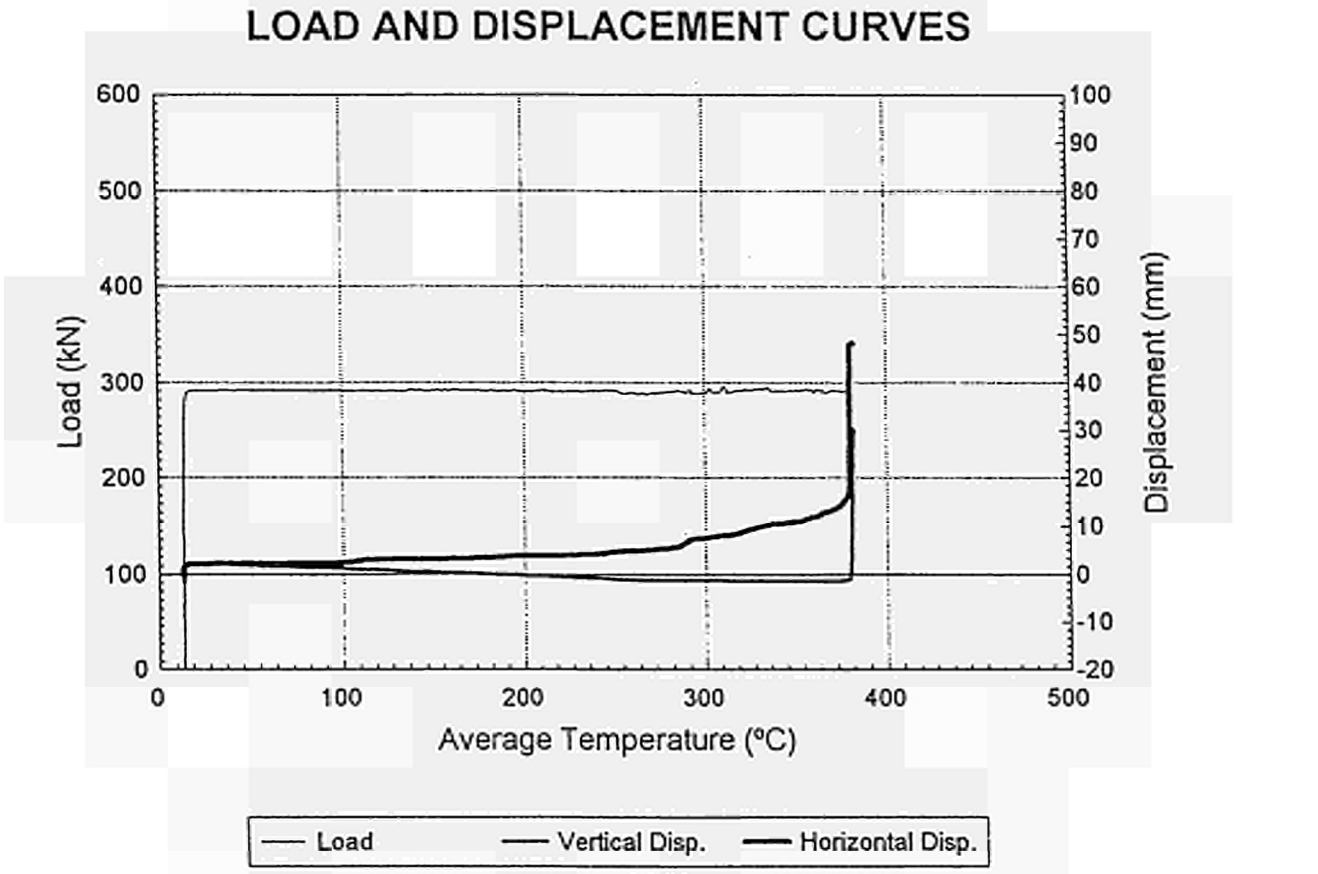

FIGURE 4.11 SPECIMEN CL3

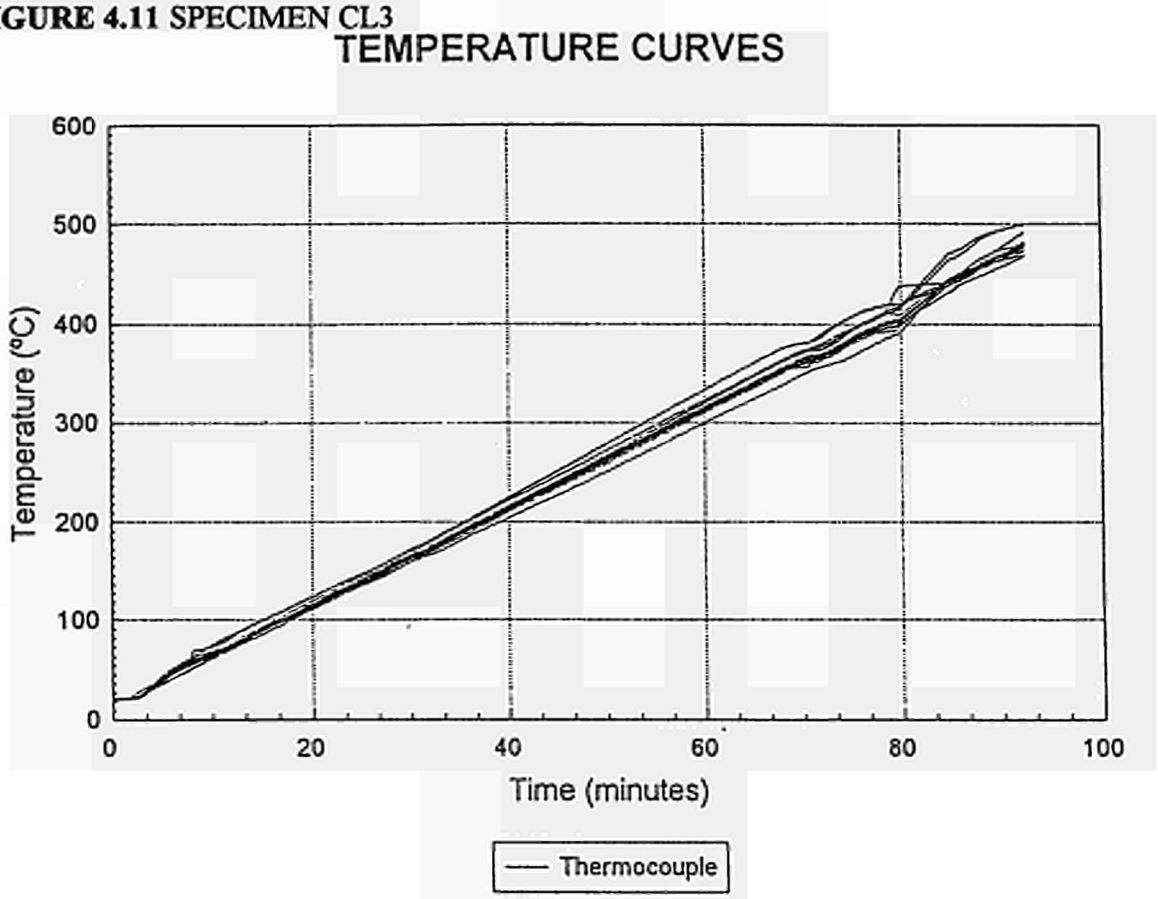

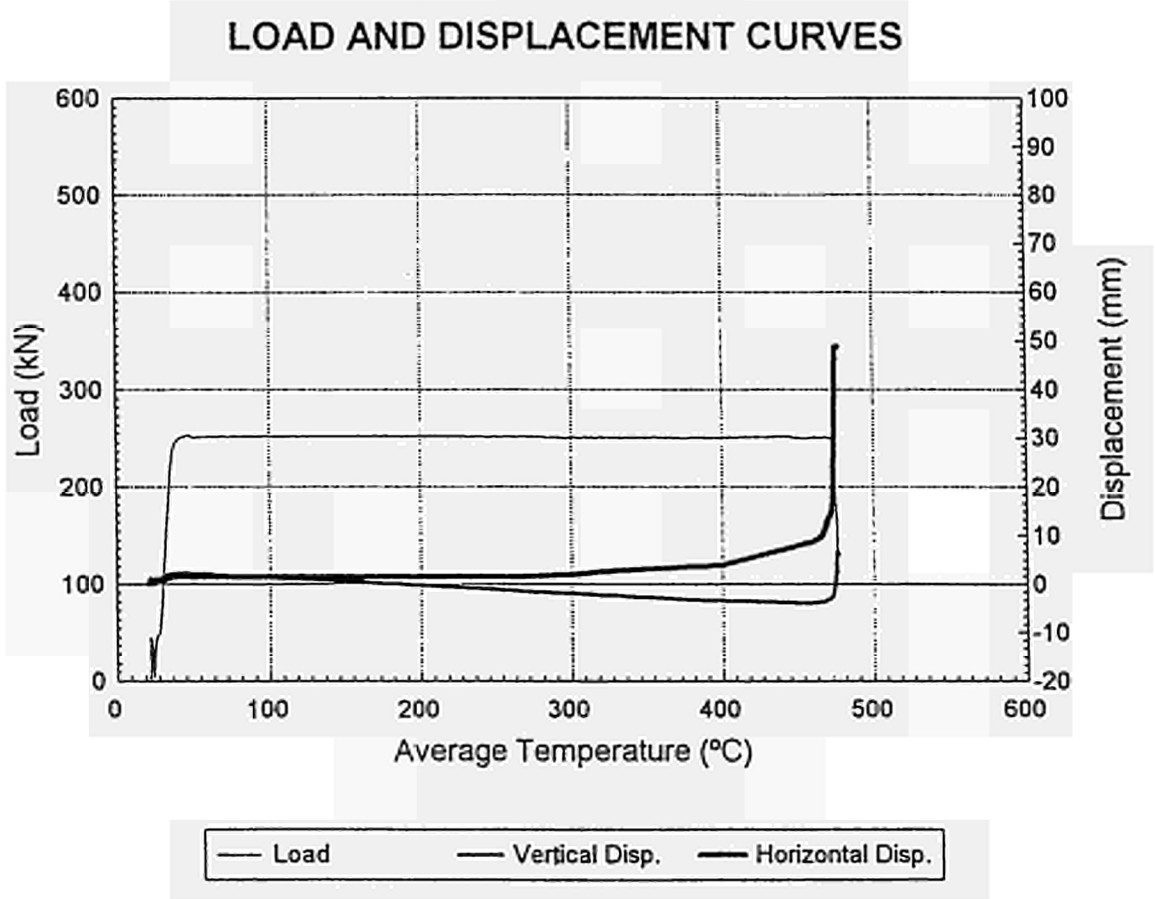

FIGURE 4.12 SPECIMEN DL3

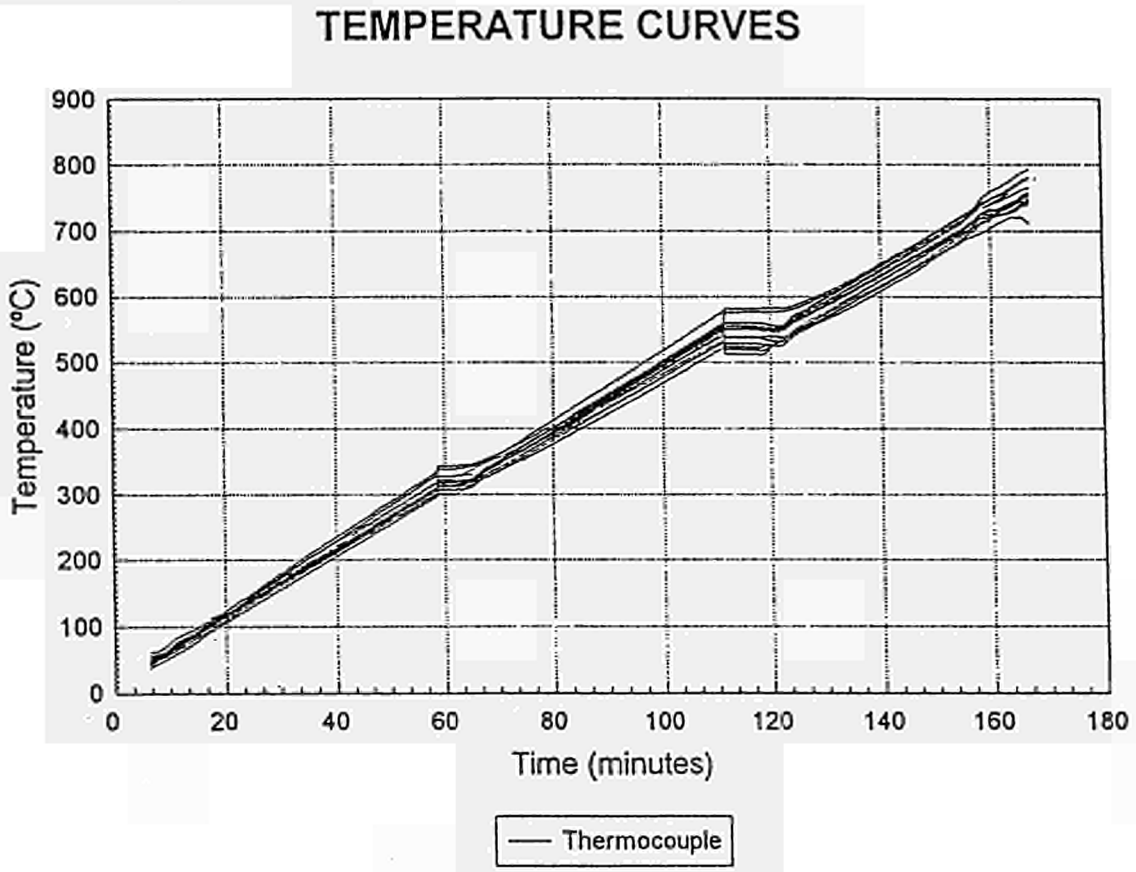

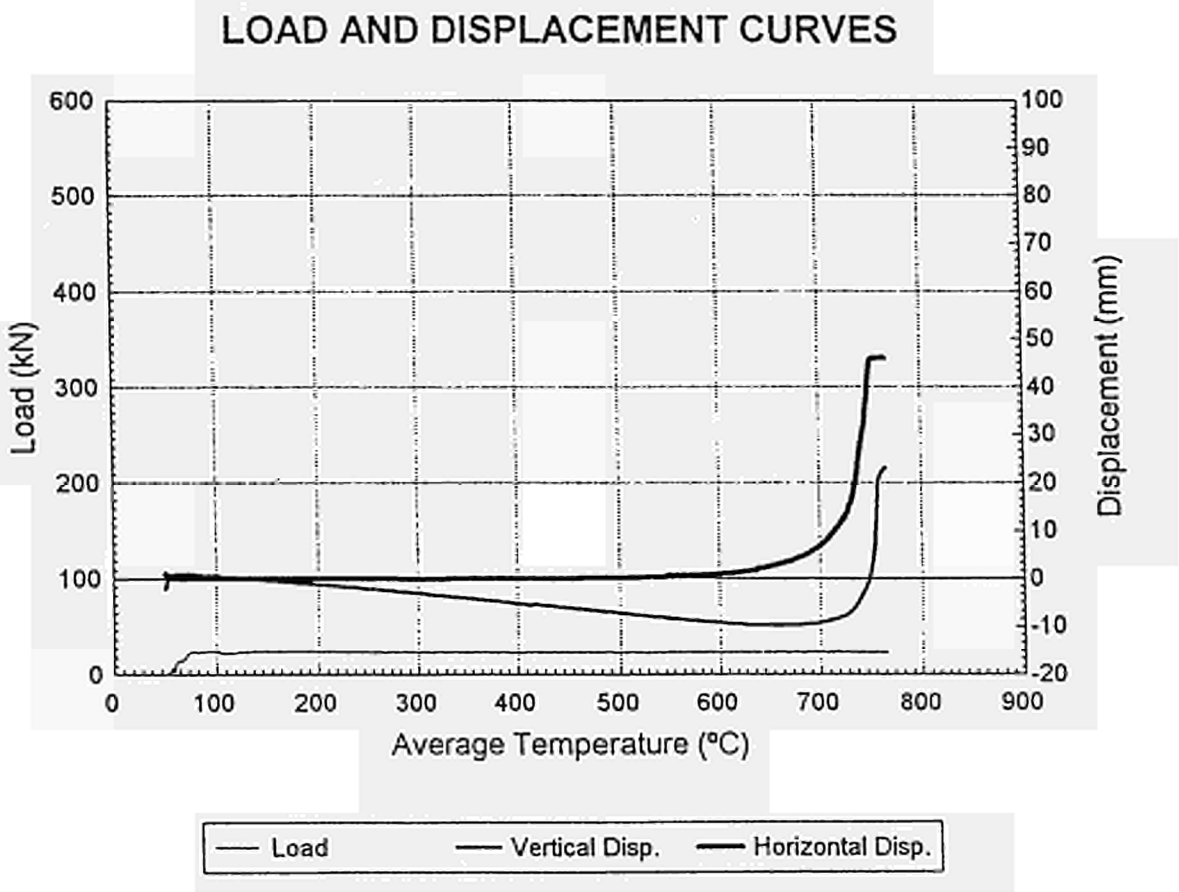

FIGURE 4.13 Thermocouples and resistors distribution for 2020 mm length specimens

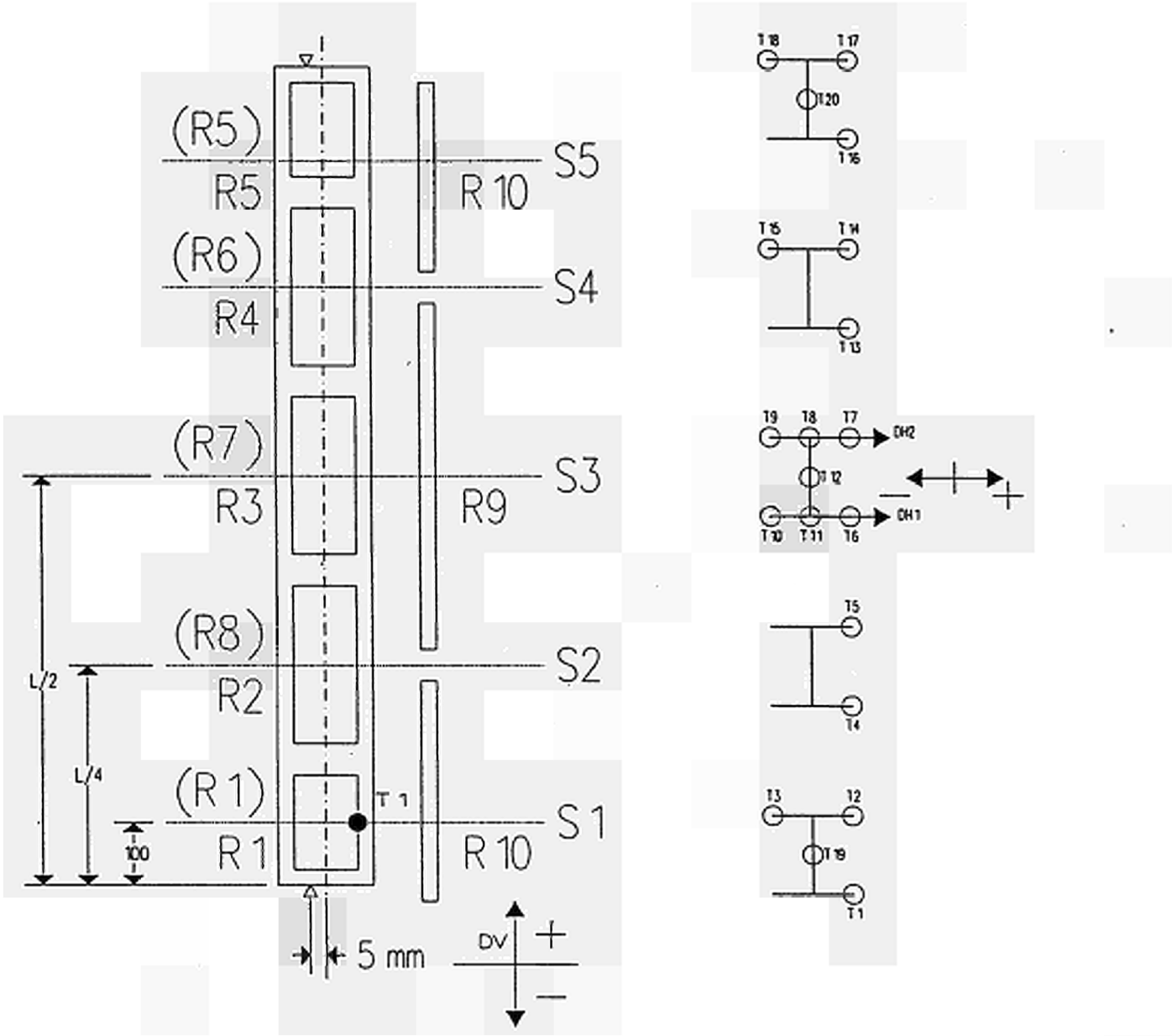

FIGURE 4.14 SPECIMEN SL4.0

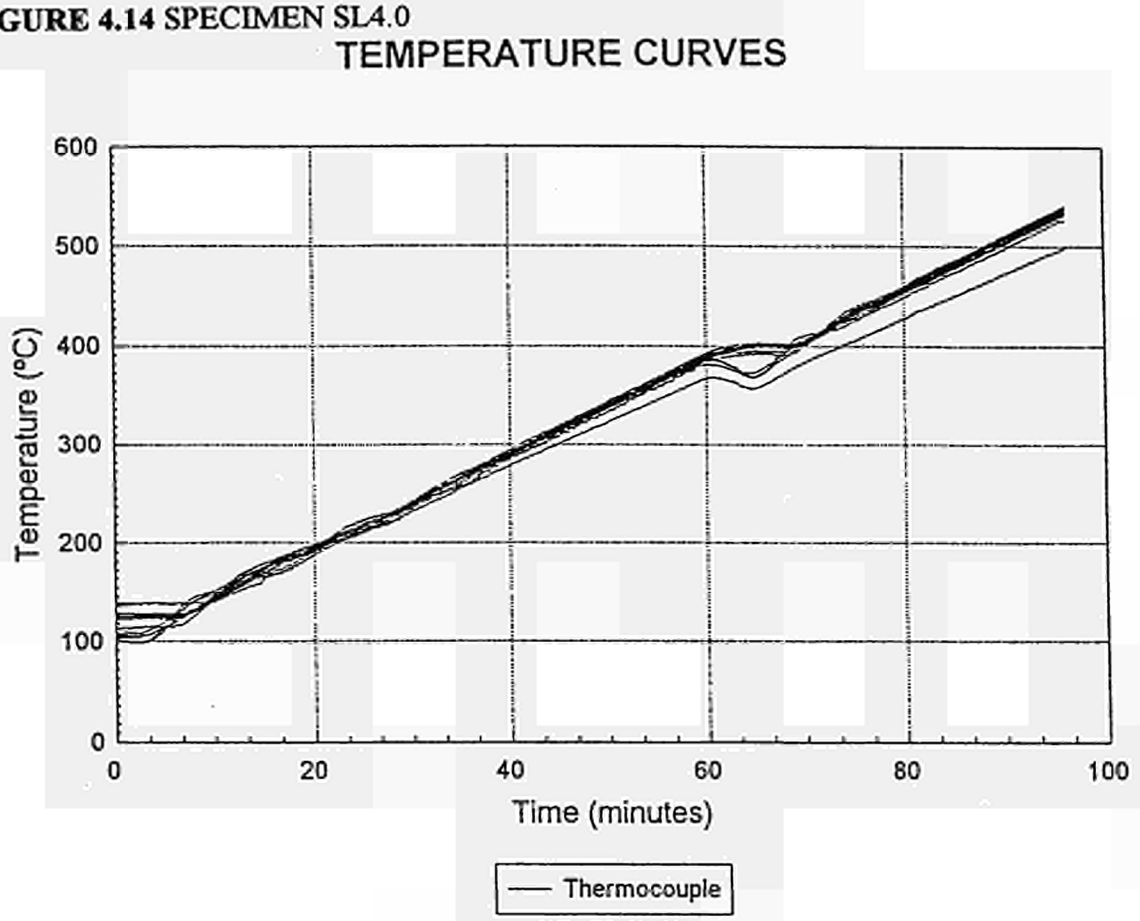

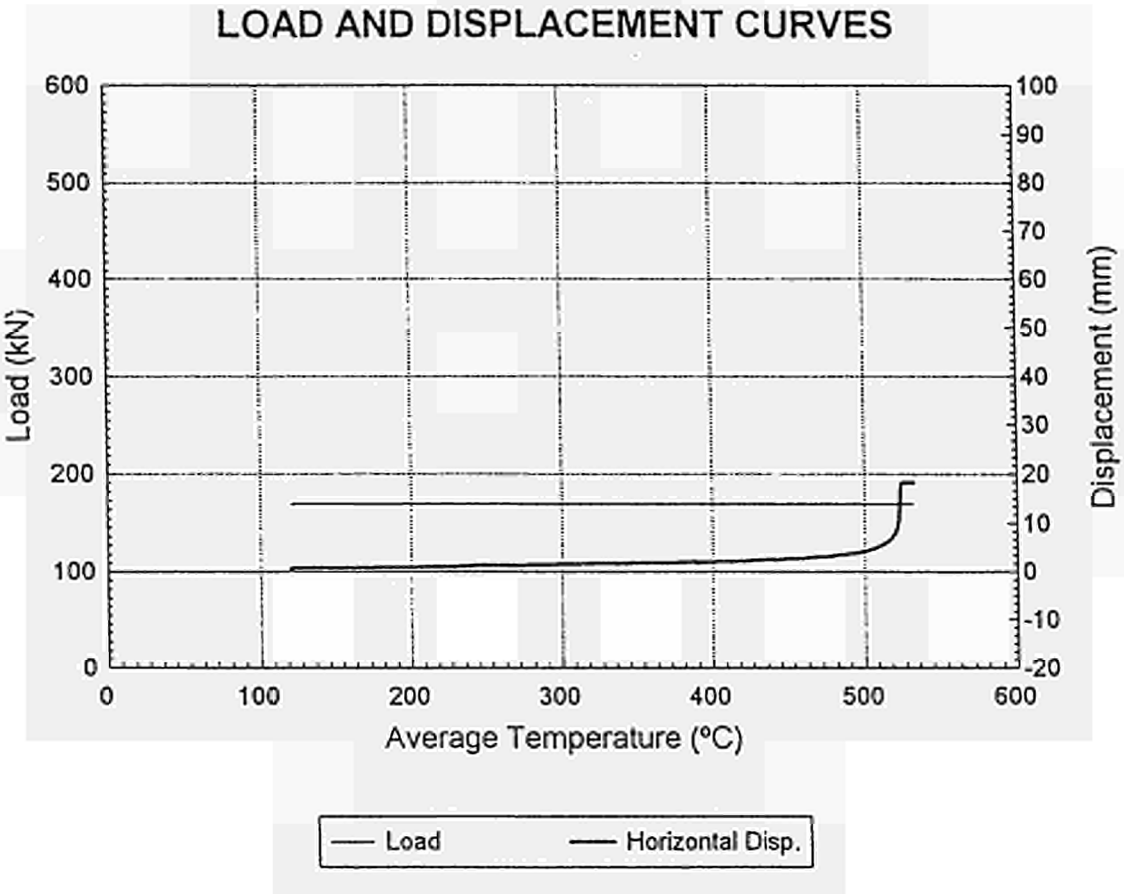

FIGURE 4.15 SPECIMEN SL4.1

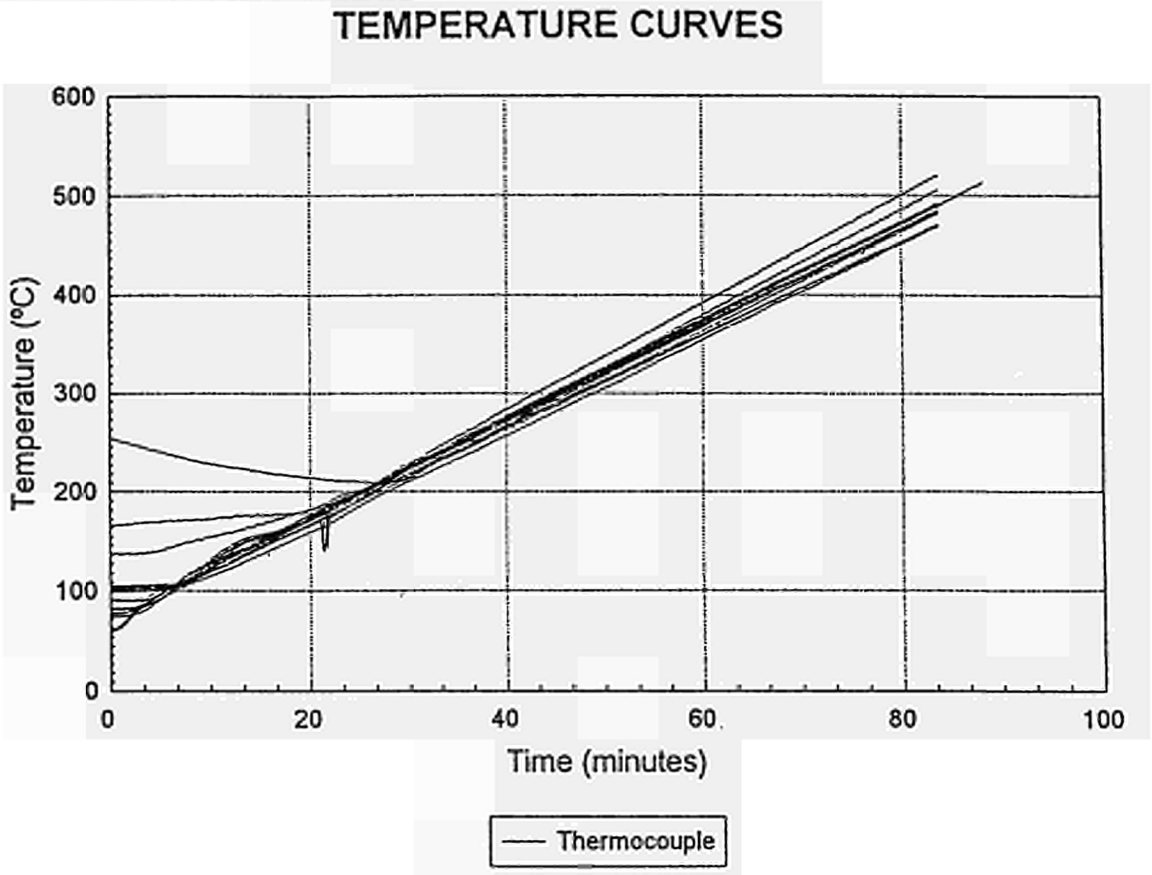

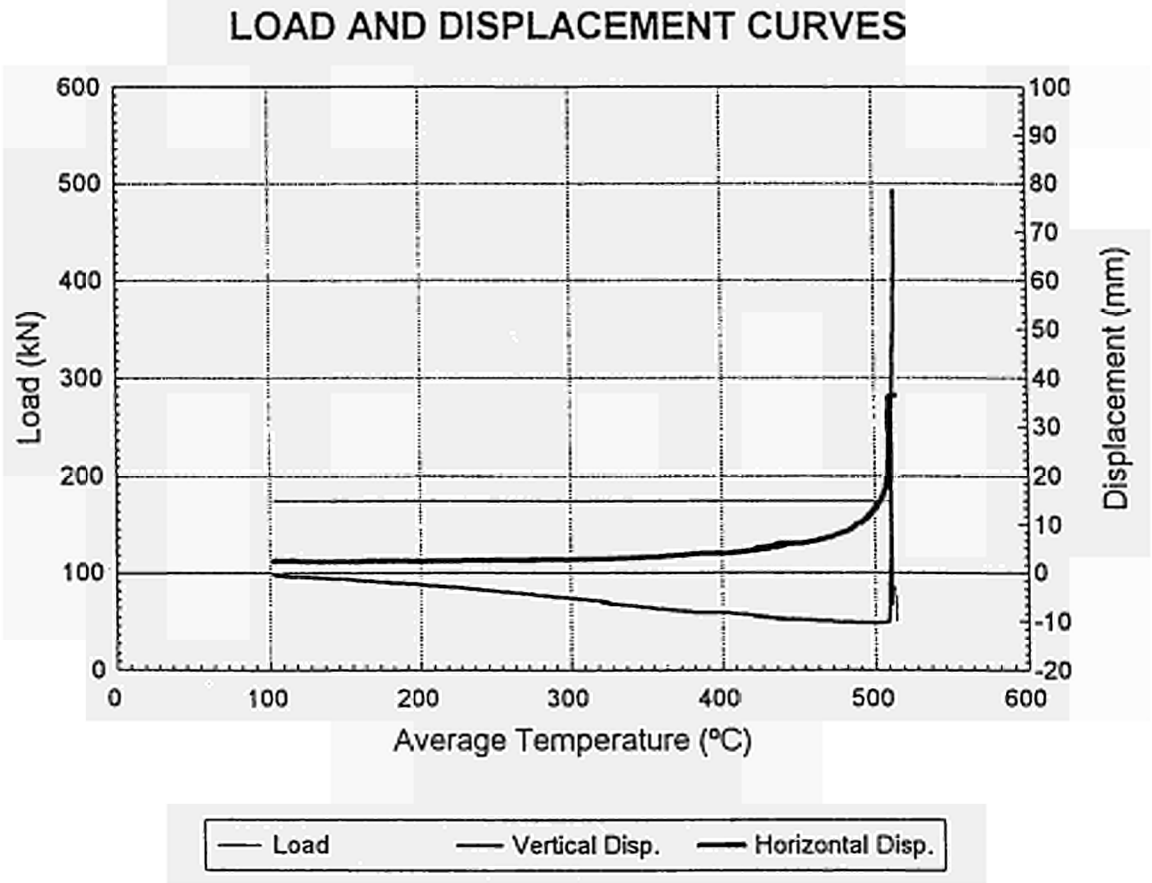

FIGURE 4.16 SPECIMEN SL4.2

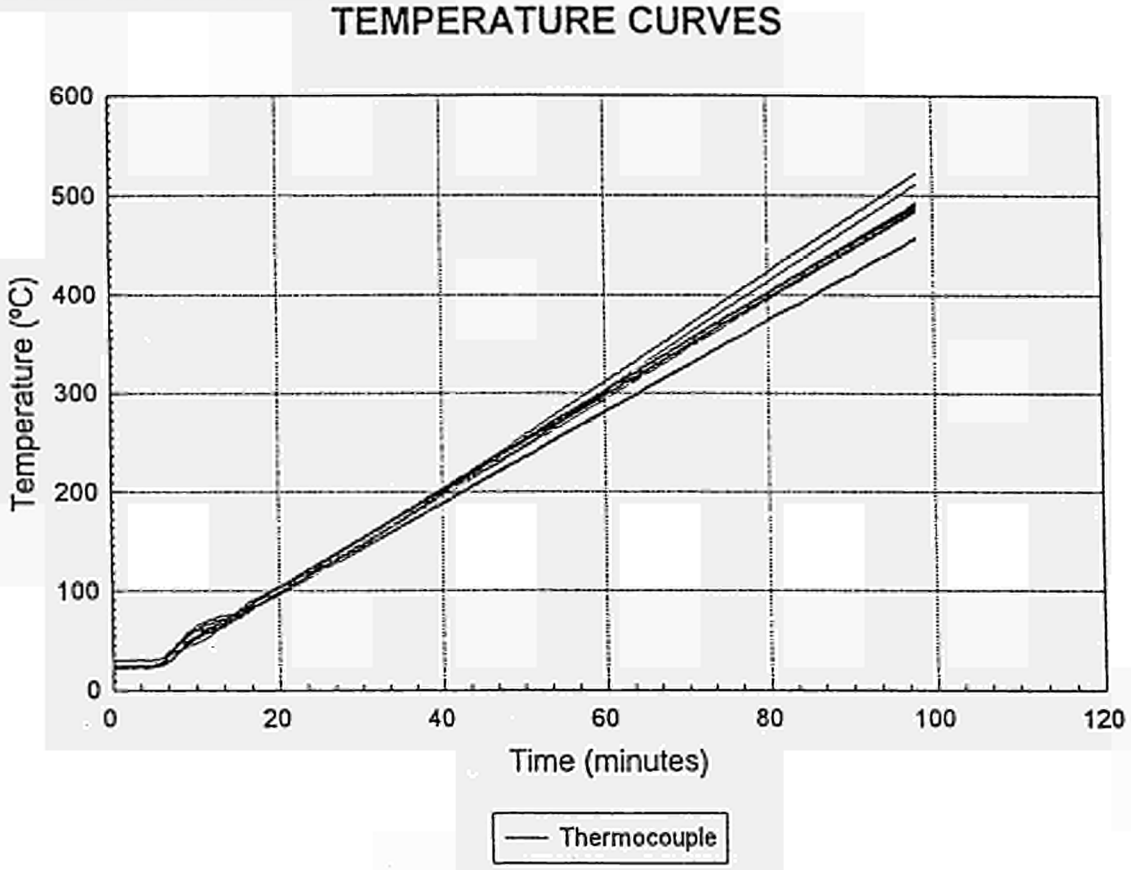

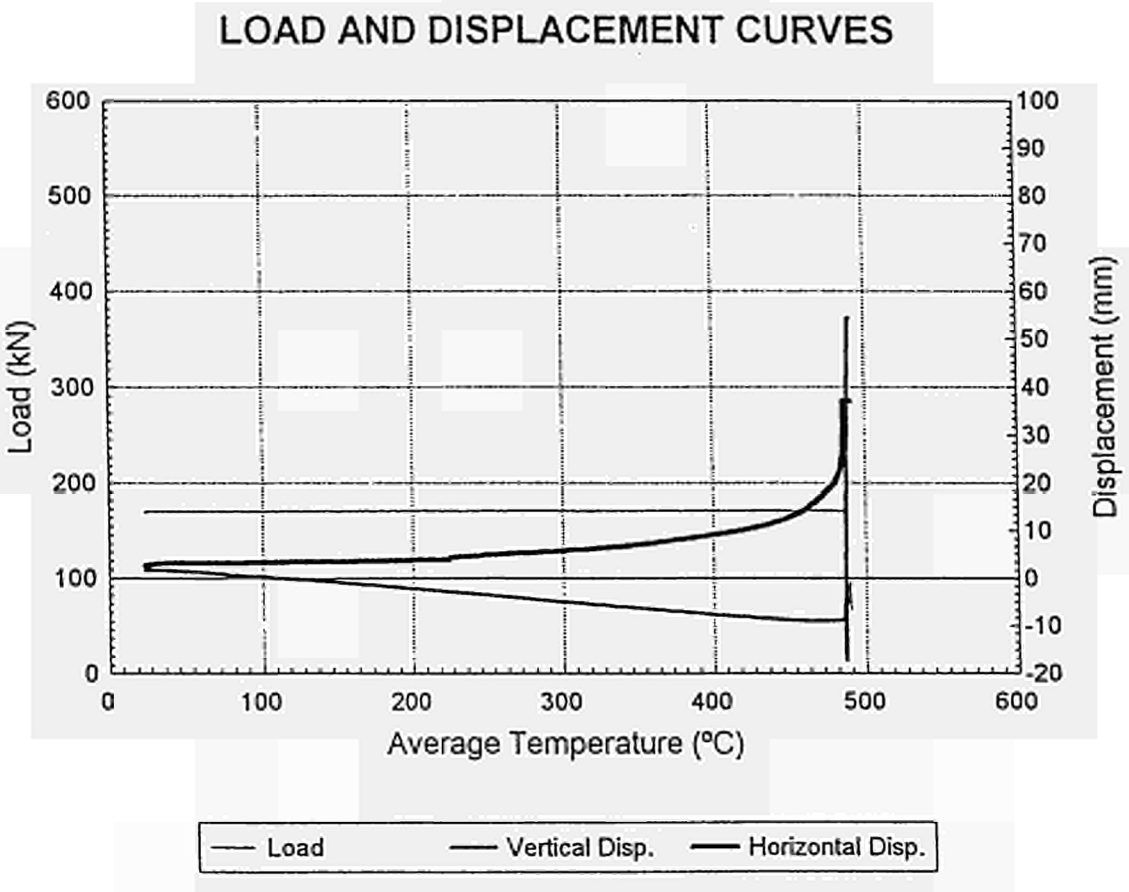

FIGURE 4.17 SPECIMEN SL4.3 (cold test)

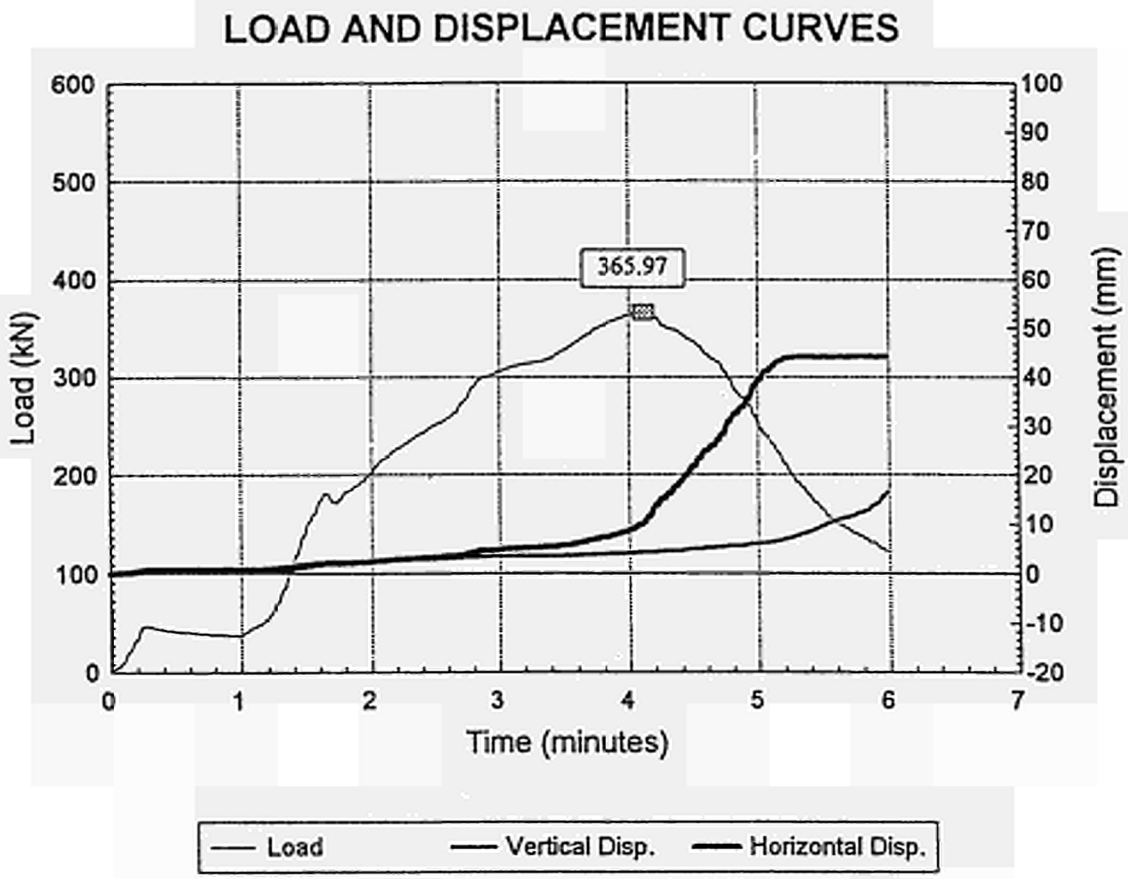

FIGURE 4.18 SPECIMEN SL4.4

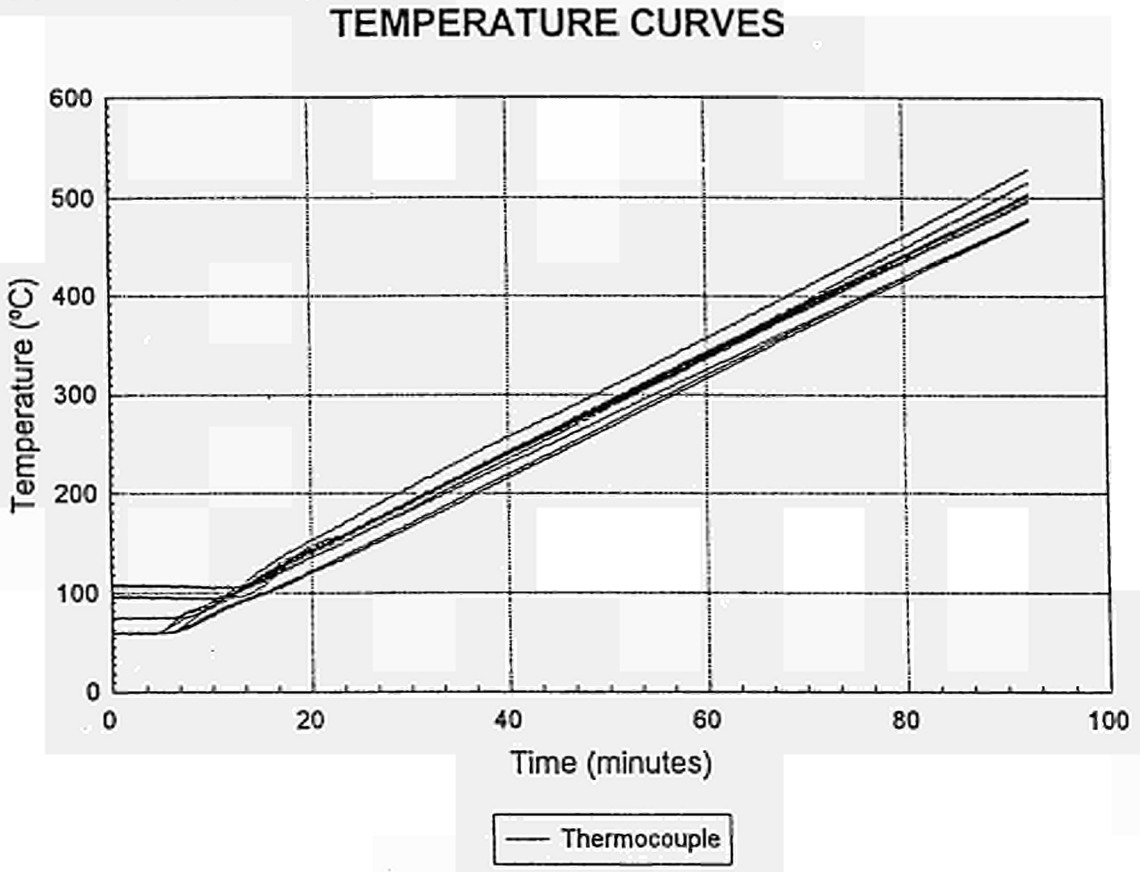

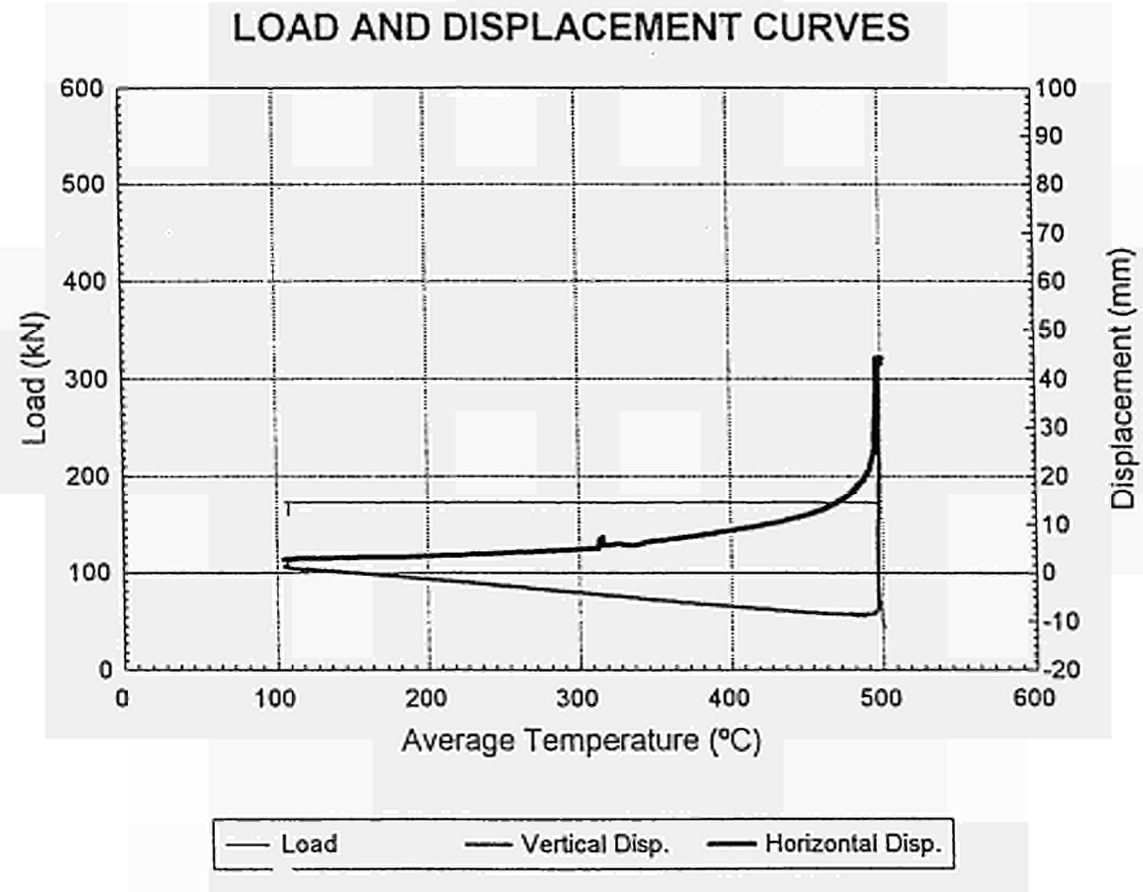

FIGURE 4.19 Thermocouples and resistors distribution for 2770 mm length specimens (AL5 and CL5)

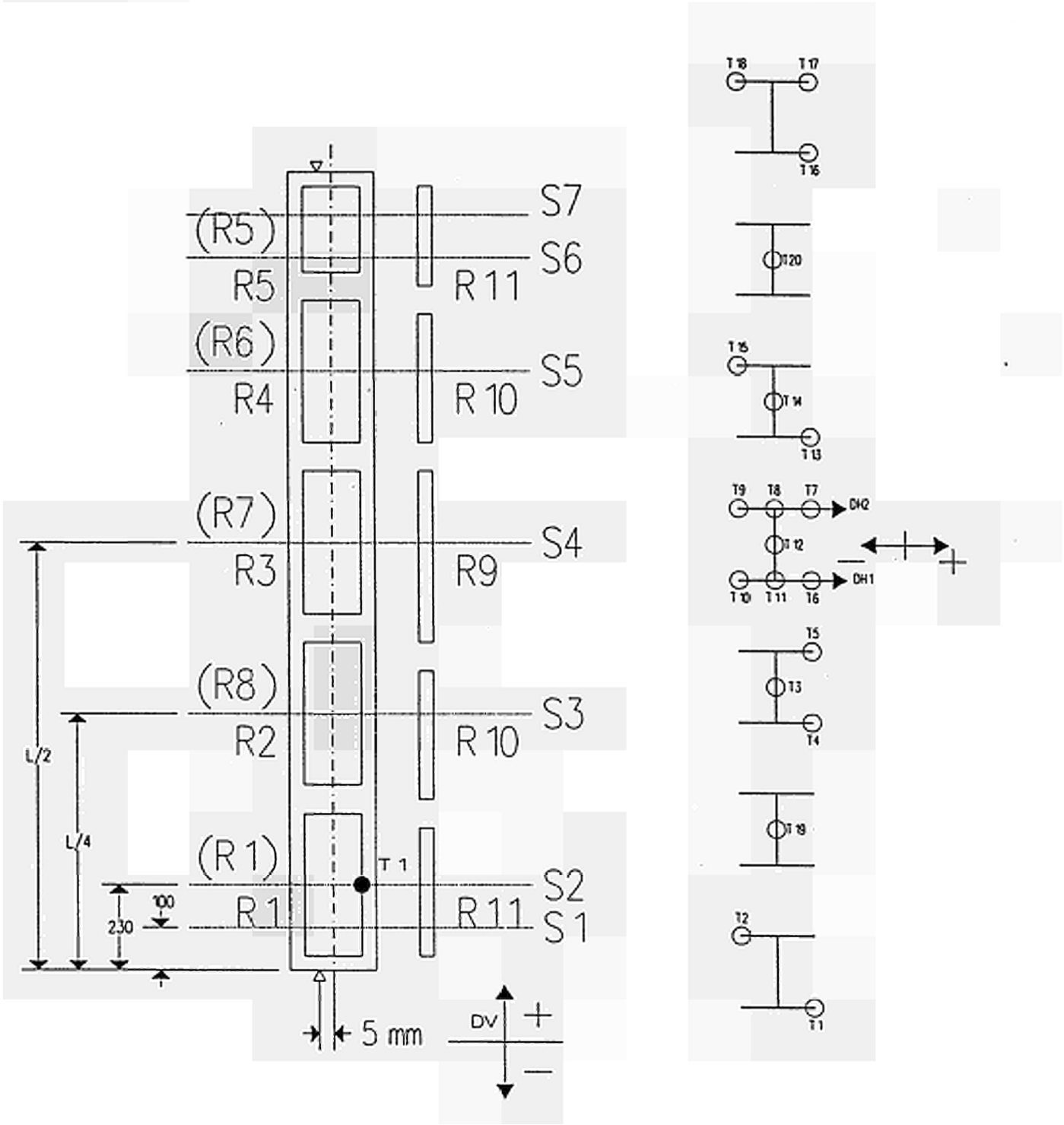

FIGURE 4.20 Thermocouples and resistors distribution for 2770 mm length specimens (BL5 and DL5)

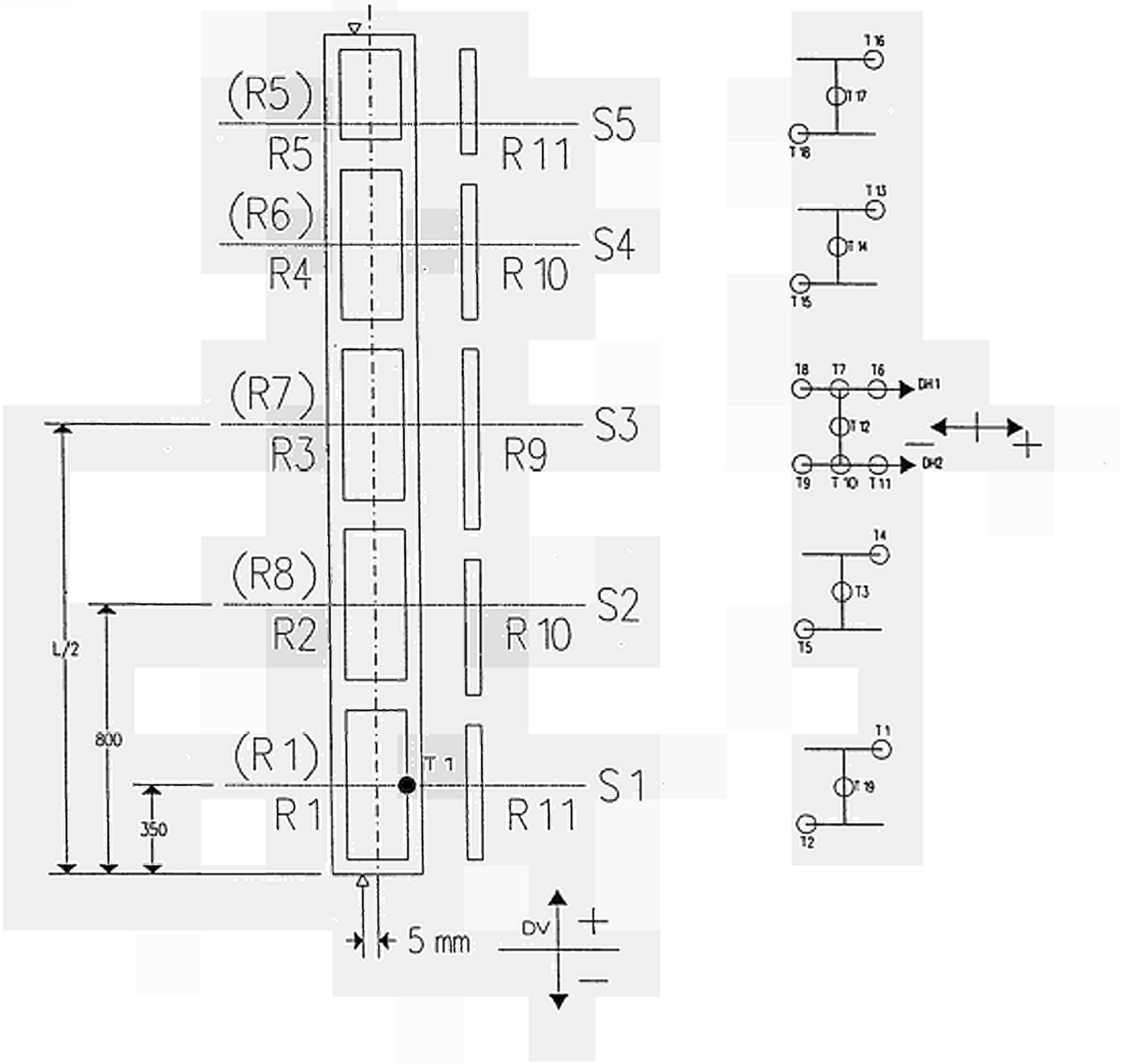

FIGURE 4.21 SPECIMEN AL5

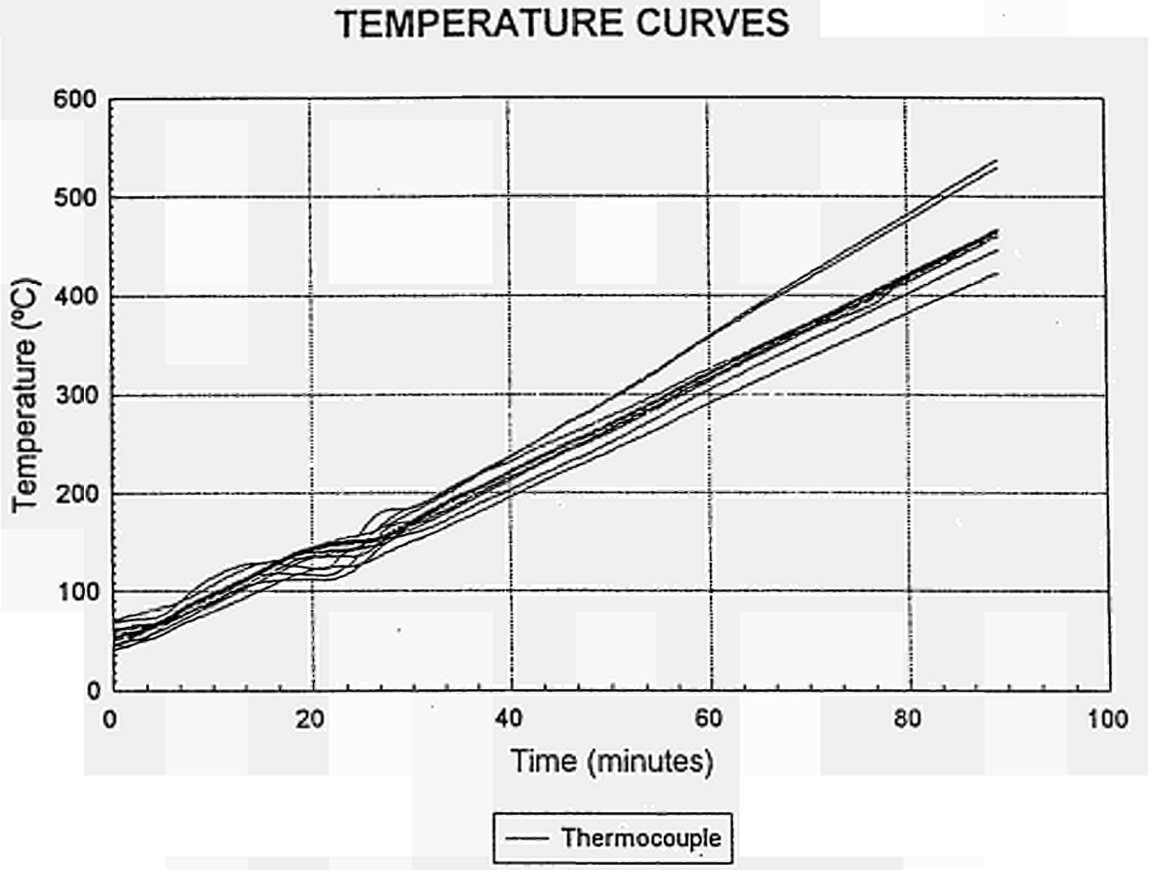

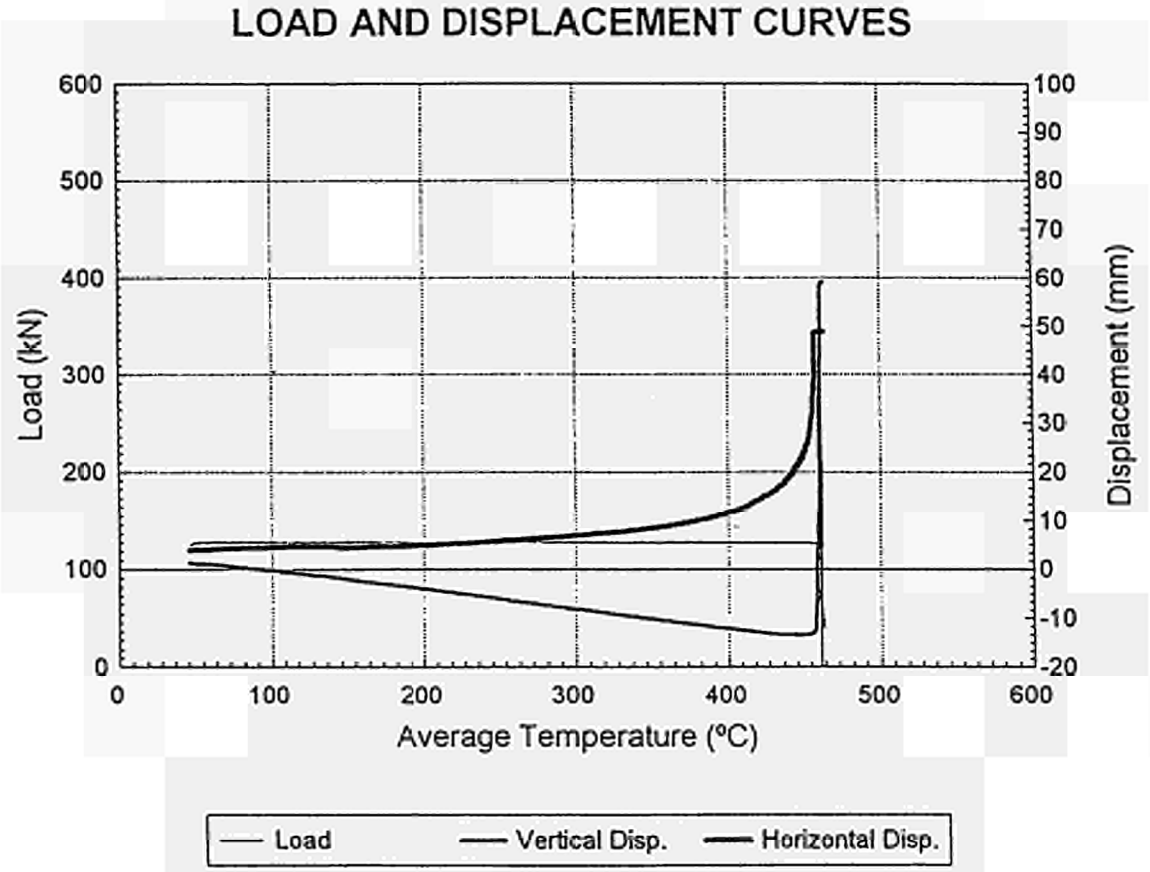

FIGURE 4.22 SPECIMEN BL5

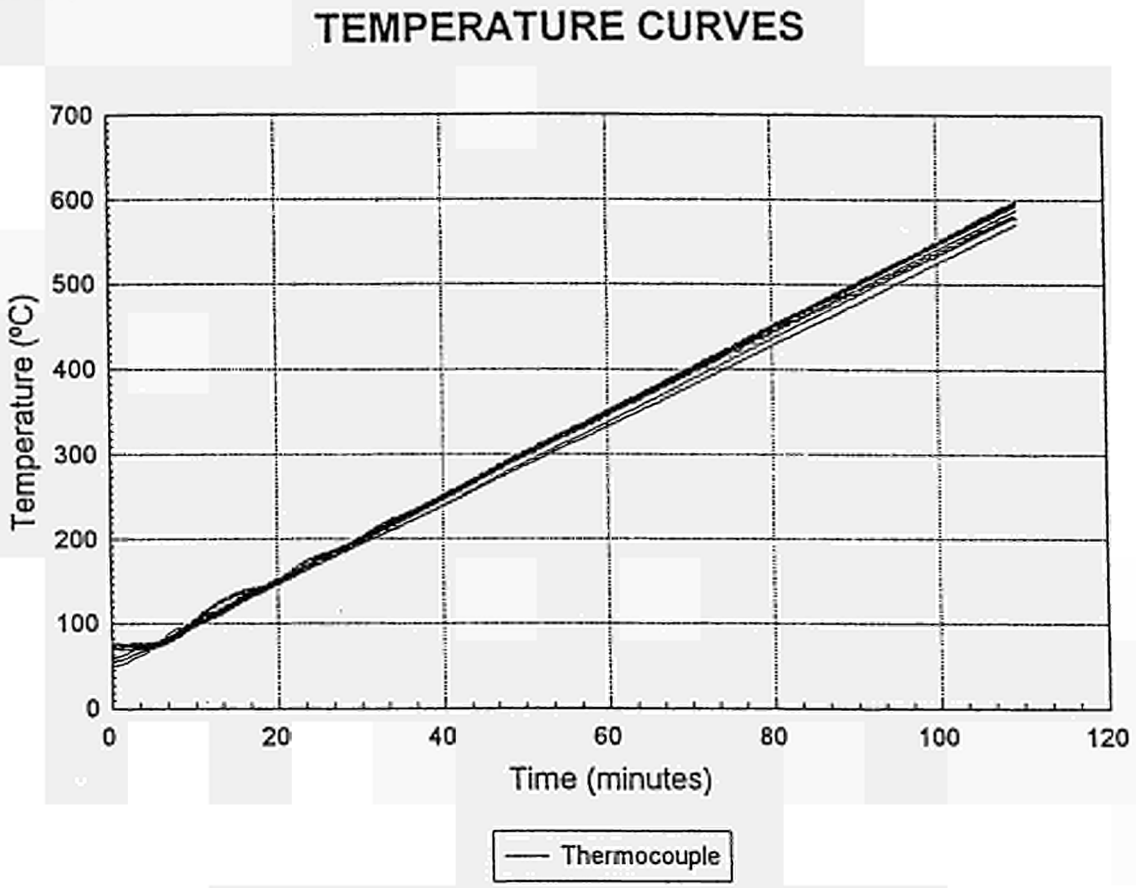

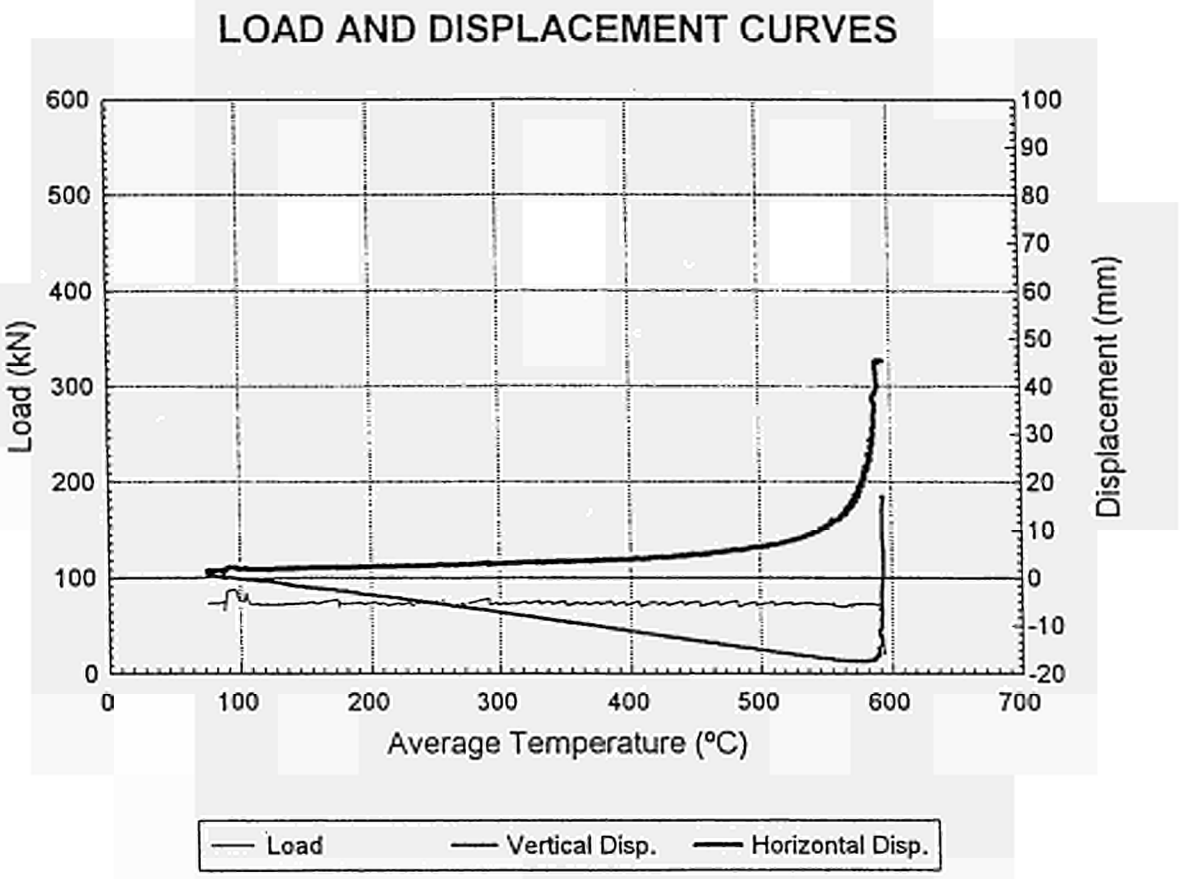

FIGURE 4.23 SPECIMEN CL5

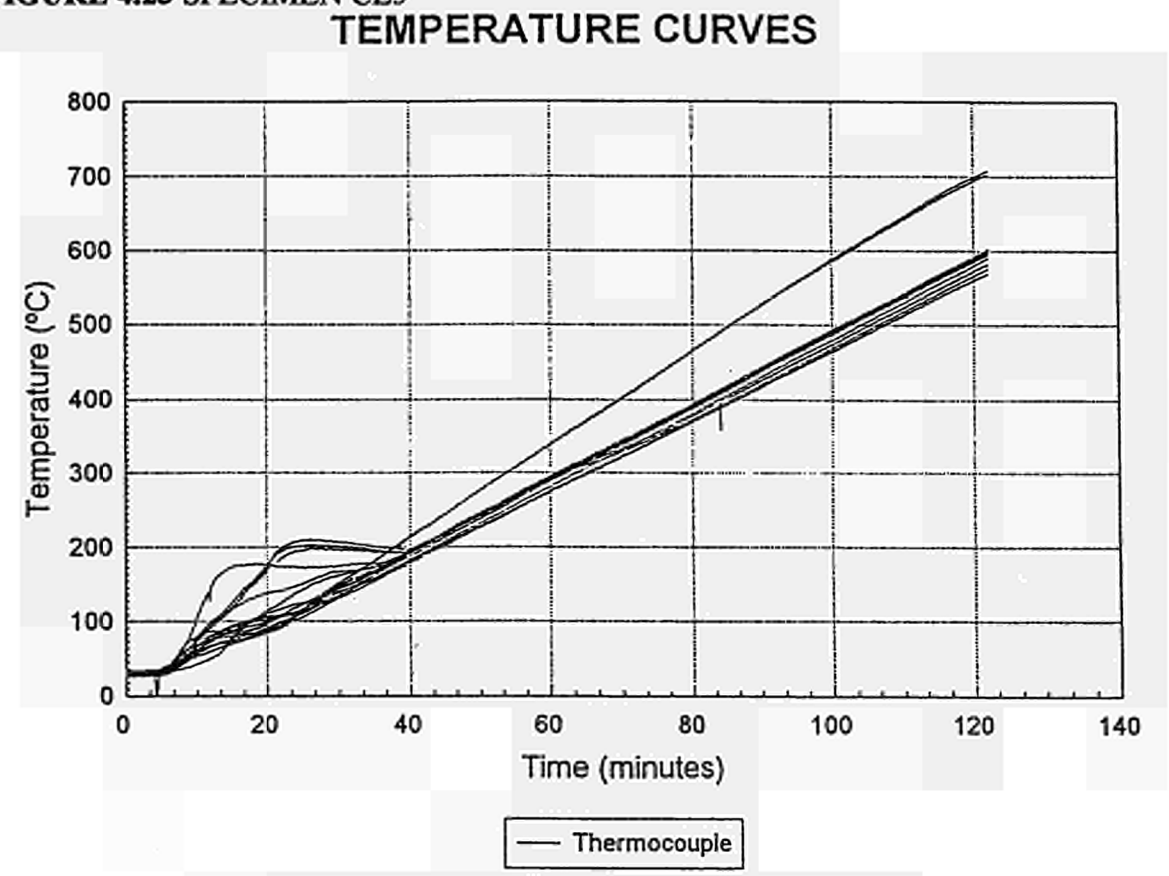

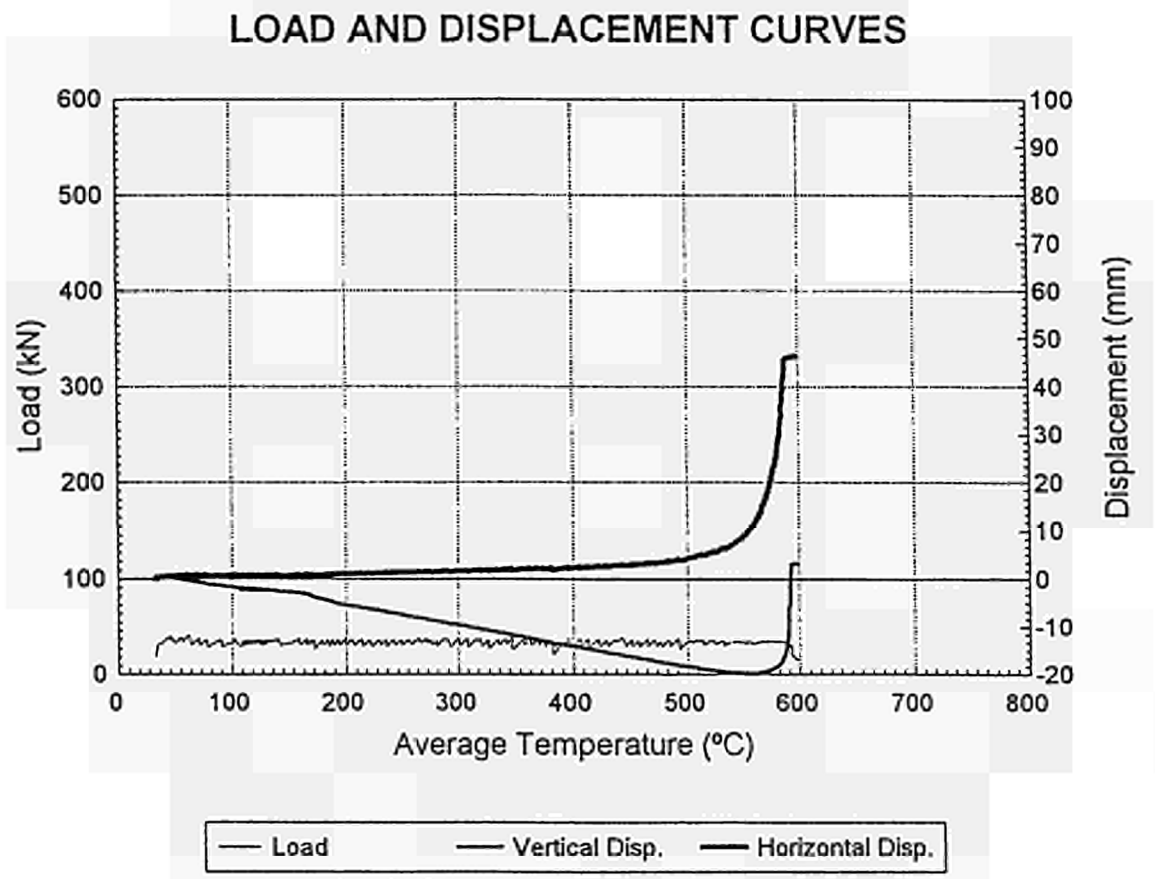

FIGURE 4.24 SPECIMEN DL5

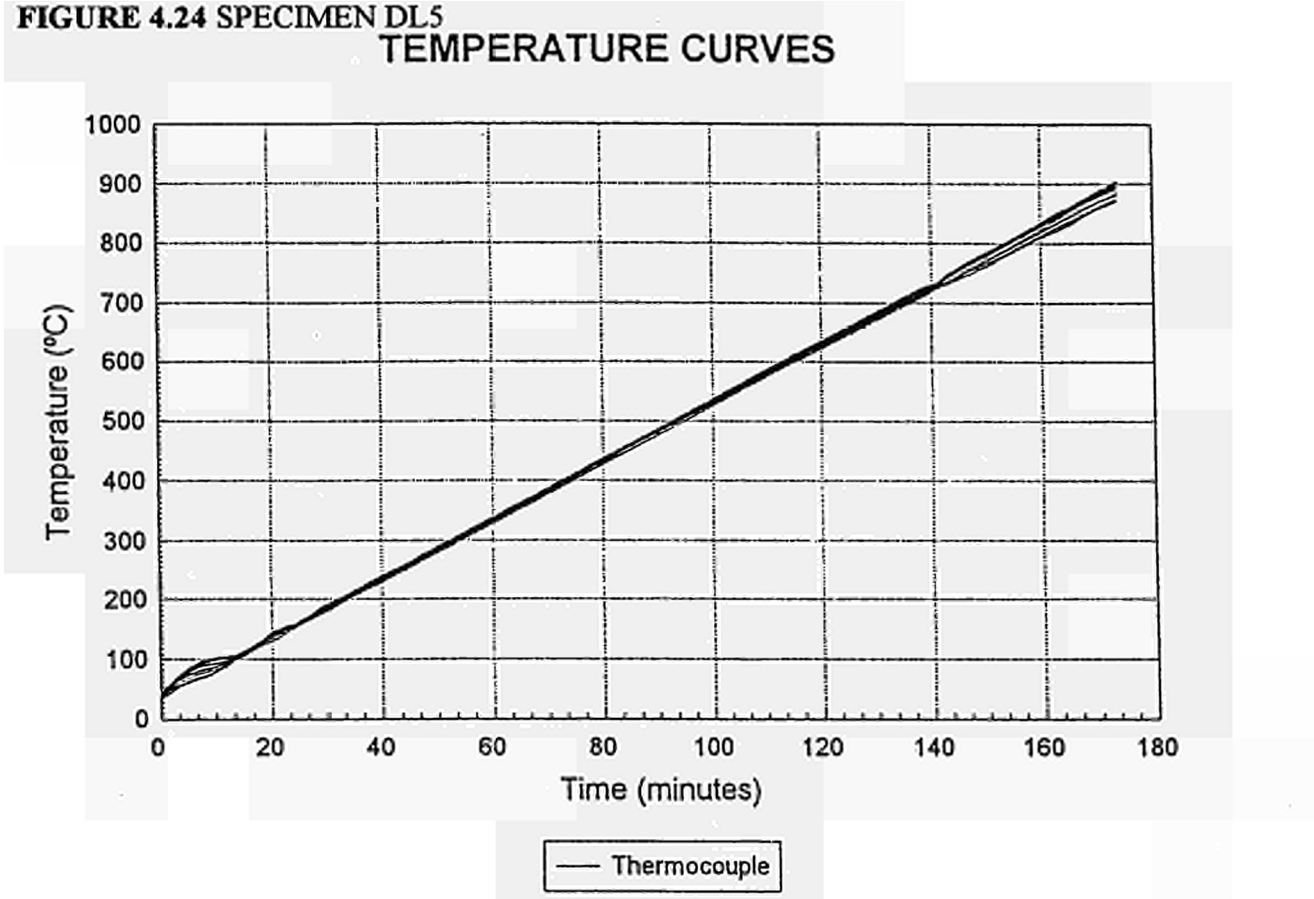

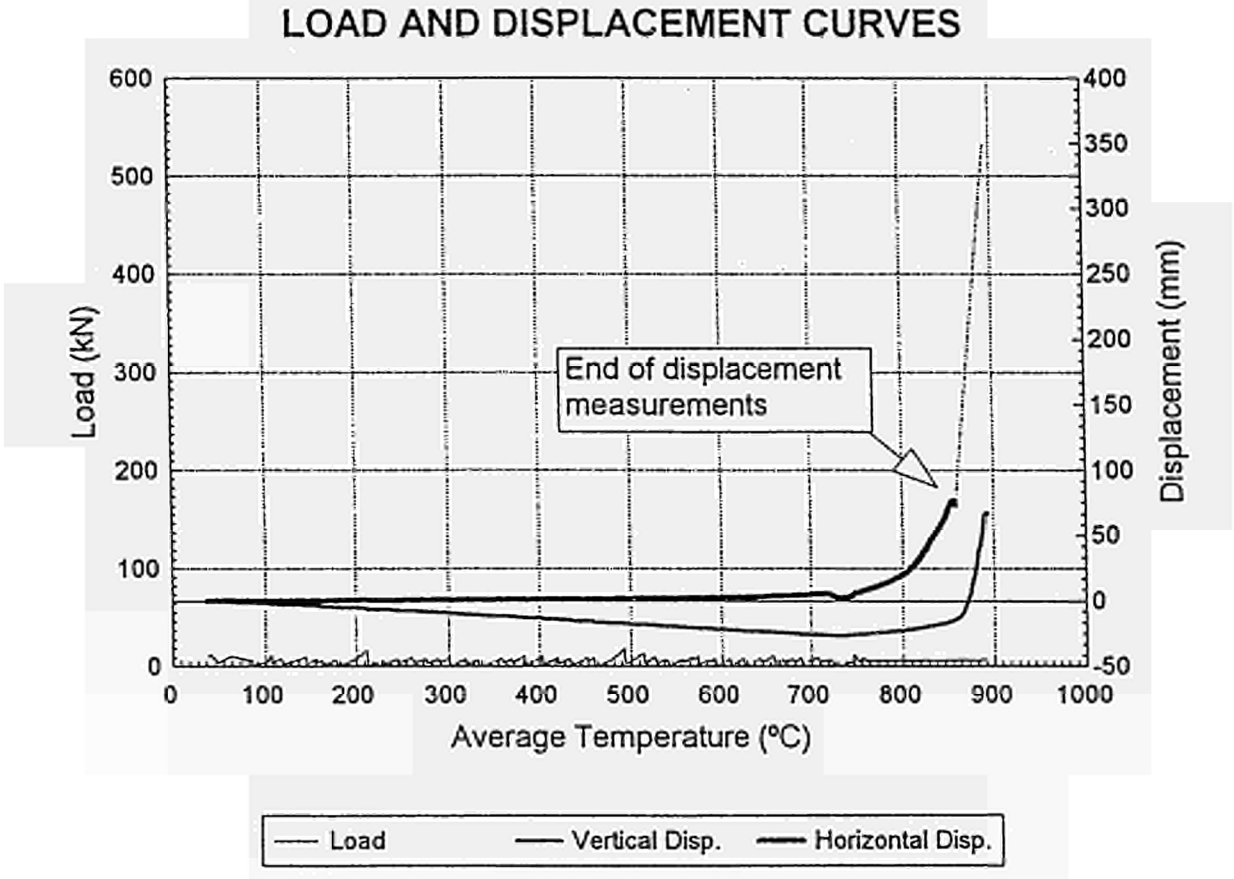

FIGURE 4.25 Thermocouples and resistors distribution for 3520 mm length specimens

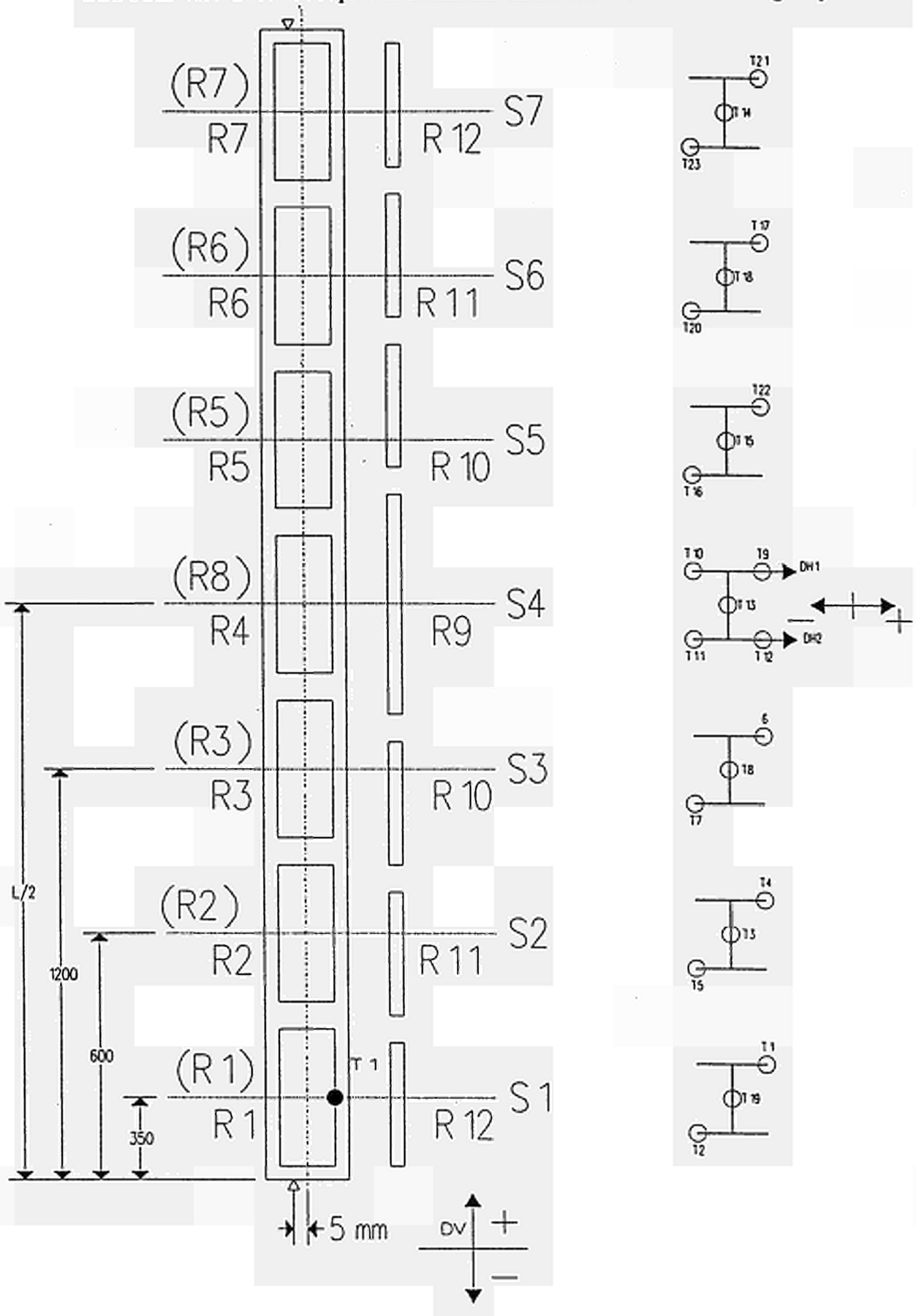

FIGURE 4.26 SPECIMEN AL6 (cold test)

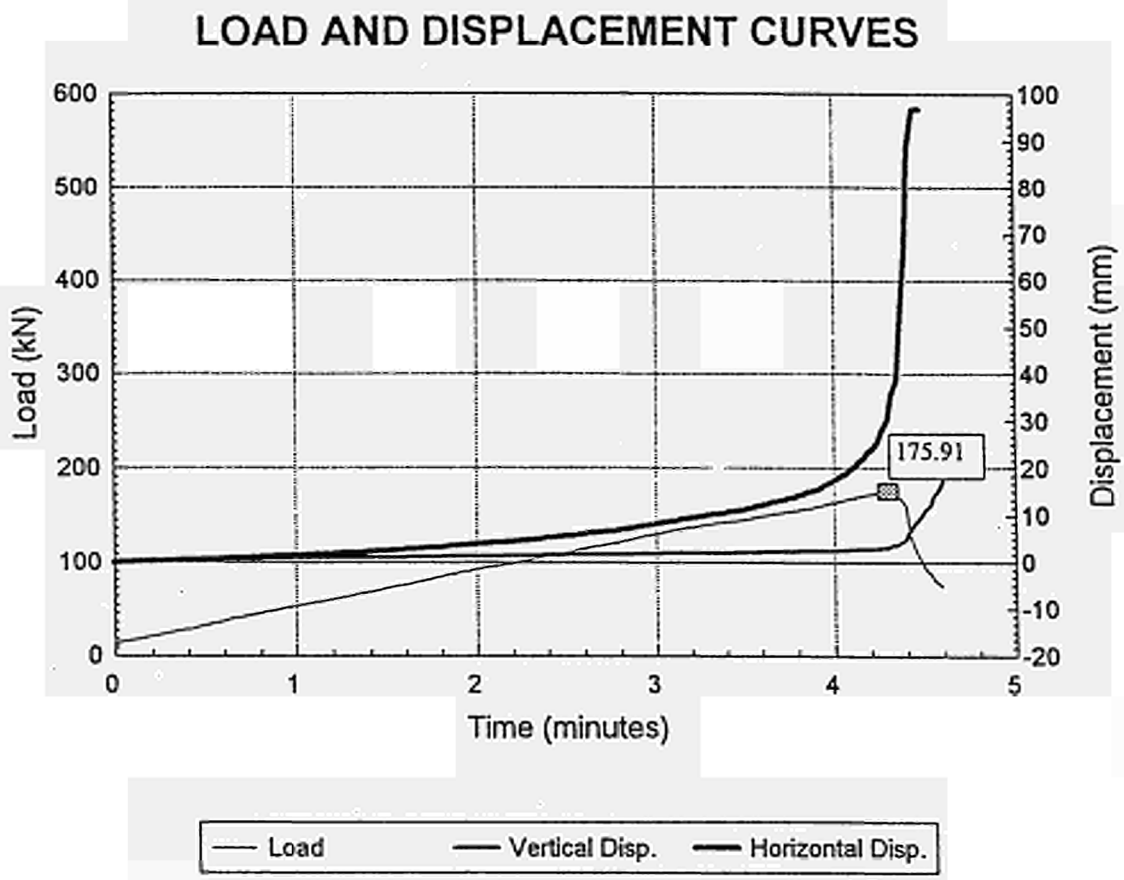

FIGURE 4.27 SPECIMEN BL6

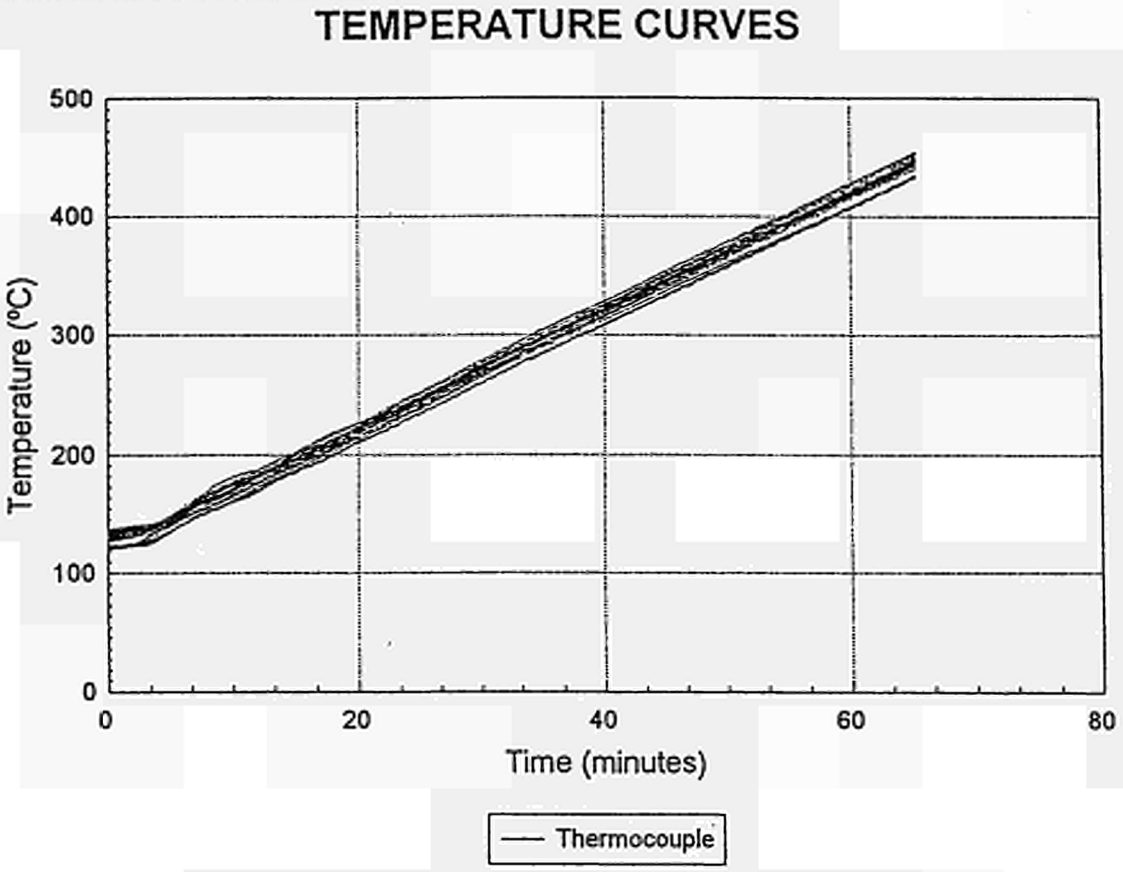

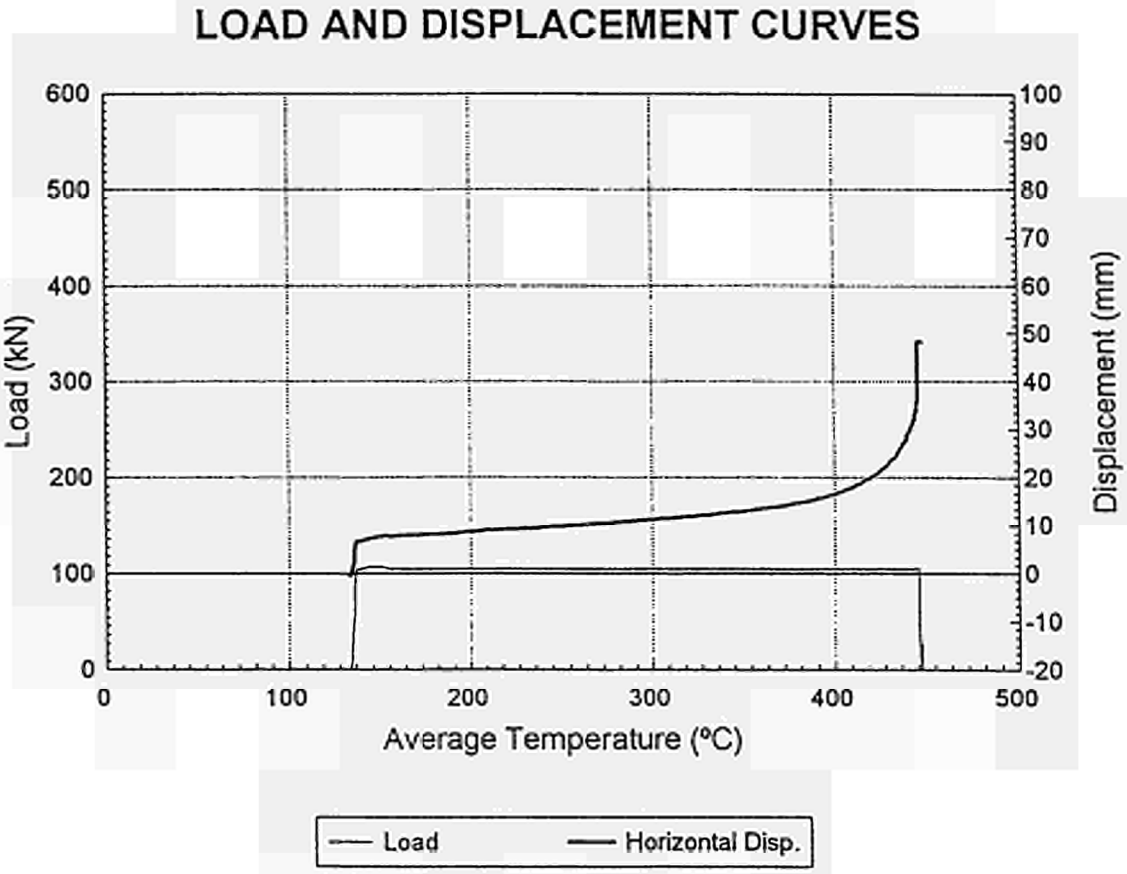

FIGURE 4.28 SPECIMEN CL6

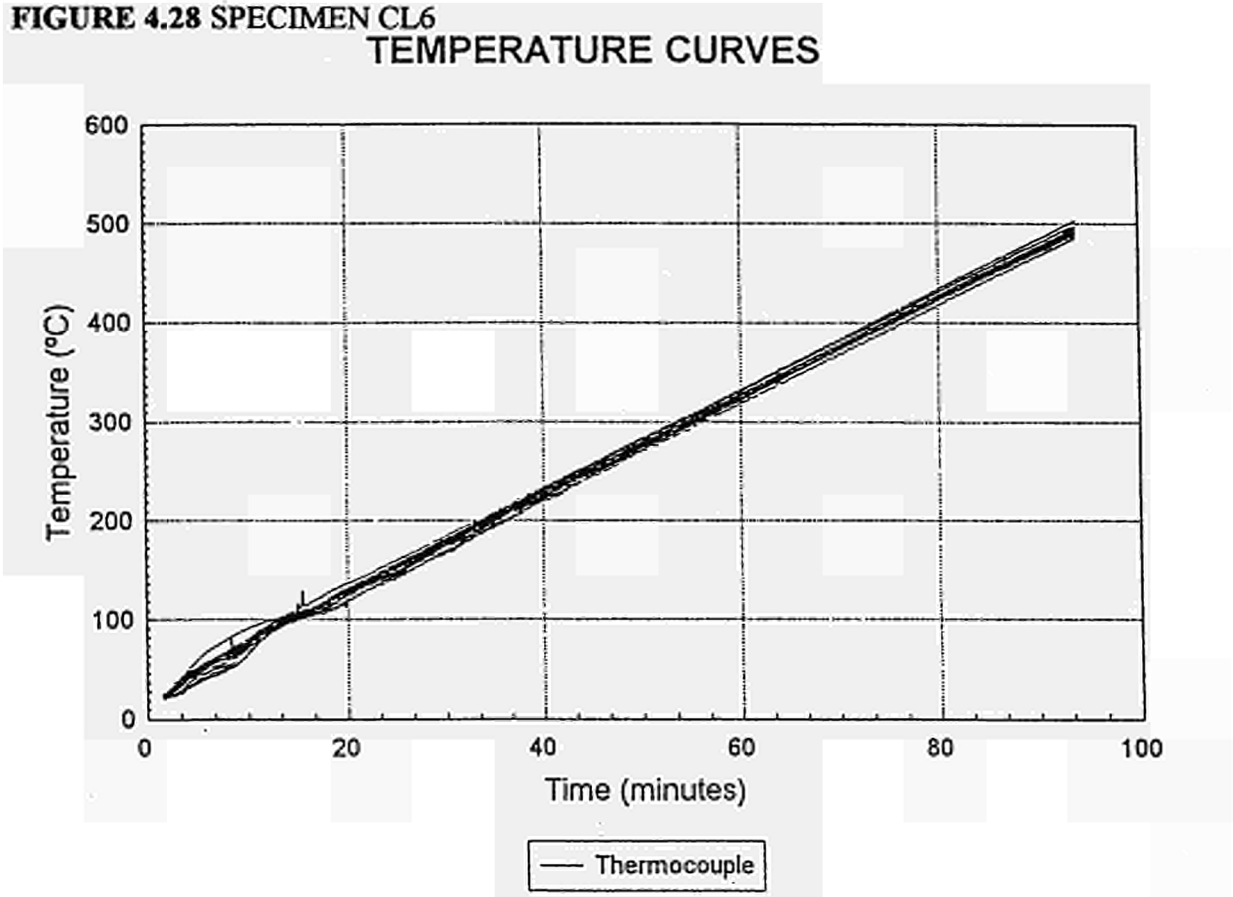

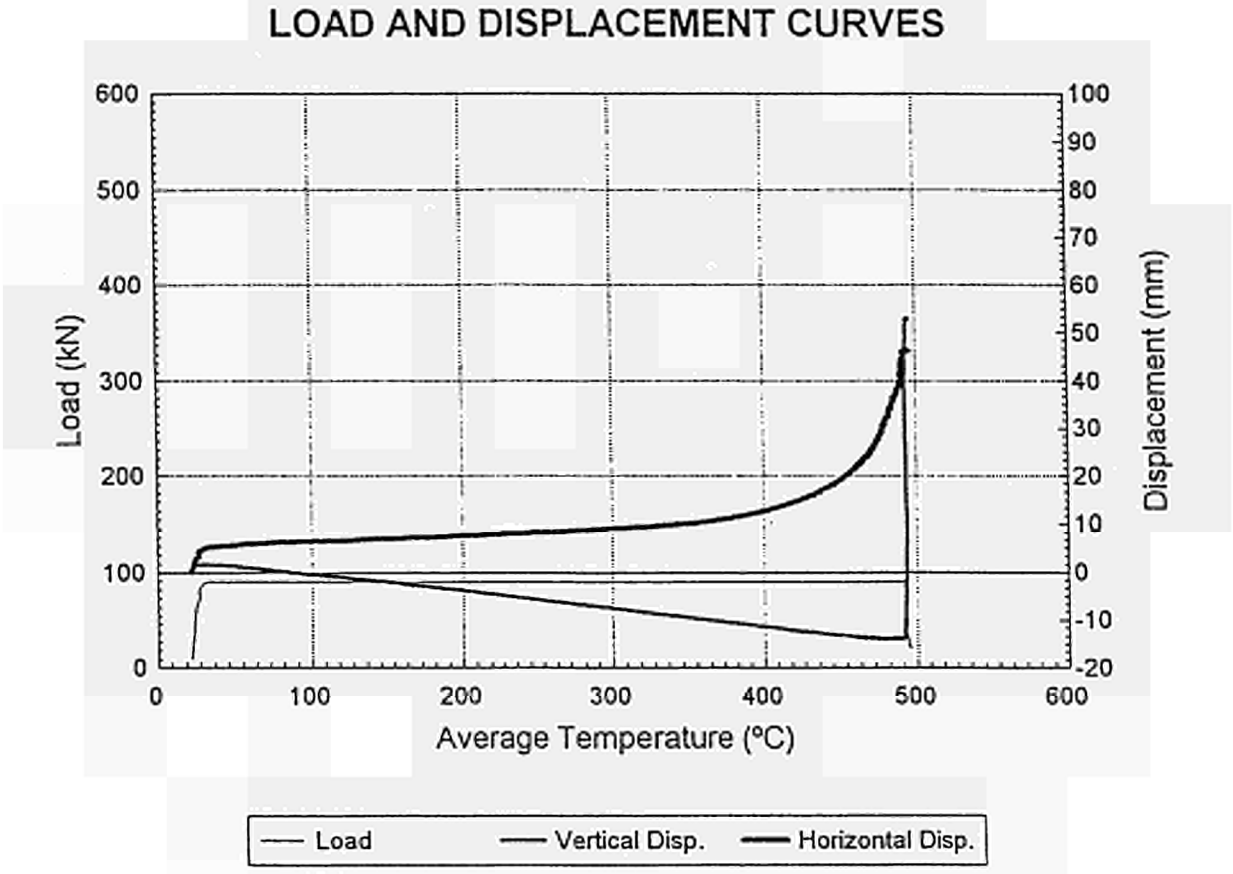

FIGURE 4.29 SPECIMEN DL6

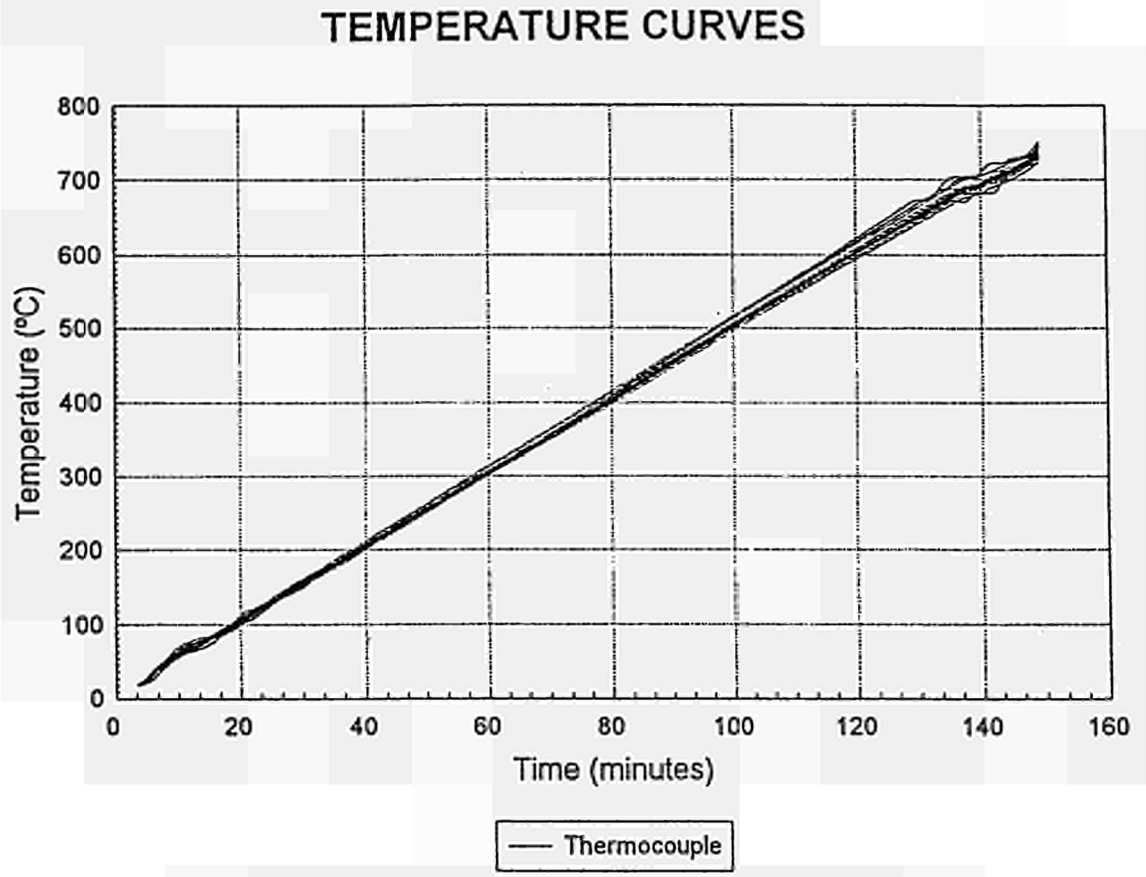

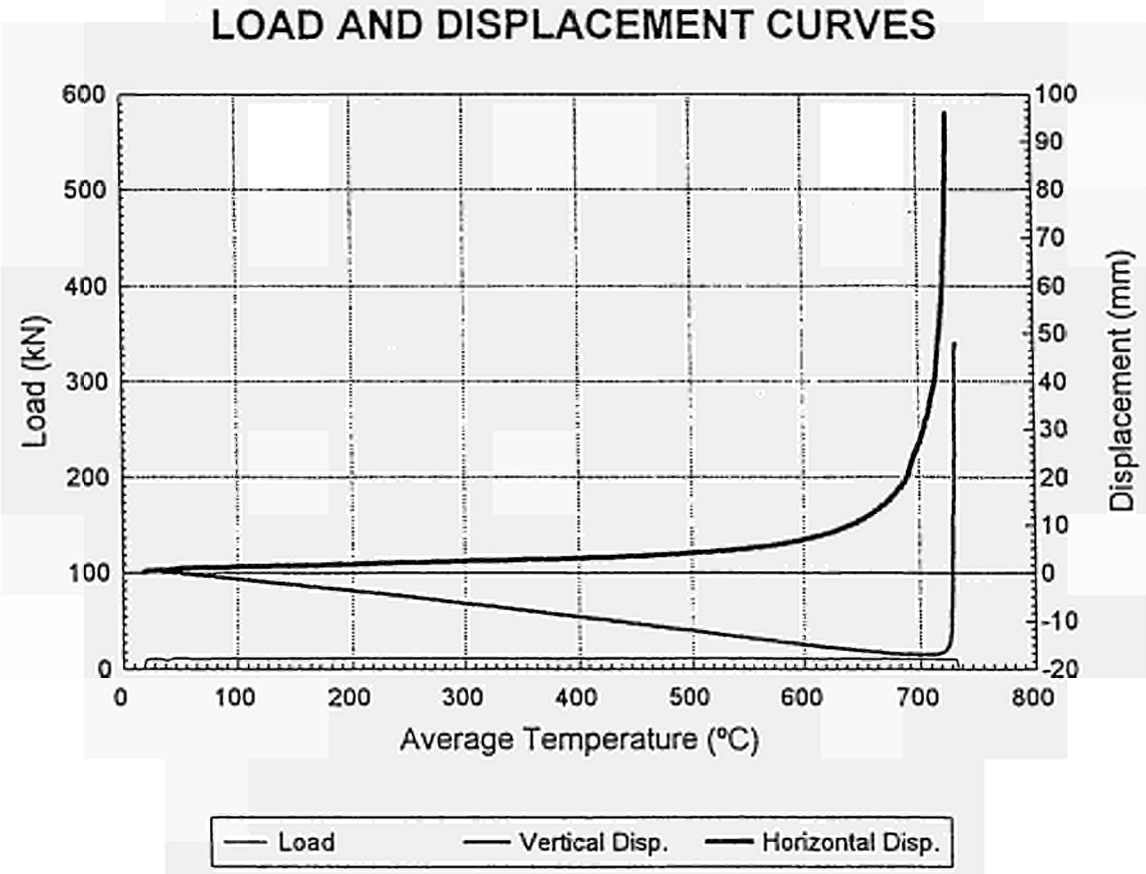

ANNEX 5:

5. CTICM TESTS

5.1 PURPOSE

Eight tests were carried out on columns subject to an axial force and to a bending moment in order acquire knowledge about the behavior of the columns in these conditions and to achieve a validation of the thermal-elastic-plastic finished element analysis software (LENAS) used to simulate the buckling of eccentrically loaded columns with rising temperatures. They also allowed to check the design assumptions such as the value of the initial deformation or the value of the yield point.

5.2 TESTS

The tests were carried out in the laboratory of the Station d'Essais du C.T.I.C.M. in Maizières-lès-Metz [13 to 20]. For the tests, it was necessary to determine :

- The heating system of the columns in order to reach a sufficiently uniform temperature.

- The type of the testing frame (according to the heating system in use).

- The dimension of the test specimens.

- The location of the measuring points (for temperatures, displacements, and the applied force).

5.2.1 HEATING SYSTEM

To heat the columns, three solutions were possible : using conventional furnaces, building a special furnace for columns, or using electric heating elements (resistors).

5.2.1.1 Conventional furnace

The laboratory of the Station d'Essais du C.T.I.C.M. is equipped with furnaces for the fire resistance testing of building elements. It seemed logical to use the existing furnaces, but this solution included practical problems which were too complex :

- Limitation of the height of the columns at 4 m.

- The temperature inside the furnaces is not uniform enough (slightly higher in the upper part)

- The base of the column must rest at about 50 cm below the furnace ground level for a proper support, which creates a considerable thermal gradient over the length of the column.

- It is difficult to measure the lateral displacements of a post at the center of a 4x3m² rectangular furnace, since a large part of the wires of the fleximeters will be heated up to 1000°C, thus leading to hardly measurable parasitic expansions.

- This solution is difficult to use, and it requires a lot of time.

5.2.1.2 Special furnace

Another solution may be to build a special furnace for our tests. It was then necessary to build a circular furnace, with a small diameter (in relation to the surface of a furnace) and the required height. To control the temperature over the length of the column, it is necessary to distribute the burners properly over the height. This solution is also difficult to use, and does not insure the uniformity of temperature within the column, even if the displacement sensors can be placed more easily and with a greater measurement reliability.

5.2.1.3 Electric heating elements

Finally, a simpler solution was chosen: it consisted of heating the column with electric heating elements. This solution has various advantages :

- The use of an existing static test frame used for the determination of the ultimate load of columns in the cold state.

- The tested columns may be up to 5 m long.

- The temperature within the column is much more uniform since it may be controlled with each resistor.

- A good reliability of the lateral distortion measurements.

- This system is very easy to use, which allows to carry out the tests with a high rhythm.

5.2.2 TEST ASSEMBLY

The columns were tested vertically to avoid an additional distortion of the column generated by its dead weight. The testing frame was made with H-sections (FIGURE 5.1) with sufficient stiffness.

Electric heating elements (FIGURE 5.2) were attached on the columns as follows : one resistor on the outer sides of the flanges and one on one side of the web, and so over the whole length of the column. Then, the column was wrapped in insulating wool. This wrapping was intended to limit the thermal losses during the heating of the column, and to reach perfect uniformity of the temperatures.

The electric heating elements were controlled by means of a programmable controller equipped with a P.I.D. system (Proportional Integral Derivative) which regulated the electric tension in the resistors in order to reach the required temperature. This required temperature was determined from the heating up curve entered into the programmable controller. The required temperature was compared with the temperature measured on the column (by means of thermocouples). If the required temperature was lower than that measured, the tension in the resistors was increased, otherwise, it was reduced (FIGURE 5.3).

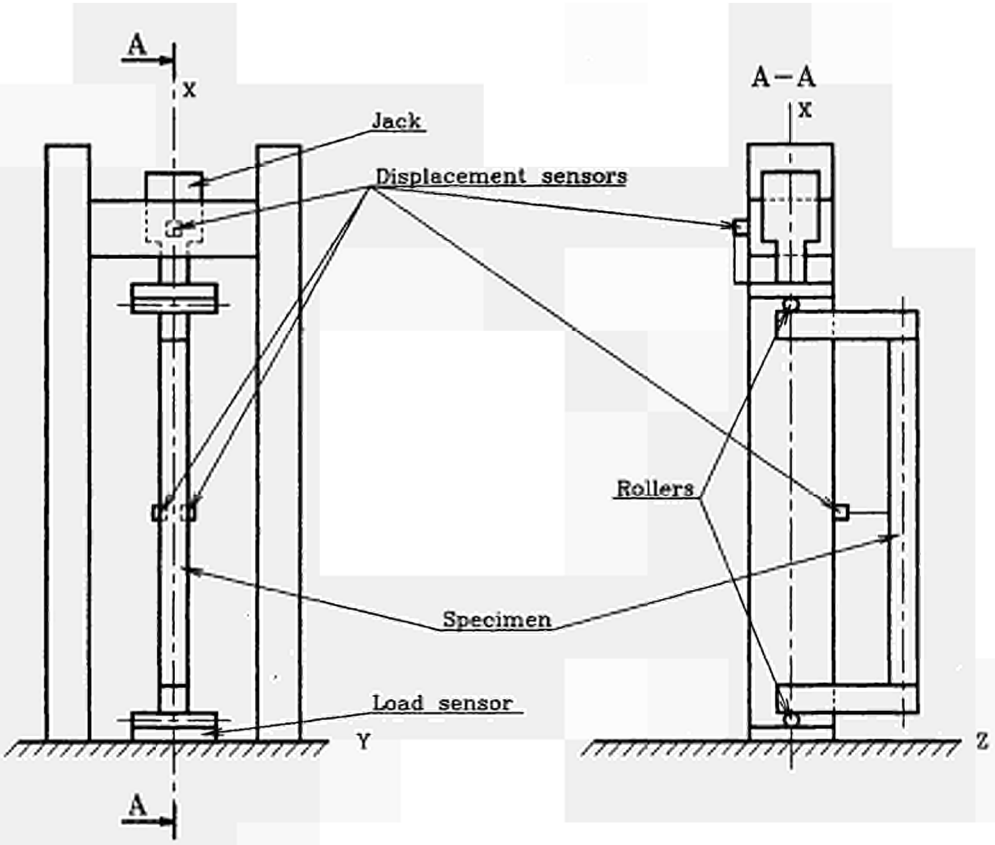

FIGURE 5.1 Test assembly

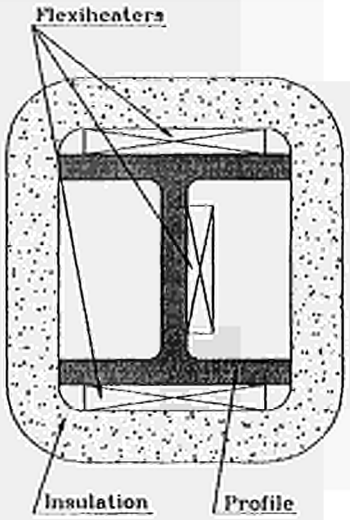

FIGURE 5.2 Location of the electric heating elements and of the insulating material

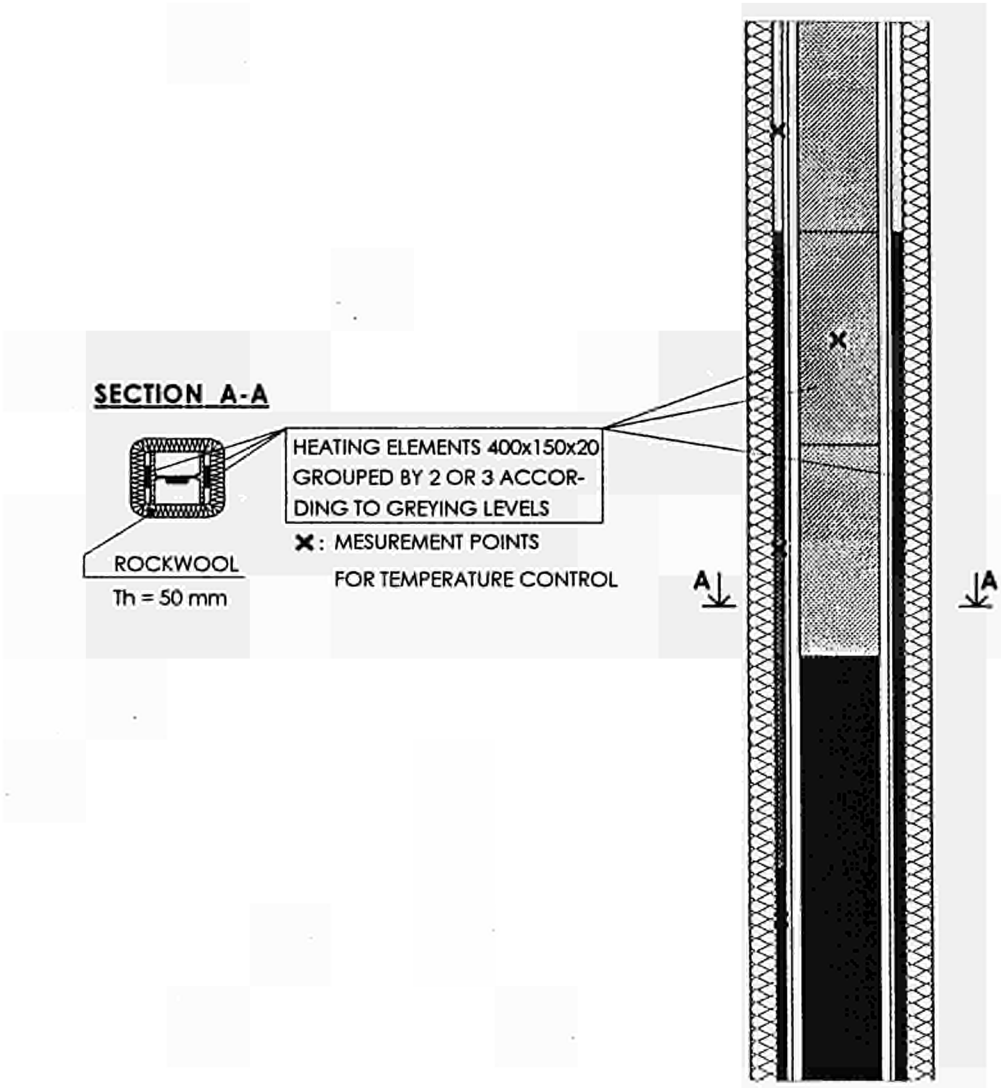

FIGURE 5.3 Location of control thermocouples and electric heating elements on the columns

5.2.3 MEASUREMENT SYSTEM

During the tests, the columns were equipped with several measurement devices, such as : load sensor, displacement sensors, thermocouples (FIGURE 5.5).

A load sensor was placed at the base of the column to record the load applied on the column continuously. Since the weight of the column was negligible in relation to the applied load, the sensor reading was reset after the column was erected. The sensor was placed in the lower part of the frame to avoid heating due to ascending hot air streams from the heated column, and thus avoid wrong readings. In addition, during the tests, the sensor was continuously cooled by a cold air stream. Two displacement sensors were positioned half-way up the column (FIGURE 5.4) in the buckling direction of the column. These double sensors allow to record any torsion of the column. A third displacement sensor was positioned at the same height, but it measured the displacements in the perpendicular direction to that of the buckling. It allowed to check that the column would not be subject to lateral torsional buckling about its second axis of inertia. A fourth sensor was positioned at the top of the column to record the axial displacement of the column under the action of the load and of the thermal expansion when the temperature increased.

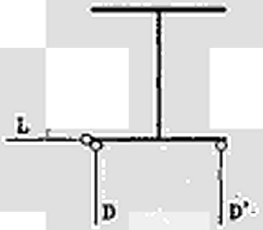

Buckling about the major axis

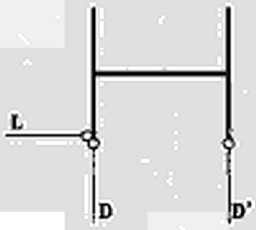

Buckling about the minor axis

FIG [redacted] **e 3 displacement sensors half-way up the columns, according to the most likely buckling axis**

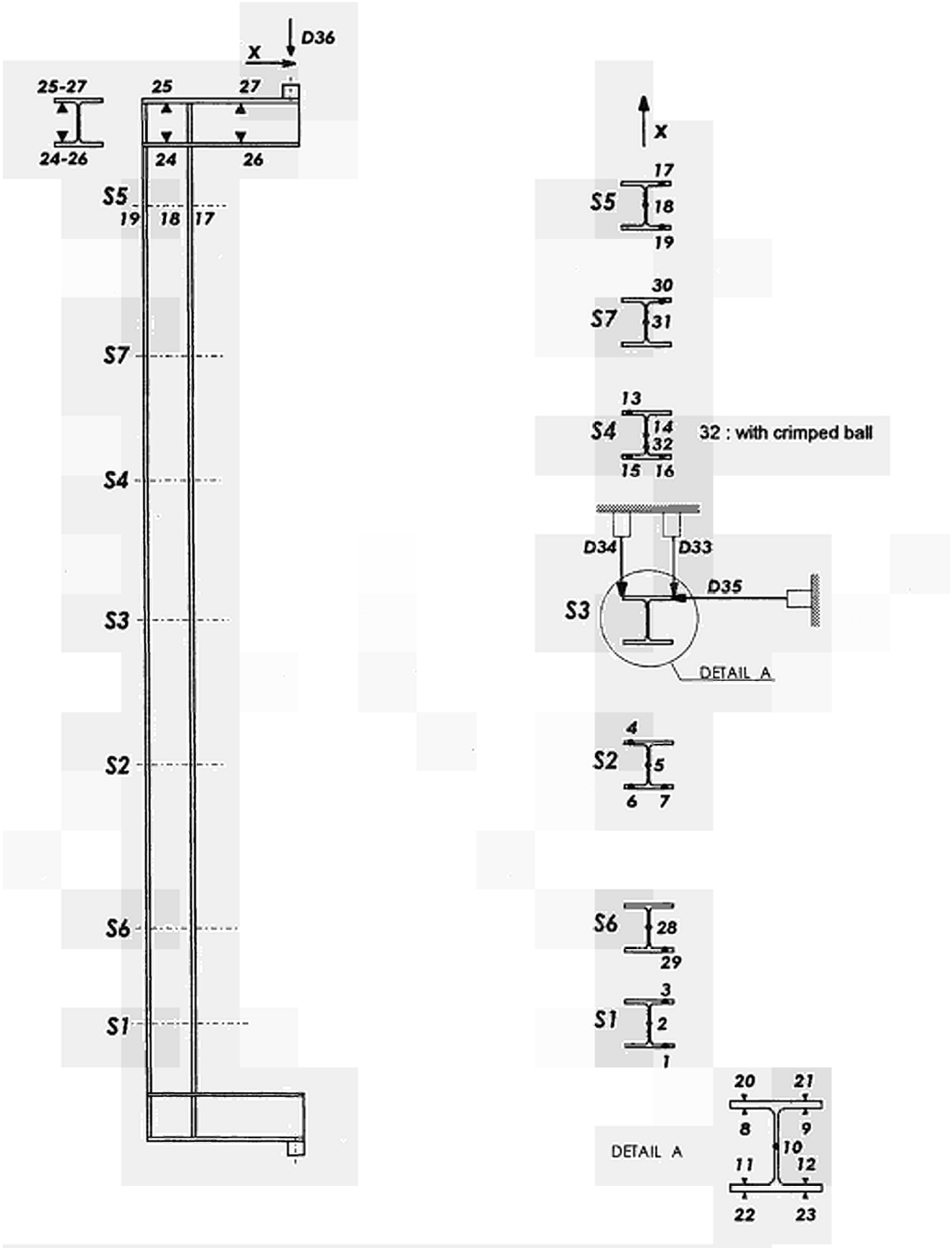

FIGURE 5.5 Location of the thermocouples and displacement sensors on P3

5.2.4 DIMENSIONS OF THE SPECIMENS AND MECHANICAL PROPERTIES

In a first stage, the type of steel section to use was determined for the eight tests, taking into account the selected buckling axis, the column length, the applied load and its eccentricity. Measurements were carried out on each specimen to find out its initial deformation, its actual section dimensions, and the yield point of the flanges and of the web.

5.2.4.1 Definition of the specimens

The test specimens were chosen so as to be representative of the structural sections (TABLE 5.1), but with reduced massiveness to avoid problems during the heating of the columns (insufficient power of the electric supply, or poor uniformity of the temperature). The loading percentage of the columns (ratio of the applied load to the failure load at ambient temperature) ranged from 24% to 72%. That allowed to cover a rather large range of failure temperatures. Very low ($\lambda < 25$) and rather high ($\lambda > 85$) slenderness ratios were chosen to cover a large enough range of slenderness ratios.

Ref.	Section	Test n°	Length [m]	λ	Applied load [kN]	Load eccentricity [m]	Loading %	Steel grade	Buckling axis
P1	HE200B	94-S-190	4	78.9	10	0.1	24	S 235	minor
P2	HE200B	94-S-186	4	78.9	10	0.3	54	S 235	minor
P3	HE200B	94-S-200	2	23.4	10	0.65	48	S 235	Major
P4	HE200B	94-S-199	2	39.5	15	0.3	72	S 235	minor
P5	HE160M	94-S-201	2	27.6	10	0.25	20	S 235	Major
P6	HE160M	94-S-197	5	70.6	10	0.5	39	S 235	Major
P7	HE140A	94-S-202	2	34.9	16	0.1	65	S 235	Major
P8	HE140A	94-S-194	5	87.3	10	0.1	53	S 235	Major

TABLE 5.1 Dimensions of the specimens and applied loads

5.2.4.2 Preliminary measurements

Some measurements were carried out before the tests. The dimensions of the sections, the column deformations (about the major axis and the minor axis) were recorded at the quarter, half and three quarters of the length of each column. TABLE 5.2 shows the values of these deformations (l / 4 represents a quarter of the column length from the base, l / 2 represents half the height of the column, and 3l / 4 represents three quarters of the length from the base).

	$\Delta_{yy'}$ (mm)			$\Delta_{zz'}$ (mm)		
Column	3l / 4	l / 2	l / 4	3l / 4	l / 2	l / 4
P1	0.5	1.5	1.5	-0.5	-0.5	-0.5
P2	1.5	2	1.5	-3	-3	-1
P3	0	1	0.5	-0.5	-0.5	-0.5
P4	1	1	0.5	0.5	0.5	1.5
P5	0	1	1	0	0	0.5
P6	1	2.5	2.5	1.5	3	2
P7	1	0.5	0.5	-0.5	0	0
P8	0.5	0.5	1	0.5	0.5	1

NOTE: The bending moment generates a displacement in directions zz' or yy' (fig. 2.1). If the measured imperfection is in the same direction as the displacement generated by the bending moment, the sign of this imperfection will be positive, otherwise it will be negative.

TABLE 5.2 Initial column straightness imperfection

The actual dimensions of the sections were measured on the specimens at the quarter of the height, at half the height, and at three quarters of the height of the columns. FIGURE 5.6 shows the average value of these three measurements recorded on each specimen.

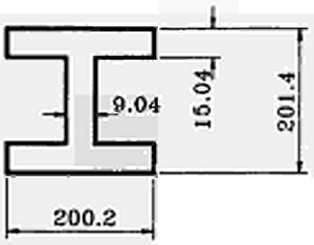

Section of column P1

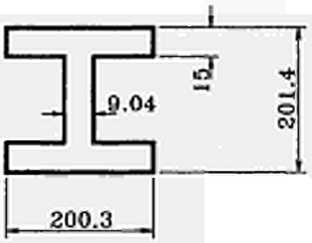

Section of column P2

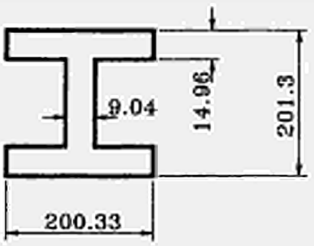

Section of column P3

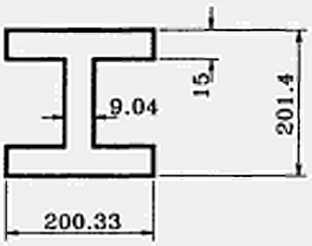

Section of column P4

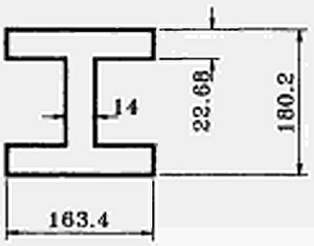

Section of column P5

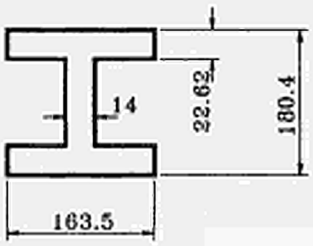

Section of column P6

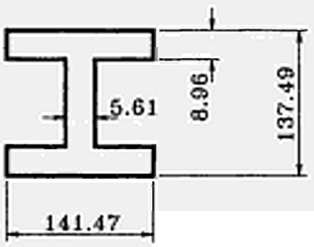

Section of column P7

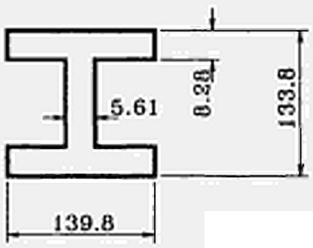

Section of column P8

FIGURE 5.6 Sections of the columns (values in mm)

The yield point was measured (TABLE 5.3) in the web and in each flange half (i.e. five measurements). These measurements were carried out only once for each section type, since

the HE160M and HE140A columns were made each time from the same member, and the HE200B columns were made with two members produced with the same metal tapping. The average value of the yield point of the flanges ($\sigma_{y\_aver\_flan}$) was worked out from the four values measured in each part of the flanges.

	STEEL SECTION		
	HE200B	HE160M	HE140A
σ_{flange_1}	265 MPa	273 MPa	264 MPa
σ_{flange_2}	279 MPa	266 MPa	262 MPa
σ_{flange_3}	279 MPa	271 MPa	261 MPa
σ_{flange_4}	274 MPa	274 MPa	253 MPa
σ_{web}	314 MPa	344 MPa	304 MPa
$\sigma_{y\_aver\_flan}$	275 MPa	271 MPa	260 MPa

TABLE 5.3 Yield point of the steel sections

5.2.5 TESTING CONDITIONS

In order to simulate the average heating conditions of protected metal columns, the thermal program consisted of two stages : a first heating up to 400°C with a temperature increase of 10°C per minute, and beyond that temperature, of only 5°C per minute, except for column P2 where the temperature increase was 10°C per minute until the end of the test.

An example of temperature recorded on column P3 is shown on FIGURE 5.7

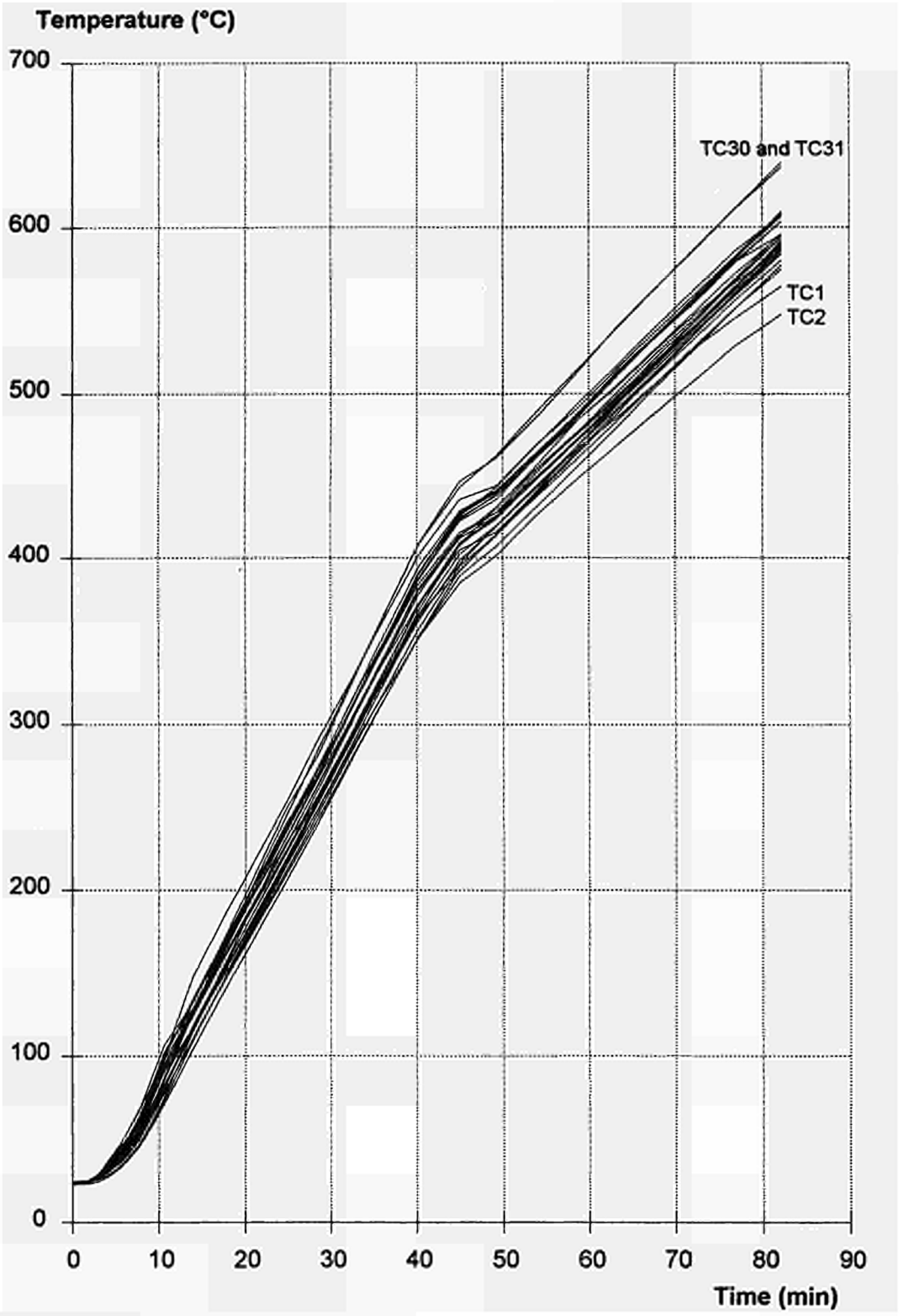

FIGURE 5.7 Temperatures recorded on P3

All the temperatures measured during the eight tests, the applied loads and the measured displacements are recorded in each test report [13 to 20].

5.2.6 DETERMINATION OF THE FAILURE TEMPERATURE

The time of failure was defined as the time when the column can no longer support the applied load. This corresponds to the time when the displacement half-way up the column becomes larger and larger, and when the deformation rate increases rapidly. The critical temperatures of the columns were calculated from the temperatures recorded in the columns at the time of failure, using two different methods:

- The first method consists of taking the average value of oall the recorded temperatures, i.e. :

$$\theta_{moy} = \frac{\sum_{i=1}^{n} \theta_i}{n} \qquad 2.1$$

- The second method consists of assigning each temperature a weighting factor. This factor is equal to the steel area taken into account :

$$\theta_{moy} = \frac{\sum_{i=1}^{n} \theta_i \, S_i}{\sum_{i=1}^{n} S_i} \qquad 2.2$$

where :

S_i is the area of the web if the i^{th} thermocouple is located in the web, and half the area of a flange is it is located in a flange

θ_i is the temperature of the i^{th} thermocouple.

In both cases, the temperatures recorded in each section nearer the ends were not taken into account, since these values are lower because of heat dissipations. FIGURE 5.7 shows that the lowest temperature was recorded by thermocouples TC1 and TC2 (see location on FIGURE 5.5), and that this temperature is 547°C. The highest temperatures, approximately 638°C, were recorded by thermocouples TC30 and TC31. The effect of the heat dissipation made the temperature decrease to 580°C for thermocouples TC17, TC18 and TC19, i.e. the thermocouples located in the highest section of the column.

On an average, the heat gradient was about 50°C on a column, and 30°C for a given section.

TABLE 5.4 shows the values recorded for the failure temperature calculated with the formulae above. These two methods lead to very similar results, and the values retained for further analysis are shown in the last column of the table.

		Critical temperature [°C]		
	Time (min)	Average	Weighted average	Retained value
P1	96.85	664.30	664.31	664
P2	58.50	575.03	575.41	575
P3	81.72	598.90	599.43	599
P4	70.68	537.64	537.99	537
P5	122.67	752.78	753.39	753
P6	76.37	572.33	572.12	572
P7	67.08	539.18	538.55	539
P8	66.22	506.82	507.56	507

TABLE 5.4 Experimental critical temperatures

ANNEX 6:

6. COMPARISON BETWEEN NUMERICAL RESULTS OF LENAS AND CTICM TESTS

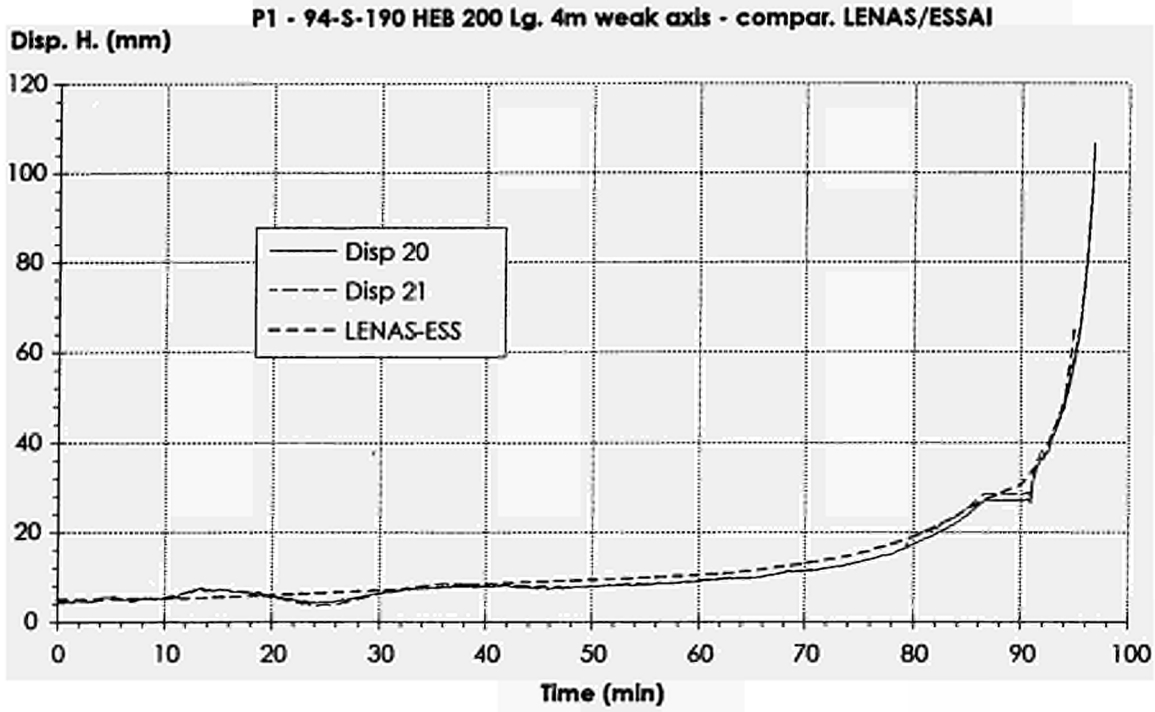

FIGURE 6.1 Horizontal displacement of column P1

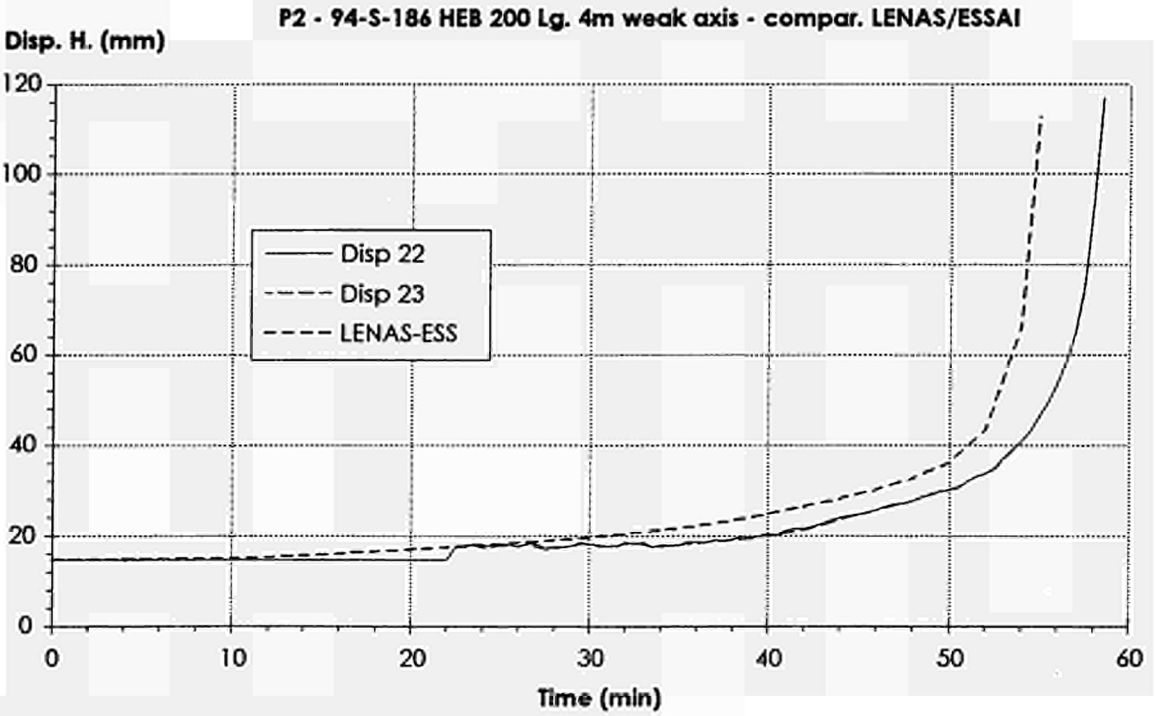

FIGURE 6.2 Horizontal displacement of column P2

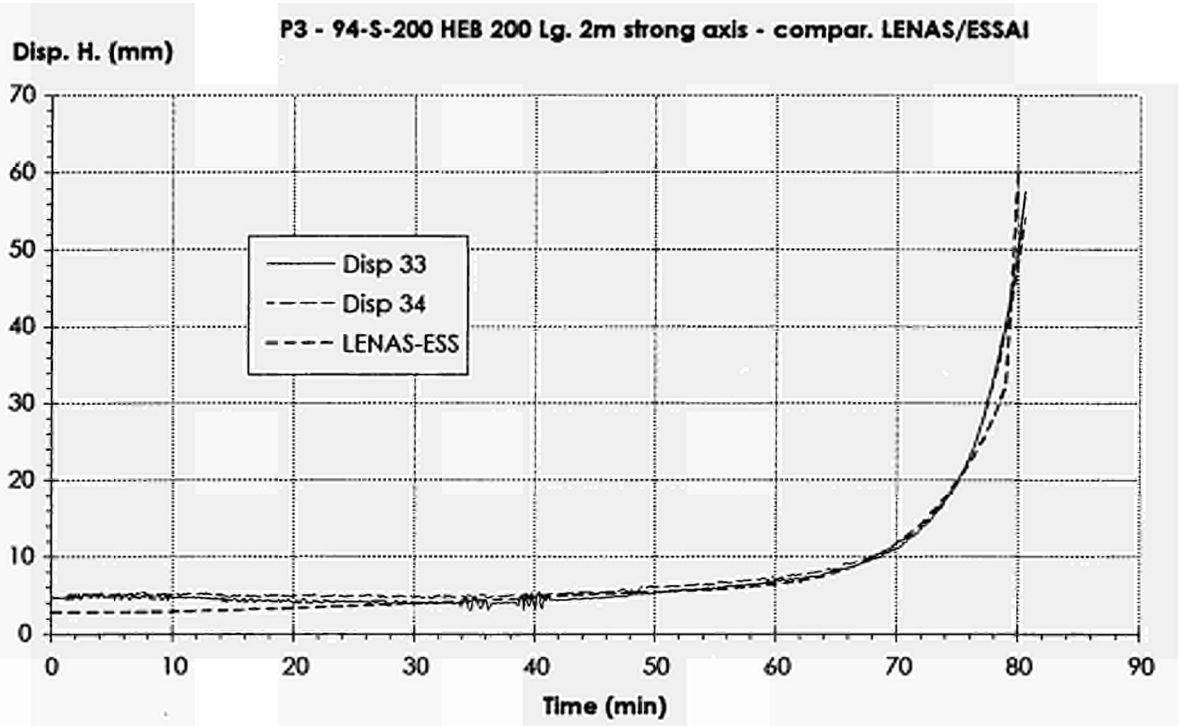

FIGURE 6.3 Horizontal displacement of column P3

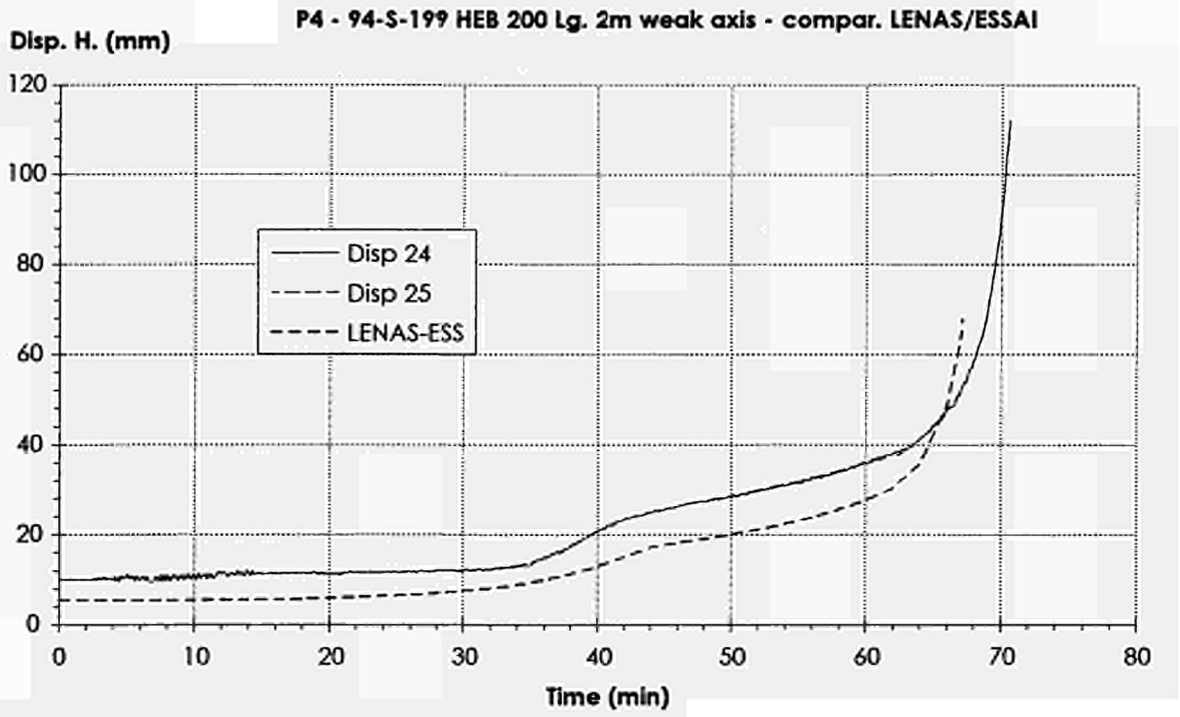

FIGURE 6.4 Horizontal displacement of column P4

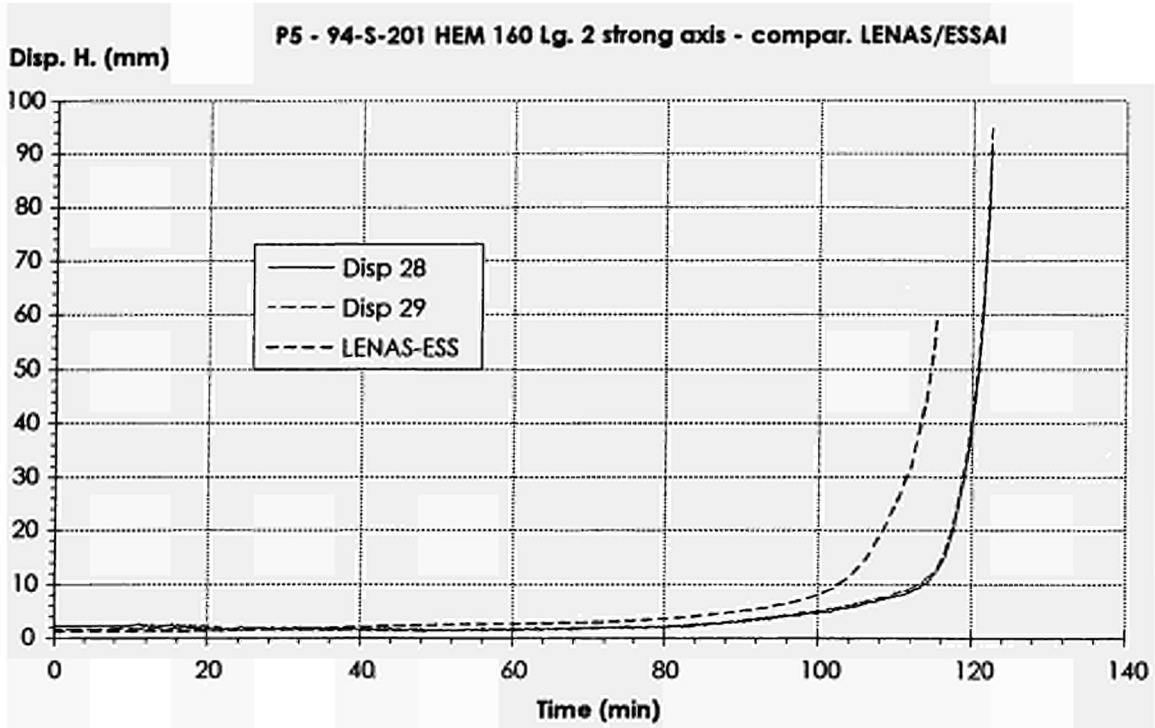

FIGURE 6.5 Horizontal displacement of column P5

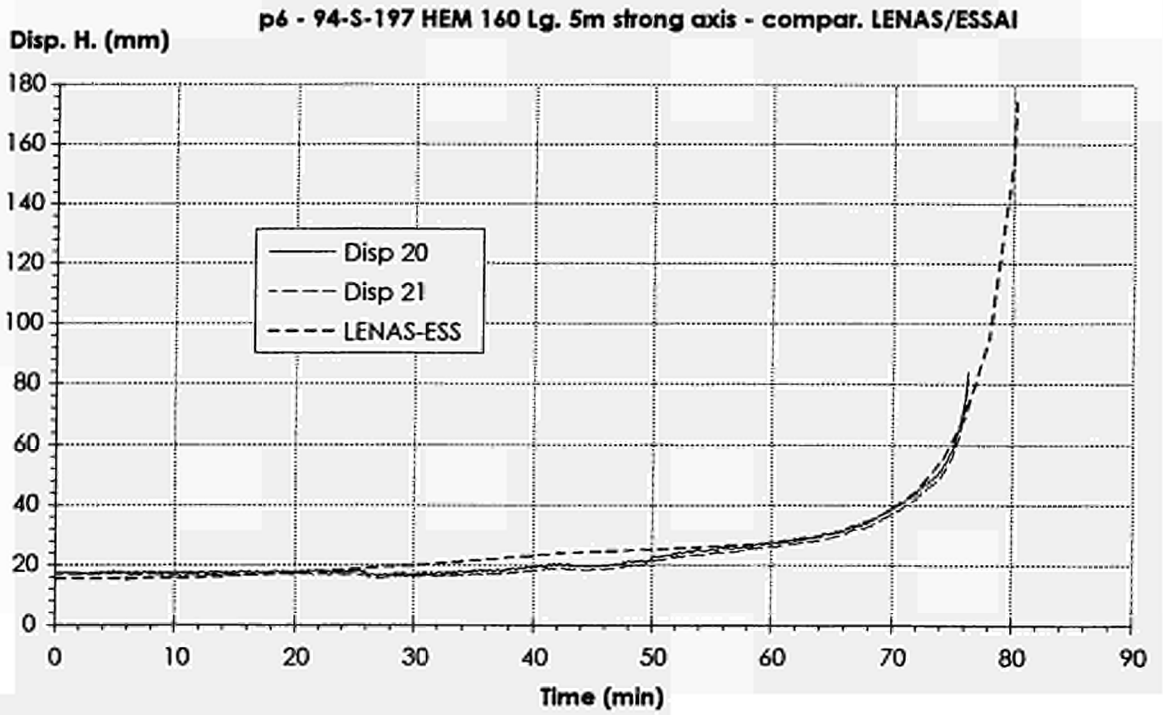

FIGURE 6.6 Horizontal displacement of column P6

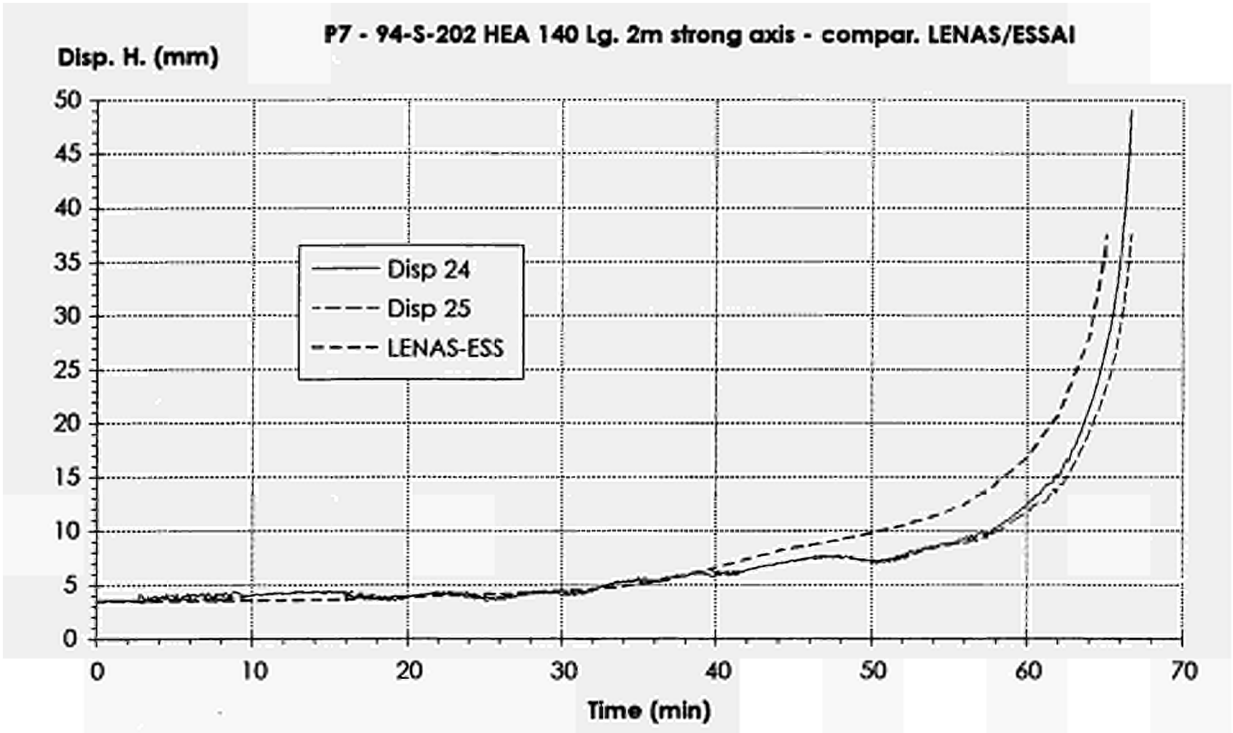

FIGURE 6.7 Horizontal displacement of column P7

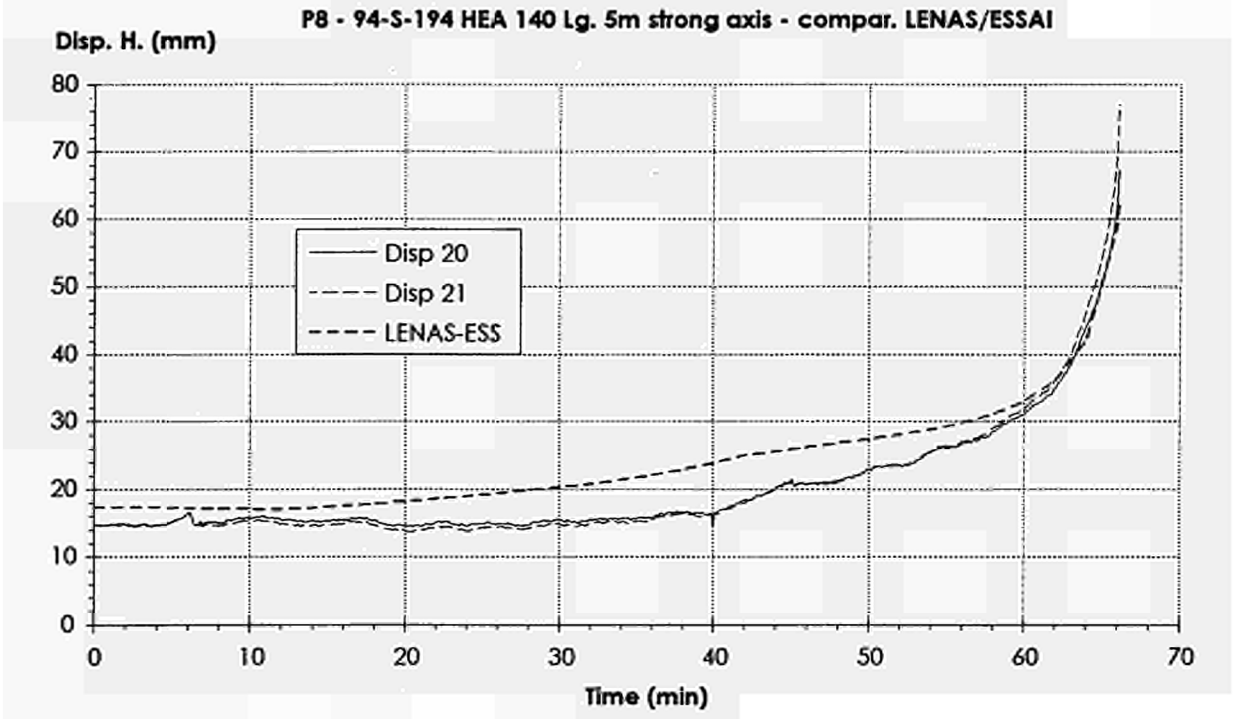

FIGURE 6.8 Horizontal displacement of column P8

ANNEX 7:

7. COMPARISON BETWEEN NUMERICAL PROGRAMS (SAFIR, CEFICOSS, LENAS, SISMEF, DIANA)

This annex is a paper made by the partners of this research and published in "Fire Safety Science" [1]

ABSTRACT

A comparison program has been established concerning the simulation of the static behaviour of steel columns submitted to fire [1]. The stress strain relationships in steel are those recommended in EC3, part 10 [2]. The five numerical codes used in this comparison are briefly described, namely CEFICOSS, DIANA, LENAS, SAFIR and SISMEF. A description of 8 tests is given: Lee's frame at ambient and at elevated temperatures, an eccentrically loaded column at ambient temperature, at uniform elevated temperature and under ISO heating and finally an axially loaded column in the same three cases (ambient, uniform and ISO).
The evolution of the horizontal displacement is graphically given for each test, as well as a table summarising the results in term of ultimate resistance.
The five programs compare reasonably well when the final resistances are considered, which would be the case in a situation of design for a real structure. In all the tests, the maximum difference between two different programs is 6%.
Differences may occur in the evolution of displacements, mainly due to the way that the residual stresses are considered, or to the fact that the non uniform temperature distribution has sometimes been replaced by a uniform temperature equal to the average value of the non uniform distribution.

Keywords : Fire resistance, Steel, Simulation, Comparison, Residual stress, Column.

INTRODUCTION

Since the first of July 1992, a research program [1] is running with the financial support of the ECSC with the aim of determining the buckling curves of hot rolled H steel sections submitted to fire, in the hypotheses of Eurocode 3, part 10 [2]. The stress strain relationships and thermal properties of steel presented in [2] are still present in the last version of EC3 part 1.2. issued in July 1993 [3]. The four organisations of the authors are responsible for the theoretical and numerical aspects, whereas LABEIN and ENSIDESA in Spain are in charge of the experimental program. As different fire codes from different organisations would be used as numerical tools in this research project, it was decided to check the consistency of the results when those different programs are applied on the same structural elements.
The main results of this comparison are presented here in order to show what level of consistency or what differences appeared, and to provide a series of points of comparison to be used by other developers of codes. Readers wishing to receive the results files can contact the first author at fax number int. + 32.41.66.95.34. Those points of comparison could also be a first help to verify the validity of the general calculation models, as required under 4.3.4., P(1) of EC3, part 10 [2].

THE CODES

The five codes are;
CEFICOSS[4,5,...,10], ProfilARBED-Recherches, Luxembourg. CEFICOSS stands for Computer Engineering of the FIre resistance of COmposite and Steel Structures.
DIANA, T.N.O. Delft. DIANA, an acronym for DIsplacement ANAlyser, is a general purpose package for structural analyses, transient potential (heat) flow problems and fluid dynamics.
LENAS-MT [11], C.T.I.C.M. Saint Rémy lès Chevreuse and TAKENAKA Tokyo. Large deflection Elasto plastic Numerical Analysis of Structures - Member in Transient state.
SAFIR, University of Liege, Belgium. This software is, after CEFICOSS, the second generation of structural fire codes developed in Liège.
SISMEF, C.T.I.C.M. Saint Rémy lès Chevreuse. Simulation a l' Incendie des Structures Mixtes par Elements Finis. Composite frame analysis considering partial connections between concrete slab and steel beam.

Some features are common for the five programs : evolution of the structure under constant load simulated as the temperatures increase, large displacements, non linear and temperature dependent material properties (structural and thermal if relevant). The main differences are identified in table 1.

TABLE 1. Main differences between the codes.

	CEFICOSS	DIANA	LENAS-MT	SAFIR	SISMEF
Thermal analysis	2D	3D	*1	3D	*1
Formulation	finite difference	finite element	-	finite element	-
Structural analysis	2D	3D	3D	3D	2D
Beam formulation	Bernoulli	Mindlin	Bernoulli	Bernoulli	Bernoulli
Nodes	2	3	2	3	2
DOF per node	3-3	6-6-6	7-7	7-1-7	3-3
Sectional discretization	rectangular fibres	Gauss-Simpson	rectangular fibres	triang. or quadr. fibres	rectangular fibres
Longitudinal integration	Gauss	Gauss	linear between the nodes	Gauss	Gauss
Large displacements	updated lagrangian	total lagrangian	updated lagrangian	total corrotational	updated lagrangian
Resid. stresses	initial strains	initial stresses	initial strains	initial strains	initial strains
Material law	uni axial	multi axial *2.	multi axial *2	uni axial	uni axial

*1 Thermal results are taken from TASEF, written by Wickström [12]
*2 Von Mises yield-criterion and isotropic strain hardening

THE TESTS.

No imposition was made concerning the discretization. Each author was responsible to chose a sufficiently fine discretization as to ensure convergence of the result with respect to the discretization, according to his experience with his own program.

STRUCTURE A : LEE'S FRAME [13].

FIGURE 1. Lee's frame (consistant units).

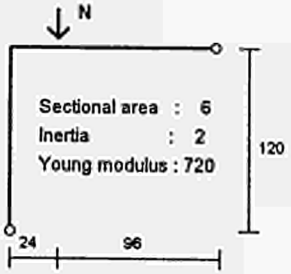

A-1 : LEE'S FRAME AT AMBIENT TEMPERATURE.

Lee's frame is often used as a reference structure to check the geometrical non linearity of programs at ambient temperature. The material is elastic, but the displacements are very large. It was analysed at ambient temperature. Fig. 2 presents the evolution of the horizontal displacement of the point where the load is applied, as a function of this vertical load.

FIGURE 2. Lee's frame at ambiant temperature.

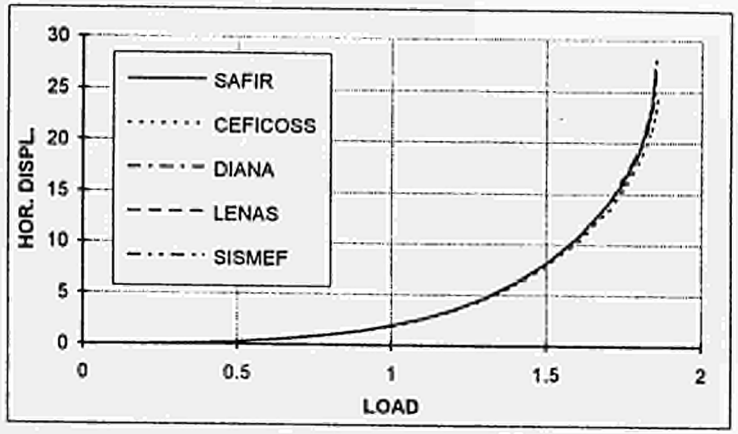

A-2 : LEE'S FRAME UNDER UNIFORMLY INCREASING TEMPERATURE.

The same structure is supposed to be made of EC3 steel with $E_s = 720$ and $f_y = 3$ (consistent units). A load of 0.2 is applied and maintained as the frame is uniformly heated. This test allows to check whether the thermal strains are correctly considered, whether redistribution of the solicitations is correct and what the effects of plasticity are at elevated temperatures. Fig. 3 presents the evolution of the horizontal displacement of the point where the load is applied, as a function of the temperature in the section.

FIGURE 3. Lee's frame under uniformly increasing temperature.

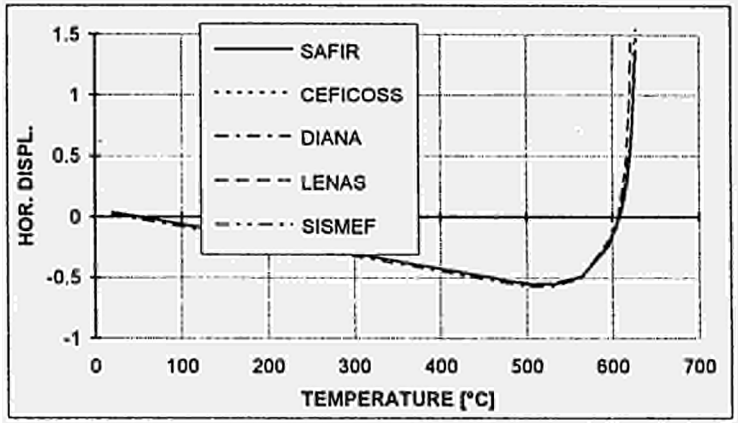

STRUCTURE B : ECCENTRICALLY LOADED COLUMN.

Description :
- simply supported column, H = 4 m, buckling around the minor axis,
- sinusoidal imperfection of 4 mm, dead weight neglected.
- HE 200 B, EC3 steel, f_y = 235 MPa, bitriangular residual stress distribution with a maximum value of 117.5 MPa.
- Loading : at both ends, axial load N + bending moment M = N x 100 mm (effects adding to the imperfection).

This column was analysed because a further step of the aforementioned research project [1] is to analyse the interaction formula R(5) from 4.2.2. in EC3 [2], proposed for members with combined axial force and moment.

B-1 : ECCENTRICALLY LOADED AT AMBIENT TEMPERATURE.

The column is analysed under increasing load and Fig. 4 provides the evolution of the horizontal displacement at mid height as a function of the vertical load.

FIGURE 4. Eccentrically loaded column at ambiant temperature.

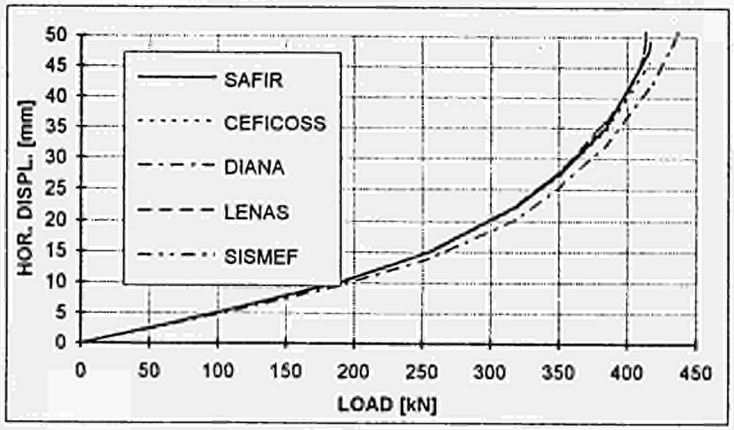

B-2 : ECCENTRICALLY LOADED AT UNIFORMLY INCREASING TEMPERATURE.

This case of uniform temperature is representative of a thermally insulated column, where the insulation gives time to the high thermal diffusivity of steel to homogenise the thermal distribution in the section. A load of 250 kN (+ M = 25 kN m) is applied and maintained as the column is uniformly heated. Fig. 5 gives the evolution of the horizontal displacement at mid height as a function of the uniform temperature in the section.

FIGURE 5. Eccentrically loaded column under increasing uniform temperature.

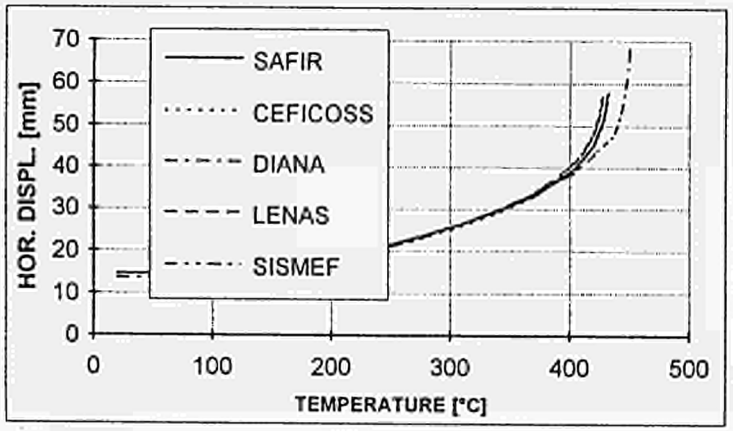

B-3 : ECCENTRICALLY LOADED UNDER ISO HEATING.

With the same load applied, the column is submitted to the ISO curve. The temperature distribution is calculated according to Eurocode[14]. The thermal gradients arising in the section can be considered as an additional structural imperfection. The evolution of the horizontal displacement as a function of time is presented on Fig. 6.

FIGURE 6. Eccentrically loaded column under ISO heating.

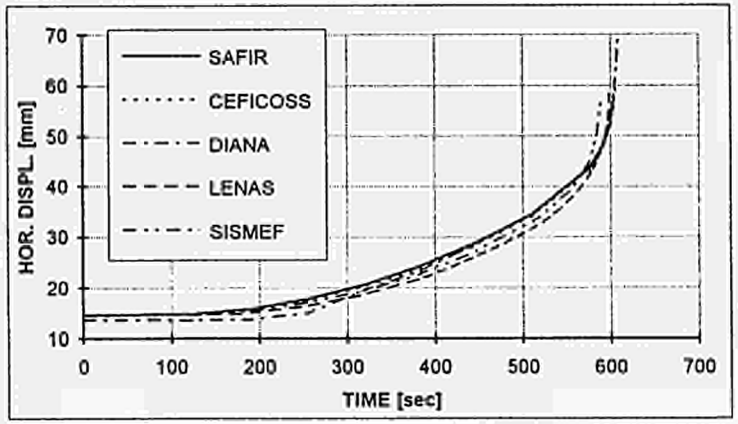

STRUCTURE C : AXIALLY LOADED COLUMN.

The column and the section are the same as for structure B.
Loading : axial load N.

C-1 : AXIALLY LOADED AT AMBIENT TEMPERATURE.

The column is analysed under increasing load and Fig. 7 provides the evolution of the horizontal displacement at mid height as a function of the axial load.

FIGURE 7. Centrically loaded column at ambiant temperature.

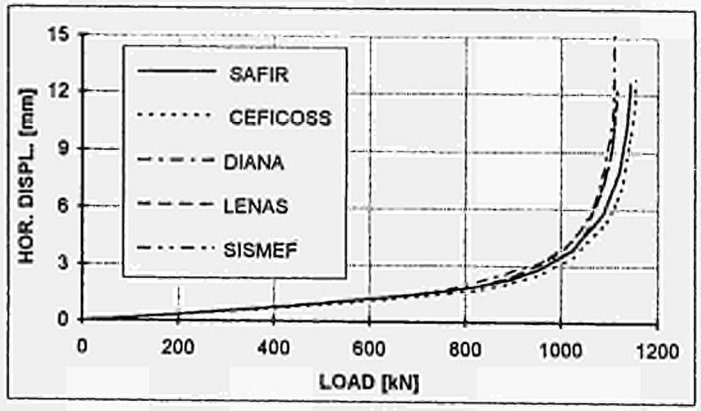

C-2 : AXIALLY LOADED AT UNIFORMLY INCREASING TEMPERATURE.

An axial load of 500 kN is applied and maintained as the column is uniformly heated. Fig. 8 gives the evolution of the horizontal displacement at mid height as a function of the uniform temperature in the section.

FIGURE 8. Centrically loaded column under increasing uniform temperature.

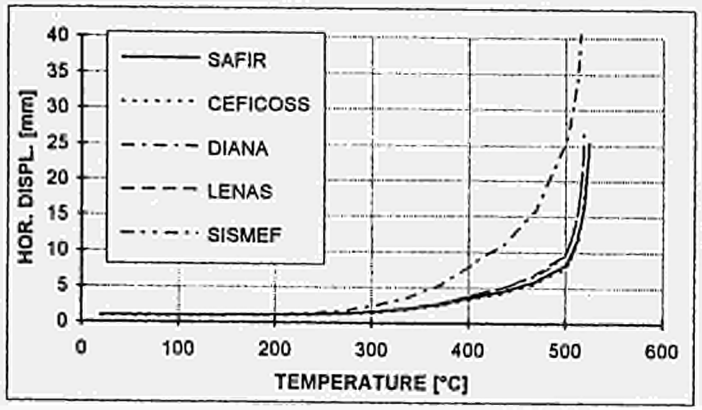

C-3 : AXIALLY LOADED UNDER ISO HEATING.

With the same load applied, the column is submitted to the ISO curve. The evolution of the horizontal displacement as a function of time is presented on Fig. 9.

FIGURE 9. Eccentrically loaded column under ISO heating.

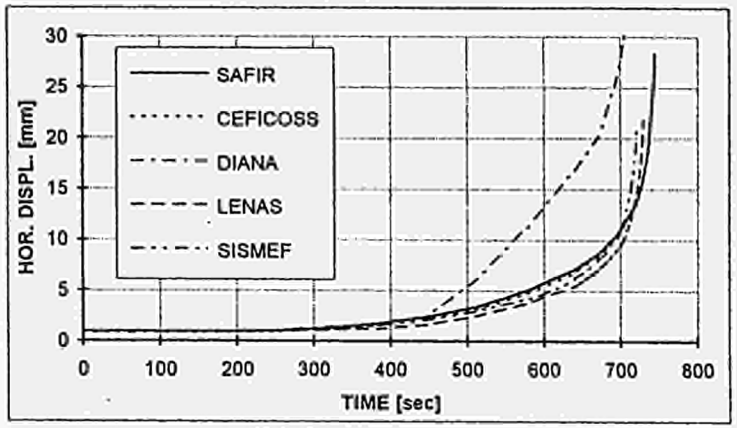

COMMENTS ON THE RESULTS

General comment :

Some of the curves presented in Fig. 2 to Fig. 9 appear as made of linear segments, not because the programs really predicted such a discontinuous behaviour (sudden plastification of the section, for example), but because only discrete points have been calculated in the diagrams and linear interpolation applied on the results when plotting the drawings.

A summary of the results is presented in table 2.

TABLE 2 : Summary of the results.

	A-1	A-2	B-1	B-2	B-3	C-1	C-2	C-3
	Load	Temp.	Load	Temp.	Time	Load	Temp.	Time
SAFIR	1,85	626°C	417 kN	432°C	604 sec	1144 kN	524°C	745 sec
CEFICOSS	1,86	625°C	416 kN	433°C	606 sec	1154 kN	524°C	745 sec
DIANA	1,855	628°C	437 kN	450°C	609 sec	1113 kN	515°C	717 sec
LENAS	1,84	621°C	414 kN	428°C	599 sec	1116 kN	518°C	730 sec
SISMEF	1,84	625°C	414 kN	427°C	589 sec	1117 kN	519°C	722 sec
Analytical	1.855					1170 kN		

For test C-1 the analytical value is provided by EC3, part 1. For a slenderness of78.90,European buckling curve c gives : Nult = 0.657 x Npl = 0.657 x 1835 kN = 1170 kN.

LEE'S FRAME.

The results of test A-1 compare very well with the analytical solution from [13], where the ultimate load is given as 1.855. All program find a result that differs by less than 1% from this analytical value. This comes as no surprise considering that Lee's frame is a commonly analysed structure for the validation of non linear codes at ambient temperature. The success with this test is therefore a minimum requirement for non linear fire codes.
When analysed at elevated temperature (test A-2), Lee's frame has also the same response according to the five programs which differ by no more than 1% considering the ultimate temperature. This gives some confidence that the law of thermal elongation and the stress-strain relationship have been similarly (and hopefully correctly) introduced in the five codes.

ECCENTRICALLY LOADED COLUMN.

The eccentrically loaded column introduces the effect of residual stresses. The four program specifically dedicated to fire analysis differ by less than 3 %. The differences between DIANA and the average value of the results given by the other four codes is 5%, 5% and 2% for the tests B-1, B-2 and B-3 respectively.

AXIALLY LOADED COLUMN.

The structure C has the same structural imperfections as the structure B (residual stresses and non uniform temperature distribution). The maximum difference between the five programs is, in term of ultimate value, less than 4%. The displacement history calculated by DIANA is significantly different from the results provided by the other programs for tests C-2 and C-3, with large displacements appearing earlier and being more important at the end of the simulations, while the results by DIANA are close to the others at the beginning of the simulations.
The reason of this difference has not been clearly identified. Some possible reasons might be;
1. The non uniform temperature distribution in case of ISO heating.
SAFIR and CEFICOSS have their own thermal routines directly linked to the static routines.
LENAS and SISMEF simulations are based on thermal results from TASEF[15].
DIANA has its own thermal routines, but not linked as a standard option to the static routines. The transfer of the thermal results to the static calculation has not been made here in order to reduce the amount of work to be done and the tests B-3 and C-3 have been calculated with uniform temperature distribution. This is yet not thought to be a major cause of the difference because, firstly the uniform temperature calculated by DIANA was similar to the average value of the non uniform temperature calculated by the other programs, secondly there is much less difference in test B-3, *although the test B-3 has also been simulated by DIANA with a uniform temperature distribution instead of a really non uniform distribution.*
2. The way how the residual stresses are considered could be the main factor.
SAFIR, CEFICOSS, LENAS and SISMEF consider initial values of residual strains, which are then naturally kept constant during the simulation [15, 16].
DIANA considers initial values of residual stresses, which are kept constant during the simulation, except if they are larger than the maximum stress allowed at each temperature.
The influence of the residual stresses and the influence of the way in which they are accounted for is illustrated in Fig. 10 for the case C-2. In this figure, the horizontal displacement calculated by DIANA and SAFIR is plotted, with and without taking into account the residual stresses. It can be seen that both codes provide very similar results when the residual stresses are not accounted for. The effect of the residual stresses on the failure temperature is not as significant as it is on the deformation behaviour. The way in which the residual stresses are taken into account does not lead to important differences for the eccentrically loaded column (see Fig. 5). Apparently the effect of the eccentricity overrules the effect of the different assumptions with regard to the residual stresses.

FIGURE 10. Influence of the residual stresses and of the way in which they are modelled..

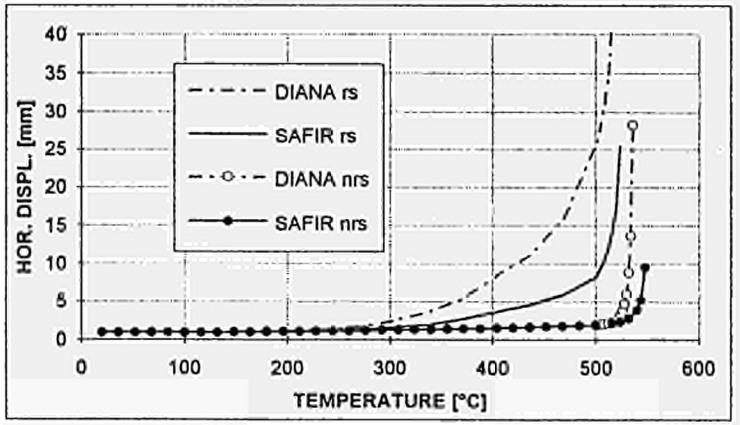

CONCLUSIONS

When applied to a structure where bending is predominant, this comparison confirmed what has already been reported elsewhere [17 p. 8.4.], that most of the simulation programs provide very similar results.
When applied to structures with important axial loads, the different five programs show differences in term of ultimate resistance that would probably be acceptable in a situation of practical design (maximum difference between two programs for all the tests : 6%). LENAS and SISMEF generally lead to very slightly lower ultimate values than SAFIR and CEFICOSS, and DIANA's results are situated either on the safe or on the unsafe side of the results of the four others.
Some differences could be observed in the evolution of displacements, probably due to the different ways that the residual stresses are considered when temperatures increase. The effects of those residual stresses appear to be the most significant in the case of centrically loaded column. This structure is indeed very sensitive to structural imperfections because any additional lateral displacement, even if small, rapidly leads the column toward instability. The effects of the residual stresses tend to decrease when the load is applied with an eccentricity.

REFERENCES

1. ProfilARBED-Recherches (Research Manager), SPCH Univ. of Liège, LABEIN-Bilbao, CTICM St Rémy lès Chevreuse, TNO - Delft. "Buckling curves in case of fire", C.E.C. Research 7210-SA/515/931/316/618, 1992-95
2. Kruppa, J., Law, M. and Twilt, L., Eurocode No. 3 Design of Steel Structures. Part 10: Structural Fire Design, Commission of the European Communities, Draft April 1990.
3. prENV 1993-1-2. Eurocode 3. Design of steel structures. Draft part 1.2. Structural fire design July 1993 version, CEN, 1993.
4. Schleich J.B., "REFAO-CAFIR , Computer assisted Analysis of the Fire Resistance of Steel and Composite Steel-Concrete Structures", C.E.C. Research 7210 SA/502 : Final Report EUR 10828 EN, Luxembourg, 1987.
5. Cajot L.G., Mathieu, J. and Schleich J.B. "REFAO-II. Practical Design Tools for Composite Steel Concrete Construction Elements Submitted to ISO-FIRE, Considering the Interaction Between Axial Load N and Bending Moment M", C.E.C. Research 7210-SA/504. Final Report EUR 13309 EN., RPS Report N° 3/90, Luxembourg, 1991.
6. Cajot L.G., Chantrain Ph., Mathieu J. and Schleich J.B.,"REFAO-III. Practical Design Tools for Unprotected Steel Columns Submitted to ISO-Fire", C.E.C. Research 7210-SA/505 : Final Report Eur 14348 EN, RPS Report N°11/91, Luxembourg, 1992
7. Cajot L.G., Franssen J.M. and Schleich J.B., "Computer Model for the fire resistance of Composite Structures", IABSE Symposium, Mixed Structures : Bruxelles, 5-7 September 1990
8. Cajot L.G.and Schleich J.B, "New Developments in the Fire Research, Resistance after fire, Effective width of composite beams during fire, Frames under natural fire conditions", Nordic Steel Colloquium on Resarch and Development within the Field of Steel Construction; Odense, Denmark, 9-11 September 1991, ProfilARBED, Luxembourg, RPS Report N° 15/91.
9. Brasseur M., Cajot L.G., Scherer M. and Schleich J.B., "Integrated Fire Safety Engineering applied to NBA", ProfilARBED Research, Luxembourg, RPS Report N°16/92, 1992.
10. Schleich, J.B., "Brandschutzkonzepte aus europäischer Sicht", Das moderne Stahlbauunternehmen, Deutscher Sthahlbautag, Berlin, Deutschland, 15-17 Oktober 1992, DSTV, Köln, pp.5-26, 1992.
11. Kaneka H. "Etude par la méthode des éléments finis du comportement mécanique d'éléments plaques en acier soumis à l'incendie", Construction Métallique, N°1, 1990.
12. Sterner, E., Wickström, U., TASEF - Temperature analysis of structures exposed to fire-user's manuel, SP Report 1990:05, Swedish National Testing Inst., Boras, Sweden, 1990..
13. Lee, S. L., Manuel, F. S. and Rossow, E. C., "Large deflections and stability of elastic frames", J. of Eng. Mech. Div., A.S.C.E., Vol. 94, EM2, p 521, 1968
14. Eurocode on Ations on Structures. Chapter 20: Actions on Structures Exposed to Fire, Draft April 1990, Commission of the European Communities, 1990.
15. Franssen, J. M., "Modélisation et influence des contraintes résiduelles dans les profils métalliques soumis à l'incendie", Construction Métallique: 3, 35-42, 1989.
16. Franssen J.M., "Residual stresses in steel profiles submitted to the fire. An analogy", Proc. of the 3rd CIB/W 14 FSE Workshop on Modelling held in Delft on the 25th and 26th of January 1993. To be published.
17 ECCS - Technical Committe 3 - Fire Safety of Steel Structures, "Fire safety in open car parks. Modern fire engineering", ECCS Technical note N° 75, 1993.

ANNEX 8:

8. N-M INTERACTION CURVESFOR A TEMPERATURE OF 400°C

The figures in this annex show the points of the M-N interaction curves calculated with LENAS for a failure temperature of 400°C.

The calculations were carried out for buckling about the minor and major axes and on the following steel sections :

- HE AA 100, 200, 400, 600 and 1000

- HE A 100, 200, 400, 600 and 1000

- HE B 100, 200, 400, 600 and 1000

- HE M 100, 200, 400, 600 and 1000

- IPE 80, 200, 400, 600, IPE 750x137, IPE 750x147, IPE 750x173, and IPE 750x193

Three load cases are presented :

- A uniform moment distribution.

- A triangular moment distribution.

- A bi-triangular moment distribution.

Ten buckling lengths were analyzed, from $\overline{\lambda}_{20} = 0.2$ to 2

These graphs represent on the x-axis the value of moment M divided by the plastic moment M_{pl}, and on the y-axis the value of axial force N divided by the failure load N_u, at temperature θ, under a centered load.

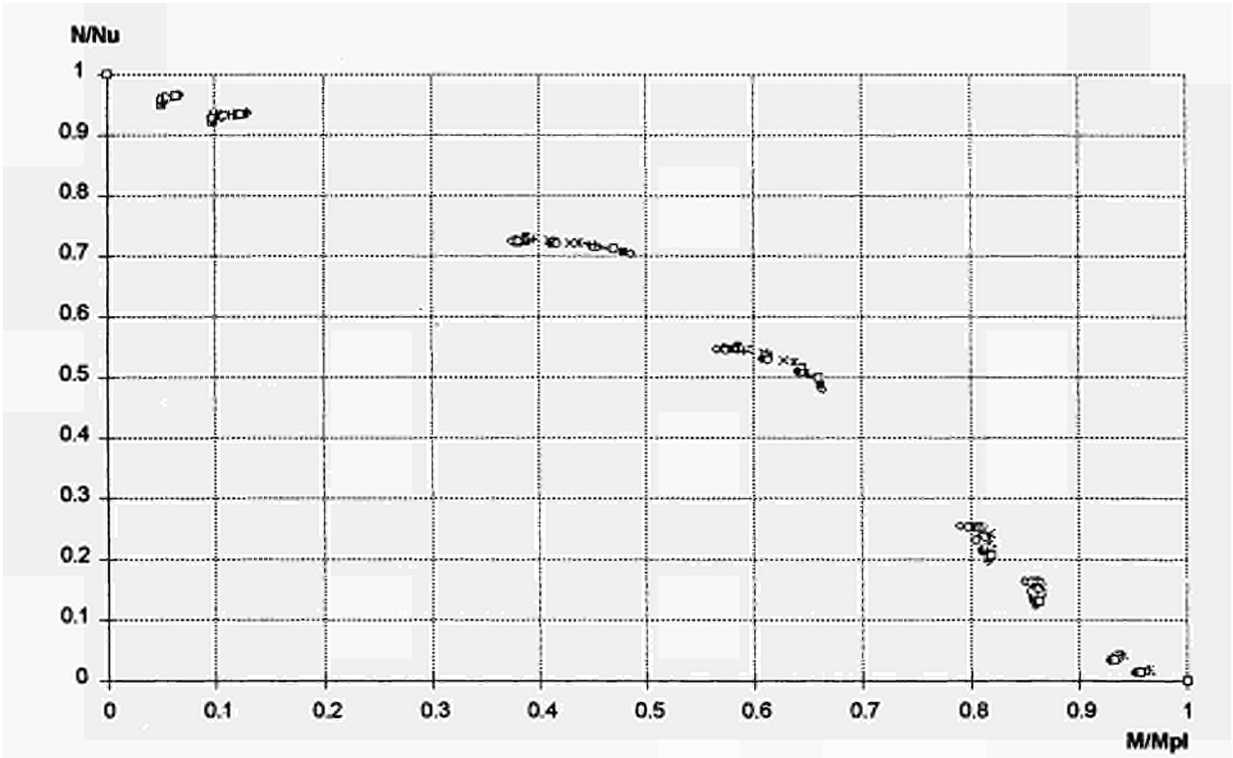

FIGURE 8.1 Points calculated for buckling about the minor axis, uniform moment distribution, and $\bar{\lambda}_{20} = 0.2$

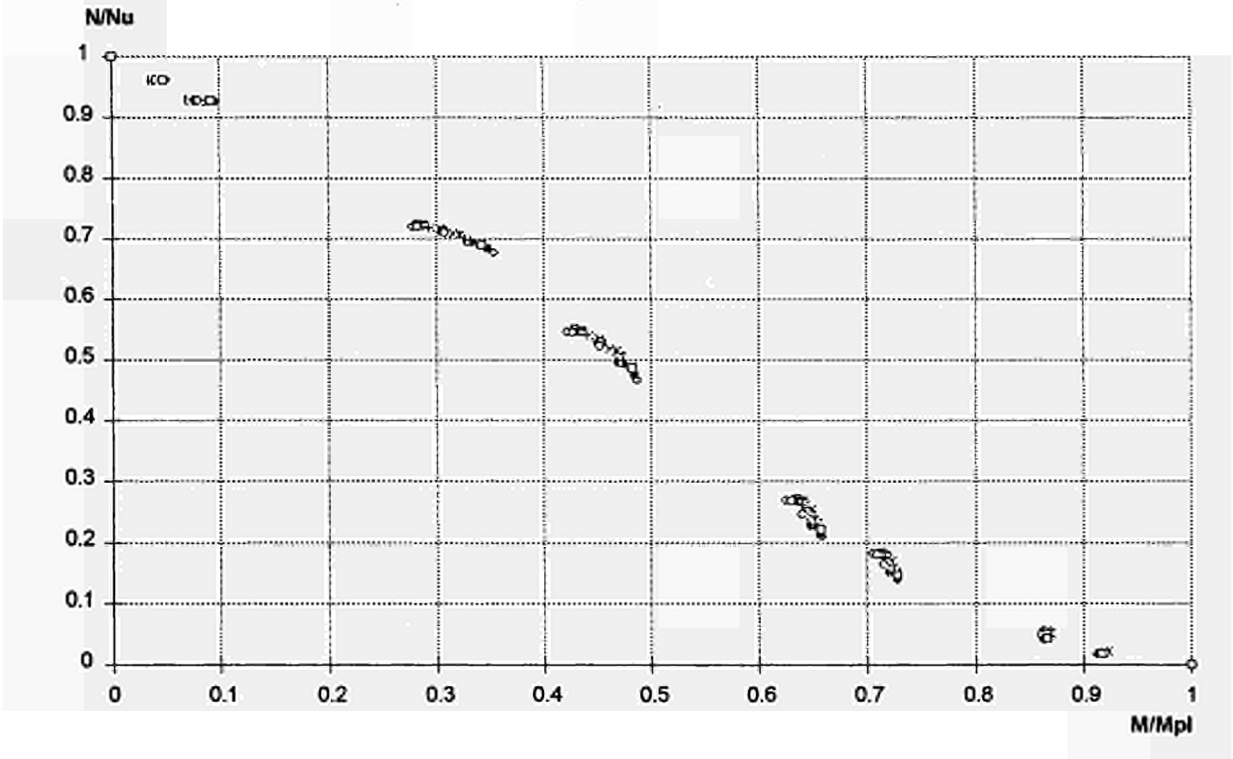

FIGURE 8.2 points calculated for buckling about the minor axis, uniform moment distribution, and $\bar{\lambda}_{20} = 0.4$

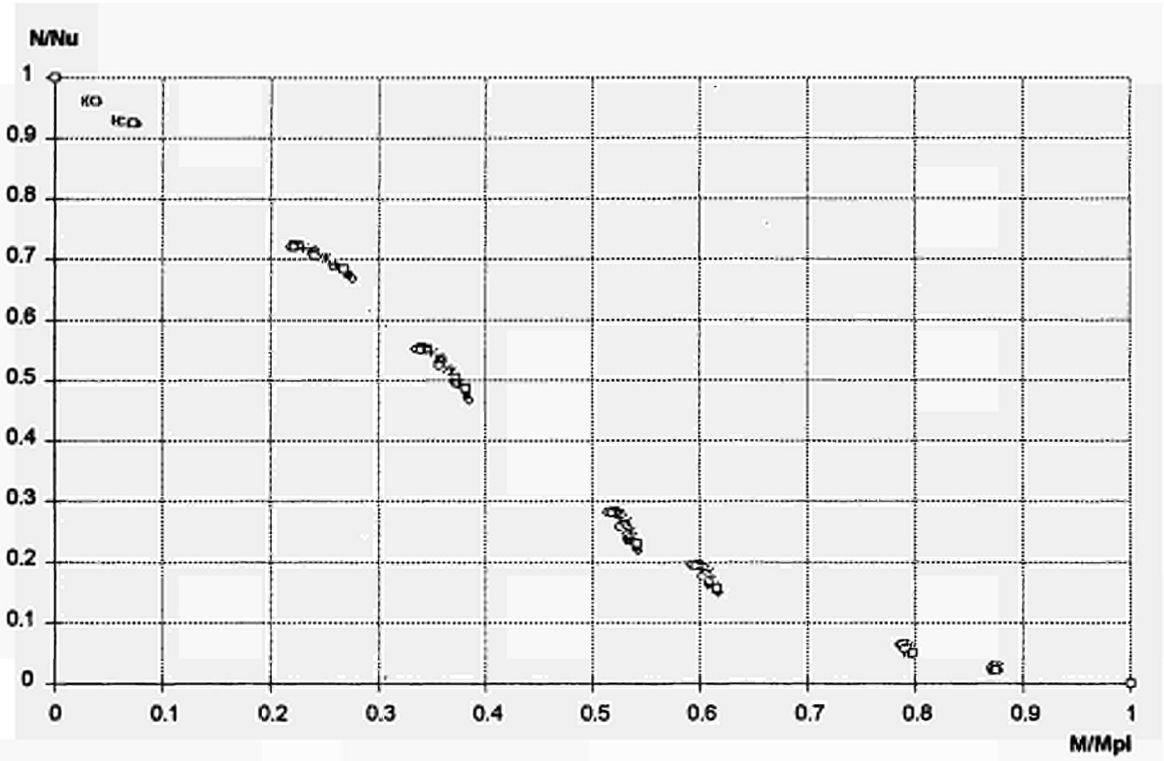

FIGURE 8.3 Points calculated for buckling about the minor axis, uniform moment distribution, and $\bar{\lambda}_{20} = 0.6$

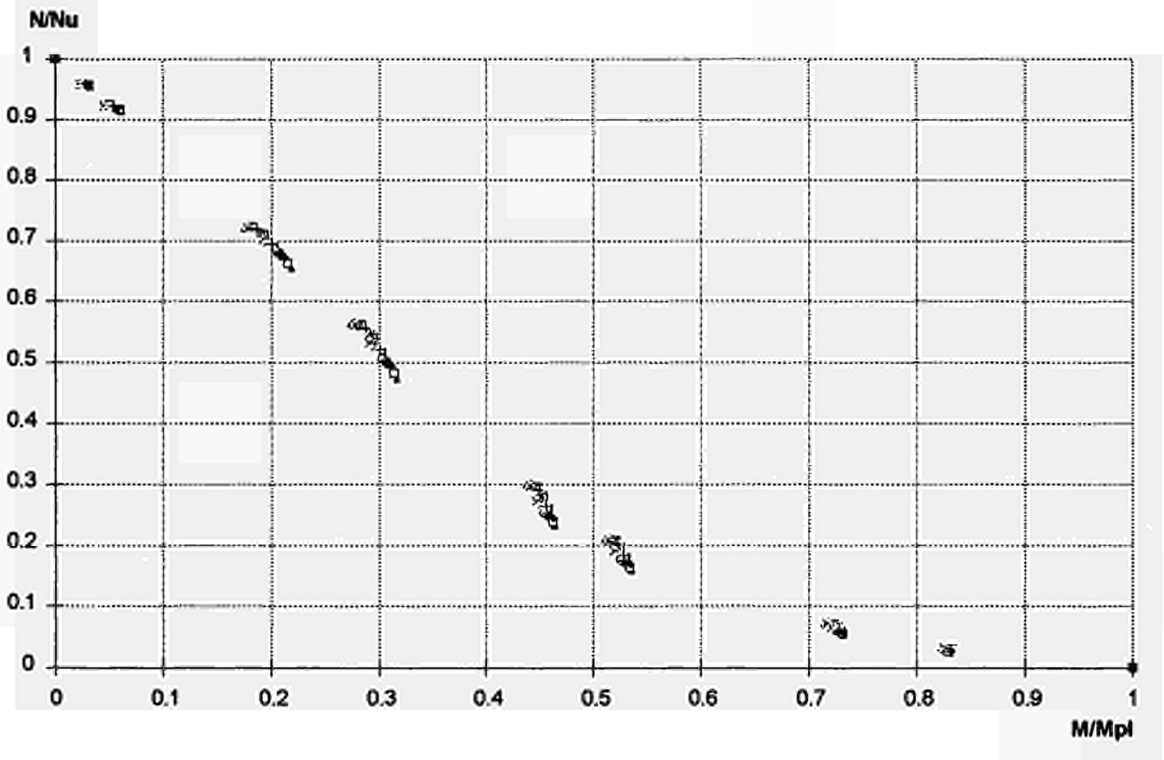

FIGURE 8.4 Points calculated for buckling about the minor axis, uniform moment distribution, and $\bar{\lambda}_{20} = 0.8$

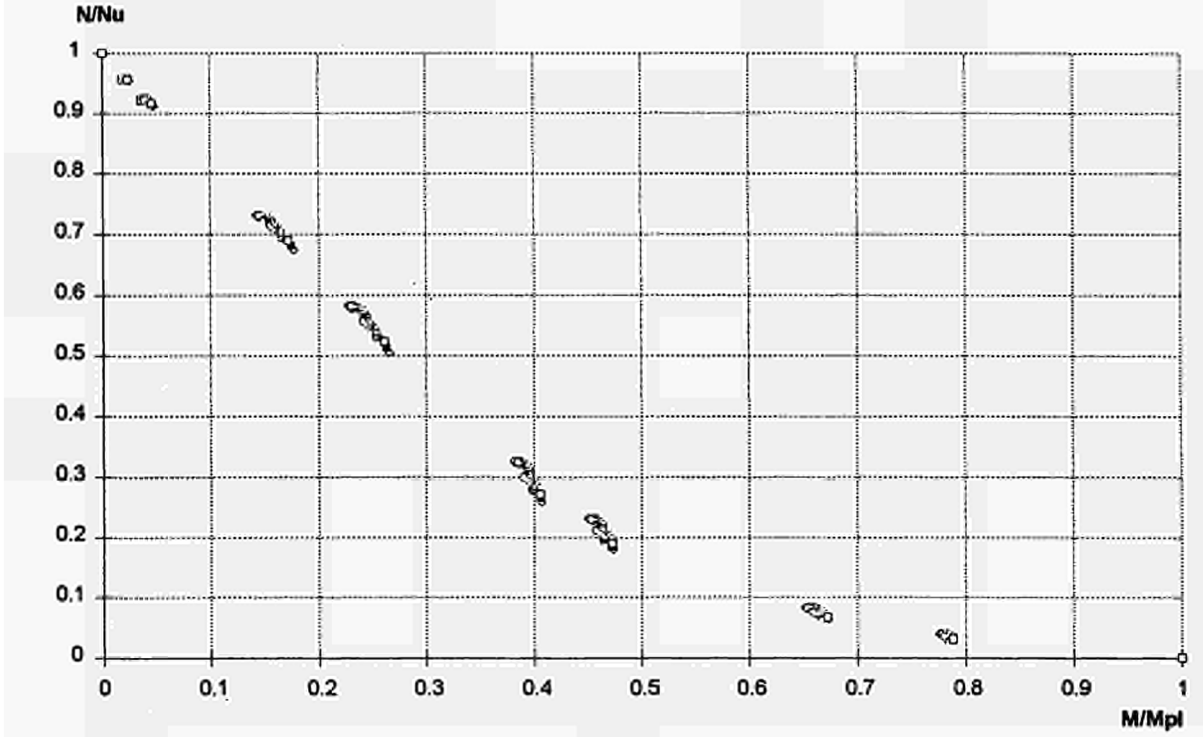

FIGURE 8.5 Points calculated for buckling about the minor axis, uniform moment distribution, and $\bar{\lambda}_{20} = 1$

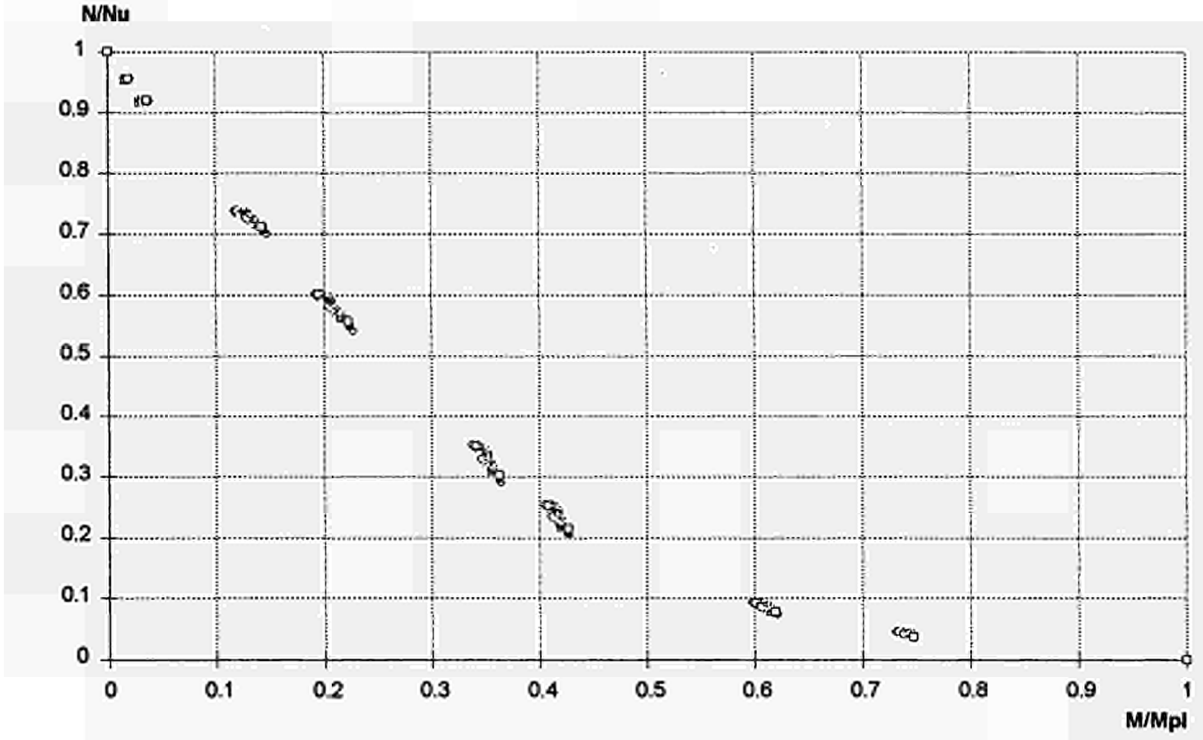

FIGURE 8.6 Points calculated for buckling about the minor axis, uniform moment distribution, and $\bar{\lambda}_{20} = 1.2$

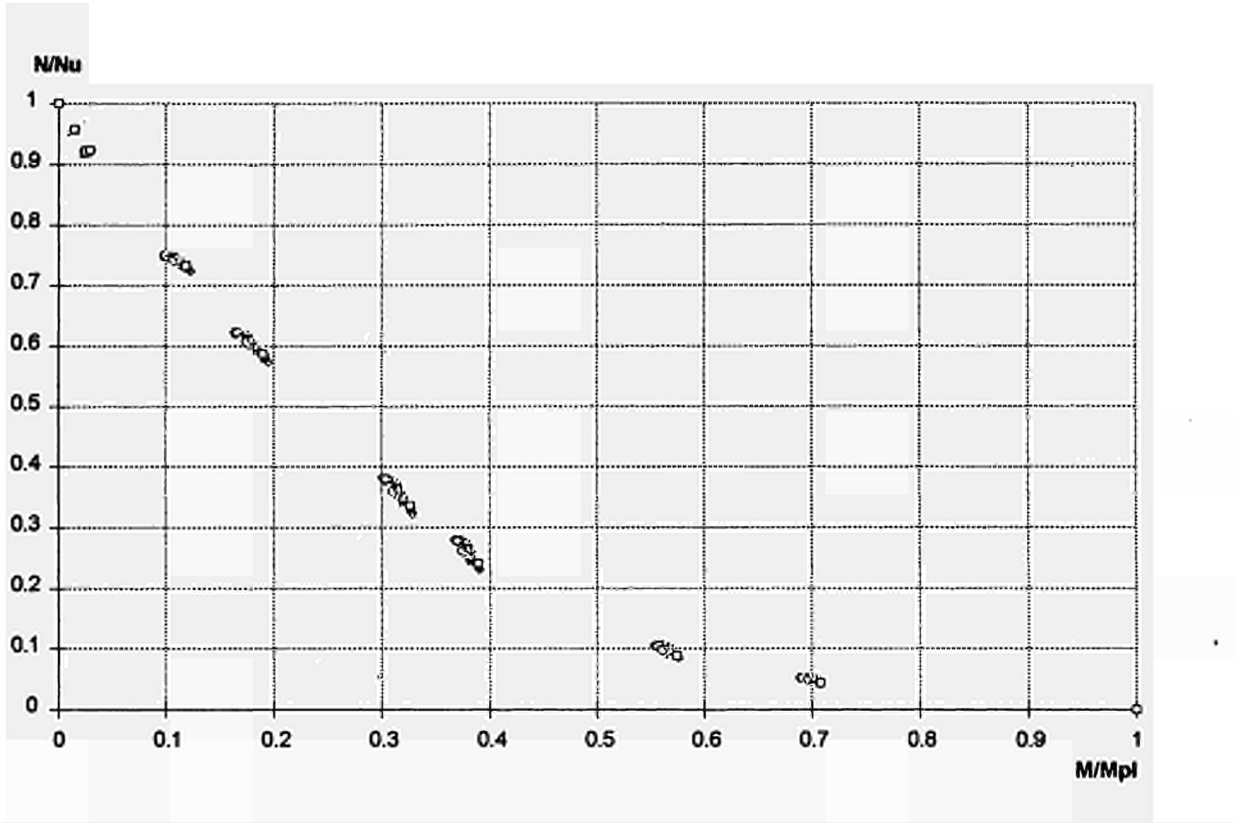

FIGURE 8.7 Points calculated for buckling about the minor axis, uniform moment distribution, and $\bar{\lambda}_{20} = 1.4$

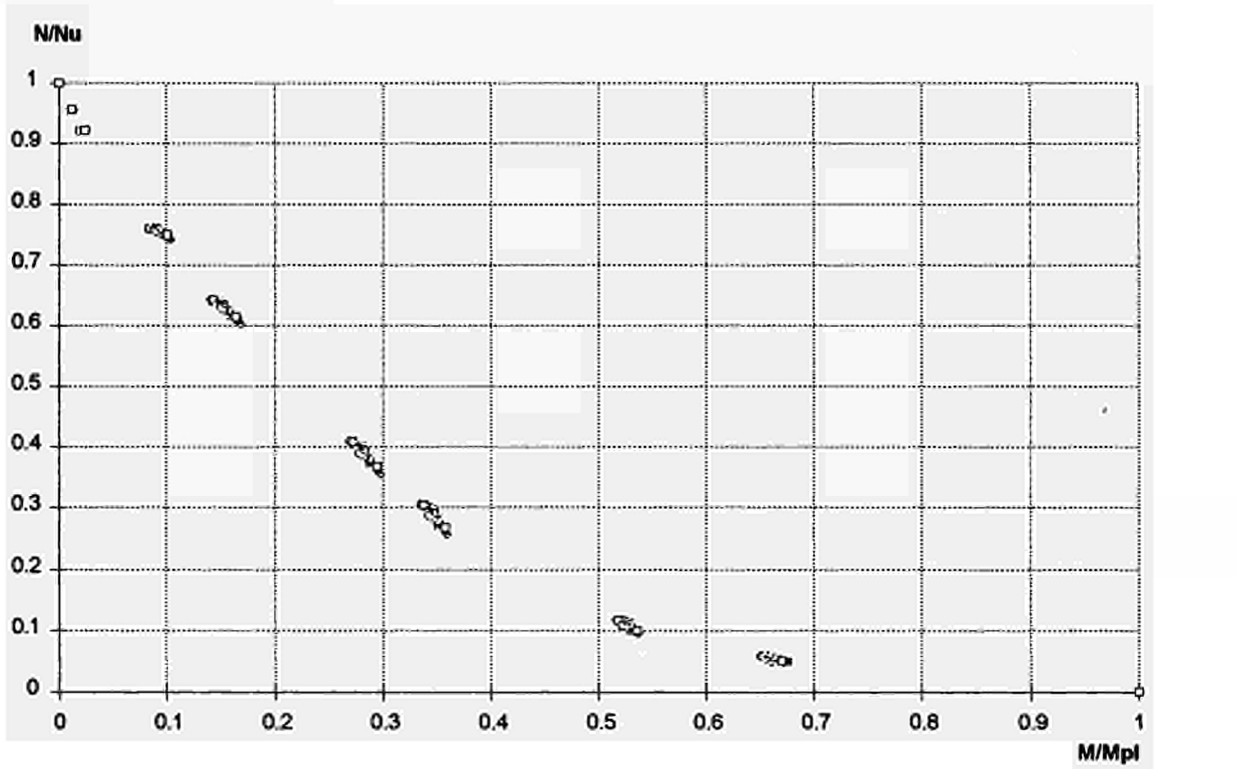

FIGURE 8.8 Points calculated for buckling about the minor axis, uniform moment distribution, and $\bar{\lambda}_{20} = 1.6$

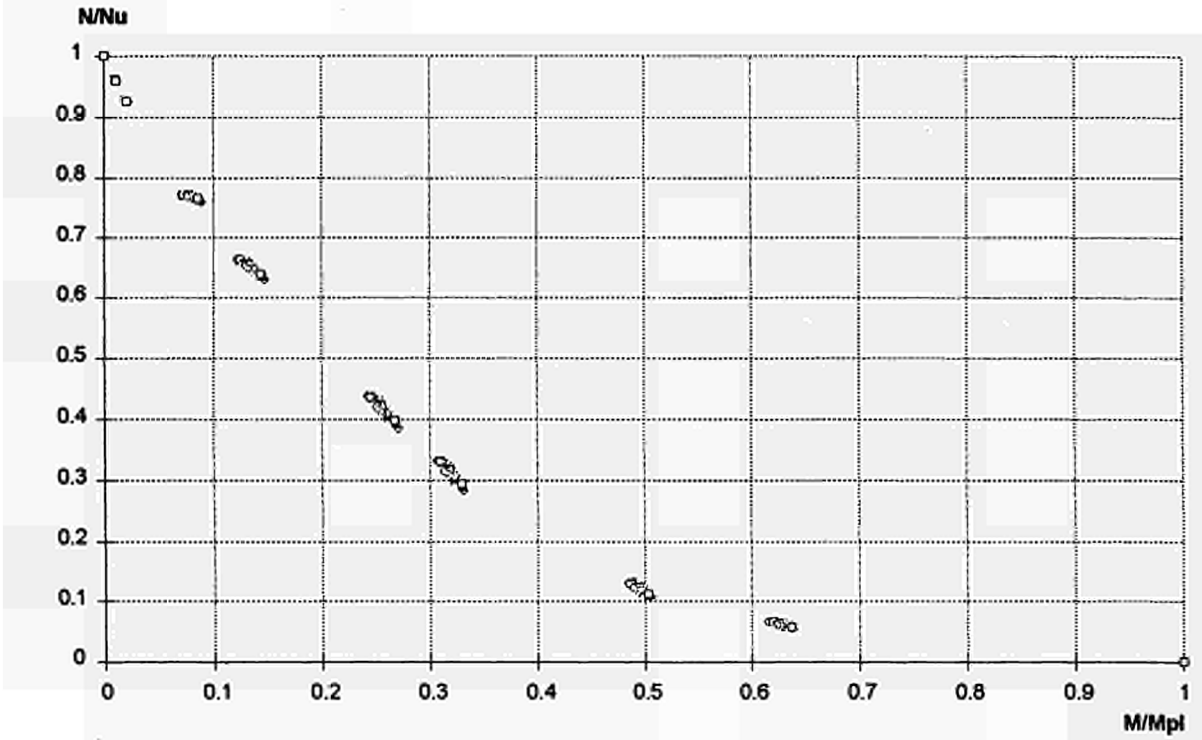

FIGURE 8.9 Points calculated for buckling about the minor axis, uniform moment distribution, and $\overline{\lambda}_{20} = 1.8$

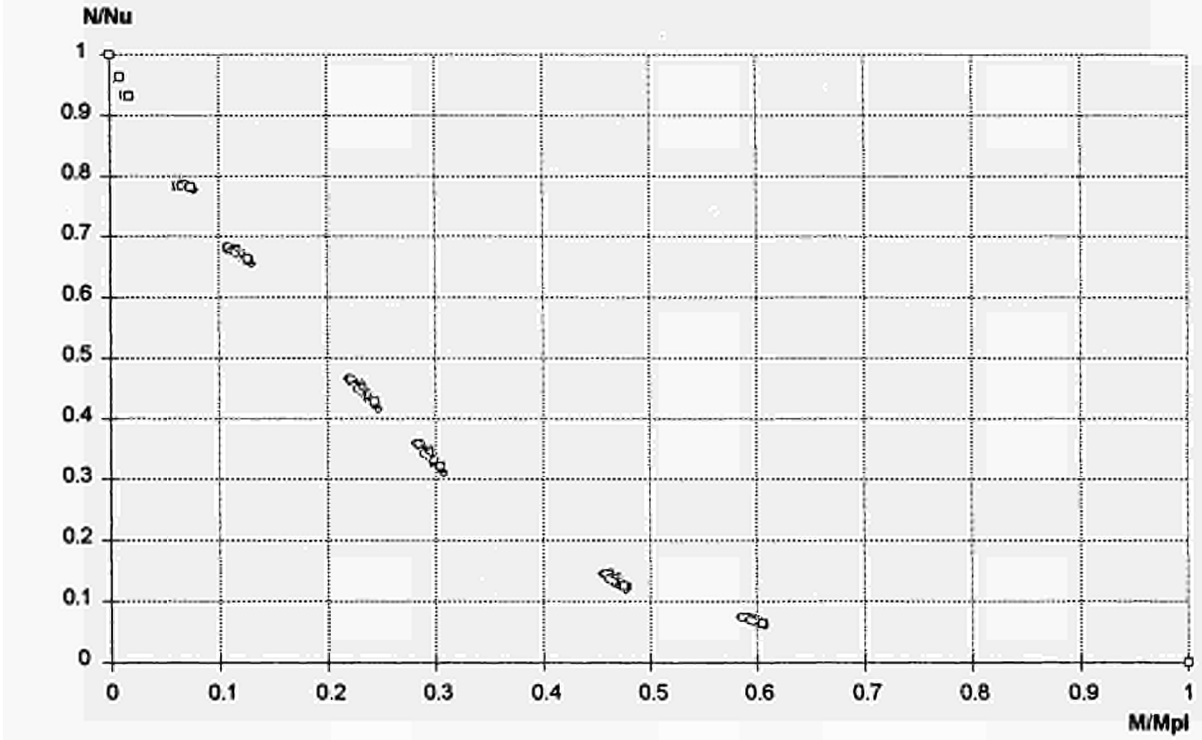

FIGURE 8.10 Points calculated for buckling about the minor axis, uniform moment distribution, and $\overline{\lambda}_{20} = 2$

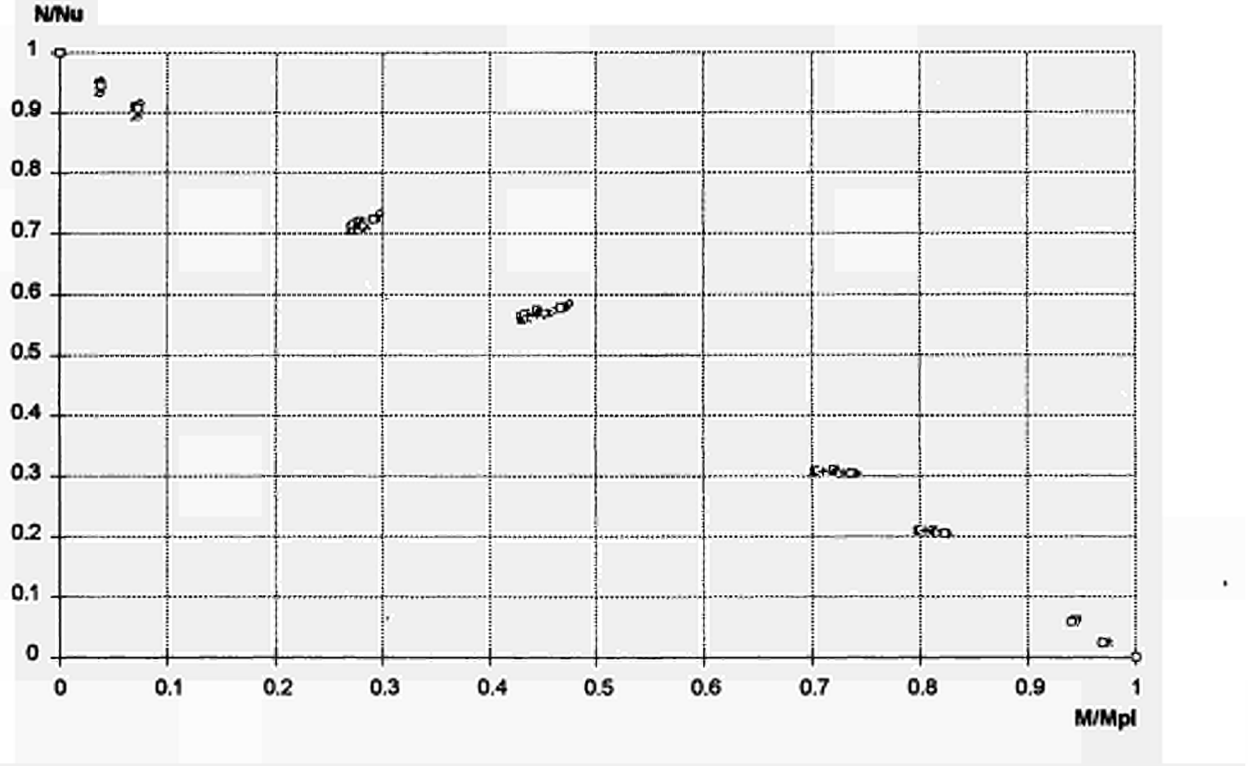

FIGURE 8.11 Points calculated for buckling about the major axis, uniform moment distribution, and $\bar{\lambda}_{20} = 0.2$

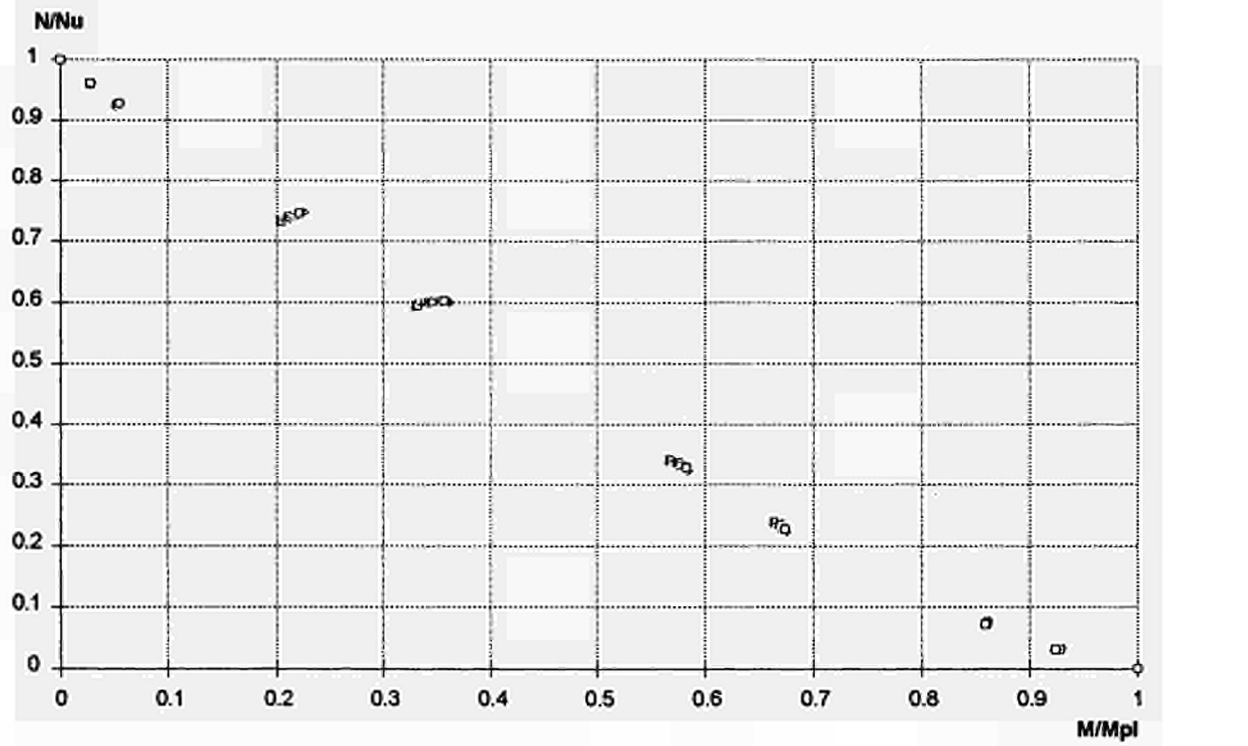

FIGURE 8.12 Points calculated for buckling about the major axis, uniform moment distribution, and $\bar{\lambda}_{20} = 0.4$

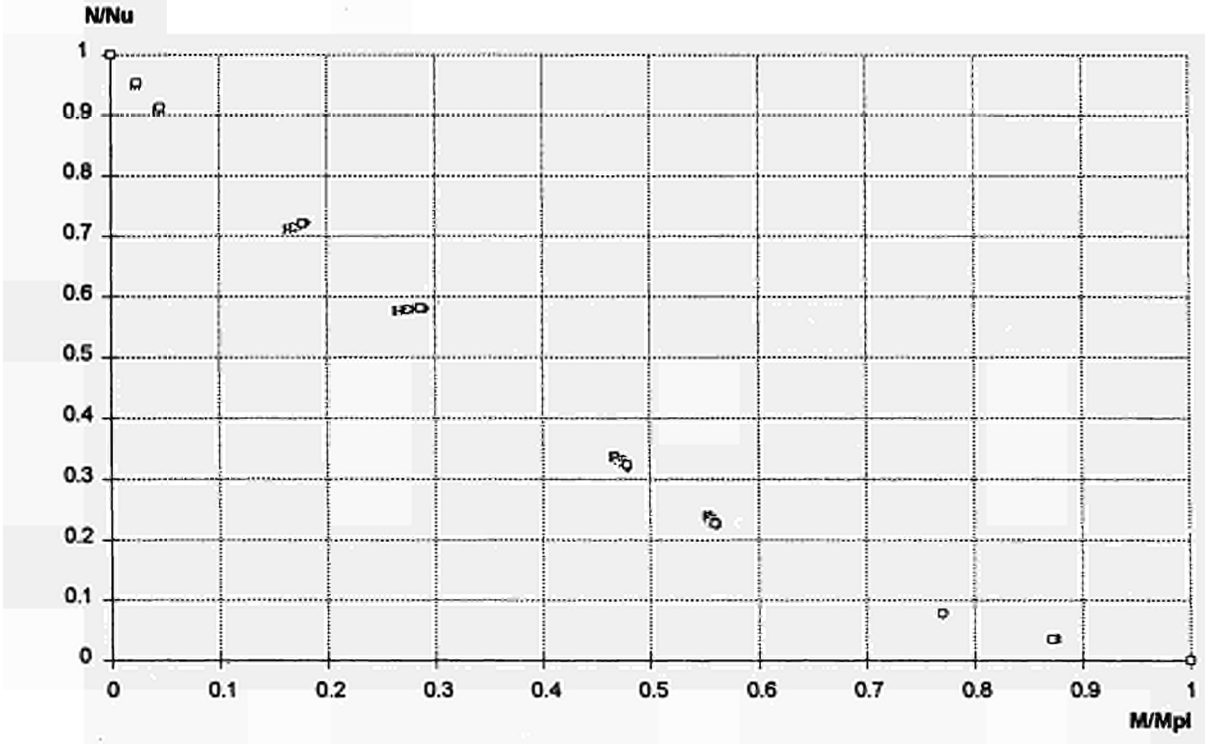

FIGURE 8.13 Points calculated for buckling about the major axis, uniform moment distribution, and $\bar{\lambda}_{20} = 0.6$

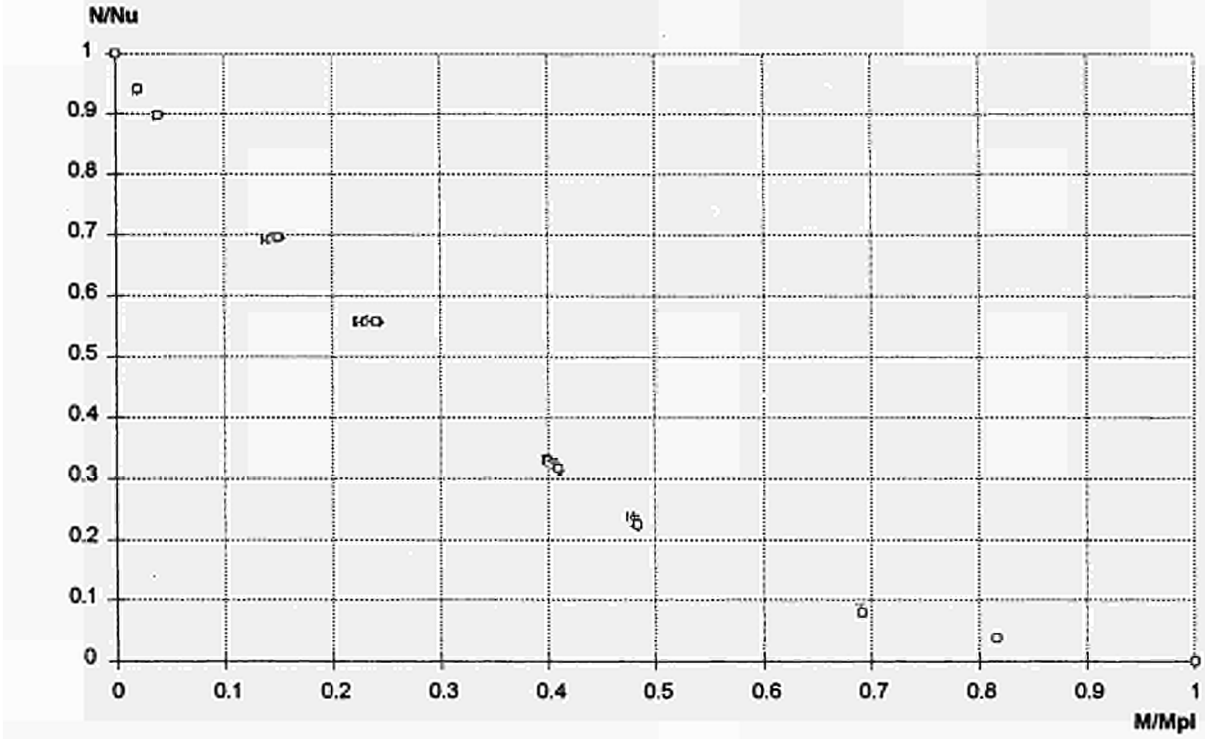

FIGURE 8.14 Points calculated for buckling about the major axis, uniform moment distribution, and $\bar{\lambda}_{20} = 0.8$

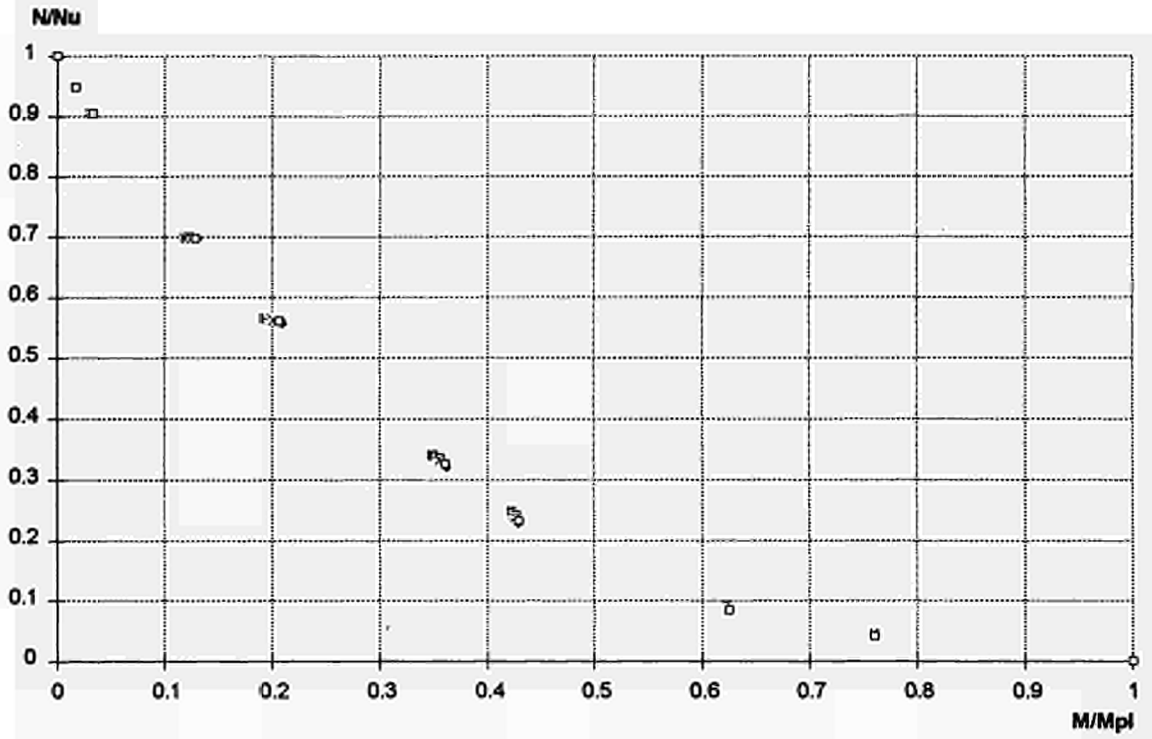

FIGURE 8.15 Points calculated for buckling about the major axis, uniform moment distribution, and $\bar{\lambda}_{20} = 1$

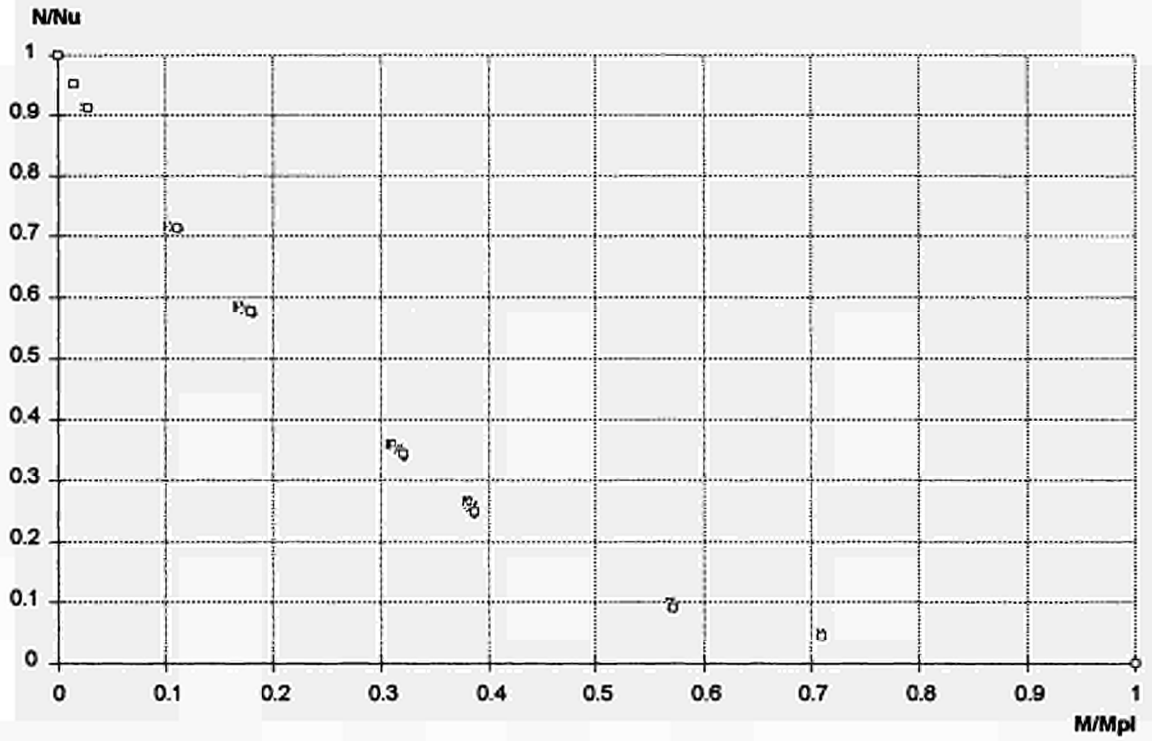

FIGURE 8.16 Points calculated for buckling about the major axis, uniform moment distribution, and $\bar{\lambda}_{20} = 1.2$

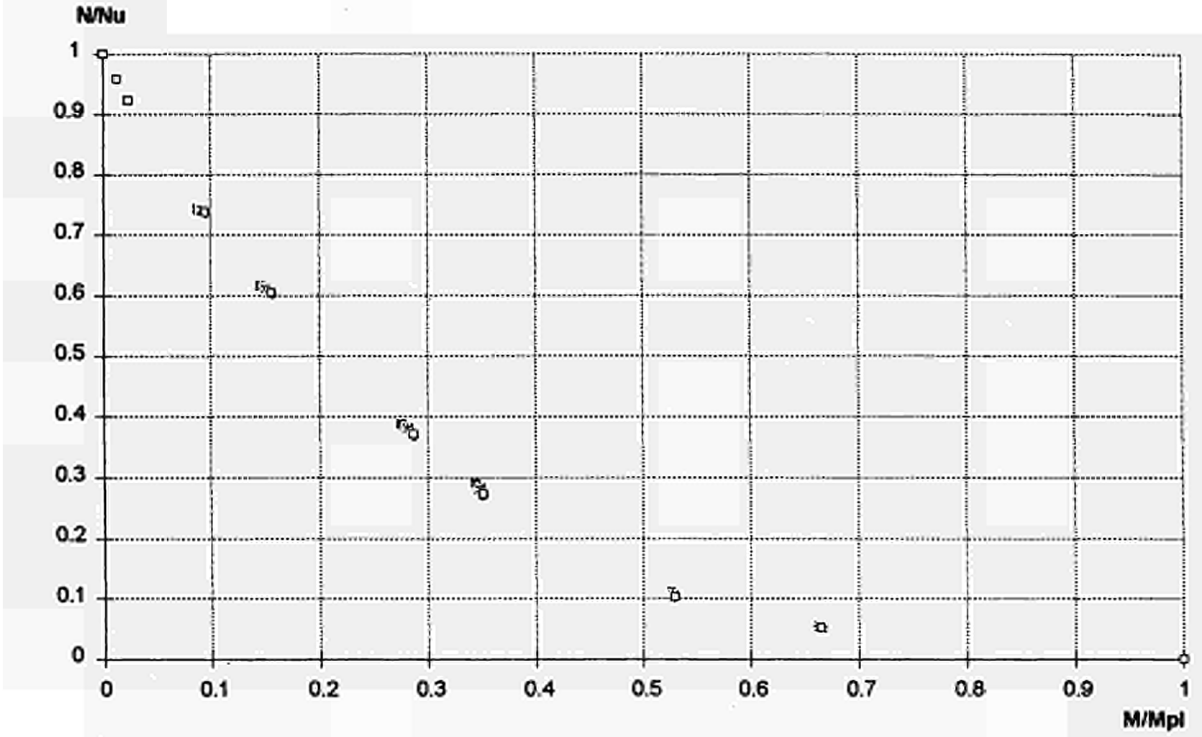

FIGURE 8.17 Points calculated for buckling about the major axis, uniform moment distribution, and $\bar{\lambda}_{20} = 1.4$

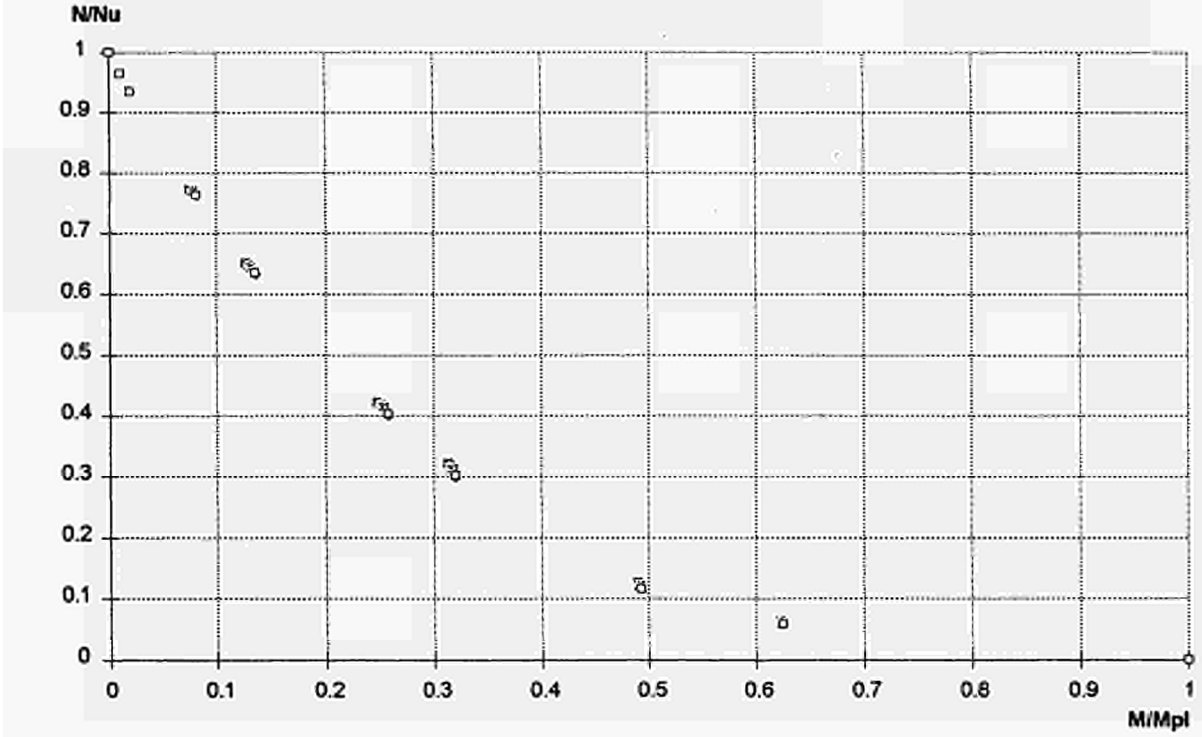

FIGURE 8.18 Points calculated for buckling about the major axis, uniform moment distribution, and $\bar{\lambda}_{20} = 1.6$

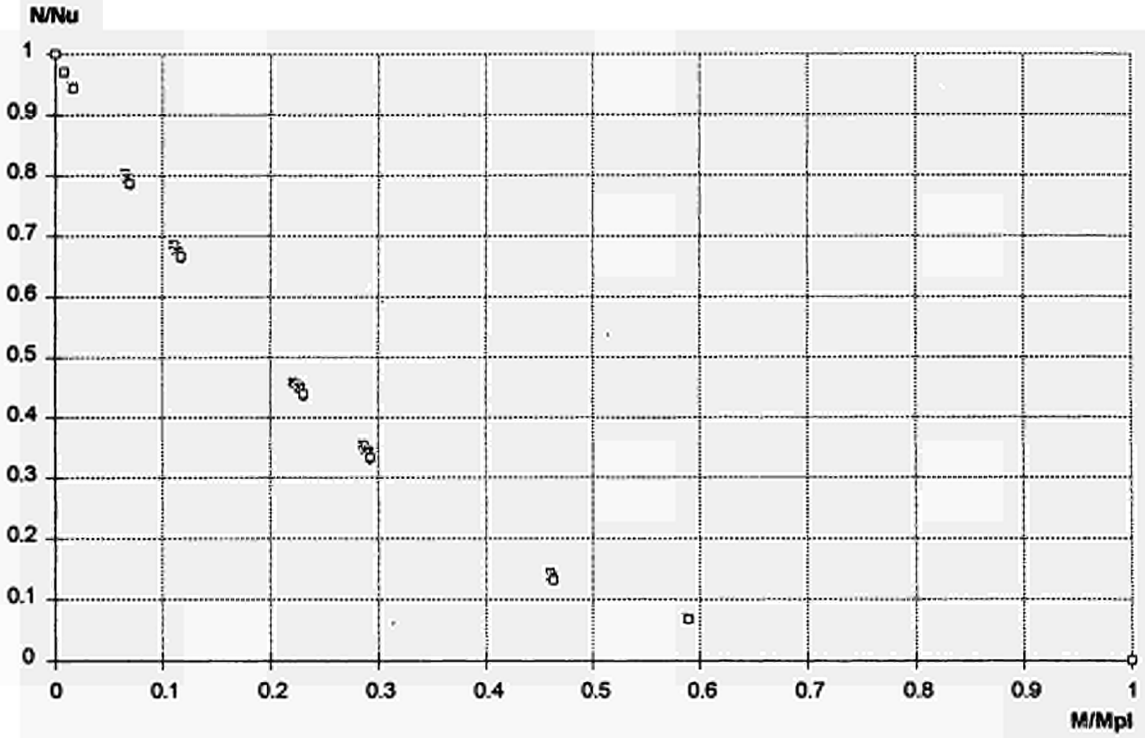

FIGURE 8.19 Points calculated for buckling about the major axis, uniform moment distribution, and $\bar{\lambda}_{20} = 1.8$

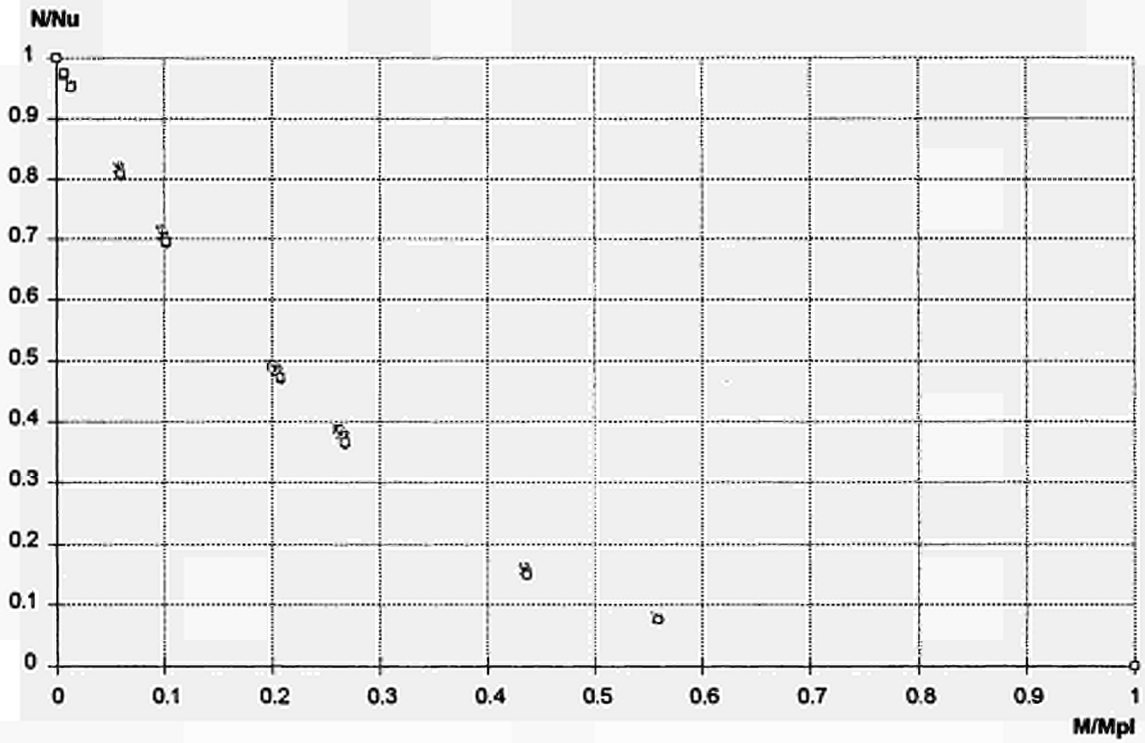

FIGURE 8.20 Points calculated for buckling about the major axis, uniform moment distribution, and $\bar{\lambda}_{20} = 2$

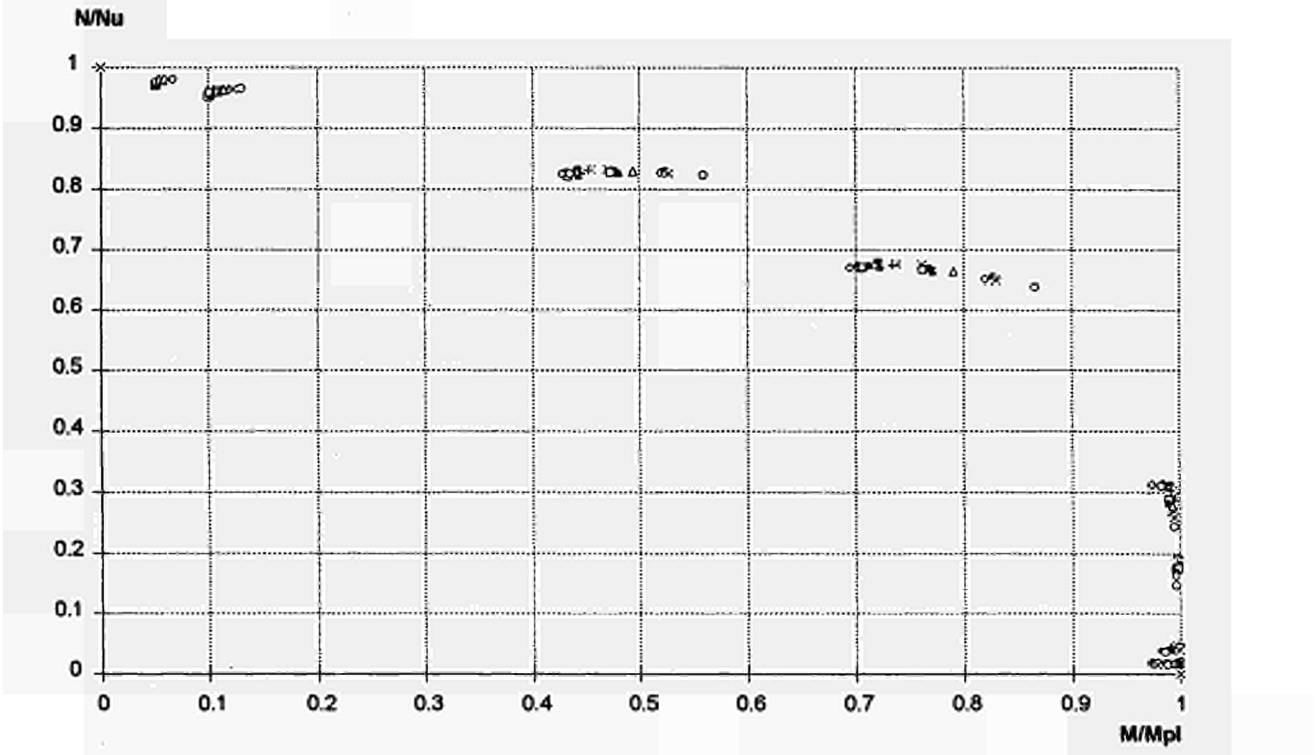

FIGURE 8.21 Points calculated for buckling about the minor axis, triangular moment distribution, and $\bar{\lambda}_{20} = 0.2$

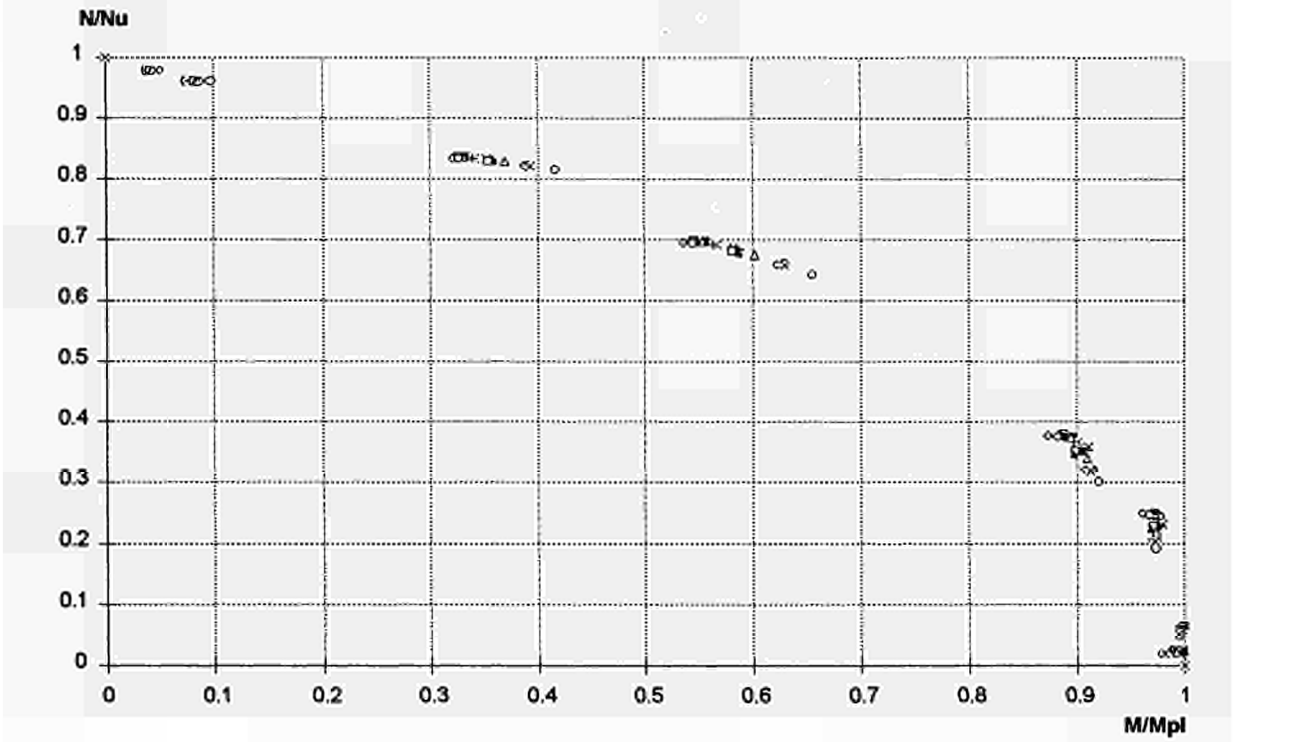

FIGURE 8.22 Points calculated for buckling about the minor axis, triangular moment distribution, and $\bar{\lambda}_{20} = 0.4$

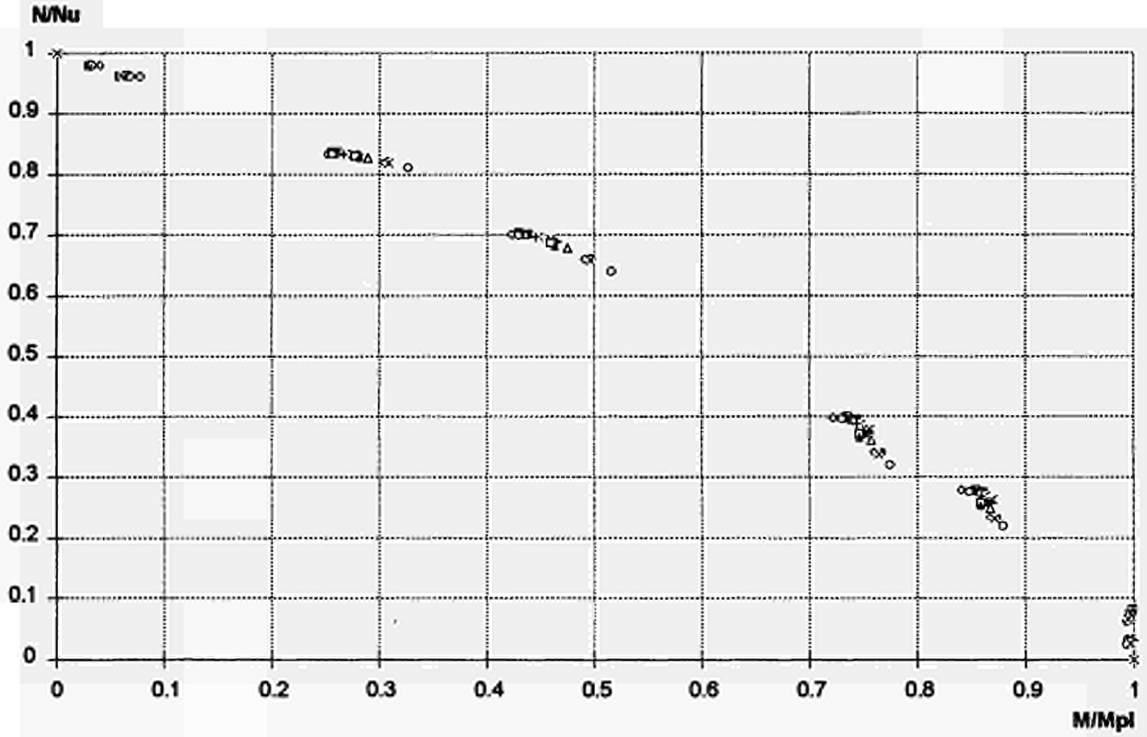

FIGURE 8.23 Points calculated for buckling about the minor axis, triangular moment distribution, and $\bar{\lambda}_{20} = 0.6$

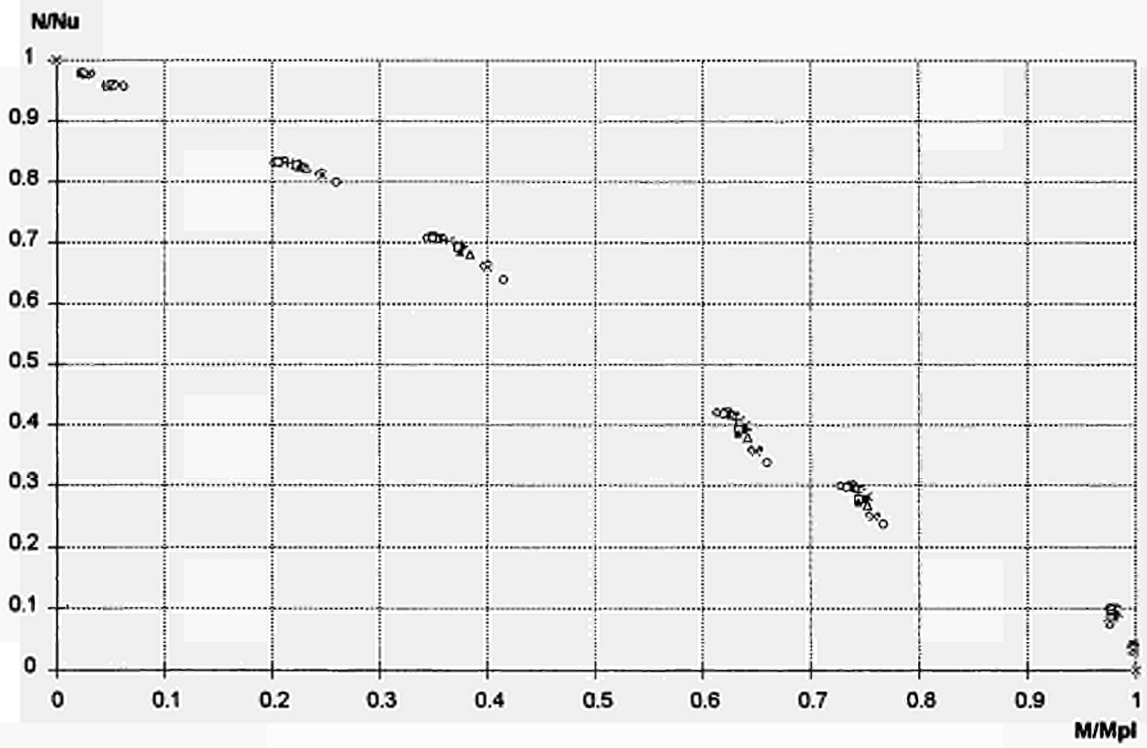

FIGURE 8.24 Points calculated for buckling about the minor axis, triangular moment distribution, and $\bar{\lambda}_{20} = 0.8$

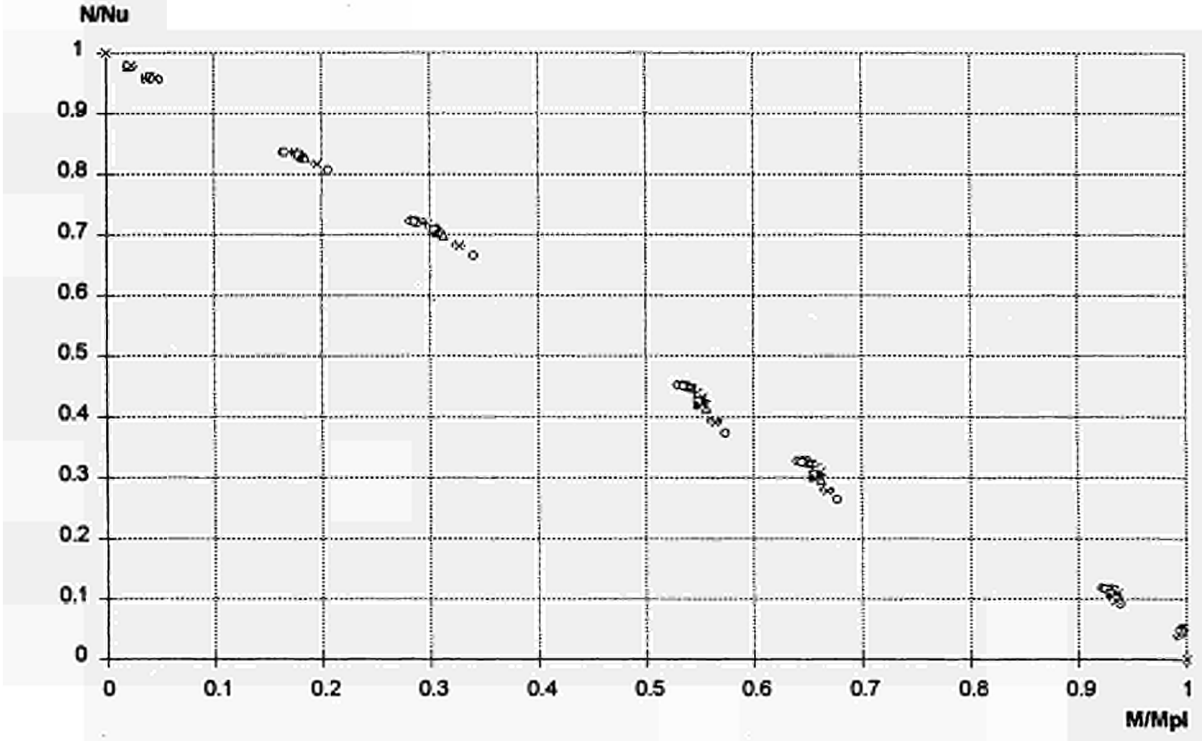

FIGURE 8.25 Points calculated for buckling about the minor axis, triangular moment distribution, and $\bar{\lambda}_{20} = 1$

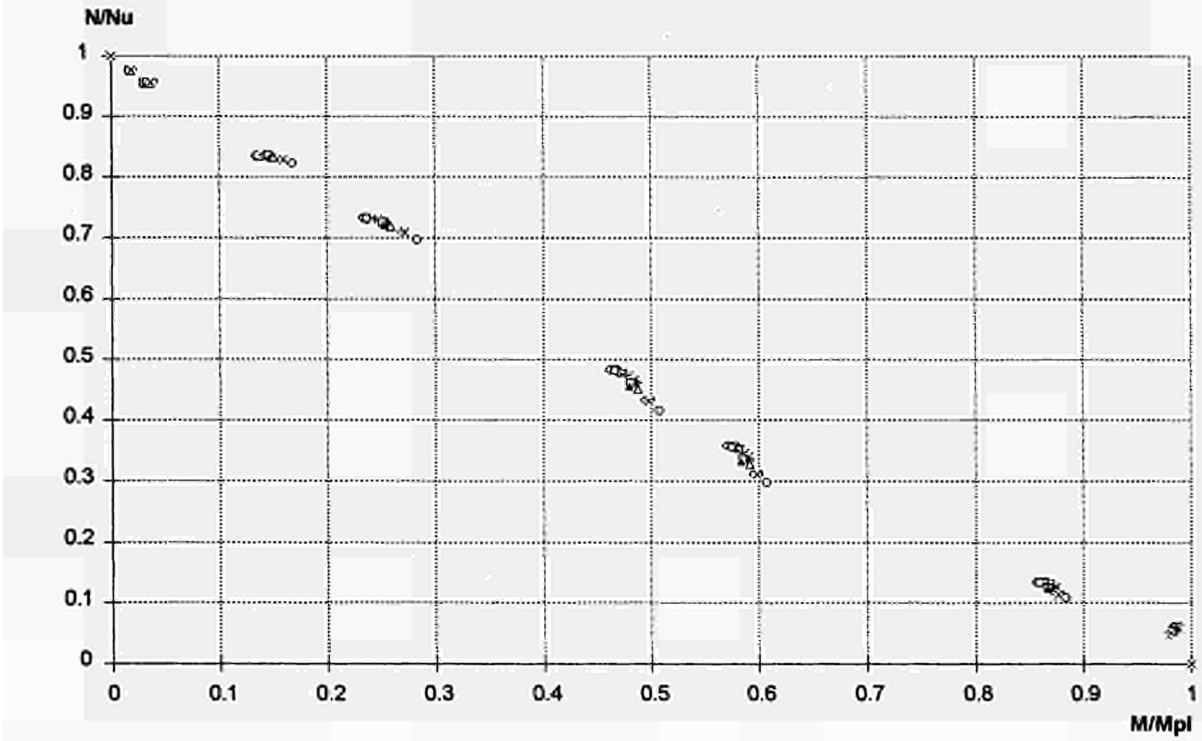

FIGURE 8.26 Points calculated for buckling about the minor axis, triangular moment distribution, and $\bar{\lambda}_{20} = 1.2$

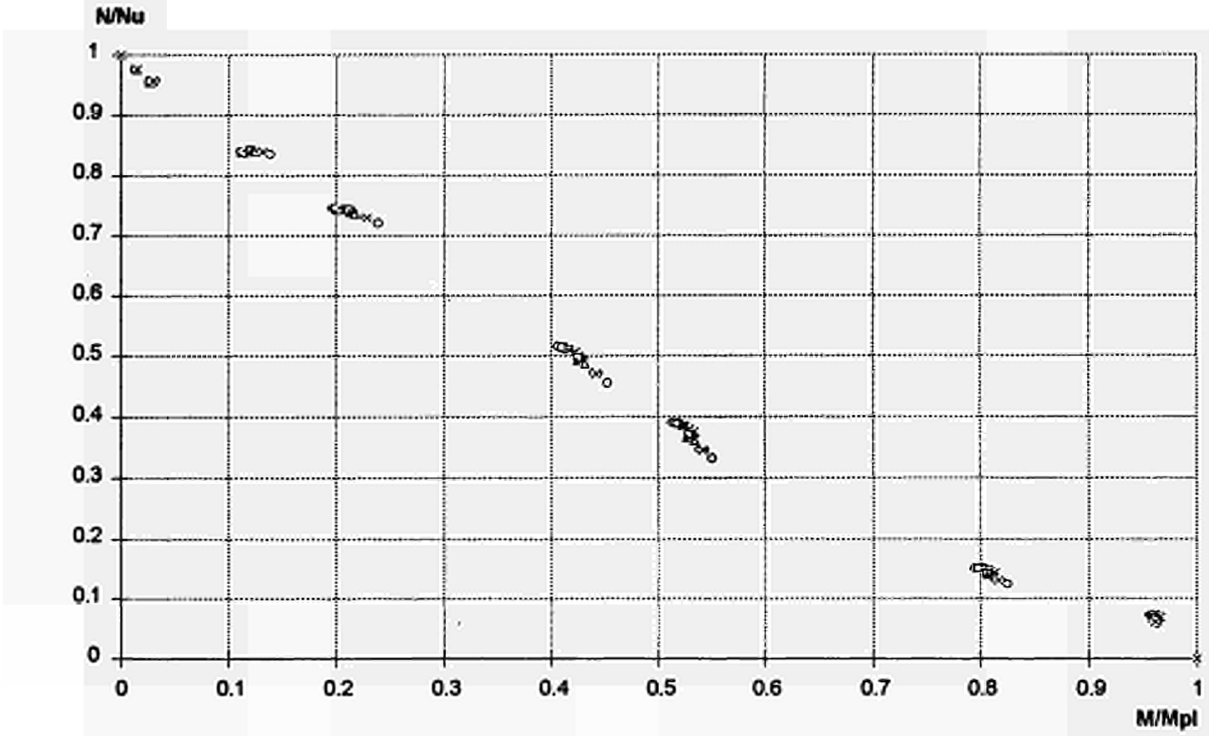

FIGURE 8.27 Points calculated for buckling about the minor axis, triangular moment distribution, and $\bar{\lambda}_{20} = 1.4$

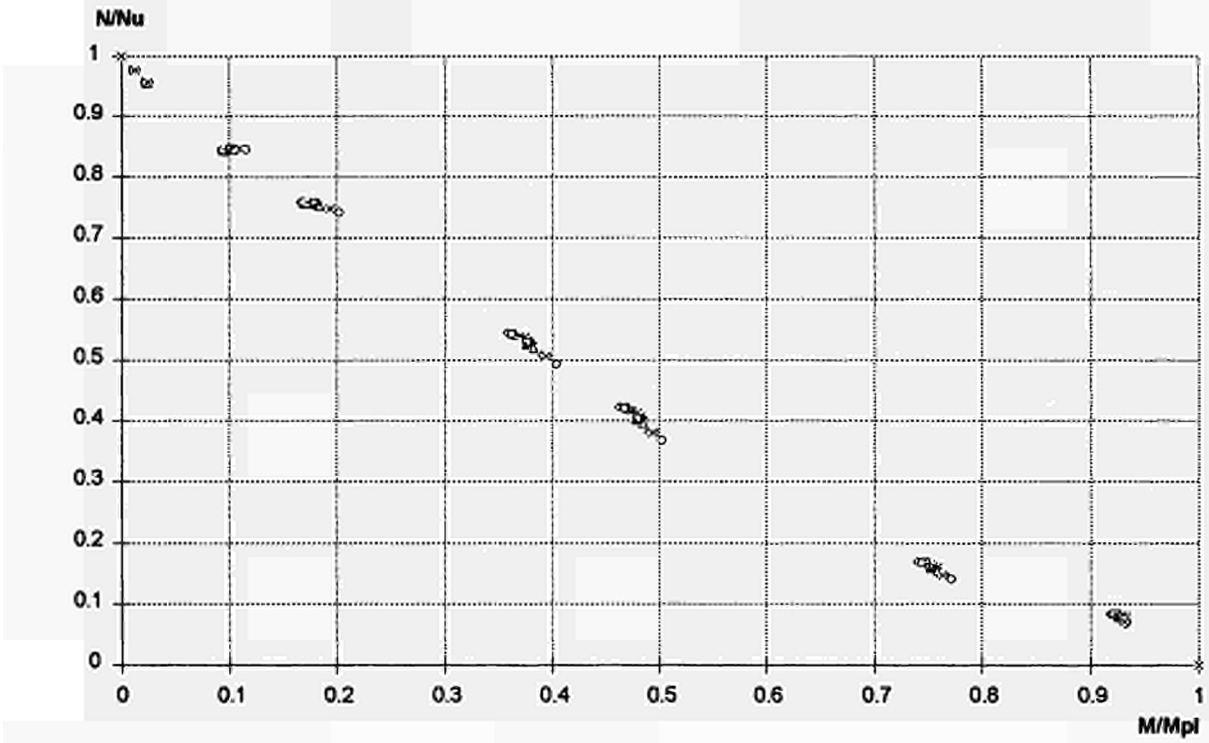

FIGURE 8.28 Points calculated for buckling about the minor axis, triangular moment distribution, and $\bar{\lambda}_{20} = 1.6$

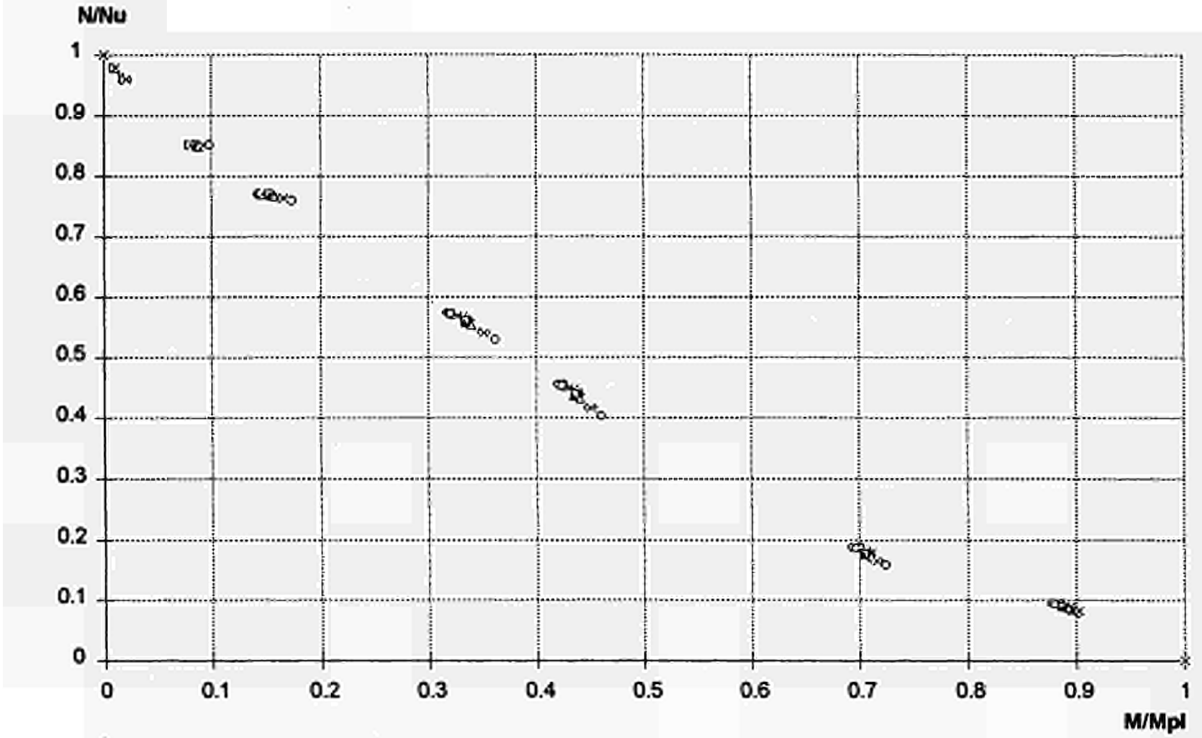

FIGURE 8.29 Points calculated for buckling about the minor axis, triangular moment distribution, and $\bar{\lambda}_{20} = 1.8$

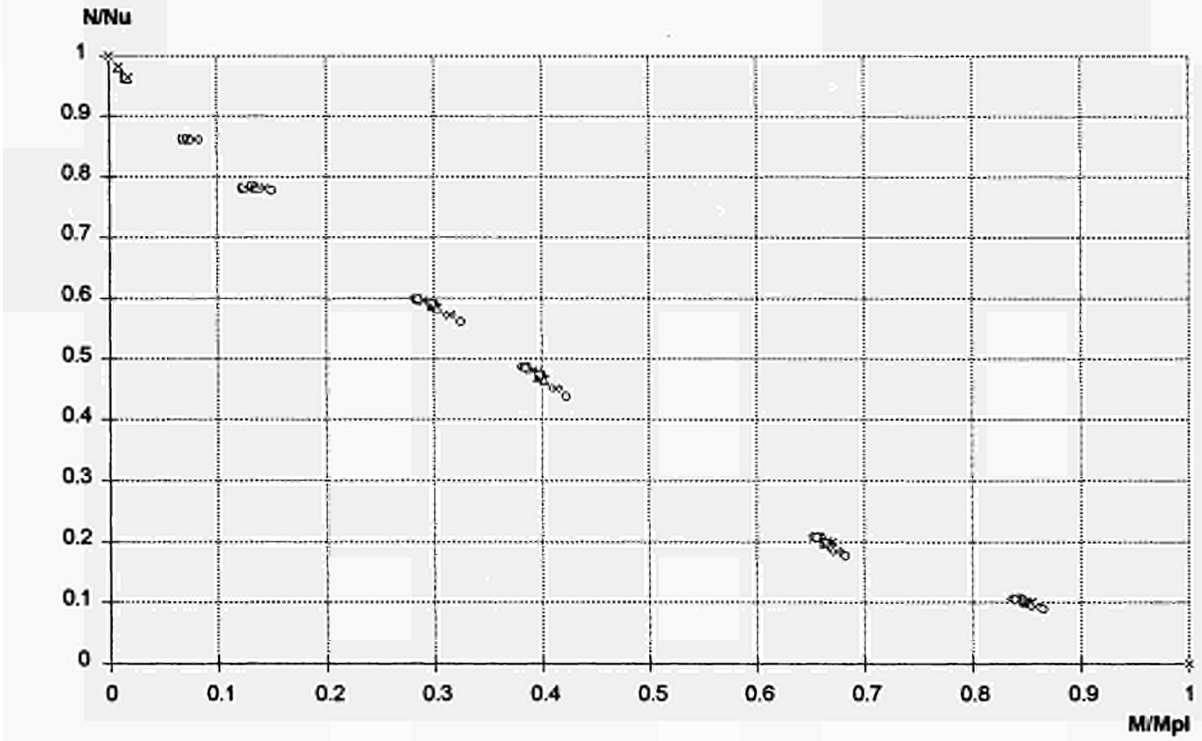

FIGURE 8.30 Points calculated for buckling about the minor axis, triangular moment distribution, and $\bar{\lambda}_{20} = 2$

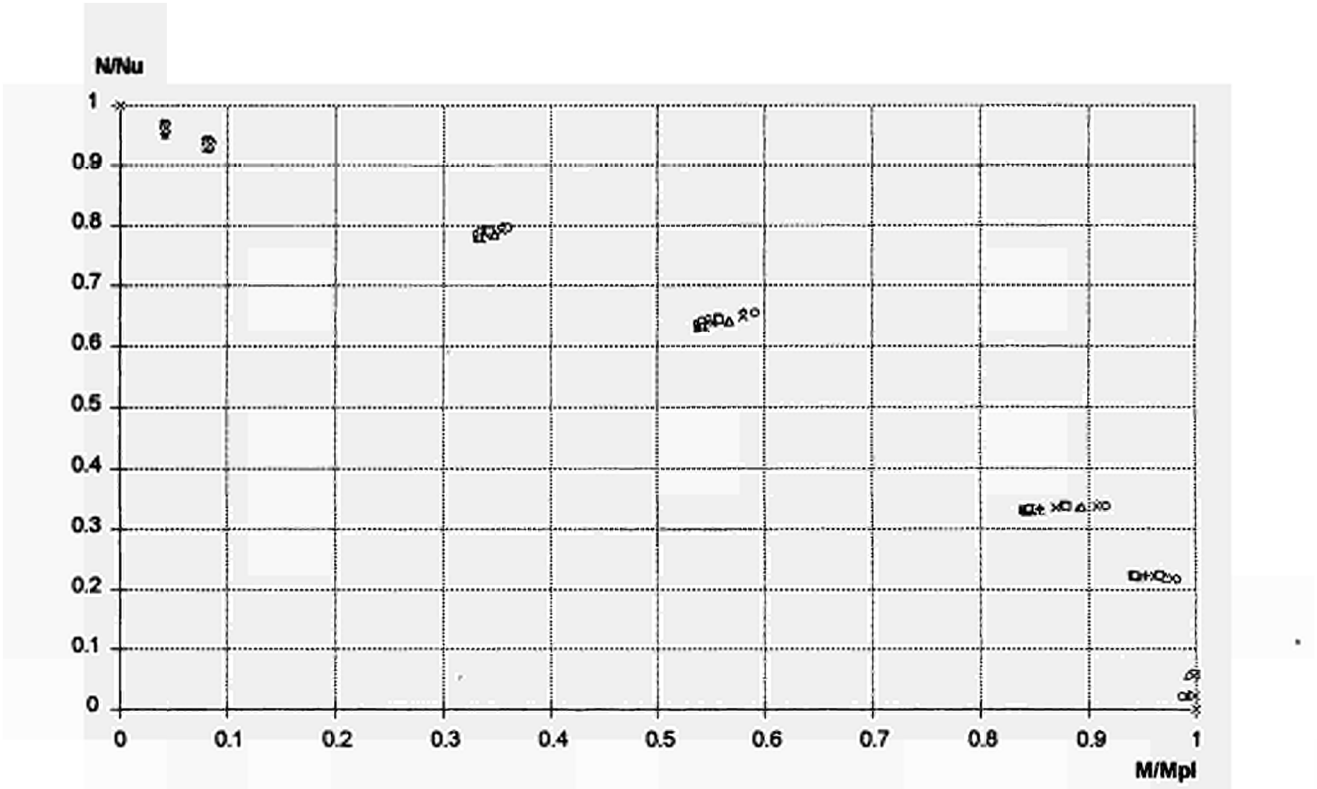

FIGURE 8.31 Points calculated for buckling about the major axis, triangular moment distribution, and $\bar{\lambda}_{20} = 0.2$

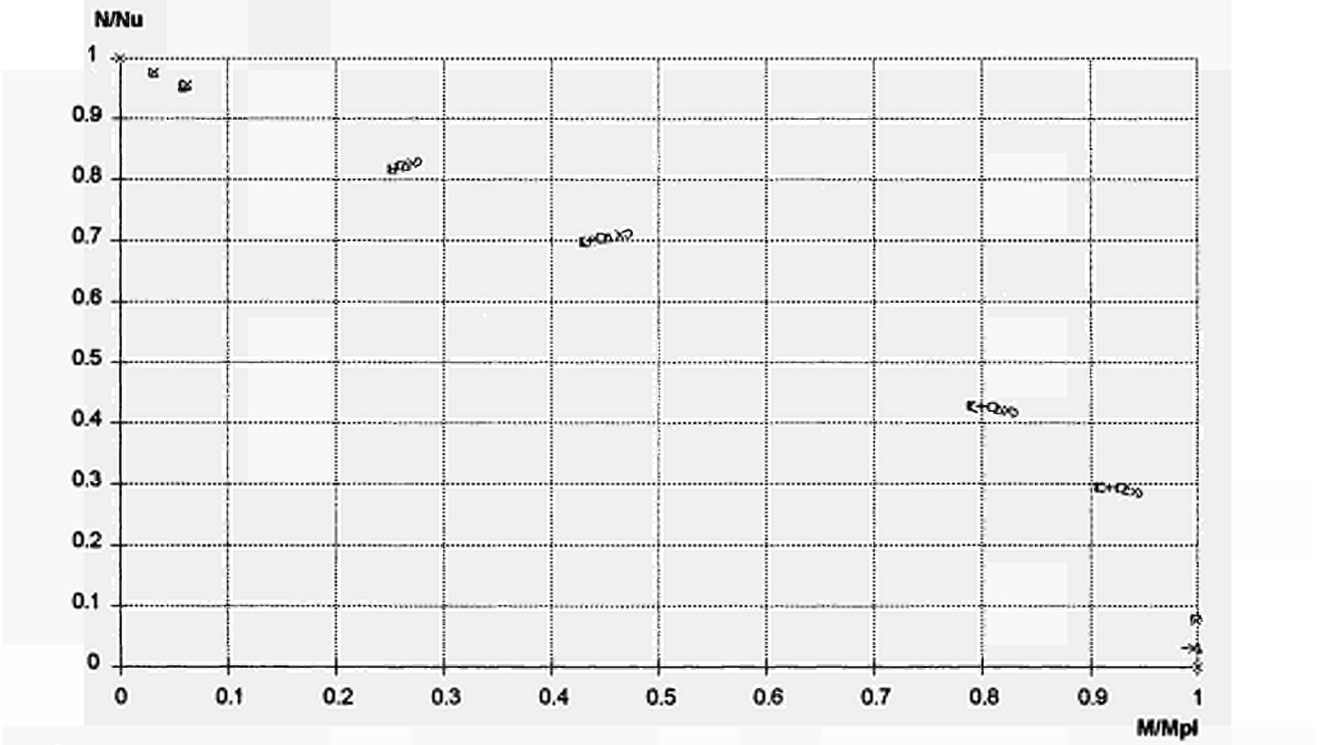

FIGURE 8.32 Points calculated for buckling about the major axis, triangular moment distribution, and $\bar{\lambda}_{20} = 0.4$

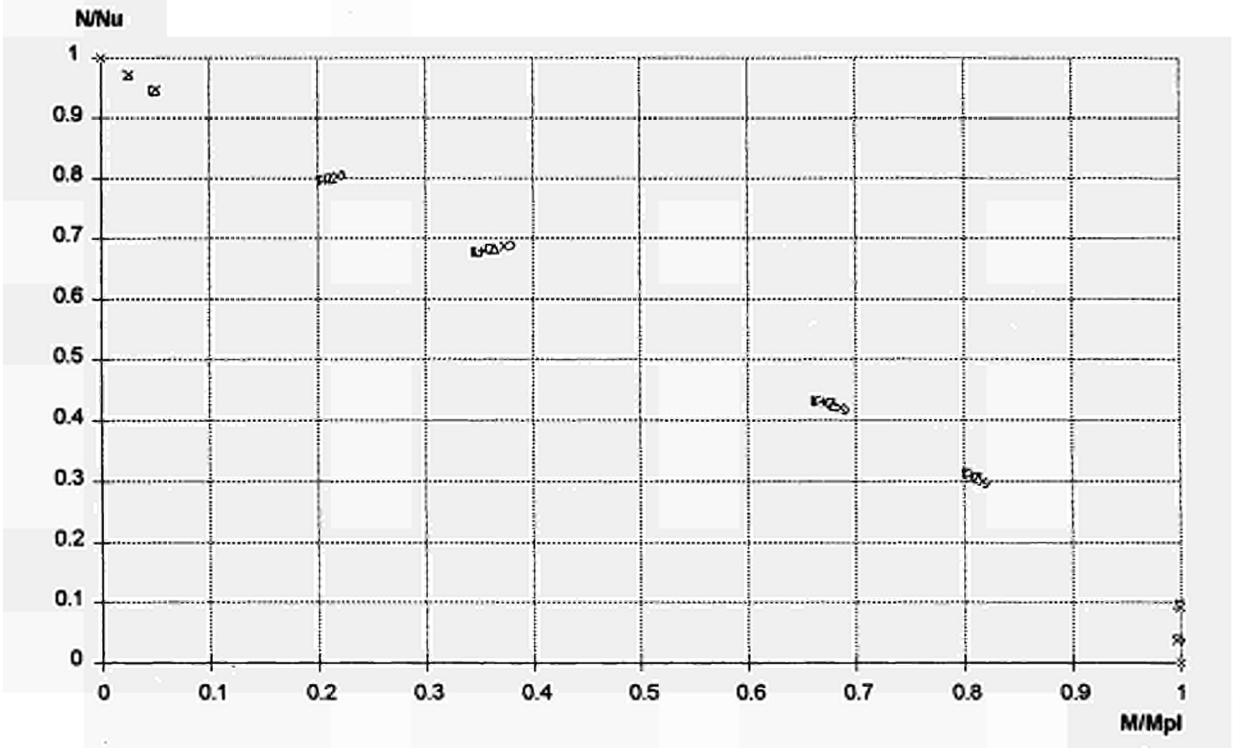

FIGURE 8.33 Points calculated for buckling about the major axis, triangular moment distribution, and $\bar{\lambda}_{20} = 0.6$

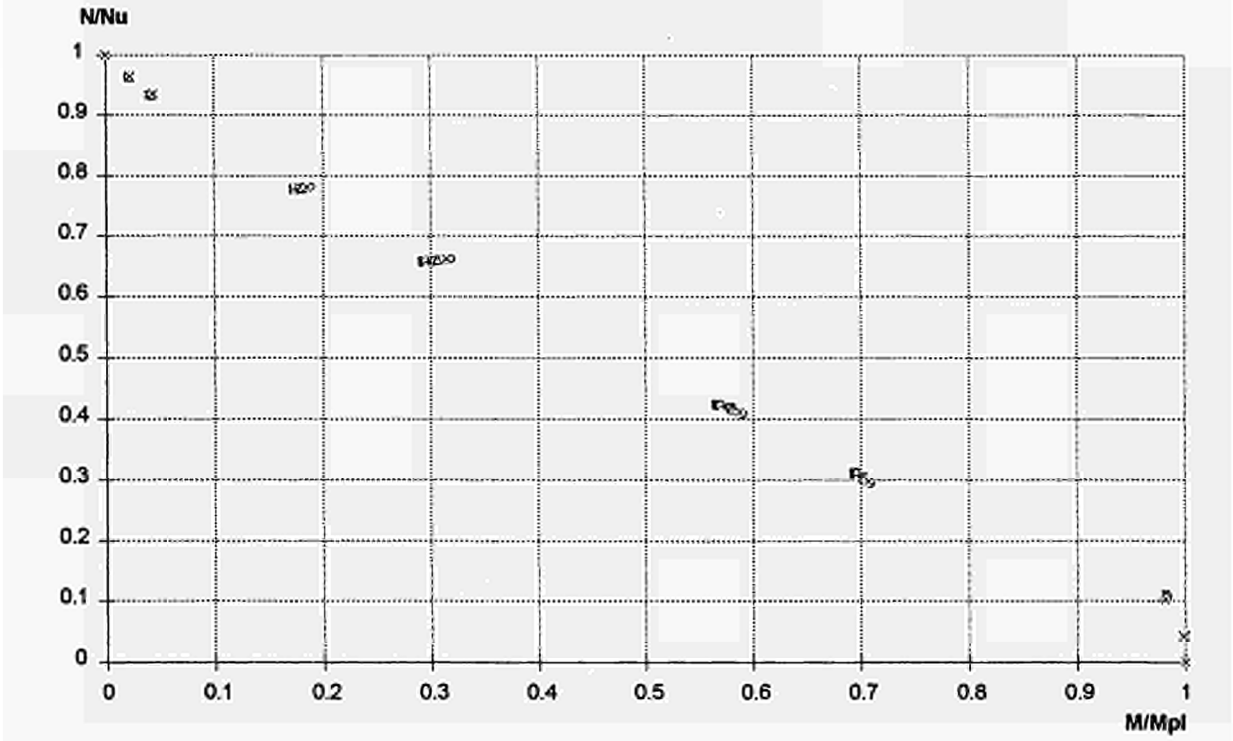

FIGURE 8.34 Points calculated for buckling about the major axis, triangular moment distribution, and $\bar{\lambda}_{20} = 0.8$

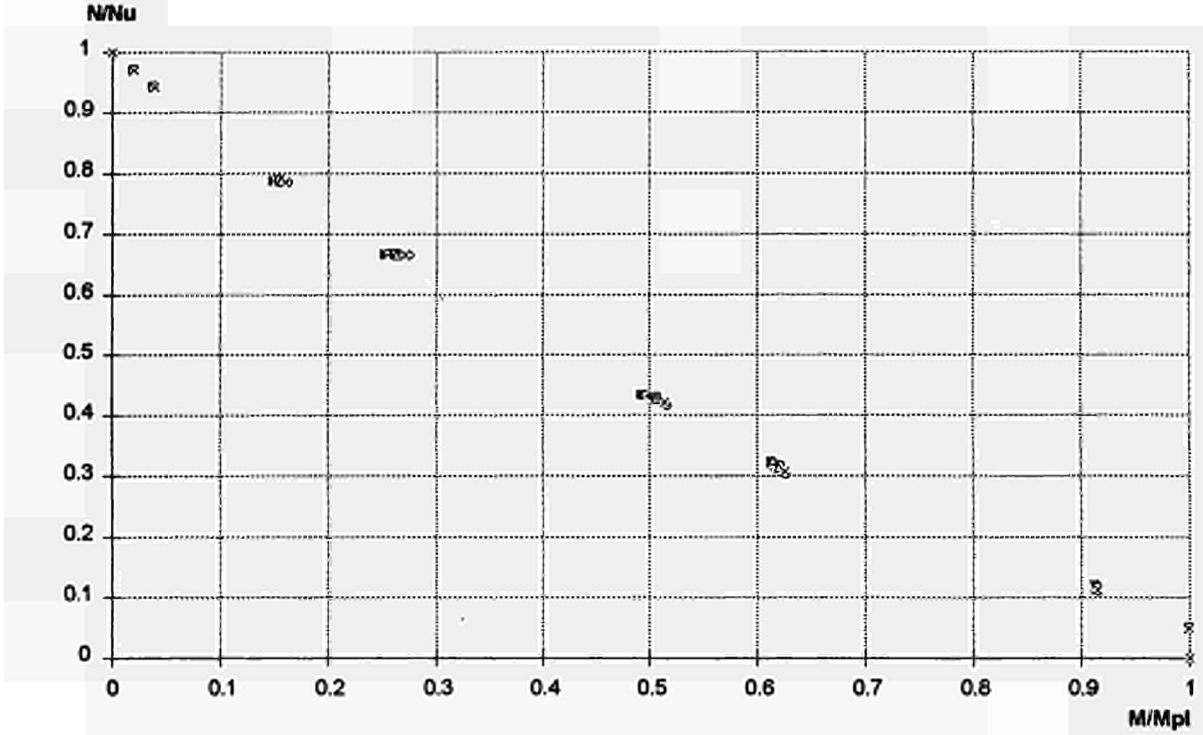

FIGURE 8.35 Points calculated for buckling about the major axis, triangular moment distribution, and $\bar{\lambda}_{20} = 1$

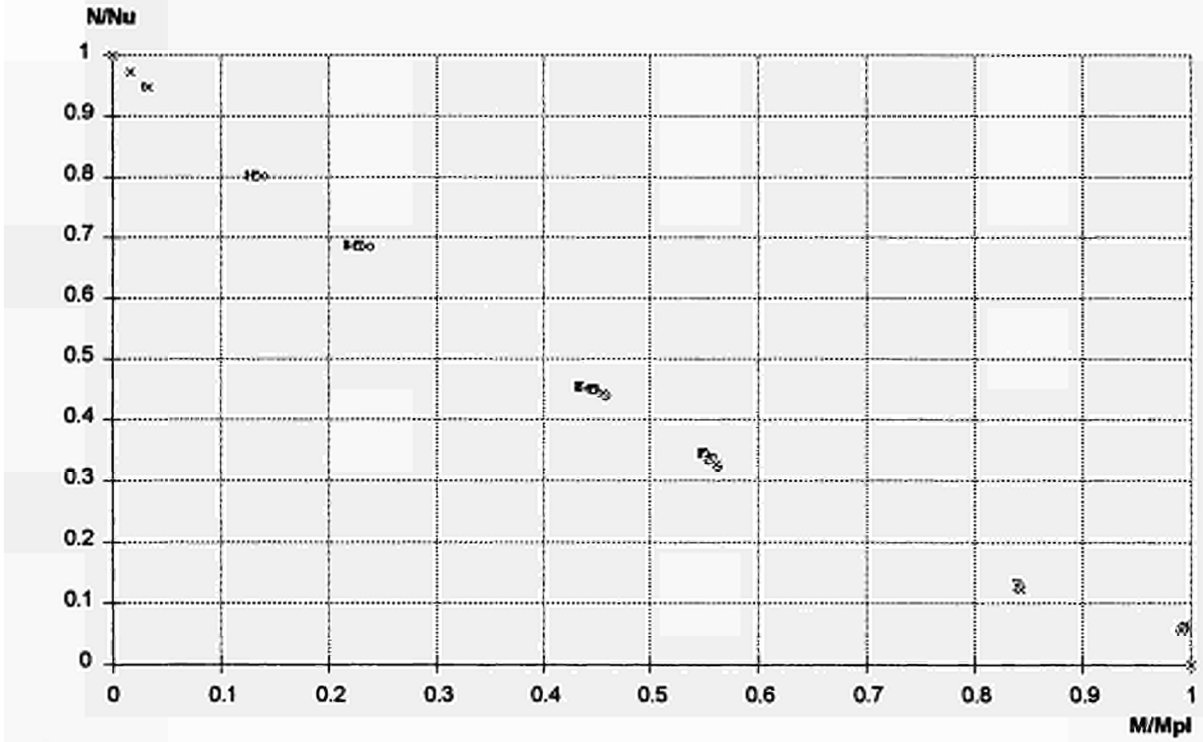

FIGURE 8.36 Points calculated for buckling about the major axis, triangular moment distribution, and $\bar{\lambda}_{20} = 1.2$

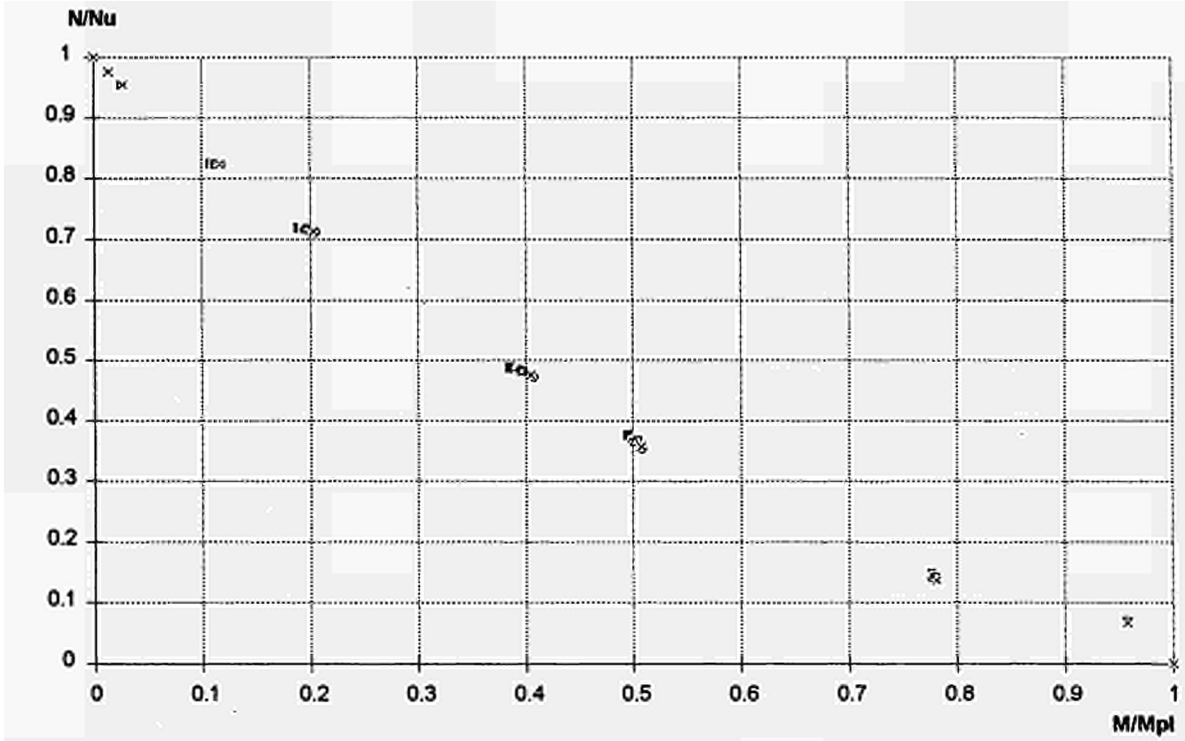

FIGURE 8.37 Points calculated for buckling about the major axis, triangular moment distribution, and $\bar{\lambda}_{20} = 1.4$

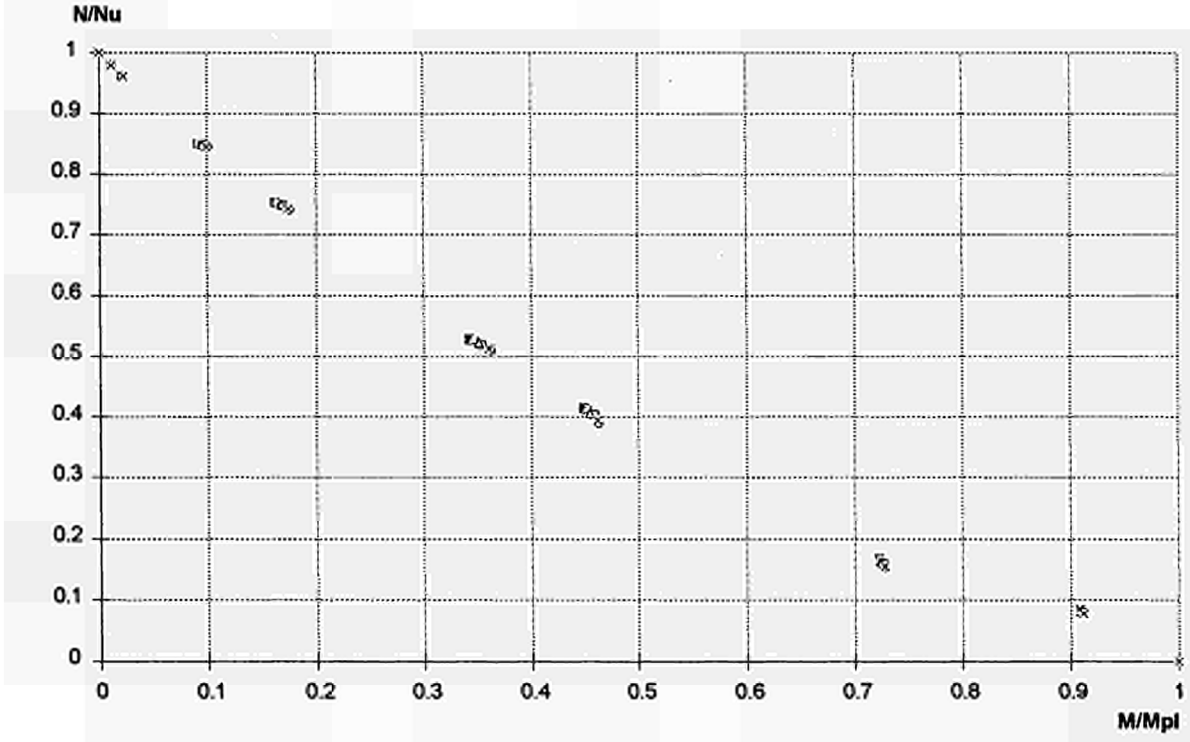

FIGURE 8.38 Points calculated for buckling about the major axis, triangular moment distribution, and $\bar{\lambda}_{20} = 1.6$

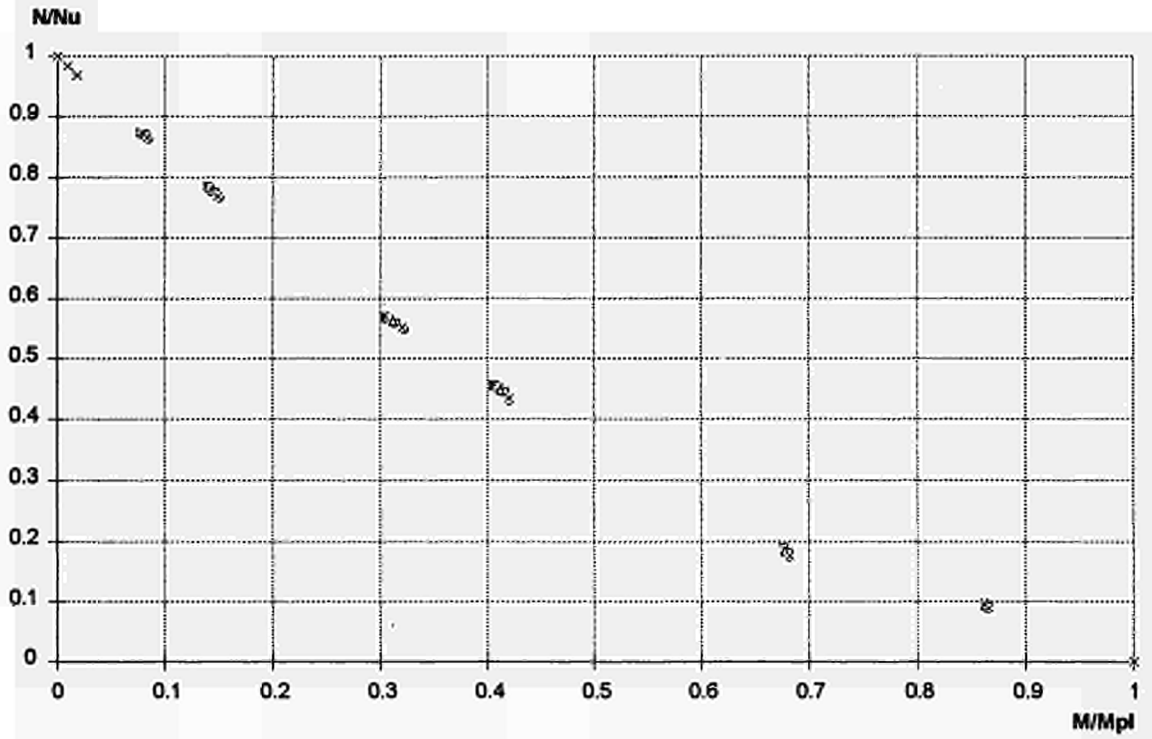

FIGURE 8.39 Points calculated for buckling about the major axis, triangular moment distribution, and $\bar{\lambda}_{20} = 1.8$

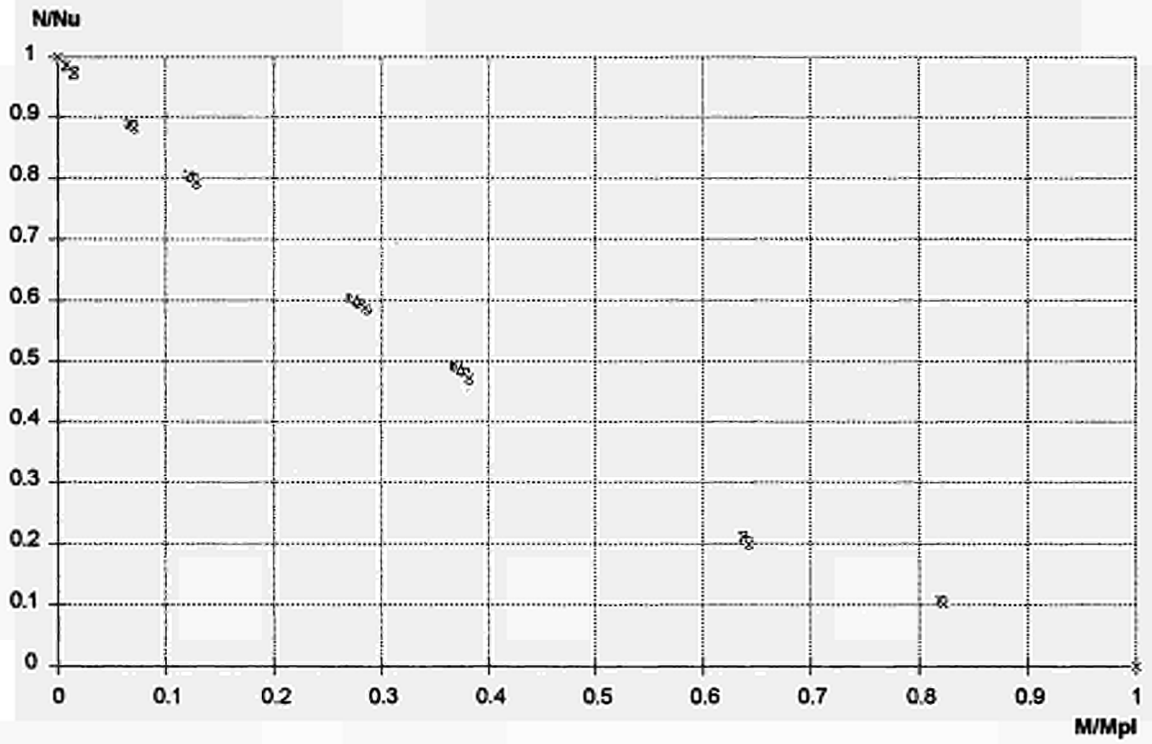

FIGURE 8.40 Points calculated for buckling about the major axis, triangular moment distribution, and $\bar{\lambda}_{20} = 2$

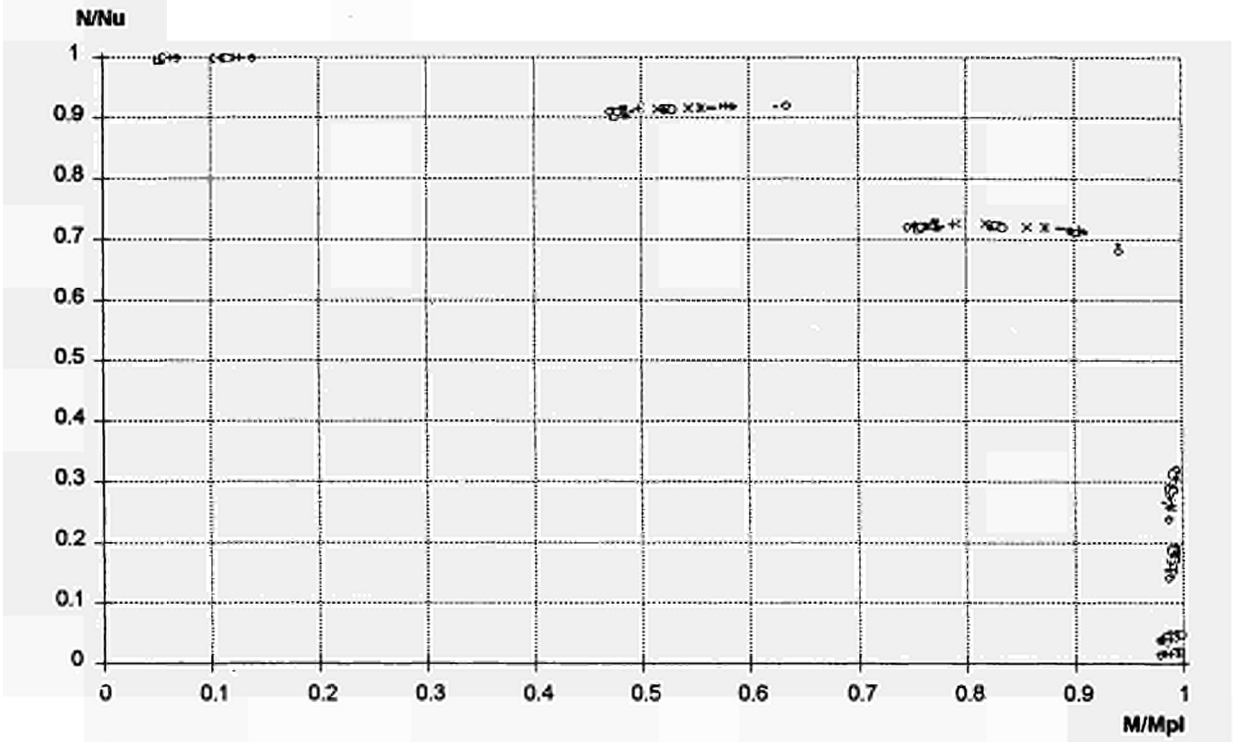

FIGURE 8.41 Points calculated for buckling about the minor axis, bi-triangular moment distribution, and $\bar{\lambda}_{20} = 0.2$

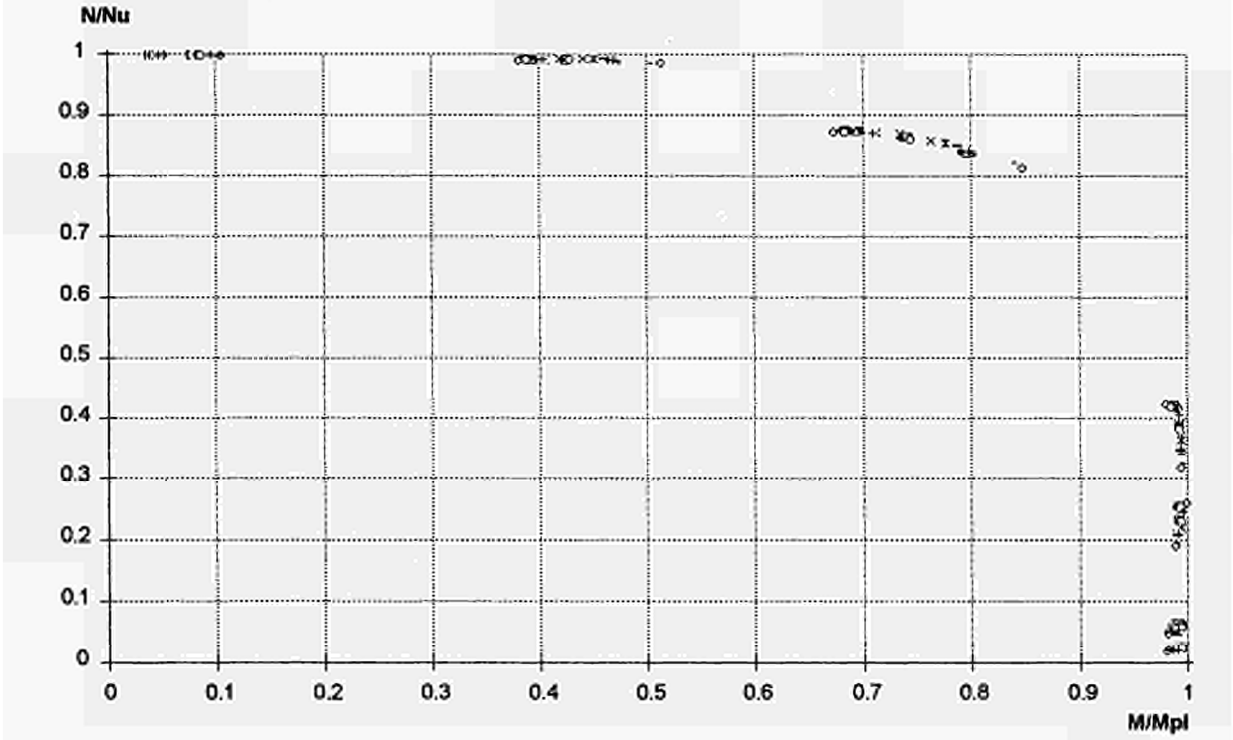

FIGURE 8.42 Points calculated for buckling about the minor axis, bi-triangular moment distribution, and $\bar{\lambda}_{20} = 0.4$

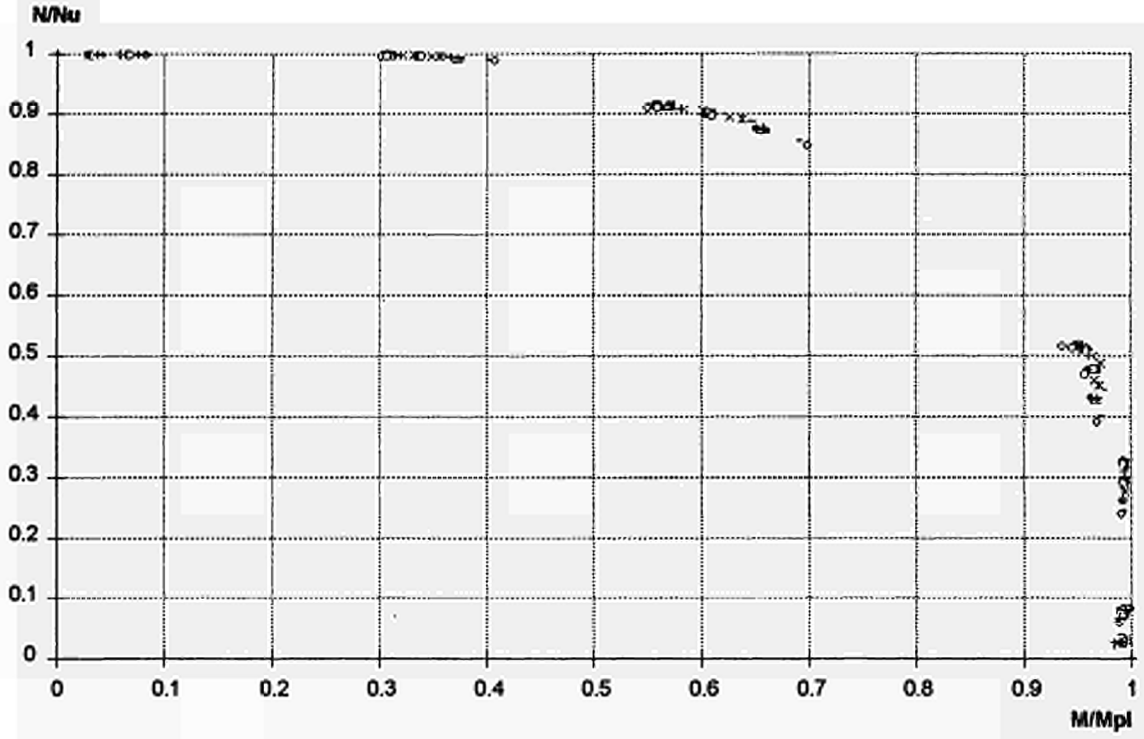

FIGURE 8.43 Points calculated for buckling about the minor axis, bi-triangular moment distribution, and $\overline{\lambda}_{20} = 0.6$

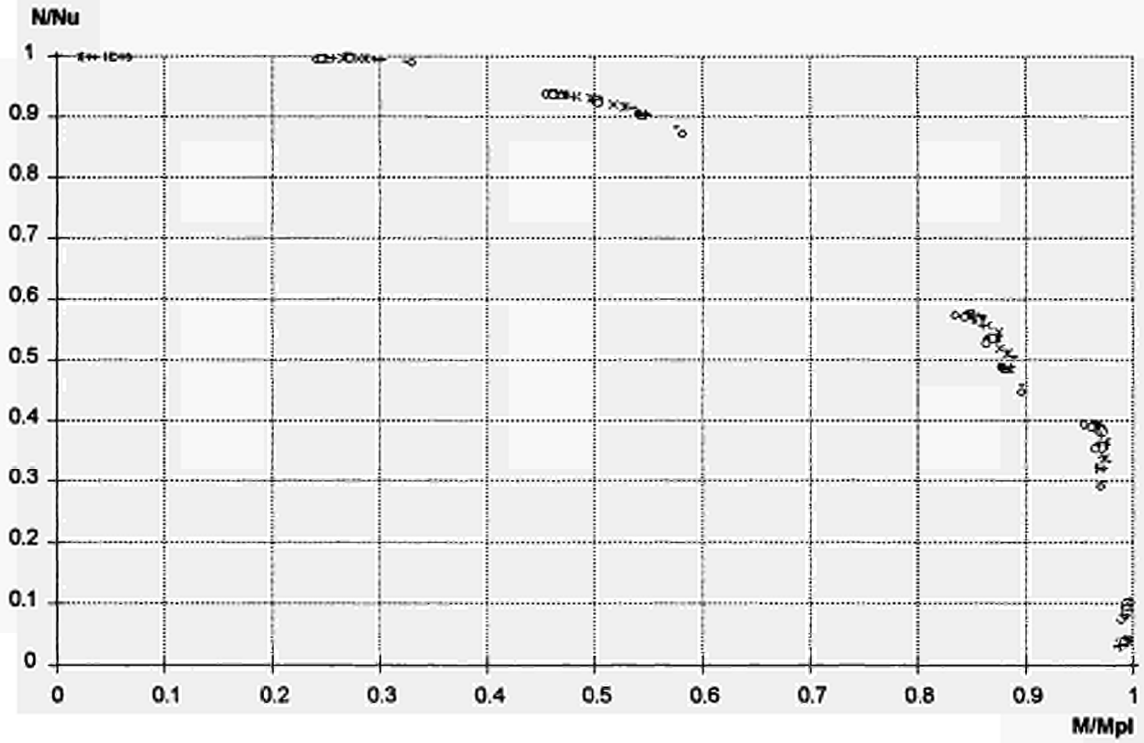

FIGURE 8.44 Points calculated for buckling about the minor axis, bi-triangular moment distribution, and $\overline{\lambda}_{20} = 0.8$

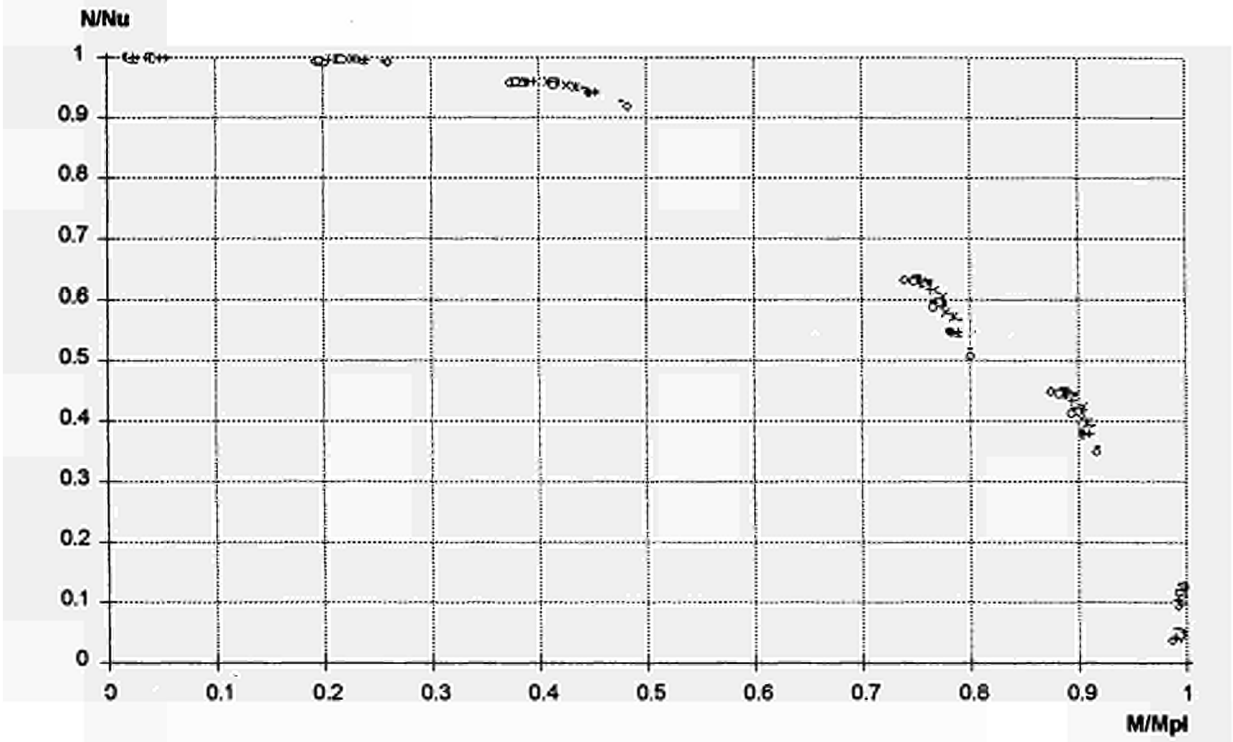

FIGURE 8.45 Points calculated for buckling about the minor axis, bi-triangular moment distribution, and $\bar{\lambda}_{20} = 1$

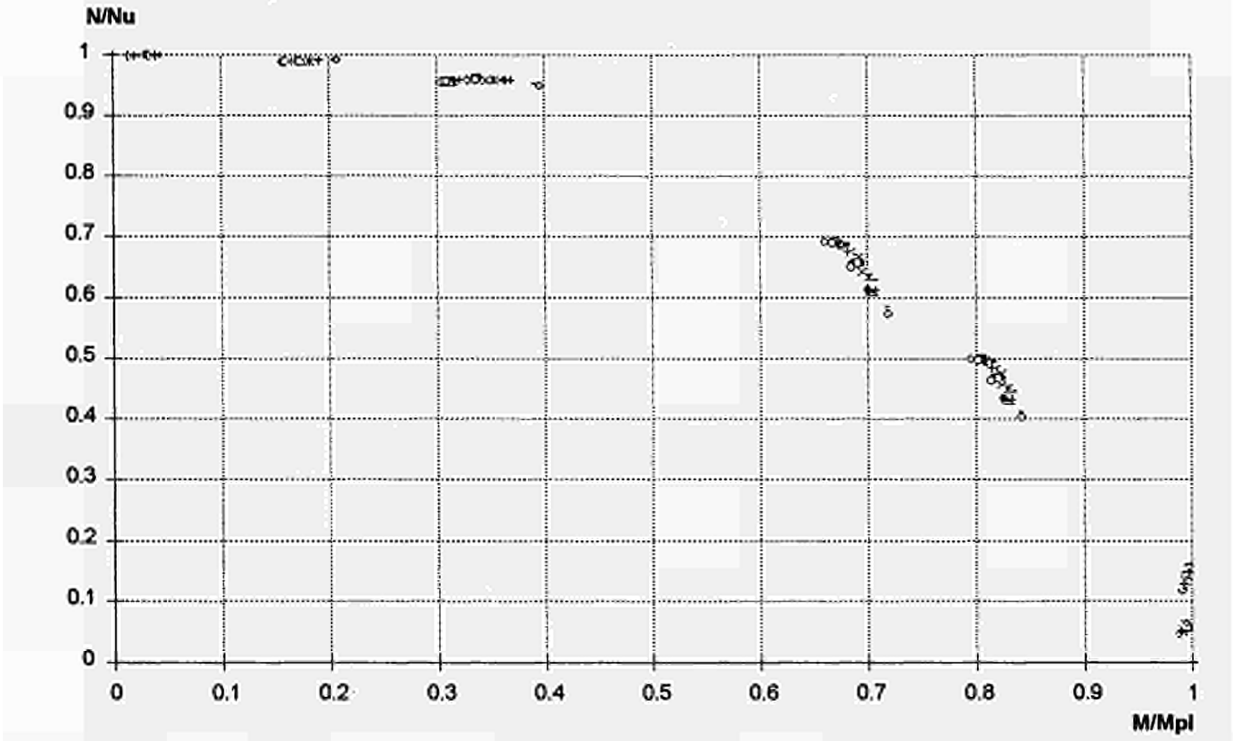

FIGURE 8.46 Points calculated for buckling about the minor axis, bi-triangular moment distribution, and $\bar{\lambda}_{20} = 1.2$

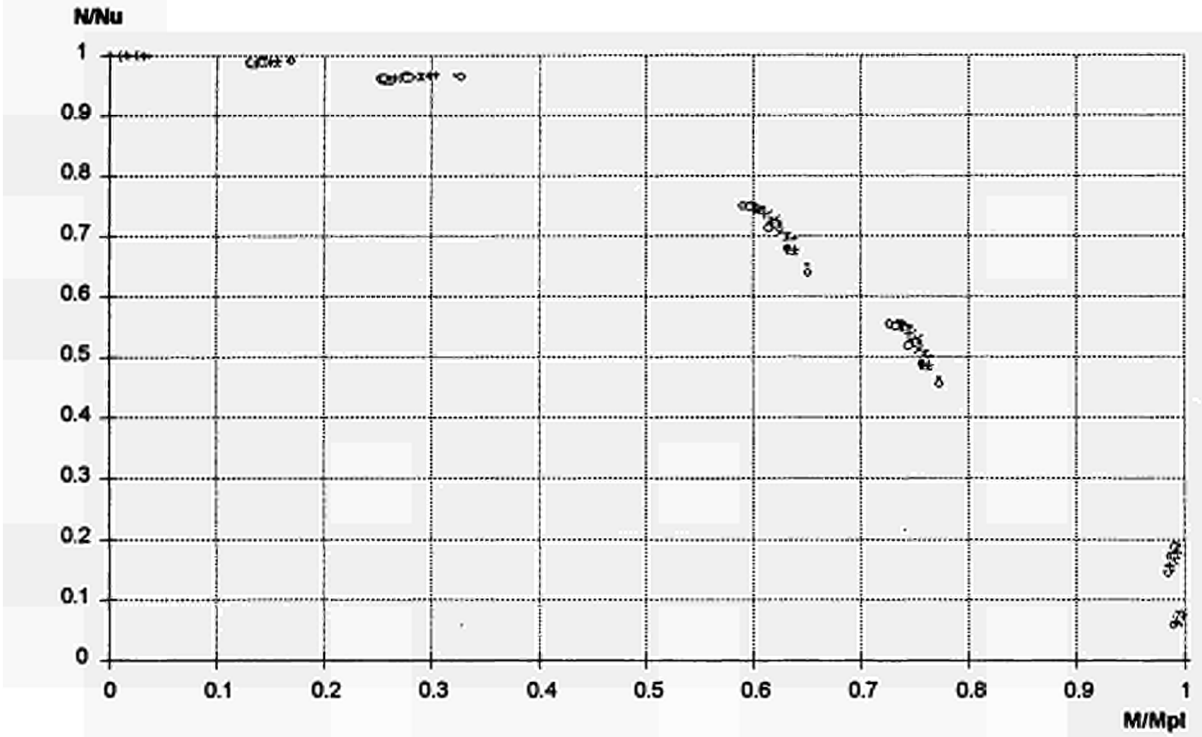

FIGURE 8.47 Points calculated for buckling about the minor axis, bi-triangular moment distribution, and $\overline{\lambda}_{20} = 1.4$

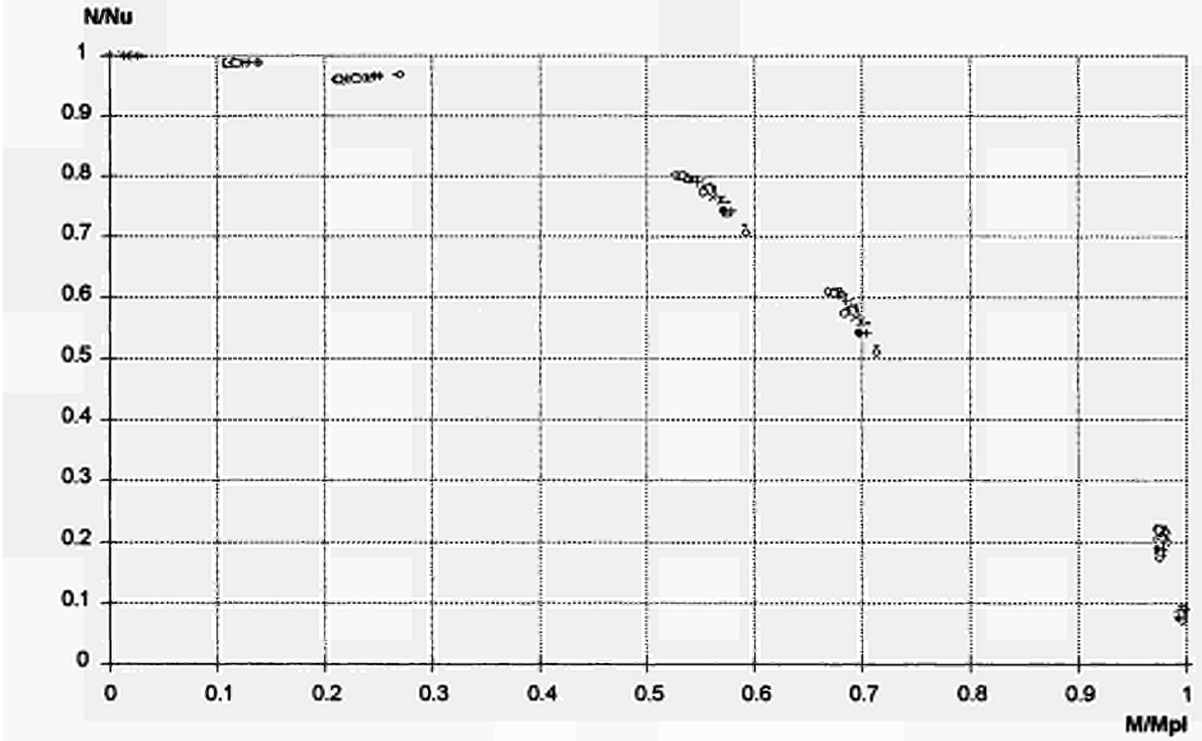

FIGURE 8.48 Points calculated for buckling about the minor axis, bi-triangular moment distribution, and $\overline{\lambda}_{20} = 1.6$

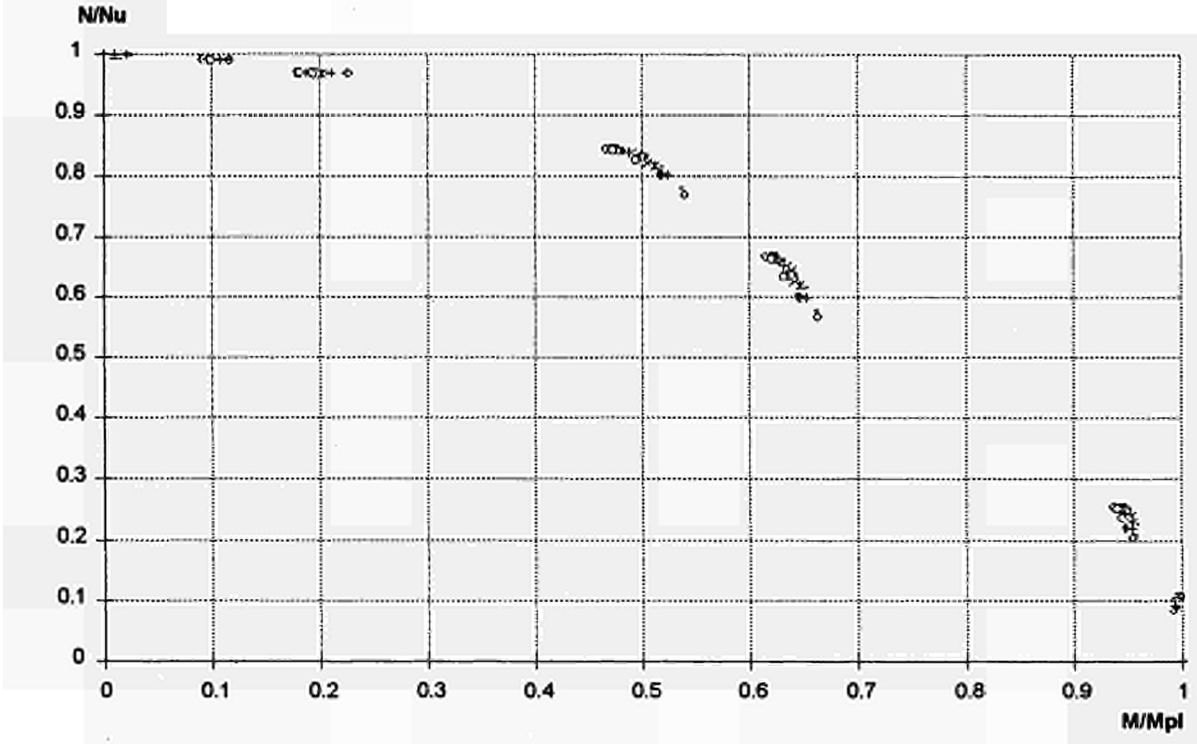

FIGURE 8.49 Points calculated for buckling about the minor axis, bi-triangular moment distribution, and $\bar{\lambda}_{20} = 1.8$

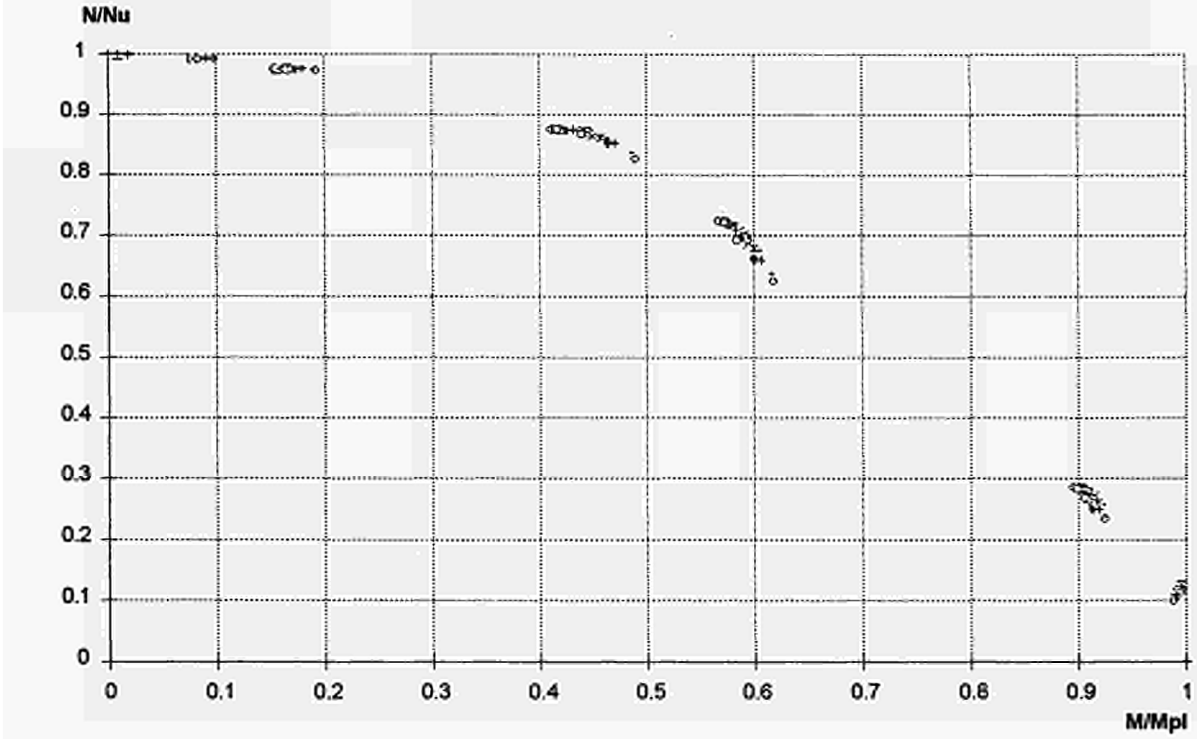

FIGURE 8.50 Points calculated for buckling about the minor axis, bi-triangular moment distribution, and $\bar{\lambda}_{20} = 2$

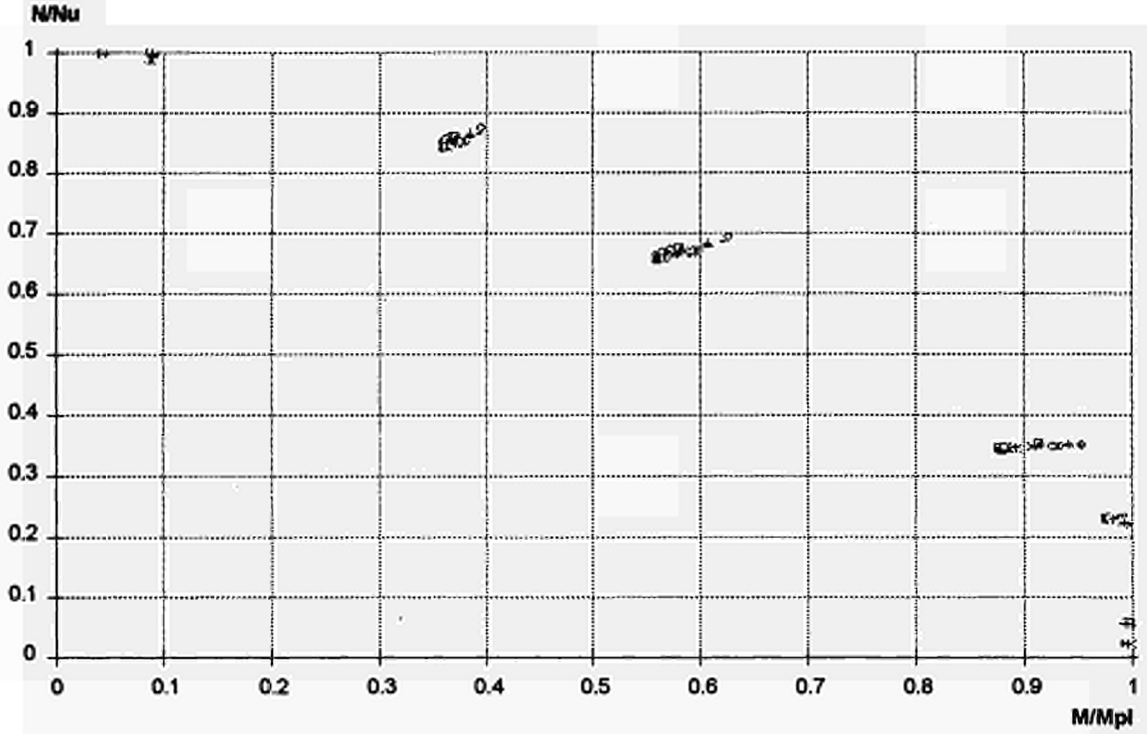

FIGURE 8.51 Points calculated for buckling about the major axis, bi-triangular moment distribution, and $\overline{\lambda}_{20} = 0.2$

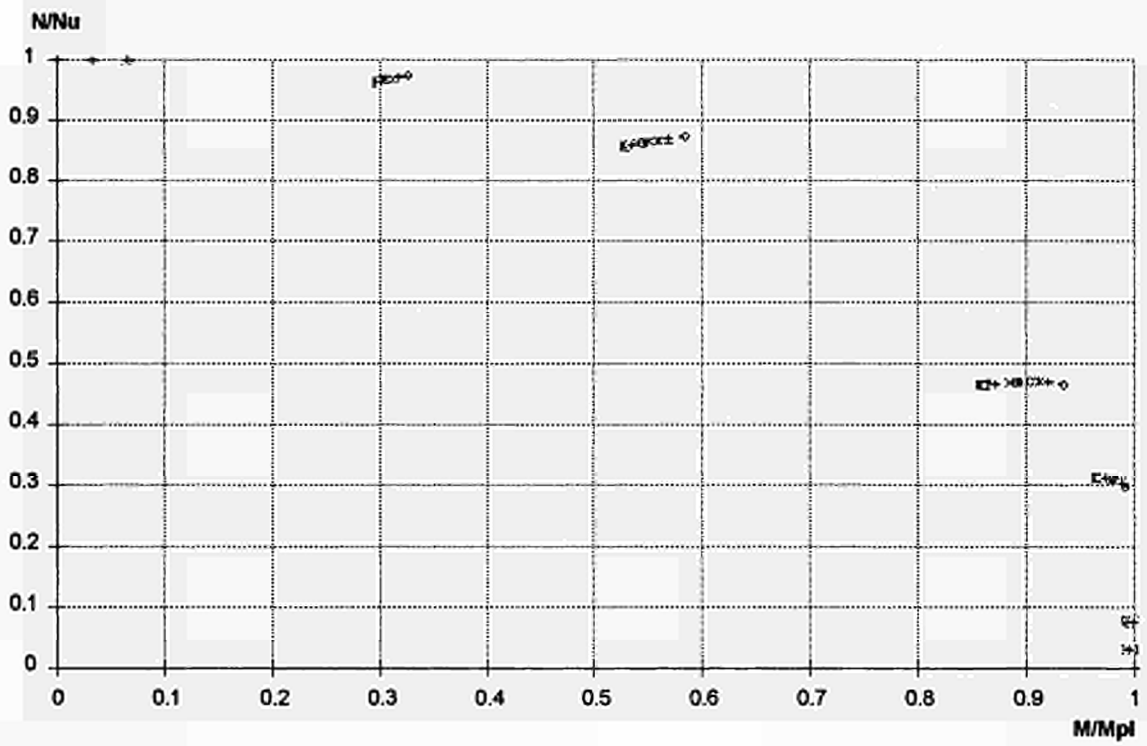

FIGURE 8.52 Points calculated for buckling about the major axis, bi-triangular moment distribution, and $\overline{\lambda}_{20} = 0.4$

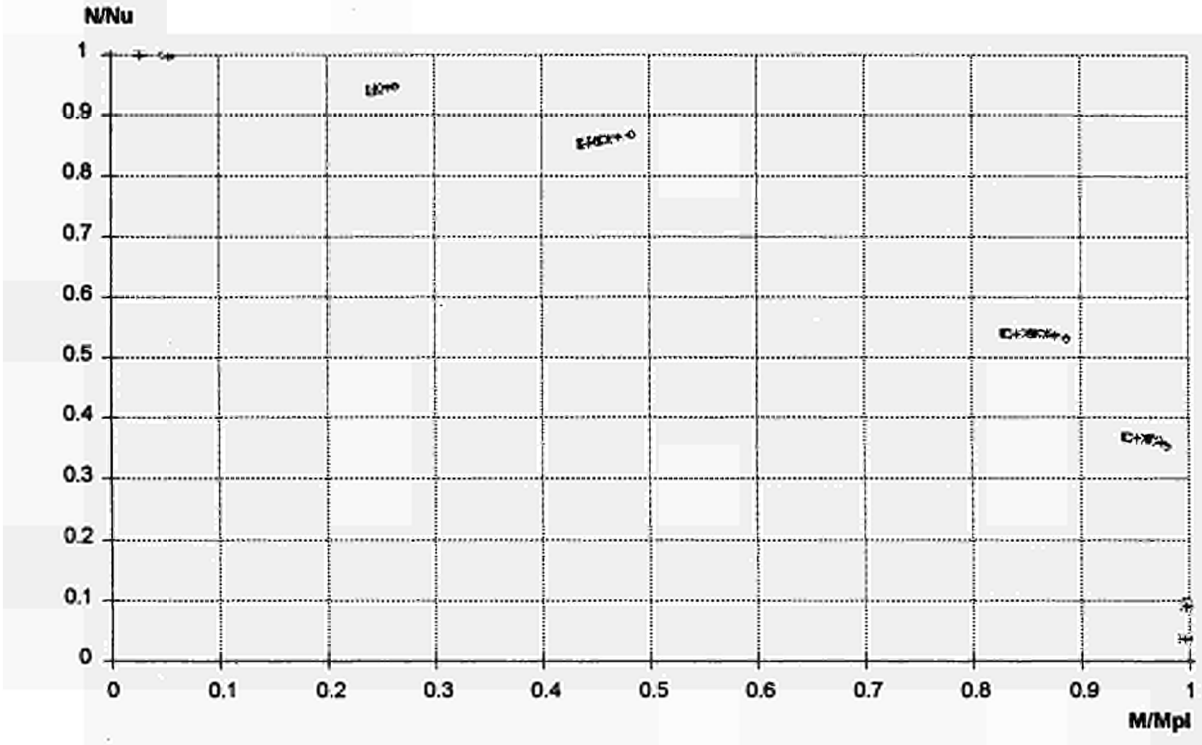

FIGURE 8.53 Points calculated for buckling about the major axis, bi-triangular moment distribution, and $\bar{\lambda}_{20} = 0.6$

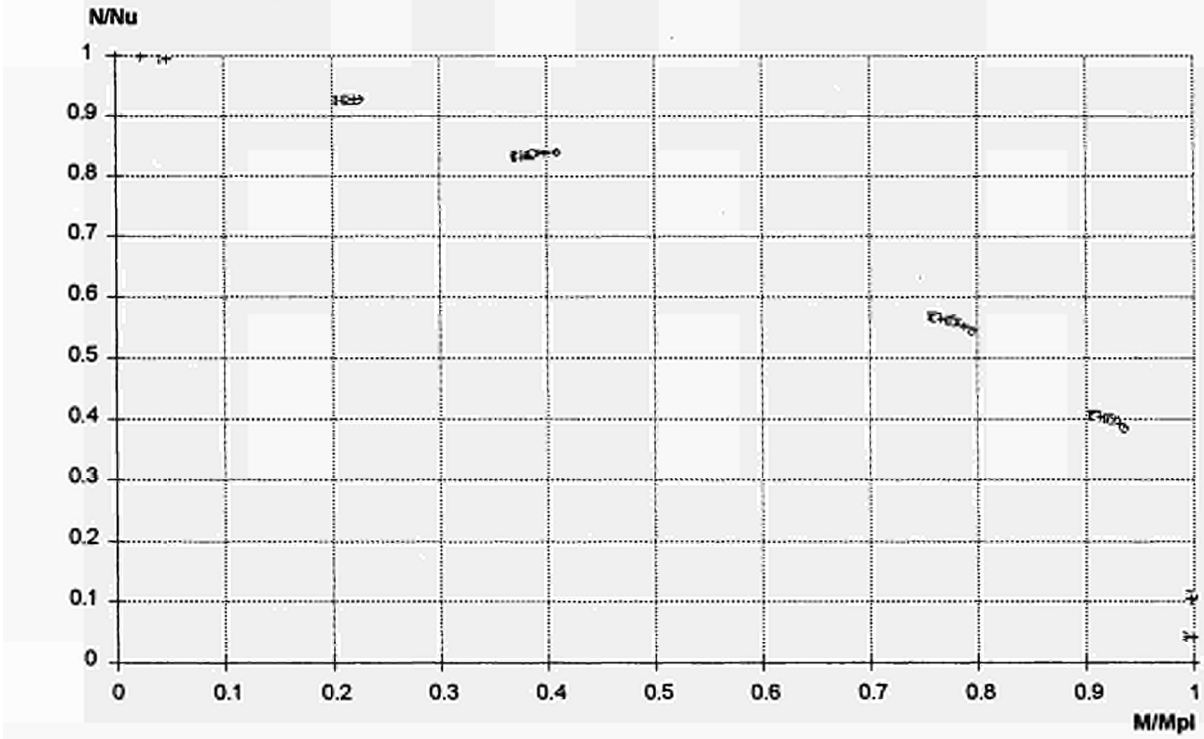

FIGURE 8.54 Points calculated for buckling about the major axis, bi-triangular moment distribution, and $\bar{\lambda}_{20} = 0.8$

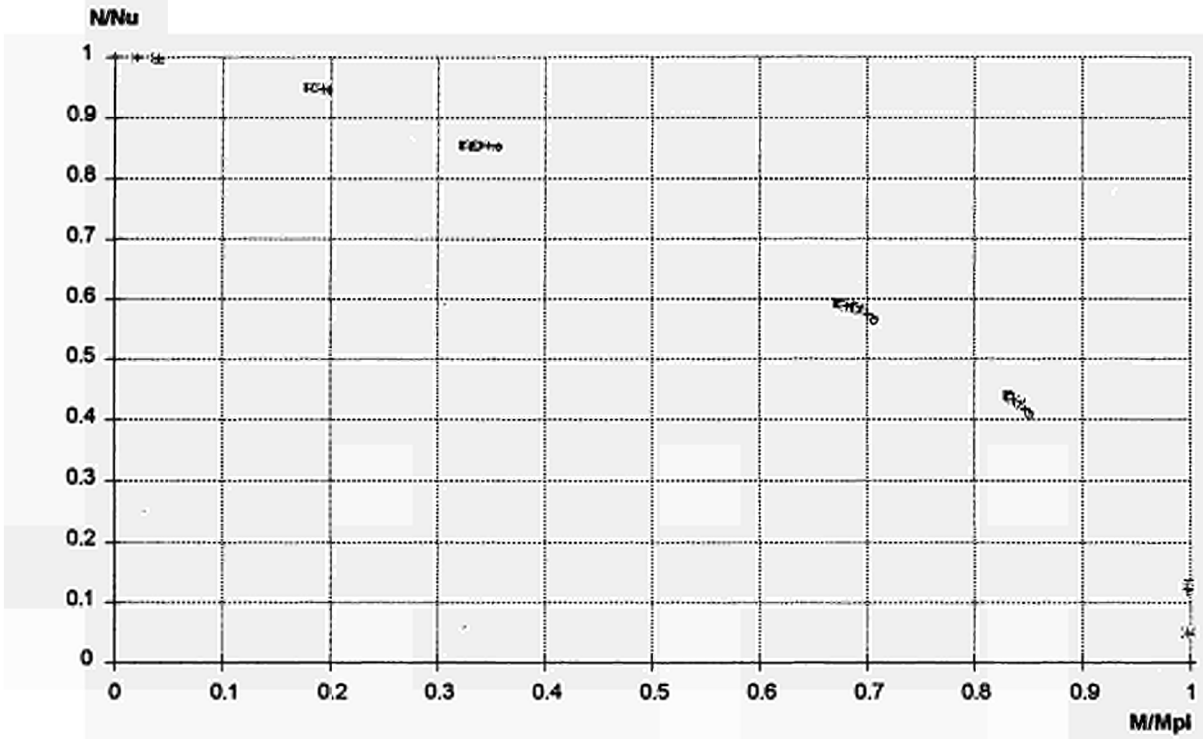

FIGURE 8.55 Points calculated for buckling about the major axis, bi-triangular moment distribution, and $\overline{\lambda}_{20} = 1$

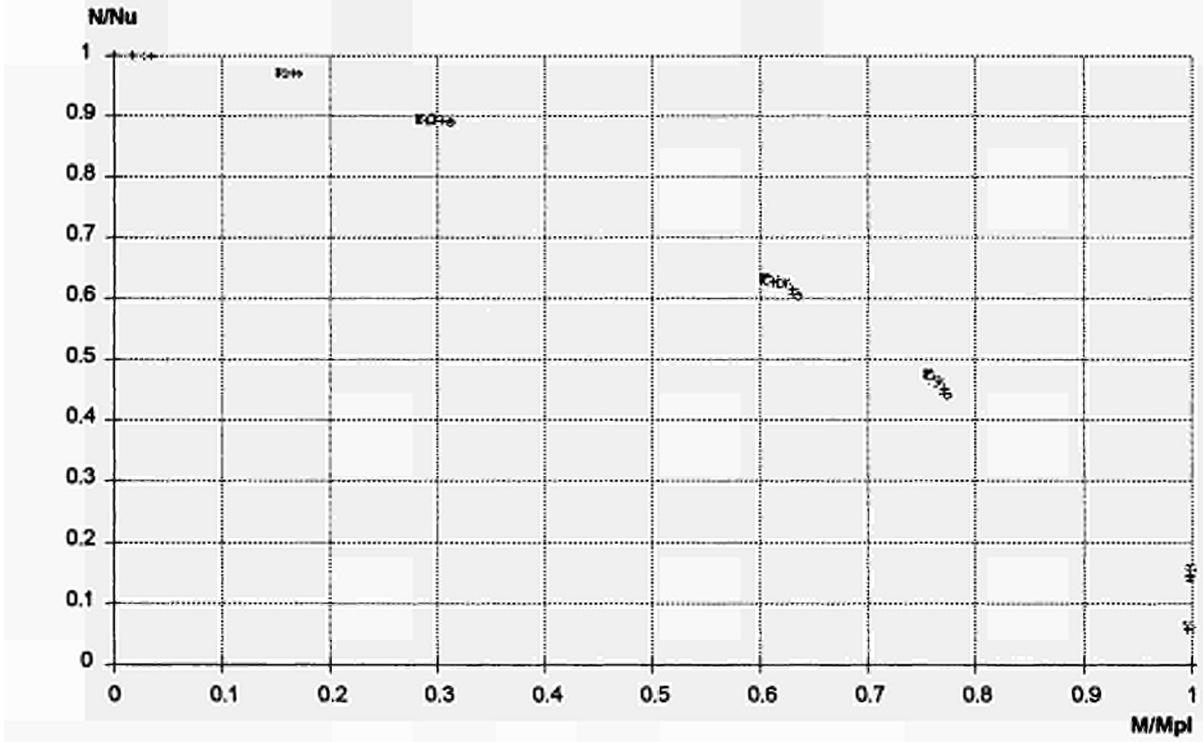

FIGURE 8.56 Points calculated for buckling about the major axis, bi-triangular moment distribution, and $\overline{\lambda}_{20} = 1.2$

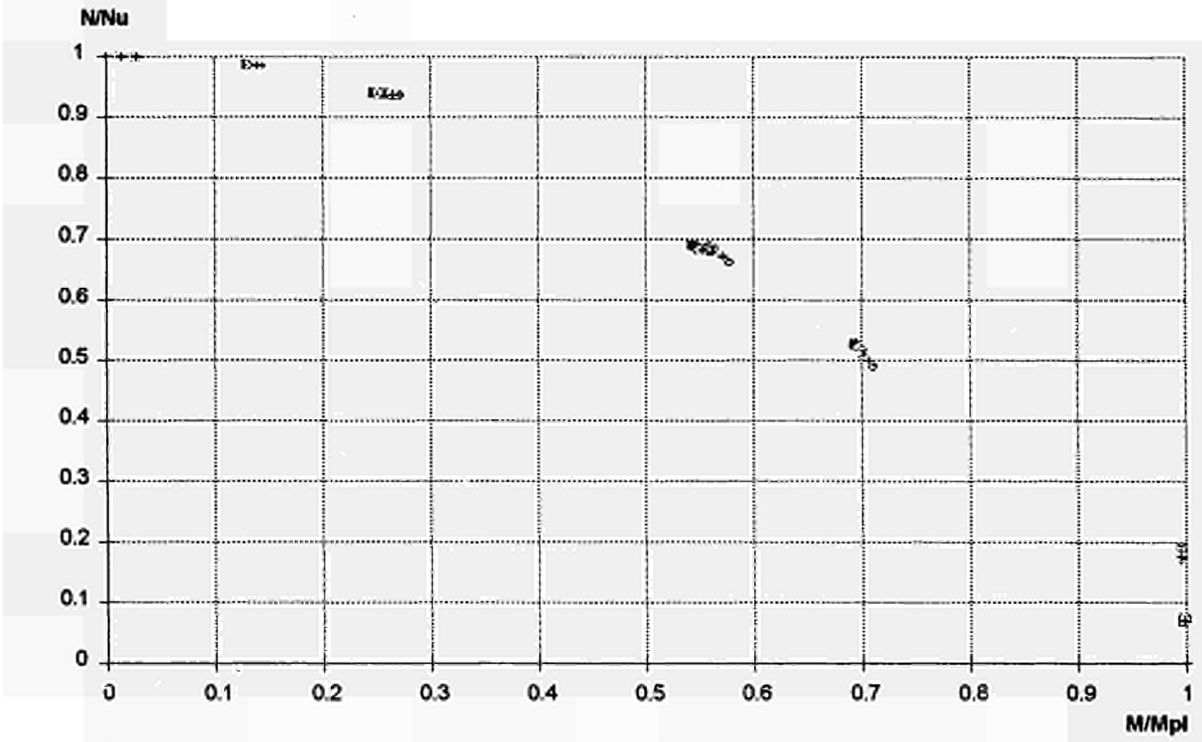

FIGURE 8.57 Points calculated for buckling about the major axis, bi-triangular moment distribution, and $\bar{\lambda}_{20} = 1.4$

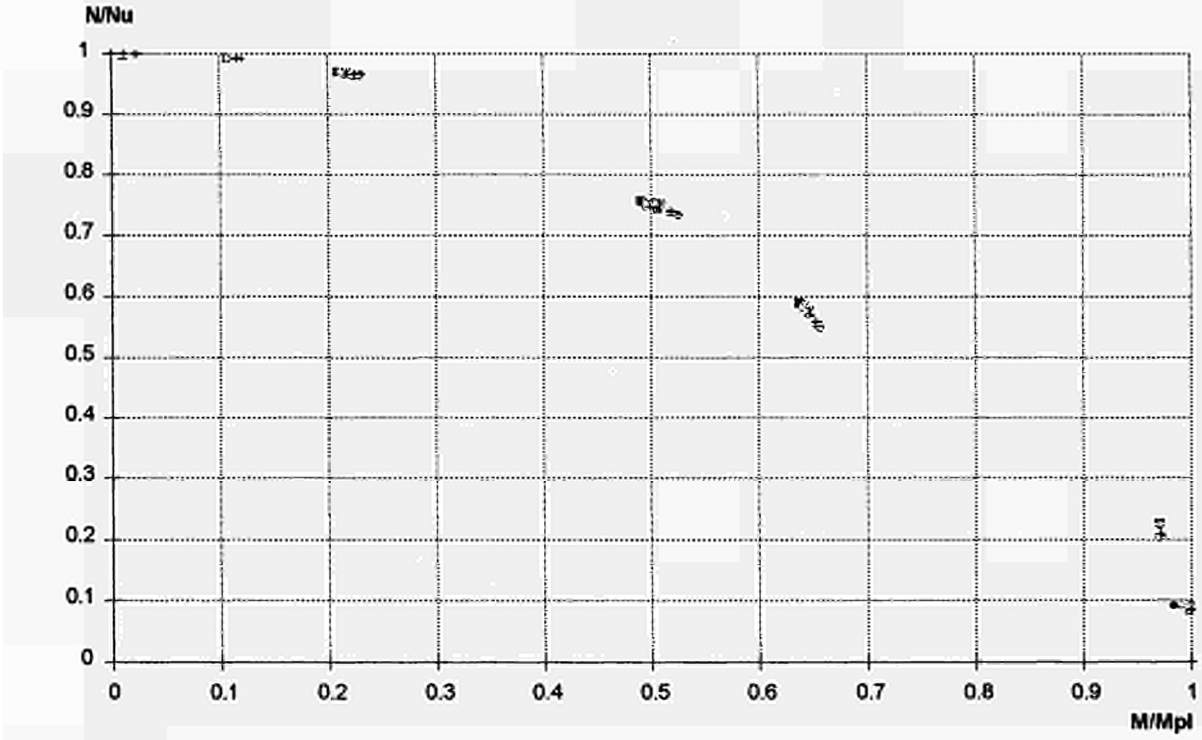

FIGURE 8.58 Points calculated for buckling about the major axis, bi-triangular moment distribution, and $\bar{\lambda}_{20} = 1.6$

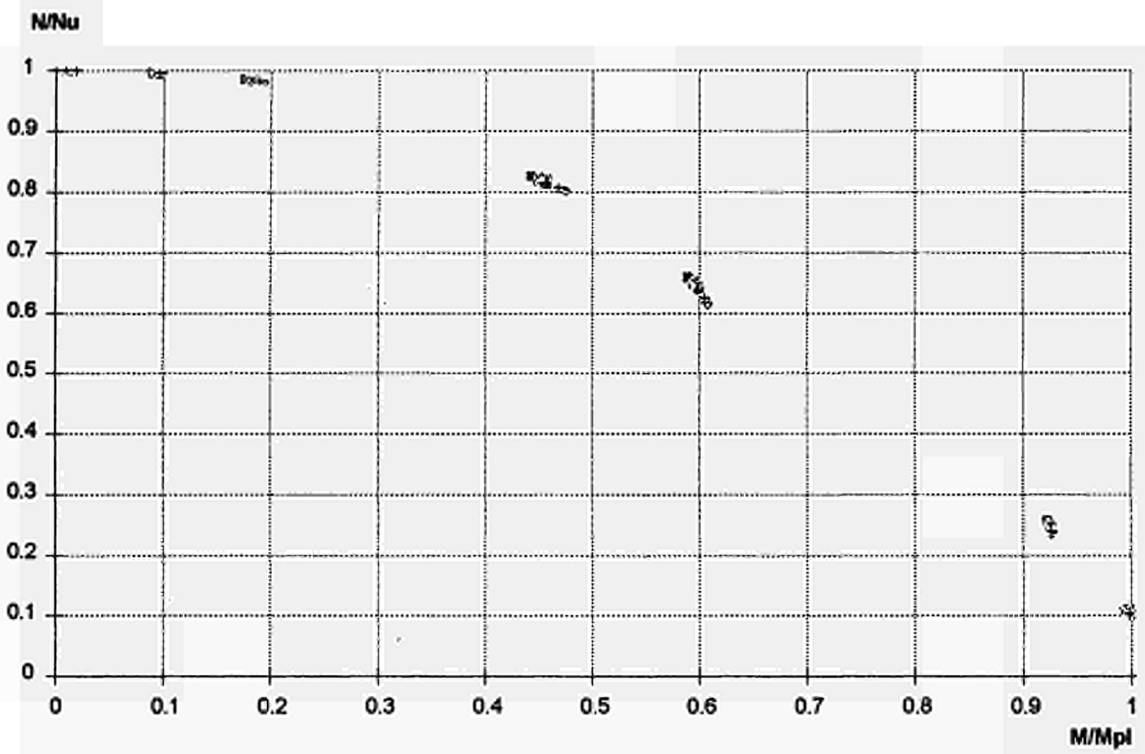

FIGURE 8.59 Points calculated for buckling about the major axis, bi-triangular moment distribution, and $\overline{\lambda}_{20} = 1.8$

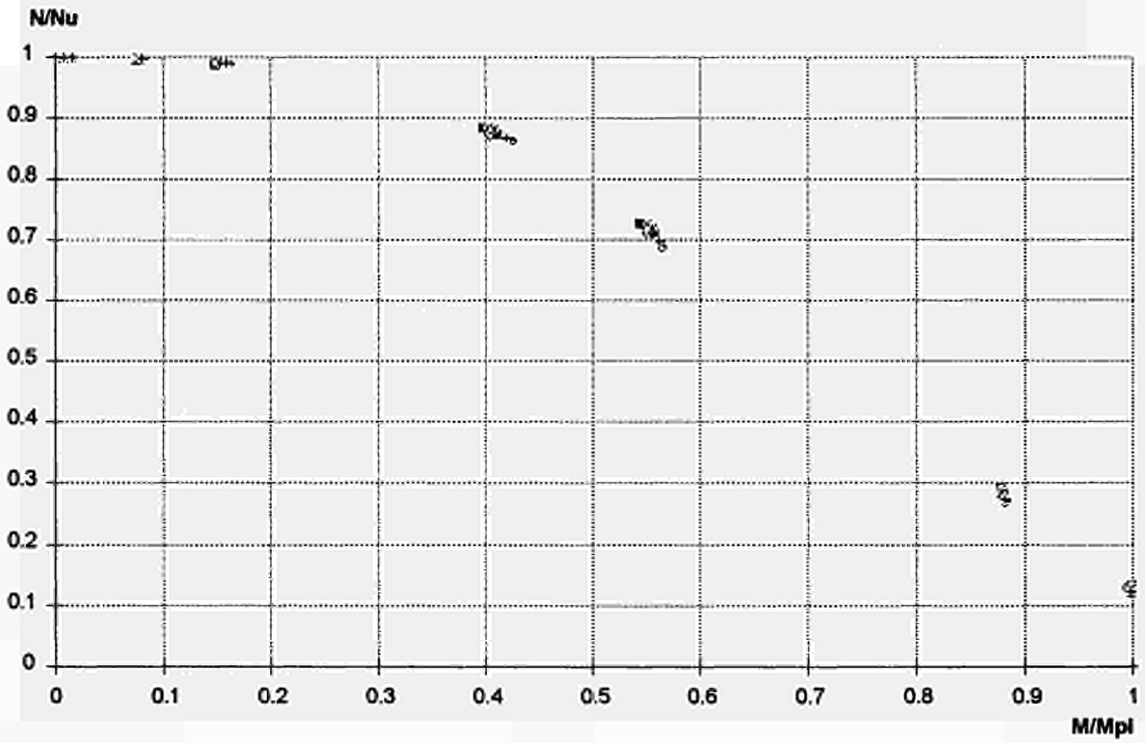

FIGURE 8.60 Points calculated for buckling about the major axis, bi-triangular moment distribution, and $\overline{\lambda}_{20} = 2$

ANNEX 9:

9. N-M INTERACTION CURVES PROVIDED BY DIANA

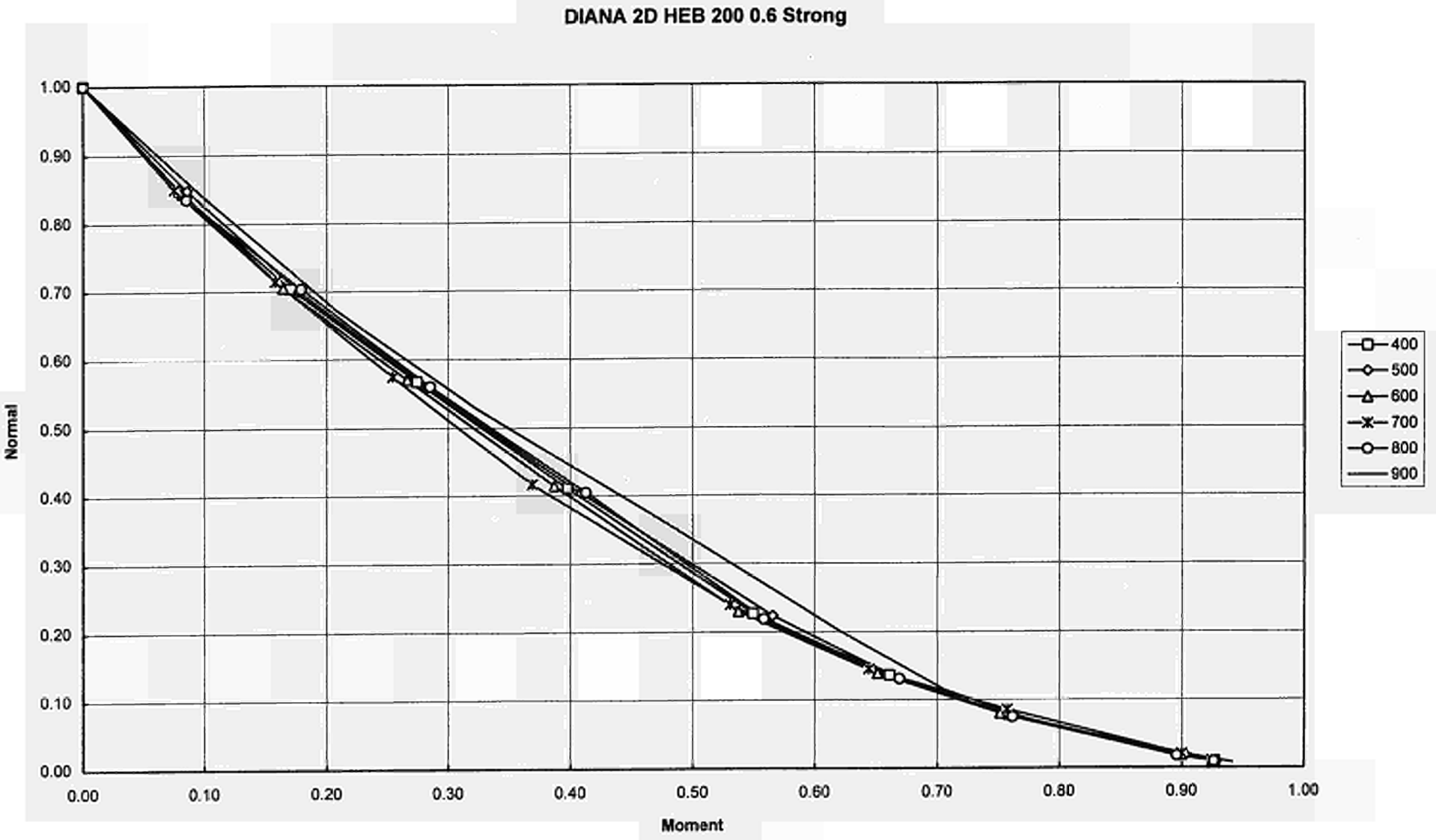
DIANA 2D HEB 200 0.6 Strong
Normal
Moment
1.00
0.90
0.80
0.70
0.60
0.50
0.40
0.30
0.20
0.10
0.00
0.00
0.10
0.20
0.30
0.40
0.50
0.60
0.70
0.80
0.90
1.00
400
500
600
700
800
900

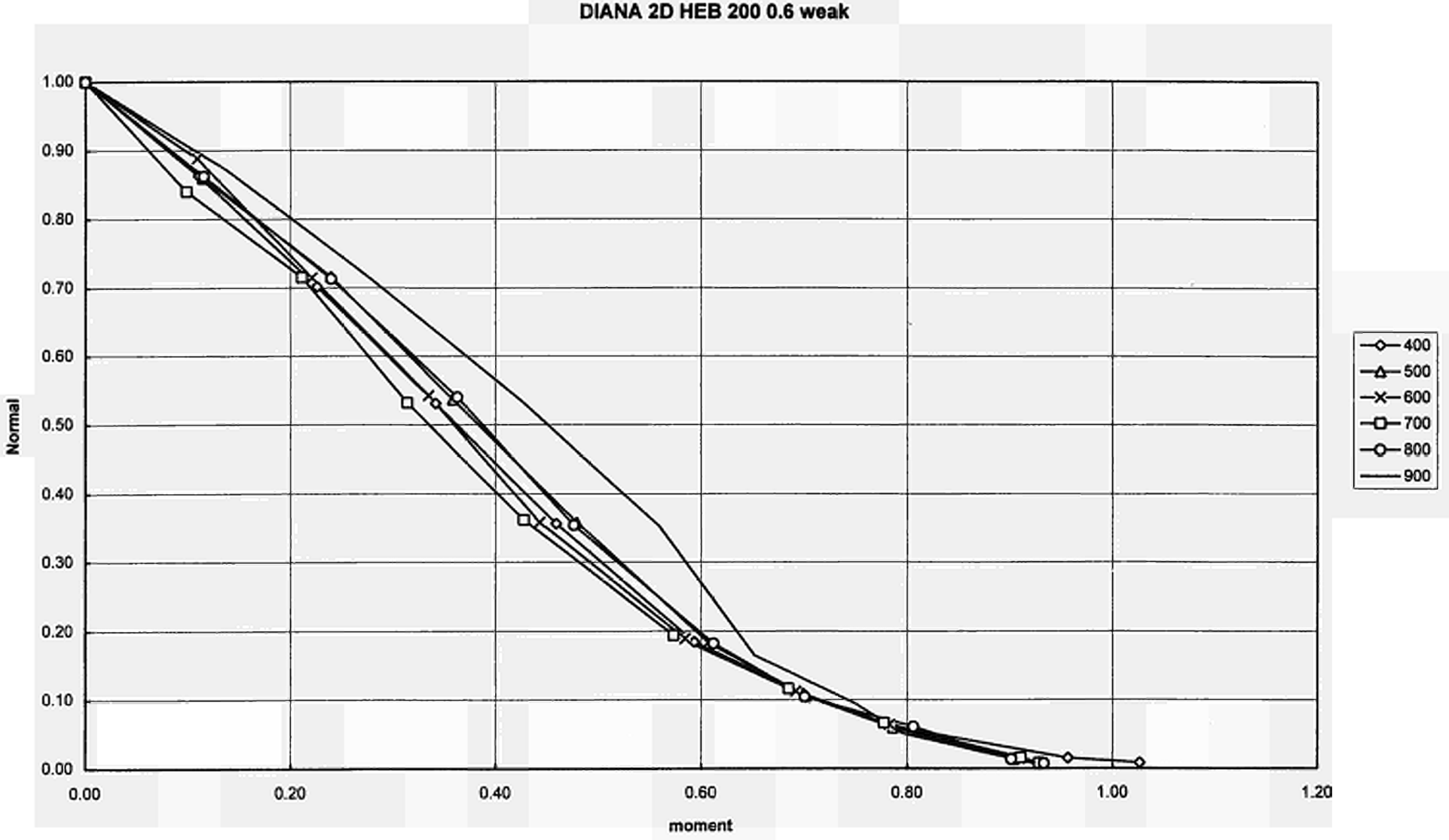
DIANA 2D HEB 200 0.6 weak
Normal
1.00
0.90
0.80
0.70
0.60
0.50
0.40
0.30
0.20
0.10
0.00
0.00
0.20
0.40
0.60
0.80
1.00
1.20
moment
400
500
600
700
800
900

ANNEX 10:

10. VALUES OF μ_y FOR BUCKLING AROUND WEAK AND STRONG AXIS AND FOR THREE TYPES OF BENDING MOMENT DISTRIBUTION (UNIFORM, TRIANGULAR AND BI-TRIANGULAR)

This annex shows the values of μ_y which were calculated from the results obtained numerically for a failure temperature of 400°C, so as to comply with the following equation:

$$\mu_y = \left[\frac{N_{Sd}}{\chi_{min} A f_y} + \frac{M_{y,Sd}}{W_{pl,y} f_y} - 1 \right] \frac{\chi_{min} A f_y}{N_{Sd}} \frac{W_{pl,y} f_y}{M_{y,Sd}}$$

μ_y was calculated for buckling about the major and minor axes, with three types of moment distribution:

- Uniform
- Triangular
- Bi-triangular

All the points calculated with LENAS are shown on FIGURE 10.1 to FIGURE 10.6, while the points obtained for both largest eccentricities were eliminated from FIGURE 10.7 to FIGURE 10.12 (we retained this assumption during the development of a simplified formula).

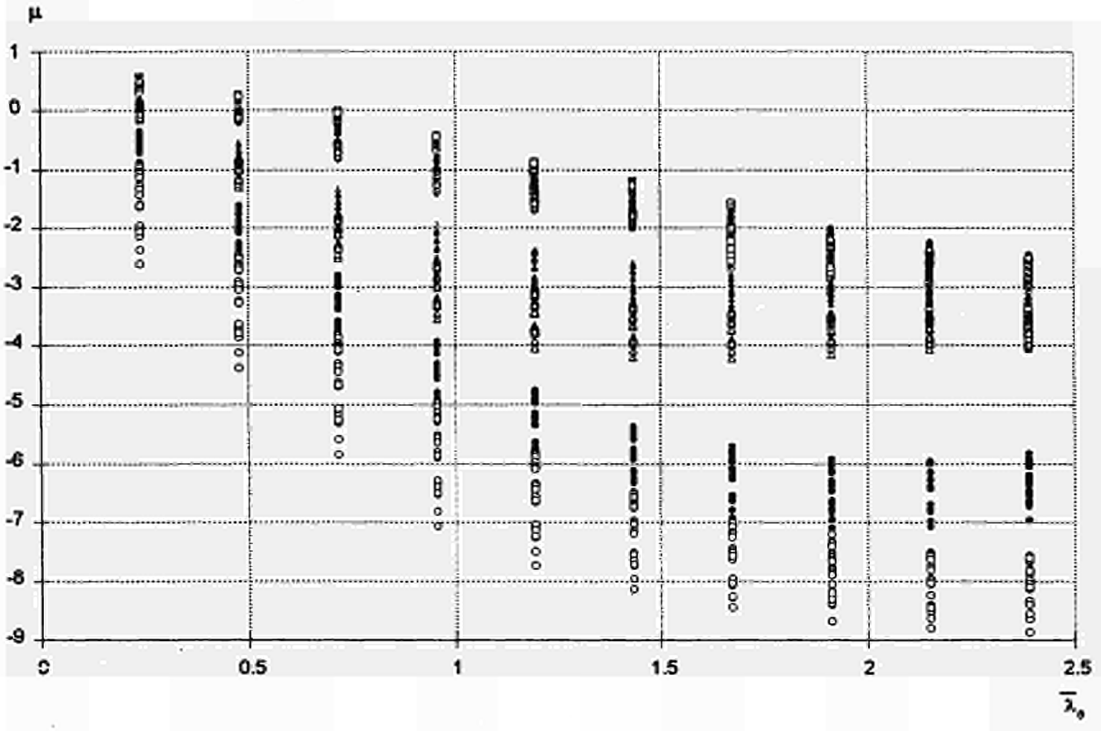

FIGURE 10.1 Evolution of μ according to the slenderness ratio (buckling about minor axis - uniform moment)

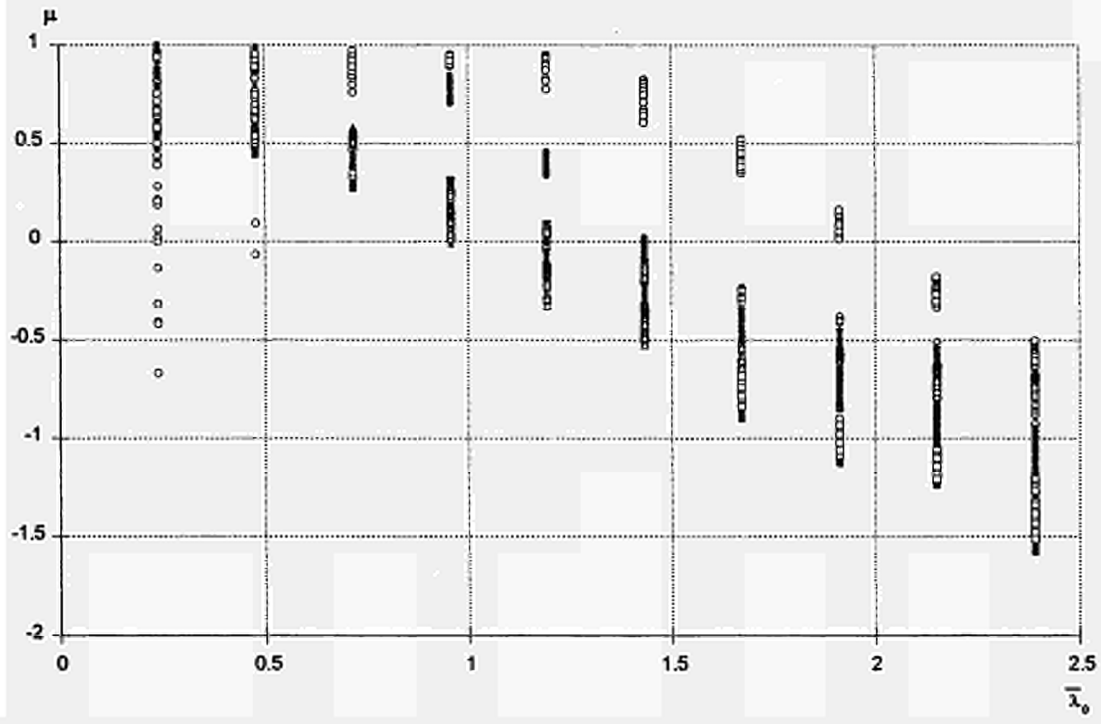

FIGURE 10.2 Evolution of μ according to the slenderness ratio (buckling about minor axis - triangular moment)

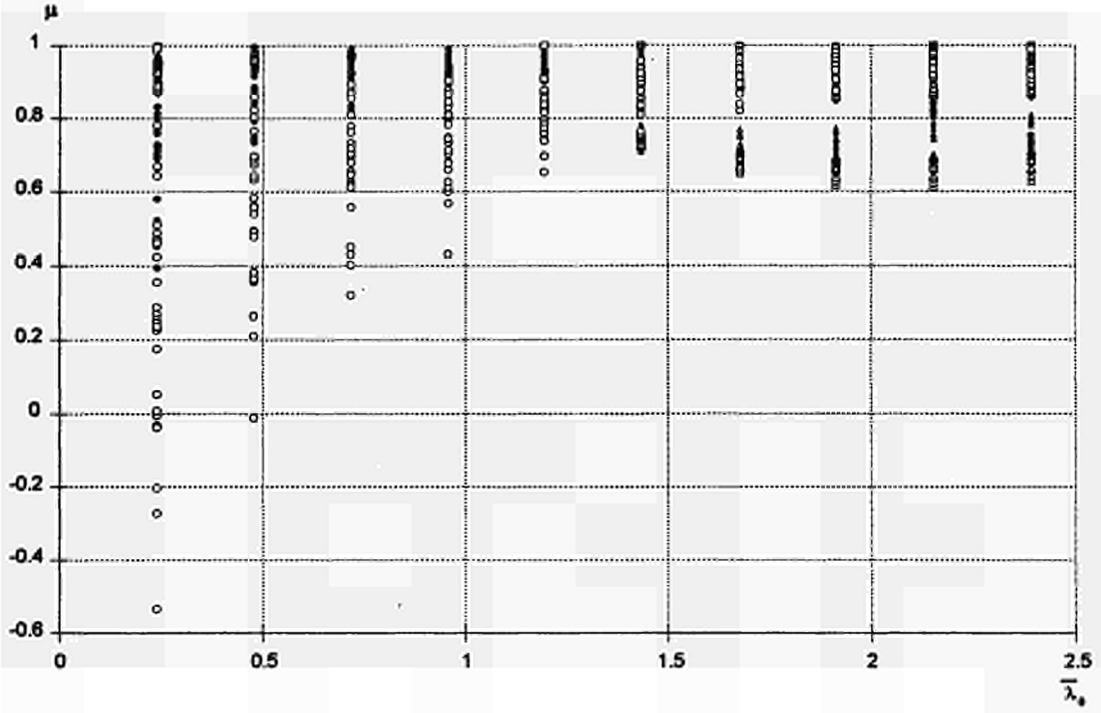

FIGURE 10.3 Evolution of μ according to the slenderness ratio (buckling about minor axis - bi-triangular moment)

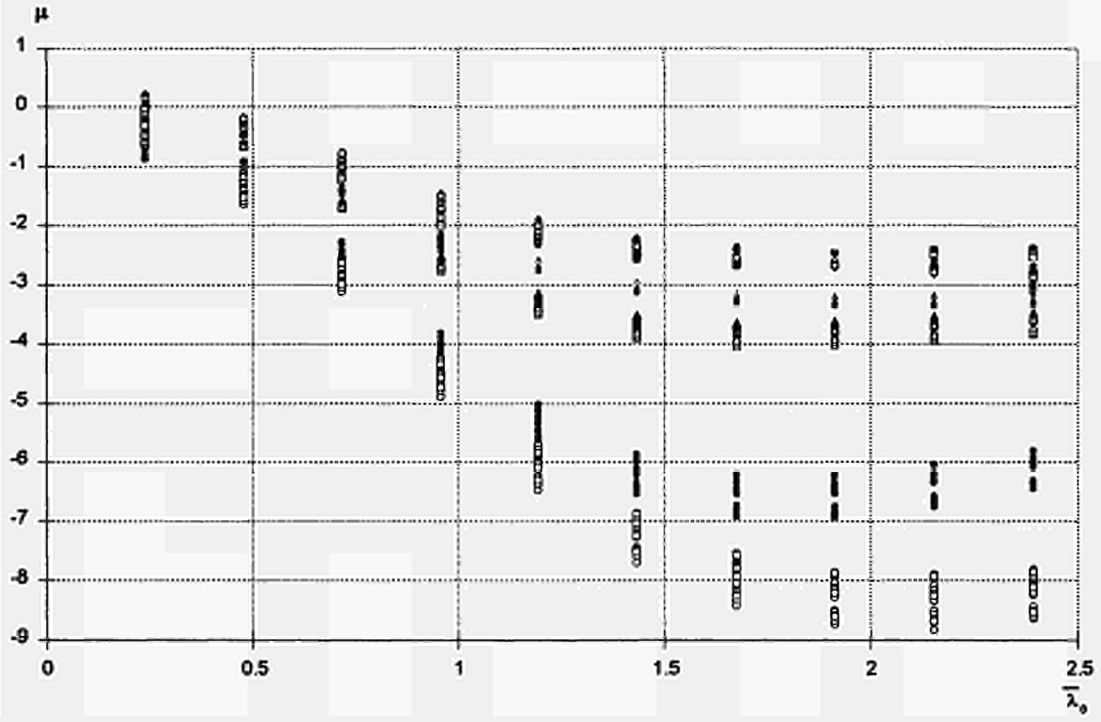

FIGURE 10.4 Evolution of μ according to the slenderness ratio (buckling about major axis - uniform moment)

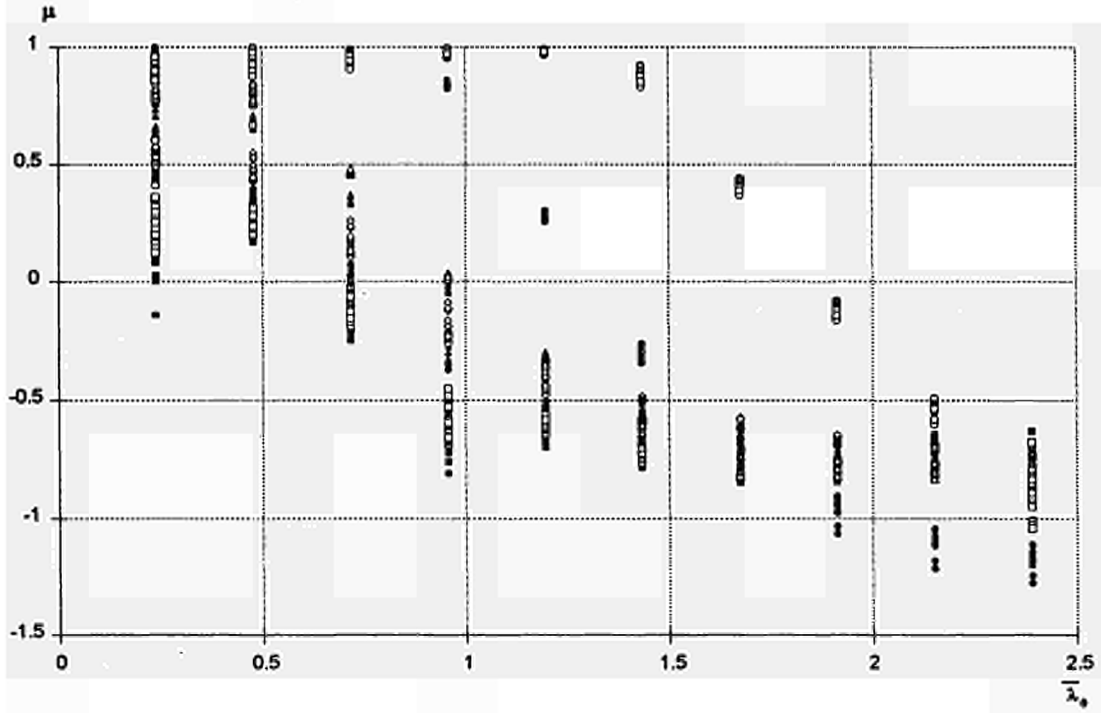

FIGURE 10.5 Evolution of μ according to the slenderness ratio (buckling about major axis - triangular moment)

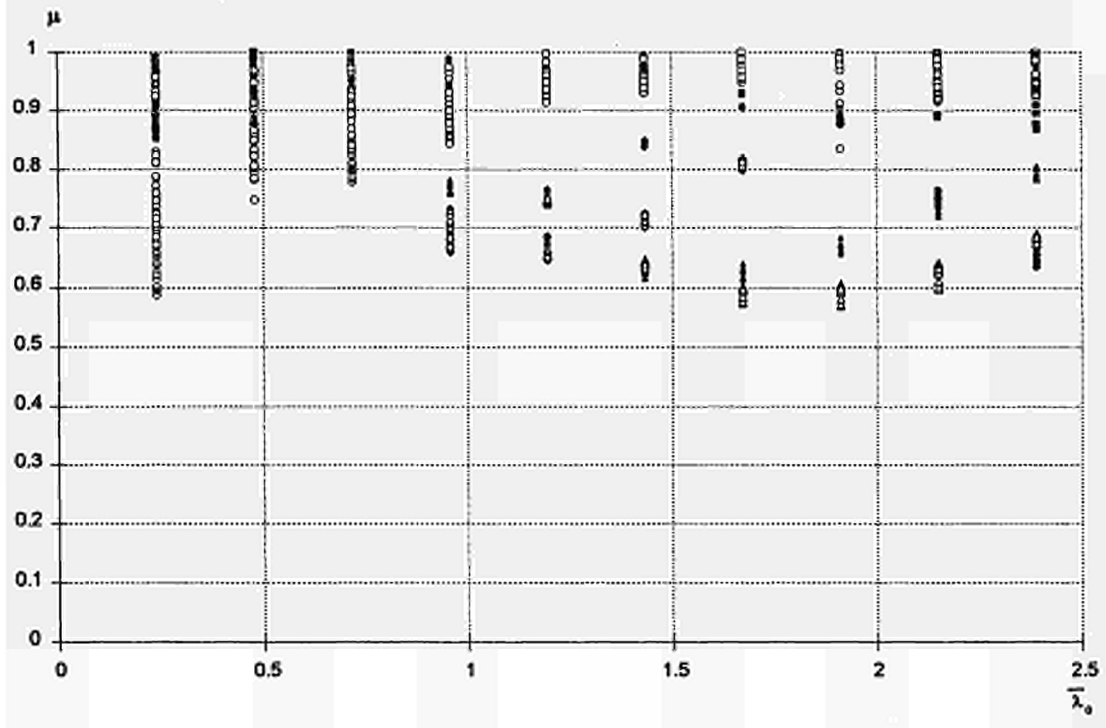

FIGURE 10.6 Evolution of μ according to the slenderness ratio (buckling about major axis - bi-triangular moment)

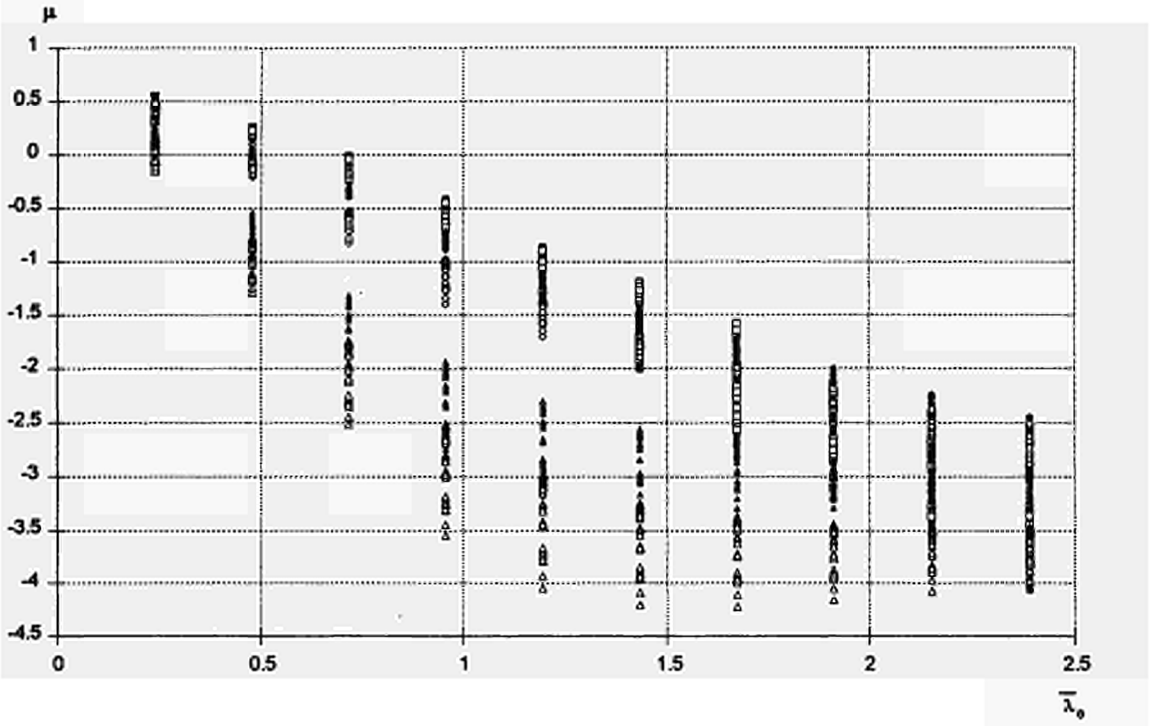

FIGURE 10.7 Evolution of μ according to the slenderness ratio (buckling about minor axis - uniform moment)

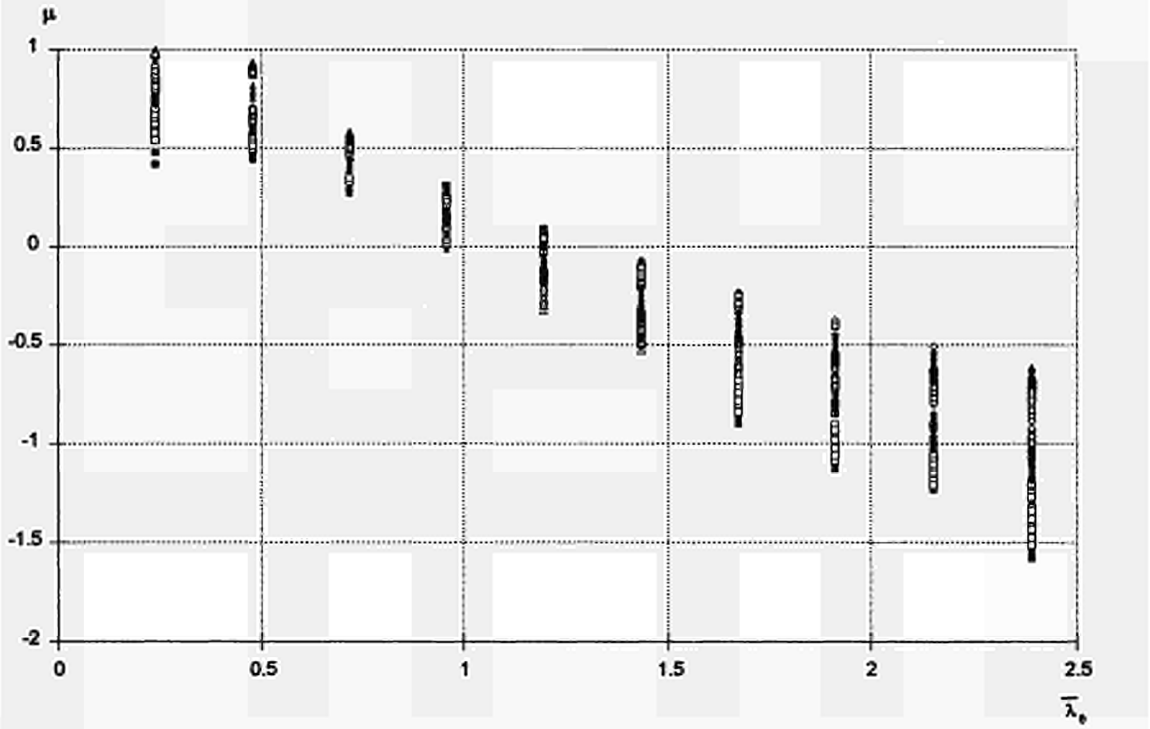

FIGURE 10.8 Evolution of μ according to the slenderness ratio (buckling about minor axis - triangular moment)

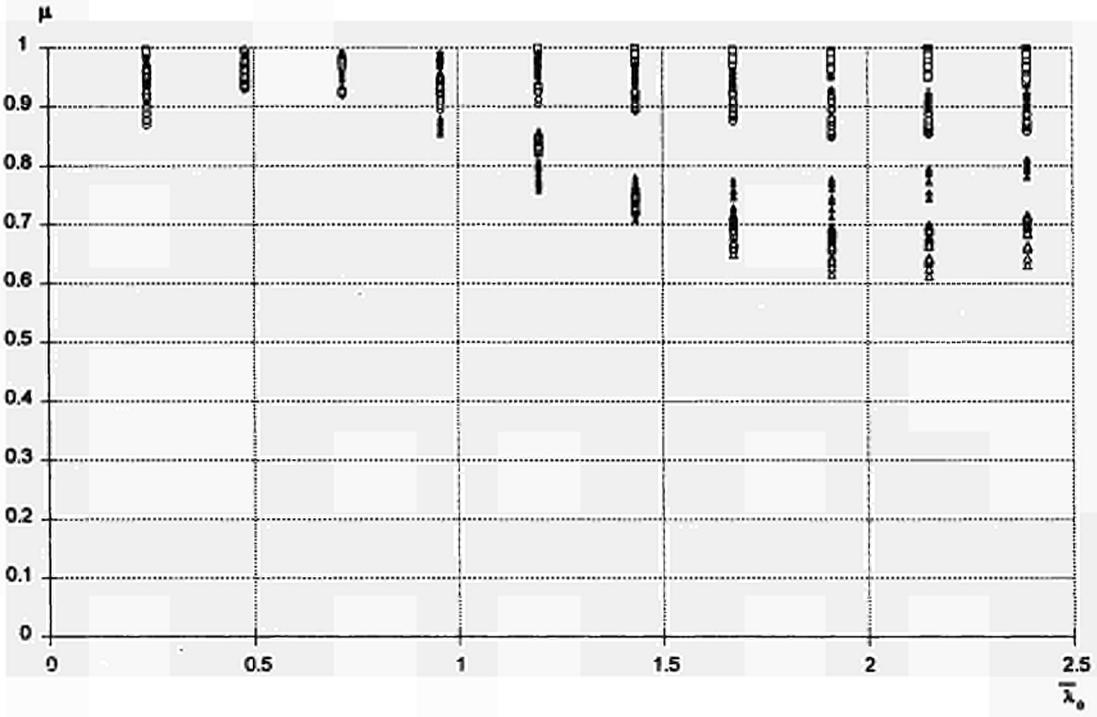

FIGURE 10.9 Evolution of μ according to the slenderness ratio (buckling about minor axis - bi-triangular moment)

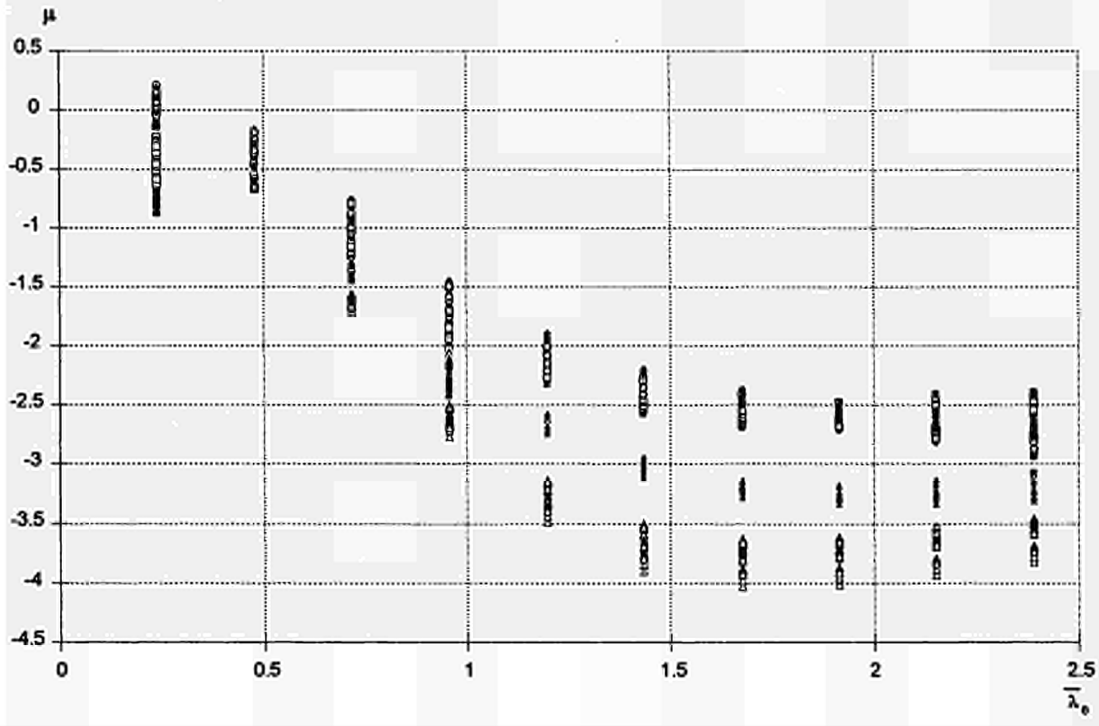

FIGURE 10.10 Evolution of μ according to the slenderness ratio (buckling about major axis - uniform moment)

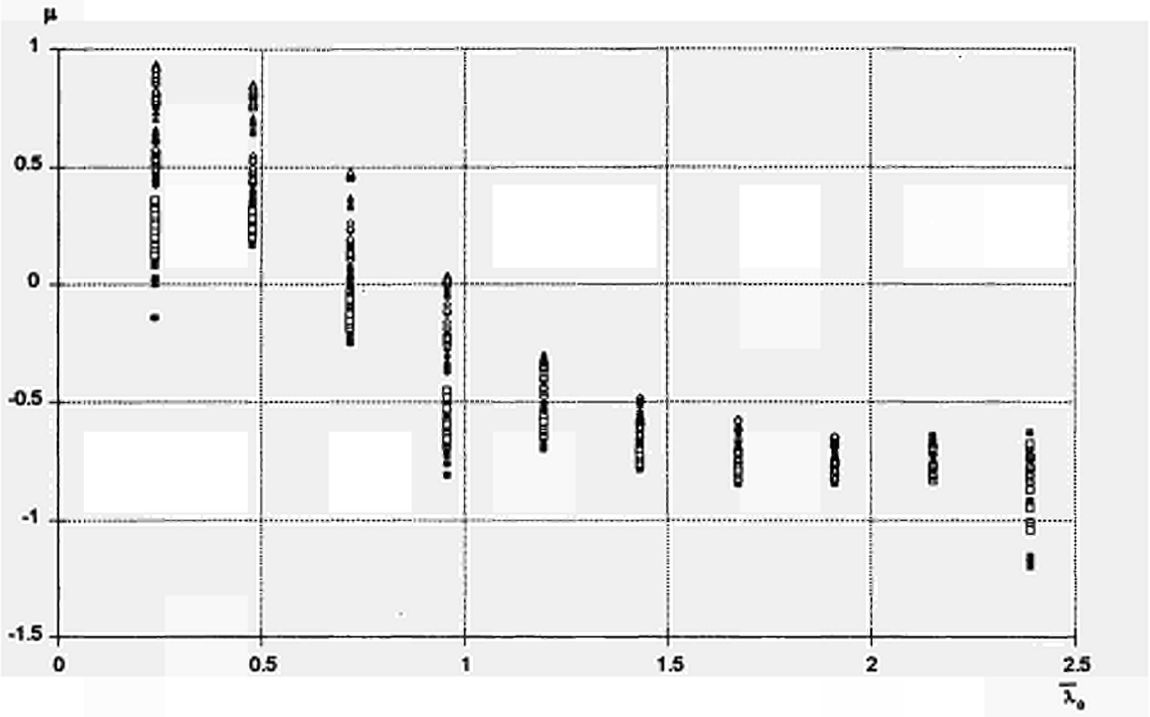

FIGURE 10.11 Evolution of μ according to the slenderness ratio (buckling about major axis - triangular moment)

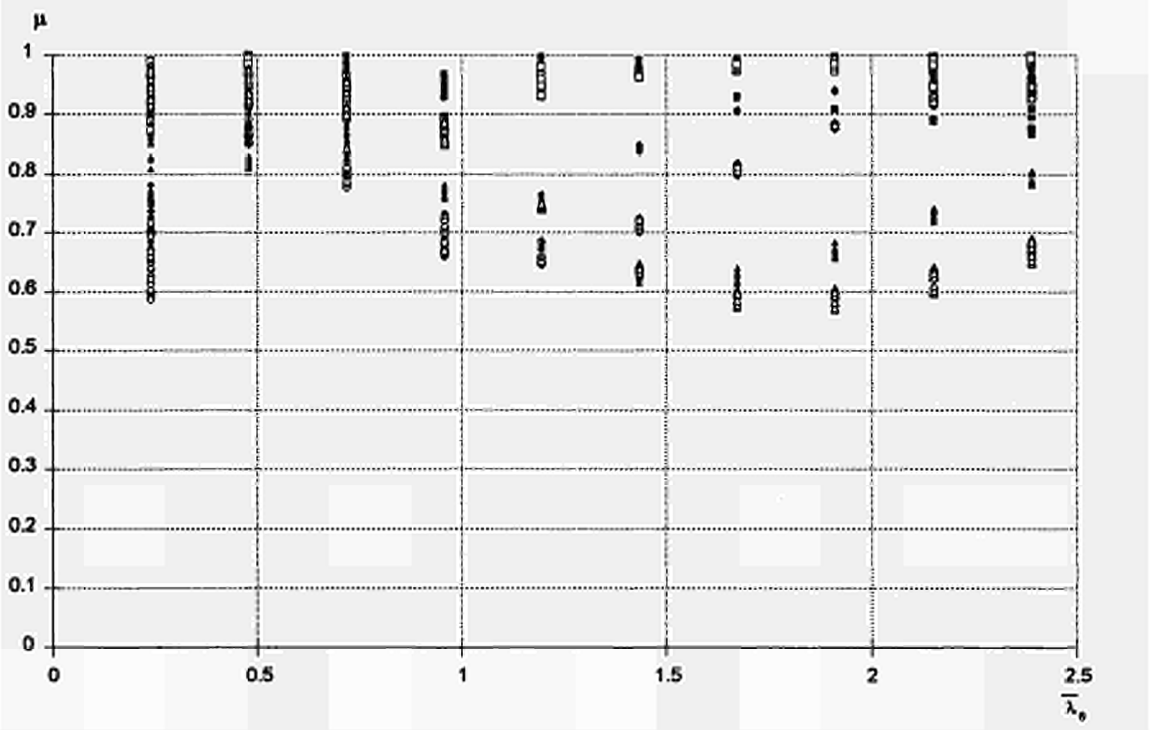

FIGURE 10.12 Evolution of μ according to the slenderness ratio (buckling about major axis - bi-triangular moment)

ANNEX 11:

11. COMPARISON BETWEEN THE NUMERICAL SIMULATION RESULTS AND THE M-N INTERACTION FORMULA (CHAPTER 4)

A comparison between all the results obtained numerically (from 400 to 900°C) and the analytical formulae (hereunder) is carried out in Annex 11.

$$\frac{N_{Sd}}{\chi(\theta)_{min}\, A\, f_{y,\theta}} + k_y \frac{M_{y,Sd}}{W_{pl,y}\, f_{y,\theta}} \leq 1$$

with:

$$k_y = 1 - \frac{\mu_y\, N_{Sd}}{\chi(\theta)_y\, A\, f_{y,\theta}} \qquad \text{but } k_y \leq 3$$

If buckling occurs about the minor axis:

$$\mu_y = \left(1.2\, \beta_{M,y} - 3\right) \bar{\lambda}_\theta + 0.71\, \beta_{M,y} - 0.29 \qquad \text{with } \mu_y \leq 0.8$$

If buckling occurs about the major axis:

$$\mu_y = \left(2\, \beta_{M,y} - 5\right) \bar{\lambda}_\theta + 0.44\, \beta_{M,y} + 0.29 \qquad \text{with } \mu_y \leq 0.8 \text{ and } \bar{\lambda}_{20} \leq 1.1$$

The value of standard $D_{numerical}$ = (calculated numerically, FIGURE 11.1) is shown on the x-axis (proposition_1), and the value of standard $D_{analytical}$ = (obtained from the above defined formula) is shown on the y-axis (LENAS). The 45° straight line represents a perfect equality between these two values. While the straight line which is slightly above represents an error of +10% of the analytical value as compared to the numerical value (therefore unconservative), the straight line which is slightly below the bisectrix represents, on the other hand, an error of -10% of the analytical value as compared to the numerical value (conservative).

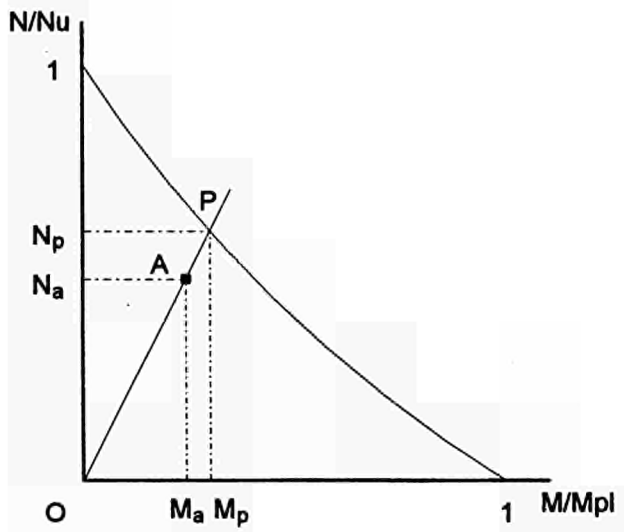

FIGURE 11.1 Calculation of $D_{numerical}$ and $D_{analytical}$

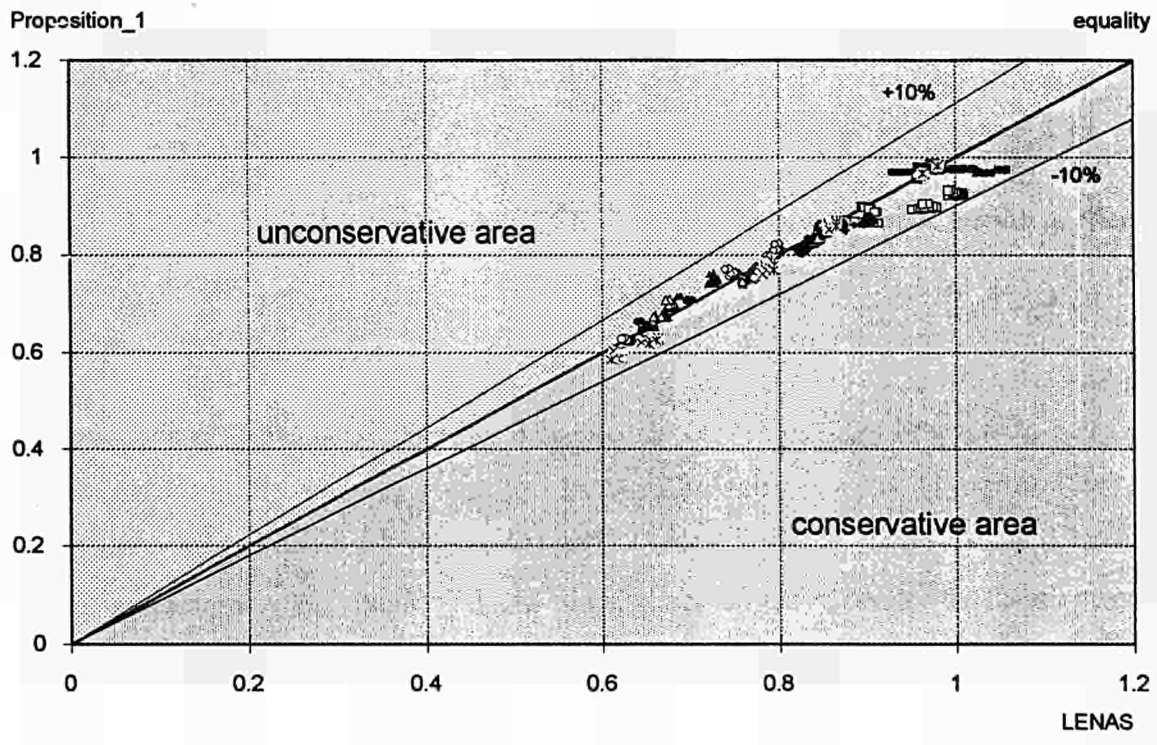

FIGURE 11.2 Formula - numerical results comparison at 400°C

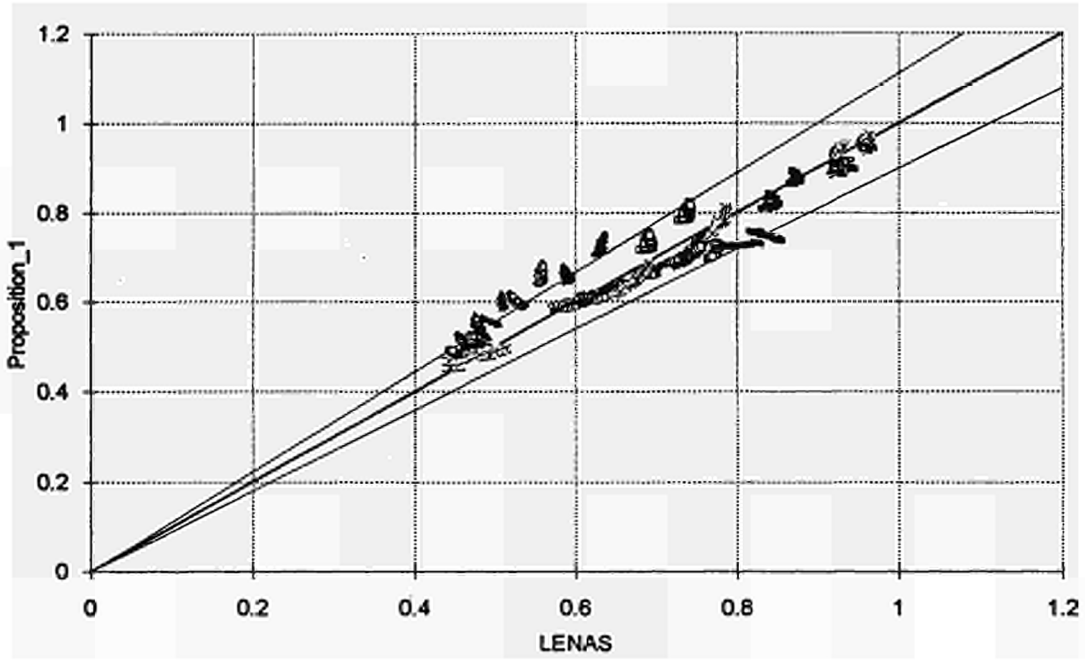

FIGURE 11.3 Formula - numerical results comparison at 400°C for buckling about minor axis and uniform moment distribution

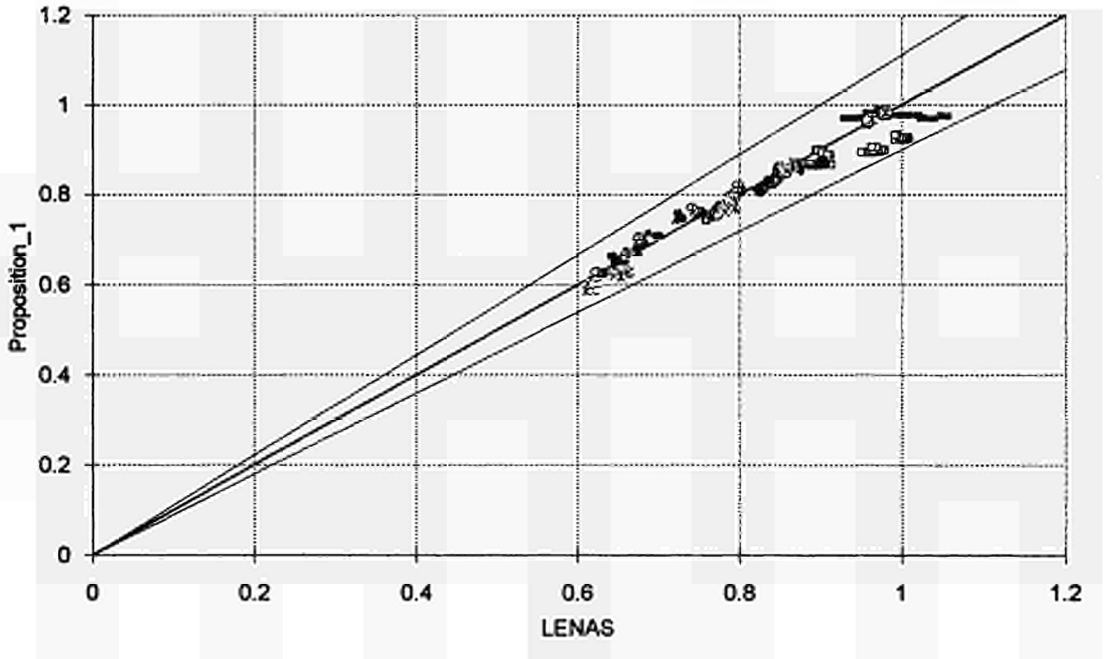

FIGURE 11.4 Formula - numerical results comparison at 400°C for buckling about minor axis and triangular moment distribution

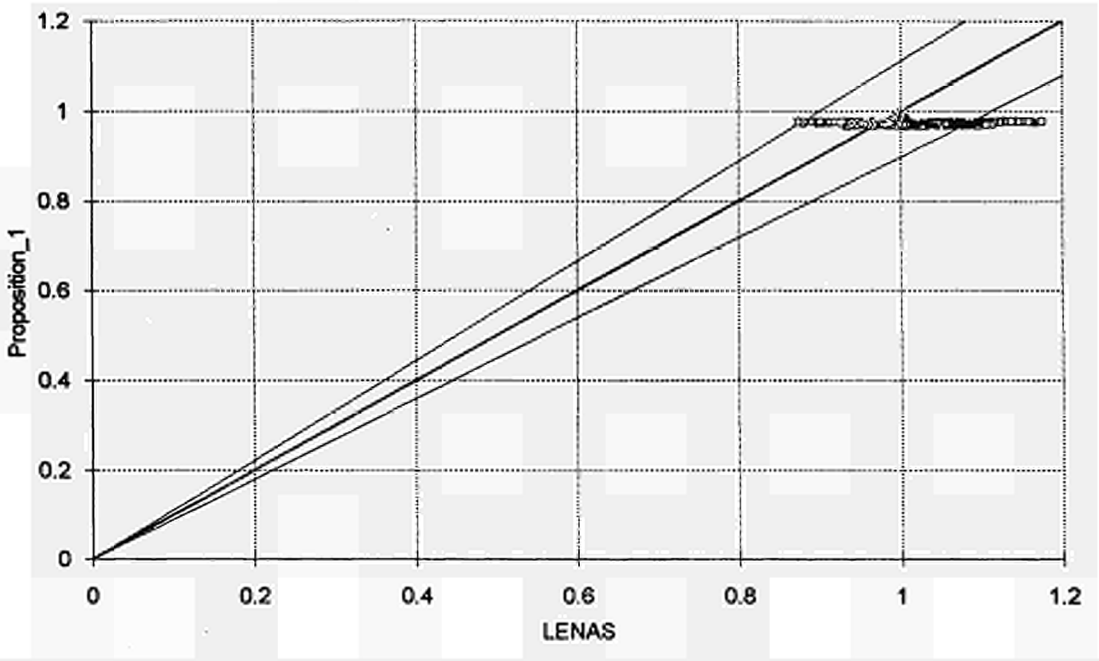

FIGURE 11.5 Formula - numerical results comparison at 400°C for buckling about minor axis and bi-triangular moment distribution

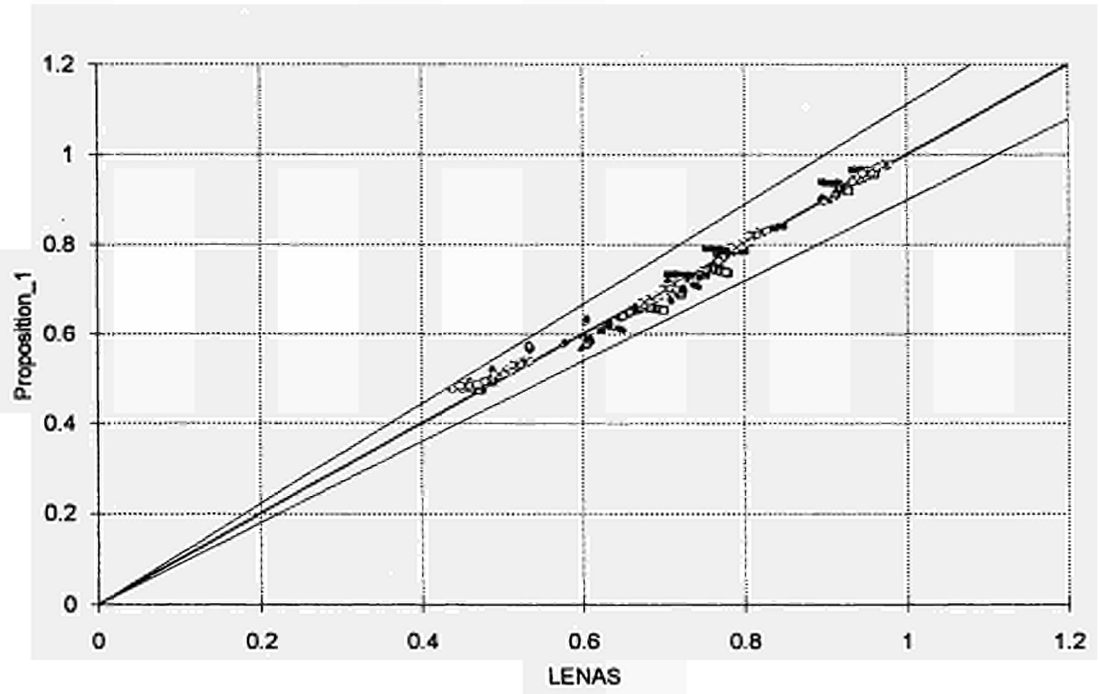

FIGURE 11.6 Formula - numerical results comparison at 400°C for buckling about major axis and uniform moment distribution

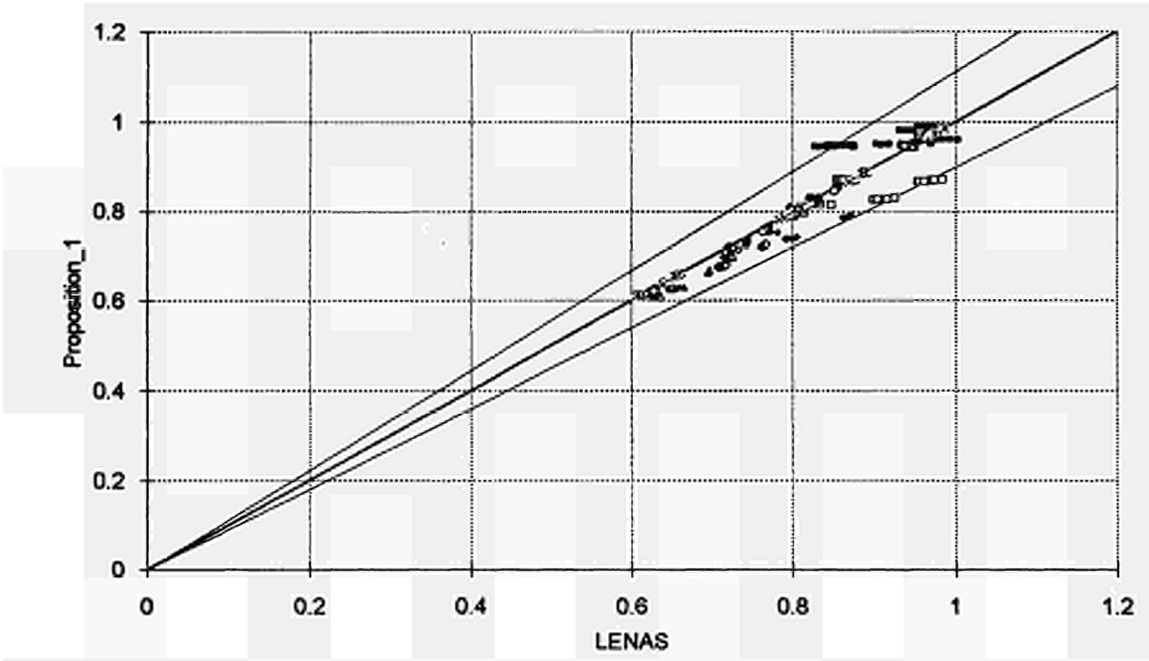

FIGURE 11.7 Formula - numerical results comparison at 400°C for buckling about major axis and triangular moment distribution

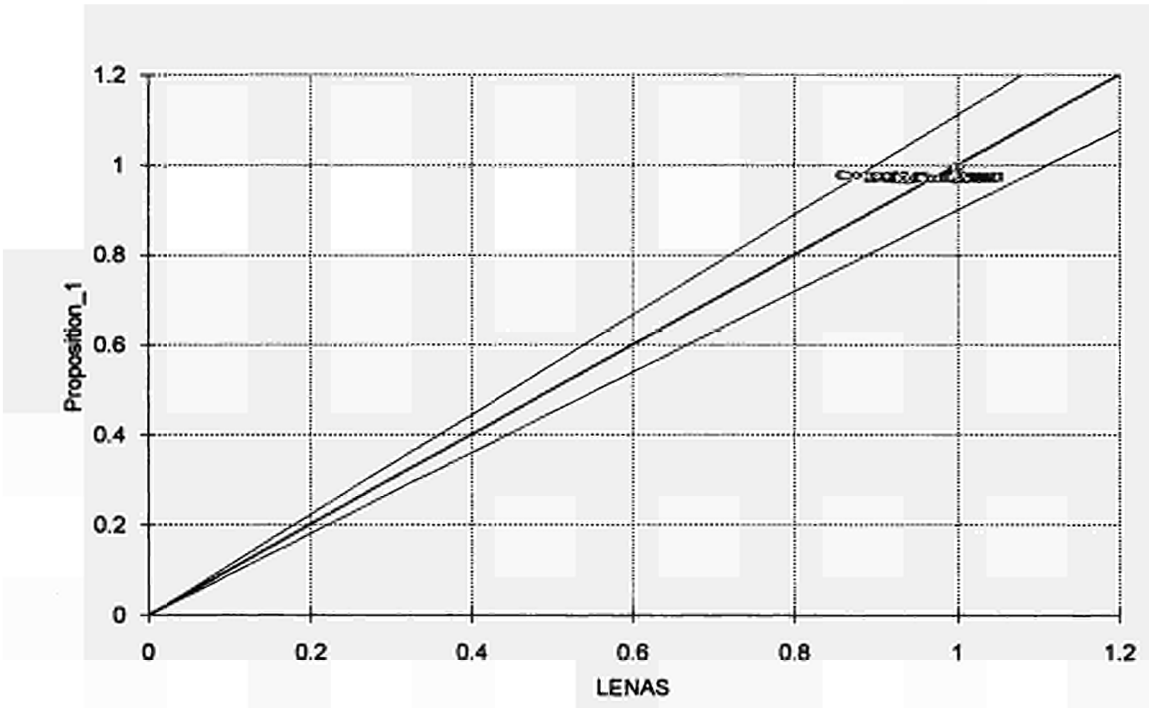

FIGURE 11.8 Formula - numerical results comparison at 400°C for buckling about major axis and bi-triangular moment distribution

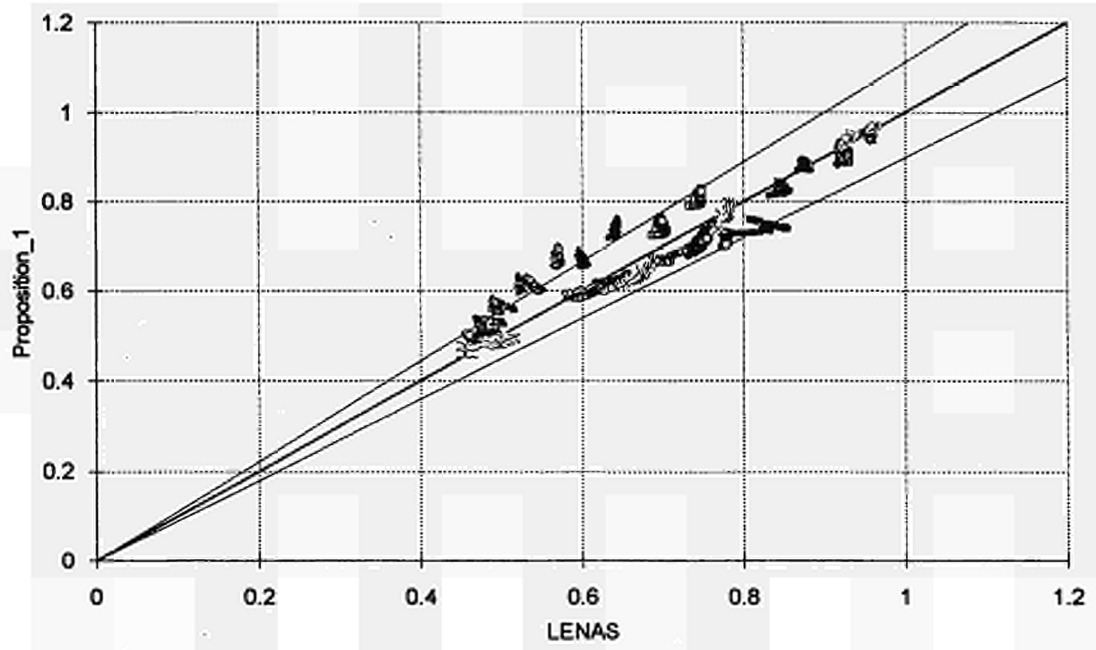

FIGURE 11.9 Formula - numerical results comparison at 500°C for buckling about minor axis and uniform moment distribution

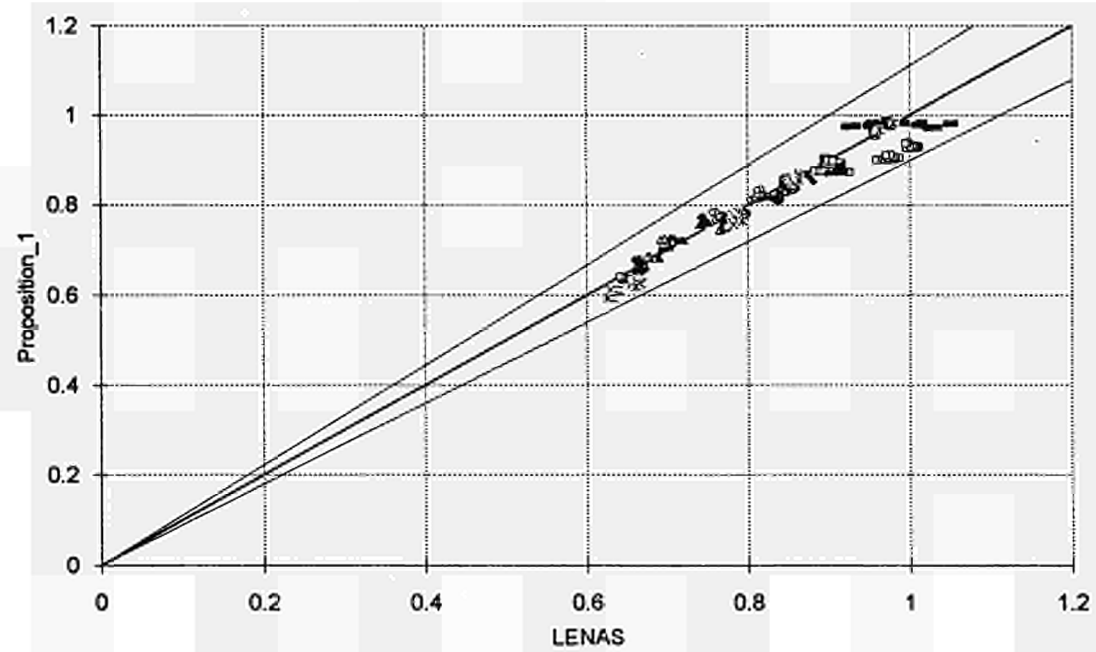

FIGURE 11.10 Formula - numerical results comparison at 500°C for buckling about minor axis and triangular moment distribution

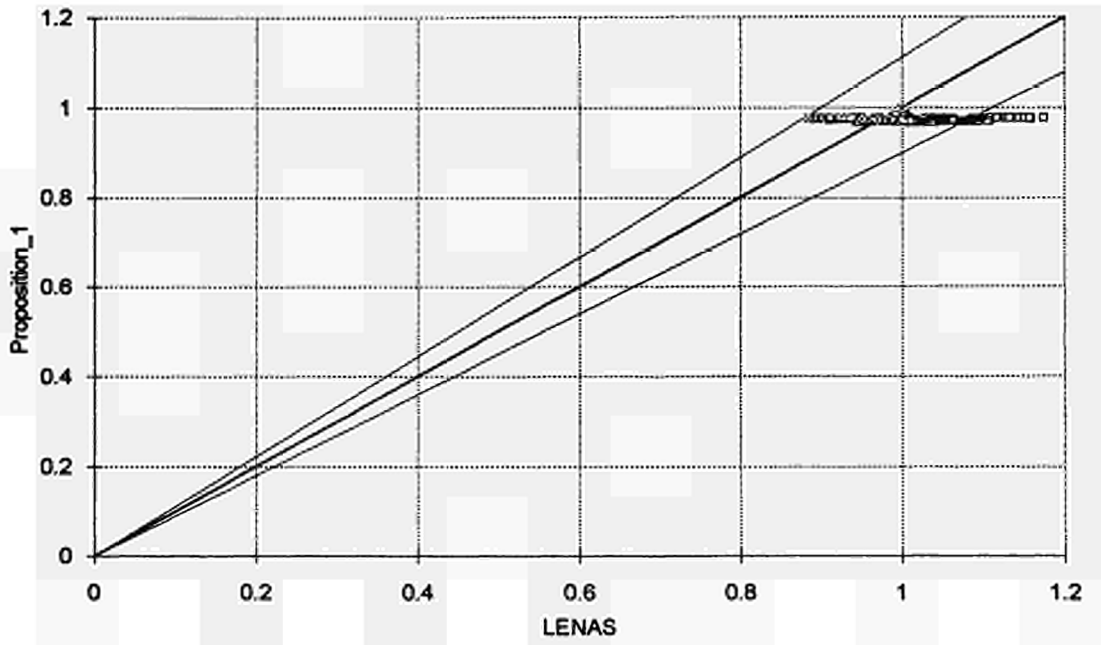

FIGURE 11.11 Formula - numerical results comparison at 500°C for buckling about minor axis and bi-triangular moment distribution

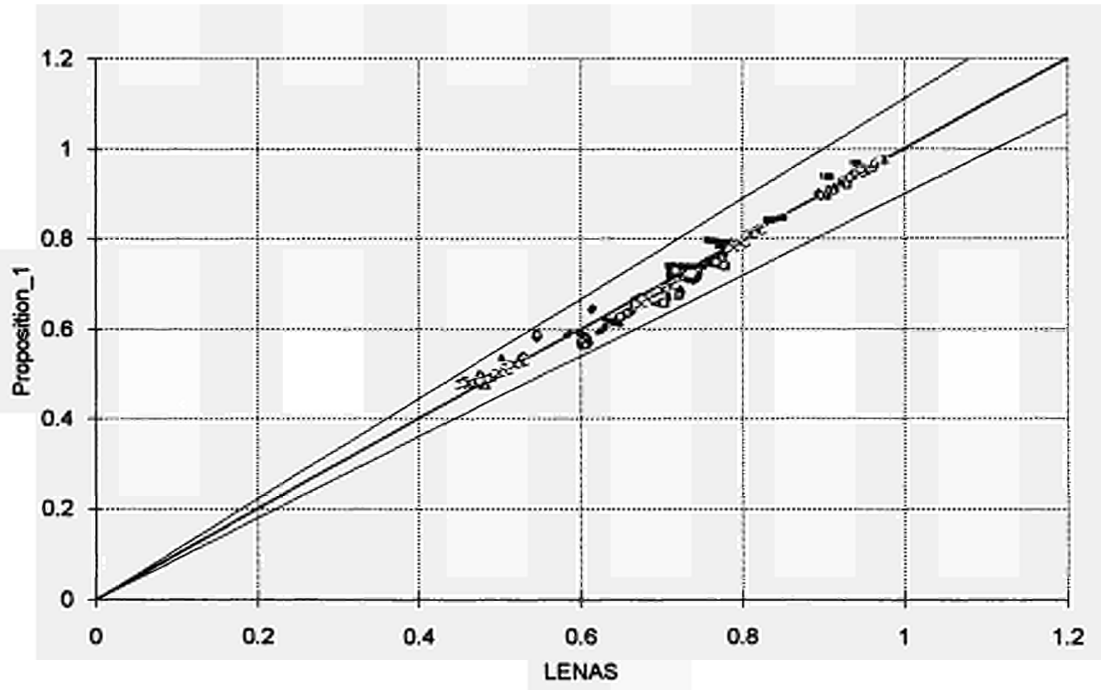

FIGURE 11.12 Formula - numerical results comparison at 500°C for buckling about major axis and uniform moment distribution

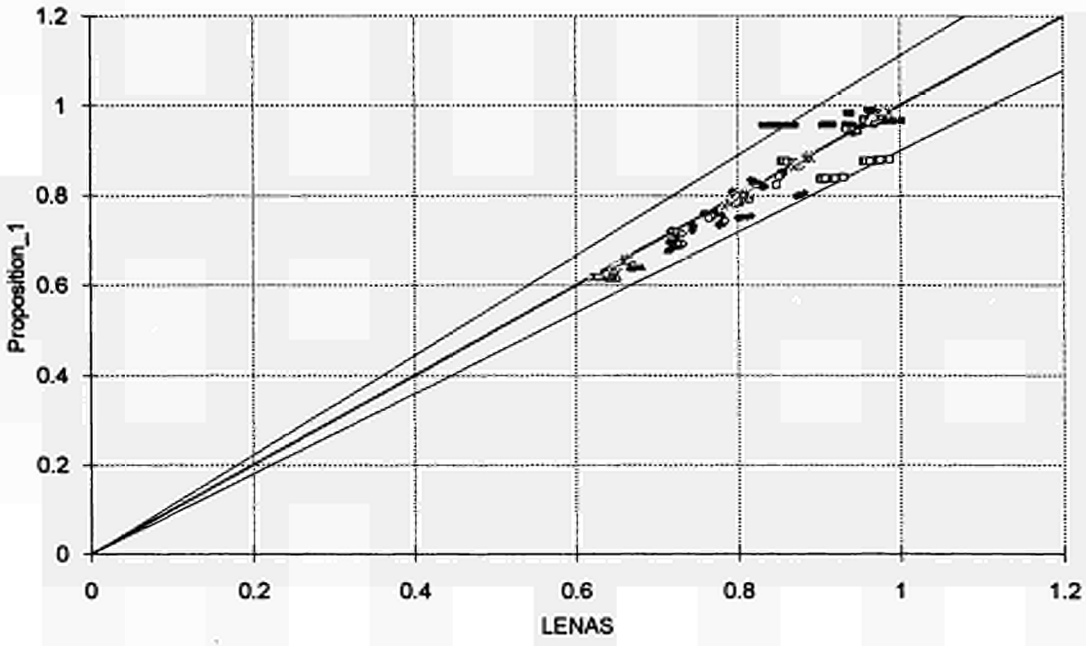

FIGURE 11.13 Formula - numerical results comparison at 500°C for buckling about major axis and triangular moment distribution

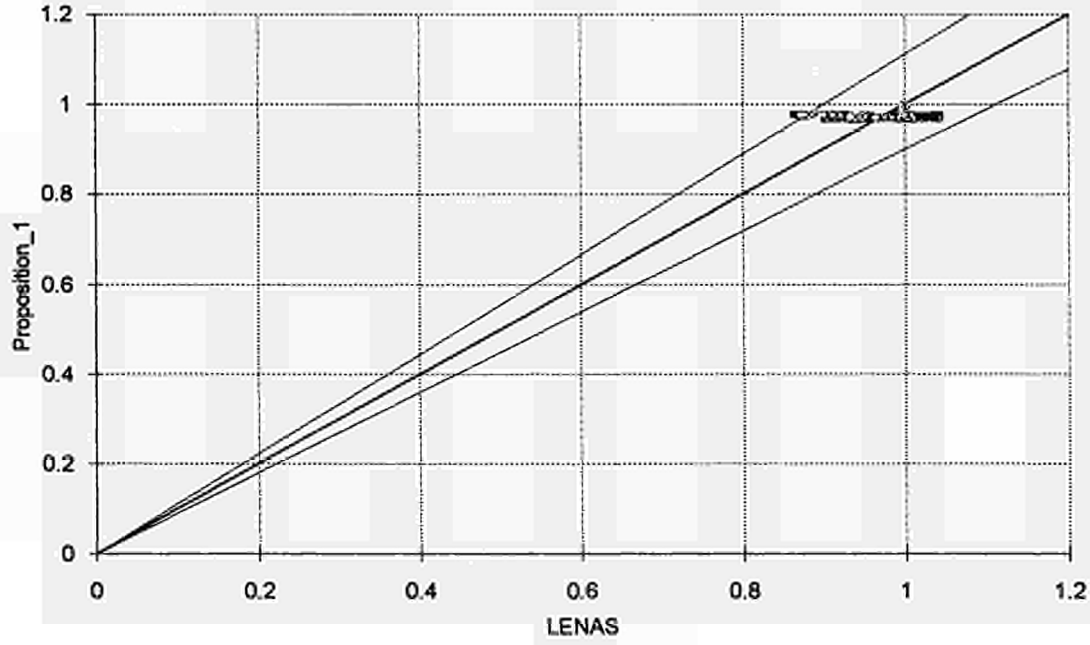

FIGURE 11.14 Formula - numerical results comparison at 500°C for buckling about major axis and bi-triangular moment distribution

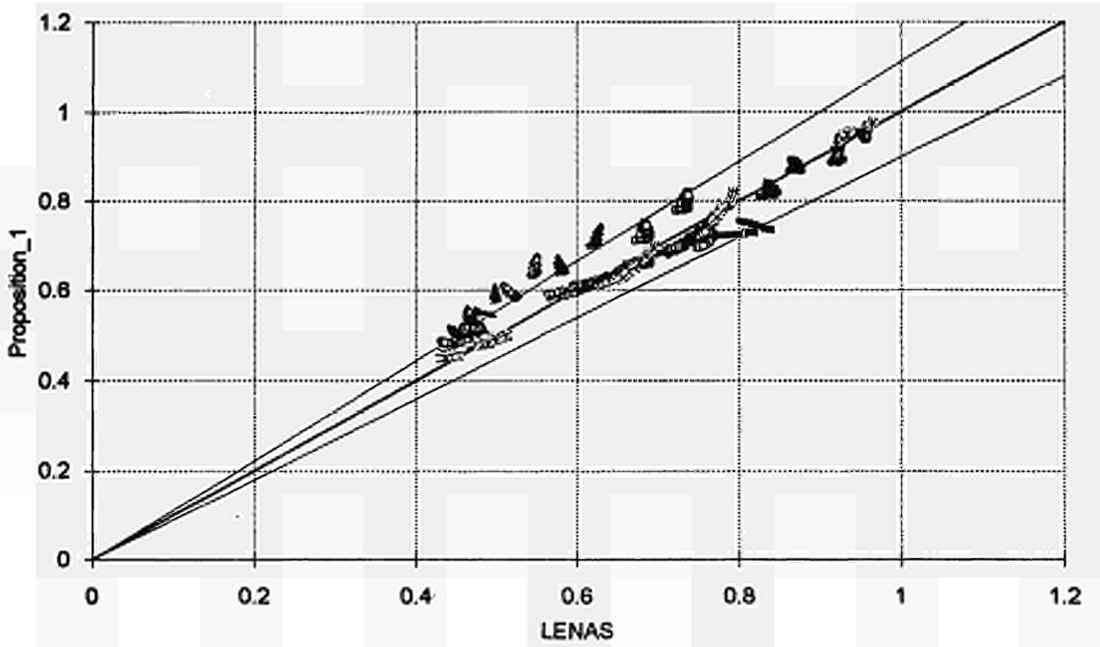

FIGURE 11.15 Formula - numerical results comparison at 600°C for buckling about minor axis and uniform moment distribution

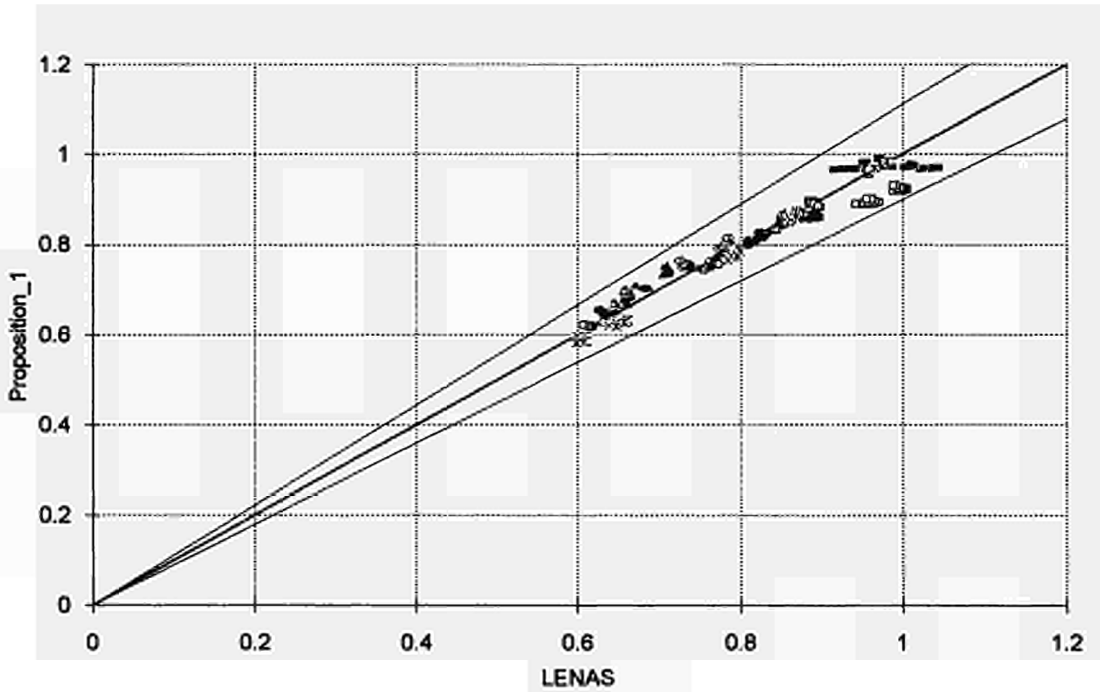

FIGURE 11.16 Formula - numerical results comparison at 600°C for buckling about minor axis and triangular moment distribution

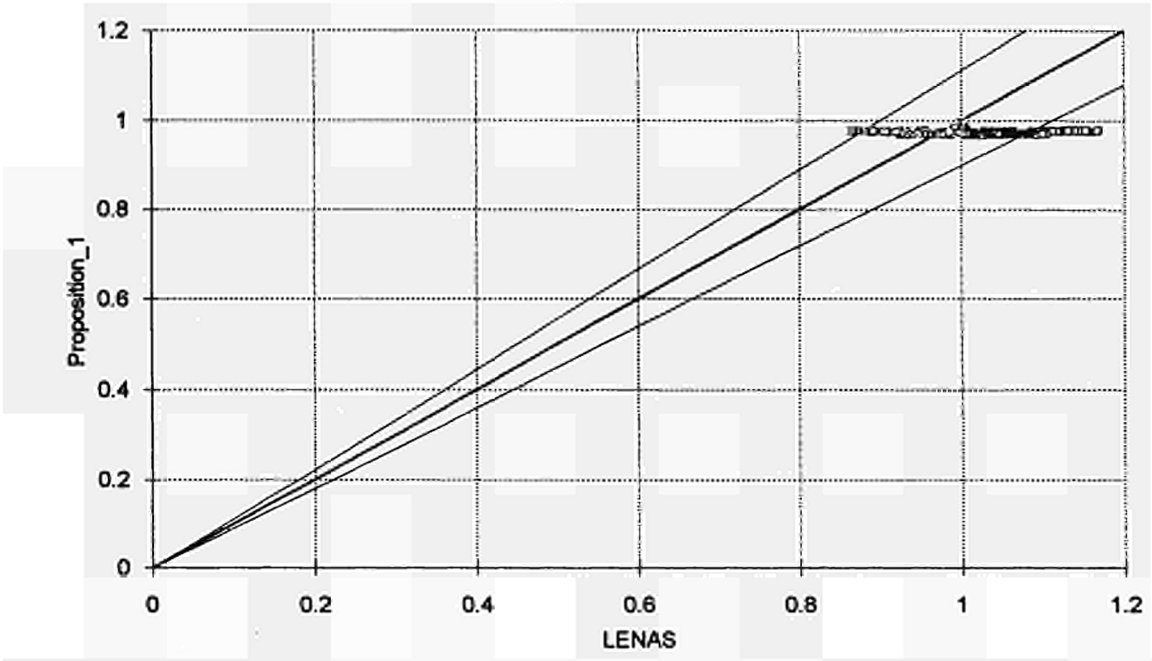

FIGURE 11.17 Formula - numerical results comparison at 600°C for buckling about minor axis and bi-triangular moment distribution

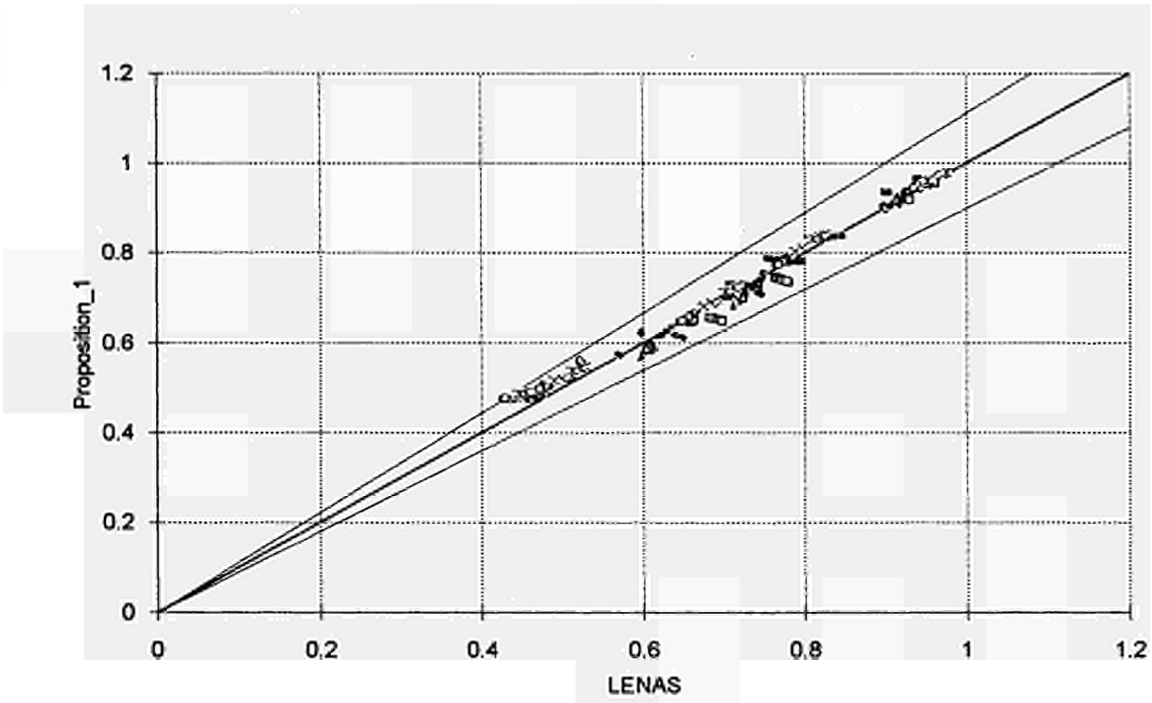

FIGURE 11.18 Formula - numerical results comparison at 600°C for buckling about major axis and uniform moment distribution

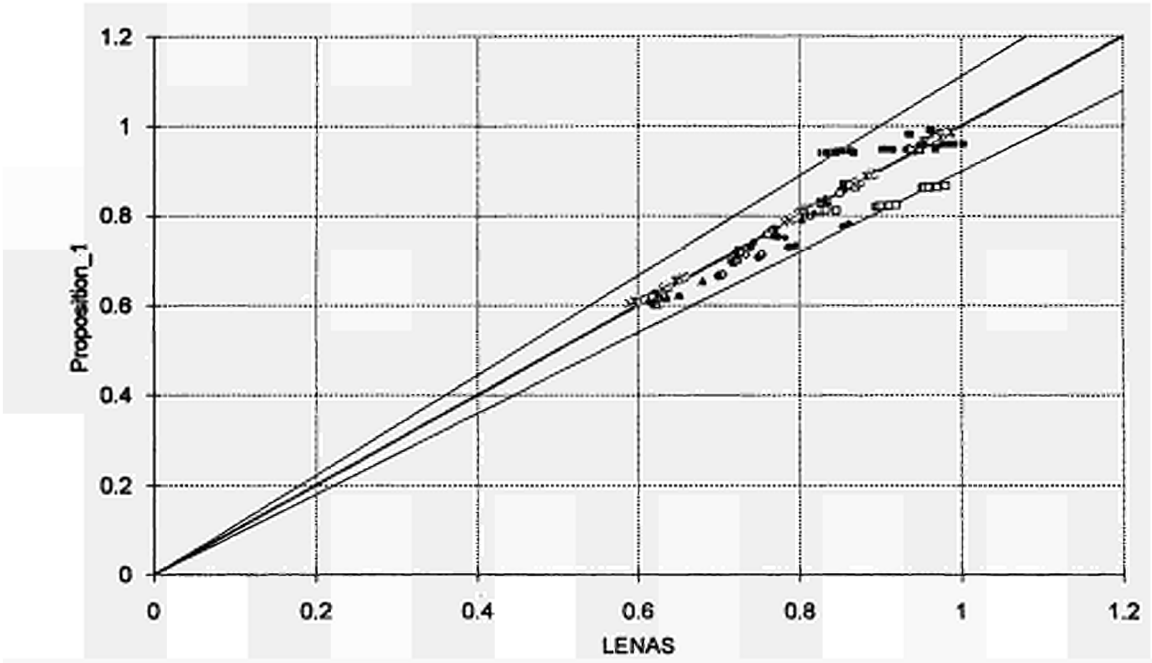

FIGURE 11.19 Formula - numerical results comparison at 600°C for buckling about major axis and triangular moment distribution

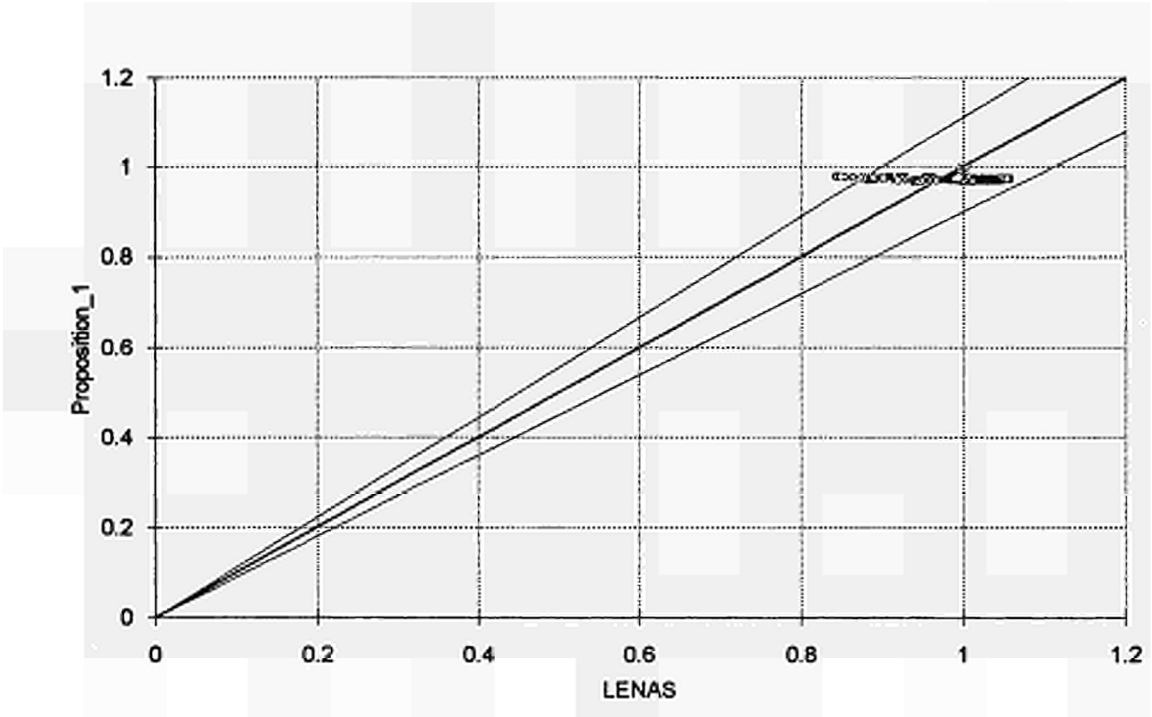

FIGURE 11.20 Formula - numerical results comparison at 600°C for buckling about major axis and bi-triangular moment distribution

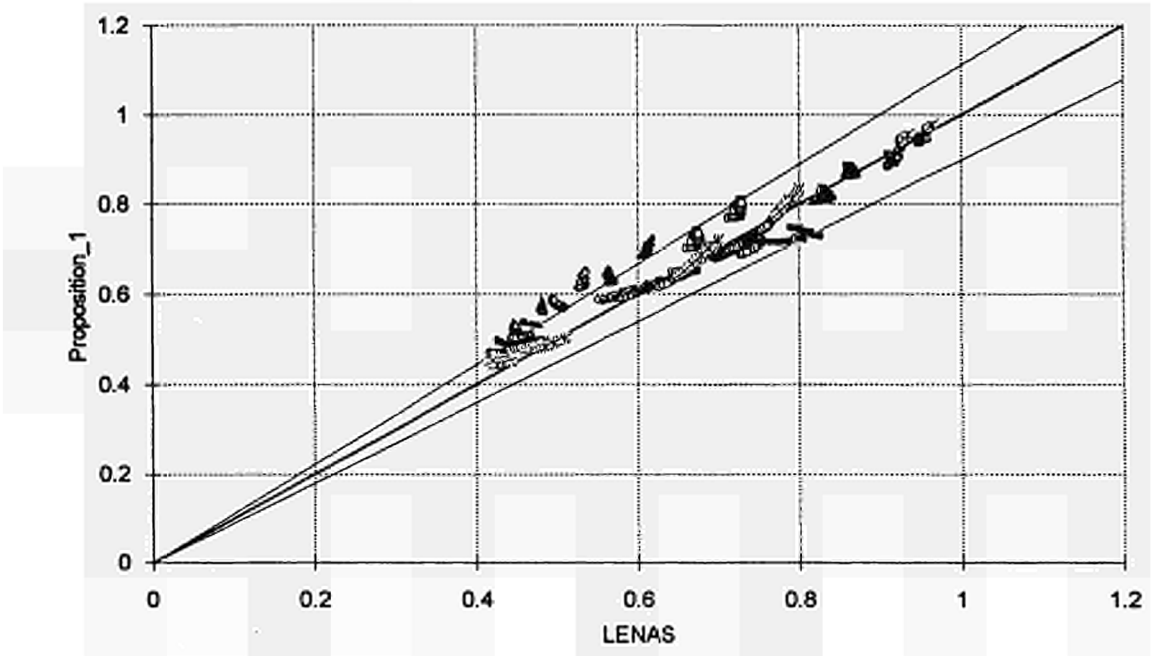

FIGURE 11.21 Formula - numerical results comparison at 700°C for buckling about minor axis and uniform moment distribution

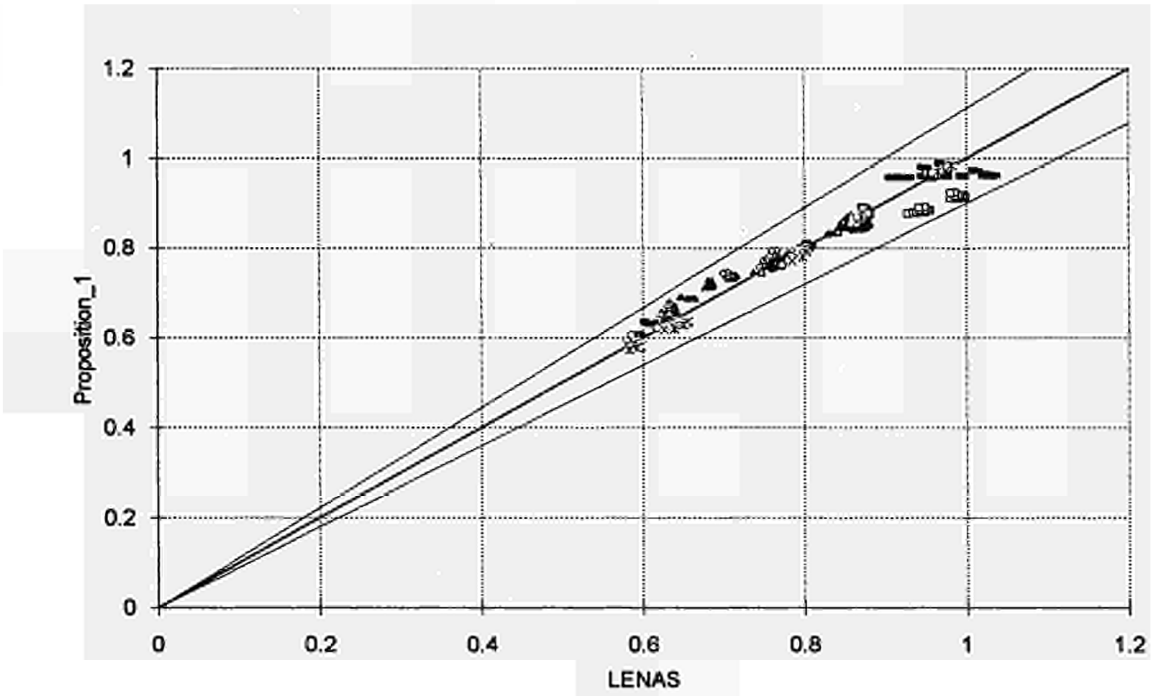

FIGURE 11.22 Formula - numerical results comparison at 700°C for buckling about minor axis and triangular moment distribution

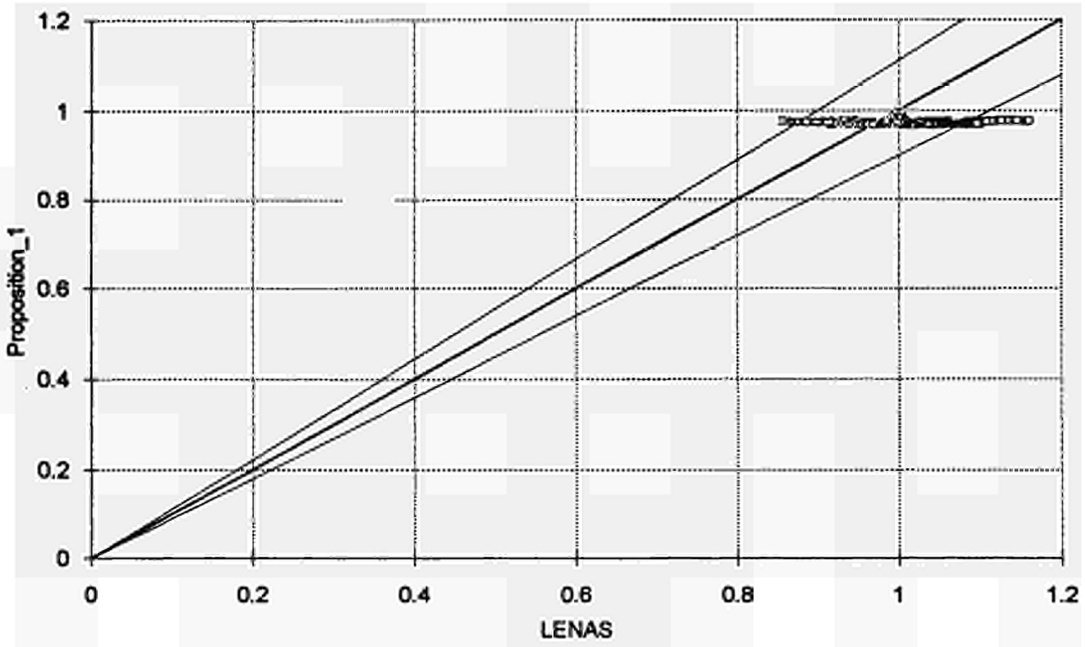

FIGURE 11.23 Formula - numerical results comparison at 700°C for buckling about minor axis and bi-triangular moment distribution

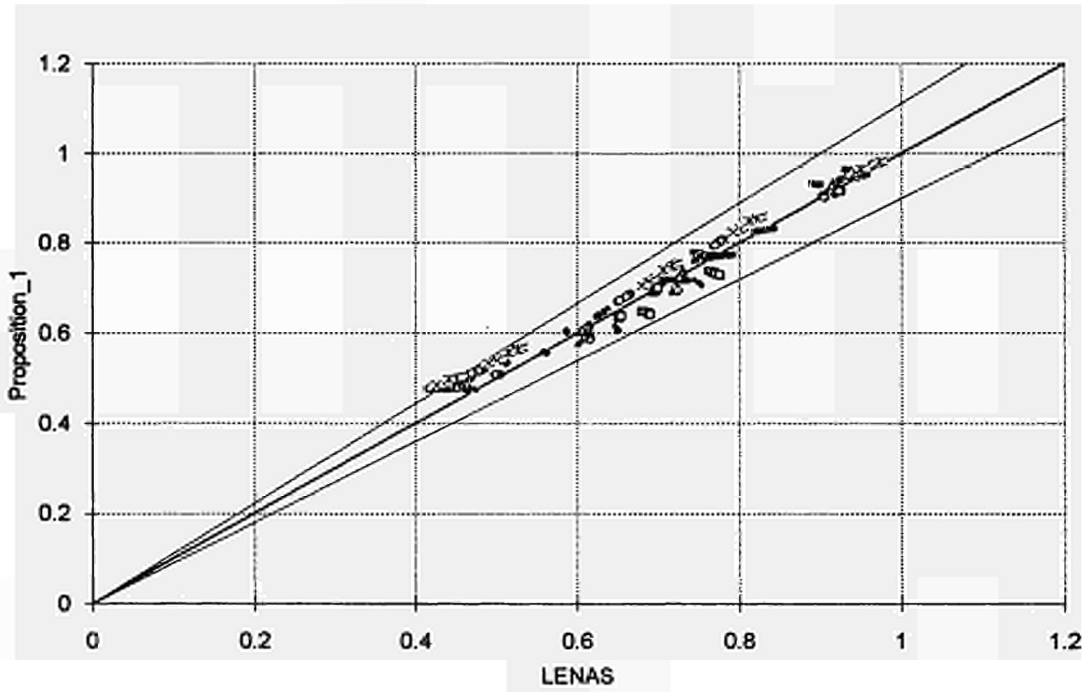

FIGURE 11.24 Formula - numerical results comparison at 700°C for buckling about major axis and uniform moment distribution

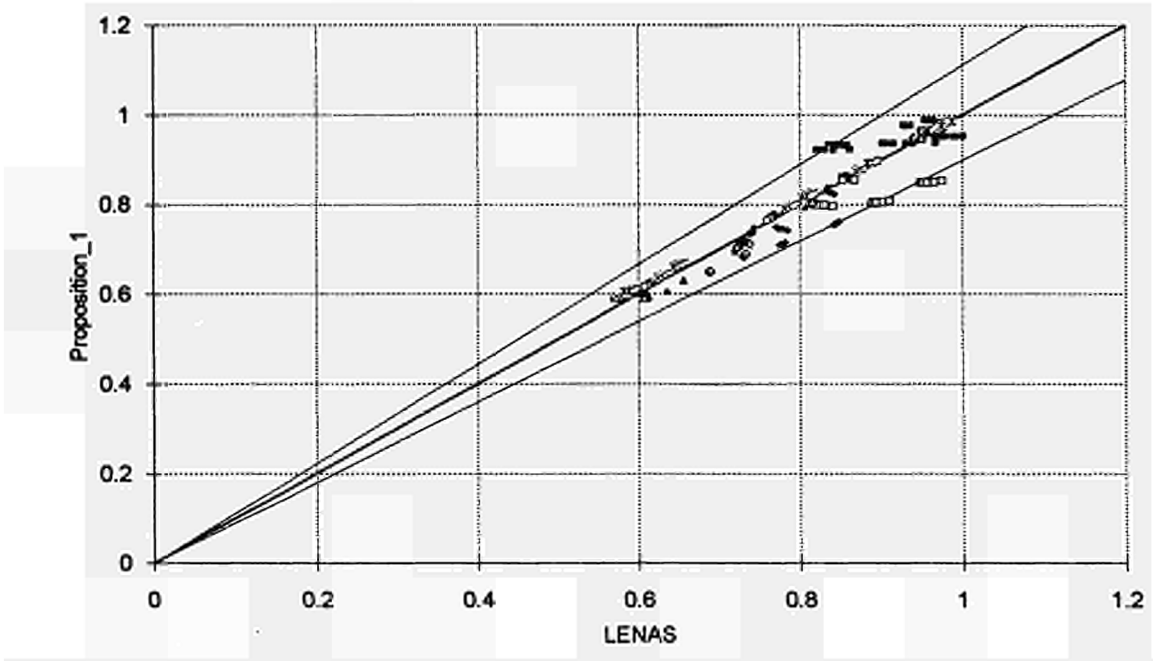

FIGURE 11.25 Formula - numerical results comparison at 700°C for buckling about major axis and triangular moment distribution

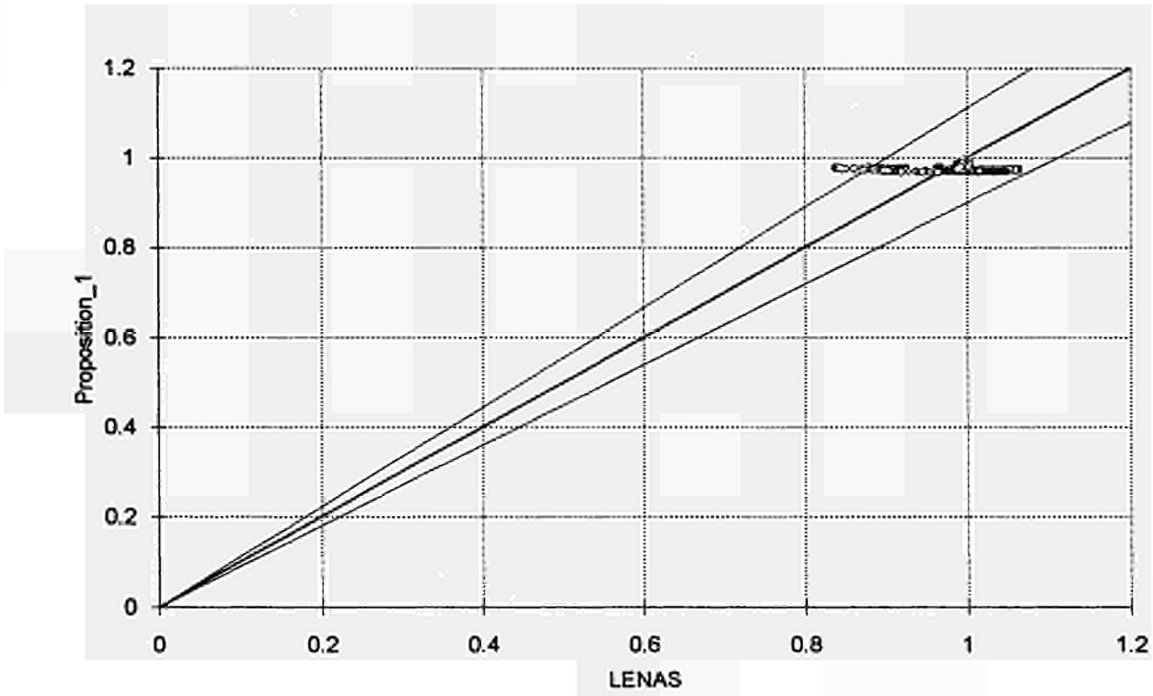

FIGURE 11.26 Formula - numerical results comparison at 700°C for buckling about major axis and bi-triangular moment distribution

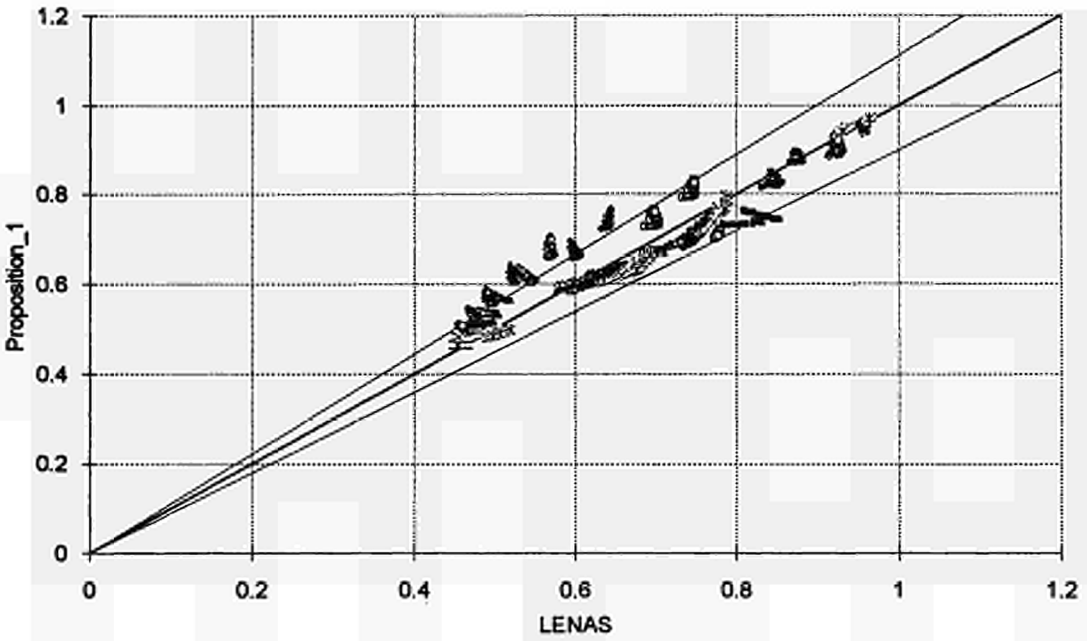

FIGURE 11.27 Formula - numerical results comparison at 800°C for buckling about minor axis and uniform moment distribution

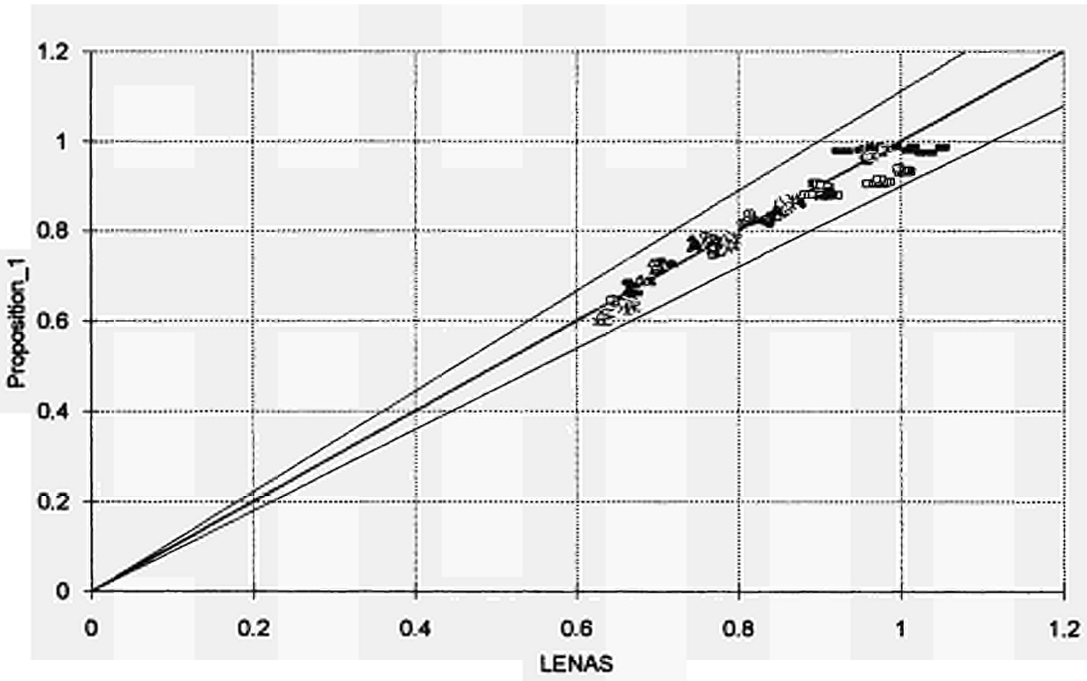

FIGURE 11.28 Formula - numerical results comparison at 800°C for buckling about minor axis and triangular moment distribution

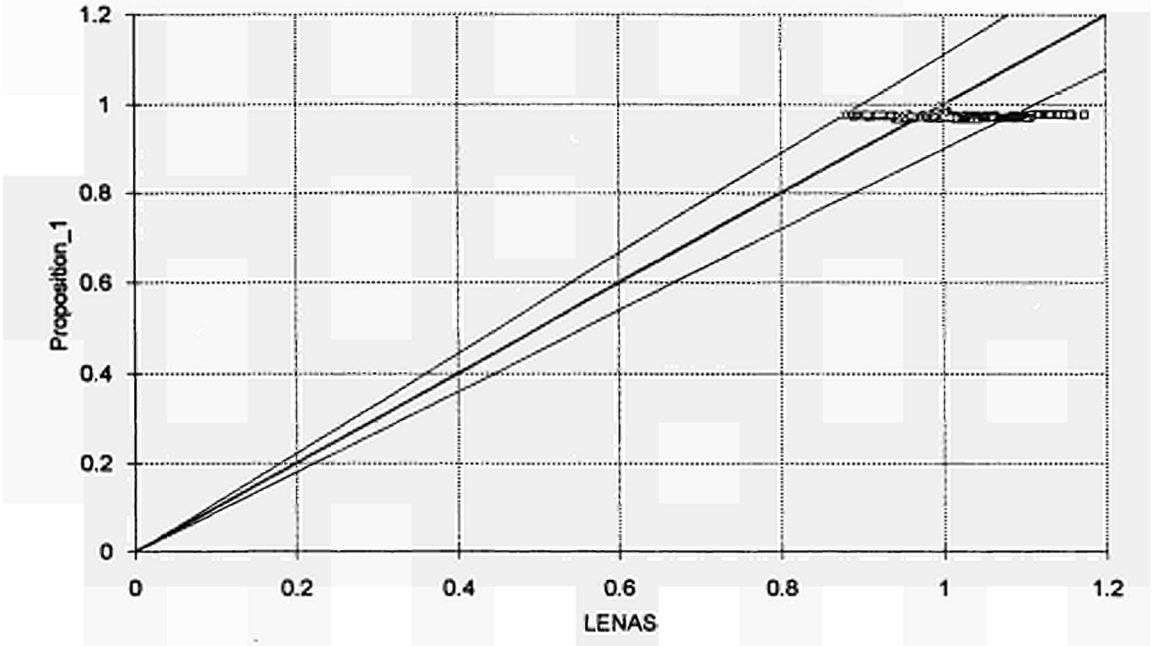

FIGURE 11.29 Formula - numerical results comparison at 800°C for buckling about minor axis and bi-triangular moment distribution

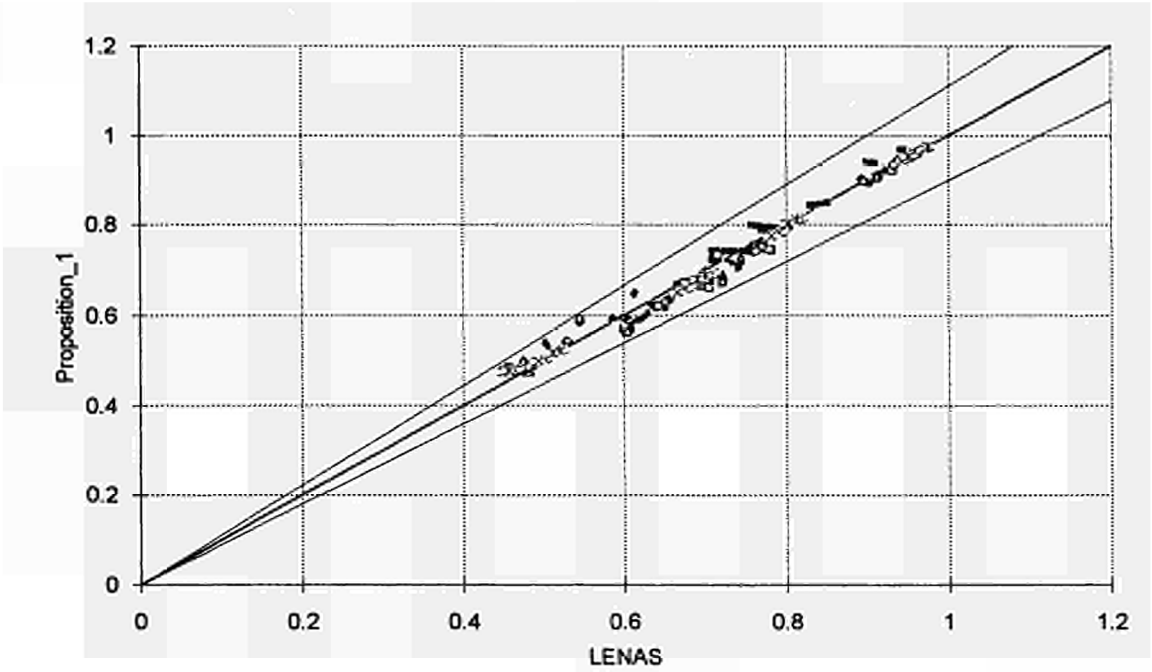

FIGURE 11.30 Formula - numerical results comparison at 800°C for buckling about major axis and uniform moment distribution

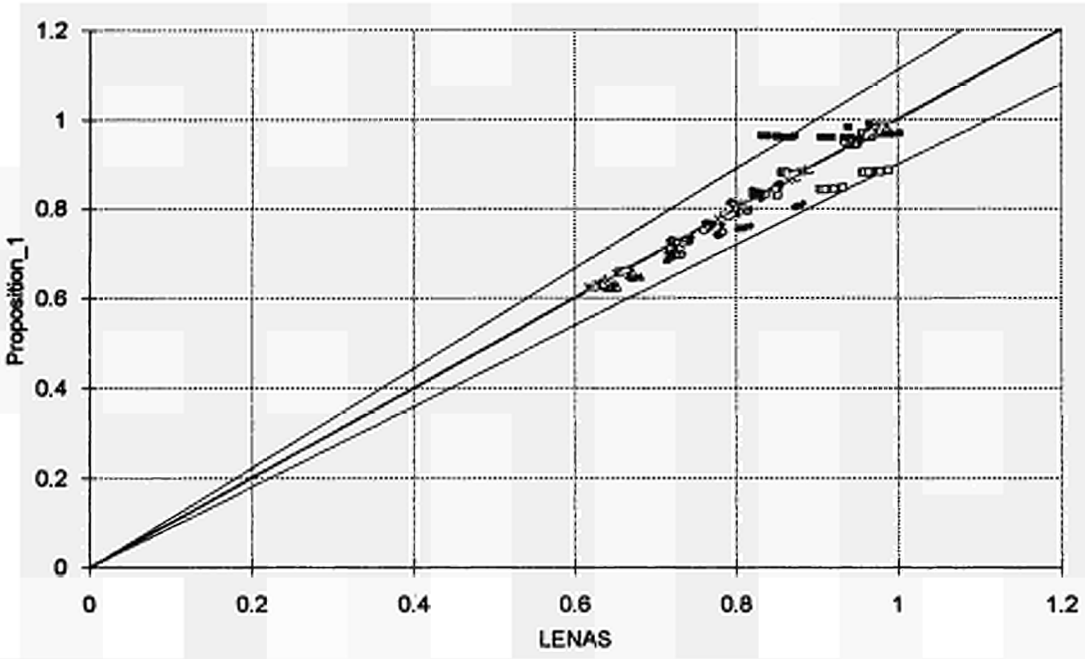

FIGURE 11.31 Formula - numerical results comparison at 800°C for buckling about major axis and triangular moment distribution

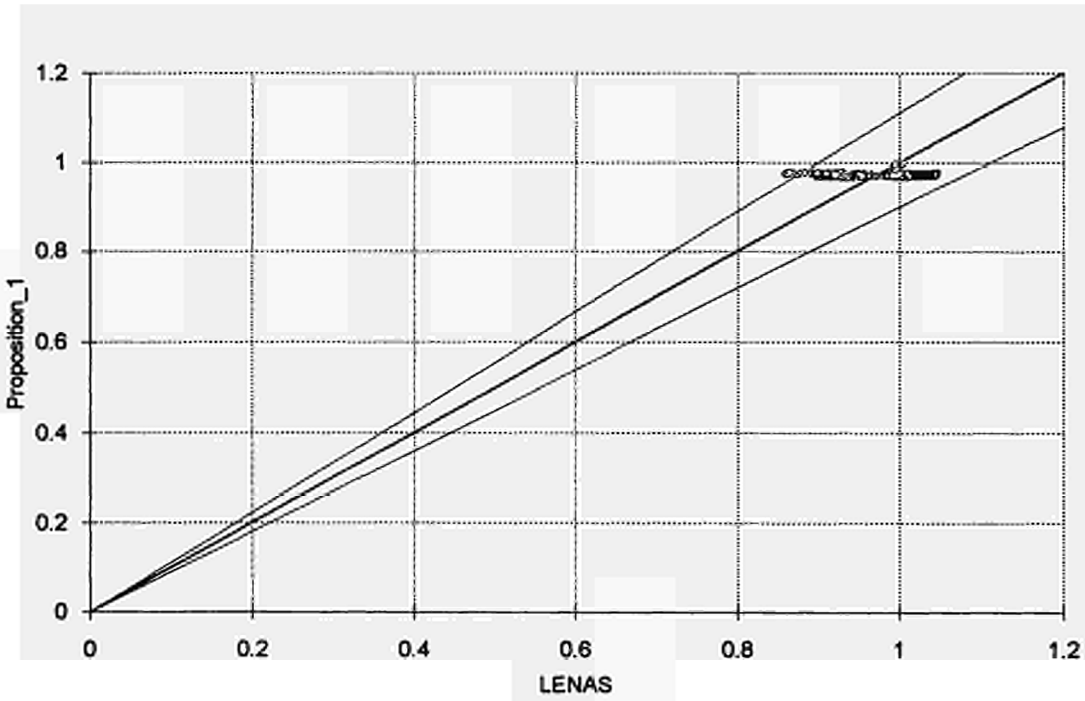

FIGURE 11.32 Formula - numerical results comparison at 800°C for buckling about major axis and bi-triangular moment distribution

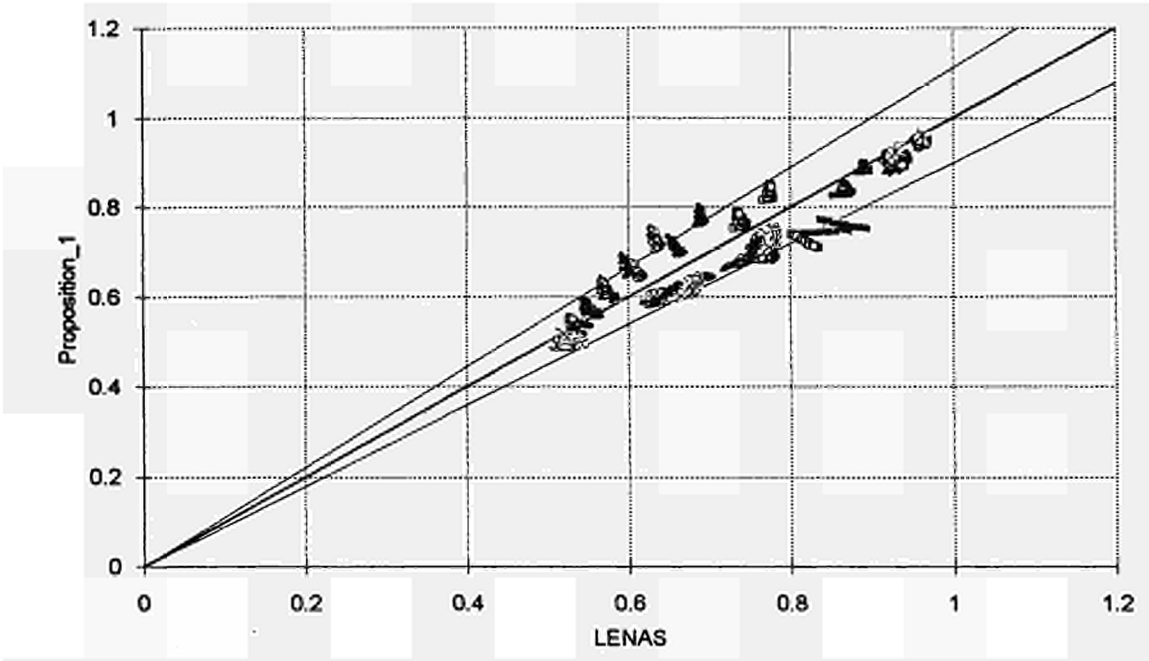

FIGURE 11.33 Formula - numerical results comparison at 900°C for buckling about minor axis and uniform moment distribution

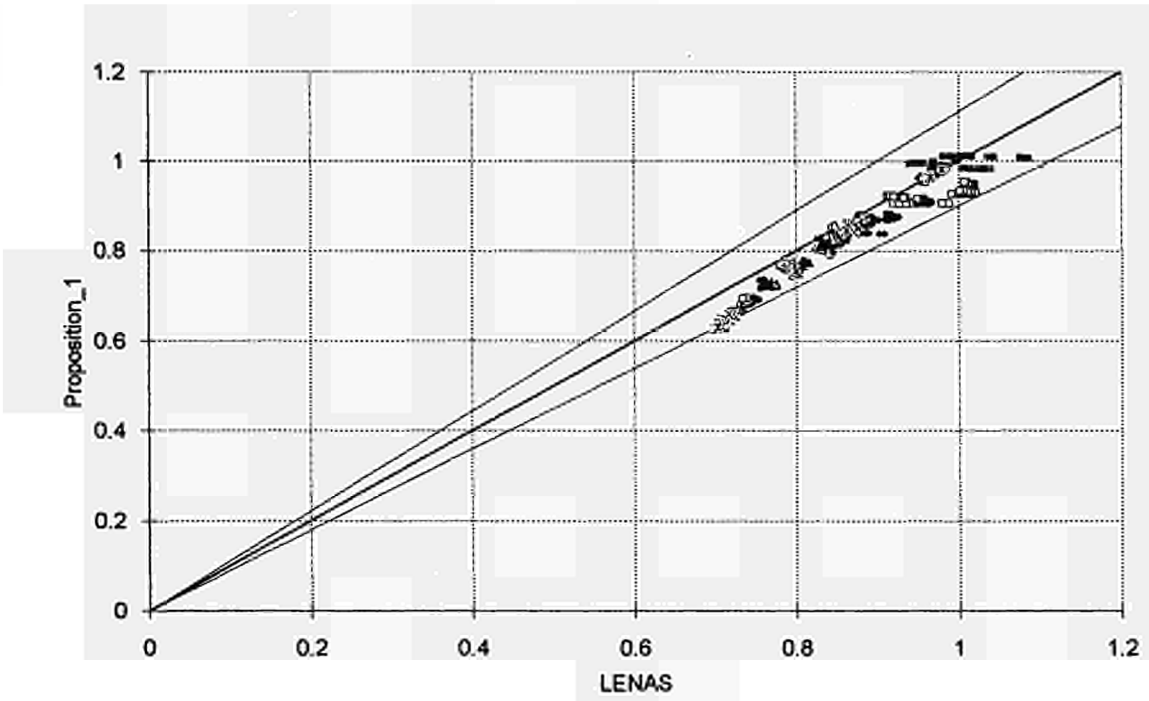

FIGURE 11.34 Formula - numerical results comparison at 900°C for buckling about minor axis and triangular moment distribution

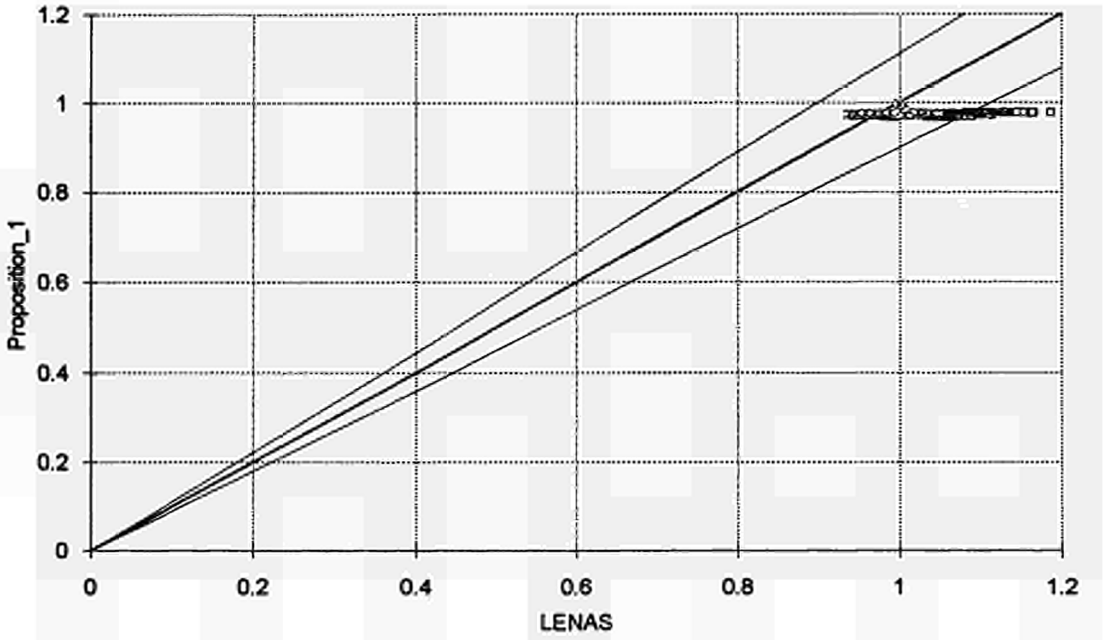

FIGURE 11.35 Formula - numerical results comparison at 900°C for buckling about minor axis and bi-triangular moment distribution

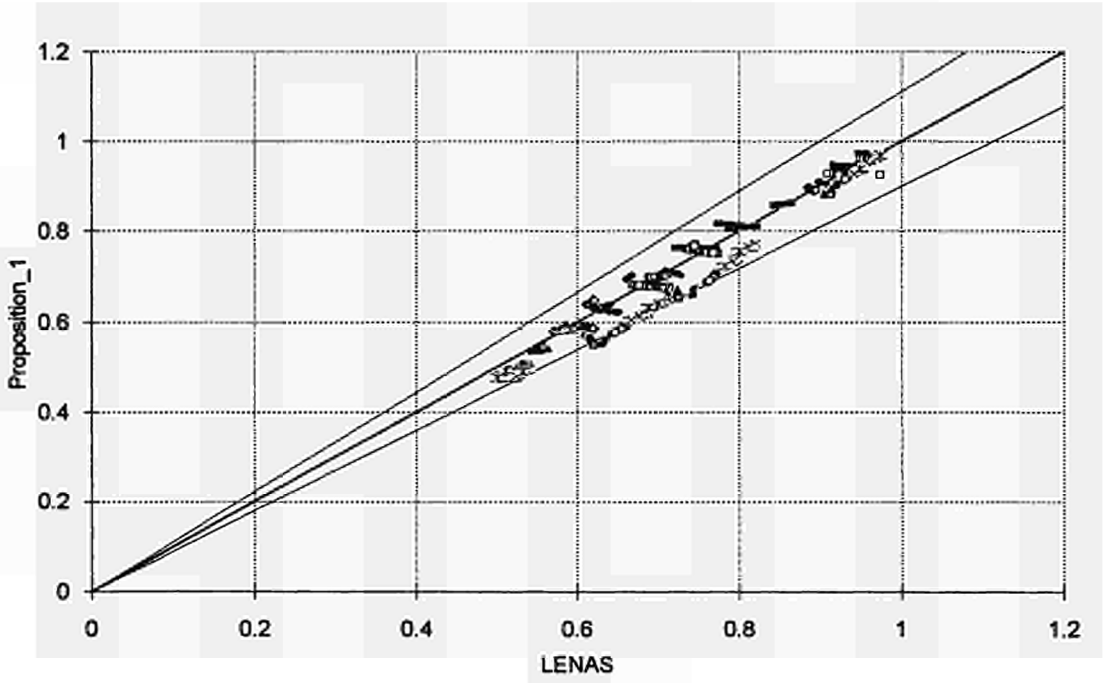

FIGURE 11.36 Formula - numerical results comparison at 900°C for buckling about major axis and uniform moment distribution

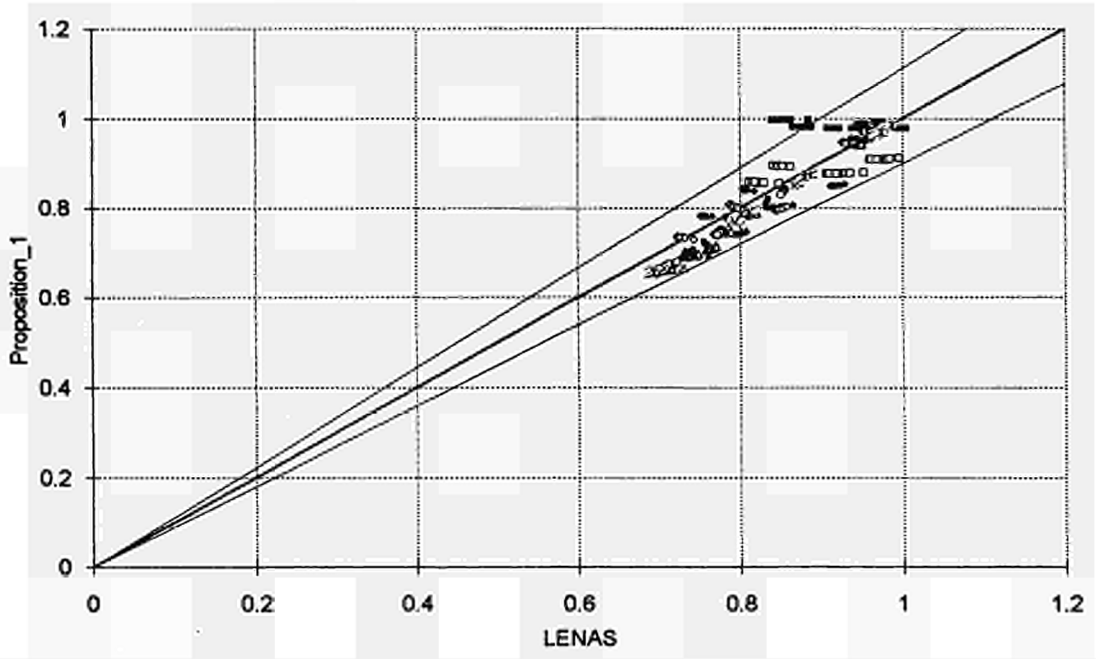

FIGURE 11.37 Formula - numerical results comparison at 900°C for buckling about major axis and triangular moment distribution

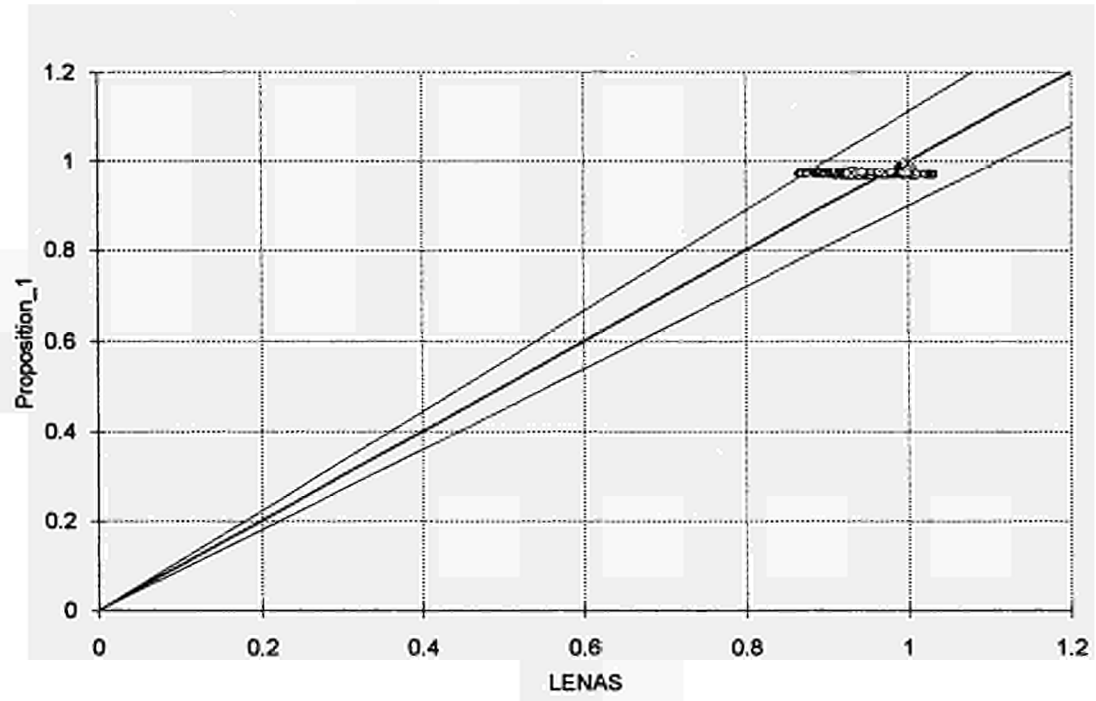

FIGURE 11.38 Formula - numerical results comparison at 900°C for buckling about major axis and bi-triangular moment distribution

ANNEX 12:

12. ANOTHER FORMULA FOR THE M-N INTERACTION

The M-N interaction law may also be written differently from the formulation of Eurocode 3 Part 1.2. This formulation is of the following type :

$$\left(\frac{N_{Sd}}{\chi_{min}\ A\ f_{y,\theta}}\right)^{\alpha} + \frac{M_{y,Sd}}{W_{pl,y}\ f_{y,\theta}} \leq 1 \qquad (12.1)$$

12.1 ANALYSIS ACCORDING TO α

The sensitiveness of this type of curves to a variation of α may be determined by drawing various curves (FIGURE 12.1) for α = 0.1, 0.2, 0.5, 1, 2, 4, 8, and 10.

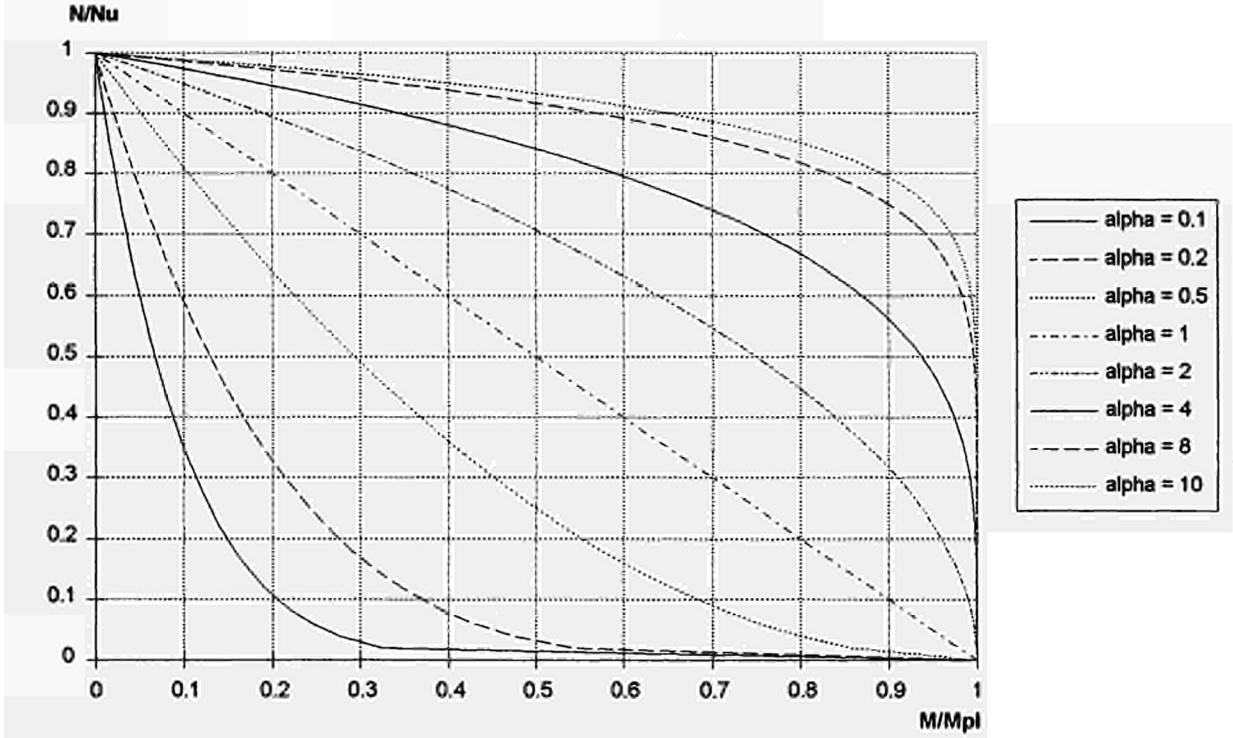

FIGURE 12.1 Evolution of the M-N interaction curve according to α

It can be noted that, for low values of α (from 0.1 to 0.2), the variation of the interaction curve is very large, while for a variation of α from 8 to 10, the difference between the curves is low.

12.2 FORMULA FOR EACH LOAD CASE

By solving equation 12.1, by dichotomy, α can be determined for all the points which were numerically calculated.

As previously, the values calculated for large eccentricities are conspicuous as compared to the other values (FIGURE 12.2), and they will therefore be neglected once more. For a low slenderness ratio and a uniform or triangular moment distribution, the dispersion of the points is greater than for large slenderness ratios. This phenomenon is not disturbing since, as we observed in section 12.1., the influence of α on the shape of the curve becomes lower and lower as α increases. Now, for low slenderness ratios, α varies between 1 and 2 for buckling about the minor axis and uniform moment distribution (and between 2 and 4.5 if the moment distribution is triangular).

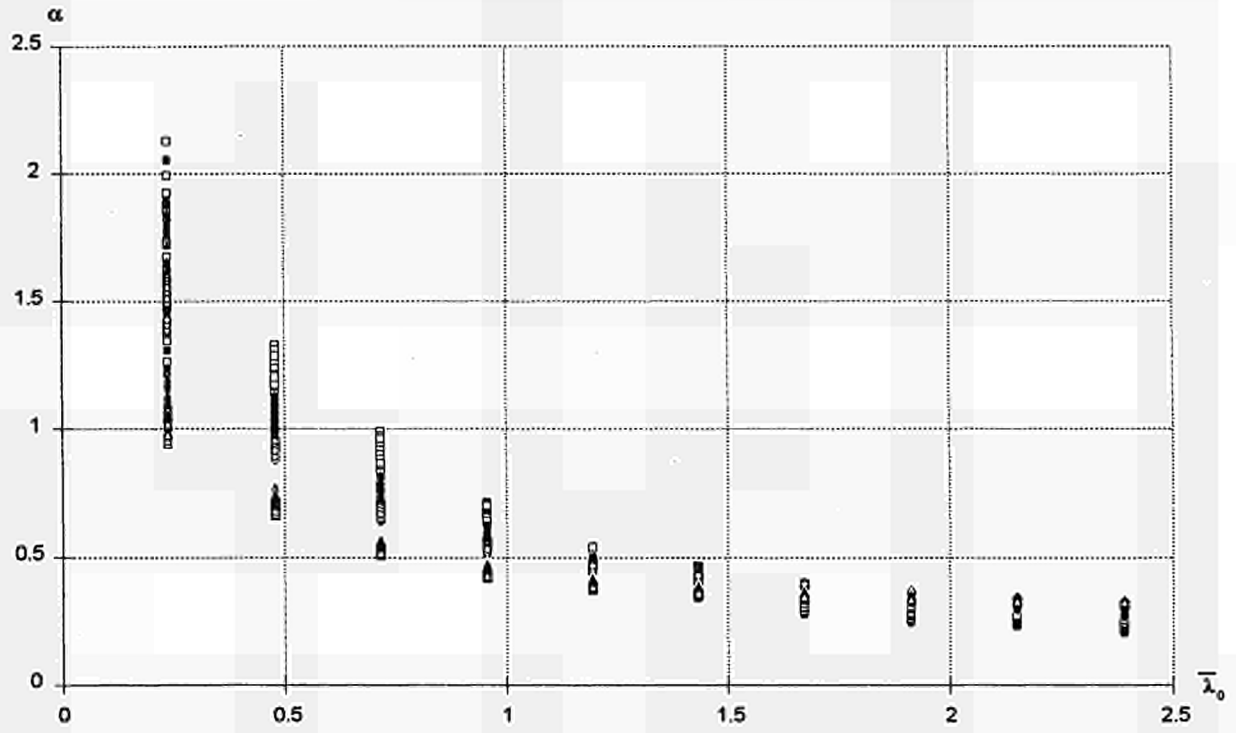

FIGURE 12.2 Evolution of α according to the slenderness ratio (buckling about minor axis - triangular moment) see also Annex 13

On the other hand, in the case of a bi-triangular moment distribution (FIGURE 12.3), the dispersion of the points is very high since α varies between 2 and 1200 . These very high values of α are due to the results concerning small eccentricities : in fact, the calculated value of N is near the ultimate value of N, which leads the interaction curve to have a very low curvature when M is small. This is obtained only if α is high.

Actually, for these points, if we take α as much smaller (2 or 3 as compared to 1200), the error is very low.

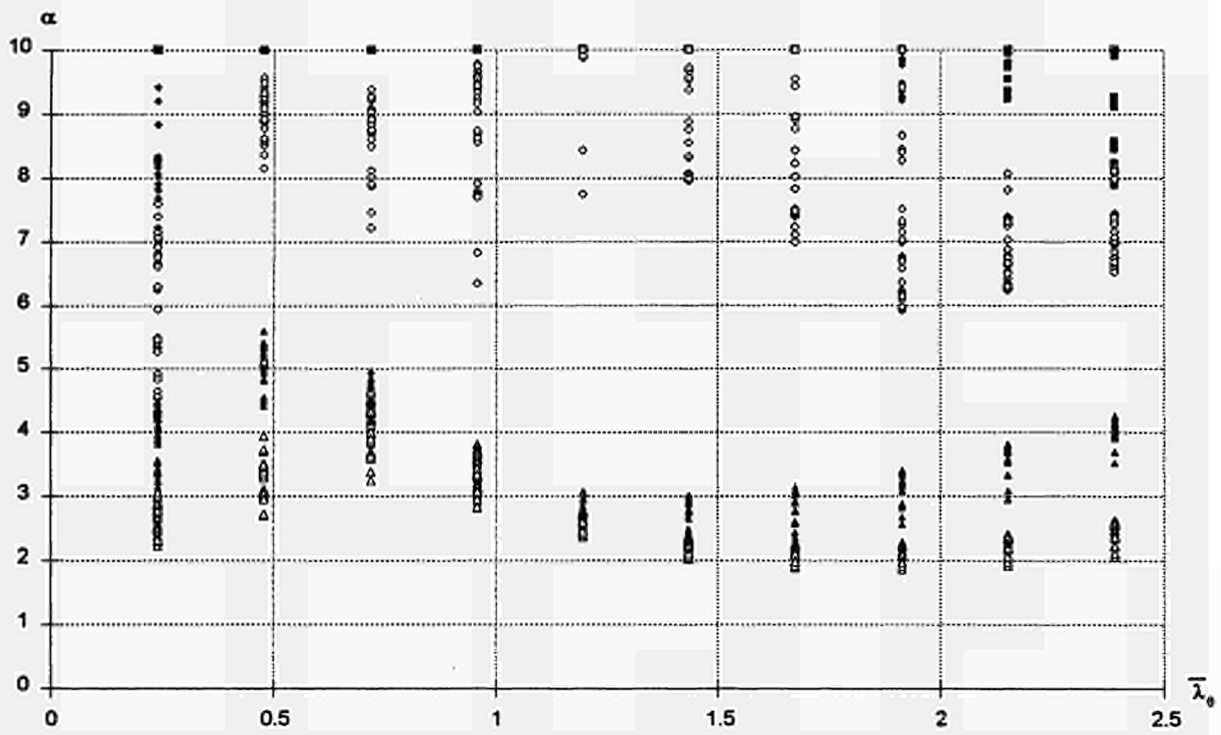

FIGURE 12.3 Evolution of α according to the slenderness ratio (buckling about minor axis - bi-triangular moment) see also Annex 13

In order to determine the curves which allow to approximate α, in a first stage, the average of the values of α is calculated for each slenderness ratio (after having first eliminated the excessively deviating values), by means of a numerical solving software; we try to find the function which best corresponds to those points.

From the evolution of the average of the points according to the slenderness ration, we try to find out a curve of the following type:

$$-\alpha = Ae^{B\bar{\lambda}_\infty} + C \qquad (12.2)$$

These calculations lead to the development of the following formulae:

- Buckling about the minor axis:

- Uniform moment distribution:

$$\alpha = 1.5e^{-2\bar{\lambda}_\theta} + 0.25 \qquad (12.3)$$

- Triangular moment distribution:

$$\alpha = 4e^{-2\bar{\lambda}_\theta} + 0.5 \qquad (12.4)$$

- Bi-triangular moment distribution:

$$\alpha = 2.5 \qquad (12.5)$$

– Buckling about the major axis:

– Uniform moment distribution:

$$\alpha = e^{-2\bar{\lambda}_\theta} + 0.28 \tag{12.6}$$

– Triangular moment distribution:

$$\alpha = 2e^{-2\bar{\lambda}_\theta} + 0.56 \tag{12.7}$$

– Bi-triangular moment distribution:

$$\alpha = 2.5 \tag{12.8}$$

Equations 5.27 and 5.30 may also be written under the form $\alpha = 6.5e^{-2\bar{\lambda}_\theta} + 2.5$ and $\alpha = 3e^{-2\bar{\lambda}_\theta} + 2.5$ with $\alpha \leq 2.5$. This does not alter the value of α but allows an easier interpolation on factor A (equation 12.2).

12.3 FINAL EQUATION

A global formula, i.e. allowing for $\beta_{M,y}$, may be determined by carrying out a linear interpolation on factor A (of equation 12.2) with a function of the exponential type for the interpolation on constant C (of equation 12.2). Factor B is immediately determined, since it is equal to -2 in all cases.

The global formulae are then as follows:

$$\left(\frac{N_{Sd}}{\chi_{min}\, A\, f_{y,\theta}}\right)^{\alpha} + \frac{M_{y,Sd}}{W_{pl,y}\, f_{y,\theta}} \leq 1 \tag{12.9}$$

If buckling occurs about the minor axis:

$$\alpha = \left(3.57\,\beta_{M,y} + 2.43\right) e^{-2\bar{\lambda}_\theta} + 0.03\, e^{\left(3.1\left(\beta_{M,y} - 1.1\right)\right)} + 0.23 \quad \text{but } \alpha \leq 2.5 \tag{12.10}$$

If buckling occurs about the major axis:

$$\alpha = \left(1.43\,\beta_{M,y} - 0.57\right) e^{-2\bar{\lambda}_\theta} + 0.047\, e^{\left(2.77\left(\beta_{M,y} - 1.1\right)\right)} + 0.23 \quad \text{but } \alpha \leq 2.5 \tag{12.11}$$

ANNEX 13:

13. VALUES OF α FOR BUCKLING AROUND WEAK AND STRONG AXIS AND FOR THREE TYPES OF BENDING MOMENT DISTRIBUTION (UNIFORM, TRIANGULAR AND BI-TRIANGULAR)

The values of α which were calculated so as to comply with the following equation:

$$\left(\frac{N_{Sd}}{\chi_{min}\ A\ f_y}\right)^{\alpha} + \frac{M_{y,Sd}}{W_{pl,y}\ f_y} = 1$$

are shown on the x-axis on the graphs in this annex, while the slenderness ratio at failure temperature is shown on the y-axis.

The values of N_{sd} and $M_{y,Sd}$ are derived from the results obtained with LENAS for a failure temperature of 400°C. These calculations were carried out for buckling about the major and minor axes and for three load types:

- Axial force + uniform moment distribution
- Axial force + triangular moment distribution
- Axial force + bi-triangular moment distribution

All the calculated values of α are shown on FIGURE 13.1 to FIGURE 13.6, while the values calculated for both maximum eccentricities were eliminated from FIGURE 13.7 to FIGURE 13.12.

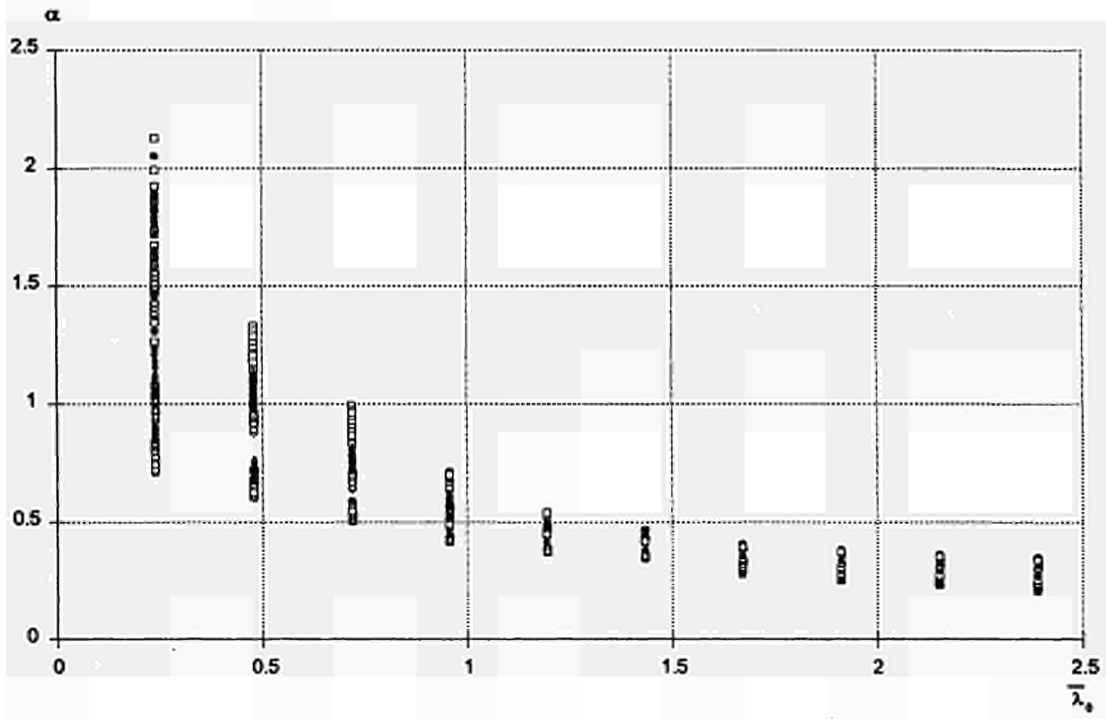

FIGURE 13.1 Evolution of α according to the slenderness ratio (buckling about minor axis - uniform moment)

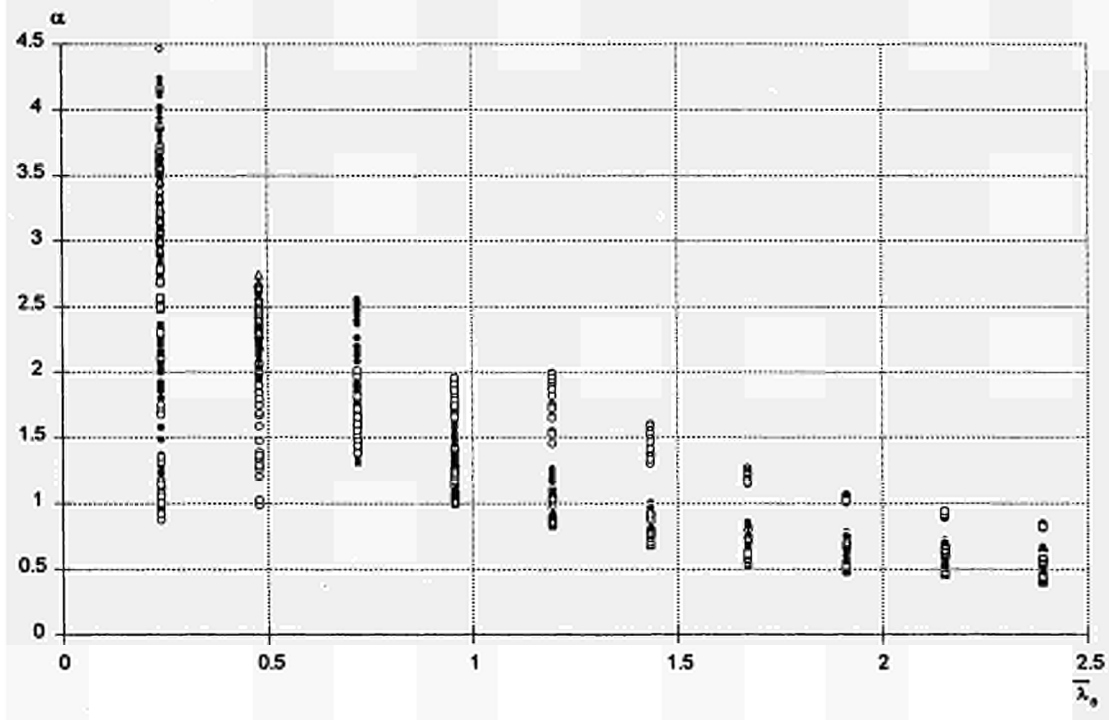

FIGURE 13.2 Evolution of α according to the slenderness ratio (buckling about minor axis - triangular moment)

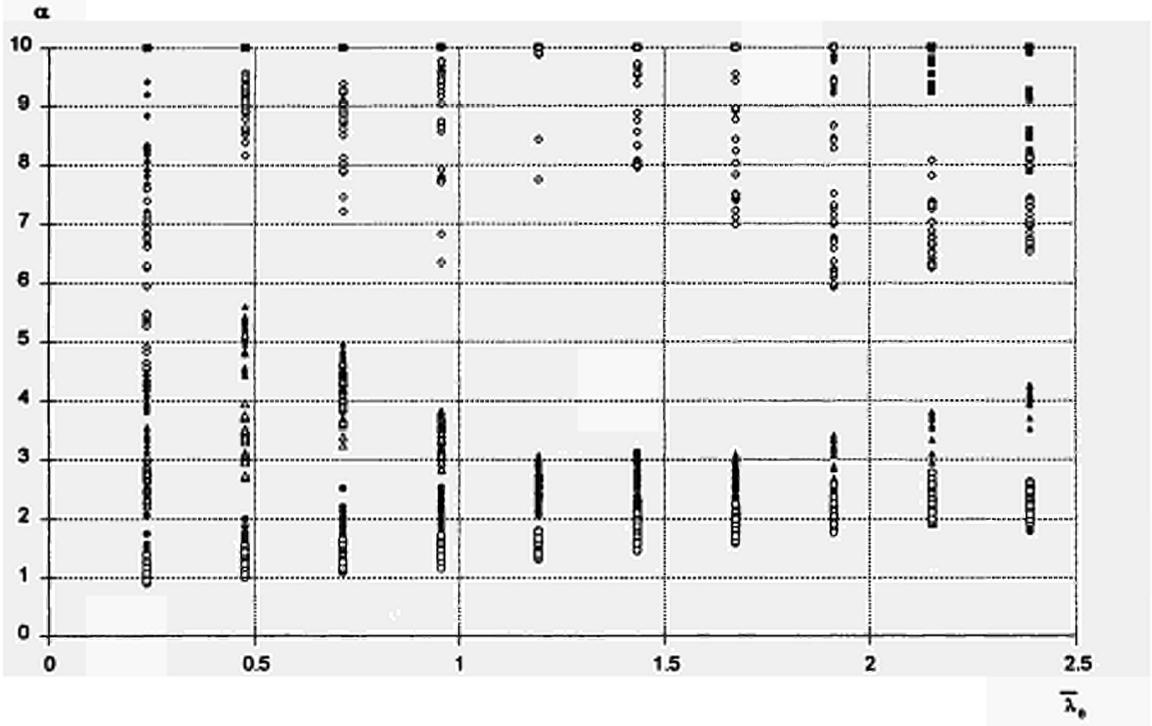

FIGURE 13.3 Evolution of α according to the slenderness ratio (buckling about minor axis - bi-triangular moment)

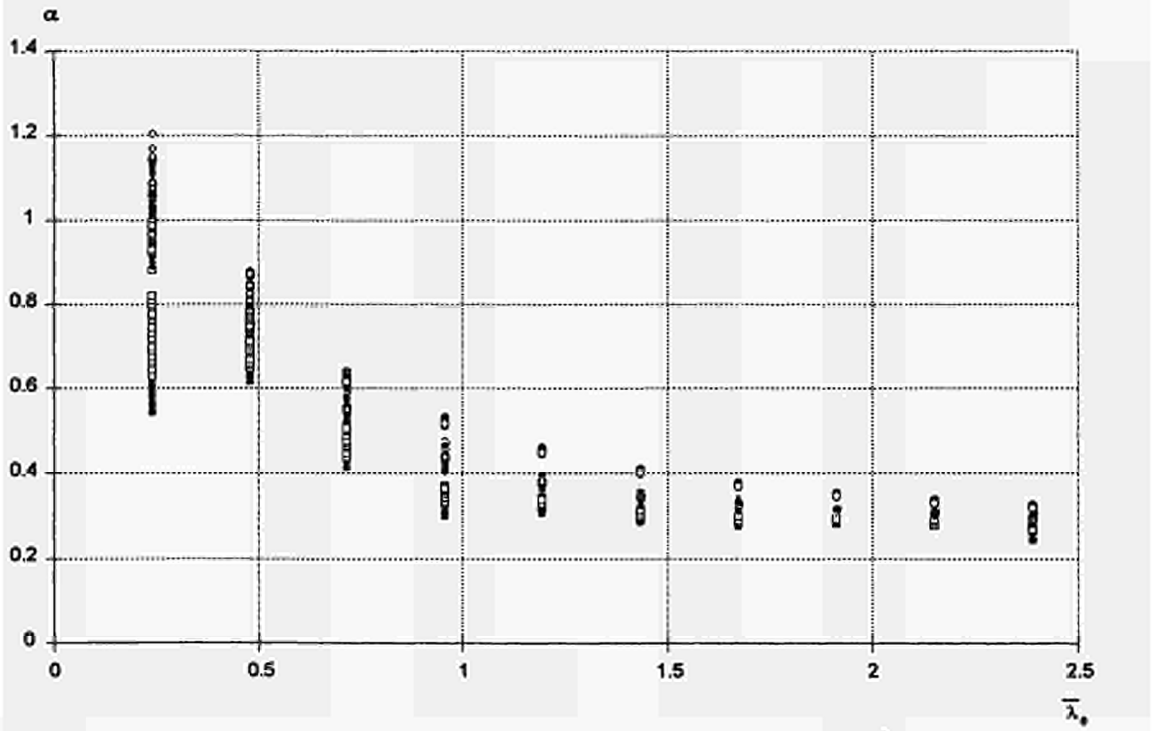

FIGURE 13.4 Evolution of α according to the slenderness ratio (buckling about major axis - uniform moment)

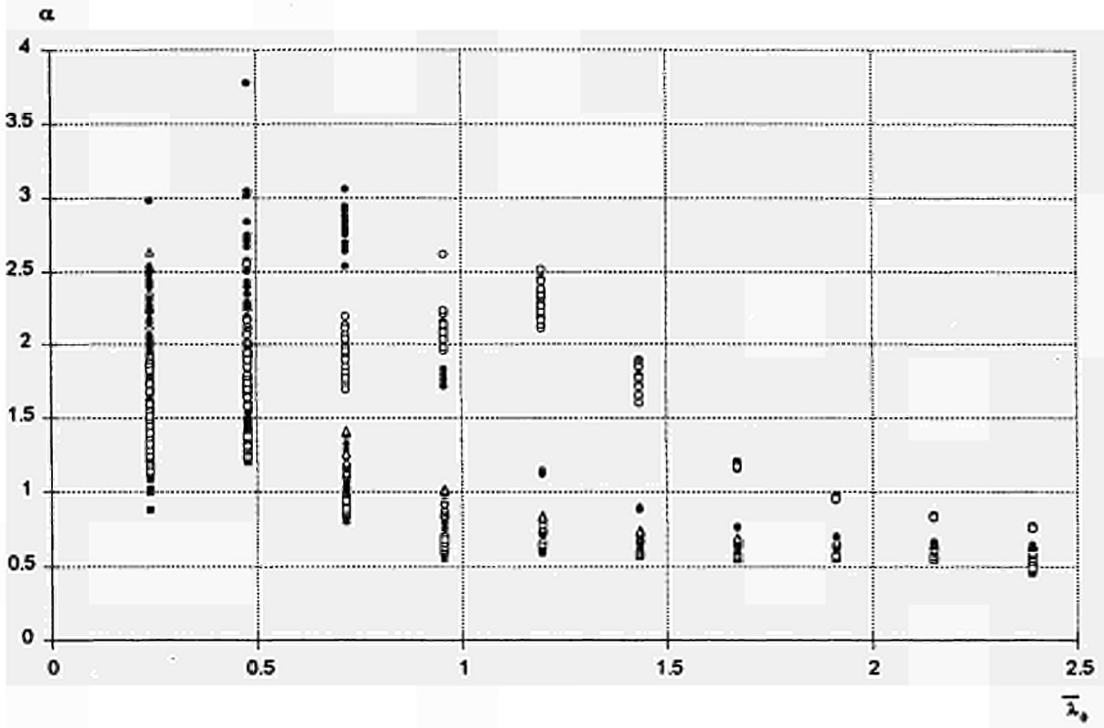

FIGURE 13.5 Evolution of α according to the slenderness ratio (buckling about major axis - triangular moment)

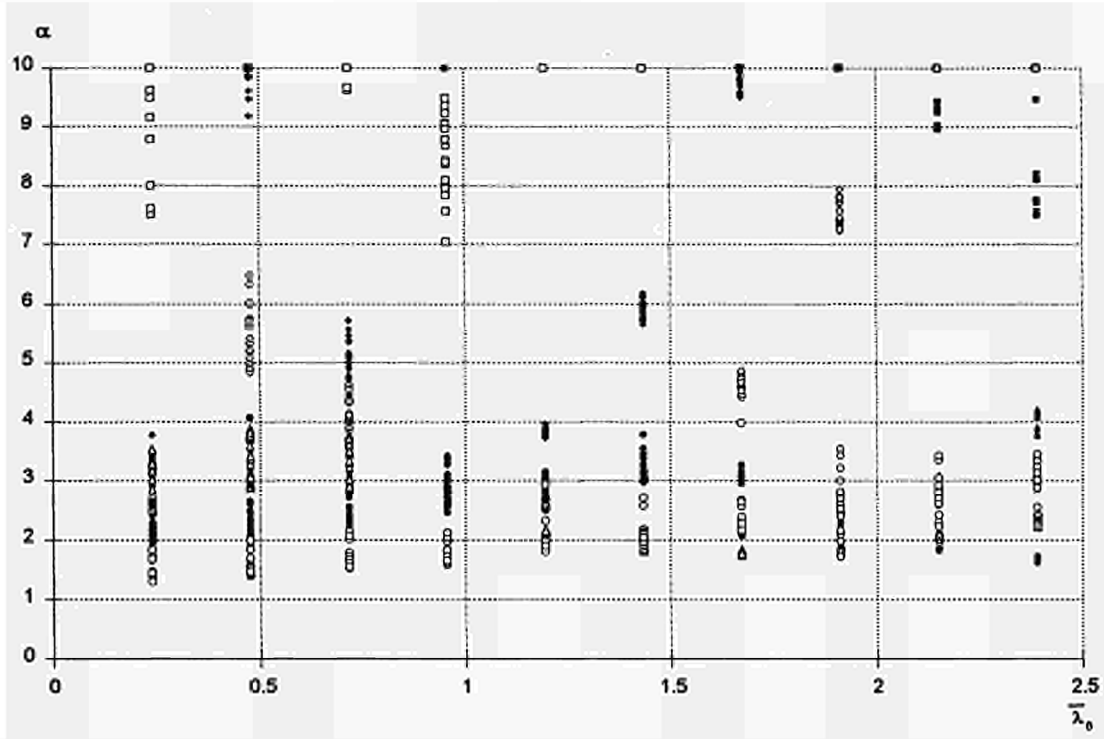

FIGURE 13.6 Evolution of α according to the slenderness ratio (buckling about major axis - bi-triangular moment)

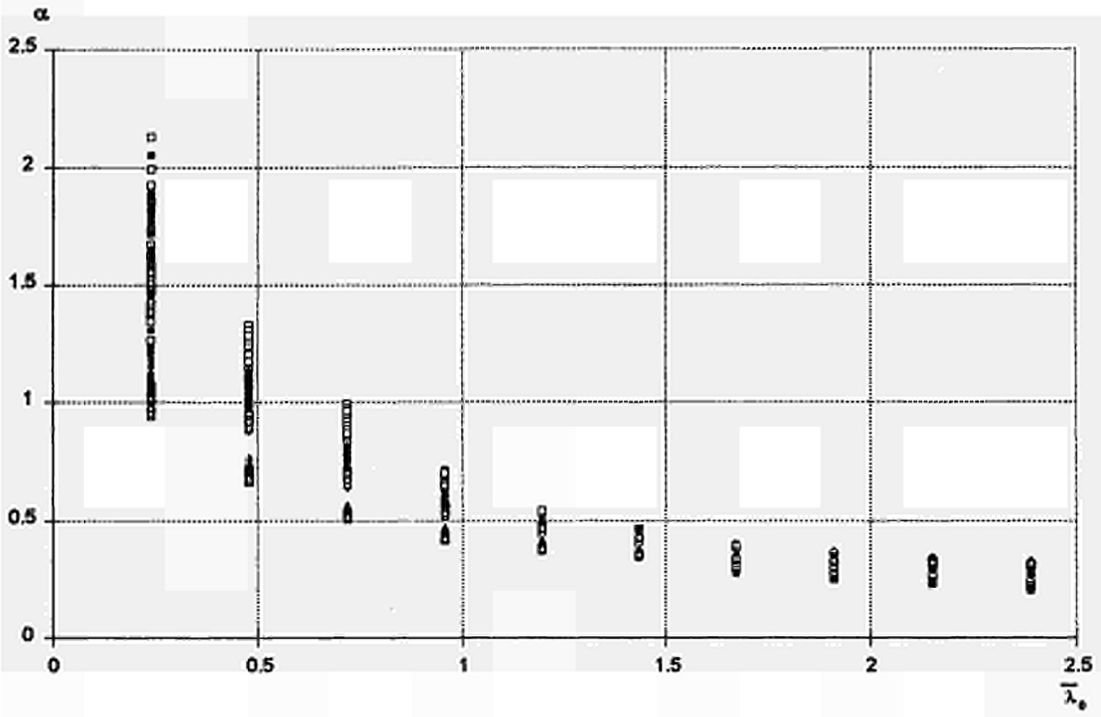

FIGURE 13.7 Evolution of α according to the slenderness ratio (buckling about minor axis - uniform moment)

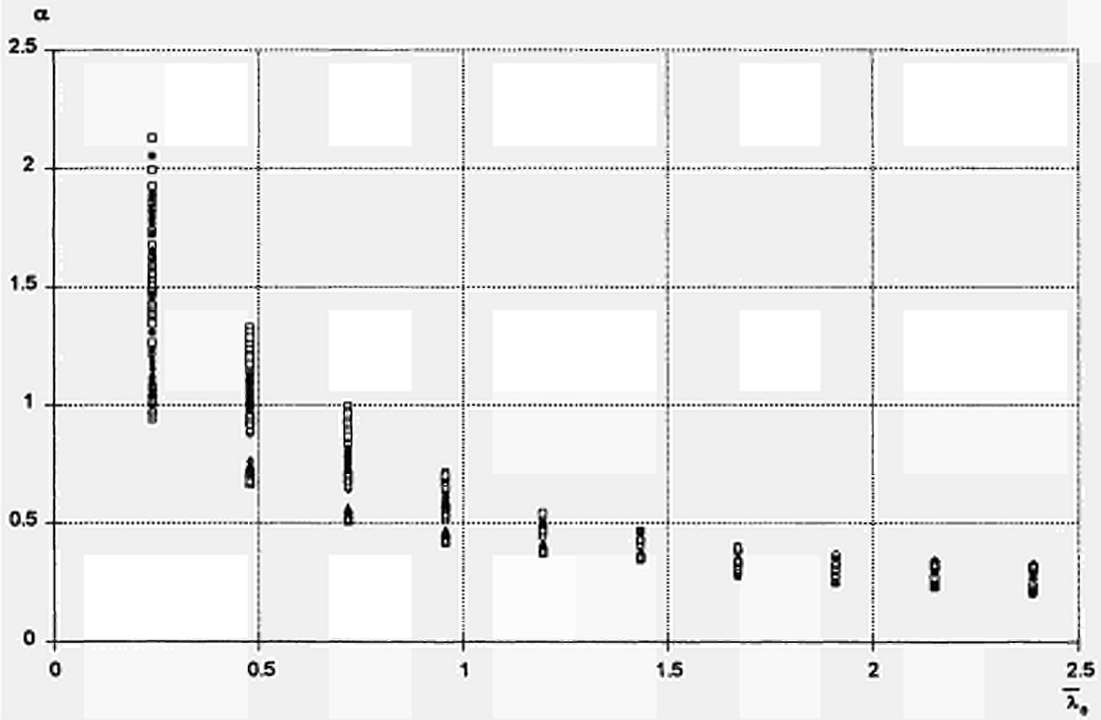

FIGURE 13.8 Evolution of α according to the slenderness ratio (buckling about minor axis - triangular moment)

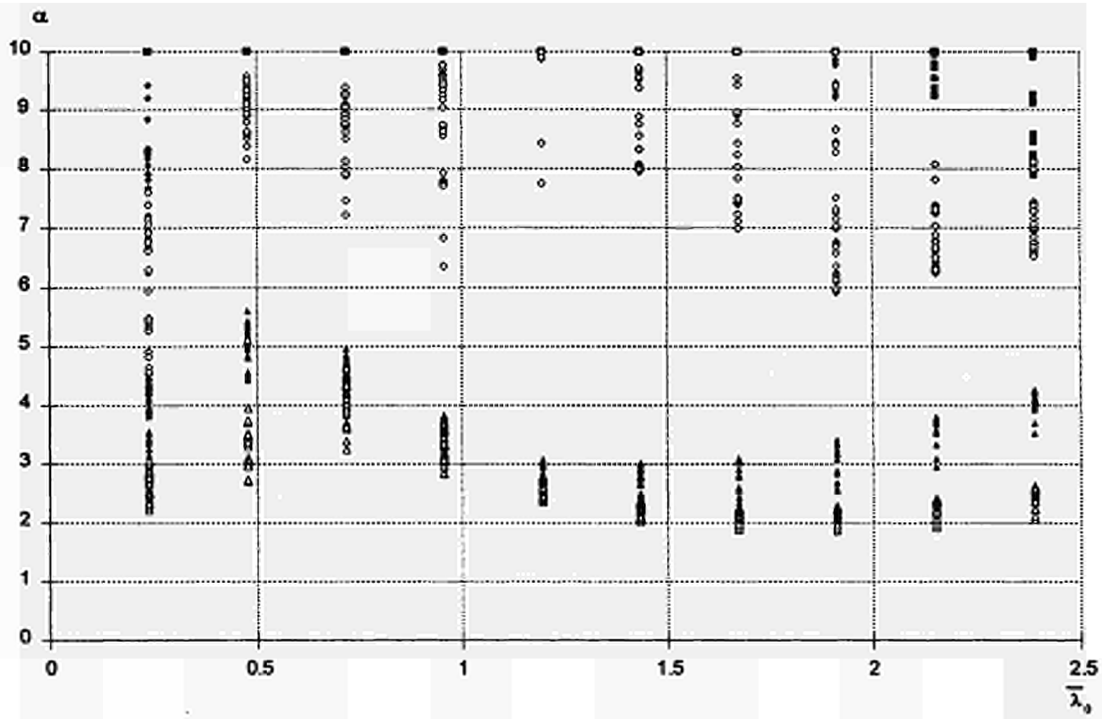

FIGURE 13.9 Evolution of α according to the slenderness ratio (buckling about minor axis - bi-triangular moment)

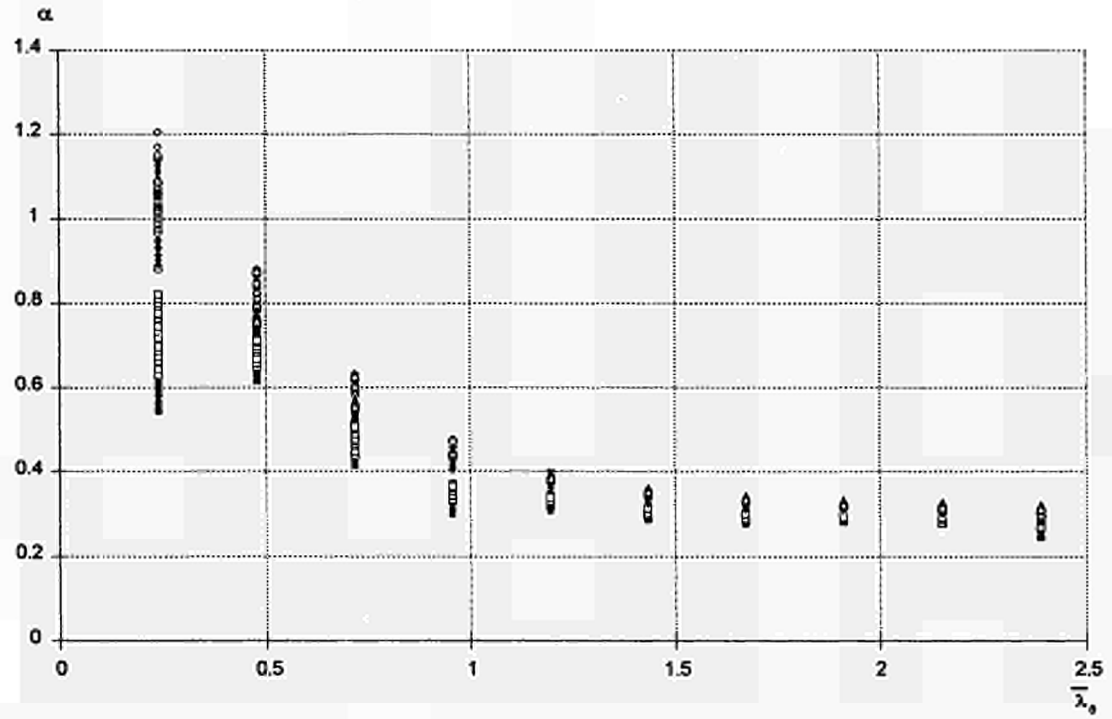

FIGURE 13.10 Evolution of α according to the slenderness ratio (buckling about major axis - uniform moment)

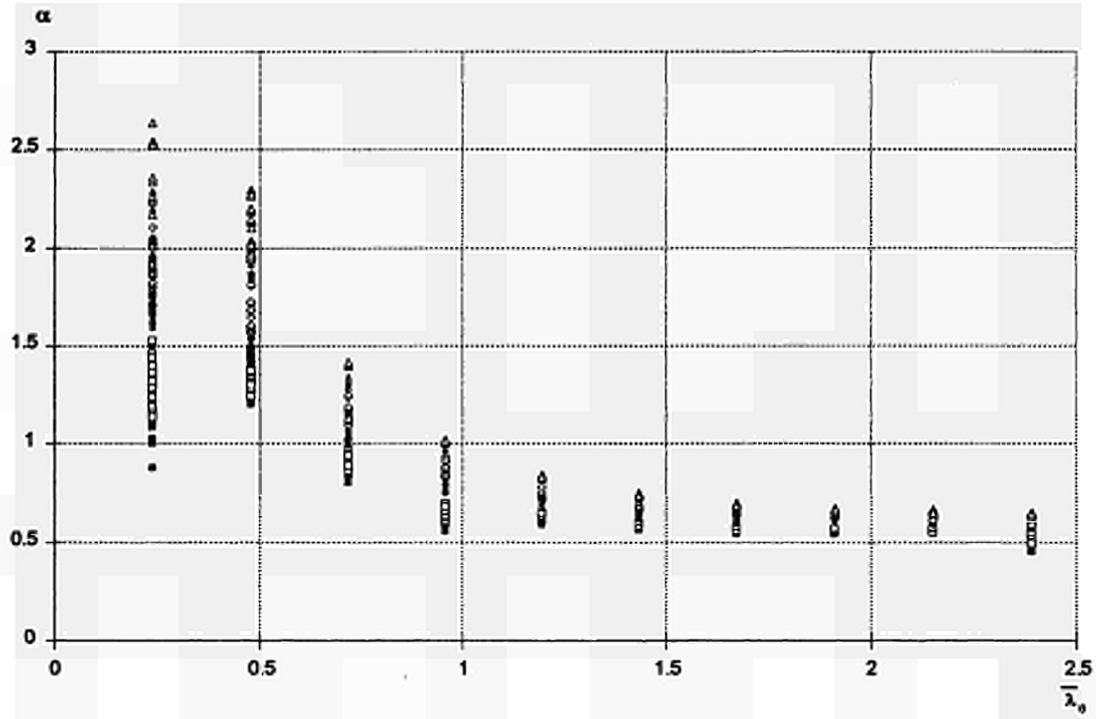

FIGURE 13.11 Evolution of α according to the slenderness ratio (buckling about major axis - triangular moment)

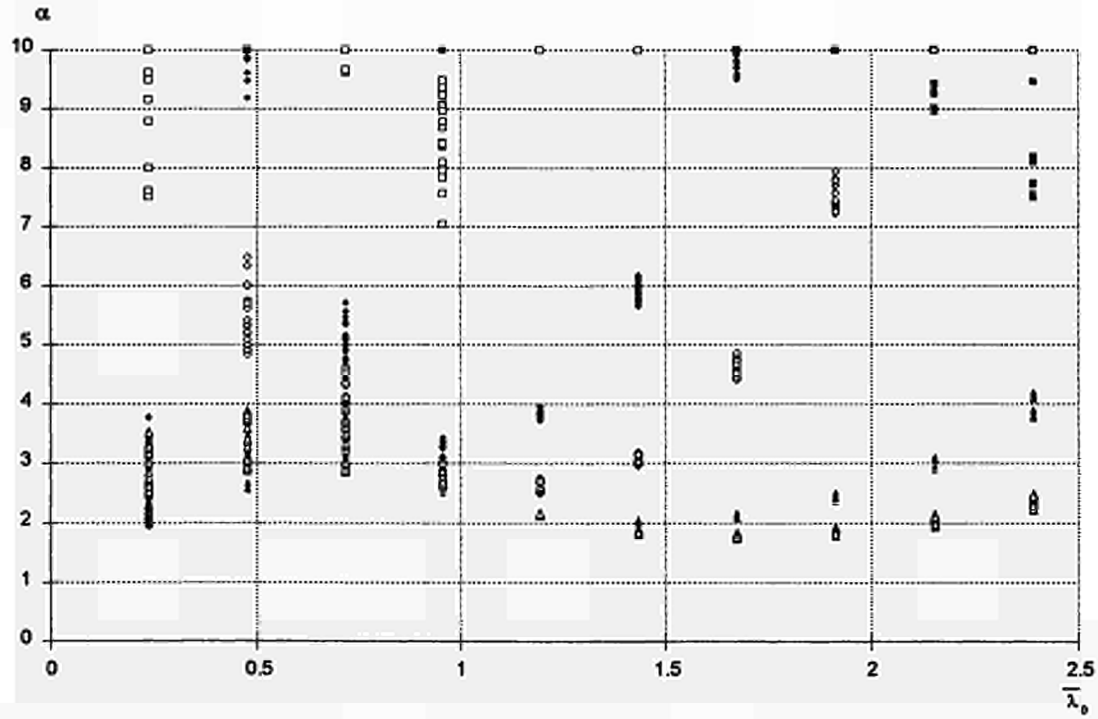

FIGURE 13.12 Evolution of α according to the slenderness ratio (buckling about major axis - bi-triangular moment)

ANNEX 14:

14. COMPARISON BETWEEN THE NUMERICAL SIMULATION RESULTS AND THE N-M INTERACTION FORMULA (ANNEX 12)

A comparison between all the results obtained numerically (from 400 to 900°C) and the analytical formulae (hereunder) is carried out in Annex 14.

$$\left(\frac{N_{Sd}}{\chi_{min}\ A\ f_{y,\theta}}\right)^{\alpha} + \frac{M_{y,Sd}}{W_{pl,y}\ f_{y,\theta}} \leq 1$$

With:

If buckling occurs about the minor axis:

$$\alpha = \left(3.57\ \beta_{M,y} + 2.43\right) e^{-2\bar{\lambda}_{\theta}} + 0.03\ e^{\left(3.1\left(\beta_{M,y} - 1.1\right)\right)} + 0.23 \qquad \text{but } \alpha \leq 2.5$$

If buckling occurs about the major axis:

$$\alpha = \left(1.43\ \beta_{M,y} - 0.57\right) e^{-2\bar{\lambda}_{\theta}} + 0.047\ e^{\left(2.77\left(\beta_{M,y} - 1.1\right)\right)} + 0.23 \qquad \text{but } \alpha \leq 2.5$$

The value of standard $D_{numerical}$ = (calculated numerically, FIGURE 14.1) is shown on the x-axis (proposition_2), and the value of standard $D_{analytical}$ = (obtained from the above defined formula) is shown on the y-axis (LENAS). The 45° straight line represents a perfect equality between these two values. While the straight line which is slightly above represents an error of +10% of the analytical value as compared to the numerical value (therefore unconservative), the straight line which is slightly below the bisectrix represents, on the other hand, an error of -10% of the analytical value as compared to the numerical value (conservative).

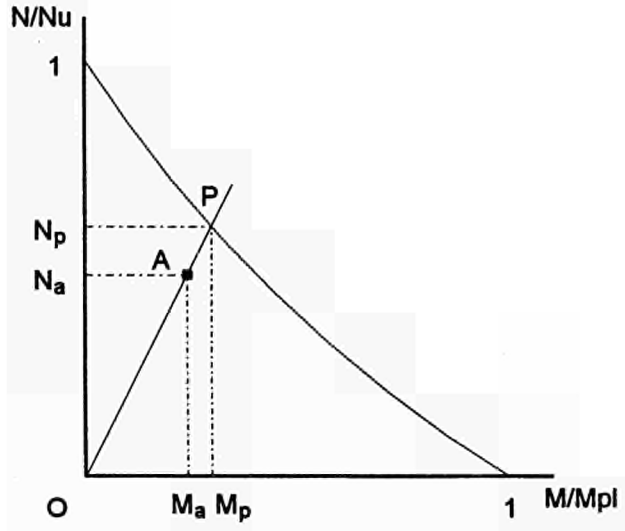

FIGURE 14.1 Calculation of $D_{numerical}$ and $D_{analytical}$

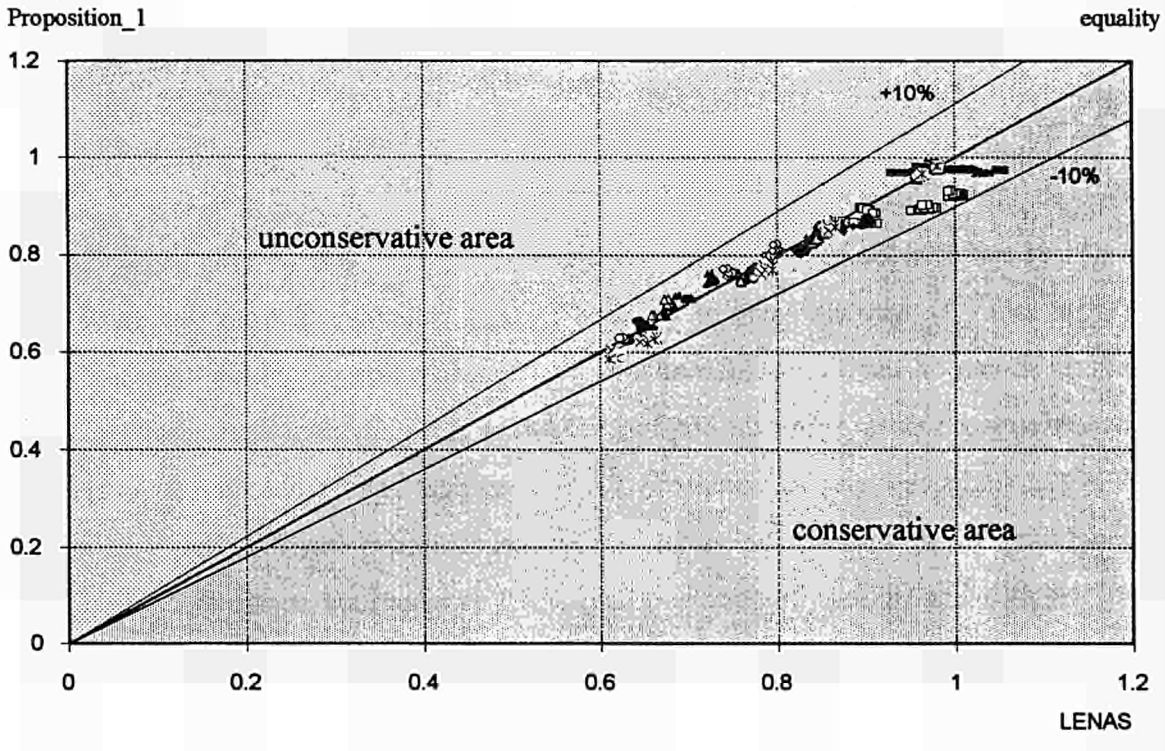

FIGURE 14.2 Formula - numerical results comparison at 400°C

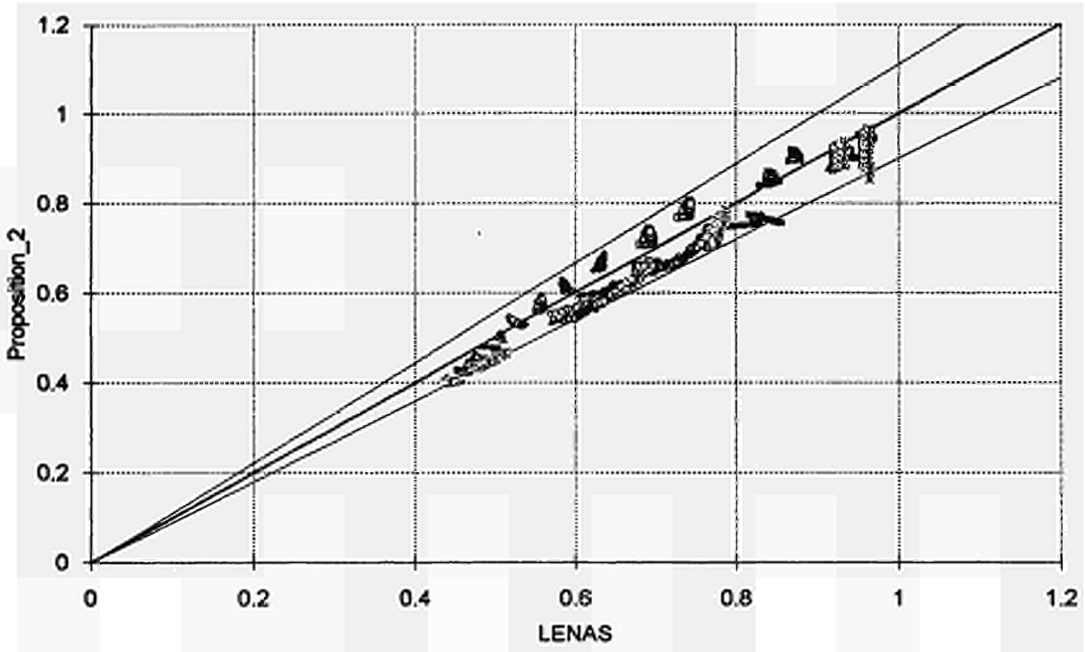

FIGURE 14.3 Formula - numerical results comparison at 400°C for buckling about minor axis and uniform moment distribution

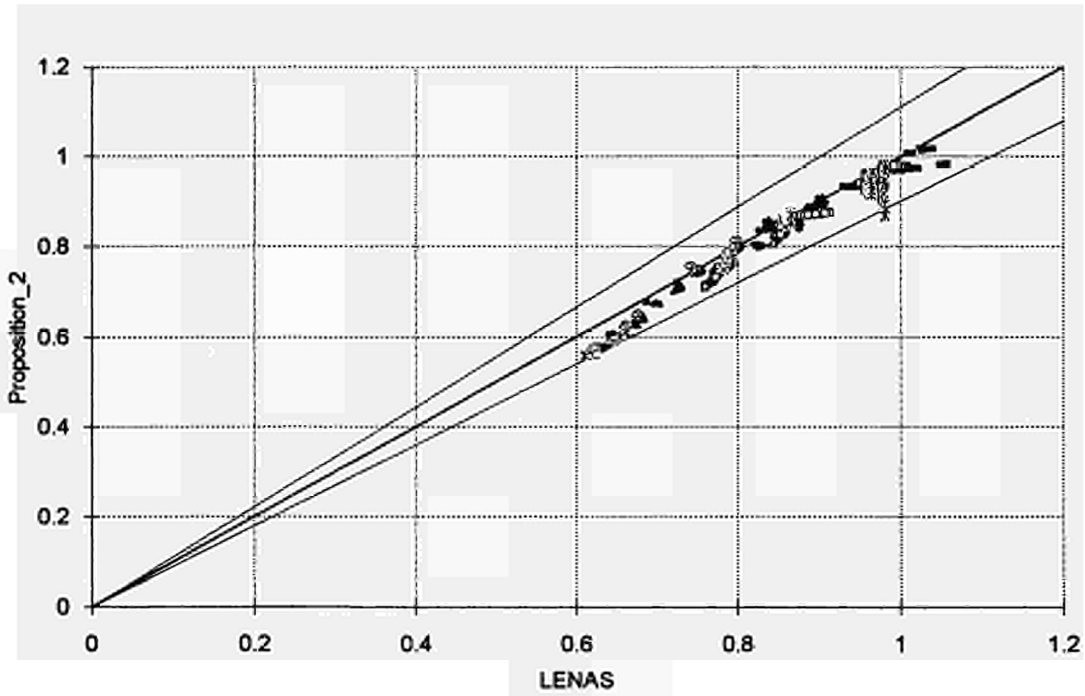

FIGURE 14.4 Formula - numerical results comparison at 400°C for buckling about minor axis and triangular moment distribution

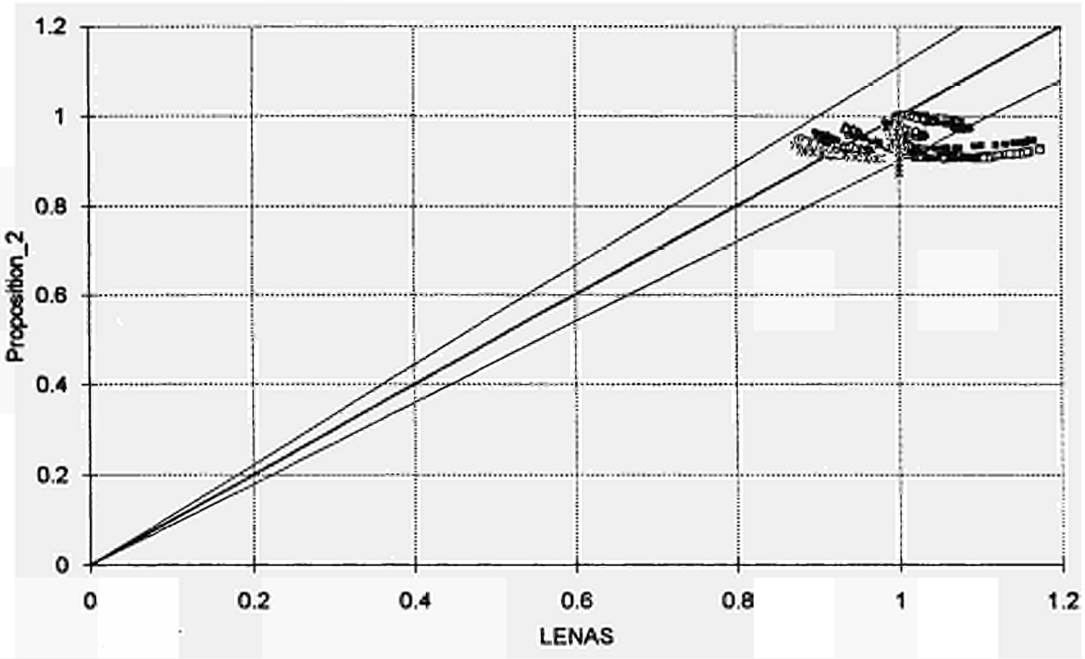

FIGURE 14.5 Formula - numerical results comparison at 400°C for buckling about minor axis and bi-triangular moment distribution

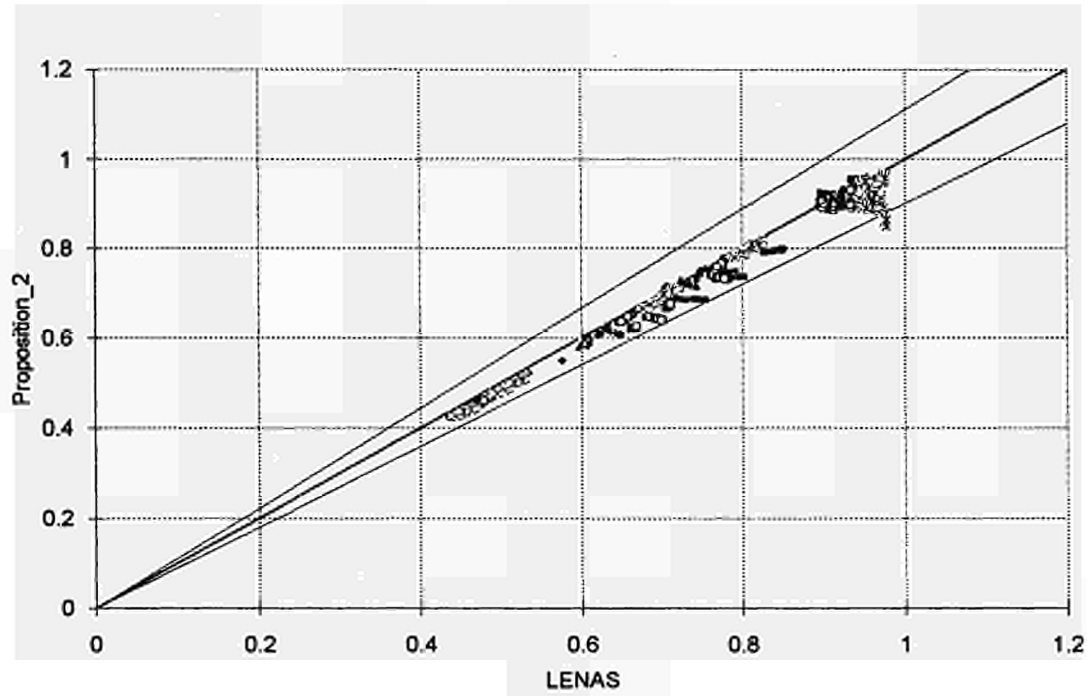

FIGURE 14.6 Formula - numerical results comparison at 400°C for buckling about major axis and uniform moment distribution

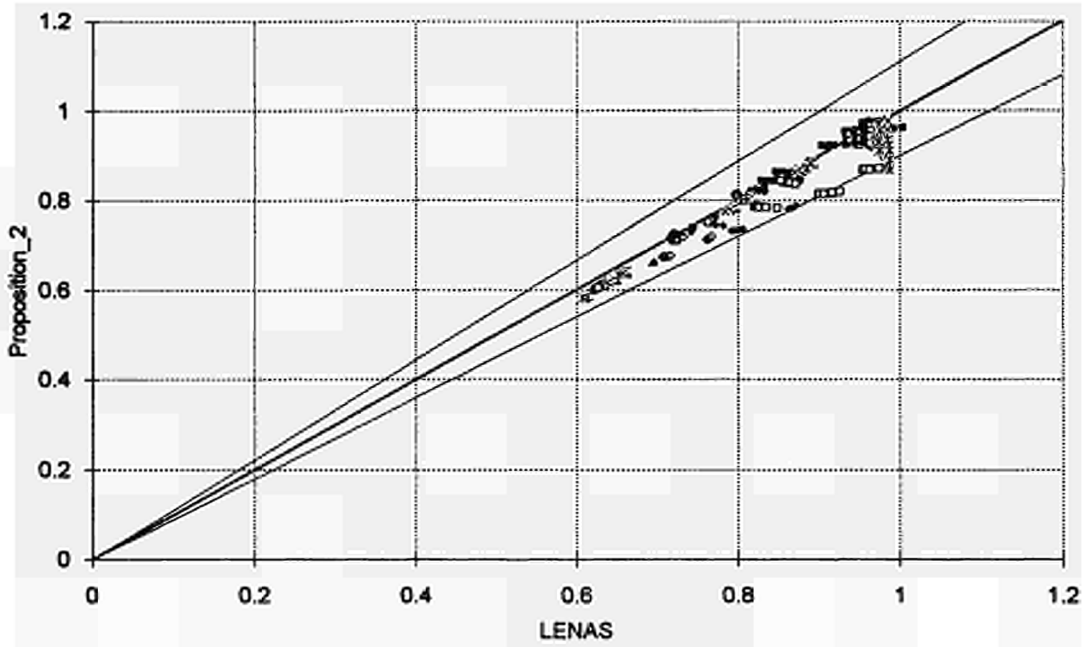

FIGURE 14.7 Formula - numerical results comparison at 400°C for buckling about major axis and triangular moment distribution

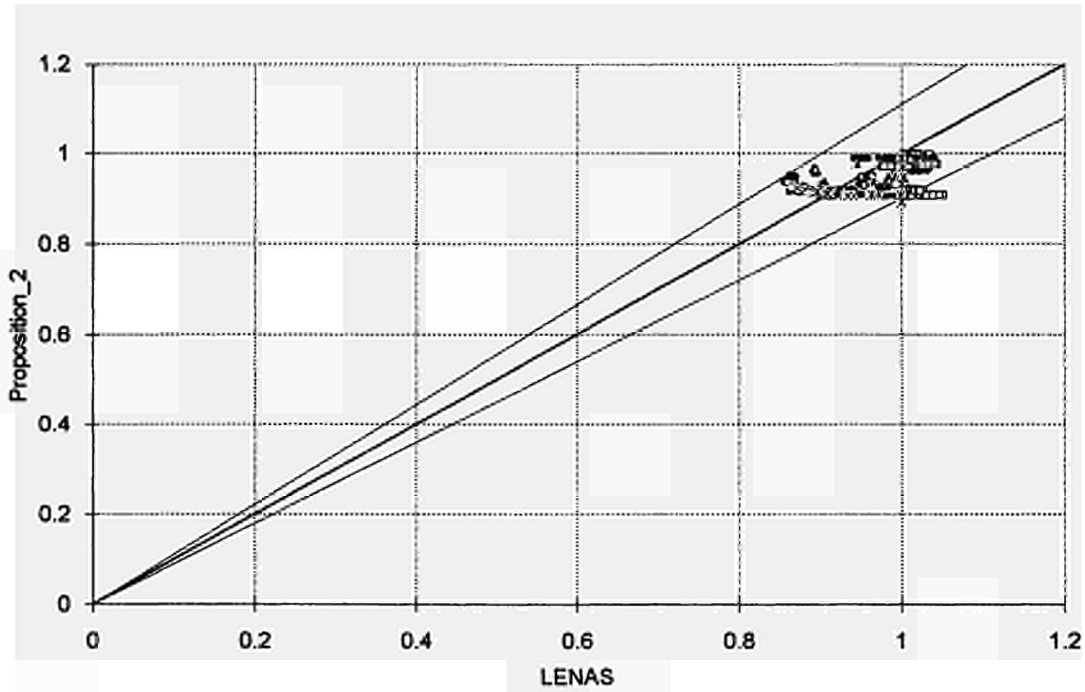

FIGURE 14.8 Formula - numerical results comparison at 400°C for buckling about major axis and bi-triangular moment distribution

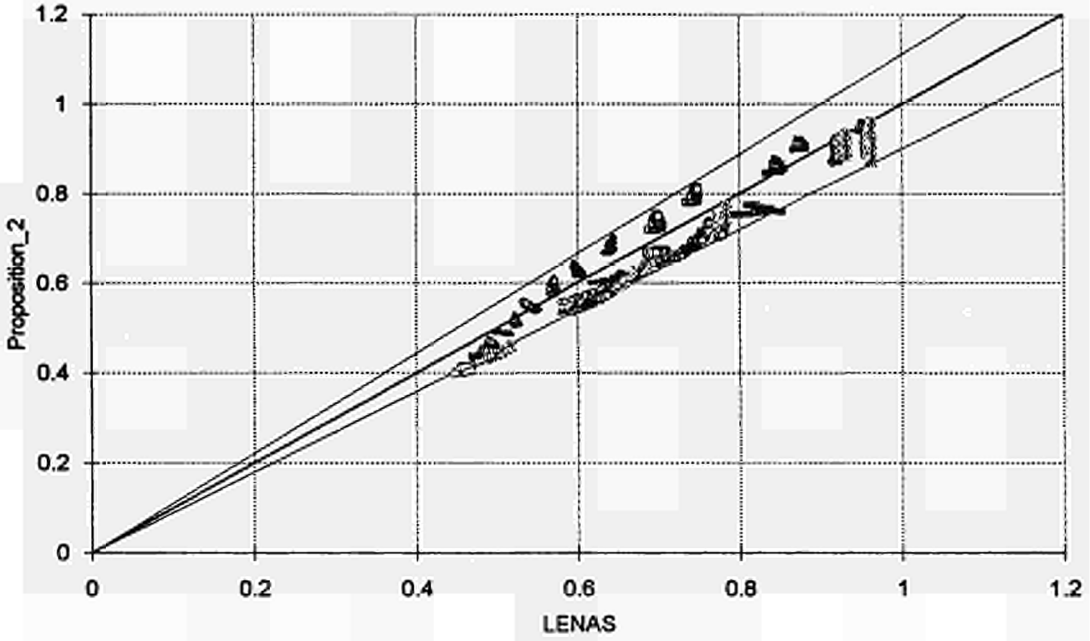

FIGURE 14.9 Formula - numerical results comparison at 500°C for buckling about minor axis and uniform moment distribution

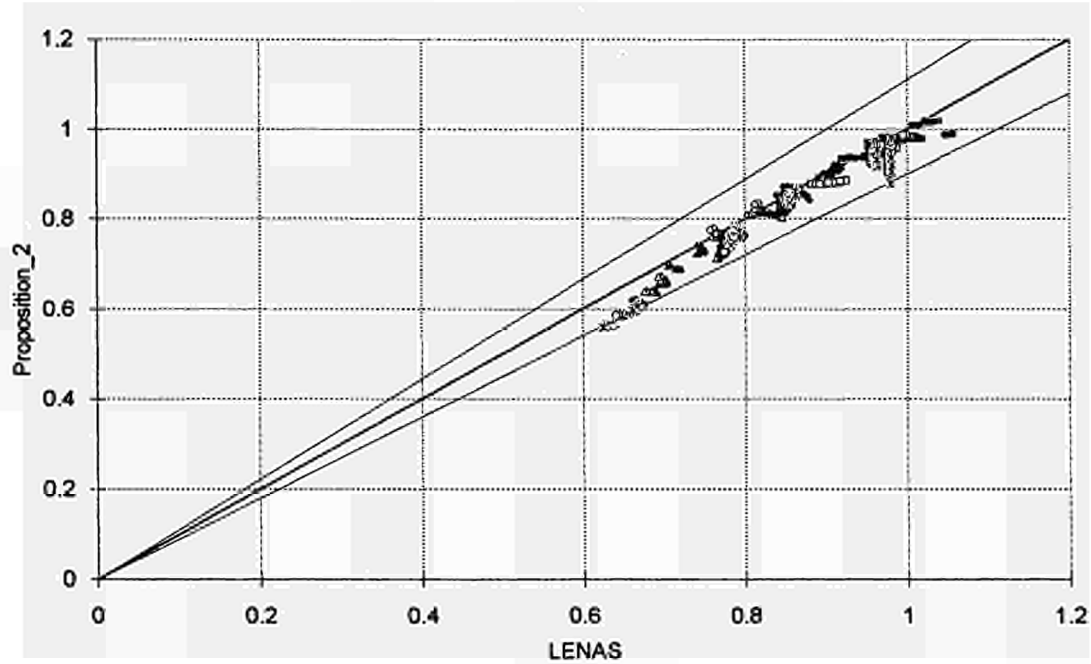

FIGURE 14.10 Formula - numerical results comparison at 500°C for buckling about minor axis and triangular moment distribution

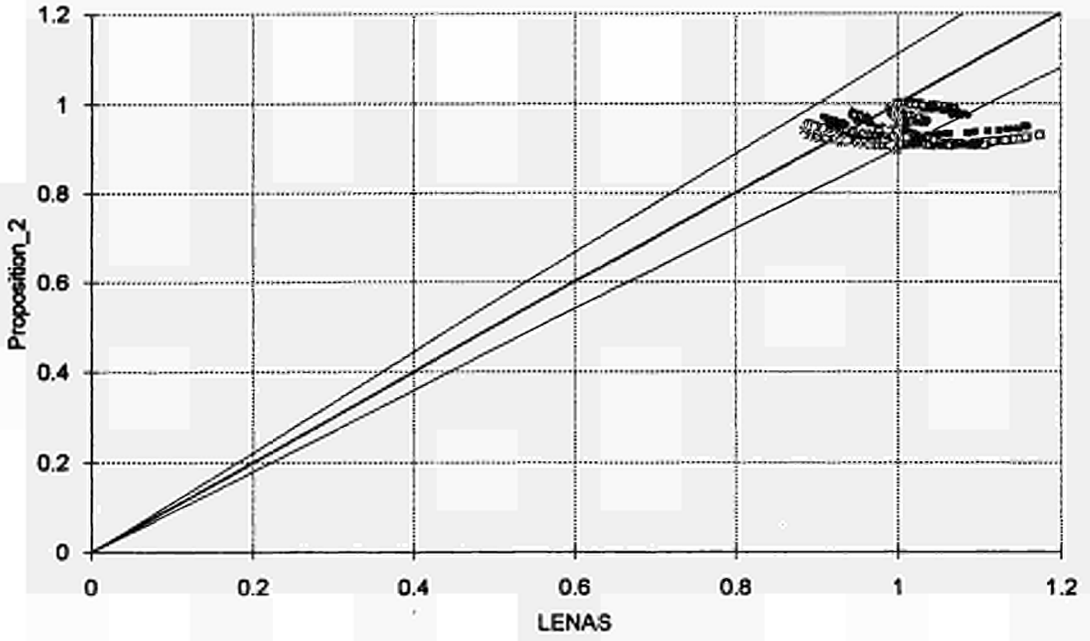

FIGURE 14.11 Formula - numerical results comparison at 500°C for buckling about minor axis and bi-triangular moment distribution

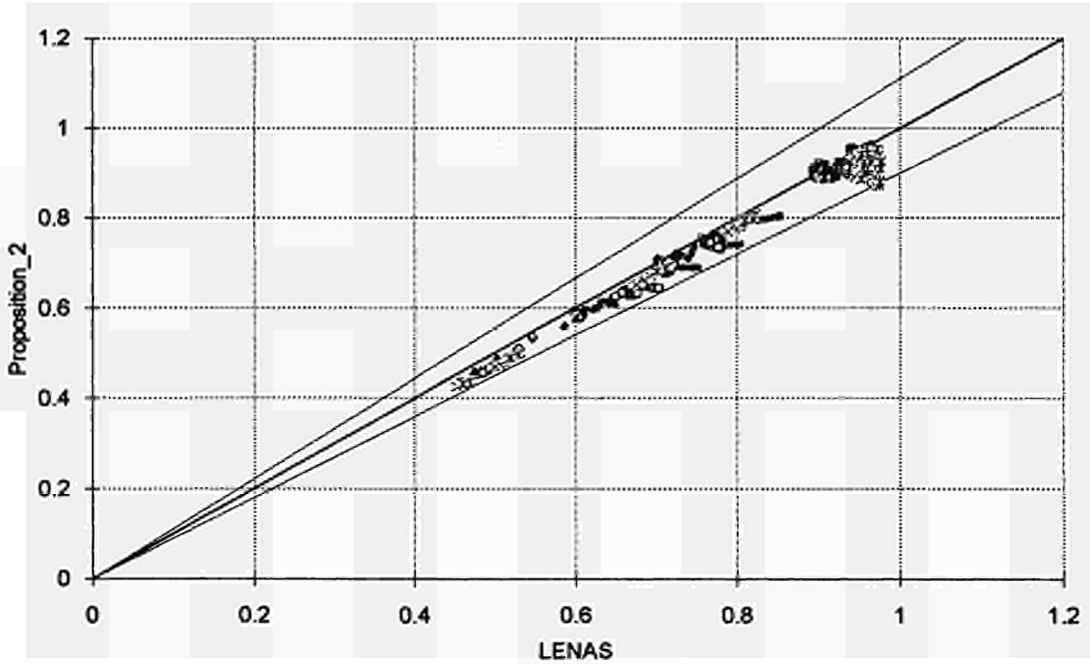

FIGURE 14.12 Formula - numerical results comparison at 500°C for buckling about major axis and uniform moment distribution

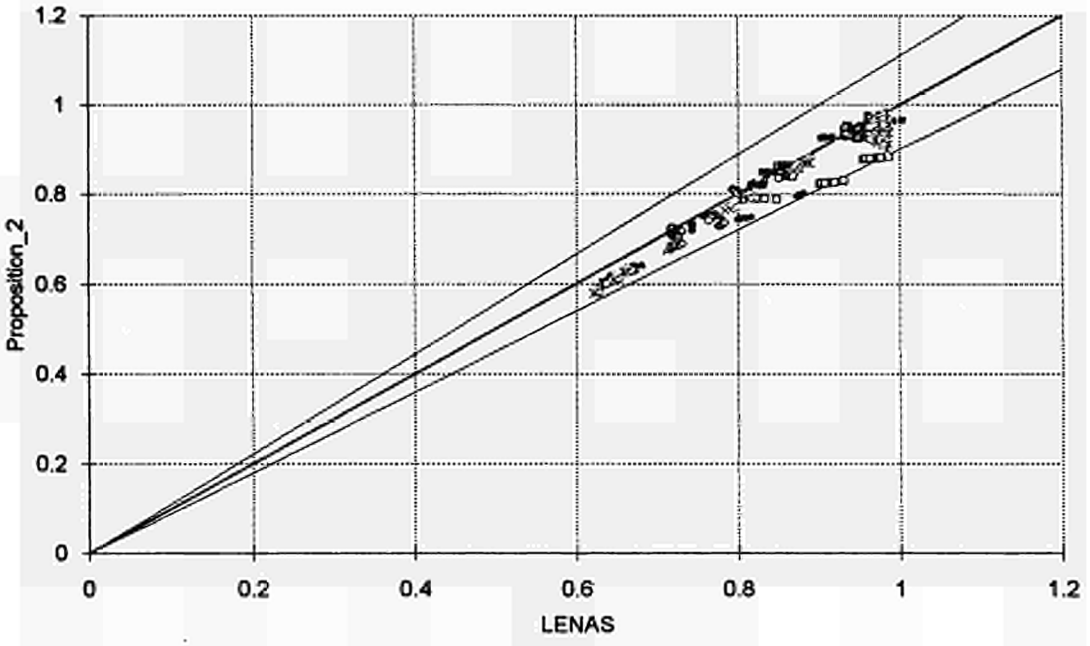

FIGURE 14.13 Formula - numerical results comparison at 500°C for buckling about major axis and triangular moment distribution

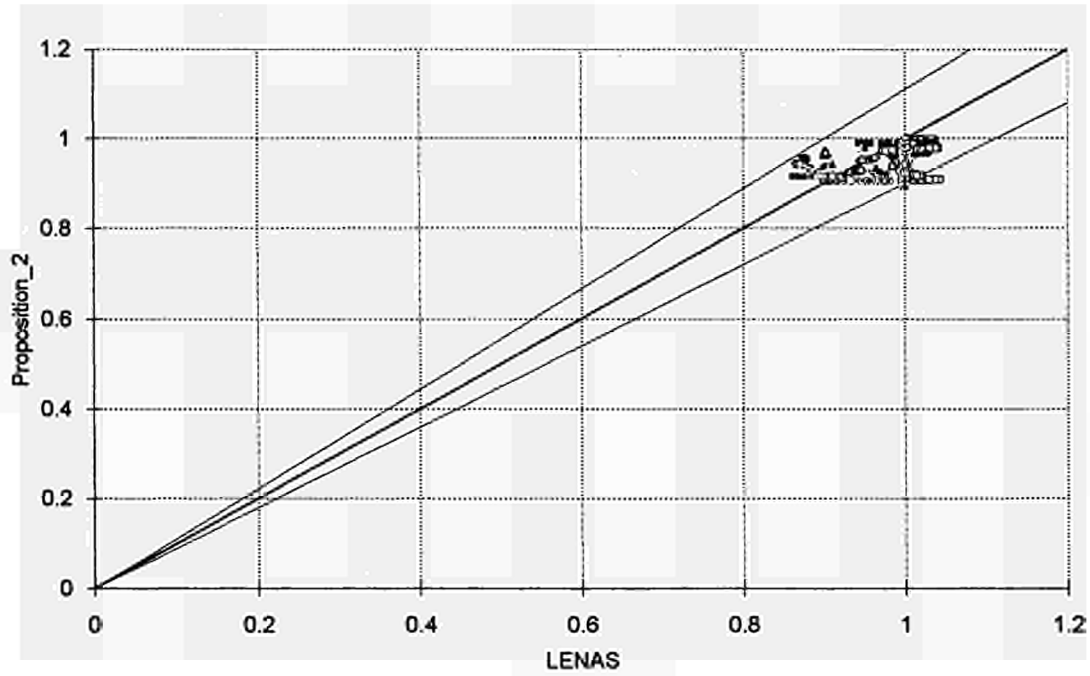

FIGURE 14.14 Formula - numerical results comparison at 500°C for buckling about major axis and bi-triangular moment distribution

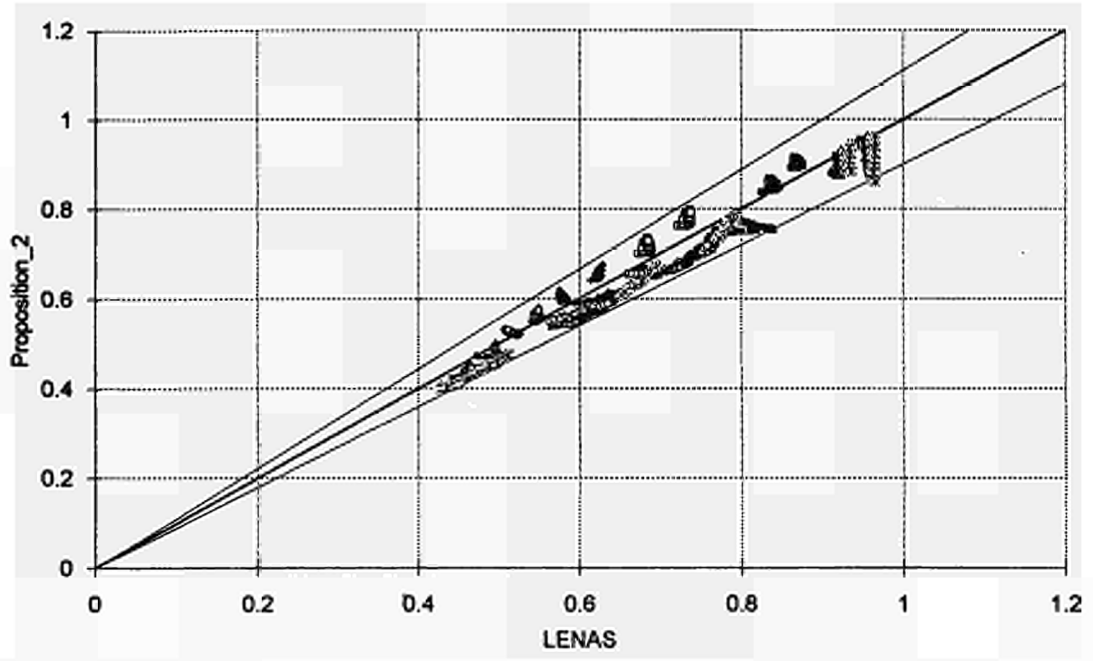

FIGURE 14.15 Formula - numerical results comparison at 600°C for buckling about minor axis and uniform moment distribution

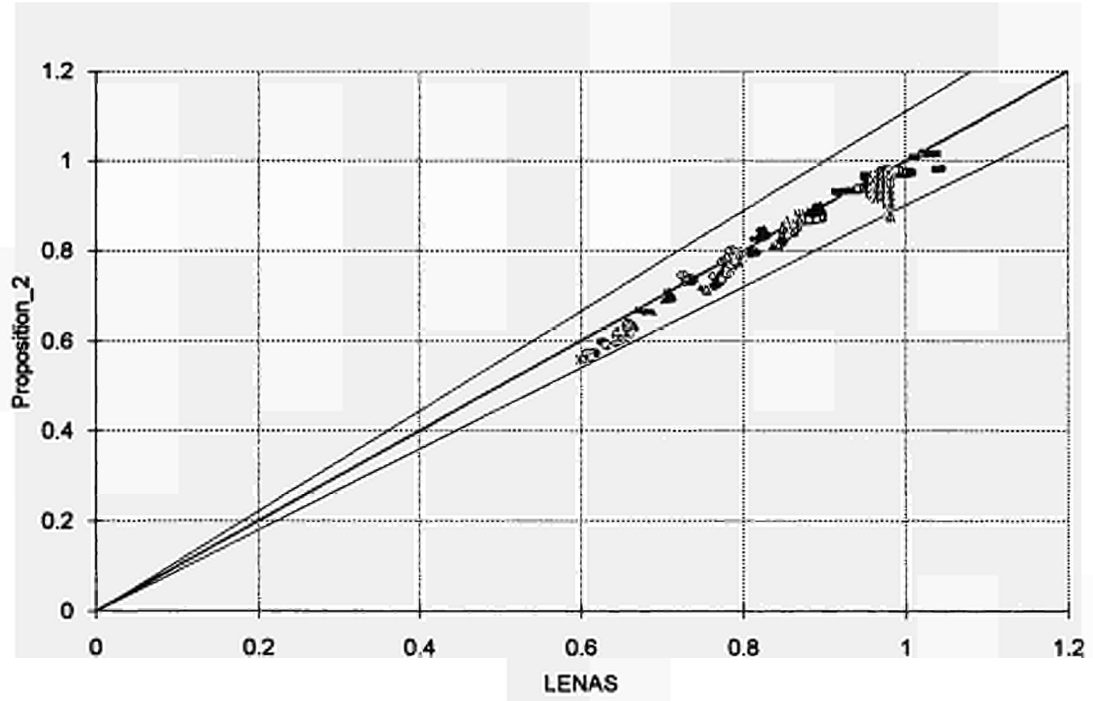

FIGURE 14.16 Formula - numerical results comparison at 600°C for buckling about minor axis and triangular moment distribution

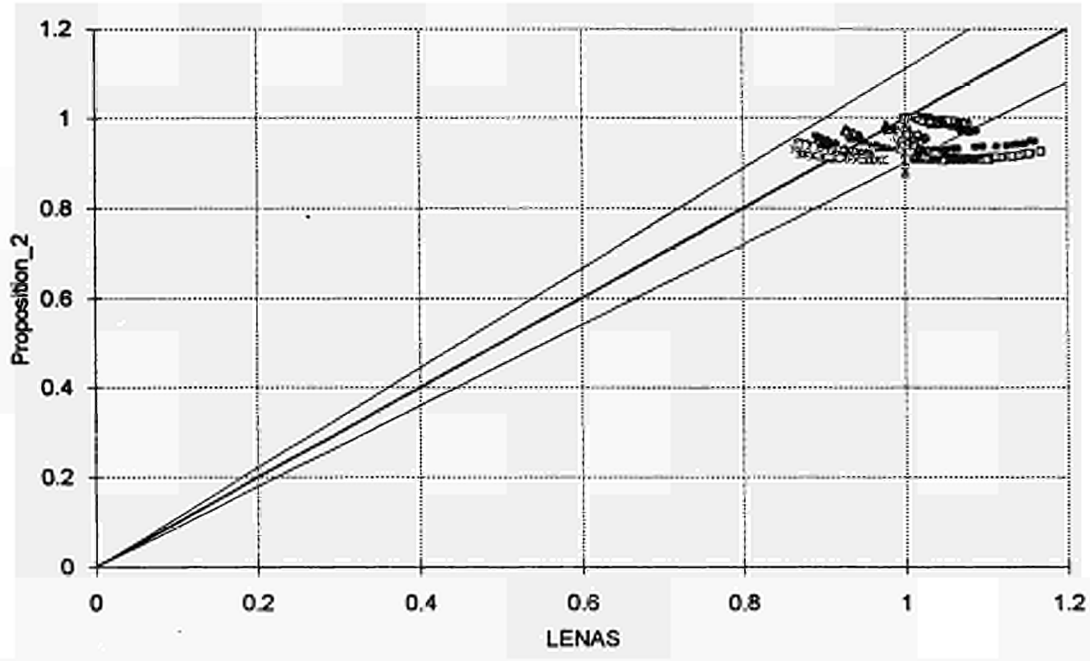

FIGURE 14.17 Formula - numerical results comparison at 600°C for buckling about minor axis and bi-triangular moment distribution

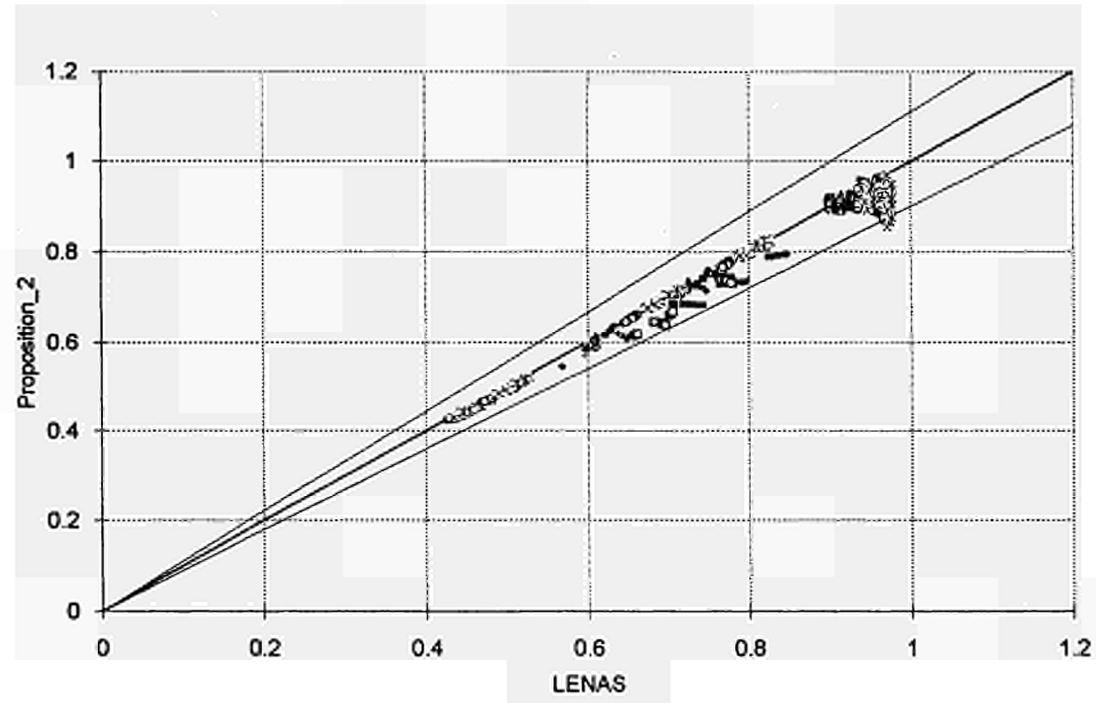

FIGURE 14.18 Formula - numerical results comparison at 600°C for buckling about major axis and uniform moment distribution

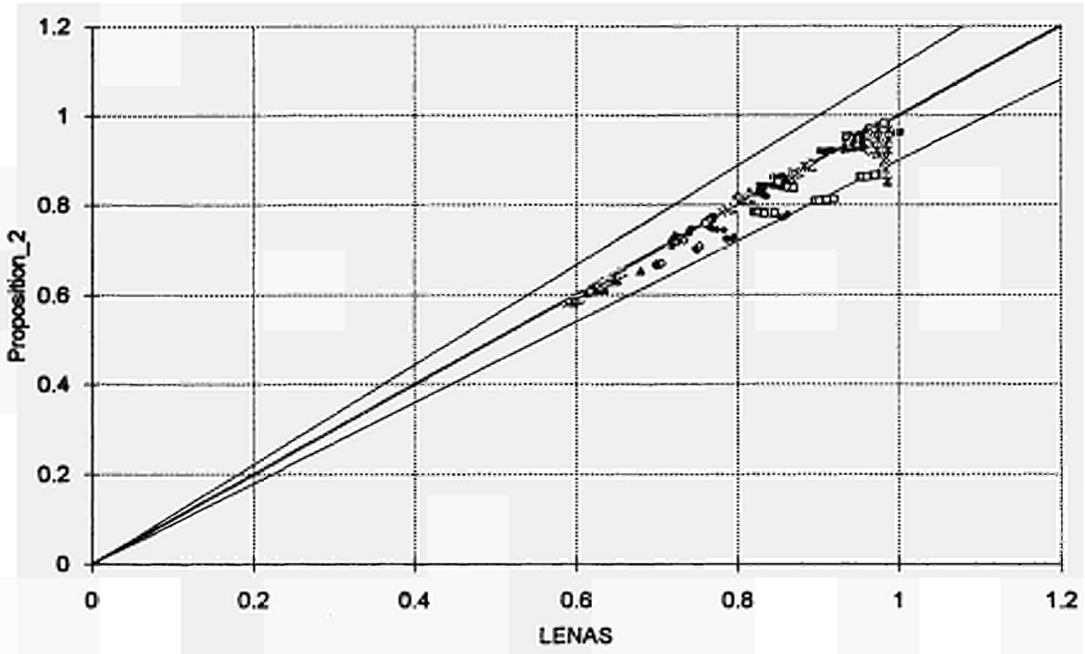

FIGURE 14.19 Formula - numerical results comparison at 600°C for buckling about major axis and triangular moment distribution

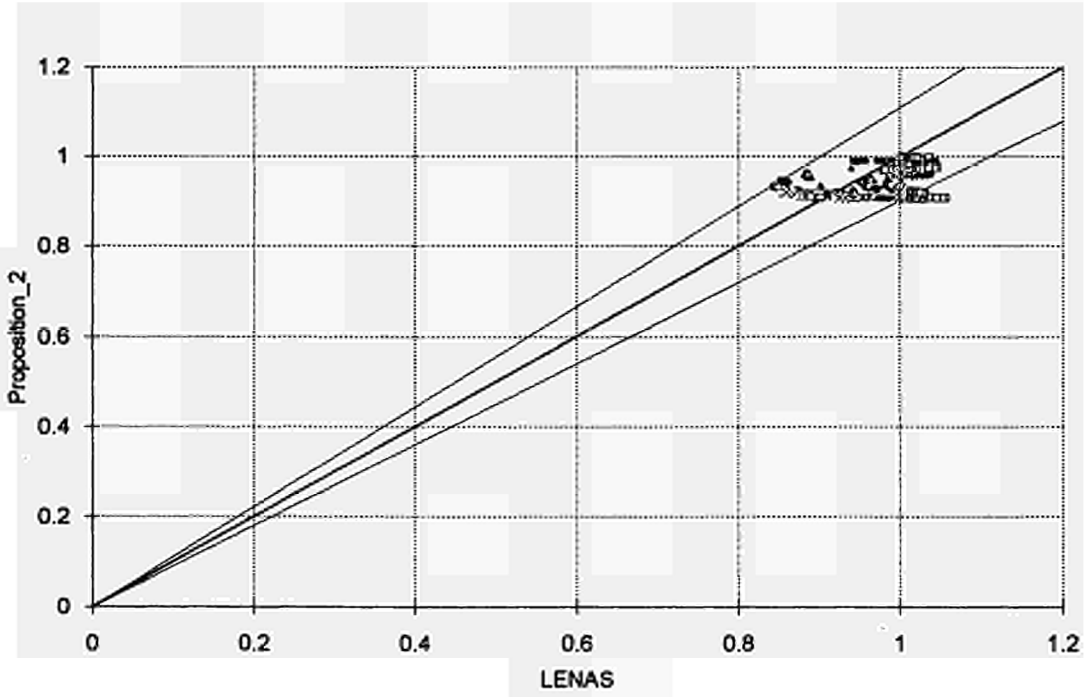

FIGURE 14.20 Formula - numerical results comparison at 600°C for buckling about major axis and bi-triangular moment distribution

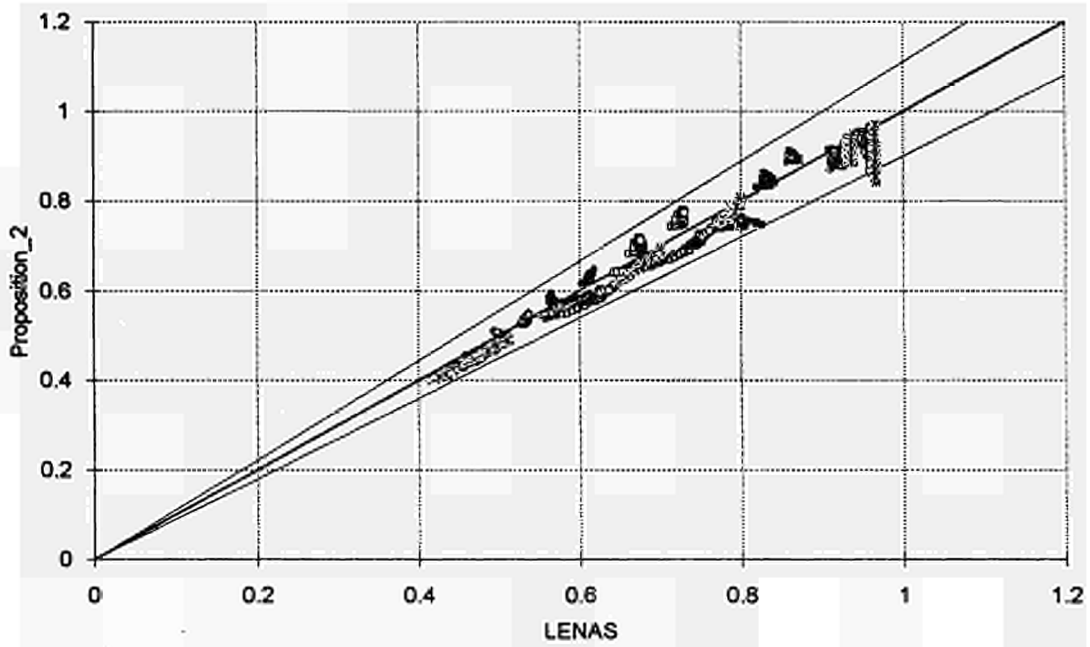

FIGURE 14.21 Formula - numerical results comparison at 700°C for buckling about minor axis and uniform moment distribution

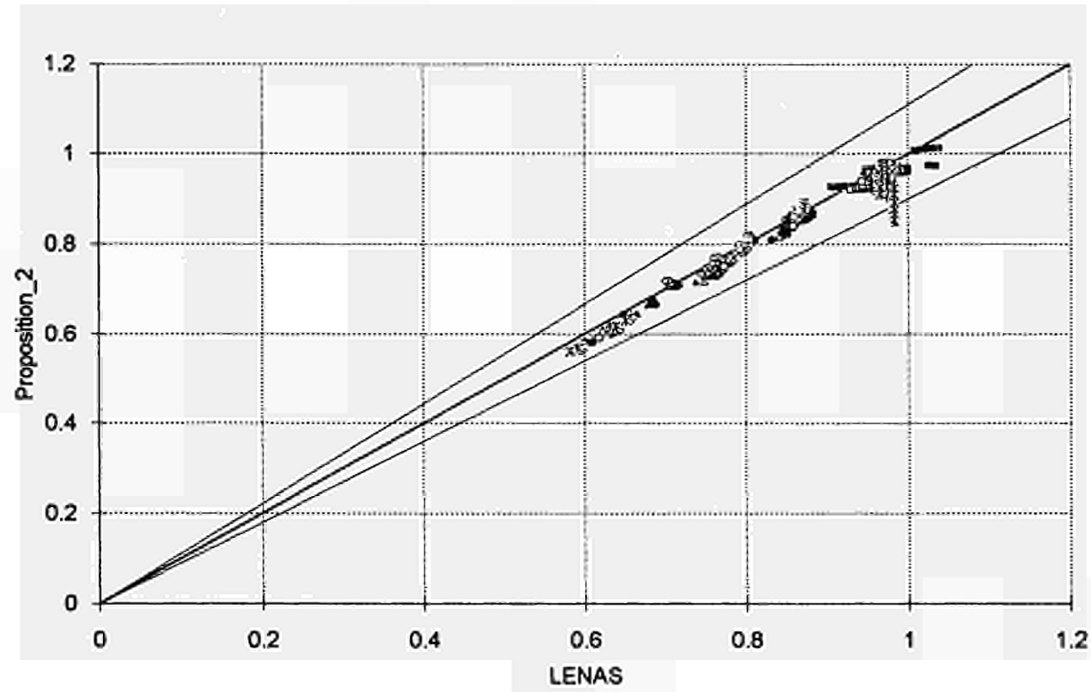

FIGURE 14.22 Formula - numerical results comparison at 700°C for buckling about minor axis and triangular moment distribution

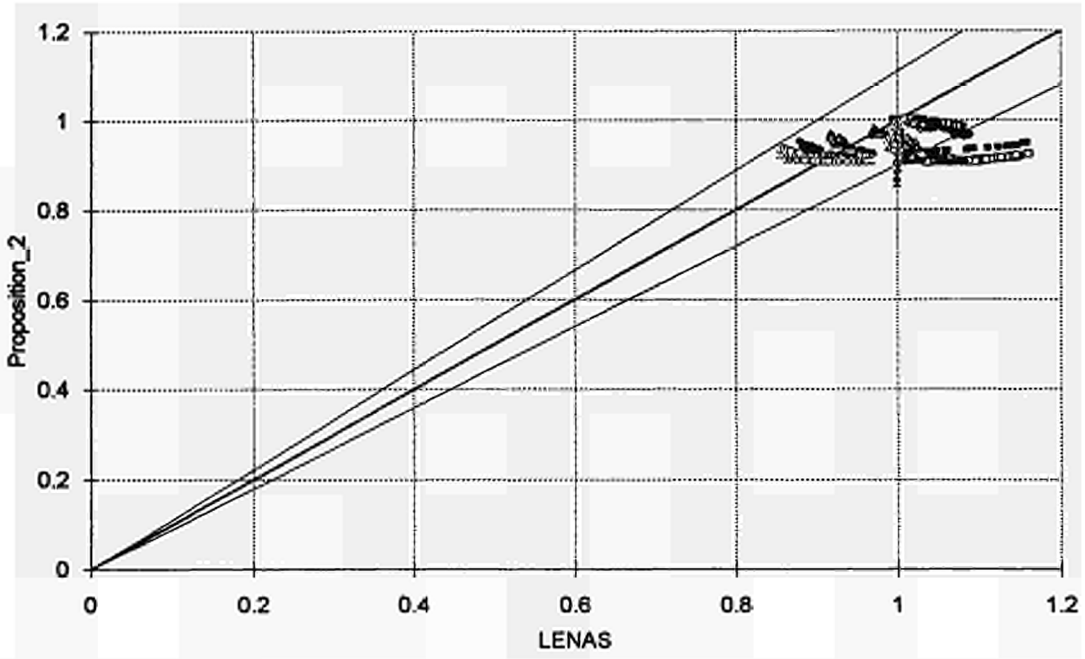

FIGURE 14.23 Formula - numerical results comparison at 700°C for buckling about minor axis and bi-triangular moment distribution

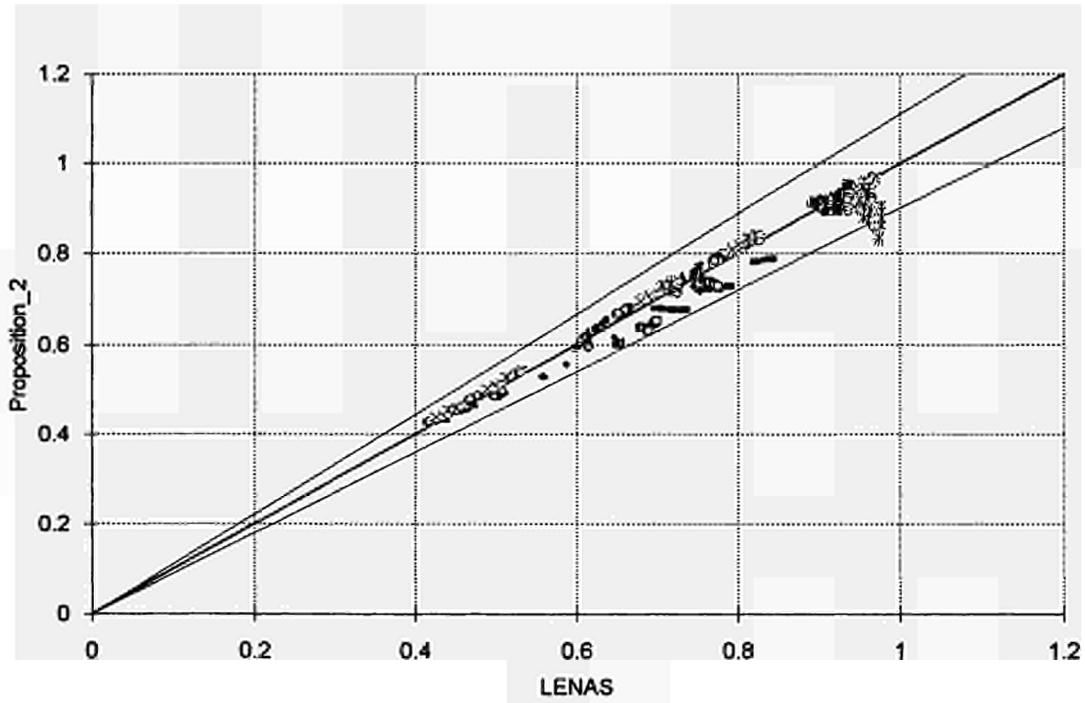

FIGURE 14.24 Formula - numerical results comparison at 700°C for buckling about major axis and uniform moment distribution

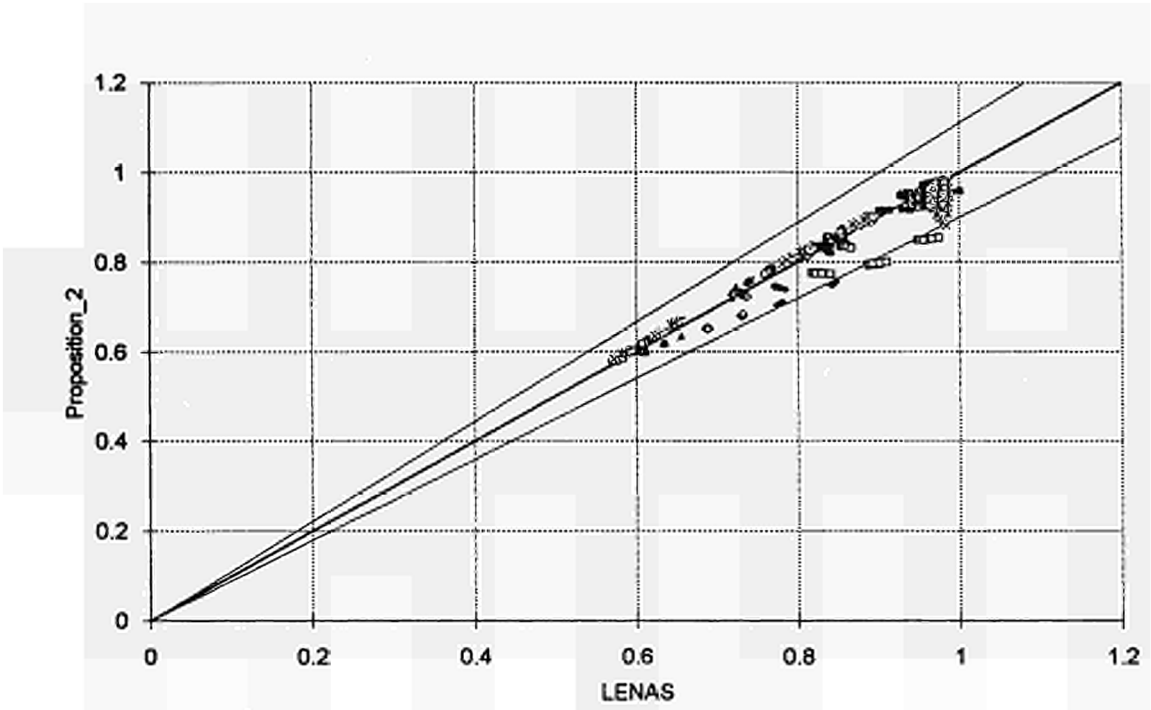

FIGURE 14.25 Formula - numerical results comparison at 700°C for buckling about major axis and triangular moment distribution

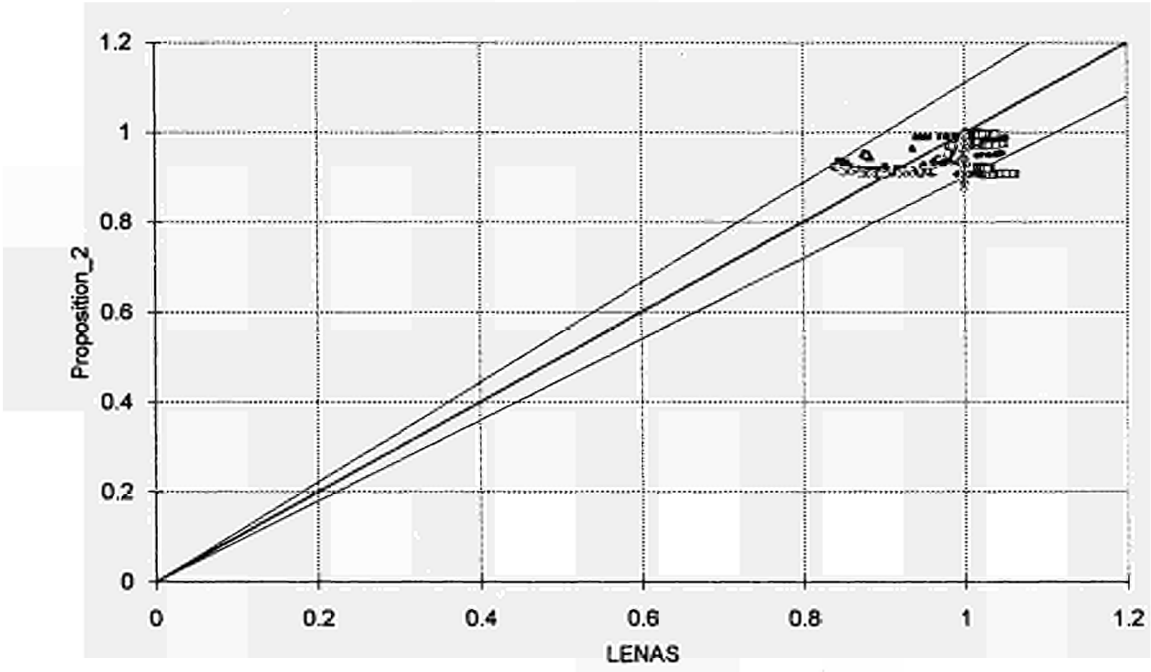

FIGURE 14.26 Formula - numerical results comparison at 700°C for buckling about major axis and bi-triangular moment distribution

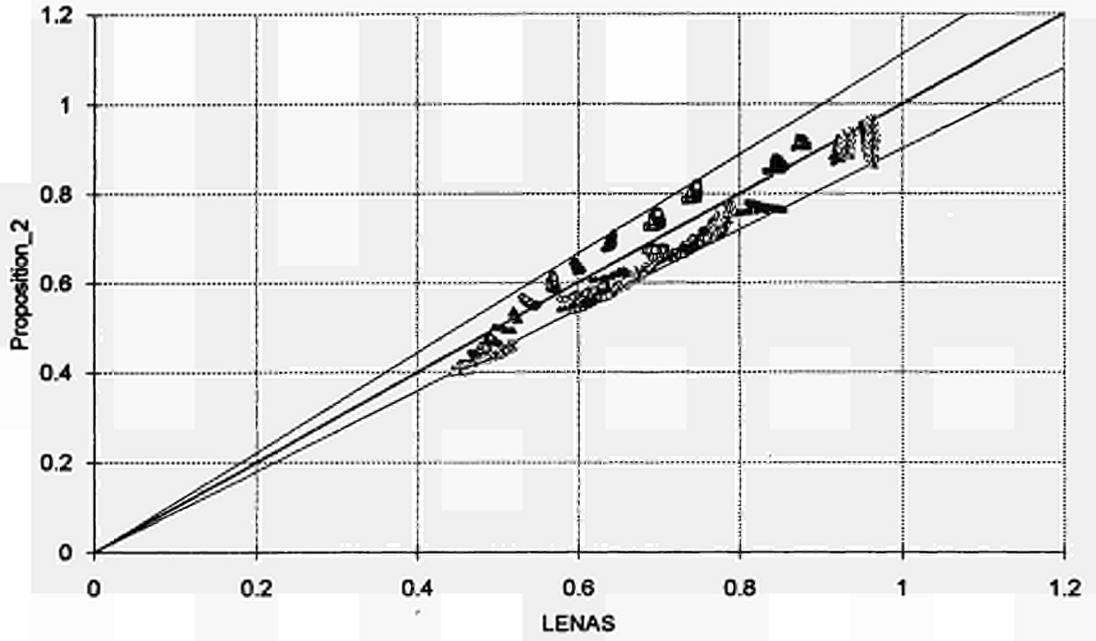

FIGURE 14.27 Formula - numerical results comparison at 800°C for buckling about minor axis and uniform moment distribution

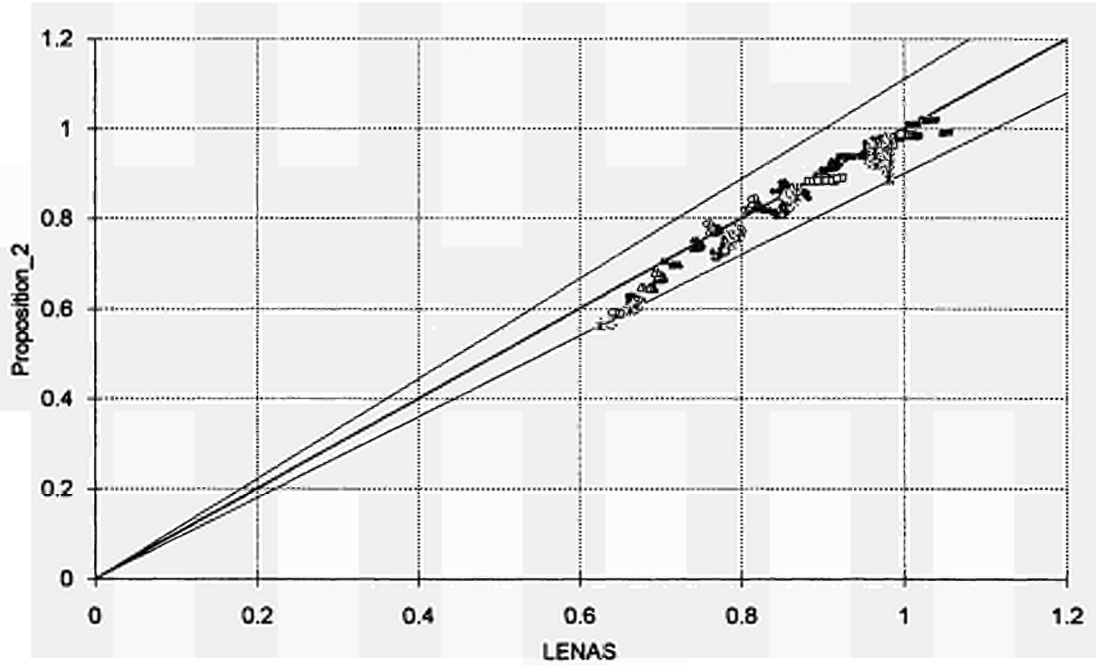

FIGURE 14.28 Formula - numerical results comparison at 800°C for buckling about minor axis and triangular moment distribution

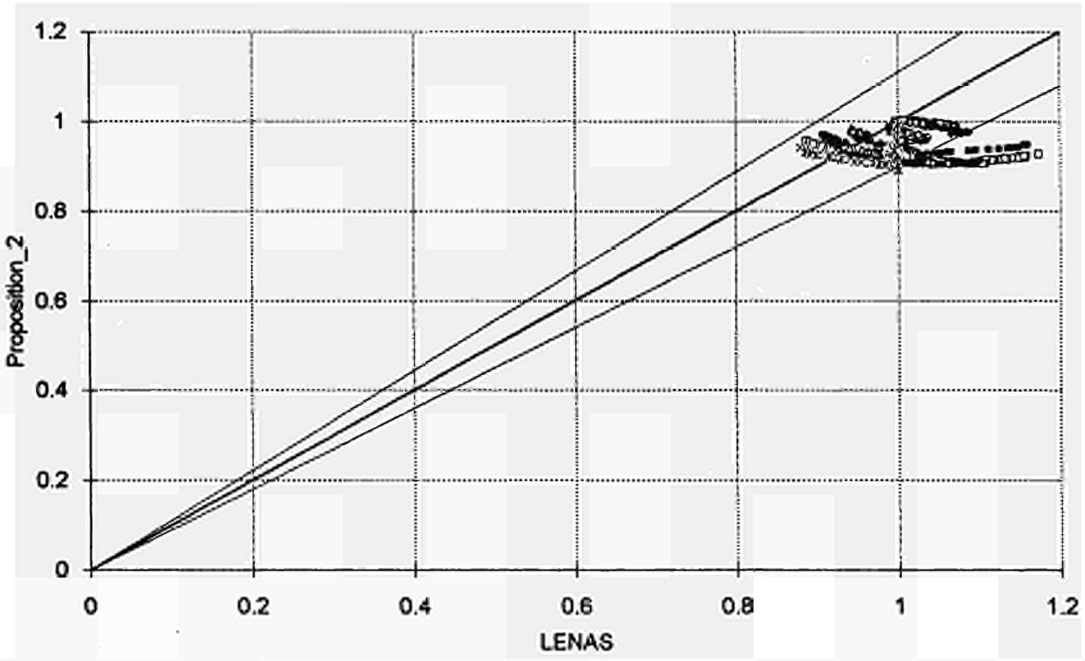

FIGURE 14.29 Formula - numerical results comparison at 800°C for buckling about minor axis and bi-triangular moment distribution

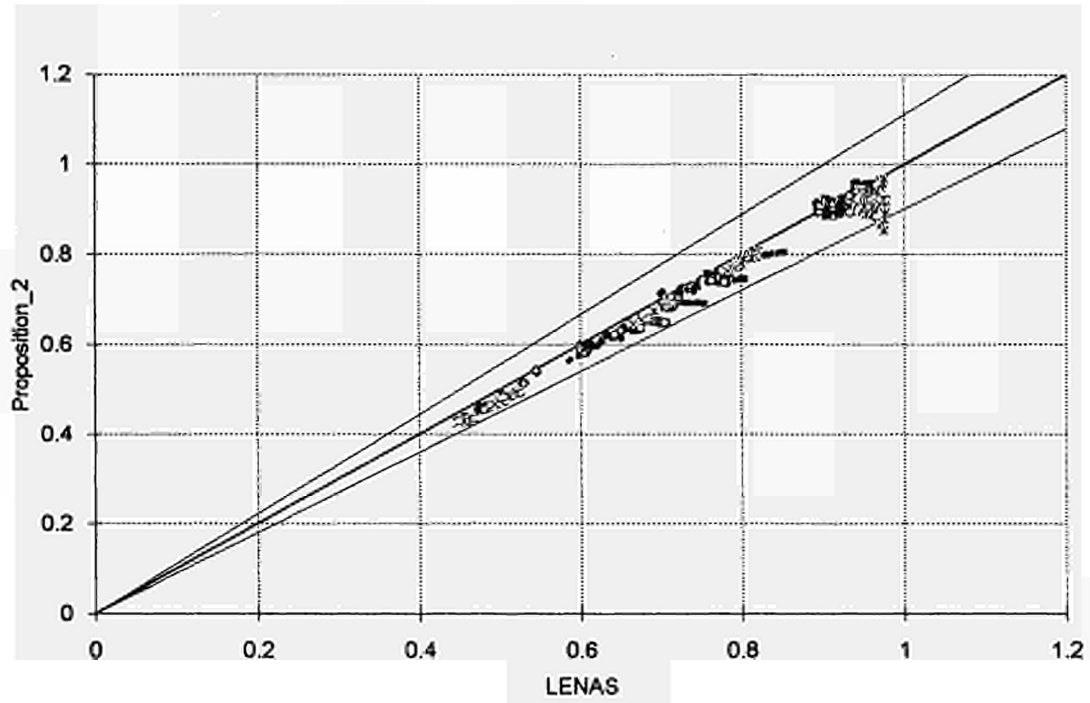

FIGURE 14.30 Formula - numerical results comparison at 800°C for buckling about major axis and uniform moment distribution

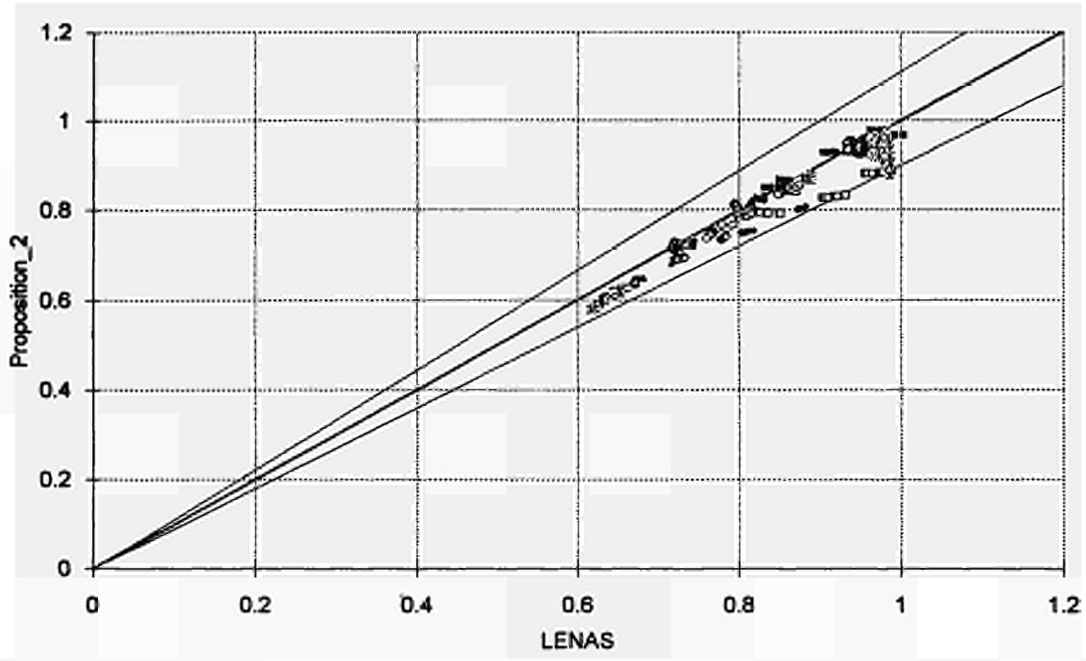

FIGURE 14.31 Formula - numerical results comparison at 800°C for buckling about major axis and triangular moment distribution

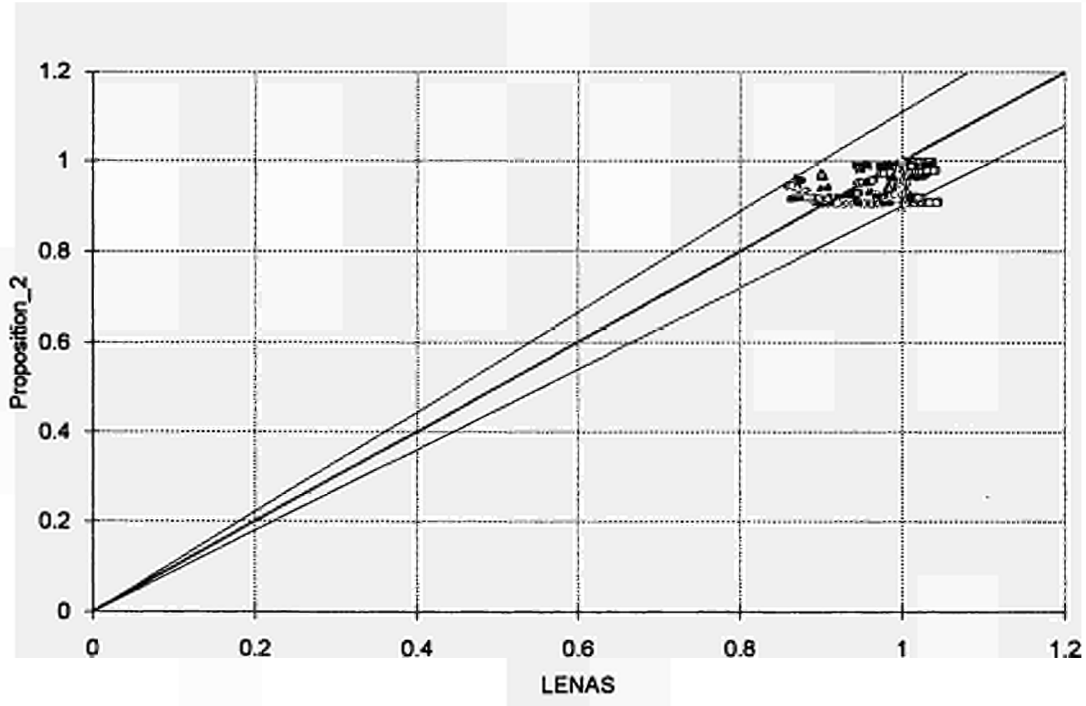

FIGURE 14.32 Formula - numerical results comparison at 800°C for buckling about major axis and bi-triangular moment distribution

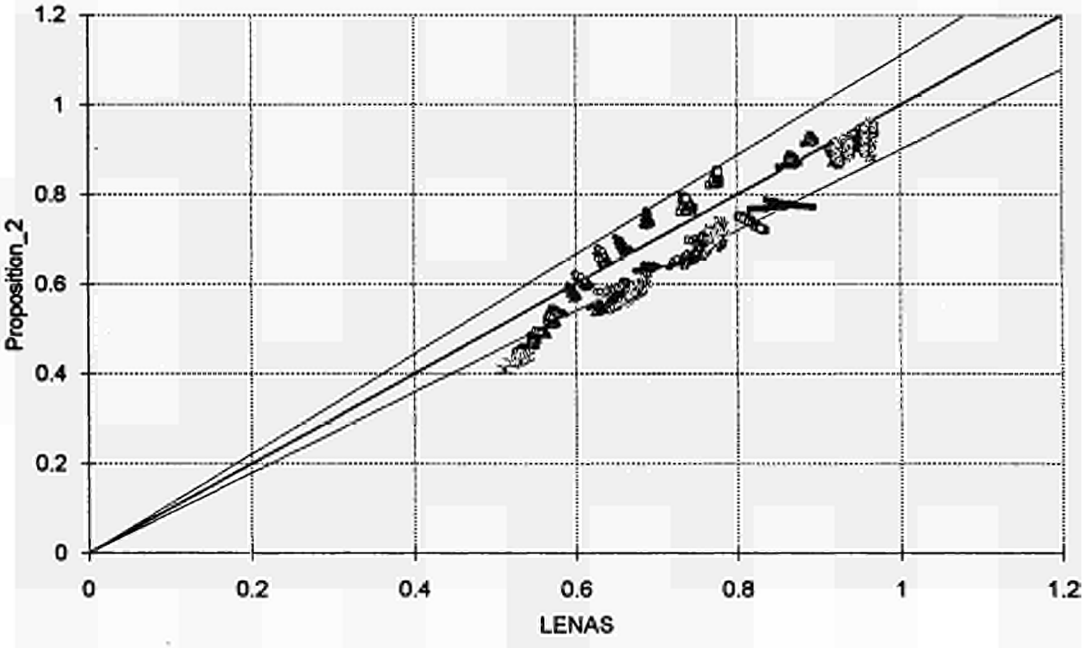

FIGURE 14.33 Formula - numerical results comparison at 900°C for buckling about minor axis and uniform moment distribution

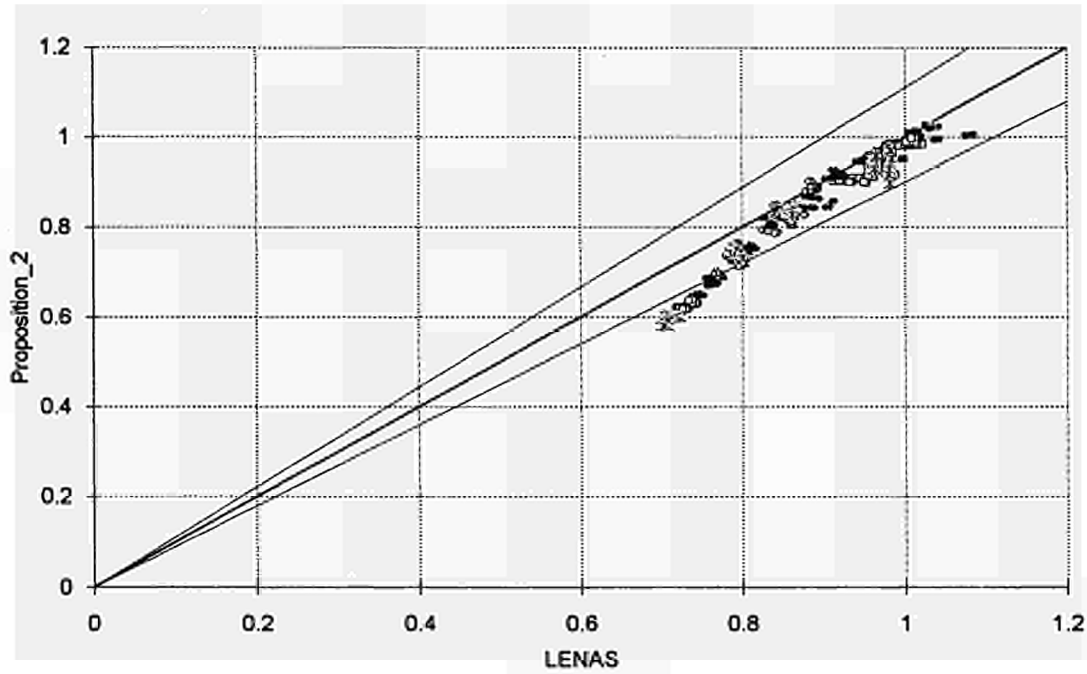

FIGURE 14.34 Formula - numerical results comparison at 900°C for buckling about minor axis and triangular moment distribution

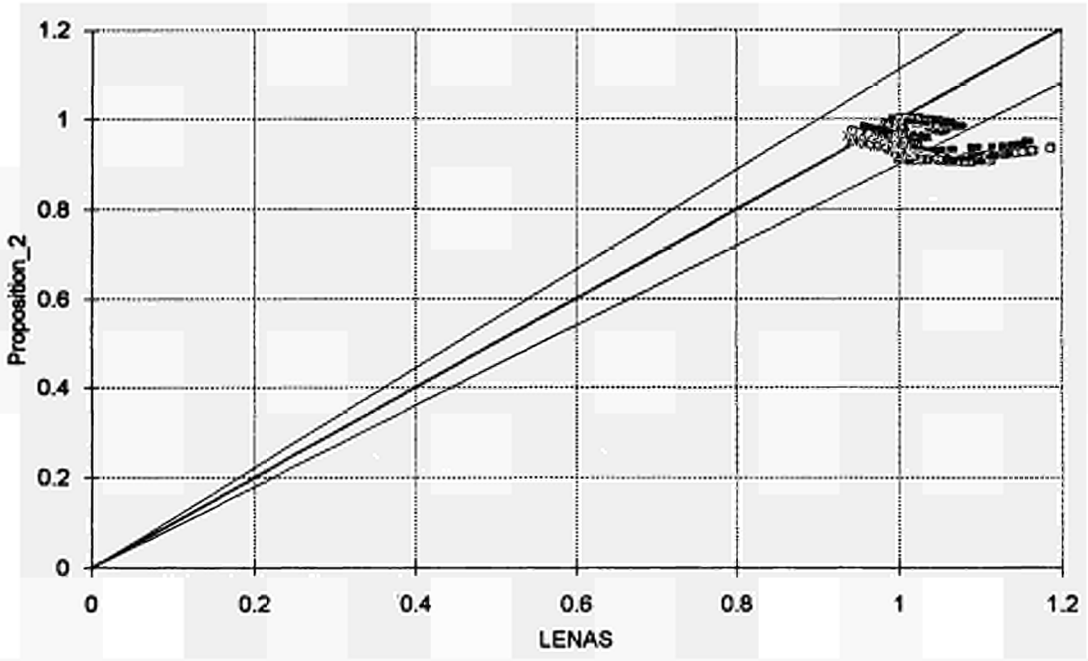

FIGURE 14.35 Formula - numerical results comparison at 900°C for buckling about minor axis and bi-triangular moment distribution

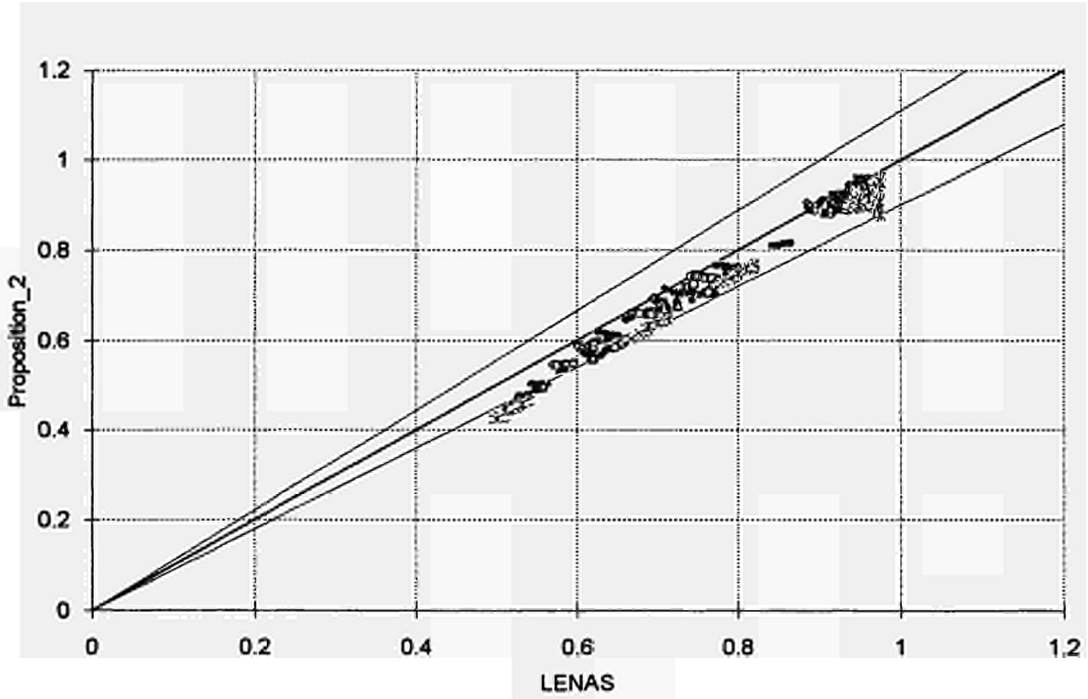

FIGURE 14.36 Formula - numerical results comparison at 900°C for buckling about major axis and uniform moment distribution

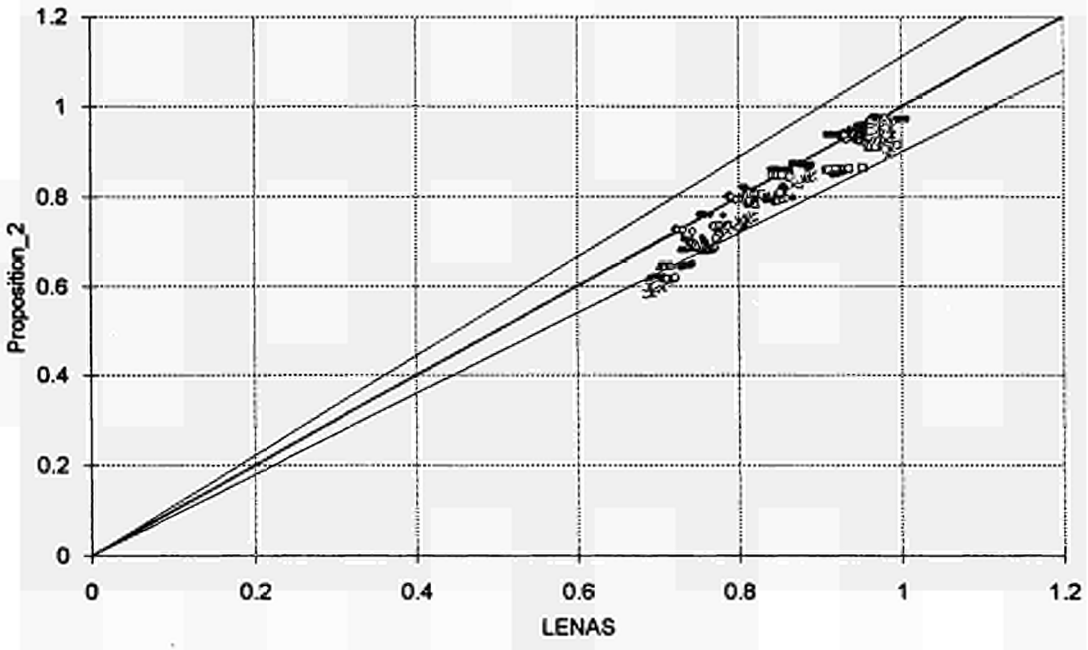

FIGURE 14.37 Formula - numerical results comparison at 900°C for buckling about major axis and triangular moment distribution

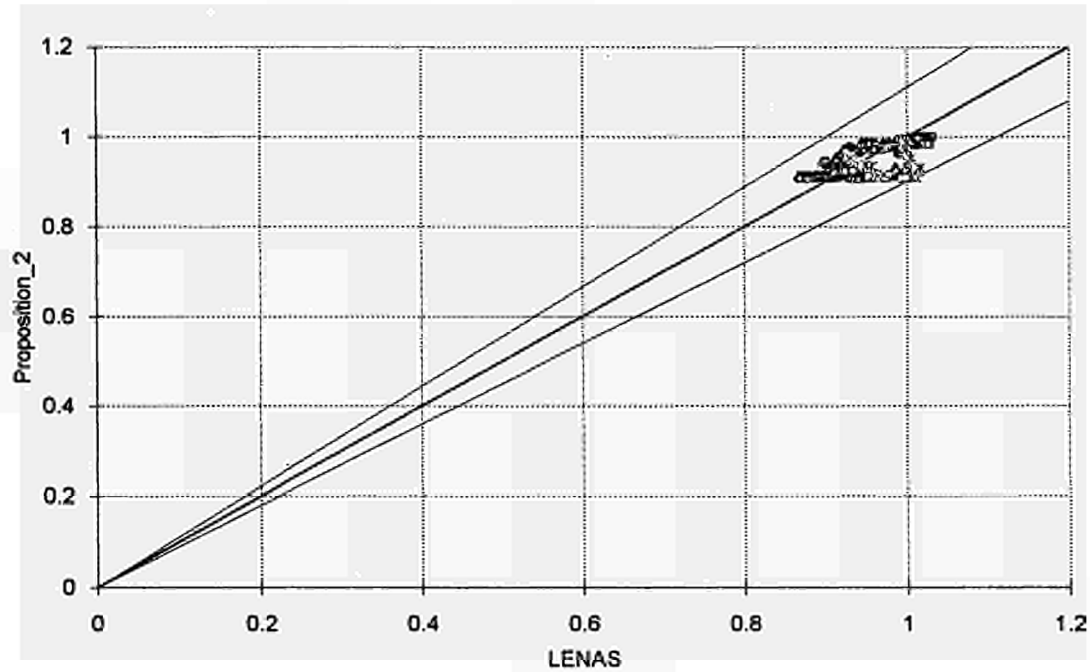

FIGURE 14.38 Formula - numerical results comparison at 900°C for buckling about major axis and bi-triangular moment distribution

ANNEX 15:

15. SIMPLIFICATION IN THE FORMULAE FOR CENTRALLY LOADED COLUMN FOR $\overline{\lambda} < 0,8$

In the formulae $\overline{\lambda}_\theta$ is dependent upon the temperature, which implies that the procedure is iterative if the critical temperature is unknown. That's why it is interesting to study the influence on the formula if the relative slenderness ratio $\overline{\lambda}$ at room temperature is considered instead of $\overline{\lambda}_\theta$.

If the method with $\overline{\lambda}$ at room temperature is applied to the database, the severity factor becomes 1,0 and it appears that method is, in an average, safe for slenderness smaller than 0,9 and unsafe for higher slenderness (see FIGURE 15.1 and FIGURE 15.2). The FIGURE 15.3 represents $\frac{100\left[N(\overline{\lambda_\theta}) - N(\overline{\lambda})\right]}{N(\overline{\lambda_\theta})}$ as a function of $\overline{\lambda}$ the slenderness at 20 °C. For small slenderness ($\overline{\lambda} < 0,5$), the use of $\overline{\lambda}$ is on the safe side for all the temperatures. If $\overline{\lambda}$ is replaced by 1,2 $\overline{\lambda}$, then the FIGURE 15.4 is obtained. Up to a value of 0,8 for $\overline{\lambda}$, the differences remain less than 10 %. That's why it can be concluded that $\overline{\lambda}_{(\theta)}$ can be taken equal to 1,2 $\overline{\lambda}$ for the calculation of χ_θ if $\overline{\lambda}$ is smaller than 0,8.

FIGURE 15.1

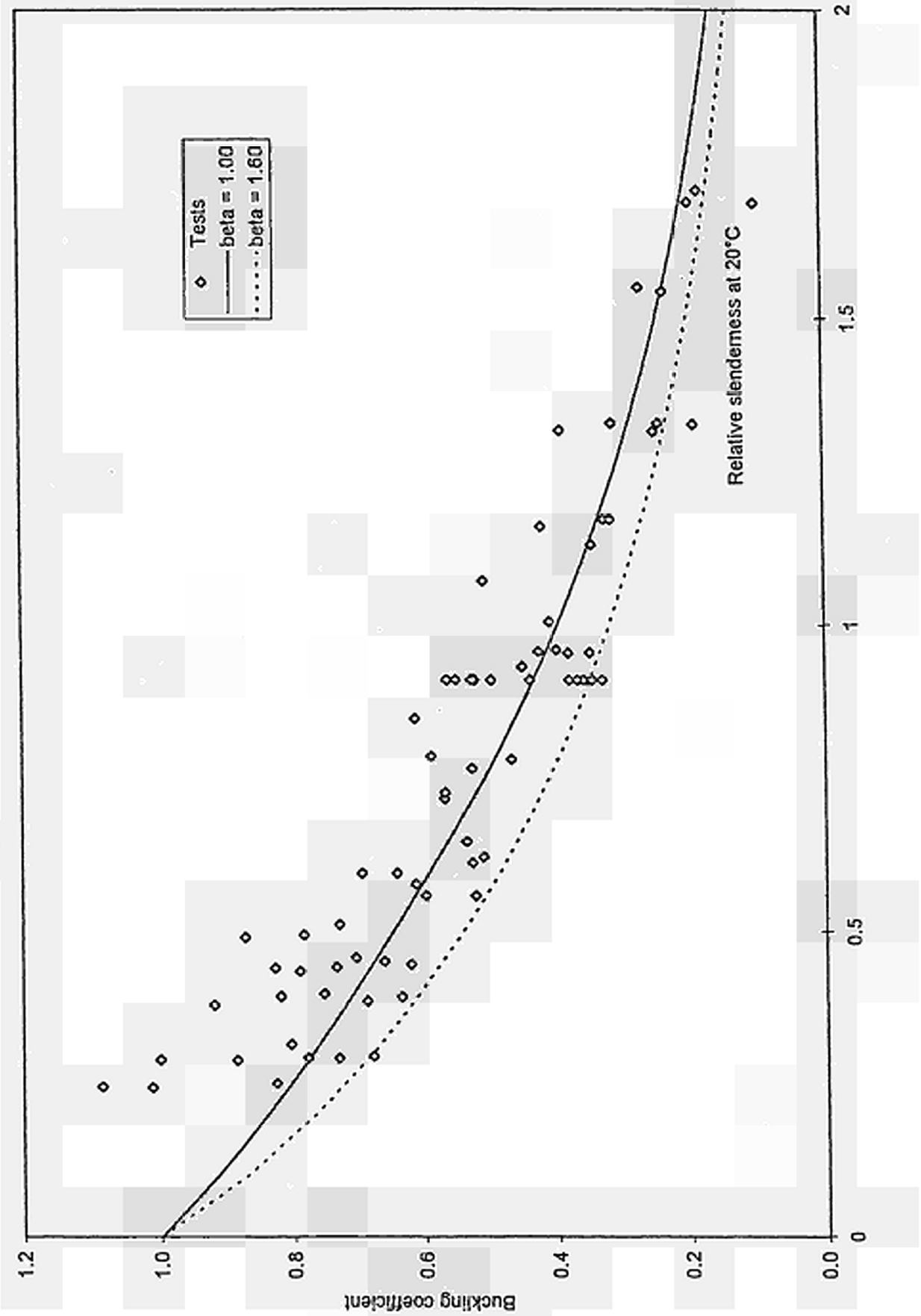
Tests
beta = 1.00
beta = 1.60
Buckling coefficient
Relative slenderness at 20°C
1.2
1.0
0.8
0.6
0.4
0.2
0.0
0
0.5
1
1.5
2

FIGURE 15.2

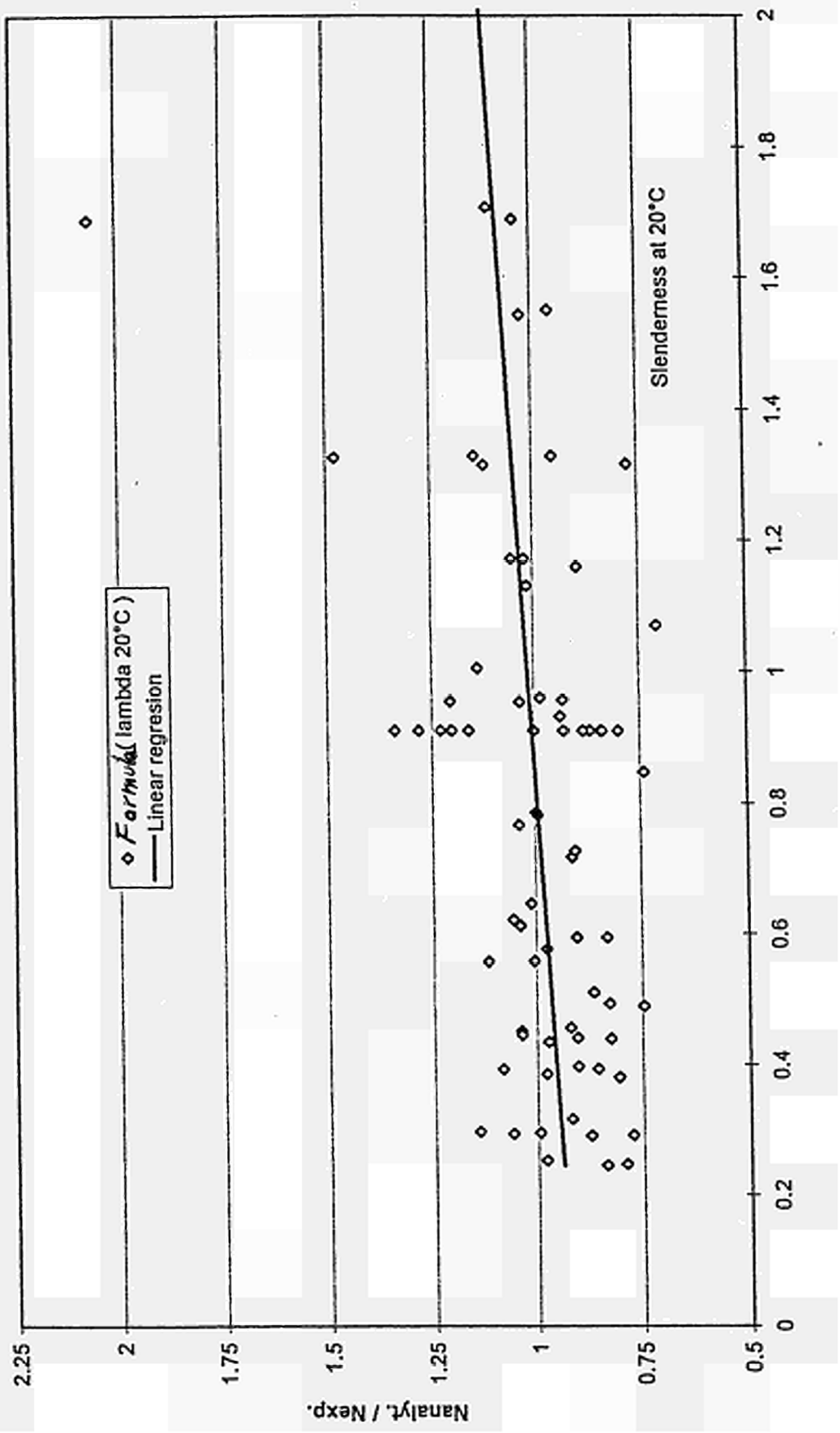
Nanalyt. / Nexp.
Slenderness at 20°C
Farwati(lambda 20°C)
Linear regresion
2.25
2
1.75
1.5
1.25
1
0.75
0.5
0
0.2
0.4
0.6
0.8
1
1.2
1.4
1.6
1.8
2

FIGURE 15.3

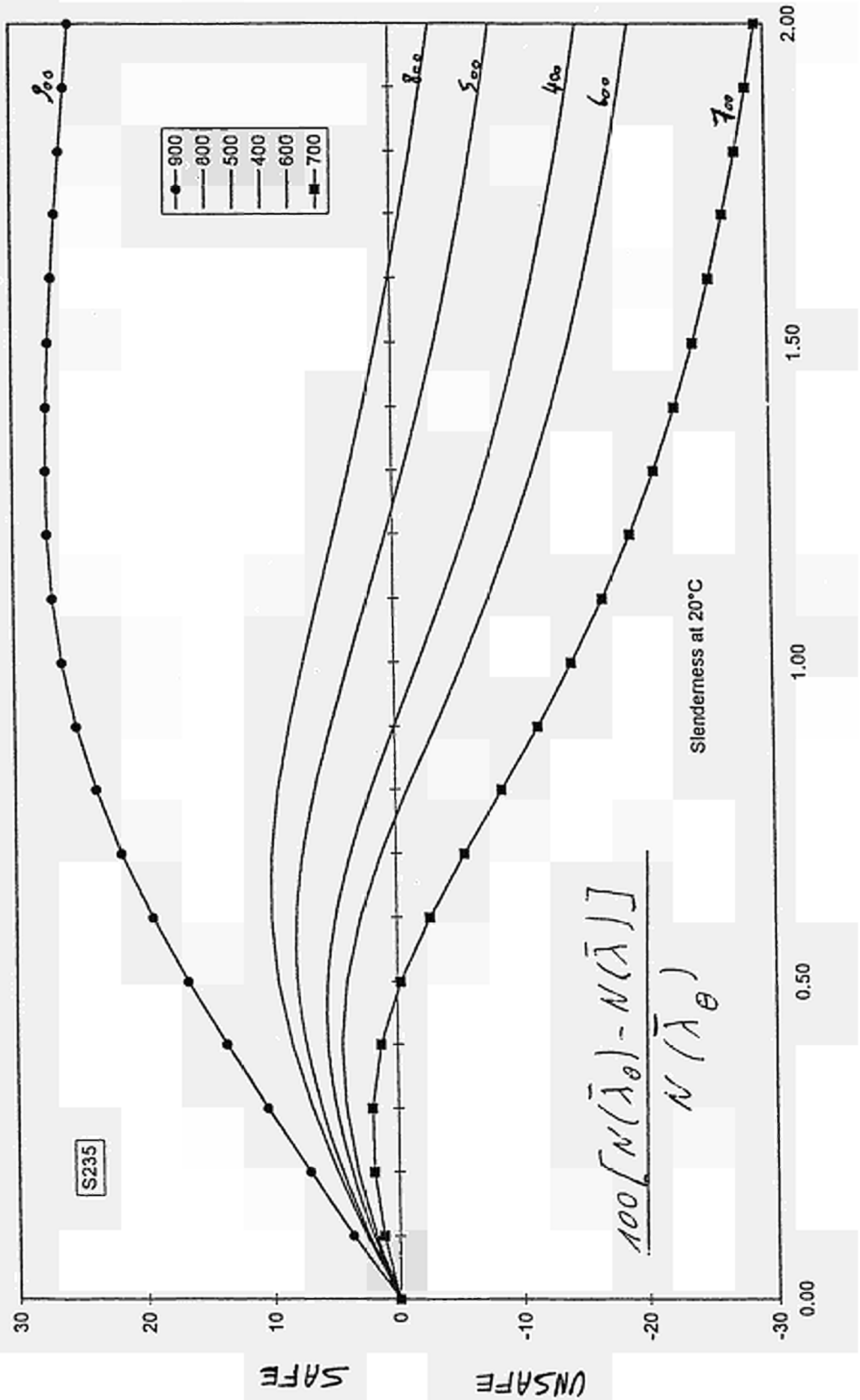
900
800
500
400
600
700
S235
Slenderness at 20°C
SAFE
UNSAFE
30
20
10
0
-10
-20
-30
0.00
0.50
1.00
1.50
2.00

FIGURE 15.4

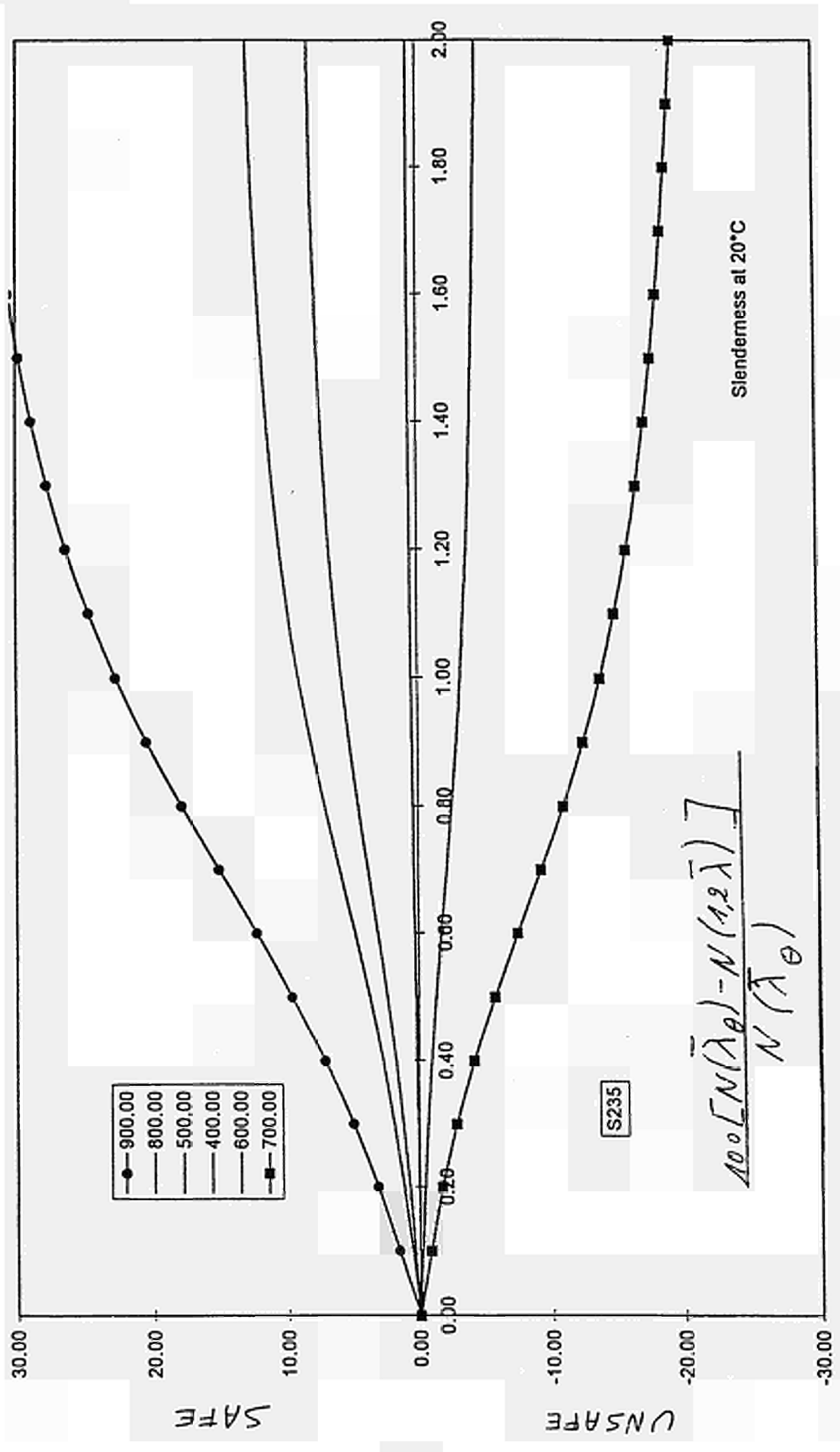
SAFE
UNSAFE
30.00
20.00
10.00
0.00
-10.00
-20.00
-30.00
0.00
0.20
0.40
0.60
0.80
1.00
1.20
1.40
1.60
1.80
2.00
900.00
800.00
500.00
400.00
600.00
700.00
S235
Slenderness at 20°C

ANNEX 16:

16. ECCS NO 89 "FIRE RESISTANCE OF STEEL STRUCTURES" - NOMOGRAM. SEPTEMBER 1995

ECCS N° 89

Fire Resistance of Steel Structures

(On the basis of ENV 1993 part 1-2 "Design of steel structures - Structural fire design") Sept. 1995

ECCS CECM E K S

1. Introduction

The required fire resistance of steel structures - in terms of fire resistance classes R30/R60/R90 etc. - is given by national regulations. These requirements should consider the number of floors, the use of the building, the fire load, the number of people and the favourable effect of active measures, such as sprinklers, automatic fire detection, and type and proximity of the fire brigade.

The assessment of the fire resistance of structural elements is based either on standard fire tests in furnaces or on calculation. This Technical Note describes calculation methods for unprotected and protected internal steelwork based on the European prestandard ENV 1993-1-2 [1], [2].

2. Principles of Calculation

2.1 Steel temperature

The increase in steel temperature is given by the following factors:

a) The section factor (A_m/V): i.e. the relation between the surface area exposed to the heat flux and the volume of the member per unit length. Calculation methods and values of (A_m/V) for common sections are given in Section 5.

b) The thermal properties of a fire protection material: i.e. thermal conductivity λ_p, its specific heat c_p and its thickness d_p. Thermal properties for various protection materials are given in Section 4. At present no European Norm is available to determine λ_p. Therefore product specifications must be obtained in each country from approved testing laboratories, or other expert institutes on condition that they are based on officially approved tests (Section 10).

c) For fire protection material containing water, the evaporation of the water causes a delay of the temperature increase of the steel when the temperature of the steel reaches 100°C (Example A1).

2.2 Mechanical properties of steel at elevated temperatures

Steel properties change with temperature (Fig. 1). For a member at a uniform temperature, called critical temperature Θ_{cr}, the load bearing capacity becomes equal to the effect of the applied loads. Failure will then occur.

The critical temperature is determined by the level of the applied load (action), expressed as the degree of utilisation in fire, given by

$$\mu_0 = E_{fi,d} / R_{fi,d,0}$$

$E_{fi,d}$: the design effect of actions in fire

$R_{fi,d,0}$: the design resistance in fire, for time t = 0 (i.e. room temperature, $\gamma_M = \gamma_{M,fi} = 1.0$, support conditions for the fire situation: 0.5 L for intermediate, 0.7 L for top storey columns)

2.3 Temperature distribution

An adaptation factor κ is introduced to take account of a non-uniform temperature distribution over the height and alongside the steel section. The value of the adaptation factor κ should be taken as follows:

- beams:
  - exposed on all four sides: $\kappa = 1.0$
  - exposed on three sides, with a composite or concrete slab on side four: $\kappa = 0.7$
- statically indeterminate beams at support:
  - exposed on all four sides: $\kappa = 0.85$
  - exposed on three sides, with a composite or concrete slab on side four: $\kappa = 0.6$

Stability problems (to account for lower strain level) $\kappa = 1.2$

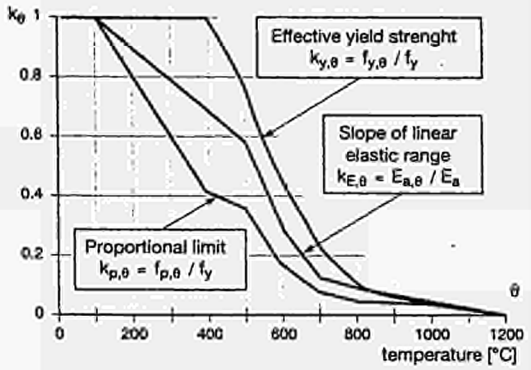

Fig. 1: Reduction factors for steel strength and stiffness at elevated temperatures

2.4 General assumptions

The calculation of the fire resistance is based on the following assumptions:

- the temperature increase follows the standard fire curve (ISO 834)
- uniform heating of the steel member. A non-uniform heat distribution is considered by the factor κ (Section 2.3)
- steel grades according to EN 10 025 (S 235, S 275, S 355) and EN 10113 (S 420, S 460)
- for member analysis, the effects of thermal expansion of the member may be neglected
- steel sections of classes 1, 2 or 3 (with $A_m/V > 10\ m^{-1}$). For sections of class 4 see example C.
- Temperature increase curves calculated for $\gamma_{n,r} = \gamma_{n,c} = 1.0$ according to ENV 1991-2-2. (If the National Application Document gives other values, see Section 10)
- Temperature increase curves for insulated steel calculated with $\phi = 0$ (Modification factors for other values see Section 4).

3. Calculation Procedure

- Calculate the degree of utilisation μ_0 (Section 2.2).
  For a preliminary design μ_0 may be taken as 0.6. This is normally a conservative assumption.
- The non-dimensional slenderness of a column is a function of the temperature Θ and has to be adapted for the calculation of μ_0:

$$\overline{\lambda}_{fi,\Theta,max} = \overline{\lambda}_{fi,0} \cdot \sqrt{k_{y,\Theta,max} / k_{E,\Theta,max}}$$

with Θ_{max} the steel temperature at failure

$$\mu_0 = E_{fi,d} / R_{fi,d,0}$$

$R_{fi,d,0}$ is calculated using $\overline{\lambda}_{fi,\Theta,max}$ as given above, the yield strength f_y at room temperature and buckling curve c.

The values of $\sqrt{k_{y,\Theta,max} / k_{E,\Theta,max}}$ are given in Table 1a.
The calculation procedure for columns is illustrated in Example D.
Table 1b gives directly the critical temperatures for intermediate columns and Table 1c for top storey columns.
For a preliminary design $\overline{\lambda}_{fi,\Theta,max} = 1.2 \cdot \overline{\lambda}_{fi,0}$ may be assumed.

- Determine the section factor. A_m/V for unprotected steel members and A_p/V for steel members insulated by fire protection material (Section 5). The thermal section factor $[(A_p/V) \cdot (\lambda_p/d_p)]$ can be derived according to Section 4 and 7.1 Example A1.
- The fire resistance time t_f is assessed by making use of the nomogram (see Section 6 and Examples in Section 7).
- A series of adaptation factors κ are considered by special curves on the left side of the nomogram.

– For a preliminary design the increase of the fire resistance time caused by the effects of moisture in the protection material may be added ($t_r = t_t + t_v$), if data is taken from Table 2. Evaporation time $t_v = (\rho \cdot \rho_p \cdot d_p^2) / (5 \cdot \lambda_p)$ [min]. No increase is allowed if the moisture is already considered implicitly in the national λ_p-values of the table in Section 10.

Tab. 1a Slenderness modification factor $\sqrt{k_{y,\Theta,max} / k_{E,\Theta,max}}$ at elevated temperatures

steel temp. Θ_a [°C]	300	400	500	600	700	800	900
$\sqrt{k_{y,\Theta,max} / k_{E,\Theta,max}}$	1.12	1.20	1.14	1.23	1.33	1.11	0.94

Tab. 1b Critical steel temperature of internal columns, for $\ell_{cr,fi,0} = 0.5\,L$, $\kappa = 1.2$

$\mu_{0,c}$	$\bar{\lambda}_{0,c}$ 0.20	0.40	0.60	0.80	1.00	1.20	1.40	1.60	1.80	2.00
0.30	642	648	658	671	686	701	717	732	744	754
0.35	618	625	635	648	664	679	691	699	710	718
0.40	597	605	615	629	645	660	673	682	688	693
0.45	579	586	597	611	628	644	657	666	673	677
0.50	561	569	580	595	613	629	642	652	659	663
0.55	545	553	565	580	598	615	629	639	646	651
0.60	529	538	550	567	585	603	617	627	635	640

Tab. 1c Critical steel temperature of top storey columns, for $\ell_{cr,fi,0} = 0.7\,L$, $\kappa = 1.2$

$\mu_{0,c}$	$\bar{\lambda}_{0,c}$ 0.20	0.40	0.60	0.80	1.00	1.20	1.40	1.60	1.80	2.00
0.30	638	640	643	648	652	656	658	660	661	662
0.35	614	617	621	626	631	635	638	640	642	642
0.40	594	596	601	606	613	617	621	623	624	625
0.45	575	578	583	589	596	601	605	608	609	610
0.50	557	561	566	573	581	586	591	593	595	597
0.55	540	544	550	558	566	573	577	580	582	584
0.60	524	528	535	544	553	560	565	568	570	572

$\mu_{0,c}$ = design load in fire / design buckling resistance for: $\Theta = 20°$, $\ell_{fi} = 1.0\,L$, buckling curve c, $\gamma_{M,fi} = 1.0$

$\bar{\lambda}_{0,c}$ = non dimensional slenderness of column for $\ell_{fi} = 1.0\,L$

4. Properties of Fire Protection Material

Table 2: General properties for preliminary design*. The following material properties may be used to calculate the modified section factor:

$$\frac{A_p}{V} \cdot \frac{\lambda_p}{d_p} \cdot \frac{1}{1 + \phi/2}; \qquad \phi = \frac{c_p \cdot d_p \cdot \rho_p \cdot A_p}{c_a \cdot \rho_a \cdot V}$$

As simplification ϕ may be taken equal to 0 (this leads to conservative results). The delay t_v caused by the moisture content of the protection material may be considered according to Example A1. The protection material must be fixed in such a way that it will keep its protective function during the required fire resistance time.

Material	unit mass ρ_p [kg / m³]	moisture content ρ [%]	thermal conductivity λ_p [W / (m·K)]	specific heat c_p [J/(kg·K)]
Sprays				
- mineral fibre	300	1	0.12	1200
- vermiculite cement	350	15	0.12	1200
- perlite	350	15	0.12	1200
High-density sprays				
- vermiculite (or perlite) and cement	550	15	0.12	1100
- vermiculite (or perlite) and gypsum	650	15	0.12	1100
Boards				
- vermiculite (or perlite) and cement	800	15	0.20	1200
- fibre-silicate or fibre-calcium-silicate	600	3	0.15	1200
- fibre-cement	800	5	0.15	1200
- gypsum board	800	20	0.20	1700
Compressed fibre boards				
- fibre silicate, mineral-wool, stone-wool	150	2	0.20	1200
Concrete	2300	4	1.60	1000
Light weight concrete	1600	5	0.80	840
Concrete bricks	2200	8	1.00	1200
Bricks with holes	1000	-	0.40	1200
Solid bricks	2000	-	1.20	1200

* Properties obtained by national fire tests of trade products are given in Section 10 on the last page of this technical note

5. Section factors

5.1 Unprotected steel members

Section factor: $\frac{A_m}{V} = \frac{\text{exposed surface area per unit length}}{\text{volume of the member per unit length}}$

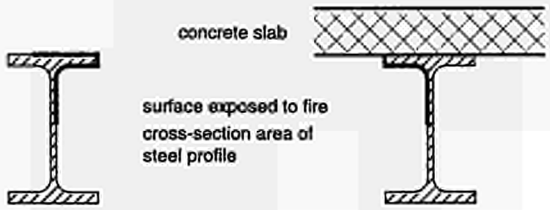

Examples:

Description	A_m / V
flat bar	exposed to fire on all sides: $= 2/t$ exposed to fire on one sides: $= 1/t$
Open section with uniform thickness	exposed to fire on all sides: $= 2/t$
Hollow section with uniform thickness	exposed to fire from outside: $= 1/t$
Solid section	exposed to fire on all sides: $= 4/d$

5.2 Steel members insulated by fire protection material

Section factor $\frac{A_p}{V} = \frac{\text{inner contour of encasement}}{\text{steel cross-section area}}$

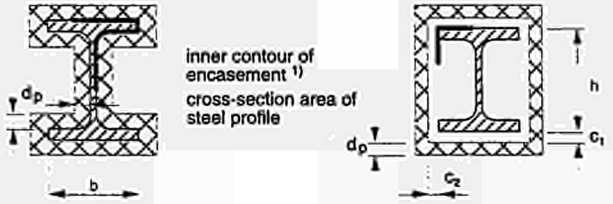

Examples:

Description	A_p / V
Contour encasement of uniform thickness. Hollow encasement 1) of uniform thickness.	Contour encasement: $\frac{\text{steel perimeter}}{\text{steel cross-section area}}$ Hollow encasement: $\frac{2\,(b + h)}{\text{steel cross-section area}}$ 1)
Contour encasement of uniform thickness, exposed to fire on three sides. Hollow encasement 1) of uniform thickness, exposed to fire on three sides.	Contour encasement: $\frac{\text{steel perimeter} - b}{\text{steel cross-section area}}$ Hollow encasement: $\frac{(2h + b)}{\text{steel cross-section area}}$ 1)

1) The clearance dimensions c_1 and c_2 should not normally exceed h/4

Legend: insulation (with thickness d_p); steel cross section; inner contour A_p

5.3 Section factors A_m/V (resp. A_p/V) in [m^{-1}] for hot rolled profiles

UNP				
80	283	227	242	186
100	275	222	238	185
120	255	205	222	173
140	239	196	210	166
160	227	187	200	160
180	218	178	193	153
200	205	170	182	147
220	192	160	170	139
240	183	153	163	133
260	172	144	154	126
280	167	140	149	122
300	161	138	144	119
320	129	110	116	97
350	135	116	122	103
380	138	119	125	107
400	129	111	117	99
UAP				
80	308	234	266	192
100	290	224	253	187
130	267	211	236	180
150	239	189	211	160
175	226	181	201	155
200	213	172	190	148
220	205	165	183	143
250	188	153	168	134
(270)	180	146	161	127
300	167	137	150	119

IPE				
80	430	329	370	269
100	389	301	335	247
120	359	278	310	230
140	335	259	290	215
160	309	240	268	200
180	292	228	254	188
200	269	210	234	175
220	253	197	221	164
240	235	184	204	153
270	226	178	197	147
300	215	167	187	139
330	199	156	174	131
360	165	145	162	122
400	174	137	152	116
450	163	129	143	110
500	150	120	132	103
550	140	113	124	97
600	129	105	115	91
750 · 137	143	116	128	101
147	134	109	120	95
173	114	93	102	81
196	102	83	91	72
IPEA				
140	408	313	354	259
160	382	295	331	244
180	354	270	308	227
200	325	253	282	210
220	298	231	259	192
240	276	214	240	178
270	265	205	222	170
300	249	192	208	160
330	228	178	199	149
360	211	165	182	138
400	200	158	175	133
450	187	149	165	126
500	172	138	152	118
550	161	129	143	111
600	147	119	131	103

INP				
80	401	321	345	286
100	349	283	301	235
120	309	250	268	209
140	274	225	238	189
160	252	205	219	172
180	229	187	200	158
200	211	173	184	146
220	195	160	171	135
240	183	150	160	127
260	169	139	148	118
280	158	130	138	111
300	149	123	131	104
320	140	115	123	99
340	132	109	116	94
360	124	103	109	88
380	118	98	104	85
400	112	94	99	80
450	100	84	89	72
500	90	76	80	85
550	84	70	75	61
600	75	64	67	55

HEA				
100	265	184	217	137
120	267	185	220	137
140	252	173	208	129
160	230	160	189	119
180	225	155	185	115
200	211	145	174	107
220	196	133	161	99
240	178	122	147	91
260	170	117	140	87
280	164	113	135	84
300	152	104	126	78
320	141	98	117	74
340	134	94	111	71
360	128	91	107	70
400	120	86	101	67
450	112	83	96	66
500	106	80	91	64
550	104	79	90	65
600	102	78	88	65
650	99	77	87	65
700	96	76	84	64
800	94	76	83	65
900	90	74	81	64
1000	89	74	80	65
HEAA				
100	354	244	290	180
120	360	246	295	182
140	341	232	280	172
160	296	202	244	150
180	278	190	229	140
200	256	174	210	129
220	242	165	199	122
240	225	153	185	114
260	213	146	176	108
280	204	139	168	103
300	191	131	158	97
320	183	127	152	95
340	176	123	146	93
360	170	119	142	91
400	160	115	135	89
450	156	114	132	90
500	151	112	129	90
550	142	107	122	87
600	138	106	120	67
650	134	104	117	87
700	129	101	113	85
800	121	97	108	84
900	113	92	101	80
1000	108	90	97	79

HEB				
100	218	153	179	115
120	201	141	166	105
140	187	130	154	97
160	169	117	139	88
180	157	110	130	82
200	147	102	121	76
220	139	96	115	72
240	130	90	107	67
260	126	87	104	65
280	123	85	102	63
300	116	80	95	60
320	109	76	91	58
340	105	74	88	57
360	102	73	85	56
400	97	70	82	55
450	91	68	77	55
500	88	67	76	54
550	87	66	75	55
600	85	66	74	55
650	84	66	74	55
700	82	65	72	55
800	81	65	72	56
900	78	64	70	56
1000	77	65	70	57
HEM				
100	116	85	96	65
120	111	80	92	61
140	103	75	85	57
160	99	71	82	54
180	96	68	79	51
200	91	64	75	49
220	88	62	73	47
240	73	51	60	39
260	71	50	59	38
280	70	49	58	37
300	60	42	50	32
320	59	42	50	32
340	60	43	50	33
360	60	44	50	34
400	61	45	52	35
450	62	46	53	37
500	63	48	54	39
550	64	49	55	40
600	65	50	56	42
HHD				
260 · 54	213	146	176	108
68	170	117	140	87
93	126	87	104	65
114	104	72	86	54
142	85	60	71	46
172	71	50	59	38
225	56	40	47	31
299	44	32	37	25
320 · 74	183	127	152	95
98	141	98	117	74
127	109	76	91	58
158	89	63	74	48
198	73	51	60	39
245	59	42	50	32
300	50	36	42	28
368	42	31	35	24
451	35	26	30	20
360 · 134	125	85	104	63
147	114	78	95	58
162	104	71	86	53
179	95	65	79	49
196	88	60	73	45
400 · 187	94	64	78	47
216	83	56	68	42
237	76	51	62	38
262	69	47	57	35
287	63	43	52	32
314	58	40	48	30
347	53	37	44	28
382	49	34	40	25
421	45	31	37	23
463	41	29	34	22
509	38	27	31	20
551	35	25	29	19
592	33	23	26	18
634	31	22	26	17
677	30	21	25	16
744	27	20	23	15
818	25	18	21	14
900	23	17	19	13
990	22	16	18	12
1086	20	15	17	11

UB				
838 · 292 · 226	100	80	90	70
838 · 292 · 194	115	90	100	80
838 · 292 · 176	125	100	110	90
762 · 267 · 197	100	85	90	70
762 · 267 · 173	115	95	105	80
762 · 267 · 147	135	110	120	95
762 · 267 · 134	150	120	135	105
686 · 254 · 170	110	90	100	75
686 · 254 · 152	120	95	110	85
688 · 254 · 140	130	105	120	90
686 · 254 · 125	150	115	130	100
610 · 305 · 238	80	65	70	50
610 · 305 · 179	105	80	95	70
610 · 305 · 149	125	95	110	80
610 · 229 · 140	120	95	105	80
610 · 229 · 125	135	105	120	90
610 · 229 · 113	145	115	130	100
610 · 229 · 101	160	130	145	110
533 · 210 · 122	125	95	110	85
533 · 210 · 109	135	110	120	95
533 · 210 · 101	145	115	130	100
533 · 210 · 92	160	125	145	110
533 · 210 · 82	180	140	160	120
457 · 191 · 98	135	105	120	90
457 · 191 · 89	145	115	130	100
457 · 191 · 82	160	125	140	105
457 · 191 · 74	175	135	155	115
457 · 191 · 67	195	150	170	130
457 · 152 · 82	145	120	130	105
457 · 152 · 74	160	130	145	115
457 · 152 · 67	175	145	160	125
457 · 152 · 60	195	160	175	140
457 · 152 · 52	225	180	200	160
406 · 178 · 74	160	125	140	105
406 · 178 · 67	175	140	155	115
406 · 178 · 60	195	155	175	130
406 · 178 · 54	220	170	190	145
406 · 140 · 46	230	185	210	160
406 · 140 · 39	270	215	245	190
356 · 171 · 67	165	125	145	105
356 · 171 · 57	190	145	170	120
356 · 171 · 51	215	160	185	135
356 · 171 · 45	240	180	210	150
356 · 127 · 39	240	195	215	165
356 · 127 · 33	280	225	250	195
305 · 165 · 54	185	140	160	115
305 · 165 · 46	215	160	185	135
305 · 165 · 40	245	185	210	150
305 · 127 · 48	180	145	160	120
305 · 127 · 42	205	160	180	140
305 · 127 · 37	230	180	205	155
305 · 102 · 33	245	200	220	175
305 · 102 · 28	280	230	255	200
305 · 102 · 25	320	255	285	225
254 · 146 · 43	200	150	175	120
254 · 146 · 37	230	170	200	140
254 · 146 · 31	270	200	235	165
254 · 102 · 28	255	200	225	175
254 · 102 · 25	285	225	250	190

UC				
305 · 305 · 283	55	40	45	30
305 · 305 · 240	65	45	55	35
305 · 305 · 198	75	50	65	40
305 · 305 · 158	95	65	75	50
305 · 305 · 137	105	70	90	55
305 · 305 · 118	120	85	100	60
305 · 305 · 97	145	100	120	75
254 · 254 · 167	75	50	65	40
254 · 254 · 132	95	65	80	50
254 · 254 · 107	115	75	95	60
254 · 254 · 89	135	90	110	70
254 · 254 · 73	160	110	135	60
203 · 203 · 86	115	80	95	60
203 · 203 · 71	135	95	115	70
203 · 203 · 60	160	110	135	80
203 · 203 · 52	185	125	150	95
203 · 203 · 46	205	140	170	105
152 · 152 · 37	190	135	165	100
152 · 152 · 30	240	160	200	120
152 · 152 · 23	310	210	255	155

6. Nomogram

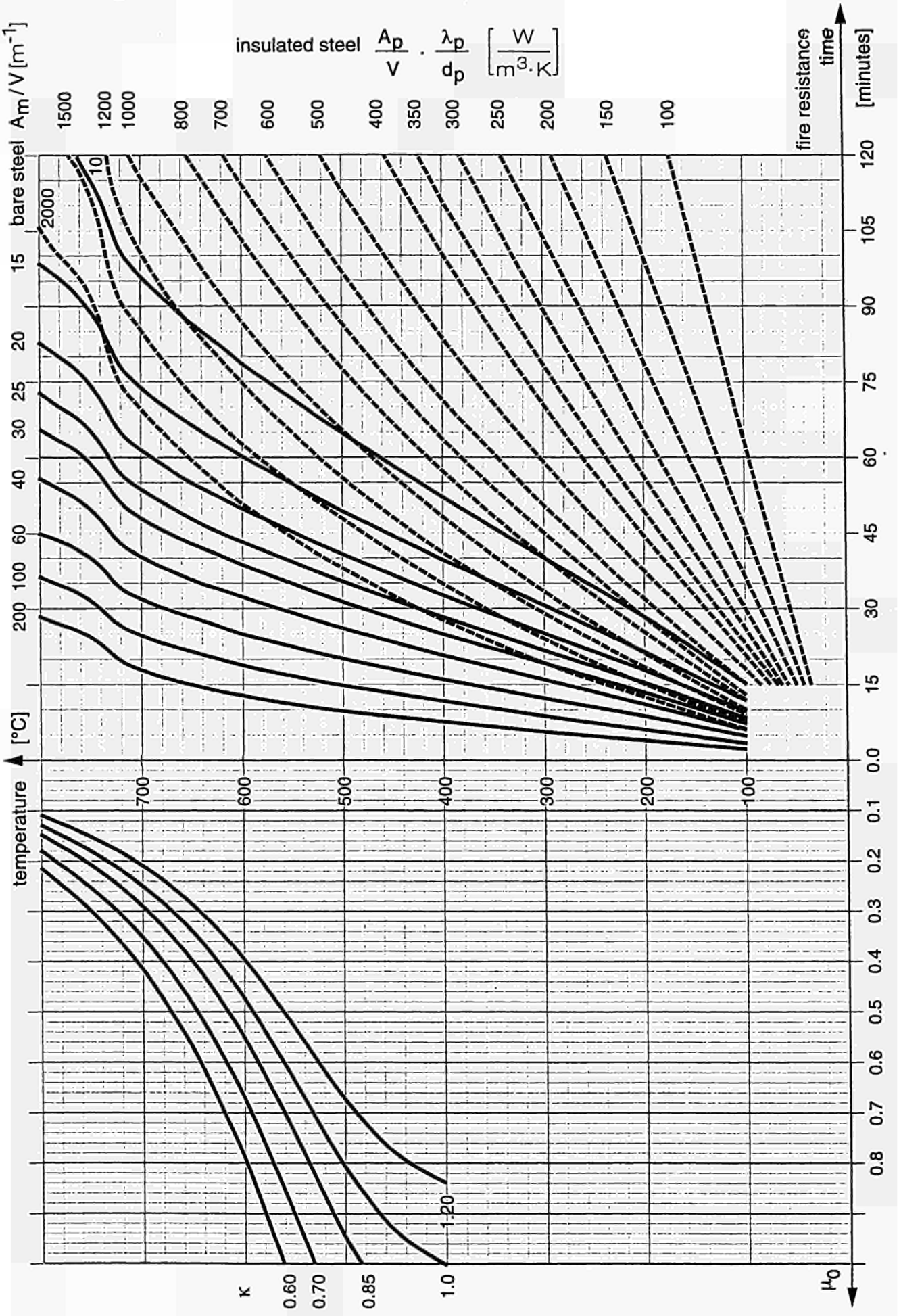
insulated steel $\frac{A_p}{V} \cdot \frac{\lambda_p}{d_p}$ $\left[\frac{W}{m^3 \cdot K}\right]$
bare steel $A_m/V\ [m^{-1}]$
temperature [°C]
fire resistance time [minutes]
κ
μ_0

7. Worked Examples

7.1 Example A

Input: degree of utilisation, thickness of fire protection and section factor.
To determine: fire resistance time.

Example A1 Column HEA 300, encased with fibre-calcium-silicate board (d_p = 25 mm, λ_p = 0.15 W/(m·K), p = 3 %, from Table 2). μ_0 = 0.6. Obtained after iteration (see Example E and Section 3). A_p/V = 104 m^{-1}, taken from Section 5.
The thermal section factor (for ϕ simplified to 0.0) is calculated as:

$$\frac{A_p}{V} \cdot \frac{\lambda_p}{d_p} = 104 \cdot \frac{0.15}{0.025} = 624\,W/(m^3 \cdot K)$$

The fire resistance time t_t can be dervied from the nomogram with μ_0 = 0.6 and κ = 1.2, as t_t = 101 minutes.
Taking into account ϕ:

$$\phi = \frac{1200 \cdot 0.025 \cdot 600}{600 \cdot 7850} \cdot 104 = 0.397$$

the modified thermal section factor is calculated as

$$\frac{A_p}{V} \cdot \frac{\lambda_p}{d_p} \cdot \frac{1}{1 + \phi/2} = 521\,W/(m^3 \cdot K)$$

The fire resistance time t_t can be found from the nomogram with μ_0 = 0.6 and κ = 1.2, as 117 minutes (a substantial increase compared to the simplified assumption ϕ = 0).
The increase in fire resistance due to the moisture content of the protection can be calculated as follows:

$$t_v = \frac{p \cdot \rho_p \cdot d_p^2}{5 \cdot \lambda_p} = \frac{3 \cdot 600 \cdot 0.025^2}{5 \cdot 0.15} = 1 \text{ minute}$$

NB: If the influence of moisture has already been included in the λ_p-values, t_v cannot be considered again.
The protected column fulfils the R90 requirement.

Example A2 Same conditions as Example A1, but a lower degree of utilisation (μ_0 = 0.4). From the nomogram the fire resistance time is extrapolated to be t_t = 121 minutes (for ϕ simplified to 0). t_t = 140 minutes for actual value of ϕ = 0.397.

7.2 Example B

Input: degree of utilisation and required fire resistance time.
To determine: required section factor and/or fire protection (type and thickness d_p of the fire protection material).

Beam IPE 300, required fire resistance R90

1. Degree of utilisation μ_0: Design bending moment (from static analysis, no lateral torsional buckling of the beam because it is stabilised by a concrete slab, steel grade S 235)

$M_{fi,d}$ = 67.5 kNm

$M_{fi,0,Rd}$ = 148 kNm (for $\gamma_{M,fi}$ = 1.0)

$\mu_0 = M_{fi,d} / M_{fi,0,Rd}$ = 0.456

The critical temperature is Θ_{cr} = 654 °C, derived from the nomogram for μ_0 = 0.459 and κ = 0.7.

2. Encasement: Beam with a concrete or composite slab on side four, i.e. section factor A_p/V = 139 m^{-1}
For a critical temperature of 654 °C, it is found from the nomogram that the thermal section factor should be smaller than 1150 W/(m^3·K) to reach R90.
For A_p/V = 139 m^{-1}, the light and dry encasement (for simplification ϕ taken as 0 on safe side) must fulfil the following condition:

$$\frac{d_p}{\lambda_p} \geq \frac{A_p/V}{1150} = \frac{139}{1150} = 0.121\,\frac{m^2 \cdot K}{W}$$

The required thickness d_p of a fibre cement board encasement (Table 2) with a thermal conductivity of λ_p = 0.15 W/(m·K) is:
$d_p \geq \lambda_p \cdot 0.121 = 0.15 \cdot 0.121 = 0.018m = 18mm$.

7.3 Example C

Input: section factor, critical temperature Θ_{cr}, fire resistance time.
To determine: Insulation thickness.

Note: A limitation of the steel temperature can be directly considered using the nomogram, e.g. for class 4 sections, Θ_{cr} = 350°C, or for strengthening of concrete with epoxy bonded flat steel reinforcement, $\Theta_{cr} \approx$ 90 °C.
Beam with class 4 section, $A_p/V \approx$ 200, fire resistance R60, Θ_{cr} = 350 °C (see ENV 1993-1-2 4.2.4).
Minimal thickness of protection by fibre-silicate boards:
According to the nomogram the thermal section factor $(A_p/V)\cdot(\lambda_p/d_p)$ must be less then 610W/(m^3·K).
With A_p/V = 200 m^{-1} the encasement must fulfil the following condition:

$$\frac{d_p}{\lambda_p} \geq \frac{A_p/V}{610} = \frac{200}{610} = 0.33\,\frac{m^2 \cdot K}{W}$$

The required thickness d_p of fibre-silicate boards (Table 2) with the thermal conductivity λ_p = 0.15 W/(m·K) results in $d_p \geq \lambda_p \cdot 0.33$ = 0.15 · 0.33 = 0.049 m = 49 mm.

7.4 Example D

Input: section factor, column length, action in fire.
To determine: fire resistance time.

Solid intermediate column 250 mm diameter, L = 4.0 m, steel grade S 235, compression force in fire $N_{fi,d}$ = 3000kN;
section factor: $A_m/V = 4/d$ = 16m^{-1}, A = 49'100mm^2
Assessment using Table 1b:
Non-dimensional-slenderness:

$$\bar{\lambda}_{0,c} = \ell_{fi}/(i \cdot \pi \cdot \sqrt{E_a/f_y}) = 4000/(62.5 \cdot \pi \cdot \sqrt{210/0.235}) = 0.68$$

Buckling resistance for 20 °C, $\gamma_{M,fi}$ = 1.0, buckling curve c:
Buckling factor χ = 0.7370; Design buckling resistance:
$N_{Rd} = \chi \cdot f_y \cdot A = 0.7370 \cdot 0.235 \cdot 49'100 = 8504$ kN
$\mu_{0,c}$ = 3000 / 8504 = 0.35 (as defined after table 1c)
Critical temperature from Table 1b (linear interpolation): Θ_{cr} = 640°C.
From the nomogram the fire resistance time for the section factor of 16 m^{-1} is found to be 63 minutes.

7.5 Example E

Input: section factor, column length, action in fire.
To determine: fire resistance time.

Solid column 250 mm diameter, L = 2.0 m, support conditions in fire ℓ_{fi} = 1.0 L, steel grade S 235, action in fire $N_{fi,d}$ = 3000 kN
Assessment using an iterative procedure:
The non-dimensional-slenderness is temperature dependant therefore the following iterative procedure must be used if the support conditions are not covered by Tables 1b (ℓ_{fi} = 0.5 L) or 1c (ℓ_{fi} = 0.7 L) (see Example D).
1. Step: normal temperature $\sqrt{k_{y,\Theta,max}/k_{E,\Theta,max}}$ = 1.0:
Non-dimensional-slenderness for 20 °C; support conditions for fire ℓ_{fi} = 1.0 L:

$$\bar{\lambda}_{fi,0} = \ell_{fi}/(i \cdot \pi \cdot \sqrt{E_a/f_y}) = 2000/(62.5 \cdot \pi \cdot \sqrt{210/0.235}) = 0.34$$

Buckling resistance for $\gamma_{M,fi}$ = 1.0, buckling curve c: Buckling factor χ = 0.929; Buckling resistance:
$N_{Rd} = \chi \cdot f_y \cdot A = 0.9286 \cdot 0.235 \cdot 49100 = 10715$ kN
μ_0 = 3000 / 10715 = 0.28
Critical temperature from the nomogram with μ_0 = 0.28 and κ = 1.2:
Θ_{cr} = 647°C.
2. Step: $\Theta_{cr} = 647°C = \Theta_{max}$ —> $\sqrt{k_{y,\Theta,max}/k_{E,\Theta,max}}$ = 1.28
(interpolation from Tab. 1a) $\bar{\lambda}_{fi,\Theta,max} = 1.28 \cdot 0.34 = 0.44$
Buckling resistance for $\gamma_{M,fi}$ = 1.0, buckling curve c: Buckling factor χ = 0.876; Buckling resistance:
$N_{Rd} = \chi \cdot f_y \cdot A = 0.876 \cdot 0.235 \cdot 49100 = 10108$ kN
μ_0 = 3000 / 10108 kN = 0.30
Critical temperature from the nomogram with μ_0 = 0.30 and κ = 1.2:
Θ_{cr} = 640°C. The iteration process can be stopped. Fire resistance time for the nomogram for Θ_{cr} = 640°C and a section factor A_m/V of 16 m^{-1} is found to be 63 minutes.

8. Symbols and Units

8.1 Symbols

A	the cross-section area	[m^2]
A_m	the surface area of a member per unit length	[m]
A_p	the area of the inner surface of the fire protection material per unit length of the member	[m]
V	the volume of a member per unit length	[m^2]
E_a	the modulus of elasticity of steel for normal temperature design 20°C ($E_a = 210 \cdot 10^3$ N/mm²)	[N/mm²]
$E_{a,\Theta}$	the slope of the linear elastic range for steel at elevated temperature Θ	[N/mm²]
c_p	the specific heat of fire protection material	[J/(kg·K)]
c_a	the specific heat of steel, $c_a \approx 600$ J/(kg·K)	[J/(kg·K)]
d_p	the thickness of fire protection material	[m]
f_y	the yield strength of steel at room temperature	[N/mm²]
$f_{y,\Theta}$	the effective yield strength of steel at elevated temperature Θ	[N/mm²]
i	the radius of gyration	[m]
$k_{y,\Theta}$	the relative value for the effective yield strength, $k_{y,\Theta} = f_{y,\Theta}/f_y$	
$k_{E,\Theta}$	the relative value for the slope of the linear elastic range, $k_{E,\Theta} = E_{a,\Theta}/E_a$	
L	system length	[m]
l_{fi}	the buckling length in fire	[m]
p	the moisture content of fire protection material	[%]
t	the thickness of steel	[m]
t_r	the total fire resistance time	[min]
t_t	the fire resistance time neglecting the influence of the moisture content	[min]
t_v	the increase of fire resistance time due to the moisture content of the fire protection material	[min]
$\gamma_{M,fi}$	the partial material safety factor in fire design	
Θ	the temperature	[°C]
Θ_{cr}	the critical steel temperature	[°C]
κ	adaption factor	
$\bar{\lambda}_{fi,0}$	the non dimensional slenderness for end conditions in fire and room temperature	
$\bar{\lambda}_{fi,\Theta,max}$	the non dimensional slenderness for end conditions in fire and steel temperature at failure	
λ_p	the thermal conductivity of the fire protection material	[W/(m·K)]
μ_0	the degree of utilisation: $\mu_0 = E_{fi,d}/R_{fi,d,0}$	[-]
ϕ	$[(c_p \cdot \rho_p \cdot d_p)/(c_a \cdot \rho_a)] \cdot A_p/V$, (see section 4)	
ρ_a	the density of steel ($\rho_a = 7850$ kg/m³)	[kg/m³]
ρ_p	the density of fire protection material	[kg/m³]

8.2 Units

SI-units are generally used.

Temperatures in Celsius [°C] are marked with Θ. For conversion temperature the following relation holds: 0 °C = 273 K, and the conversion factor between °C and K is 1.

Between Joule [J], Watt [W] and the former unit calorie [cal] the following relation holds: 1 W = 1 J/sec, 1 cal = 4.18 J.

9. References

[1] ENV 1993-1-2 ("General rules, Structural fire design"), CEN, Brussels 1995

[2] ECCS Technical Note 92, Explanatory Document to ECCS No 89,Fire resistance of steel structures, Brussels 1996

10. Rules given in the National Application Document and Properties of Proprietary Fire Protection Material According to National Test Results

Information on additional rules and changes of boxed values given in the National Application Document (NAD) and the thermal properties derived from recognised national fire tests can be ordered from the following organisations:

Austria
Österreichischer Stahlbauverband
Larochegasse 28
A-1130 Wien

Belgium
CRIF - Section Construction métallique
Université de Liège
Institut du Génie Civil
Quai Banning 6
B-4000 Liège

Croatia
Hrvatska Zajednica za Metalne Konstrukcije
Janka Rakuse 1
CRO-41000 Zagreb

Czech Republic
Czech Steelwork Fabricators Association - CSFA
Komerçni 5a
CZ-710 00 Ostrava

Denmark
Dansk Stalinstitut
Overgade 21-2
DK-5000 Odense C

Finland
Federation of Finnish Metal, Engineering and Electrotechnical Industries
P.O. Box 10
Eteläranta 10
FI-00130 Helsinki

France
CTICM
Domaine de Saint-Paul BP 64
F-78470 Saint-Rémy-lès-Chevreuse

Germany
Deutscher Stahlbau-Verbund DSTV
Ebertplatz 1
D-50668 Köln

Greece
Federation of Greek Industries
Xenofontosstreet 5
GR-105 57 Athens

Italy
Associazione fra i Costruttori in Acciaio Italiani
Viale Abruzzi 66
I-20131 Milano

Luxemburg
Profil ARBED Recherches
66 rue de Luxembourg / BP 141
L-4221 Esch/Alzette

Netherlands
TNO-Bouw, Centrum voor Brandveiligheid
Postbus 49
NL-2600 AA Delft

Norway
Den Norske Stalgruppen
Postboks 7072-Homansbyen
N-0306 Oslo 3

Spain
Empresa Nacional Siderurgica S.A. (Ensidesa)
Direccion de Asistencia a Proyectos
Paseo de la Castellana 91,la planta
ES-28046 Madrid

Sweden
The Swedish Institute of Steel Construction
Box 27751
S-11592 Stockholm

Switzerland
Schweizerische Zentralstelle für Stahlbau
Seefeldstrasse 25
CH-8034 Zürich

Turkey
Tucsa - Turkish Constructional Steelwork Association
Bahariye, Sair Latifi Sokak 29
TR-81310 Kadikoy - Istanbul

United Kingdom
The Steel Construction Institute
Silwood Park
UK-Ascot Berks SL5 7QN

BCSA
4 Whitehall Court
UK-London SW1A 2ES

Portugal
Instituto da Construçao - POLO IST
Departamento de Engenharia Civil
Instituto Superior Tecnico
Av. Rovisco Pais
PT - 1096 Lisboa codex

Slovenia
Institut za Metalne Konstrukcije
Mencingerjeva 7
Lubljana
Republika Slovenija

ANNEX 17:

17. EFFECT OF THE THERMAL GRADIENT IN EXTERNAL BARE STEEL COLUMNS

17.1 INTRODUCTION

In scope of an European Research project concenring buckling curves for bare steel columns numerical investigations are made into the thermal response of bare steel columns outside the facade.

Usually the thermal response of columns is calculated assuming an uniformly distributed thermal loading around the column according to the standard fire curve (ISO 384).

External columns are subjected to a lower thermal load than internal columns because the heating source is restricted to the windows. This means that external columns will warm up slower and reach lower temperatures than internal columns. But due to the asymmetrical loading an asymmetrical termperature distribution over the cross section of the column will occur introducing a thermal curvature. This curvature influences the buckling behaviour of the columns.

The aim of the research described in this report is the quantification of the temperatures and thermal gradient in external bare steel columns subjected to fire from the fire compartment.

The research is divided in two parts.

The thermal loading on the column is calculated with the aid of the thermal model of Eurocode 1 [54]. The model as well as the results are briefly described in chapter 2. In this part the dependence of the thermal load on the geometry of the fire compartment and the window size is investigated as well.

The results of the calculations with the model of Eurocode 1 are used as input for the FEM calculations for the thermal response of the column. In chapter 3 these numerical simulations are presented. The influence of the location of the column in respect to the windows on the thermal response of the column is determined.

Finally the conclusions of each chapter are summarized in chapter 4 to get an overview of the results. Moreover a proposal is given for a typical temperature gradient in fire exposed external steel columns.

17.2 THERMAL LOADING: MODEL OF EUROCODE 1

17.2.1 Introduction

In 1981 in England an analytical model is set up by Margaret Law and Turlogh O'Brien to calculate the flame projection from openings of buildings facades and the heat transfer from fires to external bare steel columns [51]. This model is incorporated in Eurocode 1, which describes actions on structures exposed to fire.

The model calculates flame temperatures and the temperature in the fire compartment based on the geometry of the compartment, the window sizes, the fire load and draught. Moreover the model gives assumptions for the dimensions of the flames coming out of the window and the radiative properties of the flames and the fire compartment itself.

For a complete overview of the assumptions on which the calculation with the model of Eurocode 1 is based refer to [54].

17.2.2 Description of the model

With the model a steady state calculation for a bare external steel column with a uniform temperature can be made. This means that heat flux inside the column is not taken into account.

To calculate the thermal gradient over the cross section of a column a alternative approach is needed.

With the aid of the model the flame temperature and the temperature in the fire compartment can be calculated based on the fire load and the geometry of both windows and compartment. The model includes assumptions for the geometry of the flames and the emissivities of the flames, the fire compartment, the ambient air and the facade.

The main assumptions in the model are:

1. The flames come out of upper 2/3 of the window making an angle of 45° with a vertical surface.
2. The depth of the flame is 2/3 of the window height.
3. The width of the flame is equal to the window width.
4. In the window surface the temperature equal to the calculated fire compartment temperature is assumed.
5. The emissivity of the window surface is equal to 1.
6. The emissivity of the flames depends on the thickness of the flame and the direction of the radiation.
7. For the absorpiton of the flames holds: $\alpha_{fl} = 1 - \varepsilon_{fl}$.
8. The ambient termperature remains during fire equal to 20°C.
9. The temperature in the tip of the flame is equal to 540°C. The temperature varies linearly along the flame axis.

With the model the following is calculated:

1. The length of the flame is calculated in the model (in most cases 2-3 metres above the window top).
2. The temperature of the flames.
3. The temperature of the fire compartment.

Input data for the calculation are:

1. Draught: For none calculations with this model through draught was assumed.
2. Length, width and height of the fire compartment. Assumed is [m]:
   $5.4 <$ length: $l_{com} < 14.4$

3.6 < width: w_{com} < 21.6
2.4 < height: h < 3.6

3. Number and location of windows. To avoid draught all windows are assumed to be located in the same side of the compartment. In all calculations the window ledge was assumed at 800 mm above floor level. Always just one window is assumed because two windows with a certain width result in the same calculated temperatures as one window twice as wide.
4. The window height and width: Assumed is the window top at ceiling level. So the window height depends on the compartment height:
   1.6 < height < 2.8
   1.0 < width: w_{win} < 21.0

The calculated flame and compartment temperatures in [K] are presented in TABLE 17.1.

The calculations show that the flame temperature is generally approx. 100-200 K higher than the compartment temperature. The maximum compartment temperature is about 1200-1260 K, the maximum flame temperature is about 1300-1350 K.

Moreover it can be concluded that the variation in achieved temperatures is rather small. Therefore for the calculation of the thermal gradient in bare external columns one choice is made for the flame temperature and the compartment temperature, both close to the maximum expected temperatures.

Input temperatures for the calculation of the thermal gradient:

- Compartment temperature: 1250 K
- Flame temperature: 1350 K

17.3 THERMAL RESPONSE: FEM MODEL USING DIANA

17.3.1 Model assumptions

As a typical column size a HEB 200 is chosen. Other sizes are not investigated as they are assumed to have little influence on the thermal response, since the heat is mainly transferred due to radiation. The section size has a relatively small influence on the view factors in comparison with the position of the section. The assumptions for the flame geometry and the emissivities for the flames, the window surface, the ambient air and the facade are taken from the model of Eurocode 1.

Both 2-dimensional and 3-dimensional calculations are made. With the 2D model two different configurations are investigated, see FIGURE 17.1.

1. The column is supposed to be located right in front of a window, width 2000 mm.
2. The column is supposed to be located in between two windows, both 2000 mm wide. Distance between the windows 600 mm.

With the 3D model only the latter configuration is used.

General assumptions:

- lower edge of window: 800 mm above floor level
- upper edge of window: 2600 mm above floor level
- distance between column and facade: varied among 100-2000 mm.

In the 2D model it is assumed that the maximum temperature difference will appear at the level of intersection of the column with the inclined flame surface. For configuration 1 this means that the inner flange is just reached by the flames. The outer flange is exposed to the ambient air.

The temperatures calculated with the model of Eurocode 1 are used as input values for the FEM model. Because the model of Eurocode 1 is only valid for steady state these temperatures are applied in several increments. The influence of the loading rate is investigated with the 2D model. The 3D calculations are made increasing the load linearly up to it's maximum value in 5 minutes.

17.3.2 Description of the model

With the FEM program DIANA [53] it is possible to calculate radiative heat exchange in convex voids [52]. Both configurations are modelled with multiple voids. For every side of the column convex voids are implemented to model the heat exchange among the heated surfaces. For a more detailed description of the modelling refer to appendix A[1].

17.3.3 Results of the 2D model

The main aim of the 2D model is to determine the influence of the loading rate on the thermal gradient. Only the 2D model in which the column is located in between two windows is checked with the 3D model.

The temperature differences between the inner flange (the flange nearest to the facade) and the outer flange are presented in FIGURE 17.2. The distance between the column and the facade is taken as 300 and 1200 mm. In the column located in front of the window higher temperature differences occur than in the other situation.

The time is varied in which the maximum flame and compartment temperature is reached. The results are presented in FIGURE 17.3.

As can be seen from FIGURE 17.4 the loading rate does not affect the magnitude of the temperature difference in the column. The loading speed only influences the point of time of maximum temperature difference.

17.3.4 Results of the 3D model

With the 3D model the level at which the maximum temperature difference occurs is determined. Moreover the distance among the column and the facade is varied.

The influence of the distance between the column and the facade in the steady state is presented in FIGURE 17.5 and FIGURE 17.7, showing the thermal gradient, the inner flange temperature and the outer flange temperature respectively. For all distances within the flame depth a peak appears at the intersection of the column with the inclined flame surface.

The maximum thermal gradient is larger than the gradient in the steady state. Therefore the maximum gradient is presented in FIGURE 17.4 as well. For an impression of the temperature development in time is referred to the 2D calculation shown in FIGURE 17.3.

It can be concluded that an increasing distance enlarges the thermal gradient. Both outer flange temperature and inner flange temperature decreases at increasing distance.

Generally, the peak thermal gradient will remain below 300°C and a typical value is 200°C. Along the column axis the average thermal gradient is lower. Typical values between 100-200°C are found.

17.4 CONCLUSIONS

With the model of Eurocode 1 several calculations are performed to investigate the temperatures of the flames and the fire compartment depending on the fire load and the geometry of the compartment and the windows. Within the range of the considered parameters the following conclusions are made:

- The flame temperature varies among 1100-1350 K.
- The compartment temperature varies among 840-1260 K.

With the FEM model using DIANA 2D and 3D calculations are made investigating the arising thermal gradient in external bare steel columns. Main conclusions are:

- The maximum thermal gradient is limited to approx. 300°C. The gradient increased with larger distances between the column and the facade. For a common distance of 800 mm a maximum gradient of 250°C is reached.
- Along the column axis a peak for the thermal gradient occurs near the intersection of the diagonal flame surface with the column. This peak increases for smaller distances between the column and the facade.
- The average thermal gradient along the column axis is about 100°C lower than the peak value.
- The thermal gradient depends on time as well. The thermal gradient in the steady state is generally 30°C lower than the maximum gradient.
- The loading speed does not effect the magnitude of the thermal gradient, but only the dependency on time changes, which is not relevant.
- For constructional purposes a typical value for the thermal gradient of 200°C is in reasonable accordance with the calculation results.

The results of this research can be used in a structural analysis of an external steel column. Supposed is an approach consisting of three steps. (To obtain a critical average steel temperature).

1. Put loading on member
2. Put thermal gradient of 200°C on member

3. Increase average temperature keeping the thermal gradient and the structural load constant.

With the DIANA programme some calculations have been made for a HEB 200 steel column to determine the M-N interaction curves at different ultimate temperatures. A bi-triangular bending moment distribution has been assumed (r = -1). The relative slenderness of the columns considered are 0.2, 0.6, 1.0 and 1.6. To compare the influence of the cross section HEA 600 steel column is considered but only with a relative slenderness of 0.6.

The calculations have been made with a 2D beam model, in which the radius at the flange-web connection is neglected and the residual stresses are left out.

For the column with a relative slenderness of 0.6 the M-N interaction curves have been determined to see the influence of the cross section. It appears that there is not a significant influence of the cross section shape. This was also concluded for the column with a uniform temperature.

3. The M-N interaction can be predicted by the proposal in the final report for the strong and weak axis, with the assumption that the average temperature is used in the design model. The eccentricity due to the thermal gradient has to be taken into account and the correction factor for the bending moment distribution should be used according to the actual bending moment distribution. For the thermal eccentricity bending moment r = 1 should be used and for the external bending moment r = -1.

TABLE 17.1 Fire compartment and flame temperature [K] calculated with the model of Eurocode 1 [54]

			l_{com} = 5.40 m						l_{com} = 14.4 m					
			h = 2.4 m		h = 3.0 m		h = 3.6 m		h = 2.4 m		h = 3.0 m		h = 3.6 m	
fire load [kg/m^2]			10	25	10	25	10	25	10	25	10	25	10	25
w_{com} = 3.6 m	w_{win} = 1.0 m	$T_{compartment}$	830	1117	824	1169	795	1166	775	899	817	1004	836	1076
		T_{window}	1357	1293	1258	1197	1173	1141	1341	1341	1213	1213	1146	1146
	w_{win} = 2.0 m	$T_{compartment}$	826	1206	763	1149	-	1069	864	1105	880	1193	866	1222
		T_{window}	1369	1371	1176	1249	-	1175	1373	1373	1243	1243	1174	1170
	w_{win} = 3.0 m	$T_{compartment}$	773	1161	-	689	-	947	894	1210	874	1245	830	1220
		T_{window}	1315	1417	-	813	-	1128	1404	1404	1262	1259	1134	1174
w_{com} = 12.6 m	w_{win} = 4.0 m	$T_{compartment}$	941	1264	914	1291	863	1256	913	1052	985	1196	1014	1286
		T_{window}	1380	1215	1261	1177	1133	1145	1239	1239	1169	1157	1140	1111
	w_{win} = 8.0 m	$T_{compartment}$	875	1269	785	1167	-	1062	1010	1280	1012	1353	973	1348
		T_{window}	1360	1340	813	1253	-	1173	1328	1295	1248	1208	1175	1154
	w_{win} = 12.0 m	$T_{compartment}$	786	1167	-	1024	-	913	1008	1350	955	1336	833	1269
		T_{window}	1279	1408	-	1219	-	1114	1399	1346	1222	1242	1121	1173
w_{com} = 21.6 m	w_{win} = 7.0 m	$T_{compartment}$	961	1288	929	1308	873	1266	943	1084	1021	1234	1050	1324
		T_{window}	1384	1214	1261	1179	1131	1147	1202	1196	1171	1128	1141	1091
	w_{win} = 14.0 m	$T_{compartment}$	882	1275	-	1165	-	1056	1037	1311	1376	1376	989	1361
		T_{window}	1358	1344	-	1254	-	1144	1332	1253	1183	1183	1174	1139
	w_{win} = 21.0 m	$T_{compartment}$	-	-	-	1017	-	901	-	-	966	1344	889	1268
		T_{window}	-	-	-	1218	-	1110	-		1221	1222	1119	1165
Average	$T_{compart}$	1035	859	1218	843	1108	843	1070	930	1161	949	1253	920	1263
	T_{window}	1220	1350	1325	1153	1173	1145	1141	1327	1305	1222	1206	1147	1147

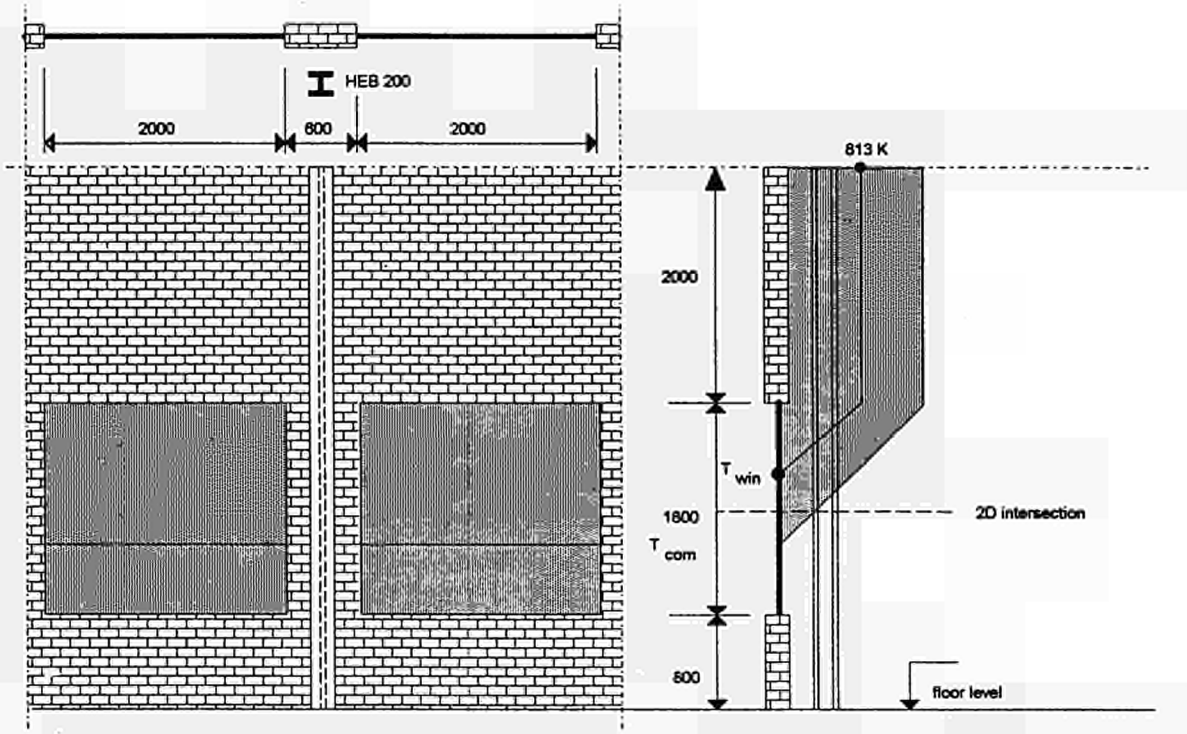

FIGURE 17.1 Location of the column relative to the window for configuration 2.

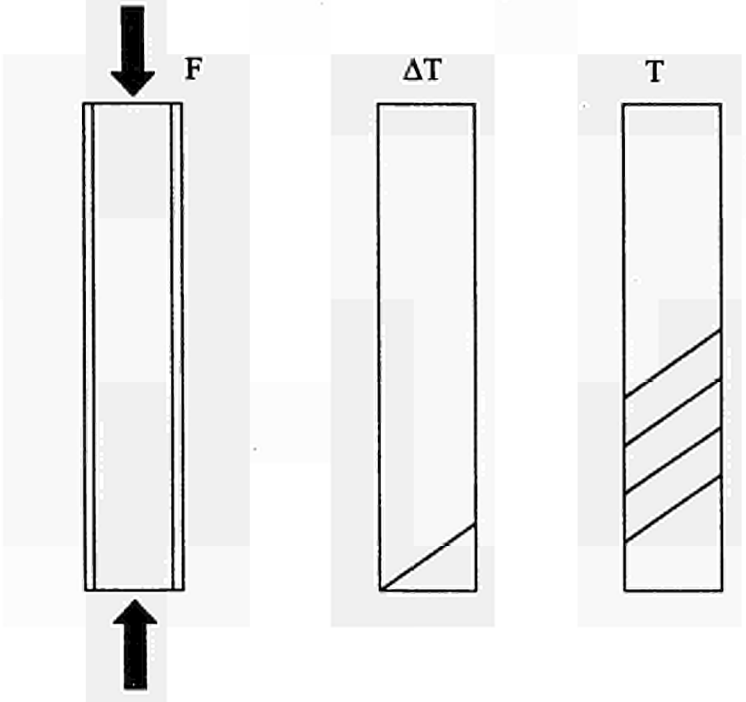

FIGURE 17.2 Approach for the structural analysis including a thermal gradient.

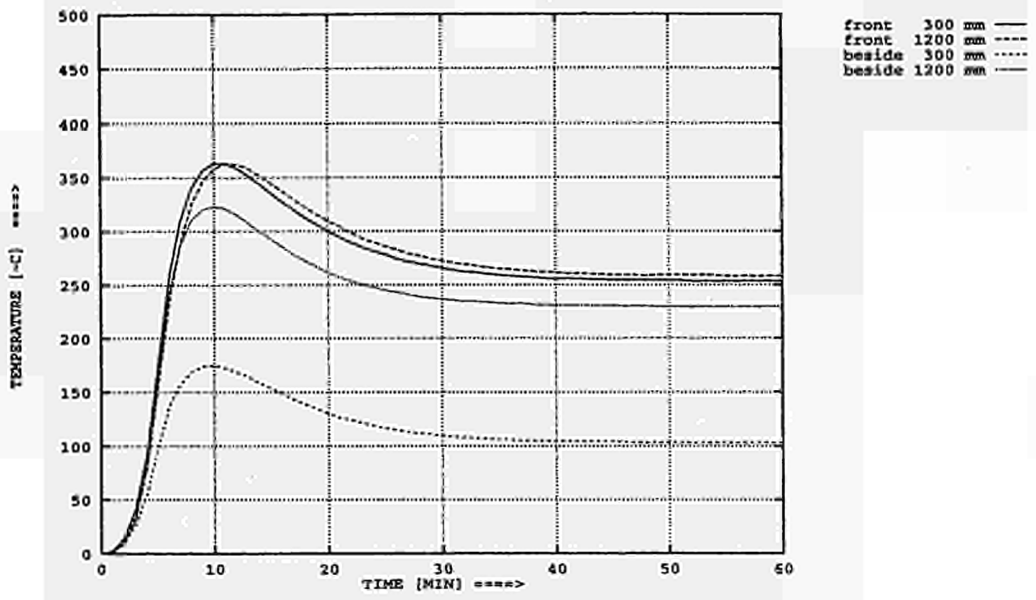

FIGURE 17.3 Thermal gradient for both configurations with 2D model. Two different distances column facade.

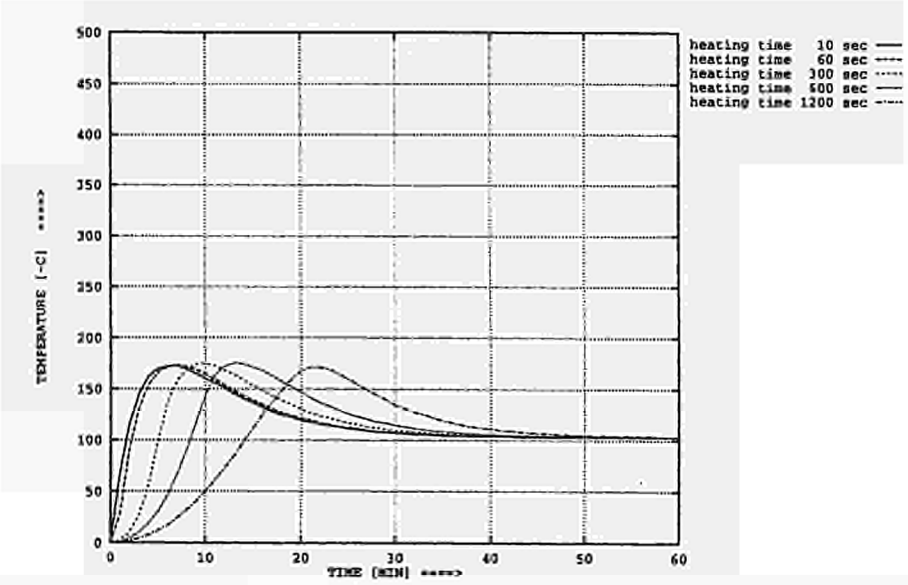

FIGURE 17.4 Thermal gradient for configuration 2 (distance 1200 mm) with 2D model, depending on loading rate.

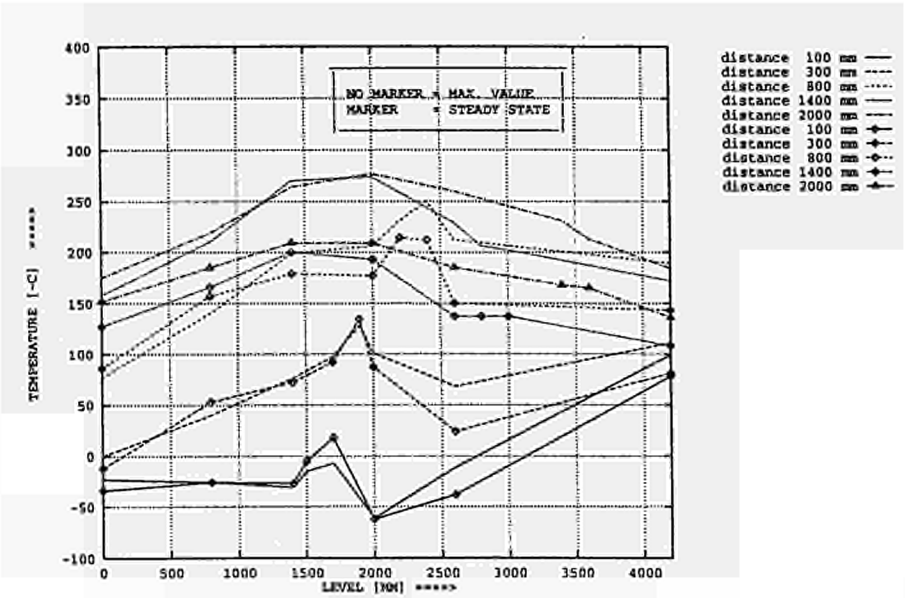

FIGURE 17.5 Thermal gradient along the column axis with 3D model, maximum value and steady state, depending on distance column-facade.

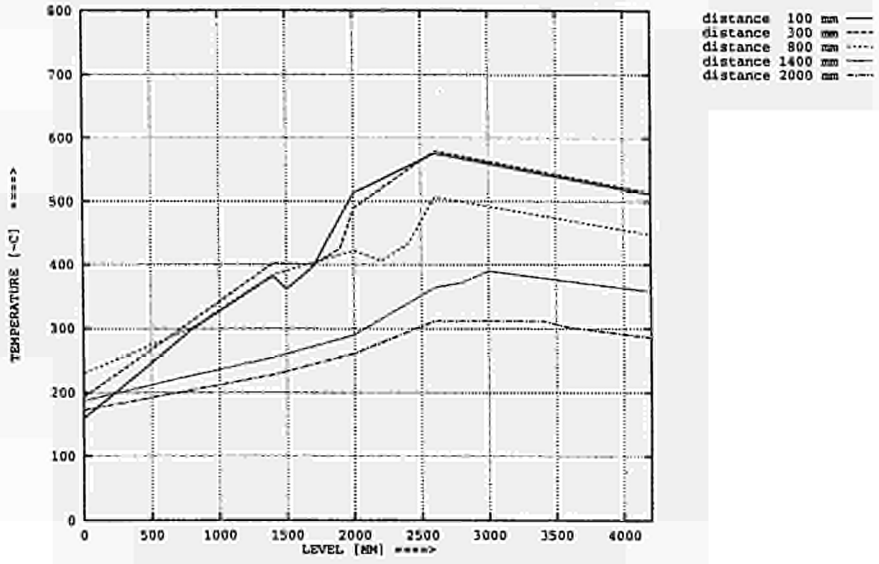

FIGURE 17.6 Outside flange temperature along the column axis for configuration 2 in steady state with 3D model. Dependency on distance column-facade.

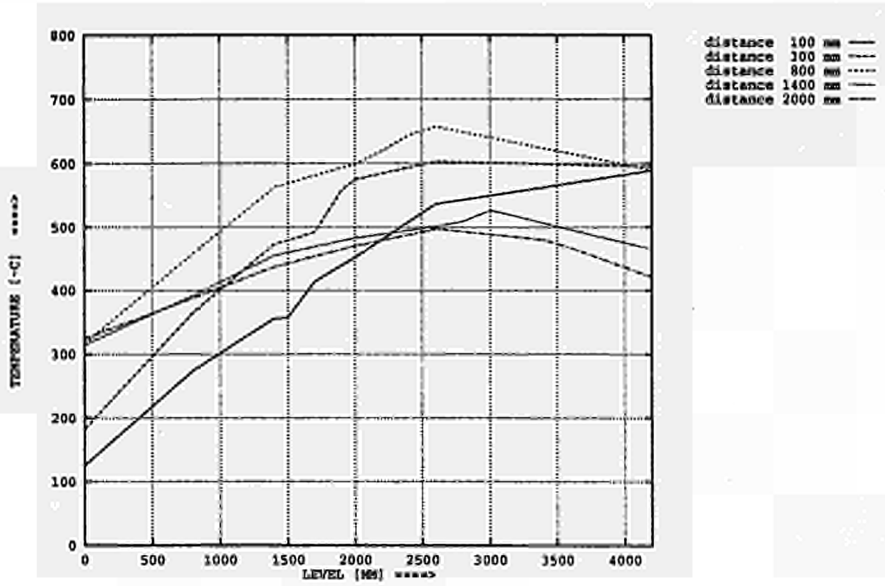

FIGURE 17.7 Inside flange temperature along the column axis for configuration 2 in steady state with 3D model. Dependency on distance column-facade.

Appendix A: Details concerning the FEM model

Radiative heat transfer from flame and compartment to section

With the FEM programme DIANA it is possible to model radiative heat transfer among surfaces in a void [52,53]. The use is restricted to convex voids. This means that each point is directly exposed to all other points in the void. For each void a matrix is solved every iteration taking into account emission and reflection of each incremental surface in the void.

Considering the configuration modelled in the research of this report it is obvious that it's impossible to model the complete radiative heat transfer within one convex void. Therefore several convex voids are modelled.

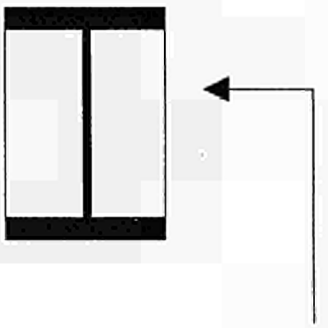

First an imaginary perfectly dark surface is modelled among the tip of the inner and outer flange (see fig). The void in between the flanges is now convex. Making this surface perfectly dark means that all radiation is passed through from both sides.

The sides of the section are heated by the window surface and the flame surfaces. For each side a convex void is modelled with each heated surface. For example, a separate void is made for the heat exchange between the vertical flame surface perpendicular to the facade and the surface formed by the flange tips and the imaginary surface between the flange tips (see fig). The additional surfaces to close the void are perfectly dark.

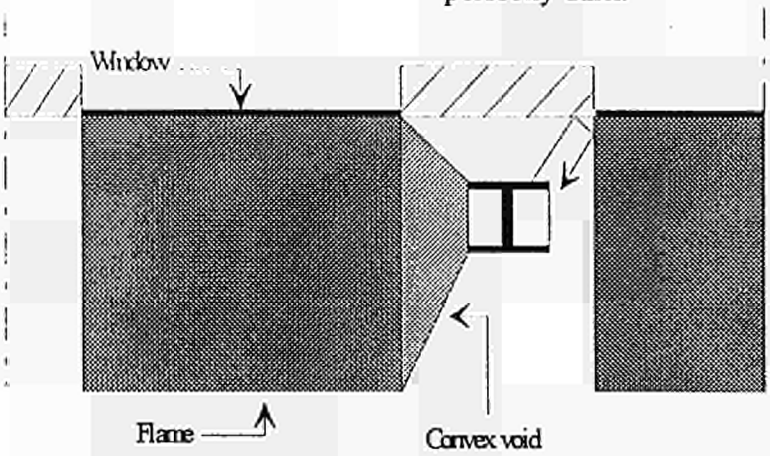

Modelling the radiation exchange in separate voids neglects the interaction between two surfaces with cannot be combined in one convex void. For example the inner flange surface radiates to the imaginary surface among the flange tips via the facade and the vertical flame surface perpendicular to the facade. (see fig).

But according to the Eurocode it is assumed that the facade surface and the ambient air have an emissivity equal to 1.0 reflecting nothing. Due to this assumption modelling the radiative heat flux from the all surfaces with separate convex voids can be done without loss of accuracy.

The emissivity of the flame surface depends on the thickness of the flame perpendicular to the flame surface. The absorption of the radiation of the window surface by the flames depends on the emissivity of the flame according to: $a_f = e_f$. This effect is taken into account reducing the emissivity of the window surface: $e_w = 1 - a_f = 1 - e_f$.

European Commission

EUR 18380 — Properties and in-service performance
Buckling curves of hot rolled H steel sections submitted to fire

J.B. Schleich, L-G. Cajot
J. Kruppa, D. Talamona
W. Azpiazu, J. Unanue
L. Twilt, J. Fellinger, R-J. Van Foeken
J-M. Franssen

Luxembourg: Office for Official Publications of the European Communities

1998 — 336 pp. — 21 x 29.7 cm

Technical steel research series

ISBN 92-828-4603-2

Price (excluding VAT) in Luxembourg: ECU 57

The research has lead to new formulae for the design of steel columns in case of fire:

— a new N/M interaction formula
— new buckling curves instead of the buckling curve c divided by 1.2 proposed in the present version of Eurocode 3 Part 1.2.

The formulae are presented in design tables useful for the practical engineer. These formulae were deduced and calibrated from a very large amount of numerical simulations (more than 300 000) and from a database comprising 141 test results including the 29 tests made within the framework of the research.

For the study of the axially loaded columns, 21 tests have been performed in the Laboratory of LABEIN in Bilbao and 8 tests have been made in the CTICM laboratory in Maizières-les-Metz to analyse columns subjected to a normal force and a constant bending moment distribution.

The numerical simulations were made by using the five programs available in the different organizations: CEFICOSS and SAFIR (ProfilARBED-Recherches and University of Liège), DIANA (TNO), LENAS and SISMEF (CTICM).

Venta • Salg • Verkauf • Πωλήσεις • Sales • Vente • Vendita • Verkoop • Venda • Myynti • Försäljning

BELGIQUE/BELGIË

Jean De Lannoy
Avenue du Roi 202/Koningslaan 202
B-1190 Bruxelles/Brussel
Tél. (32-2) 538 43 08
Fax (32-2) 538 08 41
E-mail: jean.delannoy@infoboard.be
URL: http://www.jean-de-lannoy.be

La librairie européenne/De Europese Boekhandel
Rue de la Loi 244/Wetstraat 244
B-1040 Bruxelles/Brussel
Tél. (32-2) 295 26 39
Fax (32-2) 735 08 60
E-mail: mail@libeurop.be
URL: http://www.libeurop.be

Moniteur belge/Belgisch Staatsblad
Rue de Louvain 40-42/Leuvenseweg 40-42
B-1000 Bruxelles/Brussel
Tél. (32-2) 552 22 11
Fax (32-2) 511 01 84

DANMARK

J. H. Schultz Information A/S
Herstedvang 10-12
DK-2620 Albertslund
Tlf. (45) 43 63 23 00
Fax (45) 43 63 19 69
E-mail: schultz@schultz.dk
URL: http://www.schultz.dk

DEUTSCHLAND

Bundesanzeiger Verlag GmbH
Vertriebsabteilung
Amsterdamer Straße 192
D-50735 Köln
Tel. (49-221) 97 66 80
Fax (49-221) 97 66 62 78
E-Mail: vertrieb@bundesanzeiger.de
URL: http://www.bundesanzeiger.de

ΕΛΛΑΔΑ/GREECE

G. C. Eleftheroudakis SA
International Bookstore
Panepistimiou 17
GR-10564 Athina
Tel. (30-1) 331 41 80/1/2/3/4/5
Fax (30-1) 323 98 21
E-mail: elebooks@netor.gr

ESPAÑA

Boletín Oficial del Estado
Trafalgar, 27
E-28071 Madrid
Tel. (34) 915 38 21 11 (Libros)/
913 84 17 15 (Suscripciones)
Fax (34) 915 38 21 21 (Libros)/
913 84 17 14 (Suscripciones)
E-mail: clientes@com.boe.es
URL: http://www.boe.es

Mundi Prensa Libros, SA
Castelló, 37
E-28001 Madrid
Tel. (34) 914 38 37 00
Fax (34) 915 75 39 98
E-mail: libreria@mundiprensa.es
URL: http://www.mundiprensa.com

FRANCE

Journal officiel
Service des publications des CE
26, rue Desaix
F-75727 Paris Cedex 15
Tél. (33) 140 58 77 31
Fax (33) 140 58 77 00

IRELAND

Government Supplies Agency
Publications Section
4-5 Harcourt Road
Dublin 2
Tel. (353-1) 661 31 11
Fax (353-1) 475 27 60

ITALIA

Licosa SpA
Via Duca di Calabria, 1/1
Casella postale 552
I-50125 Firenze
Tel. (39-55) 64 54 15
Fax (39-55) 64 12 57
E-mail: licosa@ftbcc.it
URL: http://www.ftbcc.it/licosa

LUXEMBOURG

Messageries du livre SARL
5, rue Raiffeisen
L-2411 Luxembourg
Tél. (352) 40 10 20
Fax (352) 49 06 81
E-mail: mdl@pt.lu
URL: http://www.mdl.lu

Abonnements:

Messageries Paul Kraus
11, rue Christophe Plantin
L-2339 Luxembourg
Tél. (352) 49 98 88-8
Fax (352) 49 98 88-444
E-mail: mpk@pt.lu
URL: http://www.mpk.lu

NEDERLAND

SDU Servicecentrum Uitgevers
Christoffel Plantijnstraat 2
Postbus 20014
2500 EA Den Haag
Tel. (31-70) 378 98 80
Fax (31-70) 378 97 83
E-mail: sdu@sdu.nl
URL: http://www.sdu.nl

ÖSTERREICH

Manz'sche Verlags- und Universitätsbuchhandlung GmbH
Kohlmarkt 18
A-1014 Wien
Tel. (43-1) 53 18 11 00
Fax (43-1) 53 18 11 67
E-Mail: bestellen@manz.co.at
URL: http://www.austria.EU.net:81/manz

PORTUGAL

Distribuidora de Livros Bertrand Ld.ª
Grupo Bertrand, SA
Rua das Terras dos Vales, 4-A
Apartado 60037
P-2700 Amadora
Tel. (351-2) 495 90 50
Fax (351-2) 496 02 55

Imprensa Nacional-Casa da Moeda, EP
Rua Marquês Sá da Bandeira, 16-A
P-1050 Lisboa Codex
Tel. (351-1) 353 03 99
Fax (351-1) 353 02 94
E-mail: del.incm@mail.telepac.pt
URL: http://www.incm.pt

SUOMI/FINLAND

Akateeminen Kirjakauppa/Akademiska Bokhandeln
Keskuskatu 1/Centralgatan 1
PL/PB 128
FIN-00101 Helsinki/Helsingfors
P./tfn (358-9) 121 44 18
F./fax (358-9) 121 44 35
Sähköposti: akstilaus@stockmann.fi
URL: http://www.akateeminen.com

SVERIGE

BTJ AB
Traktorvägen 11
S-221 82 Lund
Tfn. (46-46) 18 00 00
Fax (46-46) 30 79 47
E-post: btjeu-pub@btj.se
URL: http://www.btj.se

UNITED KINGDOM

The Stationery Office Ltd
International Sales Agency
51 Nine Elms Lane
London SW8 5DR
Tel. (44-171) 873 90 90
Fax (44-171) 873 84 63
E-mail: ipaenquiries@theso.co.uk
URL: http://www.the-stationery-office.co.uk

ÍSLAND

Bokabud Larusar Blöndal
Skólavördustig, 2
IS-101 Reykjavik
Tel. (354) 551 56 50
Fax (354) 552 55 60

NORGE

Swets Norge AS
Østenjoveien 18
Boks 6512 Etterstad
N-0606 Oslo
Tel. (47-22) 97 45 00
Fax (47-22) 97 45 45

SCHWEIZ/SUISSE/SVIZZERA

Euro Info Center Schweiz
c/o OSEC
Stampfenbachstraße 85
PF 492
CH-8035 Zürich
Tel. (41-1) 365 53 15
Fax (41-1) 385 54 11
E-mail: eics@osec.ch
URL: http://www.osec.ch/eics

BĂLGARIJA

Europress Euromedia Ltd
59, blvd Vitosha
BG-1000 Sofia
Tel. (359-2) 980 37 66
Fax (359-2) 980 42 30
E-mail: Milena@mbox.cit.bg

ČESKÁ REPUBLIKA

ÚSIS
NIS-prodejna
Havelkova 22
CZ-130 00 Praha 3
Tel. (420-2) 24 23 14 66
Fax (420-2) 24 23 11 14
E-mail: nkposp@dec.nis.cz
URL: http://www.nis.cz

CYPRUS

Cyprus Chamber of Commerce and Industry
PO Box 1455
CY-1509 Nicosia
Tel. (357-2) 66 95 00
Fax (357-2) 66 10 44
E-mail: info@ccci.org.cy

EESTI

Eesti Kaubandus-Tööstuskoda (Estonian Chamber of Commerce and Industry)
Toom-Kooli 17
EE-0001 Tallinn
Tel. (372) 646 02 44
Fax (372) 646 02 45
E-mail: einfo@koda.ee
URL: http://www.koda.ee

MAGYARORSZÁG

Euro Info Service
Európa Ház
Margitsziget
PO Box 475
H-1396 Budapest 62
Tel. (36-1) 350 80 25
Fax (36-1) 350 90 32
E-mail: euroinfo@mail.matav.hu
URL: http://www.euroinfo.hu/index.htm

MALTA

Miller Distributors Ltd
Malta International Airport
PO Box 25
Luqa LQA 05
Tel. (356) 66 44 88
Fax (356) 67 67 99
E-mail: gwirth@usa.net

POLSKA

Ars Polona
Krakowskie Przedmiescie 7
Skr. pocztowa 1001
PL-00-950 Warszawa
Tel. (48-22) 628 12 01
Fax (48-22) 826 62 40
E-mail: ars_pol@bevy.hsn.com.pl

ROMÂNIA

Euromedia
Str. G-ral Berthelot Nr 41
RO-70749 Bucuresti
Tel. (40-1) 315 44 03
Fax (40-1) 315 44 03

SLOVAKIA

Centrum VTI SR
Nám. Slobody, 19
SK-81223 Bratislava
Tel. (421-7) 531 83 64
Fax (421-7) 531 83 64
E-mail: europ@tbbl.sltk.stuba.sk
URL: http://www.sltk.stuba.sk

SLOVENIA

Gospodarski Vestnik
Dunajska cesta 5
SLO-1000 Ljubljana
Tel. (386) 611 33 03 54
Fax (386) 611 33 91 28
E-mail: repansekj@gvestnik.si
URL: http://www.gvestnik.si

TÜRKIYE

Dünya Infotel AS
100, Yil Mahallessi 34440
TR-80050 Bagcilar-Istanbul
Tel. (90-212) 629 46 89
Fax (90-212) 629 46 27

AUSTRALIA

Hunter Publications
PO Box 404
3067 Abbotsford, Victoria
Tel. (61-3) 94 17 53 61
Fax (61-3) 94 19 71 54
E-mail: jpdavies@ozemail.com.au

CANADA

Renouf Publishing Co. Ltd
5369 Chemin Canotek Road Unit 1
K1J 9J3 Ottawa, Ontario
Tel. (1-613) 745 26 65
Fax (1-613) 745 76 60
E-mail: order.dept@renoufbooks.com
URL: http://www.renoufbooks.com

EGYPT

The Middle East Observer
41 Sherif Street
Cairo
Tel. (20-2) 393 97 32
Fax (20-2) 393 97 32

HRVATSKA

Mediatrade Ltd
Pavla Hatza 1
HR-10000 Zagreb
Tel. (385-1) 43 03 92
Fax (385-1) 43 03 92

INDIA

EBIC India
3rd Floor, Y. B. Chavan Centre
Gen. J. Bhosale Marg.
400 021 Mumbai
Tel. (91-22) 282 60 64
Fax (91-22) 285 45 64
E-mail: ebic@giasbm01.vsnl.net.in
URL: http://www.ebicindia.com

ISRAËL

ROY International
PO Box 13056
61130 Tel Aviv
Tel. (972-3) 546 14 23
Fax (972-3) 546 14 42
E-mail: royil@netvision.net.il

Sub-agent for the Palestinian Authority:

Index Information Services
PO Box 19502
Jerusalem
Tel. (972-2) 627 16 34
Fax (972-2) 627 12 19

JAPAN

PSI-Japan
Asahi Sanbancho Plaza #206
7-1 Sanbancho, Chiyoda-ku
Tokyo 102
Tel. (81-3) 32 34 89 21
Fax (81-3) 32 34 69 15
E-mail: books@psi-japan.co.jp
URL: http://www.psi-japan.com

MALAYSIA

EBIC Malaysia
Level 7, Wisma Hong Leong
18 Jalan Perak
50450 Kuala Lumpur
Tel. (60-3) 262 62 98
Fax (60-3) 262 61 98
E-mail: ebic-kl@mol.net.my

PHILIPPINES

EBIC Philippines
19th Floor, PS Bank Tower
Sen. Gil J. Puyat Ave. cor. Tindalo St.
Makati City
Metro Manilla
Tel. (63-2) 759 66 80
Fax (63-2) 759 66 90
E-mail: eccpcom@globe.com.ph
URL: http://www.eccp.com

RUSSIA

CCEC
60-letiya Oktyabrya Av. 9
117312 Moscow
Tel. (70-95) 135 52 27
Fax (70-95) 135 52 27

SOUTH AFRICA

Safto
Safto House
NO 5 Esterhyzen Street
PO Box 782 706
2146 Sandton
Tel. (27-11) 883 37 37
Fax (27-11) 883 65 69
E-mail: emaistar@ide.co.za
URL: http:/www.safto.co.za

SOUTH KOREA

Information Centre for Europe (ICE)
204 Woo Sol Parktel
395-185 Seogyo Dong, Mapo Ku
121-210 Seoul
Tel. (82-2) 322 53 03
Fax (82-2) 322 53 14
E-mail: euroinfo@shinbiro.com

THAILAND

EBIC Thailand
29 Vanissa Building, 8th Floor
Soi Chidlom
Ploenchit
10330 Bangkok
Tel. (66-2) 655 06 27
Fax (66-2) 655 06 28
E-mail: eblcbkk@ksc15.th.com
URL: http:/www.eblcbkk.org

UNITED STATES OF AMERICA

Berman Associates
4611-F Assembly Drive
Lanham MD20706
Tel. (1-800) 274 44 47 (toll free telephone)
Fax (1-800) 865 34 50 (toll free fax)
E-mail: query@berman.com
URL: http://www.berman.com

ANDERE LÄNDER/OTHER COUNTRIES/ AUTRES PAYS

Bitte wenden Sie sich an ein Büro Ihrer Wahl / Please contact the sales office of your choice / Veuillez vous adresser au bureau de vente de votre choix

NOTICE TO THE READER

Information on European Commission publications in the areas of research and innovation can be obtained from:

- **CORDIS, the Community R & D Information Service**

  For more information, contact:
  CORDIS Customer Service, BP 2373, L-1023 Luxembourg
  Tel. (352) 44 10 12-2240; fax (352) 44 10 12-2248; e-mail: helpdesk@cordis.lu
  or visit the website at http://www.cordis.lu/

- **Euroabstracts**

  The European Commission's periodical on research publications, issued every two months.
  For more information, contact:
  RTD help desk, European Commission, DG XIII, L-2920 Luxembourg
  Fax (352) 43 01-32084; e-mail: rtd-helpdesk@lux.dg13.cec.be

Price (excluding VAT) in Luxembourg: ECU 57

ISBN 92-828-4603-2

OFFICE FOR OFFICIAL PUBLICATIONS
OF THE EUROPEAN COMMUNITIES

L-2985 Luxembourg